A SEDIMENTOLOGICAL AND GEOCHEMICAL APPROACH TO UNDERSTANDING CYCLES OF STRATOVOLCANO GROWTH AND COLLAPSE AT MT. TARANAKI, NEW ZEALAND

A thesis presented in partial fulfilment of the requirements
for the degree of

Doctor of Philosophy
in
Earth Science

at Massey University, Palmerston North
New Zealand

Anke Verena Zernack

2008

***Frontispiece*. Mt. Taranaki viewed from the beach.**

ABSTRACT

The long-term behaviour of andesitic stratovolcanoes is characterised by a repetition of edifice growth and collapse phases. This cyclic pattern may represent a natural frequency at varying timescales in the growth dynamics of stratovolcanoes, but is often difficult to identify because of long cycle-timescales, coupled with incomplete stratigraphic records.

The volcaniclastic ring-plain succession surrounding the 2 518 m Mt. Taranaki, New Zealand, comprises a wide variety of distinctive volcanic mass-flow lithofacies with sedimentary and lithology characteristics that can be related to recurring volcanic cycles over >190 ka. Debris-flow and monolithologic hyperconcentrated-flow deposits record edifice growth phases while polylithologic debris-avalanche and associated cohesive debris-flow units were emplaced by collapse. Major edifice failures at Mt. Taranaki occurred on-average every 10 ka, with five events recognised over the last 30 ka, a time interval for which stratigraphic records are more complete. The unstable nature of Mt. Taranaki mainly results from its weak internal composite structure including abundant saturated pyroclastic deposits and breccia layers, along with its growth on a weakly indurated and tectonically fractured basement of Tertiary mudstones and sandstones. As the edifice repeatedly grew beyond a critical stable height or profile, large-scale collapses were triggered by intrusions preceding magmatic activity, major eruptions, or significant regional tectonic fault movements.

Clasts within debris-avalanche deposits were used as a series of windows into the composition of previous successive proto-Mt Taranaki edifices in order to examine magmatic controls on their failure. The diversity of lithologies and their geochemical characteristics are similar throughout the history of the volcano, with the oldest sample suites displaying a slightly broader range of compositions including more primitive rock types. The evolution to a narrower range and higher-silica compositions was accompanied by an increase in K_2O. This shows that later melts progressively interacted with underplated amphibolitic material at the base of the crust. These gradual changes imply a long-term stability of the magmatic system. The preservation of similar internal conditions during the volcano's evolution, hence suggests that external processes were the main driving force behind its cyclic growth and collapse behaviour and resulting sedimentation pattern.

ACKNOWLEDGEMENTS

This research would not have been possible without assistance of my chief-supervisor Assoc. Prof. Shane Cronin. He suggested my research project and helped me receive a Massey and DAAD doctoral scholarship as well as other financial assistance during the course of my PhD. I would also like to thank him for helpful discussions and new ideas during my PhD. I appreciate his thorough reviews of my thesis, papers and conference abstracts.

I also wish to thank my co-supervisors Prof. Vince Neall and Dr. Bob Stewart (Massey University) and Prof Richard Price (Waikato University) for their fruitful discussions over the last four years. Vince first introduced me to Taranaki and I furthermore want to thank him for the thorough revision of a major part of my thesis and helpful criticism. Bob and Richard's help with finding the most interesting rock samples and their huge physical effort to trim them down with a sledge hammer to reasonable sizes is also greatly acknowledged, as is their guidance regarding the geochemical and analytical work afterwards. In addition, Richard organised for me to re-visit Australian National University (ANU), Canberra, for the second part of ICP-MS analyses and also arranged a stay at the University of Melbourne for isotope analysis.

I am grateful to Assoc. Prof. Ian Smith (University of Auckland) for arranging the use of the XRF and EMP equipment in Auckland as well as at ANU, Canberra for the first visit to the ICP-MS.

I would like to thank some of the people of the Soil and Earth Sciences Group. Bob Toes and Ian Furkert introduced me to the labs at the start of my PhD and helped me out during sample preparation. Mike Bretherton was there whenever my computer decided to stop working. Thanks also to Moira Hubbard who helped out with administrative and stationary problems.

At Auckland University I would especially like to thank Dr. Ritchie Sims who not only provided outstanding assistance during the use of the microprobe, but also always made me love. Thanks for all those Family Guy episodes and GBs of music, which made probing a lot more enjoyable. Mr. John Wilmhurst is thanked for his assistance in XRF analysis and sample preparation.

Roland Maas is gratefully acknowledged for his help during sample preparation and subsequent analyses of isotope sample. He made me feel at home at Melbourne University and his good sense of humour made working easy. Thanks to John Woodhead who analysed some of

my samples after I left. And a big thanks also to Jo "Tiger" Whelan who invited me to stay with her during my visit to Melbourne. She helped me get around in town and in the lab.

Thanks also to the technician and scientists at ANU, Canberra, (and Ian Smith) for help during long nights of ICP-MS analyses.

I am also grateful to all the farmers of Taranaki who allowed me to access their land and especially the Dorn family of Pihama who invited me to stay with them, introduced me to other farmers and showed me important access ways to the numerous beaches I visited during my field studies.

I furthermore want to thank fellow postgraduate students, Dr. Katherine Holt, Dr. Michael Turner, Dr. Thomas Platz and Anja Moebis for sharing our "PhD experience", listening and helping each other out during harder times.

My PhD was supported by a Massey Doctoral Scholarship and a complementary DAAD (German Academic Exchange Service) Doctoral Stipend. I would also like to thank the George Mason Trust for an additional scholarship and Education New Zealand for a New Zealand Postgraduate Study Abroad Award, which allowed me to attend the 17th International Sedimentological Congress in Fukuoka, Japan. I gratefully acknowledge FRST (MAUX0401 "Learning to live with Volcanic risk") for field and laboratory financial support and INR for a Supplementary Scholarship.

I am very grateful to my parents who have supported me all my life and encouraged me during hard years of MSc as well as PhD study, even from the other side of the globe.

Last but most important, I would like to thank my fiancé Jonathan Procter, who has supported me for the last four years in everything I did. He was my field buddy during summer field work, my drinking buddy after hard work of study and he always had an open ear for discussions as well as my complaints. I am very thankful for his help with printing the final version of this thesis. I am very grateful for his support, patience and love during the last months.

TABLE OF CONTENTS

LIST OF FIGURES

LIST OF TABLES

CHAPTER 1.

INTRODUCTION

1.1. RESEARCH PROBLEM

The volcanic history of Mt. Taranaki is characterised by a series of alternating phases of edifice construction and destruction, often through catastrophic debris avalanches (Neall 1979; Ui et al. 1986; Palmer & Neall 1991; Palmer et al. 1991; Alloway et al. 2005). This behaviour may be typical of many andesitic stratovolcanoes but is poorly understood due to the long time scales over which this process operates and the evidence for repeated/older cycles being buried. The lack of detailed long-term records from many active stratovolcanoes like Mt. Taranaki makes it difficult to understand the processes and driving forces behind their evolution. Similarly, ancient successions rarely hold full records of the history of an edifice (Monzier et al. 1999; Capra & Macias 2000, 2002; Waythomas et al. 2000; Nehlig et al. 2001; Richards & Villeneuve 2001). Hence, hazard assessment inputs and interpretations of eruption and magmatic processes on such volcanoes are traditionally concentrated on detailed interpretations of the Holocene geologic record (Siebert et al. 1995; Thouret et al. 1995; Scott et al. 1997; Ponomareva et al. 1998, 2006; Belousov et al. 1999; Waythomas 1999; Waythomas & Miller 1999; Reid et al. 2001), an interval that may be too brief to identify longer-term influences on the activity and stability of stratovolcanoes. Detailed continuous records from these volcanoes are needed in order to truly characterise probable volcanic hazards.

In addition, it is not known to what extent external factors may have influenced construction and destruction processes on volcanic edifices. The extreme climate fluctuations over the last 130 ka dramatically changed the landscape in non-volcanic areas in New Zealand (Newnham et al 1999). During periods of cold climate, major glaciers formed along the Southern Alps of the South Island, with snow-lines lowered around 600-800 m below their current levels (Porter 1975; Hellstrom et al. 1998), but only minor glaciation occurred on the North Island (McArthur & Shepherd 1990). Seasonal frozen ground occurred on the South Island while periglacial activity, along with severe fluvial, and wind erosion shaped the North Island (Pillans et

al. 1993). Thick alluvial sequences aggraded (Suggate et al. 1978; Nelson et al 1988; Eden 1989) and subsequent degradation created sets of river terraces (Suggate et al. 1978; Eden 1989). During warm climate periods, glacioeustatic high sea-level stands occurred, which, in combination with tectonic processes, resulted in uplifted marine terrace sequences with overlying regressive sediments along the New Zealand coast (Pillans 1983, 1990a, 1990b). It can thus be inferred that the climate also played an essential role in the evolution of the volcanic landscape of the Taranaki peninsula, in particular during the last glaciation. Climate conditions are not only important in controlling the rates of erosion and landscape changes, they may also influence the potential of the volcano to fail, or even trigger a collapse (McGuire 1996; Sheridan et al. 1999; Scott et al. 2005; Capra 2006).

Unusually, at Mt Taranaki an almost complete stratigraphic record of distal ring-plain successions is exposed due to continuous coastal erosion of the tectonically uplifted areas of southern Taranaki (Pillans 1986, 1994). These circumstances make Mt. Taranaki an ideal example to study the evolution of a repetitively collapsing stratovolcano in order to better understand the processes operating over its life-span. Sequences within the volcaniclastic apron surrounding the volcano have been the key to understanding the last c. 26 000 years of volcanic activity (Neall 1979; Alloway et al. 1995), yet little is known about the older volcanic history preserved in coastal ring-plain sequences in south-west and southern Taranaki. These have only been studied as a regional mapping project and were later examined from a purely sedimentological perspective (Neall 1979; Neall et al. 1986; Palmer & Neall 1991). More detailed mapping and sedimentological classification of the older parts of the succession were needed in order to establish a comprehensive reconstruction of the lifespan of this volcano for the first time.

Improved stratigraphic control was also required to extend geochemical studies into the early magmatic history of the volcano to evaluate magma evolution since inception of Mt. Taranaki volcanism. Until now geochemical work at this andesite volcano was mainly limited to the well-known succession of the last 20 ka and comparisons with products from the andesitic centres of the TVZ (Price et al. 1992, 1999, 2005; Stewart et al. 1996). Most geochemical studies concentrated on the <14 ka present-day edifice, i.e. samples from lava flows (Price et al. 1992; Stewart et al. 1996) and pyroclastic units (Platz et al. 2007a, b), and included only a few samples from the ring plain (Price et al. 1999). The debris avalanche record studied during this project allowed an insight into the geochemical composition of former edifices that existed before 20 ka and thus a better understanding of the magmatic evolution of Mt. Taranaki.

1.2. REGIONAL GEOLOGIC SETTING

The subduction of the Pacific plate under the Australian plate has formed a continuous and still highly active subduction system that extends for c. 2 800 km from the Tongan Island Arc to New Zealand (Ewart et al. 1977; Karig 1970) (Fig. 1.1). It consists of three separate segments; the Tonga and Kermadec Arcs lie within oceanic crust, whereas the New Zealand (Hikurangi) active margin is formed within continental crust (Cole 1982). The dip of the Benioff zone is around 28-30° down to a depth of c. 100 km beneath the Tongan and Kermadec Arc volcanoes, after which it steepens from 40-57° beneath the Tongan Islands to 55-71° beneath the Kermadec Islands (Sykes 1966; Isacks & Barazangi 1977) and 50-70° beneath New Zealand (Adams & Ware 1977; Ewart et al. 1977). Convergence rates increase northwards from 51-53 (Kermadec) to 75-100 mm yr^{-1} (Tonga) (Jarrard 1986; DeMets et al. 1990; Parson & Wright 1996) and as much as 240 mm yr^{-1} along the northern Tonga Arc as a result of the active opening of the Lau Basin (Bevis et al. 1995). The proto-subduction system first developed along the Tonga-Kermadec-Vitiaz Arc and is thought to have propagated southwards along the paleo-Pacific margin to north of New Zealand by 30 Ma (Ballance et al. 1982; Davey 1982; Mortimer et al. 1998; King 2000). The present plate boundary configuration dates to ~ 27 Ma with the Tonga-Kermadec sectors largely remaining intact since 45 Ma (Sdrolias & Muller 2006). A minimum age of subduction of the oceanic crust of the Pacific Plate beneath the continental crust of the Australian Plate at the Hikurangi margin of c. 25-24 Ma is given by radiometric dates of the oldest volcaniclastic deposits exposed onshore, which are attributed to the onset of arc volcanism in Northland (Hayward 1993; Herzer 1995; Mortimer et al. 1998; Chanier et al. 1999).

Chase (1978) assumed that the Pacific Plate is rotating at c. 1.27°/Ma with the relatively instantaneous pole of rotation being located at 62°S, 174°E. Later, Wallace et al. (2004) showed that deformation processes in the North Island of New Zealand are more complex and dominated by several North Island tectonic blocks that rotate at c. 0.5-3.8°/Ma relative to the Australian Plate; the poles of rotation (with the exception of that of the Wanganui block) relative to the Pacific Plate cluster where the thick and buoyant Chatham Rise impinges on the margin. As a result, the convergence between the plates decreases and the subduction becomes progressively more oblique beneath the North Island, until at the northern coast of the South Island subduction no longer occurs and strike-slip motion along the Marlborough Fault system and the Alpine Fault system dominates (Van Dissen & Yeats 1991; Cole et al. 1995; Holt & Haines 1995; Collot et al. 1996; Beavan et al. 1999; Norris & Cooper 2000). The Hikurangi

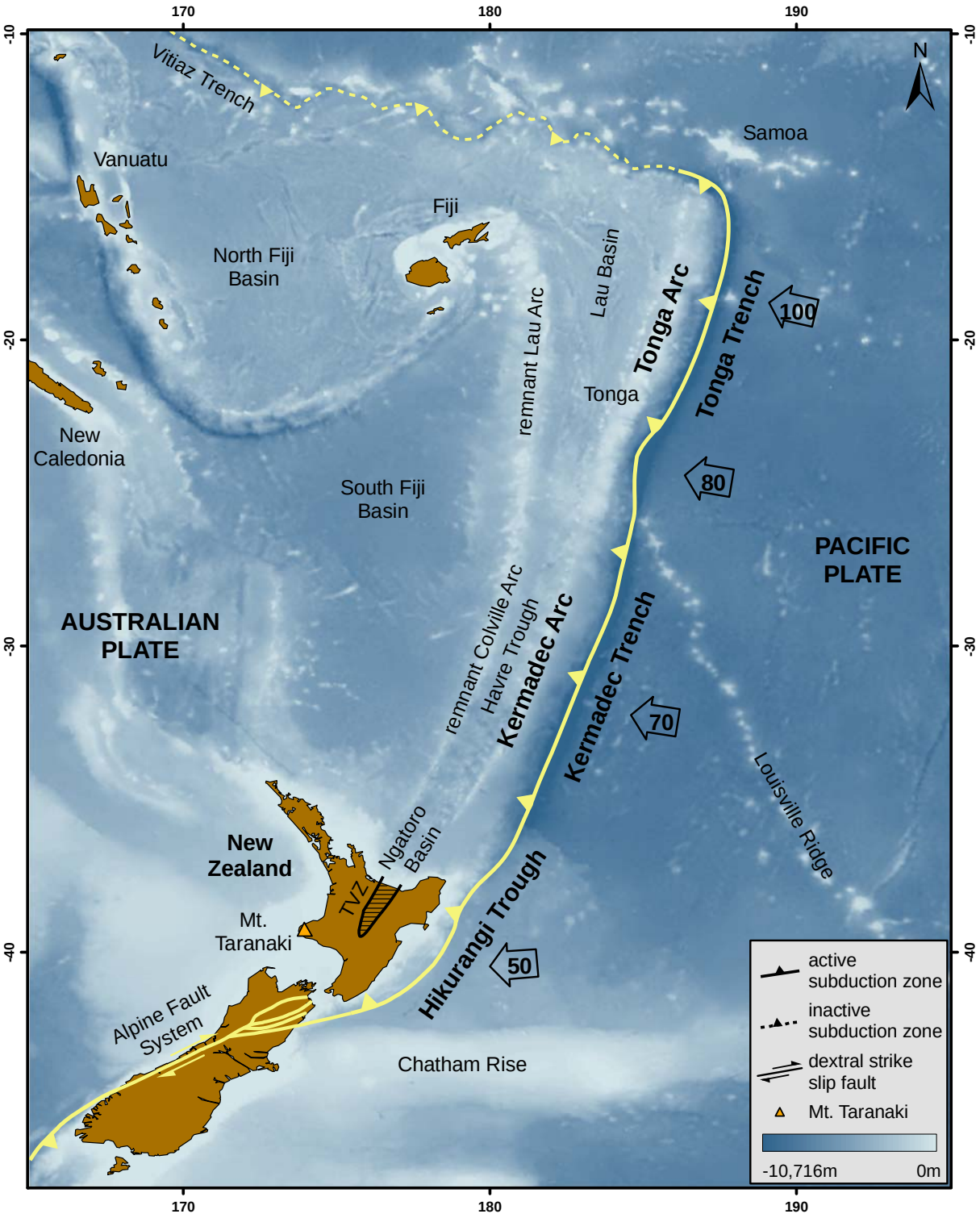

Figure 1.1 Map showing the Tonga-Kermadec-New Zealand (Hikurangi) subduction system with the Taupo Volcanic Zone at its southern end (modified from Smith & Price 2006). On the South Island the plate boundary is marked by the strike slip motion of the Alpine Fault system (location of the Alpine Fault after Norris & Cooper 2000). Arrows indicate direction and rate (mm yr^{-1}) of present-day plate convergence (from Parson & Wright 1996). Map coordinates are degrees of latitude and longitude.

margin represents a transitional region between the fast subduction along the Kermadec Arc and the intracontinental strike-slip of the South Island (Reading et al. 2001).

1.2.1. North Island setting

(i) Tectonic environment

The Taupo Volcanic Zone (TVZ) is the southern expression of the Tonga-Kermadec subduction system and the main locus of continental arc volcanism in the North Island, New Zealand (Cole 1979, 1986; Gamble et al. 1993; Wilson et al. 1995) (Fig. 1.1). The NNE-oriented zone is c. 300 km long, up to 60 km wide and characterised by thin (12-15 km), extending continental crust and exceptionally high heat flow (Stern 1987; Bibby et al. 1995; Hochstein 1995). The magnitude of total crustal heat transfer in the TVZ is highly anomalous in comparison to that of other active arcs, and with 2600 MW/100 km the highest of any subduction setting worldwide (Hochstein 1995). The rates of extension in the TVZ are about 7 mm yr^{-1} in the north and 18 mm yr^{-1} in the south; the subsidence rates are approximately 1-2 mm yr^{-1} (Cole et al. 1995). Several authors regard the TVZ as the <2 Ma part of a migrating arc, which has been active for more than 20 Ma (Stern 1985, 1987; Cole et al 1995). Over the past 4 Ma, the active volcanic front of this arc is thought to have migrated south-eastward at a rate of c. 20 mm yr^{-1} from the western part of the so-called Central Volcanic Region to its eastern half, i.e. the TVZ (Smith et al. 1989; Cole et al. 1995). This migration is considered to reflect the age and rate of asymmetric intra-continental spreading in the central North Island (Stern 1987). However, the available age-data together with geochemical and geological evidence may not support the concept of progressive southeastward migration of volcanism (Wilson et al. 1995). Instead, differences in age and type of volcanism throughout the TVZ may be a result of its variable and segmented nature (Wilson et al. 1995).

(ii) Magmatism

Volcanic activity in the TVZ started at c. 2 Ma at the Mangakino centre and has produced large volumes of rhyolite magmas in the central TVZ (Houghton et al. 1995; Wilson 1993, 2001; Wilson et al. 1995). In contrast, active andesite volcanism dominates the northern and southern extremities of the TVZ (Cole et al. 1986; Houghton & Nairn 1991; Donoghue & Neall 1996; Donoghue et al. 1999, Price et al. 2005). The Tongariro Volcanic Centre (TgVC) at the southern end comprises four major andesite massifs, Kakaramea, Pihanga, Tongariro, and Ruapehu, as well as a few satellite cones (Cole 1978). The oldest exposed lava flows on Tongariro were K-Ar dated at 230 and 273 ka respectively (Patterson & Graham 1988; Hobden et al. 1996), while the Te Herenga Formation lavas exposed in the Whakapapanui gorge on Mt. Ruapehu are

thought to be at least 300 ka (Tanaka et al. 1997). This age is consistent with andesite clasts found in the <310 ka O'Leary Conglomerate near Wanganui (Fleming 1953; Pillans 1990b; Bussell & Pillans 1992) that petrographically and geochemically match those from the Te Herenga and Waihianoa Formations (Parish 1994). Based on these studies, Gamble et al. (2003) give a maximum age of c. 340 ka for the inception of volcanism at Ruapehu and Tongariro volcanoes.

The Taranaki volcanic succession represents the most westerly expression of subduction-related volcanism in the North Island (Hatherton 1969). It is located 140 km west of the TVZ and has been assumed to lie 180 km above the westward-dipping Wadati-Benioff zone (Adams & Ware 1977; Stewart et al. 1996). Mt. Taranaki is recognised as a high-K arc volcano and was used by Dickinson and Hatherton (1967) to correlate K_2O-content to the depth of the underlying Wadati-Benioff zone (K-*h* relationship). However, more recent data showed that there is no definable seismic zone under Mt. Taranaki so that the relationship has become more enigmatic (Sherburn & White 2005). Stern et al. (2006) suggested that Taranaki magmatism might not be directly related to the present day subduction system but could instead be associated with lithospheric delamination. Other authors regarded the Taranaki volcanoes as a remnant of an earlier arc because the lineament parallels the Waitakere and Northland arcs (Hochstein et al. 1986; Briggs et al. 1989; Issac et al. 1994) rather than the NNE-trending TVZ (Cole 1982).

1.2.2. Taranaki volcanic lineament

The Taranaki volcanic succession consists of a group of four Quaternary andesite volcanoes that are spatially distinct from the contemporaneous andesitic volcanism in the Taupo Volcanic Zone (Neall et al. 1986). They form a NW-SE-trending volcanic lineament (perpendicular to the arc front) along which volcanism migrated south-eastward through time (Fig. 1.2B). The oldest and most deeply eroded centre, referred to as Paritutu Volcano (Arnold 1959), is found near New Plymouth, slightly offset from the trend defined by the other three edifices. It is represented by the remnants of several cumulodomes offshore (the Sugar Loaf Islands) and an onshore volcanic spine (Paritutu) K-Ar dated at 1.7 Ma (Stipp 1968). Kaitake Volcano is the next younger centre, which was active at c. 575 ka (Stipp 1968) and is now reduced to a series of radial ridges around a 654 m high central plateau. Ten kilometres SE of Kaitake is the eroded remnant of Pouakai Volcano, which rises up to 1 399 m asl. Volcanic activity is thought to have started at c. 670 ka (Neall 2003)and terminated with a catastrophic edifice failure producing the Maitahi debris avalanche c. 270 000 years ago (Gaylord et al. 1993). Mt. Taranaki/Egmont Volcano is the youngest and most southerly expression of volcanism

along the lineament. Volcanic activity at this centre began >130 ka (Alloway et al. 2005) with the last known eruption occurring in AD 1755 (Druce 1966; Neall et al. 1986).

1.2.3. Geology of the Taranaki peninsula

Late Cretaceous to Tertiary sedimentary basins in the western North Island include Wanganui, King Country (former North Wanganui) and Taranaki Basins (Fig. 1.2A), which are considered to be separate depocentres with similar Neogene sedimentary successions (Kamp et al. 2004). The Taranaki peninsula represents the largest onshore region within the Taranaki Basin, which is principally a subsurface feature lying offshore beneath the continental shelf (King & Thrasher 1996). The sedimentary basin sequence is built up of sand-, silt- and mudstones with intercalated shell beds, and records a period of regional transgression with higher order eustatic sea-level cycles (Kamp et al. 2004) from the late Cretaceous to early Miocene, followed by a regressive phase that is still ongoing (King & Thrasher 1996). The underlying basement can be divided into Eastern and Western Provinces that are separated by the Median Tectonic Zone (MTZ) (Mortimer et al. 1997). The western part of the Taranaki Basin is underlain by Palaeozoic and Mesozoic Gondwana rocks of the Western Province. The basement of the eastern part, including the Taranaki peninsula, consists of Carboniferous and Early Triassic to Early Cretaceous subduction-related volcanic, plutonic, and sedimentary rocks of the MTZ (Bradshaw 1993; Kimbrough et al. 1994; Sutherland 1999). The greywacke-dominated Eastern Province is separated from the MTZ by the Tongaporutu High, east of the Taranaki Fault (Mortimer et al. 1997).

The Taranaki Basin is cut by numerous active and inactive Quaternary faults (Fig. 1.2B). The Cape Egmont Fault Zone (CEFZ) marks the western limit of deformation related to the convergent plate boundary and subdivides the basin into two structural regions, the passive Western Stable Platform and the tectonically active Eastern Mobile Belt (King 1991; King & Thrasher 1996). The eastern margin of the basin is represented by the Taranaki Fault that vertically offset the basement by up to 6 km since the Late Cretaceous. The NE-SW orientation of Quaternary and active faults dates from the initial formation of the Tasman Sea (80 Ma), including the Inglewood and Norfolk Fault to the northeast of Mt. Taranaki, the Oaonui Fault to the south-west, and the Ararata Fault in the south-east (Hull & Dellow 1993). These may no longer reflect the current stress field (Sherburn & White 2006). An indicator of the more recent stress field is the alignment of volcanic vents, because these tend to lie perpendicular to the extension direction (Nakamura 1977). The SSE migration of the Taranaki volcanoes and the N-S

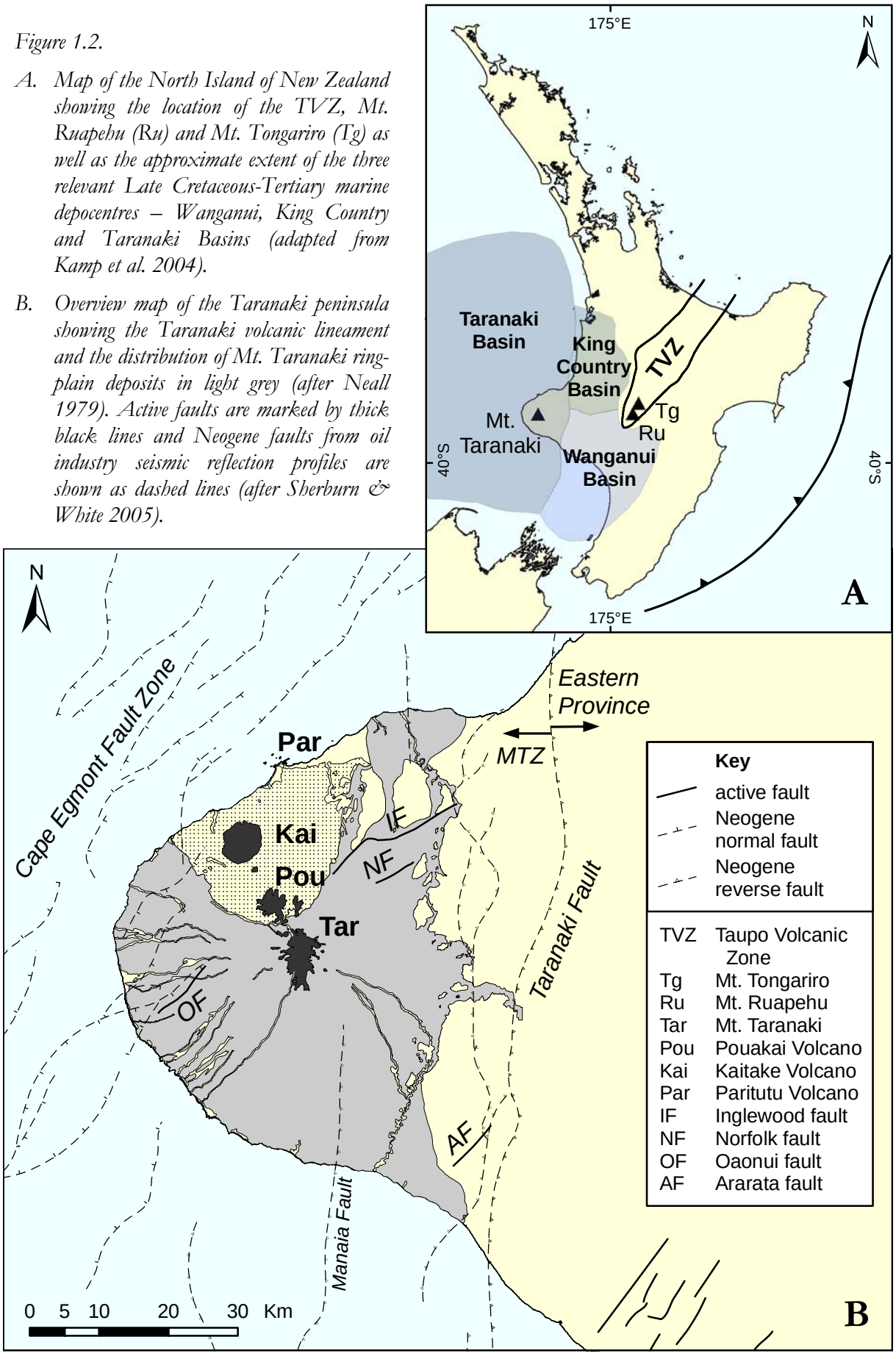

Figure 1.2.

A. Map of the North Island of New Zealand showing the location of the TVZ, Mt. Ruapehu (Ru) and Mt. Tongariro (Tg) as well as the approximate extent of the three relevant Late Cretaceous-Tertiary marine depocentres – Wanganui, King Country and Taranaki Basins (adapted from Kamp et al. 2004).

B. Overview map of the Taranaki peninsula showing the Taranaki volcanic lineament and the distribution of Mt. Taranaki ring-plain deposits in light grey (after Neall 1979). Active faults are marked by thick black lines and Neogene faults from oil industry seismic reflection profiles are shown as dashed lines (after Sherburn & White 2005).

alignment of Mt. Taranaki summit, Fanthams Peak and several lava domes (Neall 1971) might therefore represent the current stress field (Sherburn & White 2006).

The present geomorphology of the Taranaki peninsula is not related to its subsurface structure but was predominantly formed by the Quaternary volcanism and its products, which unconformably overlie the Tertiary basement. Another distinctive geomorphological feature was produced by the succession of Pleistocene sea-level high stands, which cut marine terraces into the uplifted Tertiary and volcaniclastic sequences in coastal areas of the Taranaki peninsula (Chappell 1975; Pillans 1983, 1990a, 1990b). Erosion and redistribution of the volcaniclastic deposits around the volcanoes have further shaped the landscape of Taranaki.

1.3. MT. TARANAKI/EGMONT VOLCANO

Mt. Taranaki is the second highest mountain of the North Island and volumetrically the largest andesitic stratovolcano in New Zealand. It rises up to 2 518 m asl over 25 km, resulting in steep upper slopes and a gently dipping distal surface that flattens out towards the sea. The conical shape of the volcano is broken on its southern flank by Fanthams Peak, a 1 962 m high parasitic cone that is thought to have been active over the last 7 ka (Neall et al. 1986). Exactly when the construction of Mt. Taranaki began is not known, but it is recognized as being older than 130 000 years (Alloway 1989; Alloway et al. 2005). The Motunui debris-avalanche deposit preserved in the coastal cliffs of North Taranaki represents the earliest identified activity (Alloway 1989). It was cut by the c. 127 ka Rapanui marine bench (Pillans 1983), indicating that it was deposited beforehand, and the characteristics and volume of the deposit imply that Mt. Taranaki was already a volcanic edifice of considerable height at that time.

The modern edifice of Mt. Taranaki is made up of lavas and pyroclastic deposits that are mostly younger than 14 ka (Neall 1979). These represent only a small component (c. 12 km^3) of the total volume of material erupted. The record of older volcanic activity is preserved in the surrounding ring-plain; a large (>150 km^3) apron of volcaniclastic material made up of debris-avalanche, lahar and fluvial deposits (Neall et al. 1986). It covers an area of c. 1 000 km^2 and is nearly circular in outline except in the north where the eroded remnants of the older volcanic centres formed a physiographic barrier to Mt. Taranaki-sourced mass flows (Fig. 1.3). Volcanic debris avalanches, attributed to the failure of former edifices, contributed the largest volume of volcaniclastic material to the Taranaki ring plain.

Neall (1979) and Neall et al. (1986) recognised at least four debris-avalanche deposits in west and south Taranaki, which were named Opua, Warea (the southern lobe Wr3), Pungarehu and Stratford Formations. Another three avalanche deposits (Ngaere, Okawa and Motunui Formations) of different ages were identified to the north-east and south-east of the volcano (Alloway et al. 2005), showing that collapses occurred on different sectors of the cone at different times throughout its history (Fig. 1.3). The minimum run-out distance for debris avalanches is marked by the present-day coastline of the Taranaki peninsula and generally exceeds 25 km to the west, 32 km to the south and 39 km to the north. The northern deposits can be traced for at least another 6 km offshore (Alloway et al. 2005). The debris avalanches at Mt. Taranaki were able to spread in an unconfined fashion onto the gently dissected ring-plain, forming broad fans around the volcano. This resulted in the development of three distinct surface geometries and lithofacies distributions that differ from valley-confined debris-avalanche units (Palmer et al. 1991). The deposits form a characteristic hummocky landscape with a higher density of large hills along the main dispersal axes that reduce in spatial density and size laterally and with increasing distance from source. Palmer & Neall (1991) recognised that these debris-avalanche deposits, together with their associated debris-flow deposits, record large-scale destructional events. In contrast, phases of cone growth comprised series of eruptive periods separated by intervals of quiescence. Accumulation on the ring plain during these constructional phases was dominated by lahar (debris-flow to hyperconcentrated-flow) deposits as well as tephra falls. Based on the dominant lithofacies element, the ring-plain depositional system in south-west Taranaki was split into an inferred cone-construction sequence (Opunake Fm) and a sequence representing edifice failure (Stratford Fm) (Palmer & Neall 1991). The largest known edifice failure at Mt. Taranaki produced the 20 ka Pungarehu Formation for which the calculated onshore volume is c. 7.5 km^3 (Ui et al. 1986a). Its internal structure is characterised by two major components: fragmental rock clasts (FRCs) and matrix. FRCs are shattered or deformed pieces of lava and stratified volcaniclastic material that represent intact parts of the former volcanic edifice (Alloway et al. 2005). They are surrounded by inter-clast matrix, which includes clay-sized material.

Mt. Taranaki lithologies range from vesicular red and black scorias through non-vesicular to holocrystalline, porphyric lavas of basaltic andesite to andesite composition (Neall et al. 1986; Stewart et al. 1996). Common inclusions are fragments of older eruptives and basement or cognate rocks such as diorite, gabbro, hornblendite, and Tertiary sediments, as well as rare metamorphic and mantle xenoliths (Price et al. 1999). Mt. Taranaki lavas are holocrystalline to hypocrystalline with crystal contents of 25-55%. Phenocryst assemblages are dominated by plagioclase, clinopyroxene, titanomagnetite, and hornblende with accessory apatite and zircon;

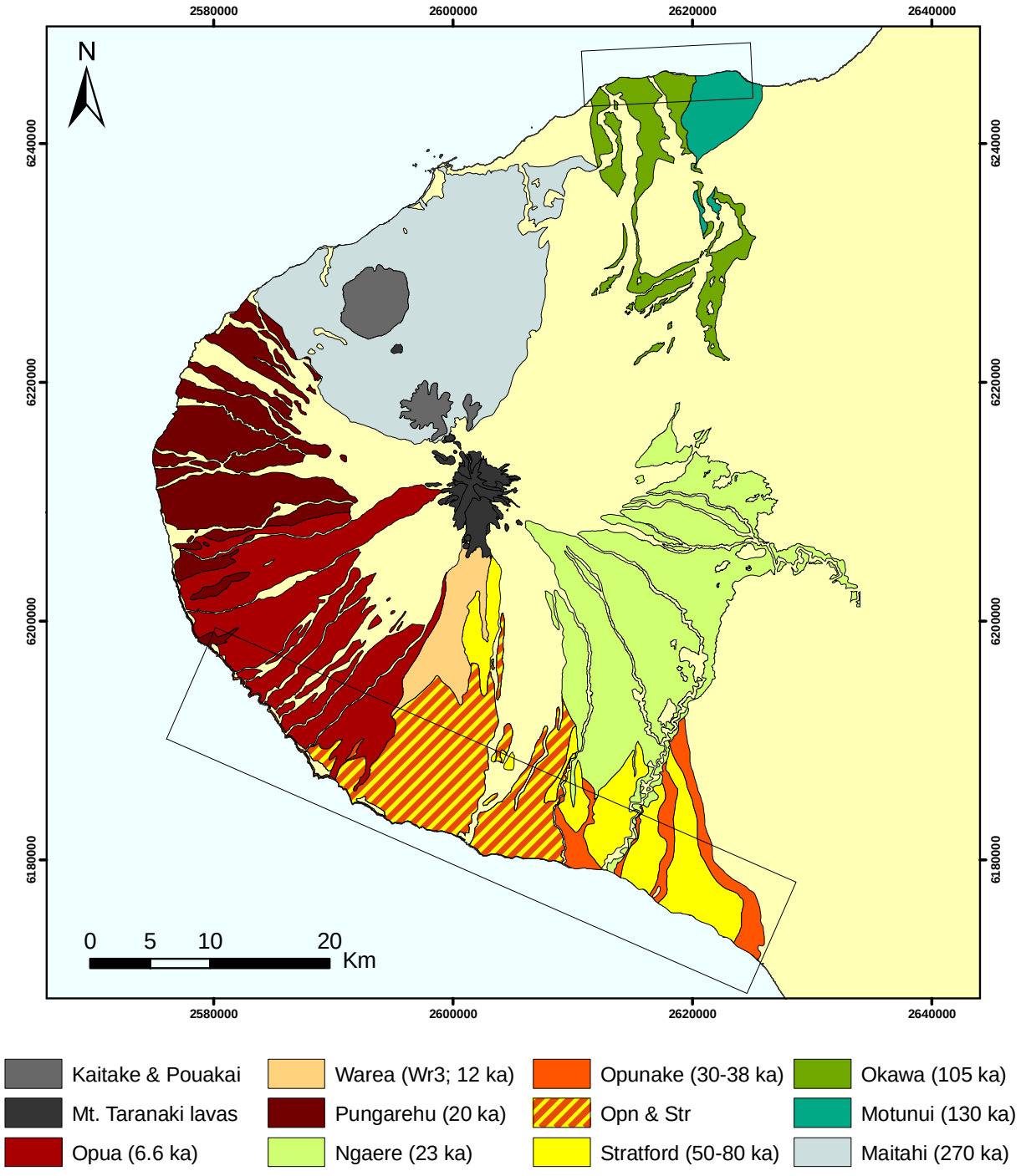

Figure 1.3. Geological map of the Taranaki Peninsula showing the distribution of identified debris-avalanche deposits and other ring-plain formations; Opn = Opunake Formation and Str = Stratford Formation (modified after Neall 1979; Neall & Alloway 2004; Alloway et al. 2005). The Maitahi Formation from Pouakai Volcano formed higher terrain, which was not inundated by Mt. Taranaki-sourced mass flows. Cone-forming lavas of Mt. Taranaki as well as lavas of the extinct volcanic centres Pouakai and Kaitake are shown in shades of grey and black. Rectangles mark the study areas in south-west and northern Taranaki.

olivine is present in more primitive lavas while orthopyroxene is extremely rare. Typical glomerocrysts comprise clinopyroxene ± titanomagnetite ± plagioclase ± olivine with rare amphibole.

The geochemical composition of Mt. Taranaki eruptives ranges from high-alumina basalt through to andesite and is dominated by high-K basaltic andesite (Price et al. 1992). K_2O abundance varies with time as magmas became progressively more K-rich with decreasing age. Overall, Taranaki lavas are markedly more potassic than equivalent andesites at Mt. Ruapehu. The trace element distribution in Taranaki volcanics shows a distinct arc-signature characteristic of subduction-related magmas, i.e. enrichment in strongly incompatible large ion lithophile elements (LILE) such as Rb, Ba and K, strong depletion in Nb relative to K and Th, enrichment in Pb over Ce, enrichment of light rare earth elements (LREE) over heavy rare earth elements (HREE) and Y (Price et al. 1999). The geochemical characteristics reflect the origin of Taranaki magmas from a depleted mantle wedge fluxed by slab fluids. They are interpreted to have evolved through a complex combination of magma mixing and assimilation and fractional crystallisation (AFC) (Price et al. 1999).

1.4. OBJECTIVES

The principle objectives of this thesis were to:

A. Use Mt. Taranaki to develop a new understanding of the growth dynamics and evolution of a stratovolcano from inception to maturity, including spatiotemporal physical development and sedimentary characteristics of construction and destruction.

B. Evaluate the geochemical development and magma evolution within this andesitic stratovolcano, through sampling within the sedimentary record.

C. Test the hypothesis that a cyclic process of edifice growth and destruction occurs at stratovolcanoes and to integrate physical, magmatic and climatic influences into a model of stratovolcano evolution and resulting sedimentation signatures.

1.5. METHODS OF STUDY

Sequences exposed along the coast in south-west Taranaki contain sedimentary records that are known to extend back to c. 100 ka (Neall 1979; Palmer & Neall 1991). This project

focused on a more detailed remapping of the Opunake and Stratford Formations in south-western and southern Taranaki. Mapping began with the northernmost and youngest units of the exposed volcaniclastic succession and proceeded southwards to the oldest units, which was possible due to a slight northward tilt of the strata related to the uplift of the Wanganui Basin to the south (Pillans 1994). Hyperconcentrated-flow and debris-flow deposits were grouped into composite stratigraphic units or packages because of the large number and narrow distribution range of single flow units. Mapping was thus focused on the correlation of deposit packages enclosed by distinct marker horizons. The key units for correlation were the easily recognised, widespread debris-avalanche deposits as well as continuous soil and peat layers.

A detailed sediment facies analysis of the exposed range of deposits was used to reconstruct volcanic events and other landscape-forming processes throughout the history of Mt. Taranaki and to interpret the growth dynamics of the volcanic edifice. Depending on their characteristics, the deposits were related to phases of cone-construction, collapse events, or periods of volcanic quiescence and landscape adjustment within the cyclic evolution of Mt. Taranaki. The events recorded in the volcaniclastic sequence were also correlated to the climatic changes that are known to have taken place over the last 130 000 years in this area, including the Last Glaciation (Pillans 1994)

The developed stratigraphy provided the basis for sampling the volcanic products for petrographic and geochemical analysis. The identified debris-avalanche deposits were used as a window into the composition of past edifices, since their clast assemblages record the geochemical character of the volcano up to the time of the collapse. Furthermore, they span the entire age range known for the volcano as they occurred from early stages of Mt. Taranaki onward. The geochemical analyses of the samples were subsequently used to gain a better understanding of long-term changes in the magmatic system of Mt. Taranaki. Geochemical data of all collected rock samples was acquired by X-ray fluorescence analysis (XRF) and inductively coupled plasma mass spectrometry (ICP-MS); in addition Strontium, Neodymium and Lead isotopic analysis of selected samples were carried out. Thin-sections of the oldest debris-avalanche sample suites were prepared for petrographic classification and analysis of mineral compositions of selected lithologies. Together, these data sets provided the basis for characterising the magmatic evolution from birth to maturity of this andesite volcano.

The geochemical data and field records combined were used to reconstruct the processes that influenced the cyclic growth and destruction of Mt. Taranaki and to elucidate the relative roles of internal and external driving forces behind the volcano's behaviour.

1.6. THESIS CONTENTS

The following Chapter 2 outlines the newly established stratigraphy of the ring-plain succession in south-west Taranaki. It describes the distribution and age of identified debris-avalanche units as well as volcanic mass-flow and reworked deposits. After developing the chronology of volcanic and other events, Chapter 3 focuses on the sedimentological characteristics of the different types of ring-plain deposits. These provide the basis for the subsequent interpretation of the ring-plain depositional system and landscape evolution. The geochemical compositions of clast assemblages, including rare earth and trace element characteristics and isotopic fingerprints, are presented in Chapter 4. Here, the debris-avalanche clasts are used to geochemically characterise past edifices in order to better understand the magmatic system and its evolution. Chapter 5 describes the clast lithologies within the Mt. Taranaki debris-avalanche deposits, their petrographic features and the mineralogy of the oldest sample suites in comparison to young eruptives to infer changes in crystallisation conditions and origin of the volcanic rocks. The stratigraphy, sedimentology and geochemical results are combined and discussed in Chapter 6 to develop a model of cyclic growth and destruction of andesitic stratovolcanoes, based on Mt. Taranaki. Chapter 7 closes with conclusions and recommendations for further work.

CHAPTER 2.

STRATIGRAPHY OF THE VOLCANICLASTIC RING-PLAIN SUCCESSION OF SOUTH-WEST TARANAKI

2.1. INTRODUCTION

Ring-plain successions of stratovolcanoes provide a significant long-term record of past eruptive and sedimentary events that may not be preserved or exposed closer to source (e.g. Cronin & Neall 1997; Lecointre et al. 1998; Belousov et al. 1999; Davidson & De Silva 2000). Deposits representing these events can often be dated by applying the radiocarbon method to intercalated soil/peat layers and ripped-up fragments of wood, as well as by identifying interbedded tephras of known age. This provides the basis for a chronological reconstruction of volcano evolution and a stratigraphic overview of volcaniclastic successions.

Previous studies on and around Mt. Taranaki mainly focused on the younger volcanic history. Deposit sequences that built up the modern edifice and younger landscape-shaping parts of the volcaniclastic apron surrounding the volcano have been the key to understanding the last c. 26 000 years of volcanic activity (Neall 1979; Neall et al. 1986; Alloway et al. 1995; Alloway et al. 2005). Yet, little is known about the history prior to this time, since older units are buried by tens to hundreds of metres of more recent volcaniclastic deposits. Due to the interplay of coastal erosion and tectonic uplift (Pillans 1994), older parts of the ring-plain succession are exposed in coastal cliffs in south-west and southern Taranaki with sedimentary records extending back to at least 100 000 years (Neall 1979; Palmer & Neall 1991). These were studied as part of a regional mapping project and later examined from a sedimentological perspective (Neall 1979; Neall et al. 1986; Palmer & Neall 1991).

More detailed mapping of these sequences has enabled a comprehensive reconstruction of the earlier volcanic history of Mt. Taranaki. This chapter presents the results from mapping of the coastal sections in south-west Taranaki and the developed stratigraphic overview of the older ring-plain succession.

2.2. STRATIGRAPHY OF MT. TARANAKI

Volcanic activity at Mt. Taranaki began more than 130 000 years ago as indicated by the earliest known volcanic products (Motunui Fm.) that closely underlie the c. 127 ka NT2/Rapanui wave cut surface (Alloway et al. 2005). The last known eruptions include the Tahurangi eruption of AD1755 (Druce 1966) and the emplacement of the summit dome, considered to be around AD1800 (Platz 2007). The volcanic history has been characterised by alternating phases of edifice construction and collapse (Neall 1976; Neall et al. 1986; Alloway 1989; Palmer & Neall 1991; Alloway et al. 2005), which accumulated a thick volcaniclastic apron around the present stratovolcanic cone. Modern Mt. Taranaki is made up of lavas and pyroclastic deposits mostly younger than 10 ka. This 12 km^3 cone represents only a small component of the total volume of material erupted compared to the c. 150 km^3 ring plain. The volcanic stratigraphy of the centre has been subdivided into two separate groupings: the edifice-forming deposits and those of the ring-plain succession (Neall 1979; Neall et al. 1986; Alloway et al. 1995; Alloway et al. 2005). These are summarised in the following sections.

2.2.1. Ring-plain stratigraphy

Early studies and geological maps of Taranaki subdivided the apron of volcaniclastic material surrounding the Taranaki volcanoes into several segments of different ages and origin based on geomorphological features and soil properties (Lensen 1959; Grant-Taylor 1964a, 1964b; Hay 1967; Grant-Taylor & Kear 1970). The formation of these so-called "ring-plains of laharic agglomerate" was thought to coincide with periods of Pleistocene glaciation, while the corresponding warm interglacial periods were marked by cutting of marine benches (Fleming 1953; Grant-Taylor 1964a, 1964b; Hay 1967). The idea that ring plain-building lahars were restricted to glacial periods was based on the hypothesis that much greater amounts of snow and ice would have been on the volcanoes during cold climate conditions. Fossil pollen from deposits below most laharic "agglomerates" indicated a warm climate, while those from within several of the laharic deposits suggested cold conditions (Grant-Taylor 1964a). The absence of laharic breccias during interglacial intervals (during periods of marine incursion) was explained by diminution of volcanic activity during warm climates (Grant-Taylor 1964a).

Five "ring-plains" were attributed to Kaitake and Pouakai Volcanoes and two younger ones to Mt. Taranaki (Grant-Taylor 1964a, 1964b; Hay 1967). Activity at Kaitake produced the New Plymouth, Eltham and Inglewood lahars (Hay 1967). Subsequently activity at Pouakai commenced, which completed the Maitahi ring plain and partly built up the Lepperton ring plain.

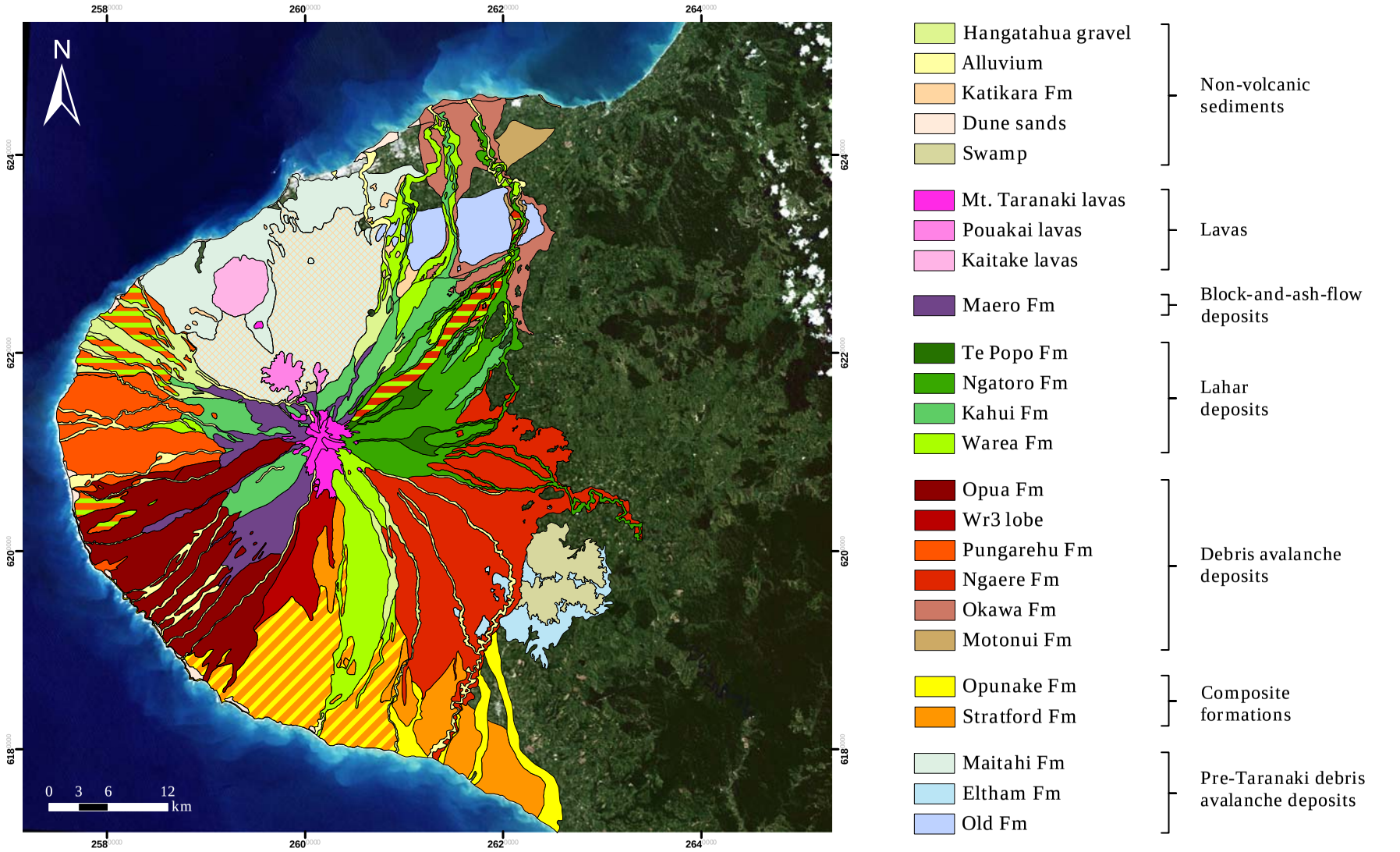

Figure 2.1. Quaternary Geological Map of Taranaki showing the distribution of volcanic, volcaniclastic and sedimentary Formations (after Neall & Alloway 2004). Grid references are in NZ map grid.

When activity at Mt. Taranaki started, it formed a ring plain that merged with the Lepperton one and two new ones; the Stratford and Opunake lahars. The >50 ka Stratford and 30-38 ka Opunake Formations were thought to represent remnants of ring plains formed during the last glaciation that were separated by a period of warm climate conditions (Grant-Taylor & Kear 1970). Erosion of the western part of the Stratford surface during this interval was followed by accumulation of the Opunake lahars, which in places lapped on to the Stratford ring plain. Distinction of the two surfaces was based on weathering differences and ash cover, with >4 m of ash above the Stratford Fm. versus >1 m of ash covering the Opunake Fm.

Later mapping projects followed a more modern approach in reconstructing the volcanic history of the Taranaki peninsula. The former laharic "agglomerates" were interpreted as individual debris-avalanche deposits resulting from major collapses of past edifices. Studies by Neall (1976, 1979), Neall et al. (1986), Alloway (1989), Gaylord et al. (1993), Neall & Alloway (2004), and Alloway et al. (2005) recognised and mapped the distribution of five debris-avalanche deposits from Mt. Taranaki and one from Pouakai Volcano. These re-defined or newly-mapped formations mostly replace the older units (Fig. 2.1). Exceptions are the oldest surfaces of unknown age, which have not been studied in detail, and the volcaniclastic sequence in south-west Taranaki that is still referred to as Stratford and Opunake Formations.

The following sections introduce previously identified and mapped stratigraphic units of the Taranaki volcanic succession from oldest to youngest:

(i) Eltham surface and Old Formation

The Old Formation was originally considered to be part of the Eltham surface (Grant-Taylor 1964; Hay 1967; Neall 1979) but was found to be older by Neall & Alloway (2004) since it forms the base of the coverbeds of the c. 520 ka Ball Marine Terrace (Q13, Kaiatea Marine Terrace of Pillans, 1983). It consists of a clay-rich diamicton that forms an elevated and highly dissected surface in north-east Taranaki.

The Eltham Formation comprises a voluminous debris-avalanche deposit in the eastern ring-plain sector near the town of Eltham. It occurs near the base of the coverbed sequence of the Ararata Marine Terrace (Q11) and is overlain by the c. 360 ka Rangitawa Tephra, suggesting an age of >400 ka and hence an origin from Pouakai Volcano (Neall & Alloway 2004).

(ii) Maitahi Formation

The Maitahi ring plain was redefined as Maitahi Formation and attributed to a catastrophic collapse of Pouakai Volcano. The youngest $^{40}Ar/^{39}Ar$ date obtained from debris-

avalanche clasts gives a maximum age of c. 240 ka for the event (Gaylord et al. 1993). A more precise age range could not be established since its base is not exposed. The voluminous debris-avalanche deposit covers a vast area around Pouakai and is best exposed along the north-western coast from Oakura to New Plymouth where it forms >40 m high cliffs.

(iii) Motunui Formation

The oldest confirmed Mt. Taranaki debris-avalanche deposit, and also the oldest known unit derived from this volcano, the Motunui Formation is exposed along the northern coast of the Taranaki peninsula (Alloway 1989; Alloway et al. 2005). Its age was estimated based on its stratigraphic position in relation to marine terraces. According to an older study, the deposit overlies and thus postdates the cutting of the c. 127 ka NT2/Rapanui Marine Terrace (Alloway 1989). A different age (210-127 ka) was specified by Alloway et al. (2005), who described the Motunui Formation as being truncated by the NT2/Rapanui and overlying the NT3/Ngarino Marine Terrace.

Near Turangi Road, a younger marine bench (NT1) is cut into the Motunui Formation. NT1 was first correlated to the 81 ka Hauriri Marine Terrace of the Wanganui District (Alloway 1989) and later to the 105 ka Inaha Marine Terrace of south Taranaki (Neall & Alloway 2004; Alloway et al. 2005). In the following, the age of the Motunui Formation is referred to as >130 ka according to its chronostratigraphic position below the Rapanui wave-cut surface (Neall & Alloway 2004; Alloway et al. 2005).

(iv) Okawa Formation

The Okawa Formation comprises a debris-avalanche deposit that was emplaced around 105 ka as indicated by its stratigraphic position below the Inaha wave cut surface and the fossil pollen record preserved in peat beds below and above (Neall 2003; Alloway et al. 2005). It has a minimum volume of c. 3.62 km^3 and covers >255 km^2 in northern and north-eastern Taranaki (Alloway 1989). The deposit was mapped from around Inglewood, where it forms a distinctive surface with numerous mounds, down the Waiongana Stream and the Manganui-Waitara Rivers to the coast.

(v) Stratford and Opunake Formations

Due to a thick soil and ash cover, the volcaniclastic sequence in south and southeast Taranaki does not exhibit distinct surface characteristics that allow detailed mapping of individual units. Hence, while areas in western and eastern Taranaki previously mapped as Stratford and Opunake Formations have been redefined, these outdated formations still occur in the southern

and south-western sector of the geological map (Neall & Alloway 2004). The main distribution of the Stratford Formation is to the east of Manaia, while the Opunake Formation covers the coastal areas from Opunake to Manaia. Both comprise similar lithofacies, i.e. laharic, debris-avalanche and alluvial deposits that accumulated between c. 80-50 ka and 38-30 ka, respectively (Grant-Taylor & Kear 1970; Neall 1979). Later sedimentological studies of the south-western ring-plain described the occurrence of three debris-avalanche deposits within the Stratford Formation and one within the lahar-dominated Opunake Formation (Palmer & Neall 1991; Palmer et al. 1991).

(vi) Ngaere Formation

The large-volume (>5.85 km^3) Ngaere debris-avalanche deposit covers c. 320-500 km^2 of the north-eastern to south-eastern Taranaki ring plain (Alloway 1989; Alloway et al. 2005) and forms an extensive hummocky landscape in the south-eastern sector. The deposit pre-dates the Kawakawa Tephra and overlies the Tuikonga Tephra, giving a ^{14}C age range of 22.6-23.4 ka for the collapse event (Alloway et al. 1995; Alloway et al. 2005). The closely underlying Poto.b tephra bed was interpreted to indicate that the triggering of the collapse and the generation of the Ngaere debris avalanche was directly related to eruptive activity (Alloway 1989; Alloway et al. 2005).

(vii) Pungarehu Formation

The Pungarehu Formation closely overlies the 22.6 ka Kawakawa Tephra and was dated at c. 22.1 ka (Neall 1979). It is the most voluminous debris-avalanche deposit known from Mt. Taranaki (>7.5 km^3) and covers at least 200-250 km^2 of the western ring-plain sector (Neall 1979; Ui et al. 1983). Its offshore extent is thought to be at least 8 km west of Cape Egmont (McDougall & Gibb 1970; Neall 1979) and bathymetric maps show the occurrence of debris avalanche mounds on the seafloor to a depth of about 60 m (Shell, BP and Todd Oil Services Ltd. 1974). To the south, its extent is obscured due to the progressive overlapping of the younger Warea and Opua Formations. The deposit thickness exceeds 60 m in proximal locations and 16 m near its main dispersal axis at medial coastal outcrops. The most distinctive feature of the Pungarehu Formation is its characteristic hummocky surface with mounds ranging in average height from 5 m near the coast to 30 m at 300 m altitude (Neall 1979).

(viii) Warea and Kahui Formations

The Warea Formation was originally defined as volcaniclastic deposits that were emplaced between 16-12 ka (Neall 1972). It consists of four lobes of different lithologies. Lobe

Wr1 to the north-west, Wr2 to the south-west and Wr4 to the south-east of Mt. Taranaki filled small paleo-channels and intermound areas of the older Pungarehu debris-avalanche deposit and were hence interpreted as lahar deposits (Neall 1979). In contrast, the southern lobe Wr3 occurs between Oeo and Otakeho Streams and is characterised by small mounds in proximal locations and hence attributed to a debris avalanche (Neall 1979). Five debris-flow and hyperconcentrated-flow deposits on the eastern and north-eastern flanks with a maximum age of 21.5 ka were also correlated to the Warea Formation (Alloway 1989). Newer studies of the north-western and south-western lobe show that several individual debris-flow and hyperconcentrated-flow deposits of various ages (22.5-14.8 ka) occur in all major catchments of the western ring-plain sector (Procter et al. 2009). Their wide range of sedimentological characteristics reflects their various origins and flow dynamics.

The Kahui Formation contains a series of block-and-ash-flow and debris-flow deposits that were emplaced from 12.5-7 ka and extend up to 20 km from the present summit of Mt. Taranaki (Neall 1979). Some debris-flow deposits occur on the north-western flank of the volcano and at least 8 were recognised on the lower western flanks, where they fill depressions between higher ridges of the Pungarehu Formation. Alloway (1989) correlated a succession of at least three cohesive and one non-cohesive debris-flow deposits on the north-eastern flank to the Kahui Formation. The units occur in channels of major tributaries and have an implied age range of c. 13-7 ka (Neall 1979; Alloway et al. 1992).

(ix) Opua Formation

The Opua debris-avalanche deposit (0.35 km^2) covers large parts of the western and south-western ring plain (Neall 1979). Its surface is covered by mounds generally <20 m in height and typically <2 m near the coast. Composite-shaped mounds and internal contacts suggest a multiple origin with some mounds consisting of Pungarehu mounds that were subsequently covered by the Opua debris-avalanche deposit. The Opua Formation overlies the c. 7 ka BP Oakura Tephra and was dated at c. 6.6 ka (Neall 1979). A large amphitheatre between Bob's Ridge and Fanthams Peak is considered to demarcate the source area, which collapsed to generate the Opua debris avalanche. The avalanche scarp has since been partly infilled by younger lava flows.

(x) Ngatoro, Te Popo and Hangatahua Formations

The Ngatoro Formation consists of two debris-flow lobes on the north-eastern and eastern flank, the latter of which shows transitions to hyperconcentrated-flow and streamflow deposits (Neall 1979; Alloway 1989). The deposits were emplaced between c. 3.5-3.6 ka.

The Te Popo Formation comprises at least two debris-flow units that occur in channels and interfluve areas on the eastern flank of Mt. Taranaki, (Alloway 1989). Their implied age is 2.9-3.1 ka because they are interbedded with Manganui tephra beds.

The Hangatahua Gravels are c. 400 year old sandy gravels that occur along the Stony River in western Taranaki (Neall 1979; Neall et al. 1986). They are thought to have formed during floods and reworking of block-and-ash flow deposits following the Maero eruptive episode (Platz 2007).

2.2.2. Tephra and edifice stratigraphy

Mt. Taranaki has experienced frequent explosive pyroclastic eruptions, with most fall units distributed in a broad NNE to SSE sector from the present summit (Neall 1972; Alloway 1989; Alloway et al. 1995; Turner et al. 2008). The oldest tephras are best preserved in peat and carbonaceous-rich sediments exposed along the northern coast, including the oldest identified tephra located above the Motunui Formation (Alloway 1989). Ring-plain records near the volcano are largely buried or have been influenced by post-depositional mixing and weathering, thus only allowing a few of the most prominent tephra beds to be identified. Distal outcrops in northern Taranaki provide a better record of eruptive activity from >130 to 28 ka (Alloway 1989). Activity between 100-80 ka produced five distinct major tephra beds and a further seven between 80-28 ka. The <28 ka record of eruptive activity is better preserved in the eastern and north-eastern ring plain and contains at least 75 individual tephras $>10^7$ m^3, resulting in an average periodicity of one eruption of this magnitude in 330 years (Alloway 1989; Alloway et al. 1995). Minor eruptive activity between 32-28 ka was followed by frequent, moderate to large magnitude eruptions from 28-23.4 ka, which produced a sequence of thirteen tephra beds in north-east and central Taranaki and several debris-flow deposits of the Opunake Formation (Alloway et al. 1995). A new cycle of intense eruptive activity started at 22.7 ka and is thought to have initiated the Ngaere collapse to the east. High-frequency eruptions rapidly rebuilt the edifice, before it collapsed to the west to form the Pungarehu debris-avalanche deposit. The collapse was followed by intense eruptive activity between 20.2-19.4 ka and sporadic moderate to small magnitude eruptions between 18.8-12.9 ka. At the same time, debris and hyperconcentrated flows of the Warea Formation were generated on all flanks of the volcano (Neall 1979; Alloway 1989; Alloway et al. 1995; Procter et al. 2009).

The present edifice of Mt. Taranaki is thought to have been predominantly constructed over the last 10 000 years, following the deposition of the Warea debris and hyperconcentrated flows (Neall et al. 1986). The edifice consists of an older bottom part and a younger symmetrical

upper cone, which is slightly offset from the centre of the lower cone (Grant-Taylor 1964a, 1964b). This is indicated by the abrupt decrease in gully depth above c. 1100 m, a steeper slope of the mountain and the termination of some older lava flows and pyroclastic deposits. Grant-Taylor (1964b) suggested that the top part of the original edifice, which was probably 300 m higher than at present, was removed and a younger cone constructed in its place.

Frequent effusive activity between 12-7 ka produced lava flows (Fig. 2.3) interspersed with dome-building episodes, and dome-collapse block-and-ash-flow emplacement on the eastern and western flanks (Neall 1979; Neall et al. 1986; Platz 2007), while intense explosive activity between 10-8 ka resulted in deposition of eight tephra beds (Alloway et al. 1995). The Warwicks grouping contains the oldest lava flows (c. 8 ka), including distinct geomorphic features such as Warwicks Castle and Bob's Ridge, that form the present upper cone (Stewart et al. 1996). Following the Opua collapse, emplacement of the Peters Lavas (7-3.3 ka) further built up the edifice (Neall 2003) and was accompanied by sporadic small to large tephra emission between 8-4.4 ka (Alloway et al. 1995). Two large subplinian eruptions produced widespread tephras at 4.1 ka (Korito Tephra) and 3.6 ka (Inglewood Tephra) as well as at least 3 pyroclastic flows (Neall 1972; Alloway 1989; Neall et al. 1986; Alloway et al. 1995). The Inglewood eruption was followed by deposition of the Ngatoro debris flows (Neall et al. 1986; Alloway 1989). Major eruptive activity from the satellite vent Fanthams Peak occurred at c. 3.3 ka and produced several lava flows (Neall 1986; Downey et al. 1994; Alloway et al. 1995) with the latest ones possibly as young as 1.4 ka (Rosenthal 2005). Frequent, small to moderate sized eruptions from Fanthams Peak deposited four closely spaced tephra beds at c. 3.1 to 2.8 ka (Alloway et al. 1995; Turner et al. 2008). Subsequently, four lava domes were extruded from subsidiary vents on the lower flanks of Mt. Taranaki: the Dome, Skinner Hill and the Beehives (Neall 1971; Neall et al. 1986). A period of dome-building and dome-collapse block-and-ash-flows on the eastern flanks at 2 ka (Neall et al. 1986) was followed by the extrusion of the 1.7 ka Staircase lavas, which partly filled the Opua amphitheatre (McGlone et al. 1988; Downey et al. 1994; Stewart et al. 1996; Neall 2003). The subplinian Kaupokonui eruption at 1.4 ka preceded the construction of the uppermost part of the modern edifice. The youngest lava flows <1.7 ka, which further filled the Opua amphitheatre, are summarised in the Skeet grouping and the Summit grouping comprising the present summit dome and the Turtle, a prominent lava coulee on the upper NW flanks (Neall 2003). The youngest (Maero) eruptive period began around 800 years BP and has been dominated by dome-forming and collapse episodes (Maero block-and-ash-flows), several smaller eruptions and the subplinian Burrell eruption (Cronin et al. 2003; Platz 2007). The Tahurangi eruption in AD1755

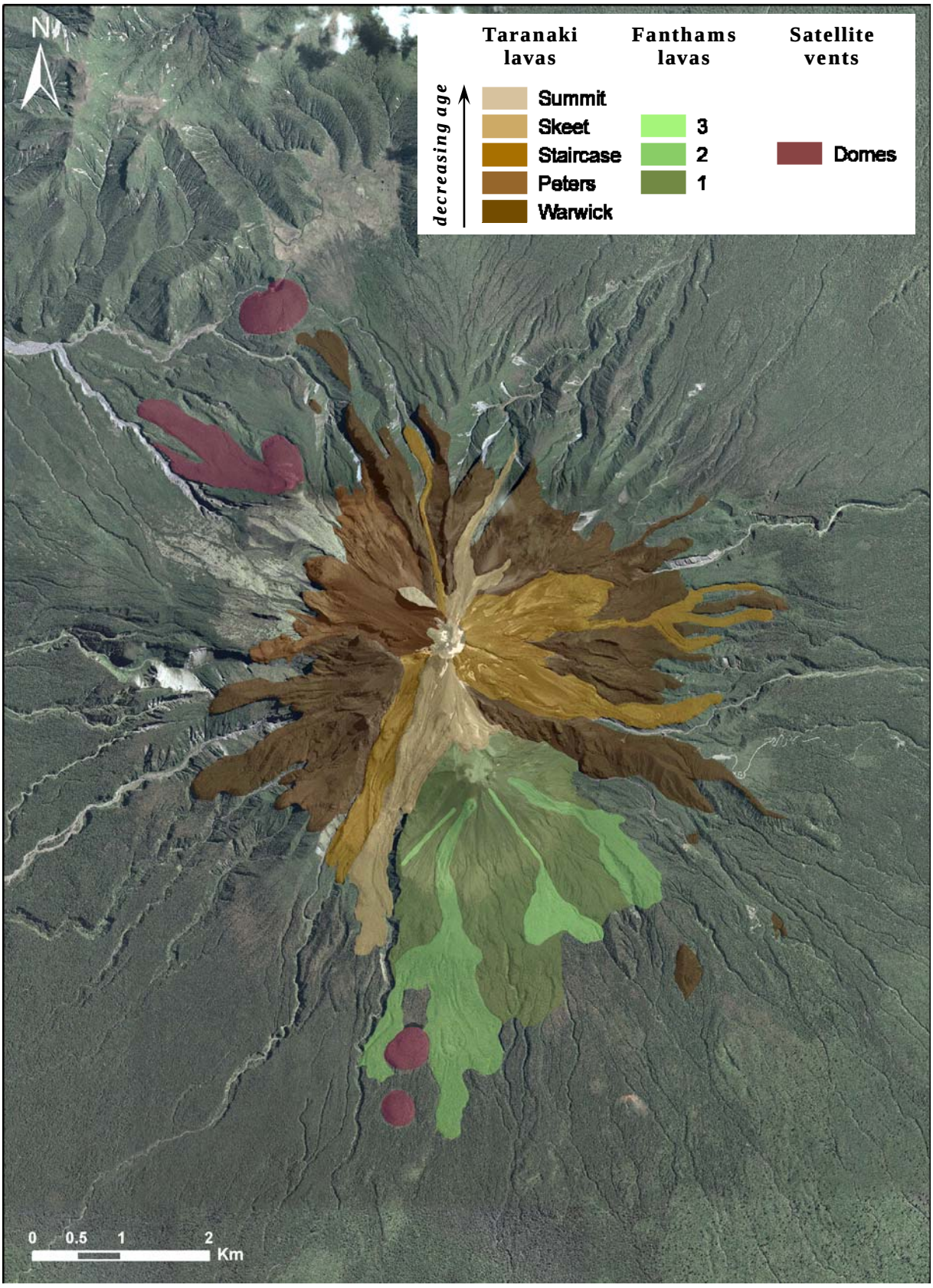

Figure 2.2. Lava flow distribution and stratigraphy of the upper portion of the Mt. Taranaki edifice (after Neall 2003). Lavas from Fanthams Peak are shown in shades of green and cumulodomes on the flanks of Mt. Taranaki in purple (The Dome and Skinner Hill to the north and the Beehives to the south).

was considered the last known eruptive activity at Mt. Taranaki (Druce 1966), until Platz (2007) suggested a later emplacement of the summit dome some time afterwards.

2.3. STRATIGRAPHIC CORRELATION (METHODS)

A stratigraphic framework and chronology of debris-avalanche and lahar deposits of the south-western ring plain has been established from detailed field mapping. Radiocarbon ages obtained from wood found within, and peat interbedded with, the deposits, and identification of rhyolitic tephra marker beds, provided timeframes and chronostratigraphic control of the younger sequence. The age of older units was estimated from their stratigraphic position in relation to mapped marine terraces as well as cover-bed stratigraphy and tephrochronology (cf. Pillans 1983; Neall 1986; Alloway et al. 2005).

Remapping of the Opunake and Stratford Formations was focused on coastal cross-sections, which provide continuous lateral exposure. Field investigations started with the northernmost and youngest units of the exposed volcaniclastic succession at Arawhata Road and proceeded southwards to the oldest units up to the Tangahoe River mouth, where the volcaniclastic sequence wedges out. The studied stretch of coastline was divided into 17 segments named after streams and rivers to allow a better overview. These segments and the locations of studied cliff sections can be found in Appendix 1.

Lahar (debris-flow to hyperconcentrated-flow) deposits in Taranaki are superficially similar in lithology, texture and fabric. This lack of individual diagnostic properties made mapping and correlation of separate flow units difficult. A closer examination of the deposits, where possible, allowed the identification of, in cases, unique sedimentological features and clast assemblages. Detailed sedimentological study was, however, dominantly focused on characterising and classifying the different types of flow deposits (cf. Chapter 3). To establish a stratigraphic overview and because of the large number and narrow distribution of single flow units, genetically related series of hyperconcentrated-flow and debris-flow deposits were grouped into stratigraphic intervals. Mapping was focused on the correlation of these deposit packages enclosed by distinctive marker horizons. Key units for correlation were the easily recognised, widespread debris-avalanche deposits, continuous paleosols and peat layers representing long hiatuses in volcaniclastic deposition, and a single rhyolitic tephra derived from the Taupo Volcanic Zone.

2.4. IDENTIFICATION AND NOMENCLATURE OF MARKER BEDS

2.4.1. Debris-avalanche deposits

Debris-avalanche deposits occur frequently in the Taranaki ring-plain succession and are easily recognised due to their distinctive sedimentological characteristics (cf. Chapter 3). The considerable thickness (typically between 0.5-6 m) of the deposits in combination with a wide, continuous lateral distribution makes them the most useful and reliable markers for correlation of the volcaniclastic sequences (Fig. 2.3).

Figure 2.3. At this location (Kaupokonui 6B), three debris-avalanche deposits (Otakeho, Rama and Ngaere) are exposed, which represent important lithological markers for correlation of the volcaniclastic sequence.

2.4.2. Important paleosols and peat sequences

Most paleosols and peat layers are thin (5-20 cm) and of limited lateral extent, which makes them inadequate for correlation. Some paleosols of greater thickness can be traced for several hundred meters, rarely up to several kilometers, in lateral exposure, thus allowing some correlation of the over- and underlying deposits. Two distinct tephric soils developed into layers of medial ash were recognised in western Taranaki by Neall (1972, 1979) and were helpful for correlations of the younger succession. The Okato Tephra separates the Pungarehu Formation from the overlying Warea debris-flow and hyperconcentrated-flow deposits, while the Oakura Tephra is interbedded between the Warea and Opua Formations.

Since peat typically accumulates in wet depressions, the resulting deposits are often of limited lateral extent and lenticular geometry. Two peat/organic soil sequences in the Taranaki succession are very thick and relatively widespread in cross-sectional coastal outcrops. Despite their variable thickness, they could easily be identified in numerous locations. The radiocarbon dates of these important peat sequences from this and former studies are summarised in Table 2.1. The younger peat sequence is here referred to as Hihiwera Peat because it is thickest in the Opunake area, where the uppermost layer was dated at c. 28.8 ka (Fig. 2.4). A correlative was also recognised in sections near Manaia. Previous workers obtained several radiocarbon dates of this significant deposit at various locations, giving an age range of 30-34.4 ka (Grant-Taylor & Rafter 1963; Grant-Taylor 1964; McGlone et al. 1984).

A second prominent organic soil represents an important marker within the oldest parts of the succession since they are past the dating limits of the radiocarbon dating method. The paleosol is exposed near the present-day sea-level at the bottom of the cliff sections from Punehu 13 (Fig. 2.5A) to Oeo 7B, where it occurs c. 2-5 m above beach level, overlying a mound of the Oeo debris-avalanche deposit (cf. Section 2.5.11). In its northernmost locations, it is characterised by the preservation of tree stumps in growth position at its top, which can be found amongst beach pebbles below the high water mark (Fig. 2.5B-C). Due to this distinctive feature, it is referred to as Puketapu buried forest. It is here assumed to be of similar age as the "Manaia Lignite", which occurs over a coastal stretch of 2.5 km near Inaha Stream (Fig. 2.6). This distinct >1 m-thick peat contains pollen assemblages that reflect a full forest cover dominated by *Dacrycarpus dacrydioides* and *Podocarpus spicatus* and was correlated with the warm interstadial conditions of MISS 5a (McGlone et al. 1984). Its age was thus estimated at c. 80 ka.

TABLE 2.1. *Radiocarbon and amino-acid racemisation dates of important peat deposits.*

Sample number	Age (yrs BP)	Stratigraphic unit	Locations[1]
Wk-19143[*]	28 824 ± 237	Hihiwera Peat (top)	Middleton Bay 9
NZ331[†]	34 400 ± 1500	Hihiwera Peat	Middleton Bay 3
NZ409[§]	31 800 ± 1800	Hihiwera Peat	Middleton Bay 8
ANU-1887[#]	33 300 ± 1100	Hihiwera Peat	Waiokura 5C
BJP-014[##]	30 000 ± 20 000	Hihiwera Peat	Waiokura 5C
Wk-19144[*]	background	Puketapu buried forest	Oeo 3A
BJP-010[##]	95 000 ± 20 000	Manaia Lignite	Waiokura 5C

[1]See Appendix for map and grid references of locations.

^{14}C dates [*]this study, [†]Grant-Taylor & Rafter (1963), [§]Grant-Taylor (1964), [#]McGlone et al. (1984).

[##]Amino acid racemisation dates McGlone et al. (1984).

Figure 2.4. A: At its type locality Middleton Bay 9, the Hihiwera Peat is c. 1.2 m thick with an upper part consisting of peat and organic soil beds while the lower part is characterised by tephric and silty paleosols. B: At location Otahi 7 it is c. 0.8 m thick and of massive appearance.

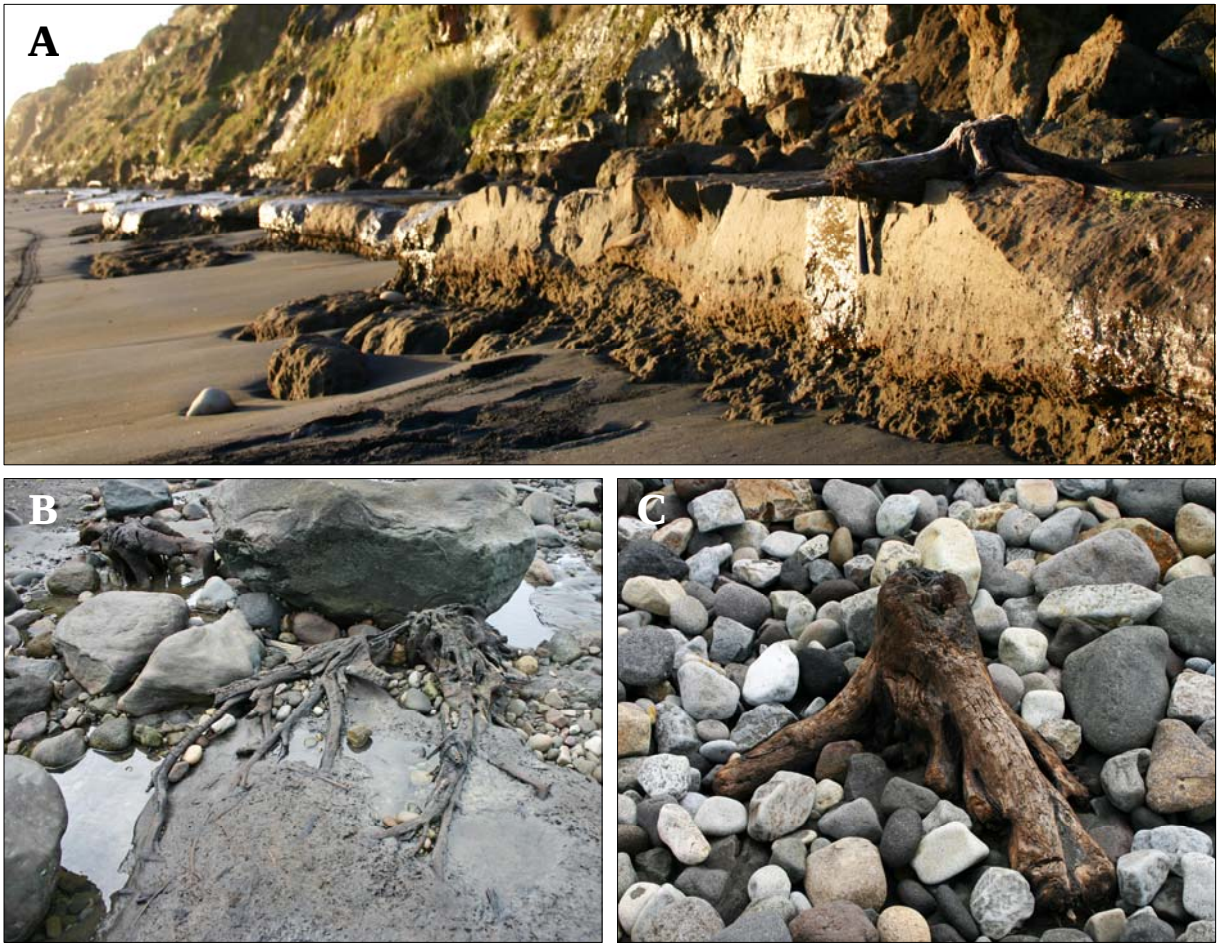

Figure 2.5. A: The Puketapu buried forest is c. 0.5 m thick at location Punehu 4, where it forms a distinct, continuous layer at the bottom of the cliff just above the high tide mark. B-C: Tree stumps in growth position surrounded by beach pebbles mark locations where the actual paleosol occurs below sea level (B: Punehu 13; C: Oeo 4).

2.4.3. Rhyolitic tephras

Four prominent rhyolitic tephras have been found in Taranaki (Wellman 1962; Aitken 1971; Stewart et al. 1977; Geddes et al. 1981; Alloway 1989; Alloway et al. 1994, 1995, 2005) the c. 4 ka Stent Tephra, the c. 22.6 ka Kawakawa Tephra/Aokautere Ash (both from Taupo Volcanic Centre; Wilson et al. 1988; Froggatt & Lowe 1990; Wilson 2001), the c. 45 ka Rotoehu Tephra from Okataina Volcanic Centre (Vucetich & Puller 1969; Lian & Shane 2000; Shane & Sandiford 2003) and the c. 350-400 ka Rangitawa Tephra (Naish et al. 1995). In this study, only the Kawakawa Tephra was identified at several coastal locations in western Taranaki. It occurs within a prominent soil sequence below the Pungarehu debris-avalanche deposit where the fine glassy ash typically forms discontinuous 1-3 cm thick yellow pods of ash (Fig. 2.7).

2.4.4. Dune sands

An up to 10 m-thick sequence of well-sorted, high-angle cross-stratified dune sands occurs in the older part of the south-western ring-plain succession (Fig. 2.8). The paleo-dune field is exposed over a broad stretch of coastline (>15 km) from Taungatara 8 to Wahamoko 10. The considerable thickness, wide distribution, intercalated hyperconcentrated-flow deposits, numerous thin peat beds, iron-stained weathering horizons and weakly developed soils in the tops of individual dune sets indicate that the sands accumulated over a long period of time. Their distribution and sedimentary characteristics (cf. Section 3.5.6) resemble those of present-day coastal dune fields. The paleo-dune sands typically occur below the Otakeho debris-avalanche deposit (cf. Section 2.5.6) to c. 1.4 m below the above described Puketapu buried forest. Such an incursion of sand dunes is likely to have been triggered by one of the higher sea-level stands of the post-Rapanui succession. From its stratigraphic position the Puketapu buried forest is likely to correlate with MISS 5a, hence the age range of the dune sands is estimated at >50 ka but <80 ka.

Figure 2.6. The prominent c. 80 ka Manaia Lignite of McGlone et al. (1984) is c. 1.2 m thick at location Waiokura 6B, near the type locality at Inaha Stream.

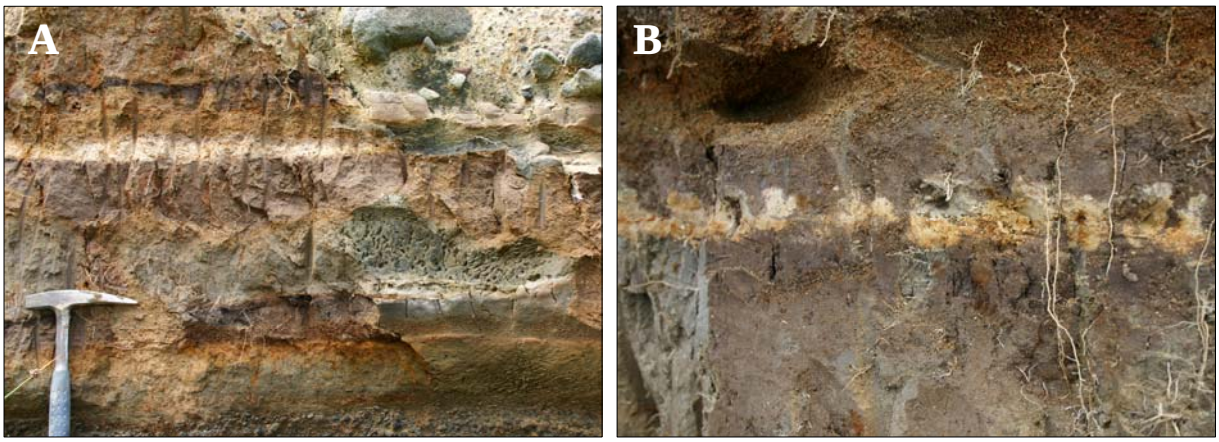

Figure 2.7. In coastal sections of south-west Taranaki, the Kawakawa Tephra occurs in a thick soil sequence below the Pungarehu debris-avalanche deposit. The tephra bed is of a distinct creamy colour and can form a continuous horizon (A) or appear patchy (B), probably due to falling on a shrubby vegetation cover. The tephra thickness in both photos is c. 2-3 cm.

Figure 2.8. Planar and high-angle cross-bedded sets of fine-grained, greyish dune sands with weathered, iron-stained tops (A) overlying three fine-grained pumiceous hyperconcentrated-flow deposits (B) at Punehu 1a.

2.5. NEW OR REDEFINED DEBRIS-AVALANCHE DEPOSITS

2.5.1. Motumate debris-avalanche deposit (redefined unit)

The Motumate debris-avalanche deposit is named after Motumate Stream in south Taranaki. The unit occurs in discontinuous exposures over a c. 10.8 km stretch of coastline from Oeo 7A to Kaupokonui 7 (Fig. 2.10). At its type locality Kaupokonui 5, the deposit forms a prominent c. 3.5 m thick, massive layer near the top of the cliff section (Fig. 2.11A). Here, it is characterised by pebble- to cobble-sized, polylithologic (cf. Section 5.3) clasts, rare small megaclast <0.5 m and small, rounded rip-up clasts in a clay-rich matrix (Fig. 2.9). Its upper and basal contacts are planar with no evidence for erosion. The Motumate debris-avalanche deposit is bracketed by two thin paleosols and overlain by a thin hyperconcentrated-flow deposit and thick soil (Fig. 2.11B). Two hyperconcentrated-flow deposits and fluvial sediment with interbedded paleosols occur directly below the unit. Near the type locality, the Motumate can be traced over c. 1.8 km, but rapidly thins to either side from 3.5 m to c. 0.8 m, suggesting that it was deposited in a relatively deep paleo-channel. The Motumate Formation was identified in three channels west of the type section, where its thickness ranges from c. 0.3-1 m. Two further reference sections are Wahamoko 1 and 4A, which also mark the margins of a c. 2.3 km wide but relatively shallow channel (Fig. 2.12A-B). Within this channel, the deposit is characterised by fewer, pebble- to small cobble-sized clasts in >90% matrix and a maximum thickness of c. 1 m (Fig. 2.12C).

Figure 2.9. The Motumate debris-avalanche deposit is exposed near the top of the cliff at its type locality Kaupokonui 5 (2602779/6180288) and separated from the underlying Ngaere Formation by hyperconcentrated-flow deposits and fluvial sediments.

The lenticular deposit geometry, minor thickness and narrow distribution range of the Motumate deposit in coastal locations indicate deposition from a relatively small lobe of a debris avalanche, which was confined to paleo-channels in these medial areas. Its distribution appears similar to that of the southern portion (ou2) of the Opua Formation, which only reached the present day coast along two major channels (Neall 1979). Due to its stratigraphic position, distribution and sedimentary characteristics, the Motumate debris-avalanche deposit is here correlated to the southern lobe of the Warea Formation (Wr3) of Neall (1979). When projected towards the volcano, the unit would overlap with the Wr3 lobe. The Wr3 unit is c. 5 km wide and >3 m thick at 350 m asl but bifurcates in two <2 m thick lobes along Oeo and Otakeho Streams below 240 m asl (Neall 1979). Between 450-250 m <5 m-high mounds occur that become progressively smaller to the south along Oeo Stream and are absent where the deposit thins to <2 m. Figure 2.10 shows the distribution of the Motumate debris-avalanche deposit in coastal locations and the inferred origin from the Wr3 lobe. The age of the Motumate debris avalanche is constrained via its correlative, the Warea Formation, which is bracketed between the c. 16 ka Okato Tephra and the c. 7 ka Oakura Tephra (Neall 1979).

Some confusion regarding the correlation of the Motumate debris-avalanche deposit has been caused by later studies. Alloway et al. (2005) interpret the south-eastern Warea lobe (Wr4) as a younger debris-avalanche deposit dated between c. 3.6-4.2 ka. The same deposit is marked as Opua Formation on the latest geological map of Taranaki (Neall & Alloway 2004). In contrast, Neall (1979) described the deposits, which were mapped to the coast along Kaupokonui Stream, as coarse conglomerates and sandstones that grade southwards into soft coarse sands and fine gravel that show fluvial bedding and form a planar surface. Based on the descriptions by Neall (1979) it is here inferred that the Wr4 lobe was deposited by young (3.6-4.2 ka) debris flows and hyperconcentrated flows. This is also implied by exposures of the deposits along Kaupokonui Stream, in the vicinity of Kaupokonui township and along the coast, which comprise massive stacks of fine-grained hyperconcentrated flow units. Another set of hyperconcentrated-flow units with interbedded fluvial sediments exposed at the bottom of the sequence indicates that an earlier paleo-stream channel existed at this location, which was subsequently filled by two massive debris-avalanche deposits. The absence of the Motumate debris-avalanche deposit in sequences near Kaupokonui Stream suggests that the present channel post-dates it. The deposition of the Motumate unit most likely filled and blocked the major paleochannel near the type section, forcing the stream to change its course. This could have led to reactivation of the Kaupokonui Stream channel, which was subsequently filled by fluvial sediments and younger lahar deposits of the Wr4 lobe.

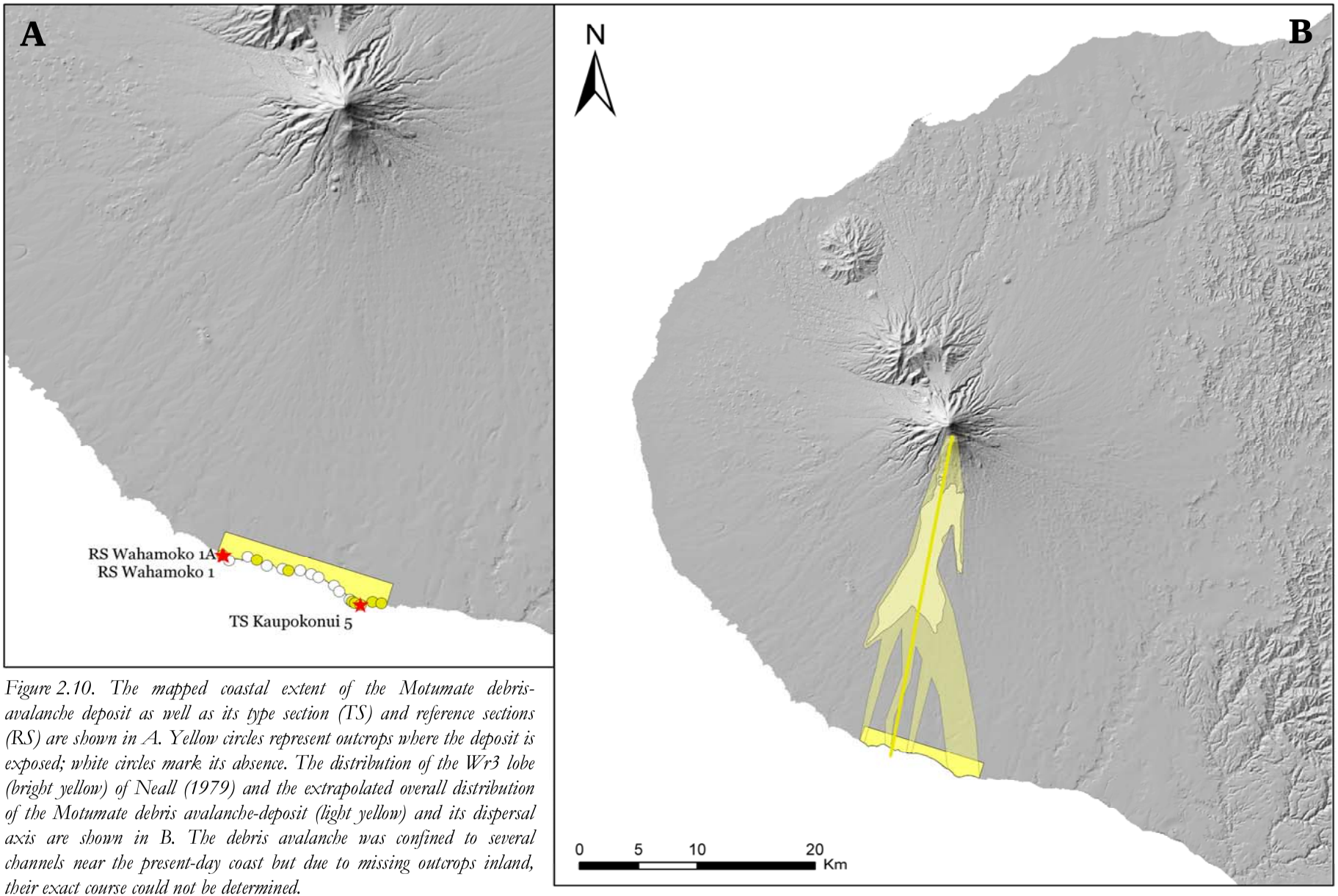

Figure 2.10. The mapped coastal extent of the Motumate debris-avalanche deposit as well as its type section (TS) and reference sections (RS) are shown in A. Yellow circles represent outcrops where the deposit is exposed; white circles mark its absence. The distribution of the Wr3 lobe (bright yellow) of Neall (1979) and the extrapolated overall distribution of the Motumate debris avalanche-deposit (light yellow) and its dispersal axis are shown in B. The debris avalanche was confined to several channels near the present-day coast but due to missing outcrops inland, their exact course could not be determined.

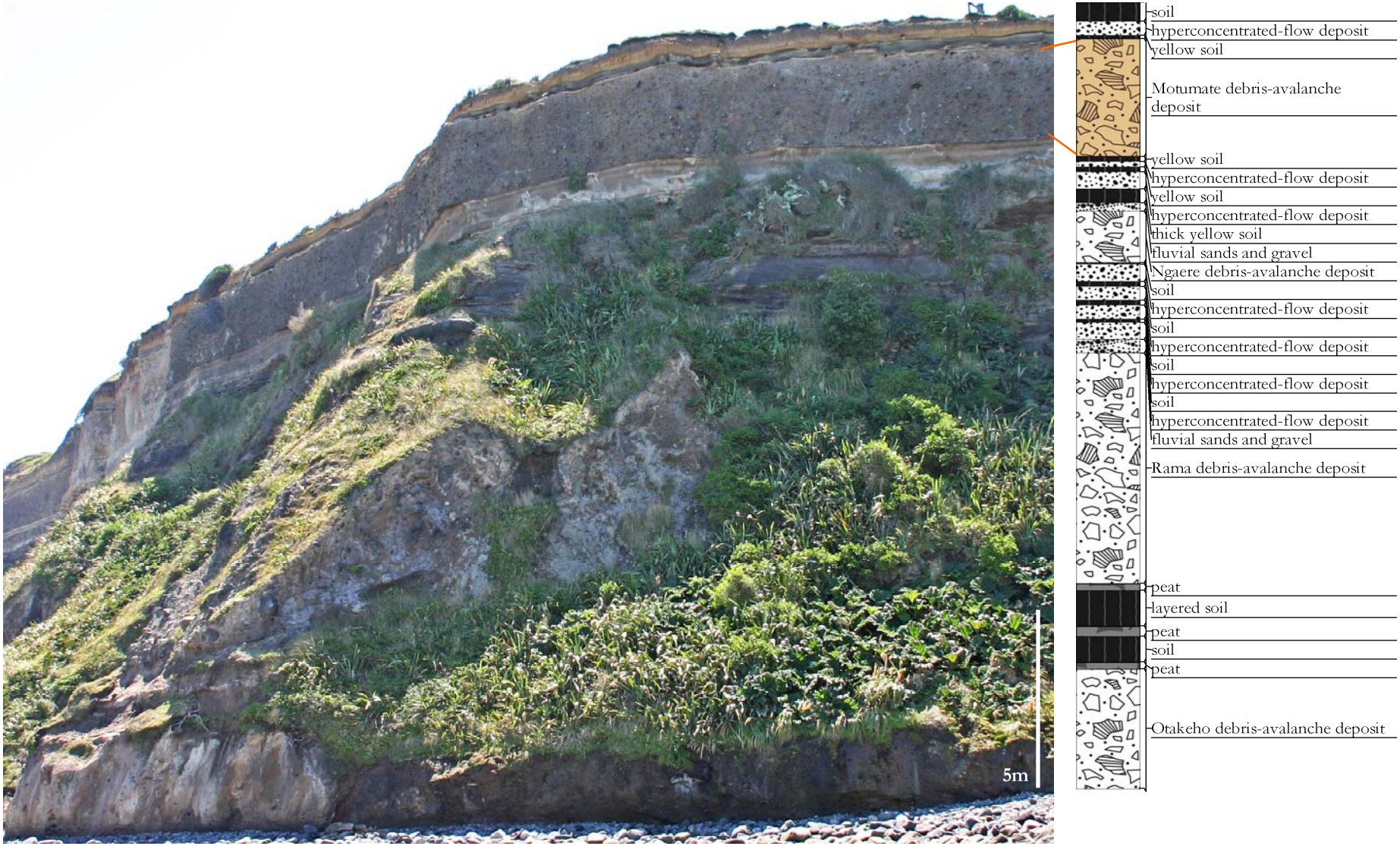

Figure 2.11. Stratigraphy of the type section for the Motumate debris-avalanche deposit (2602779/6180288). Here, the deposit occurs near the top of the cliff section and overlies the Ngaere, Rama and Otakeho debris-avalanche deposits that are interbedded with hyperconcentrated flow units and paleosols.

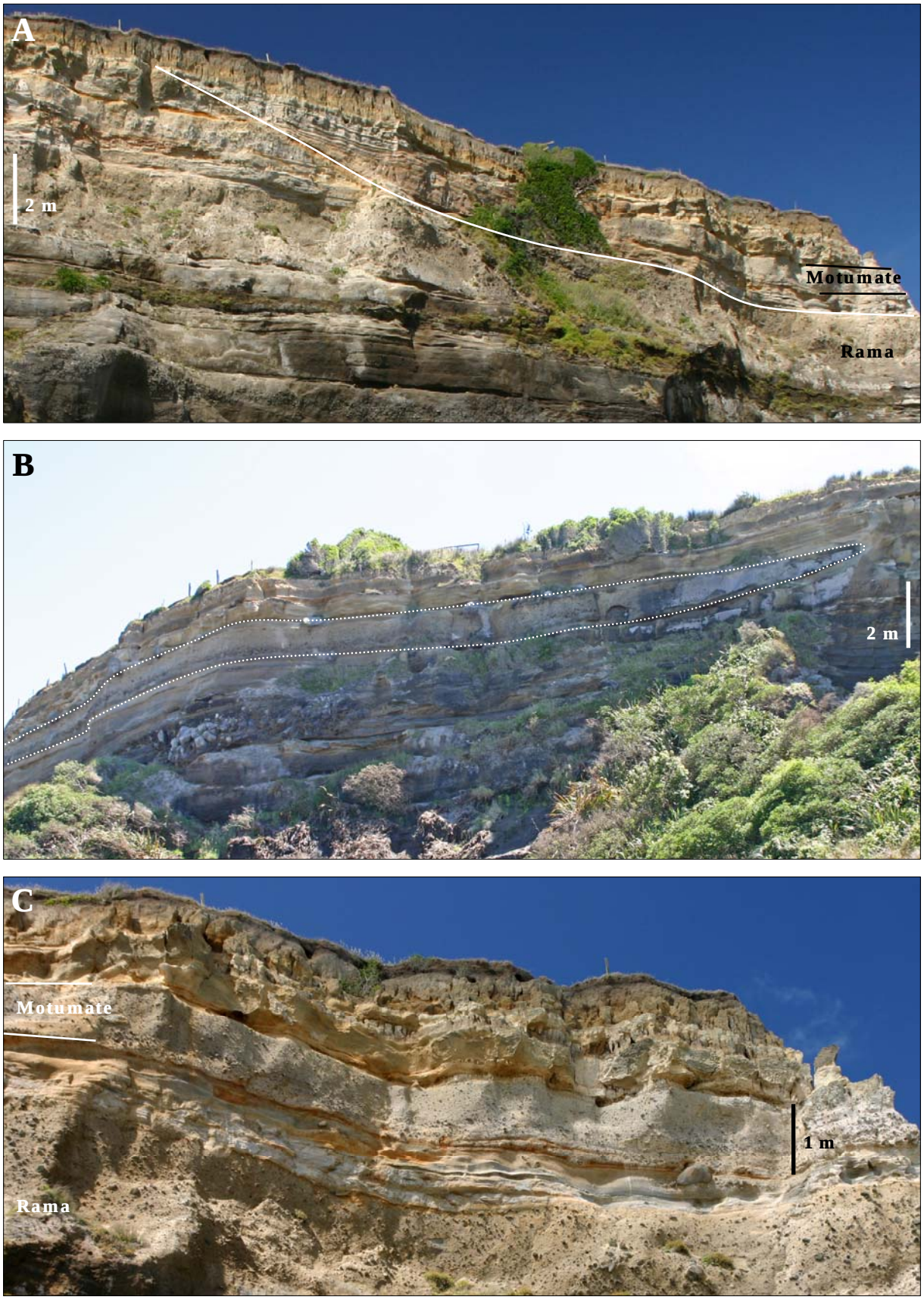

Figure 2.12. Location Wahamoko 1 marks the north-western margin of a shallow channel, to which the Motumate debris avalanche was confined (A). The deposit wedges out abruptly at Wahamoko 4a (B) and shows a maximum thickness of 1 m within the paleo-channel (C).

2.5.2. Te Namu debris-avalanche deposit (new unit)

The Te Namu debris-avalanche deposit is a formerly unknown unit named after Te Namu Pa in south-west Taranaki. The deposit first crops out just east of Okaweu Stream (Okaweu 1) at the bottom of the sequence. It forms a distinct unit from this outcrop to Middleton Bay 3 and was also identified from Waiteika 3 to Taungatara 3, i.e. over at least 8.8 km of lateral exposure (Fig. 2.13). From Mangahume 2 to Waiteika 1 only one thin debris-avalanche deposit is exposed, which could not be clearly identified. It represents either Te Namu or Pungarehu, or both deposits, without inter-beds. The Te Namu debris-avalanche deposit was also recognised further inland c. 0.8 km upstream at Waiaua Stream. Its extent farther north is unknown since the sequence dips under the present day sea-level. The deposit most likely continues for at least the same lateral distance as was observed southwards.

At its type locality Okaweu 9, the Te Namu is >5 m thick and characterised by polylithologic, pebble- to boulder-sized clasts and abundant large rip-up clasts (up to 1.5 m across) in a clay-rich matrix (Fig. 2.15A). It is overlain by a distinct soil sequence consisting of two dark organic paleosols that are separated by two andesitic tephra beds and an interbedded pale pink silt layer (Fig. 2.15B). Above the soil, four hyperconcentrated-flow deposits are exposed, separated by thin paleosols (Fig 2.14). The top of the sequence consists of the Opua debris-avalanche deposit and an underlying thick soil sequence. The strata below the Te Namu are not exposed.

At reference locality Okaweu 2, the >2 m thick Te Namu is exposed at the bottom of the cliff section and characterised by pebble- to boulder-sized clasts as well as large rip-up clasts of an underlying peat/soil layer, possibly the Hihiwera Peat (Fig. 2.16B). The sequence above the debris-avalanche deposit is more complete at this location (Fig. 2.16A). The Opua Formation forms the top of the section and is separated from the Pungarehu Formation by a thick laminated paleosol. The Kawakawa Tephra was identified in the soil sequence below the Pungarehu (cf. Fig. 2.7). It overlies a series of hyperconcentrated-flow deposits and cross-bedded fluvial sands. At Heimama 10, the strata below the Te Namu consist of several thin hyperconcentrated-flow deposits, cross-bedded fluvial pebbly sands and an intercalated normal to reverse graded transitional debris/hyperconcentrated-flow deposit. A piece of ripped-up wood from within the Te Namu debris-avalanche deposit collected at this location gave a maximum age of 29 074 ± 399 a BP (Wk-16402). At Okaweu 2, a minimum emplacement age of 25 198 ± 167 a BP (Wk-16401) was obtained from a sample of the overlying paleosol. Further details of radiocarbon dates that were obtained to infer the emplacement ages of debris-avalanche deposits from this study can be found in Table 2.2.

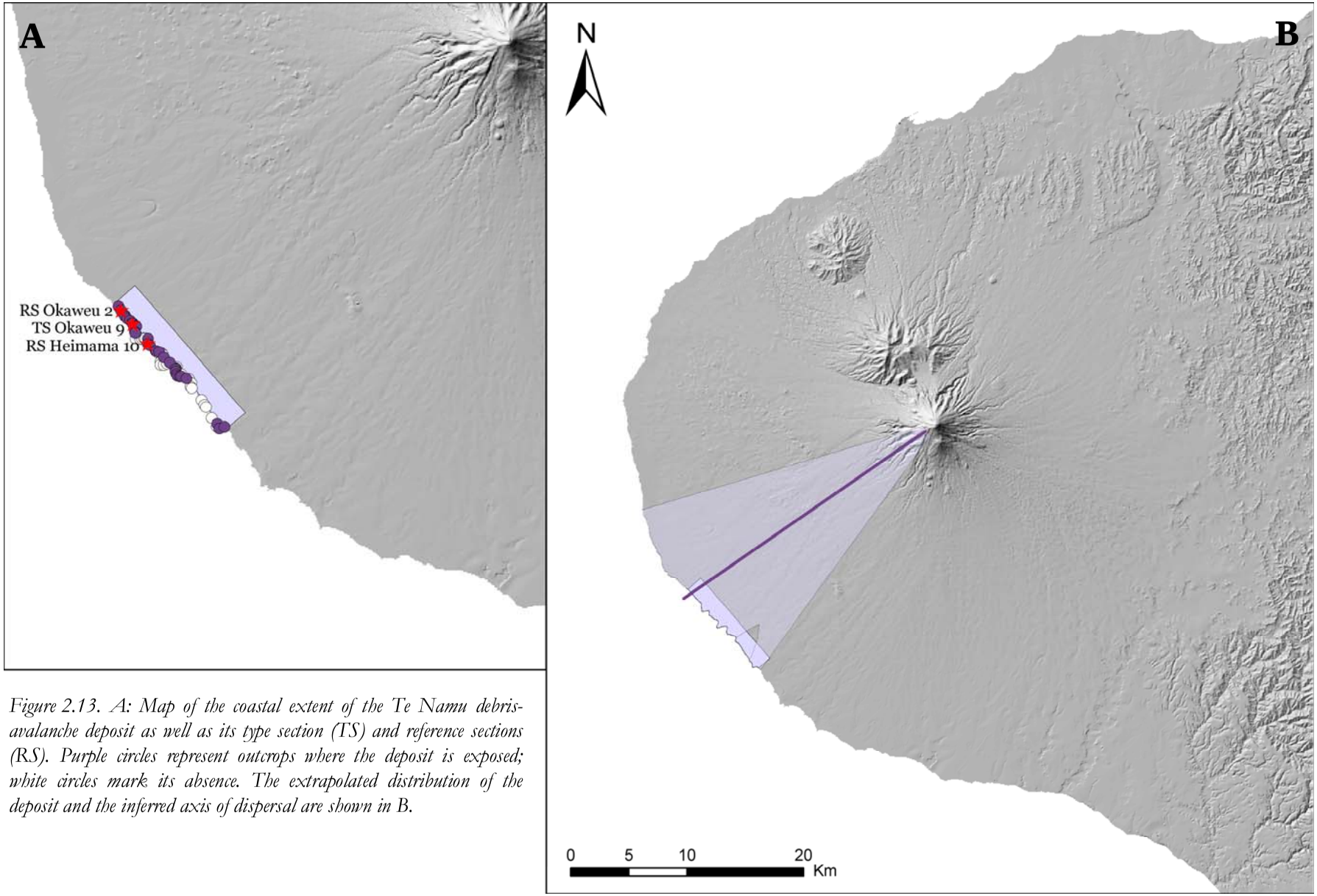

Figure 2.13. A: Map of the coastal extent of the Te Namu debris-avalanche deposit as well as its type section (TS) and reference sections (RS). Purple circles represent outcrops where the deposit is exposed; white circles mark its absence. The extrapolated distribution of the deposit and the inferred axis of dispersal are shown in B.

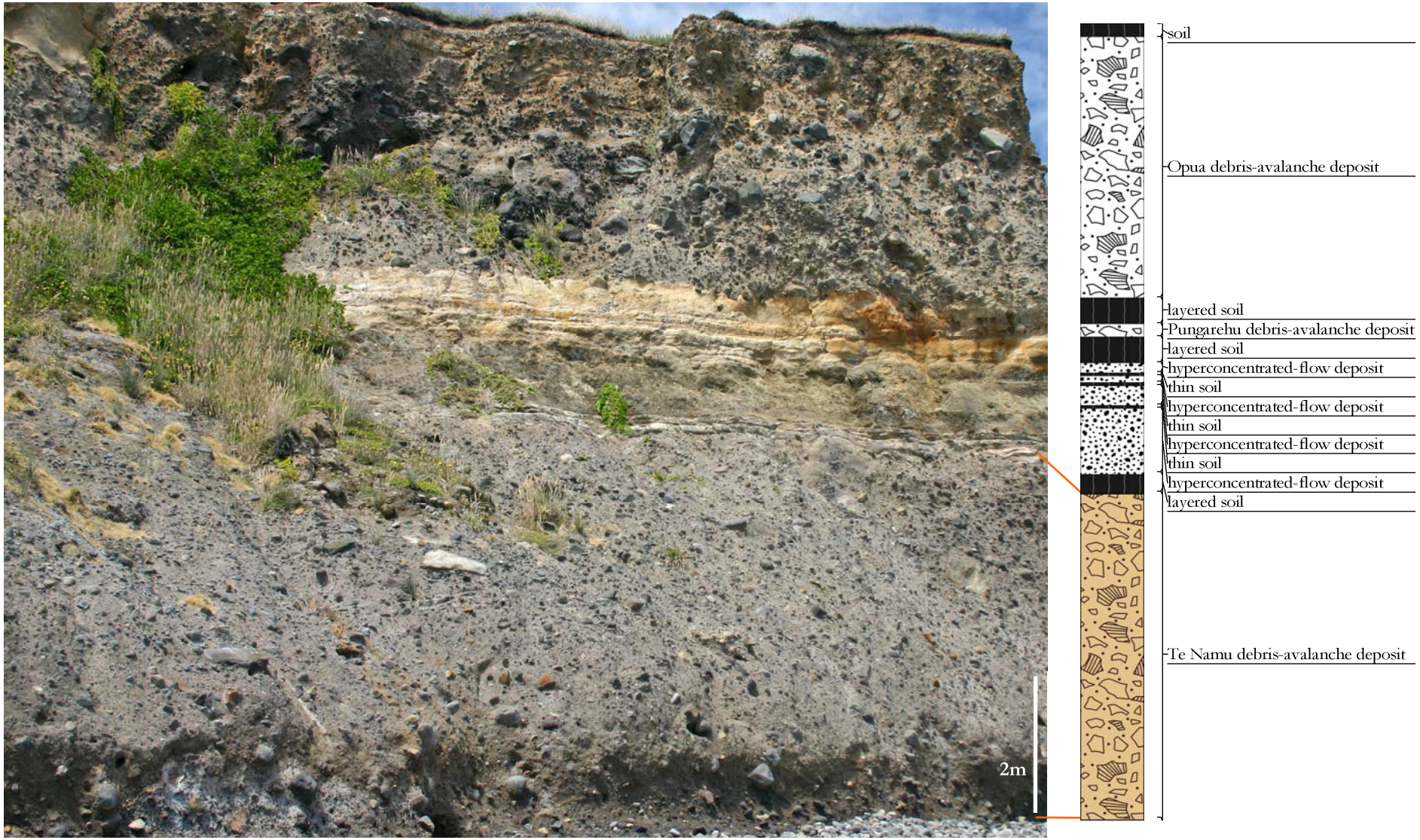

Figure 2.14. Stratigraphy of the type section for the Te Namu debris-avalanche deposit (2581432/6195939). The Te Namu is exposed at the bottom of the cliff section and overlain by hyperconcentrated-flow deposits with interbedded paleosols and the Opua Formation at the top of the section.

Figure 2.15. At its type section (2581432/6195939), the Te Namu debris-avalanche deposit is >5 m thick and contains pebble- to boulder-sized clasts as well as abundant rip-up clasts in a clay-rich matrix (A).

It is overlain by two distinct organic paleosols that embrace two andesitic tephra beds and a pale pink silt layer (B).

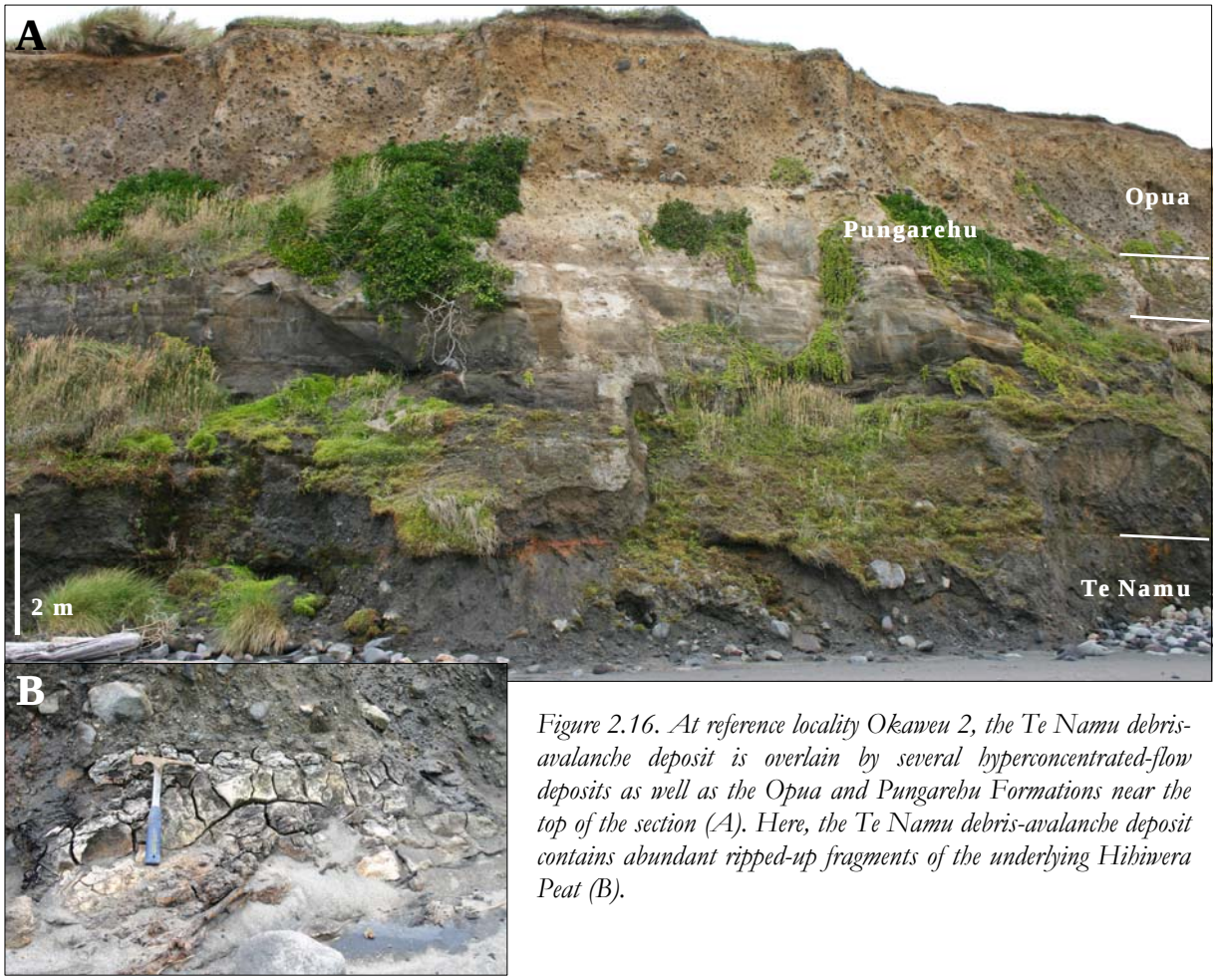

Figure 2.16. At reference locality Okaweu 2, the Te Namu debris-avalanche deposit is overlain by several hyperconcentrated-flow deposits as well as the Opua and Pungarehu Formations near the top of the section (A). Here, the Te Namu debris-avalanche deposit contains abundant ripped-up fragments of the underlying Hihiwera Peat (B).

2.5.3. Ihaia debris-avalanche / debris-flow deposit

A cohesive debris-flow or runout debris-avalanche deposit (Ihaia) is exposed over c. 3.2 km below the Hihiwera Peat from Okaweu 11 to Middleton Bay 4 (Fig. 2.17). At most outcrops it is c. 1 m thick, and up to 1.6 m at its type locality Middleton Bay 3. Here, the deposit is characterised by predominantly pebble-sized clasts and abundant pieces of wood in a clay-rich matrix (Fig. 2.18). Its base is marked by a thin layer with coarser cobble-sized clasts. A piece of wood from within the deposit at this location was dated at 31 522 ± 381 BP (Wk-19142) (cf. Table 2.2), which fits in well with the age of the directly overlying Hihiwera Peat. The deposit occurs near the bottom of the section and is underlain by fine-grained pumice-rich hyperconcentrated-flow deposits (Fig. 2.19).

The stratigraphic position and age of the Ihaia deposit indicates that it might be a lateral equivalent to the Rama debris-avalanche unit (cf. Section 2.5.4). A direct correlation was not possible because the Rama is not exposed in coastal cliffs for another 8 km to the south. The deposit characteristics on the other hand are similar to the Otakeho debris-avalanche deposit (cf.

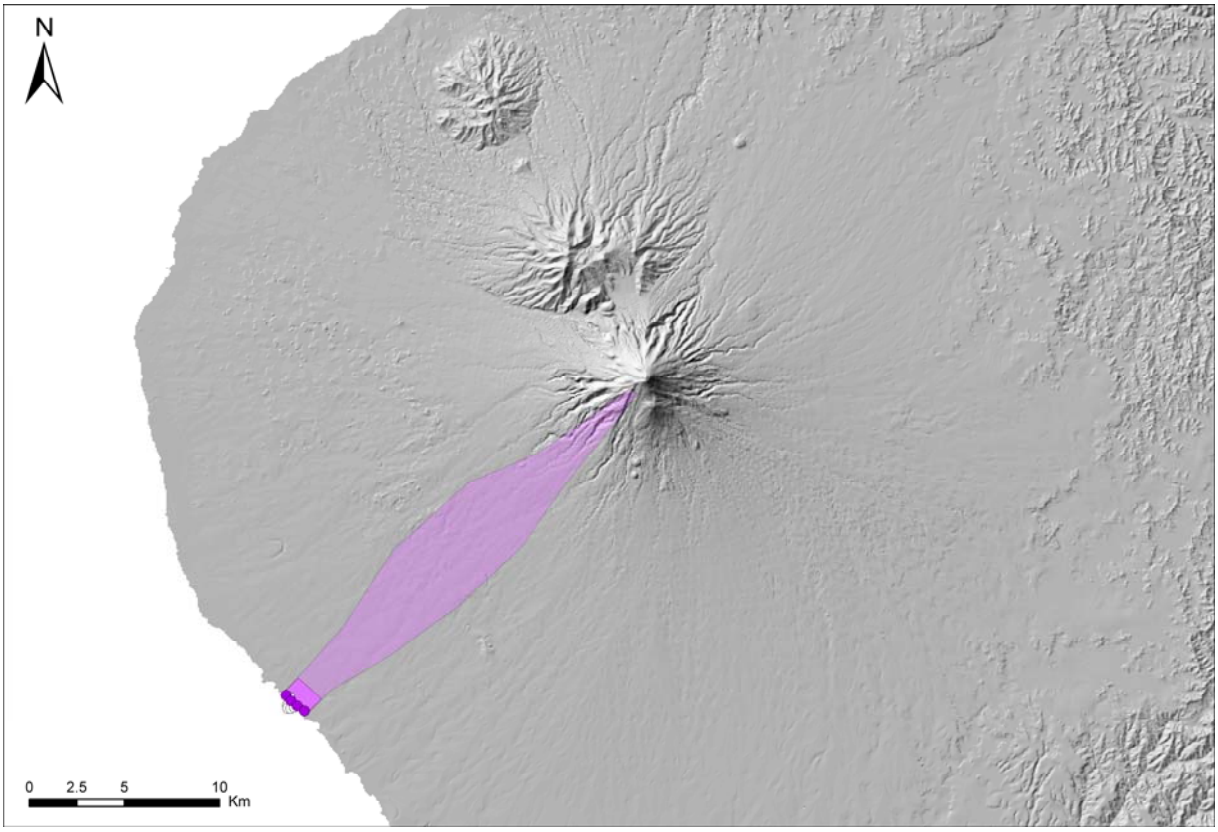

Figure 2.17. Map of the lateral coastal extent of the Ihaia debris-flow deposit and extrapolated distribution inland.

Section 2.5.6), which also contains abundant wood and shows a thin bouldery layer at some locations. The young radiocarbon age could in this case represent a dating error due to contamination with younger carbon leaching through the profile. A direct correlation with the Otakeho debris-avalanche deposit was also not possible because it first crops out 4.4 km farther south. A third and here favoured option is that the deposit was produced by a small separate debris avalanche that post-dated the Rama event and was roughly confined to the Opunake paleo-river system (cf. Chapter 3) between Heimama and Waiaua Streams. Due to its unclear origin, the debris avalanche/debris-flow deposit is here informally named Ihaia debris-flow deposit after Ihaia Road that runs roughly parallel to its interpreted dispersal axis.

Figure 2.18. The c. 1.5 m thick Ihaia debris-flow/debris-avalanche deposit (DFD) consists of >90% matrix with only a few pebble-sized clasts and abundant pieces of wood at its type section Middleton Bay 3. It is overlain by the Hihiwera Peat. The arrow points to a hammer for scale (handle c. 30 cm long).

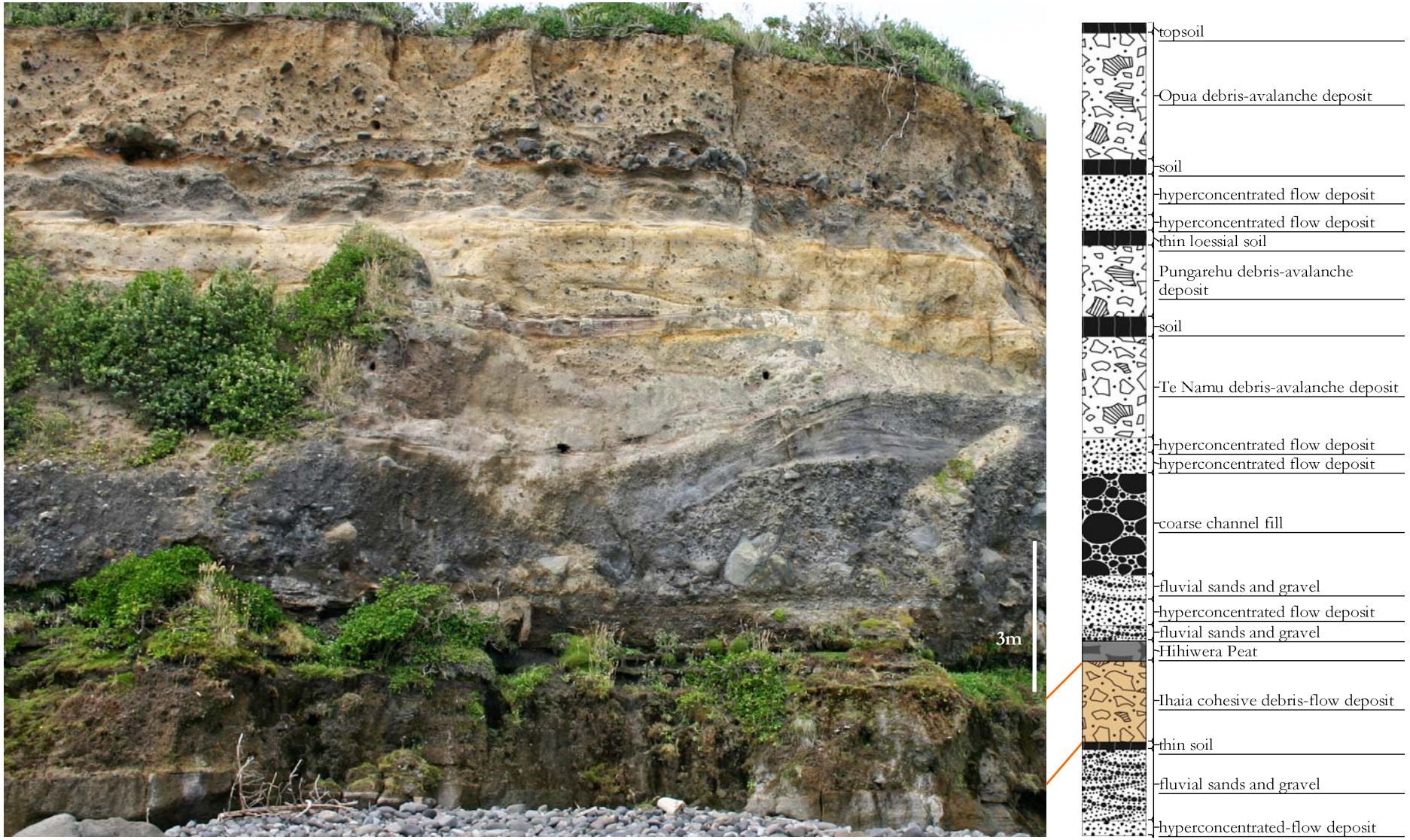

Figure 2.19. Stratigraphy of the type section for the Ihaia debris-flow deposit (2583440/6193829). The deposit is exposed at the bottom of the cliff below the Hihiwera Peat. Above the peat, a thick series of coarse channel fill and hyperconcentrated-flow deposits are exposed with an intercalated lens of the Te Namu and Pungarehu debris-avalanche deposits and a Warea hyperconcentrated-flow deposit and the Opua Formation at the top of the section.

2.5.4. Rama debris-avalanche deposit (redefined unit)

The Rama debris-avalanche deposit represents the most prominent unit within the former Stratford Formation and was described by Neall et al. (1986) as a c. 50 000 years old debris-avalanche deposit with a minimum thickness of 10 m and a minimum volume of 1.5 km^3. Later studies by Palmer & Neall (1991) and Palmer et al. (1991) referred to the deposit as Stratford Formation debris avalanche 1 with an inferred age of 48 000 years, a maximum observed thickness of 17 m, volume of 2.6 km^3, and covering an area of 510 km^2. Its lateral extent (32.1 km) was mapped by Palmer et al. (1991) and is similar to the data presented here. Redefining this debris-avalanche deposit was necessary to emphasize its distinct and mappable character and to replace the Stratford Formation with a more rigorous stratigraphic subdivision. It was named after Rama Road, which is located near Manaia township and runs roughly parallel to its interpreted dispersal axis.

In this study, the Rama debris-avalanche deposit was correlated over a c. 25.5 km long stretch of coastline from Punehu 9B to Waingongoro 3 (Fig. 2.20). At its type section, Kaupokonui 1, the deposit is c. 5.5 m thick and characterised by pebble- to cobble- and few boulder-sized clasts and rip-up clasts in a clay-rich matrix (Fig. 2.21). It also contains large brecciated megaclasts up to 5.5 m across, which are common at several locations. It overlies the Ihaia debris-flow deposit and the Otakeho debris-avalanche unit (Fig. 2.23). The sequence overlying the Rama consists of a series of at least 9 hyperconcentrated-flow deposits with interbedded paleosols. These units are also exposed along Kaupokonui Stream near Kaupokonui township (Fig. 2.22).

Reference locality Waiokura 5C corresponds to the Inaha Section described by McGlone et al. (1988). Here, the Rama debris avalanche forms a massive c. 8 m-thick marker unit near the top of the cliff with similar sedimentological characteristics to its type section (Fig 2.24A-B). Fine-grained hyperconcentrated-flow deposits, fluvial sands and interbedded peat layers occur below the Rama and overlie the Inaha marine bench (cut into the Tertiary mudstone sequence at the bottom of the cliff). The Rama is directly overlain by a prominent c. 0.8-1 m thick peat sequence (Fig. 2.24B), which is here correlated with the Hihiwera Peat. A radiocarbon date of c. 33 300 a BP (ANU-1887, McGlone et al. 1988, cf. Table 2.1) gives a minimum age for the Rama debris-avalanche deposit. The top of the cliff section is marked by fluvial sands and gravel as well as several hyperconcentrated-flow deposits that thicken in a small channel near Inaha Stream. A c. 1.5-2 m thick soil has formed into the top of the volcaniclastic sequence. The maximum observed thickness of 12 m at Kaupokonui 7A suggests that the Rama is one of the most voluminous debris-avalanche deposits of the southern ring-plain succession.

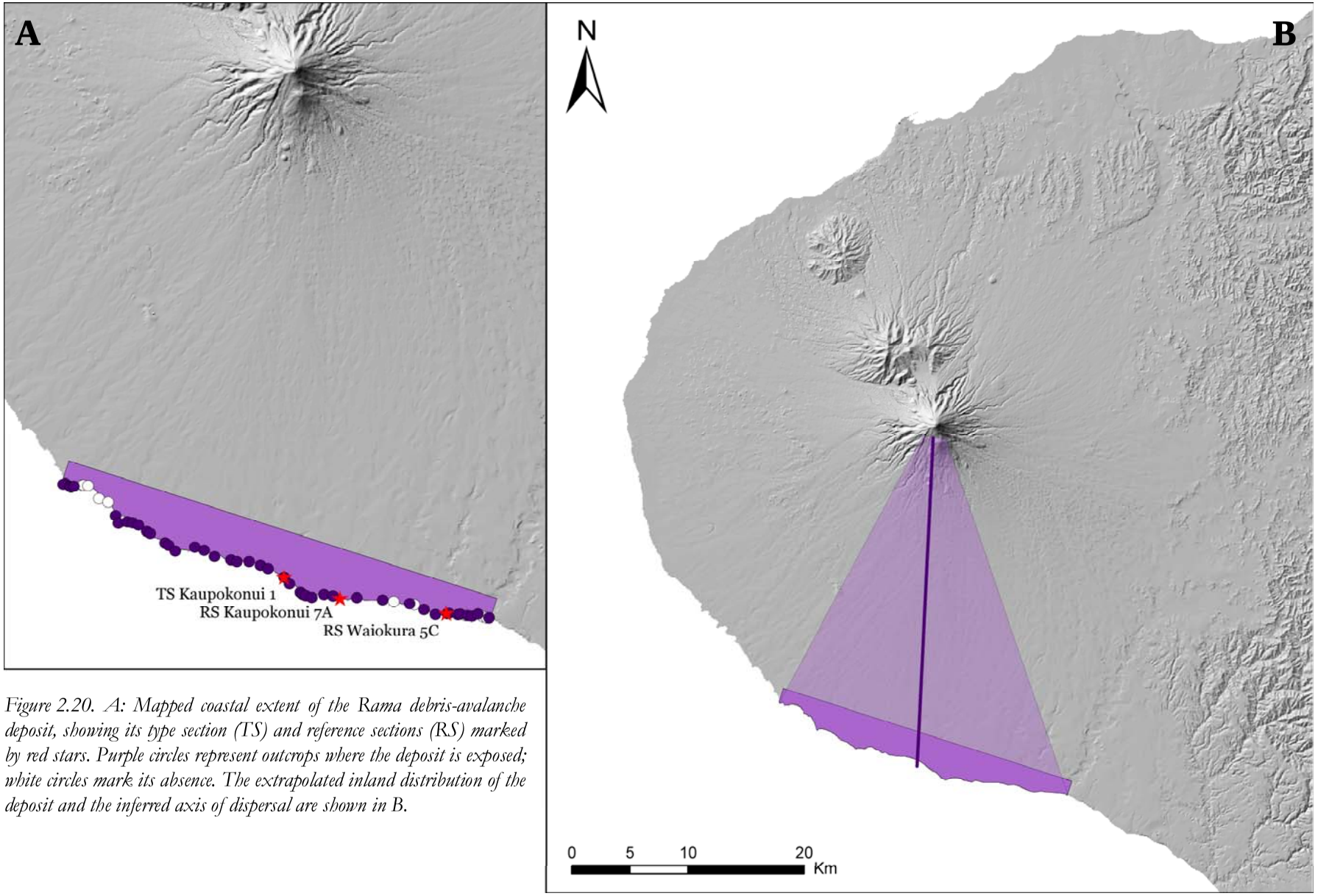

Figure 2.20. A: Mapped coastal extent of the Rama debris-avalanche deposit, showing its type section (TS) and reference sections (RS) marked by red stars. Purple circles represent outcrops where the deposit is exposed; white circles mark its absence. The extrapolated inland distribution of the deposit and the inferred axis of dispersal are shown in B.

Figure 2.21. At its type section Kaupokonui 1, the Rama debris-avalanche deposit is c. 5.5 m thick and characterised by coarse clasts, few small rip-up clasts and a large brecciated megaclast in a clay-rich matrix.

Figure 2.22. Near its type section, the Rama is overlain by stacks of fine-grained hyperconcentrated-flow deposits (HFDs) with interbedded fluvial sediments (Flu) that are best exposed further inland along Kaupokonui Stream.

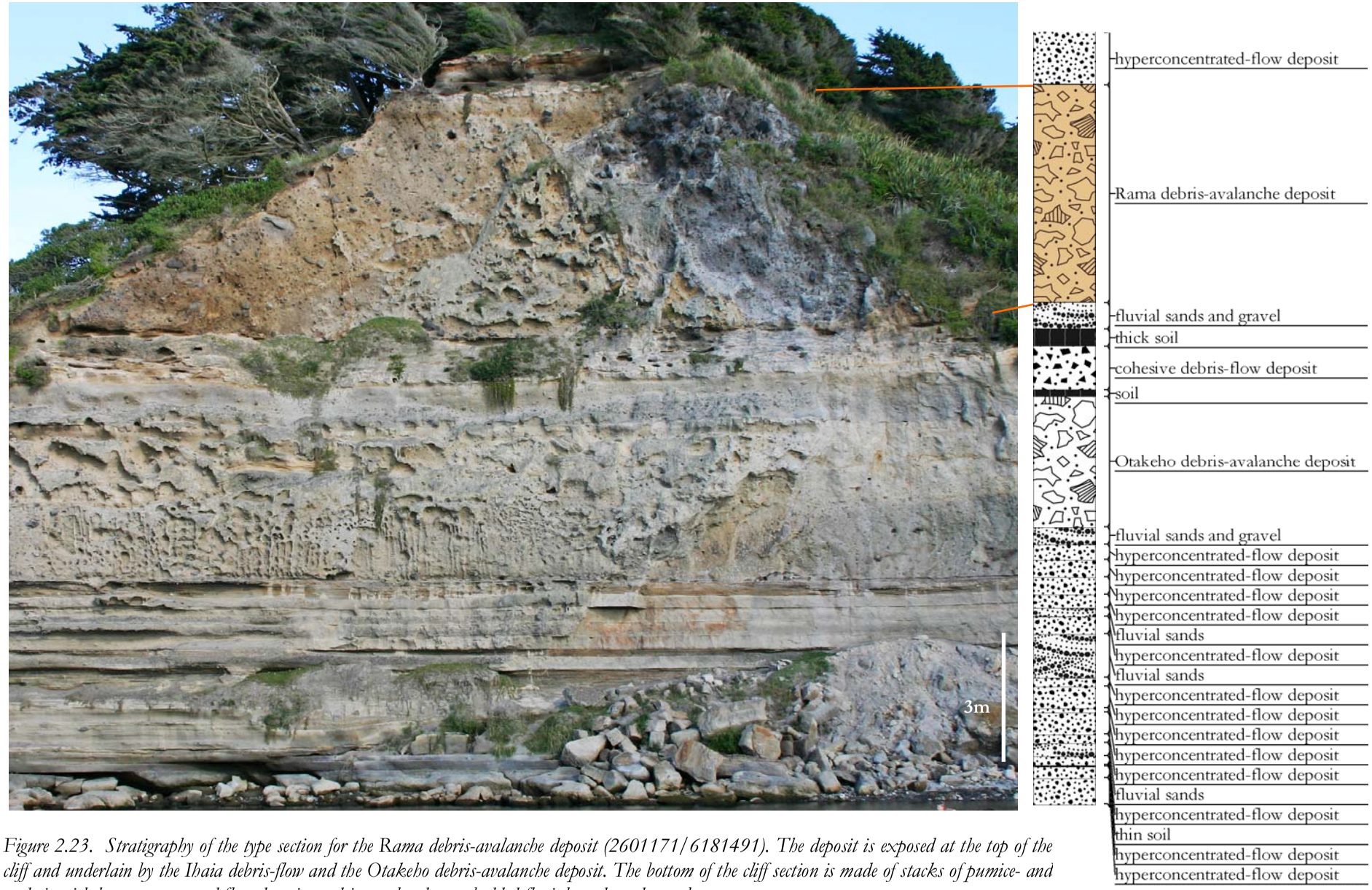

Figure 2.23. Stratigraphy of the type section for the Rama *debris-avalanche deposit (2601171/6181491). The deposit is exposed at the top of the cliff and underlain by the Ihaia debris-flow and the Otakeho debris-avalanche deposit. The bottom of the cliff section is made of stacks of pumice- and andesite-rich hyperconcentrated-flow deposits and intercalated cross-bedded fluvial sands and gravels.*

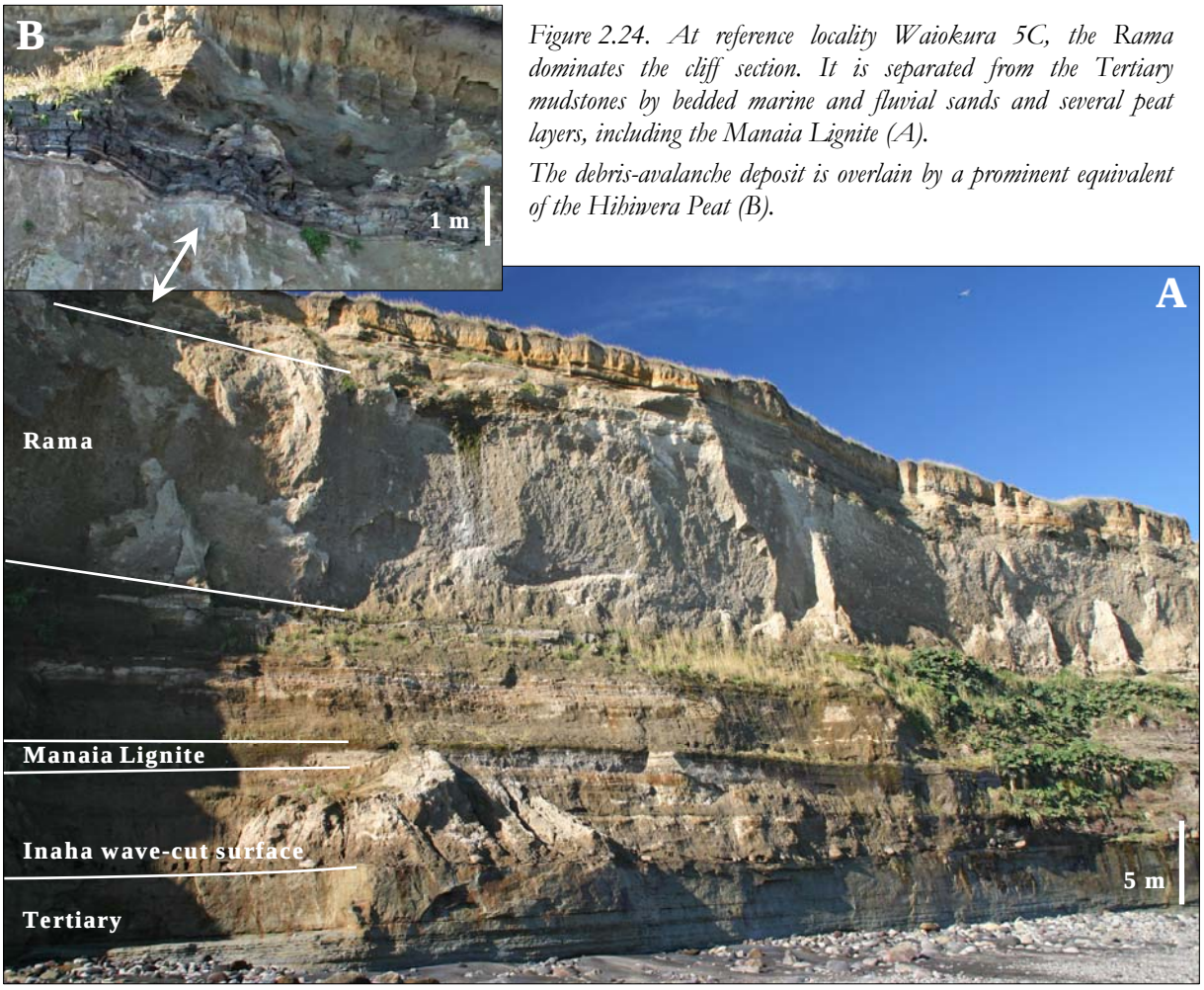

Figure 2.24. At reference locality Waiokura 5C, the Rama dominates the cliff section. It is separated from the Tertiary mudstones by bedded marine and fluvial sands and several peat layers, including the Manaia Lignite (A).

The debris-avalanche deposit is overlain by a prominent equivalent of the Hihiwera Peat (B).

Figure 2.25. An unnamed c. 1.3 m thick cohesive debris-flow deposit is exposed at Kaupokonui 1. It occurs above the Otakeho debris-avalanche deposit and is separated from the overlying Rama by cross-bedded fluvial sands.

2.5.5. Unnamed debris-flow deposit (Kaupokonui Stream)

An unnamed clay matrix-rich debris-flow deposit is exposed below the Rama debris-avalanche deposit at Kaupokonui 1. It was referred to as Stratford Fm. 2 by Palmer et al. (1991) and described as having a maximum thickness of 1.5 m, a maximum width of 10.7 km, covering an area of 90 m^2 with a volume of 0.1 km^3. Palmer & Neall (1991) attributed this "muddy diamicton" to a small debris avalanche that was channelled down the Kaupokonui and Waingongoro catchments. In this study, the debris-flow deposit could not be correlated with units that occur along the Waingongoro River but was only mapped over c. 1 km from Kaupokonui 1-2B (Fig. 2.26).

It is very matrix-rich and contains mainly pebble- and few cobble-sized clasts, which are mostly concentrated near the base of the deposit, giving it a normally graded appearance (Fig. 2.25). It has a maximum thickness of c. 1.3 m at Kaupokonui 1 but rapidly wedges out. It was most likely deposited from the distal portions of a small debris avalanche that was confined to a paleo-Kaupokonui Stream. Due to its localised distribution and minor importance, the debris-flow deposit has not been named. It was emplaced between 50-35 ka as indicated by its stratigraphic position between the Rama and Otakeho debris-avalanche deposits.

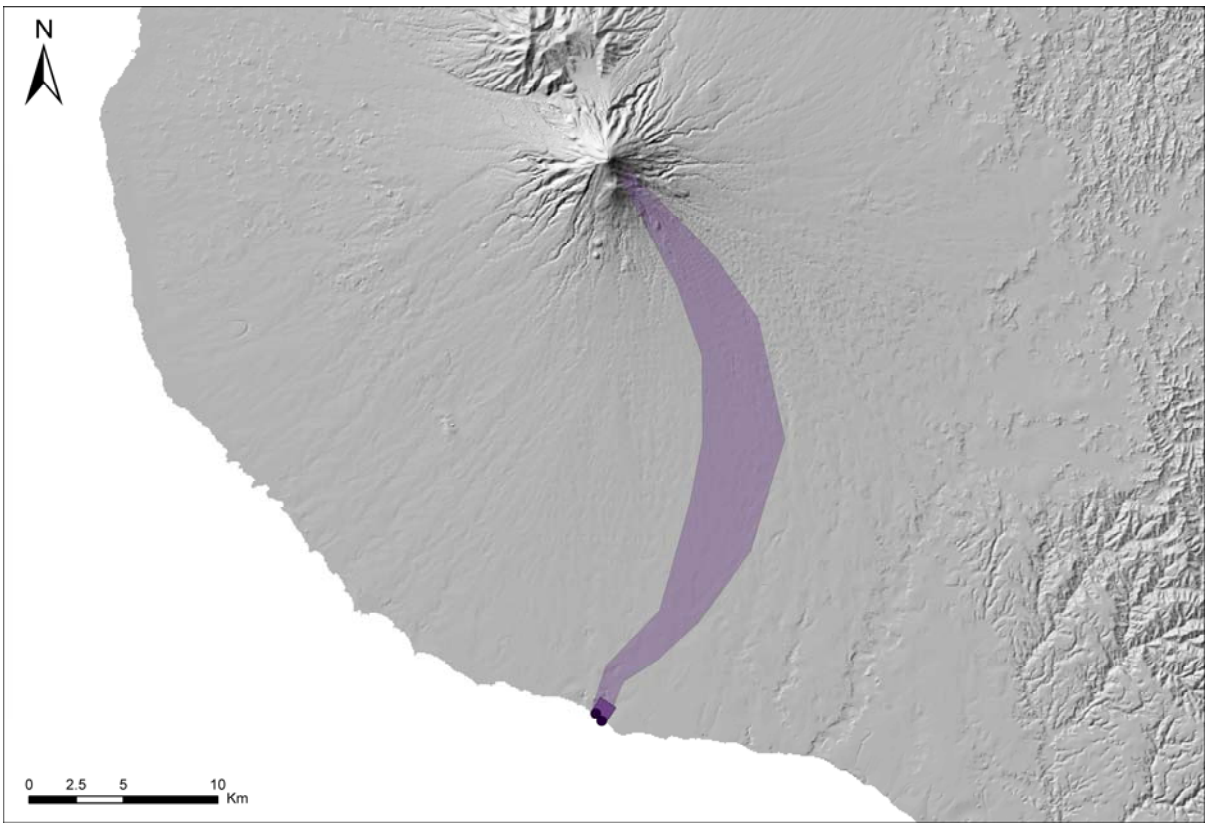

Figure 2.26. Mapped coastal extent of the unnamed debris-flow deposit and extrapolated inland distribution along a proto-Kaupokonui catchment.

2.5.6. Otakeho debris-avalanche deposit (redefined unit)

A second prominent debris-avalanche deposit was recognised within the Stratford Formation (Palmer & Neall 1991; Palmer et al. 1991). This unit was informally named Stratford Formation debris avalanche 3 and was thought to have been emplaced c. 80 000 years ago (Palmer et al. 1991). Palmer & Neall (1991) described a maximum thickness of 6 m and 32.1 km lateral width, with the deposit covering an area of 370 km^2 under >1 km^3 volcaniclastic material. The unit is here named Otakeho debris-avalanche deposit after Otakeho Stream in south Taranaki. It was mapped from Taungatara 4 to Waiokura 3A over c. 24.5 km (Fig. 2.30). At its type section Wahamoko 10, the Otakeho debris-avalanche deposit is c. 2.5 m thick, massive and contains pebble- to cobble-sized clasts and small rip-up clasts in a clay-rich matrix (Fig. 2.27). Coarser clasts are rare and the matrix makes up >85% of the deposit. At this locality, abundant large holes represent tree casts but the deposit contains only small, scattered pieces of wood. The bottom half of the Otakeho has a greenish colour in contrast to the more yellow-brownish top, which is even more evident at Kaupokonui 1 (cf. Fig. 2.25). A thin soil has developed into the top of the Otakeho, which is separated from the overlying Manaia debris-avalanche deposit by a series of thick, coarse, channelised hyperconcentrated-flow deposits that grade into finer-grained hyperconcentrated-flow deposits and fluvial sediments (Fig. 2.31). The top of the cliff consists of coarse- and fine-grained hyperconcentrated-flow deposits that are covered by a thick soil. The sequence below the Otakeho is made up of thin hyperconcentrated-flow deposits and intercalated fluvial sands. Cross-bedded dune sands crop out at the very bottom of the section.

Near reference locality Oeo 1, the Otakeho debris-avalanche deposit is only c. 1 m thick and overlies a peat layer rich in large pieces of wood and a thick yellow tephric soil (Fig. 2.28). A distinct soil was also formed within the top of the deposit. The bottom of the sequence is characterised by massive stacks of dune sands with intercalated peat beds and weakly developed paleosols. These distinct units are exposed below the Otakeho over a wide stretch of coastline from Taungatara 8 to Wahamoko 10, where they are replaced by stacks of hyperconcentrated-flow deposits with interbedded fluvial sands. Reference locality Kaupokonui 5 is the type section of the Motumate debris-avalanche deposit and was described in detail above. Here, the Otakeho debris-avalanche deposit consists almost exclusively of a clay-rich matrix and contains only scattered, pebble-sized clasts mostly <5 cm in diameter. It is characterised by abundant ripped-up fragments of trees including large logs and large stratified rip-up clasts (Fig. 2.29).

A wood sample from within the debris-avalanche deposit was collected at a location nearby but its age exceeded the limit of the radiocarbon method (cf. Table 2.2). Hence, the age of the Otakeho debris-avalanche deposit is estimated to be c. 55 ka.

Figure 2.27. The Otakeho debris-avalanche deposit is c. 2.5 m thick at its type section Wahamoko 10 (2600243/6181996).

Figure 2.28. At Oeo 1, the deposit is only c. 1 m thick and overlies a distinct peat layer and a thick paleosol.

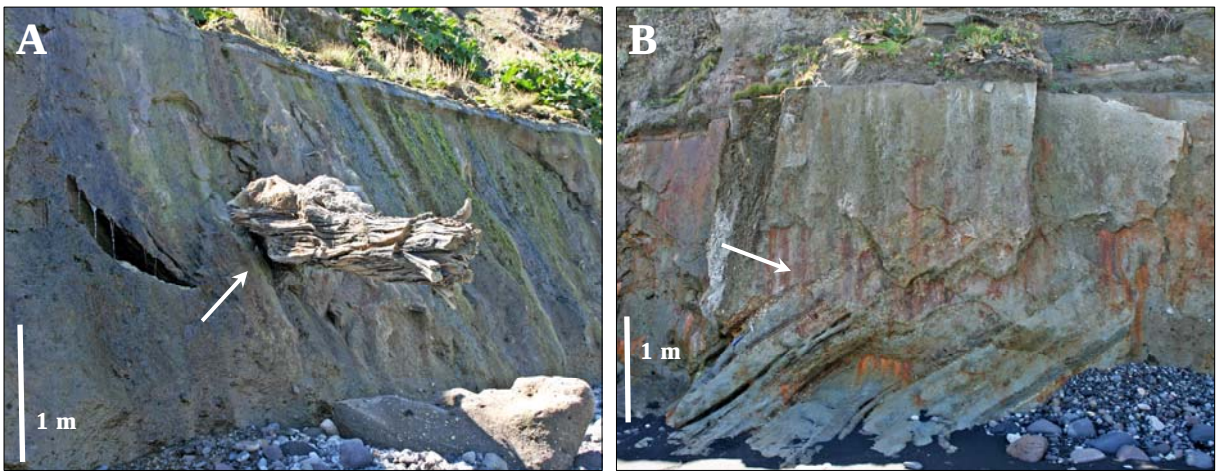

Figure 2.29 At reference locality Kaupokonui 5, the Otakeho debris-avalanche deposit is very matrix-rich and contains several large tree logs (A) and large stratified rip-up clasts >3 m in diameter (B), both marked by arrows.

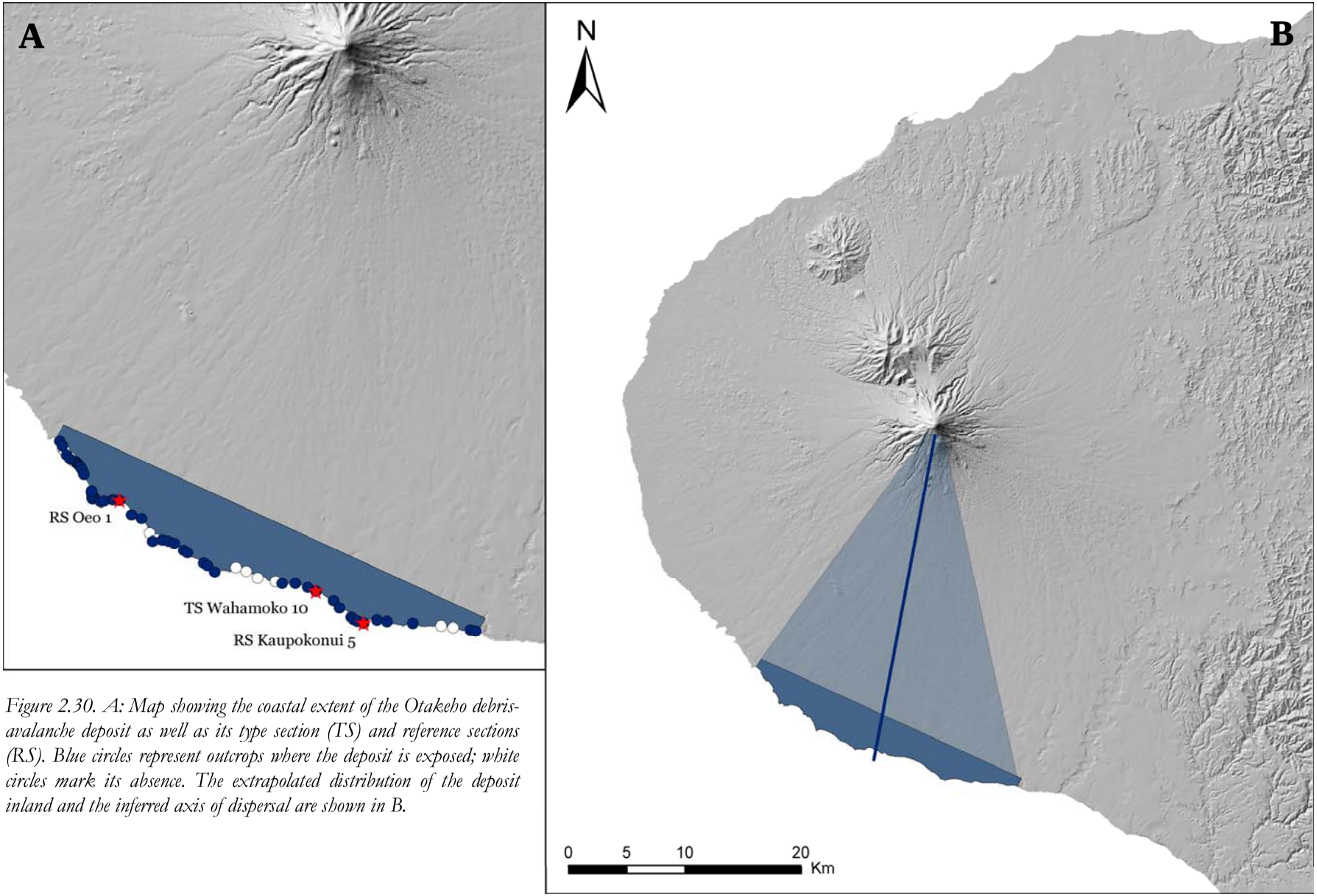

Figure 2.30. A: Map showing the coastal extent of the Otakeho debris-avalanche deposit as well as its type section (TS) and reference sections (RS). Blue circles represent outcrops where the deposit is exposed; white circles mark its absence. The extrapolated distribution of the deposit inland and the inferred axis of dispersal are shown in B.

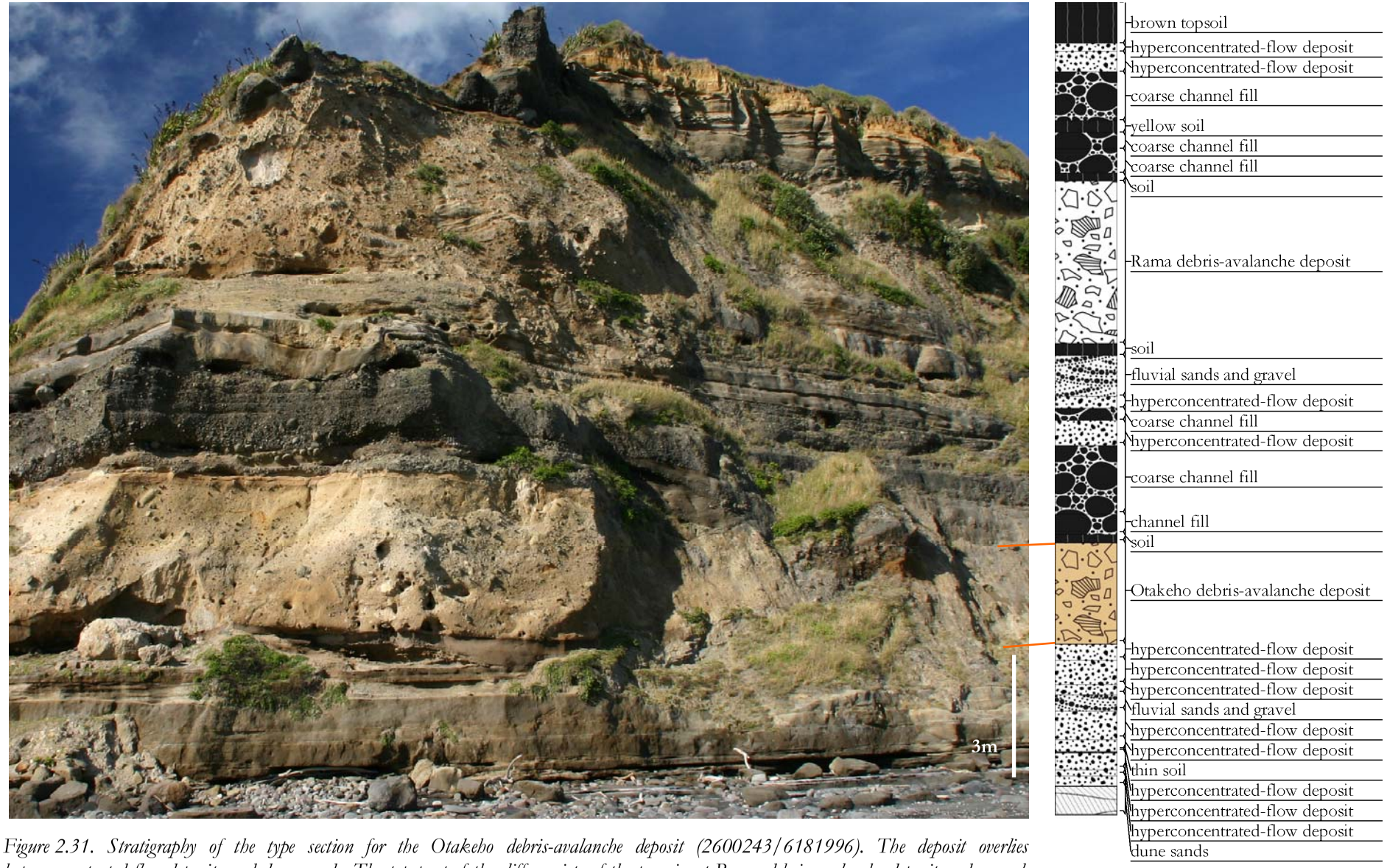

Figure 2.31. Stratigraphy of the type section for the Otakeho debris-avalanche deposit (2600243/6181996). The deposit overlies hyperconcentrated flow-deposits and dune sands. The top part of the cliff consists of the prominent Rama debris-avalanche deposit and several

2.5.7. Unnamed debris-flow deposits (Punehu and Kaupokonui Streams)

A thin clay matrix-rich debris-flow deposit occurs below the Otakeho debris avalanche deposit over a short stretch of coastline (0.7 km) from Taungatara 10 to Punehu 3A (Fig. 2.32). The deposit is c. 0.5-1 m thick, very matrix-rich (90-95%) and contains small, scattered pebble-sized clasts (Fig. 2.33). It is separated from the overlying Otakeho debris-avalanche deposit by a thin paleosol. The debris-flow deposit is underlain by a thick paleosol and stacks of dune sands at Taungatara 10, and peat and pumiceous hyperconcentrated-flow deposits at Punehu 3A. The deposit was most likely emplaced by the run-out of a very small debris avalanche that was confined to a paleo-Punehu Stream in distal areas.

Another clay-rich debris-flow deposit occurs at this stratigraphic position at Kaupokonui 1A (Fig. 2.32). It is c. 0.8 m thick and separated from the Otakeho by fluvial sediment (Fig. 2.34). It appears to have been produced by a similar process as the unnamed debris flow at Punehu, i.e. the distal run-out of a very small debris avalanche which was channelised down a paleo-Kaupokonui catchment. Both cohesive debris-flow deposits occur at a similar stratigraphic position and seem to be of similar age as the below-described Waihi debris-avalanche deposit. Since a direct correlation was not possible, it is unknown if they represent lateral equivalents of the same large debris-avalanche event or individual smaller events.

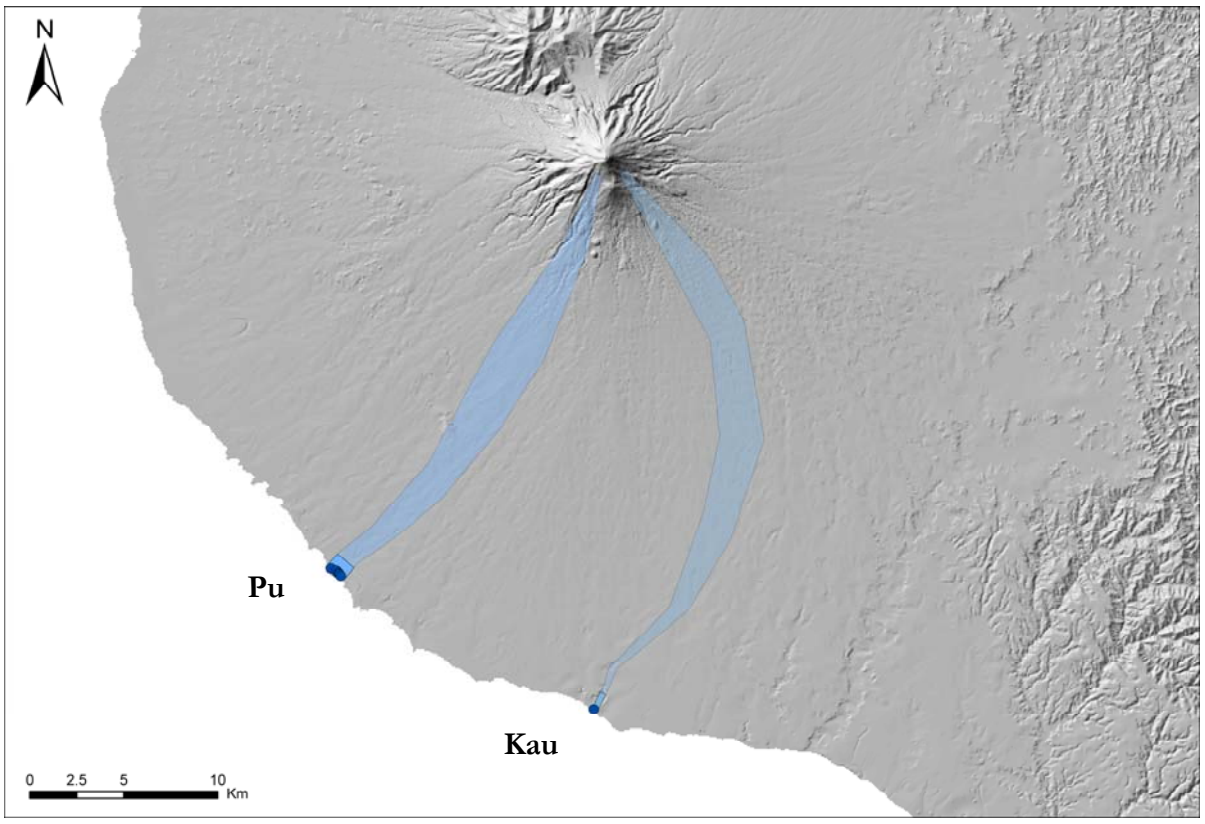

Figure 2.32. Mapped coastal extent and extrapolated inland distribution of the two unnamed debris-flow deposits along proto-Punehu (Pu) and -Kaupokonui (Kau) catchments.

Figure 2.33. In the Punehu catchment, the unnamed debris-flow deposit below the Otakeho debris-avalanche deposit is c. 0.6 m thick, very matrix-rich and characterised by small,granule- to pebble-sized clasts.

Figure 2.34. In the Kaupokonui catchment, a c. 0.8 m thick unnamed debris-flow deposit occurs below the Otakeho. It is underlain by fluvial sands (Flu) and hyperconcentrated-flow deposits (HFDs).

2.5.8. Tokaora debris-avalanche deposit (new unit)

The Tokaora debris-avalanche deposit has not been described previously and was named after Tokaora township in south Taranaki. It is exposed over c. 2 km of coastline from Waingongoro 2a-5 (Fig. 2.36). At its type section Waingongoro 5, the deposit thickens to c. 3 m in a small paleo-channel and wedges out to the east (Fig. 2.35A). It is characterised by pebble- to cobble-sized scattered clasts in a dark brownish matrix and a distinct yellowish top, separated from a darker basal part by a sharp and wavy boundary (Fig. 2.35B-C). Otherwise similar deposit characteristics and clast sizes suggest that the sharp colour difference of the matrix was produced by different degrees of weathering and diagenesis of the deposit surface rather than sedimentological differences. The Tokaora is overlain by bedded grey transitional hyperconcentrated-flow/streamflow deposits and separated from the underlying Waihi debris-avalanche deposit by a thin layer of rounded fluvial pebbles and sands (Fig. 2.37). The bottom of the cliff section is made up of bedded sands with intercalated paleosols and Tertiary mudstone.

At reference locality Waingongoro 2-2a, the Tokaora debris-avalanche deposit slopes down from the higher ridge of Tertiary mudstones into the deep Waingongoro paleo-valley, but subsequent erosion has removed it within the centre of the valley.

The small lateral extent of the Tokaora debris-avalanche deposit suggests that it was produced by the channelised run-out of either a smaller debris avalanche or the marginal portion of one that was directed to the east, similar to the Ngaere event. Its age can only be roughly estimated from its stratigraphic position below the Otakeho and above the Waihi debris-avalanche deposits suggesting approximately 60 ka.

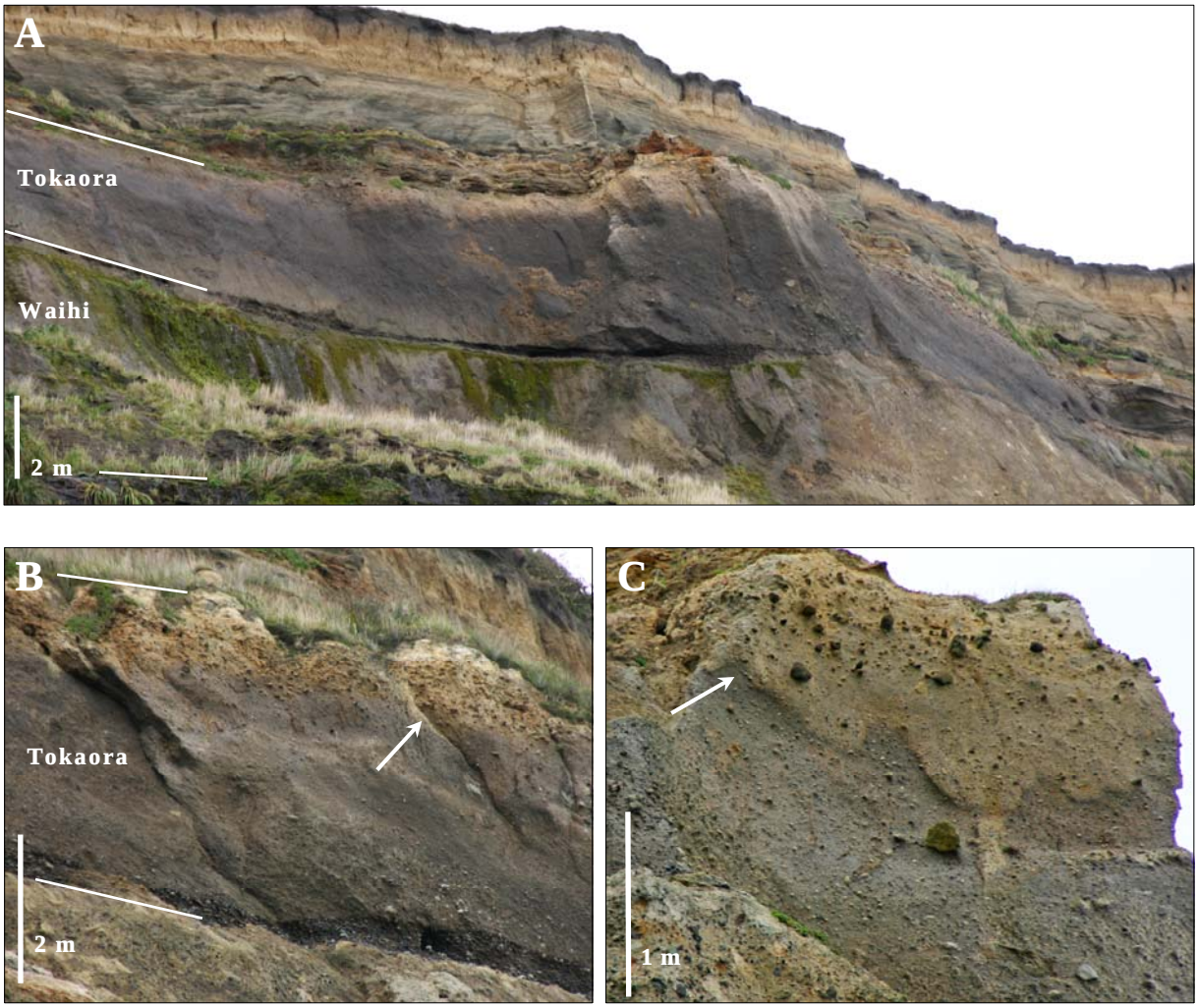

Figure 2.35. The Tokaora debris-avalanche deposit thickens in a small channel at its type section Waingongoro 5 (2614414/6178412) and is shown in A. It is characterised by small, predominantly pebble-sized clasts in a dark brownish matrix and typically has a yellowish weathered top, marked by white arrows (B-C).

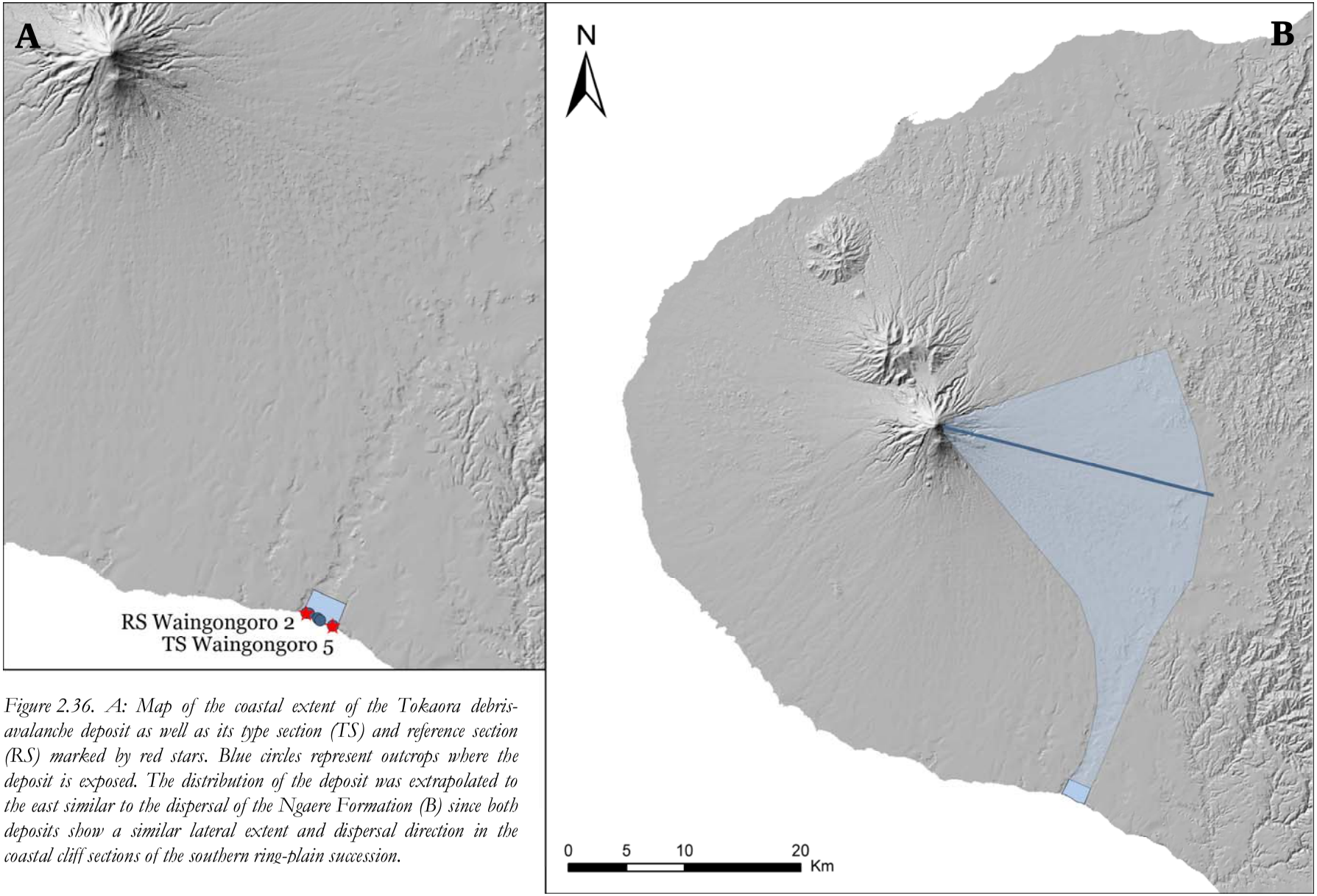

Figure 2.36. A: Map of the coastal extent of the Tokaora debris-avalanche deposit as well as its type section (TS) and reference section (RS) marked by red stars. Blue circles represent outcrops where the deposit is exposed. The distribution of the deposit was extrapolated to the east similar to the dispersal of the Ngaere Formation (B) since both deposits show a similar lateral extent and dispersal direction in the coastal cliff sections of the southern ring-plain succession.

Figure 2.37. Stratigraphy of the type section for the Tokaora debris-avalanche deposit (2614414/6178412). The deposit occurs near the top of the cliff and is underlain by the Waihi debris-avalanche deposit. The bottom of the cliff consists of bedded sands and Tertiary mudstones.

2.5.9. Waihi debris-avalanche deposit (new unit)

The Waihi debris-avalanche deposit is a formerly unknown unit, named after Waihi beach near Hawera in south Taranaki. It is exposed over 17.8 km from Waiokura 2A to Waihi 6B, where the volcaniclastic sequence wedges out and the uplifted Tertiary mud- and sandstone succession forms the entire cliff section (Fig. 2.40). The Waihi debris-avalanche deposit is c. 4 m thick at its type section Waihi 2. The deposit contains pebble- and cobble-sized clasts (typically <10 cm) in a clay-rich matrix and has a high content of pumice clasts. Larger clasts are concentrated in a c. 1 m-thick bouldery basal layer (Fig. 2.38). Secondary clasts are abundant, including ripped-up fragments of mudstone and pieces of wood. The top of the cliff consists of fluvial sands and a thin hyperconcentrated-flow deposit, capped by a thick soil (Fig. 2.41). The Waihi directly overlies the Waingongoro debris-avalanche deposit, which shows similar sedimentological characteristics (cf. Section 2.5.10).

At reference locality Waihi 5A, the Waihi debris-avalanche deposit contains pebble- to cobble- and some boulder-sized clasts including several large, rounded megaclasts (>5 m across), abundant small (c. 0.2-0.5 m in diameter) to fewer medium-sized (1-1.5 m across) rip-up clasts and pieces of wood (Fig. 2.39A-B). The deposit is c. 5 m thick and separated from the underlying Waingongoro debris-avalanche deposit by a distinct paleosol. At Waingongoro 4A, the Waihi and Waingongoro debris-avalanche deposits thicken in a small channel. Here, the Waihi appears to consist of two gradational units with different sedimentological characteristics. These most likely represent two pulses of a single collapse series. The bottom unit ranges in thickness from 3-5 m and is exceptionally coarse. It contains large cobble- to boulder-sized clasts and abundant brecciated megaclasts of the same lithology (Fig. 2.39C). In contrast, the upper unit thickens to 2-3 m and is similar to the Waihi at other locations. It is matrix-rich and contains pebble- to cobble-sized clasts as well as small rip-up clasts.

The debris-avalanche deposit is thickest at Waihi 6 (>9 m), where it filled a small channel. The overall deposit thickness, its maximum thickness of 9 m at a runout distance of c. 45 km, and its sedimentological characteristics suggest that the Waihi debris-avalanche deposit is of very large volume. The course of the debris avalanche might have been similar to that of the Ngaere debris avalanche with the main body of the flow being directed to the east and a marginal part flowing southward to the current coastline area. This distribution pattern would explain the limited lateral extent and considerable thickness of the deposit. But since there are no outcrops available that cut deep enough into the eastern ring-plain succession, the distribution of the three southern debris-avalanche deposits (Tokaora, Waihi and Waingongoro) can only be speculated.

Figure 2.38. The Waihi debris-avalanche deposit shows a distinct coarse basal layer at its type section Waihi 2 (2617078/6176430) and is sedimentologically similar to the underlying Waingongoro debris-avalanche deposit.

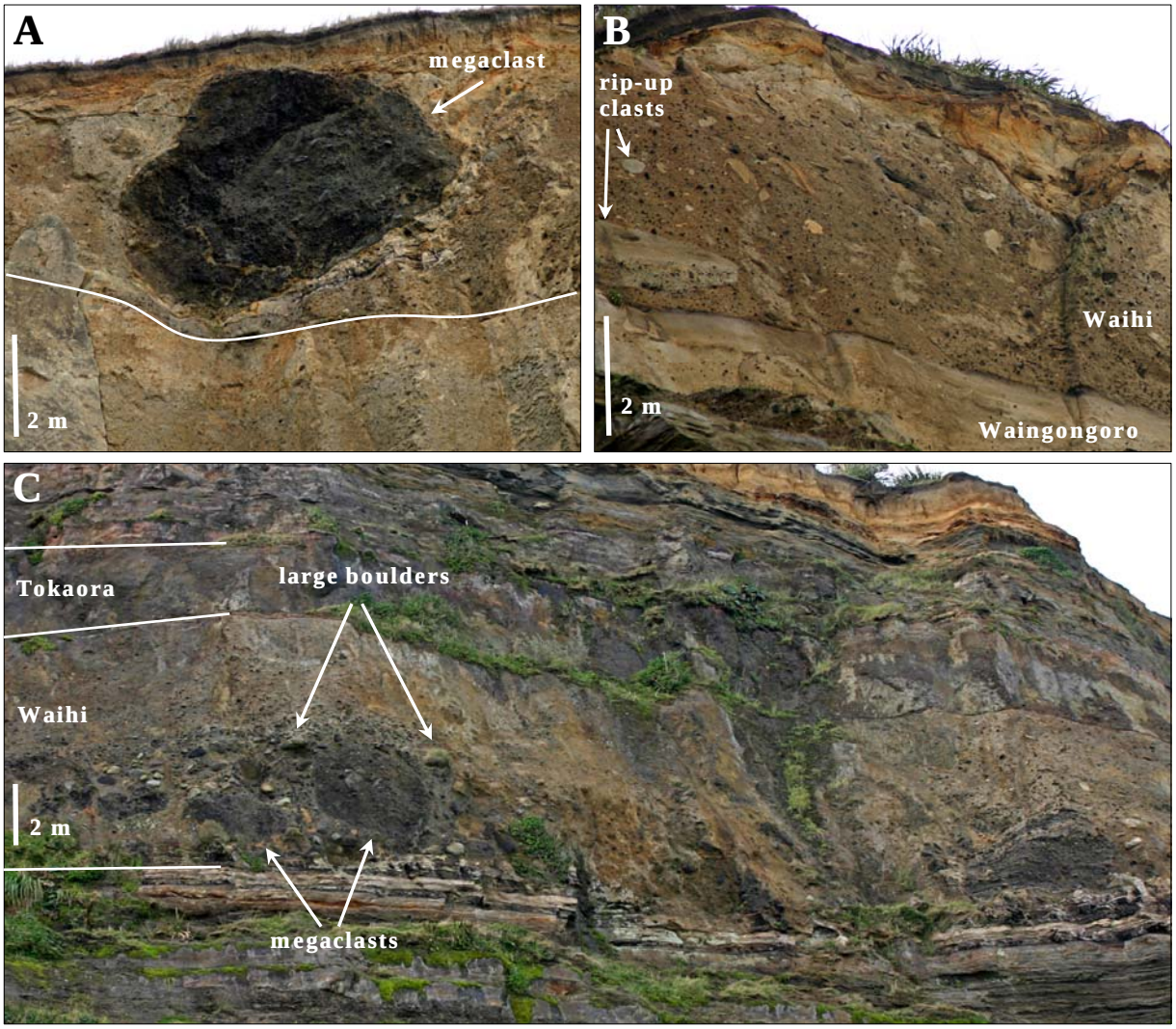

Figure 2.39. At reference locality Waihi 5A, the Waihi debris-avalanche deposit is c. 5 m thick and characterised by large, rounded megaclasts (A) and abundant rip-up clasts (B). At Waingongoro 4A, the deposit thickens in a small channel and consists of a coarse bottom unit with large cobble- to boulder-sized clasts and abundant brecciated megaclasts and a thinner upper part characterised by smaller clasts and small rip-up clasts (C).

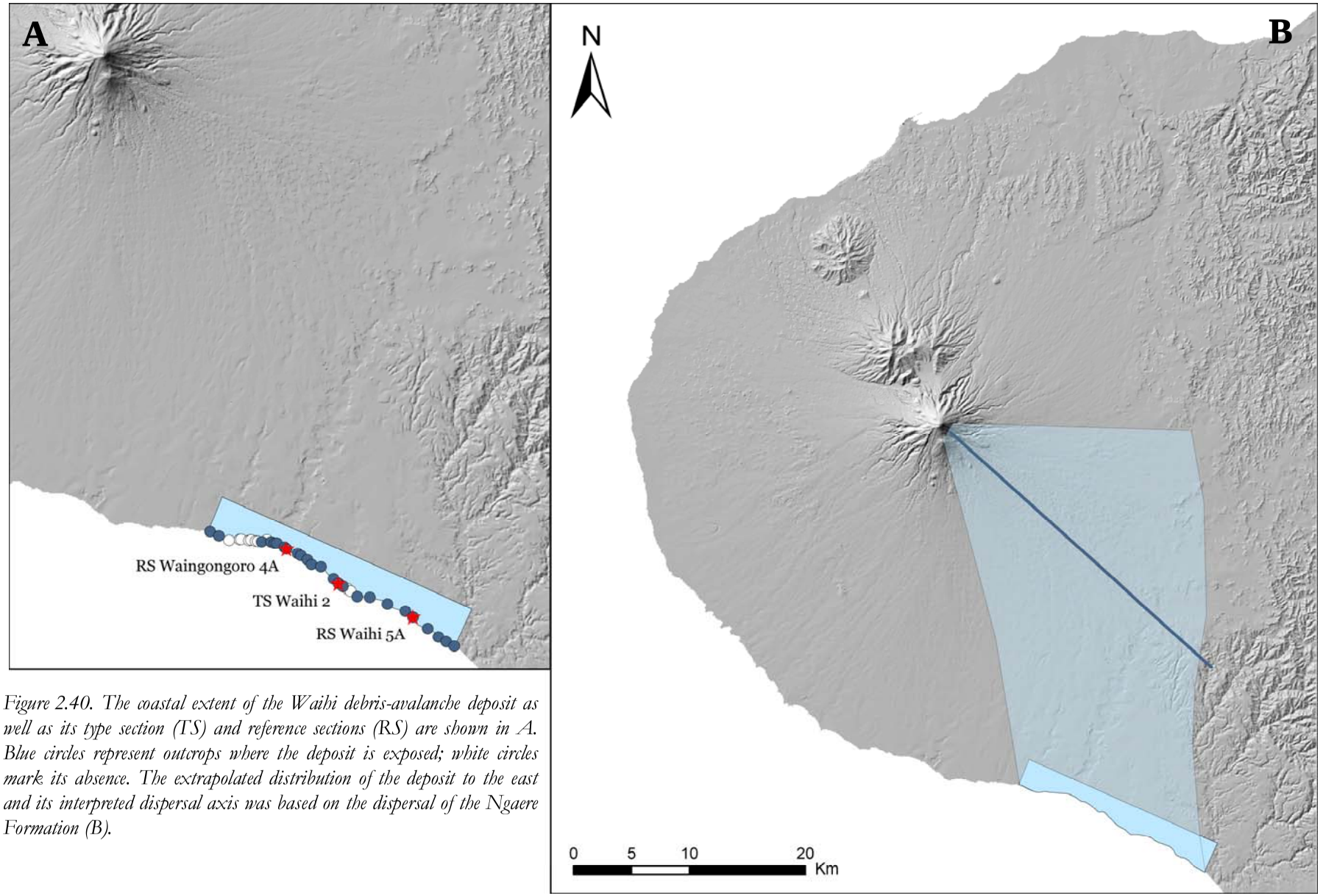

Figure 2.40. The coastal extent of the Waihi debris-avalanche deposit as well as its type section (TS) and reference sections (RS) are shown in A. Blue circles represent outcrops where the deposit is exposed; white circles mark its absence. The extrapolated distribution of the deposit to the east and its interpreted dispersal axis was based on the dispersal of the Ngaere Formation (B).

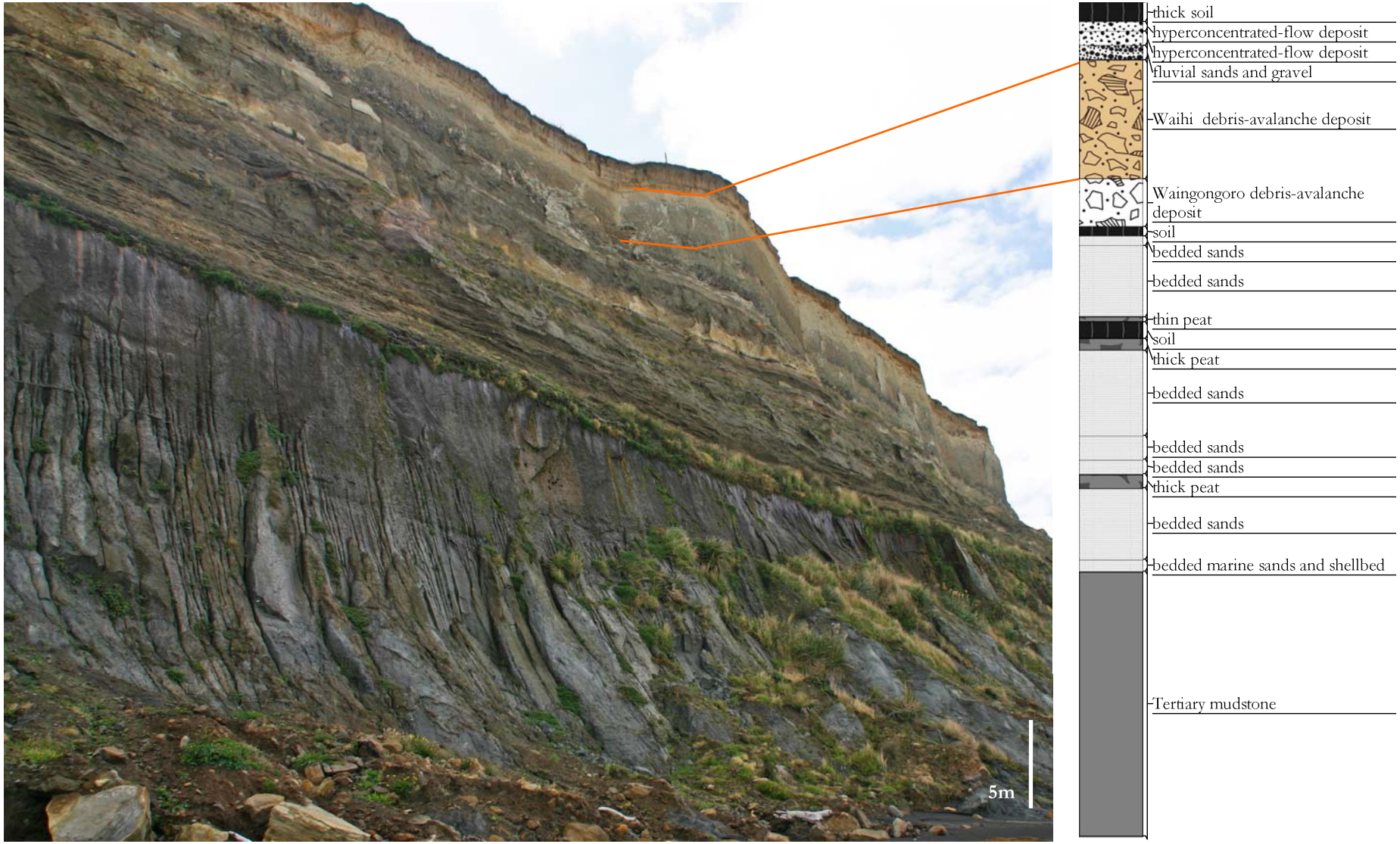

Figure 2.41. Stratigraphy of the type section for the Waihi debris-avalanche deposit (2617078/6176430). The deposit is exposed near the top of the cliff. The sequence below is made of bedded sands with two thick intercalated peat/soil layers. Marine sands and a prominent shellbed form the coverbeds of the Rapanui marine bench and separate the volcaniclastic succession from the underlying Tertiary mudstone sequence.

The emplacement age of the Waihi can only be estimated from its stratigraphic position. It predates the Otakeho and Tokaora events and overlies the Oeo and Waingongoro debris-avalanche deposits, giving an approximate age range of c. 80-50 ka (assumed to be emplaced most likely at 70 ka).

2.5.10. Waingongoro debris-avalanche deposit (new unit)

The Waingongoro debris-avalanche deposit was named after Waingongoro River and has not been described elsewhere. It shows similar distribution and deposit characteristics as the overlying Waihi unit but is of smaller volume. It was mapped over 16.6 km from Waiokura 2A to Waihi 6 (Fig. 2.44). At its type locality Waihi 5, the deposit is about 5 m thick and contains pebble- to cobble-sized clasts, including a high content of pumice clasts, few larger boulder-sized clasts as well as small rounded rip-up clasts in a clay-rich matrix (Fig. 2.42A). Rip-up clasts become more abundant a few hundred metres east at Waihi 5C (Fig. 2.42B). The deposit is underlain by a thick laminated soil and separated from the overlying Waihi debris-avalanche deposit by a thin but distinct paleosol (Fig. 2.45). A thick laminated soil/peat occurs above the Waihi, which is covered by a thick series of bedded sands with intercalated thin peat beds and a thick soil at the top of the section. The sequence below the Waingongoro debris-avalanche deposit consists of bedded sands that are interbedded with thick soil and peat layers.

In several locations, the Waingongoro debris-avalanche deposit is characterised by a coarse basal layer similar to the Waihi. At reference locality Waingongoro 6, this zone of subrounded to subangular cobble- to boulder-sized clasts is very distinct and c. 0.5 m thick (Fig. 2.43). The upper part of the 1.6 m thick deposit is characterised by smaller clasts. The sequence at this location shows a similar stratigraphy as the type section but the two debris-avalanche deposits directly overlie each other and lack a paleosol between. The thin, laminar-bedded sands above the Waihi are interpreted as being emplaced from transitional hyperconcentrated flows/dilute stream flow with interbedded fluvial sands, while the sands below the debris-avalanche deposits more likely represent dune and beach sands.

Similar to the Waihi, the age of the Waingongoro debris-avalanche deposit could only be estimated based on its stratigraphic position below the Otakeho and Tokaora and above the Oeo debris-avalanche deposits. It is thought to have been emplaced around 75 ka, with respect to the possible age of the Waihi. The interbedded thin soil appears to represent only a short time break between the two debris-avalanche deposits and is often missing, indicating that they were most likely emplaced within a relatively short period of time. However, it is impossible to precisely determine the age of these two units without further dating.

Figure 2.42. At its type section Waihi 5 (2620264/6175098), the Waingongoro debris-avalanche deposit is c. 5 m thick and characterised by abundant small rip-up clasts of the underlying bedded sands. It is overlain by the Waihi debris-avalanche deposit (A) from which it is separated by a thin paleosol (B).

Figure 2.43. In some locations, the Waignongoro debris-avalanche deposit shows a distinct basal layer of subrounded to subangular cobble- to boulder-sized clasts and has a similar appearance as the overlying Waihi.

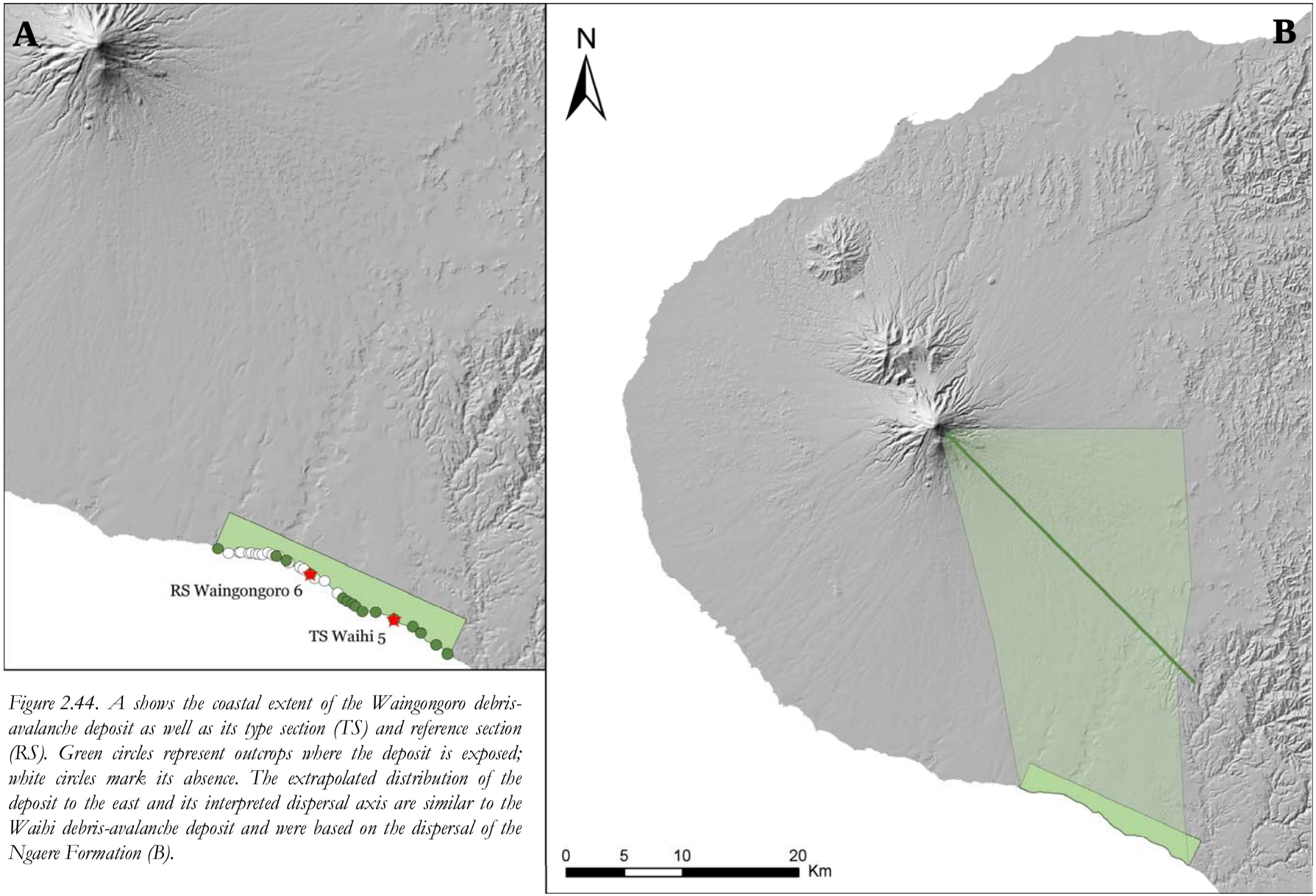

Figure 2.44. A shows the coastal extent of the Waingongoro debris-avalanche deposit as well as its type section (TS) and reference section (RS). Green circles represent outcrops where the deposit is exposed; white circles mark its absence. The extrapolated distribution of the deposit to the east and its interpreted dispersal axis are similar to the Waihi debris-avalanche deposit and were based on the dispersal of the Ngaere Formation (B).

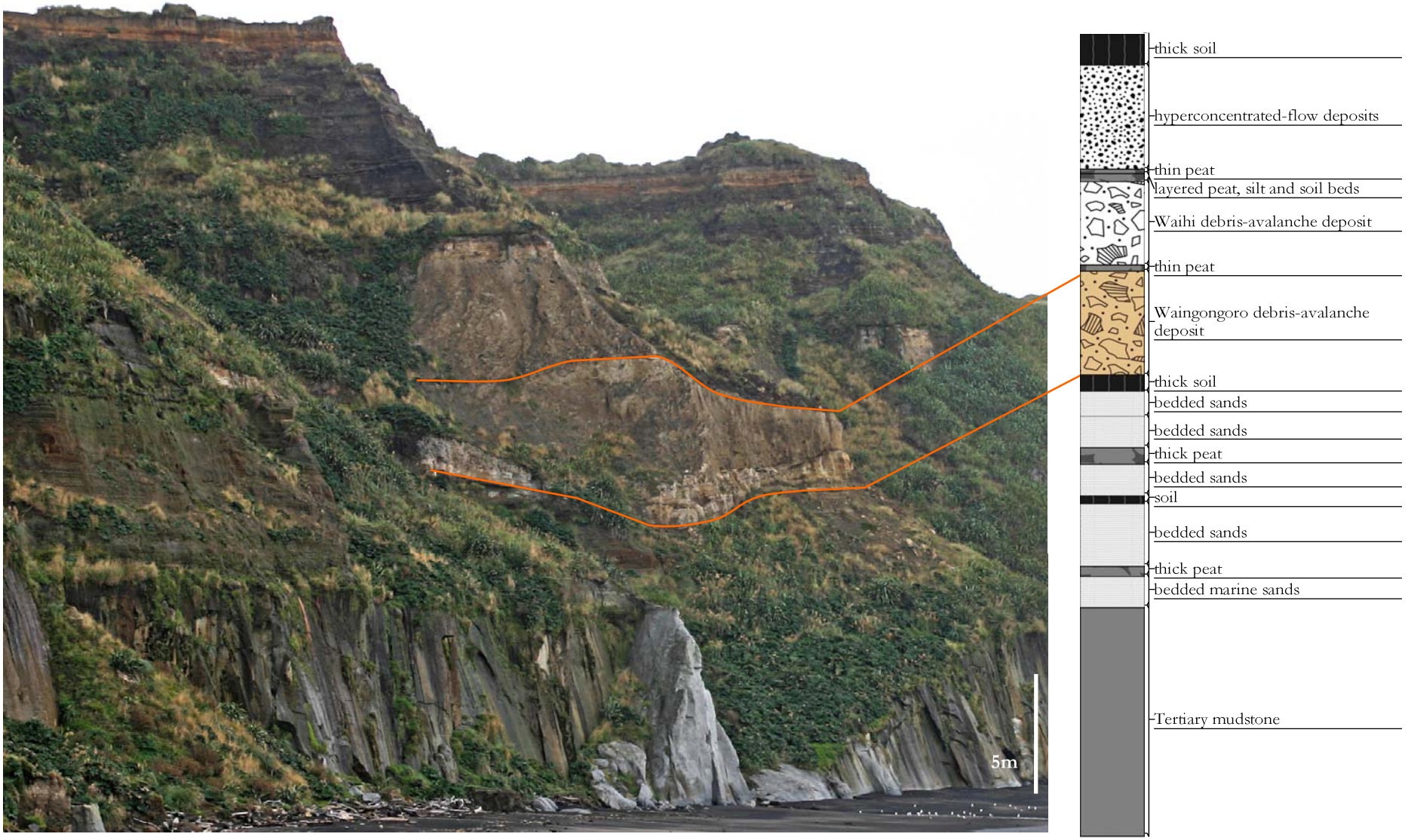

Figure 2.45. Stratigraphy of the type section for the Waingongoro debris-avalanche deposit (2620264/6175098). The deposit is overlain by the Waihi debris-avalanche unit and several hyperconcentrated –flow deposits. The bottom of the cliff section is made up of bedded sands and Tertiary mudstones.

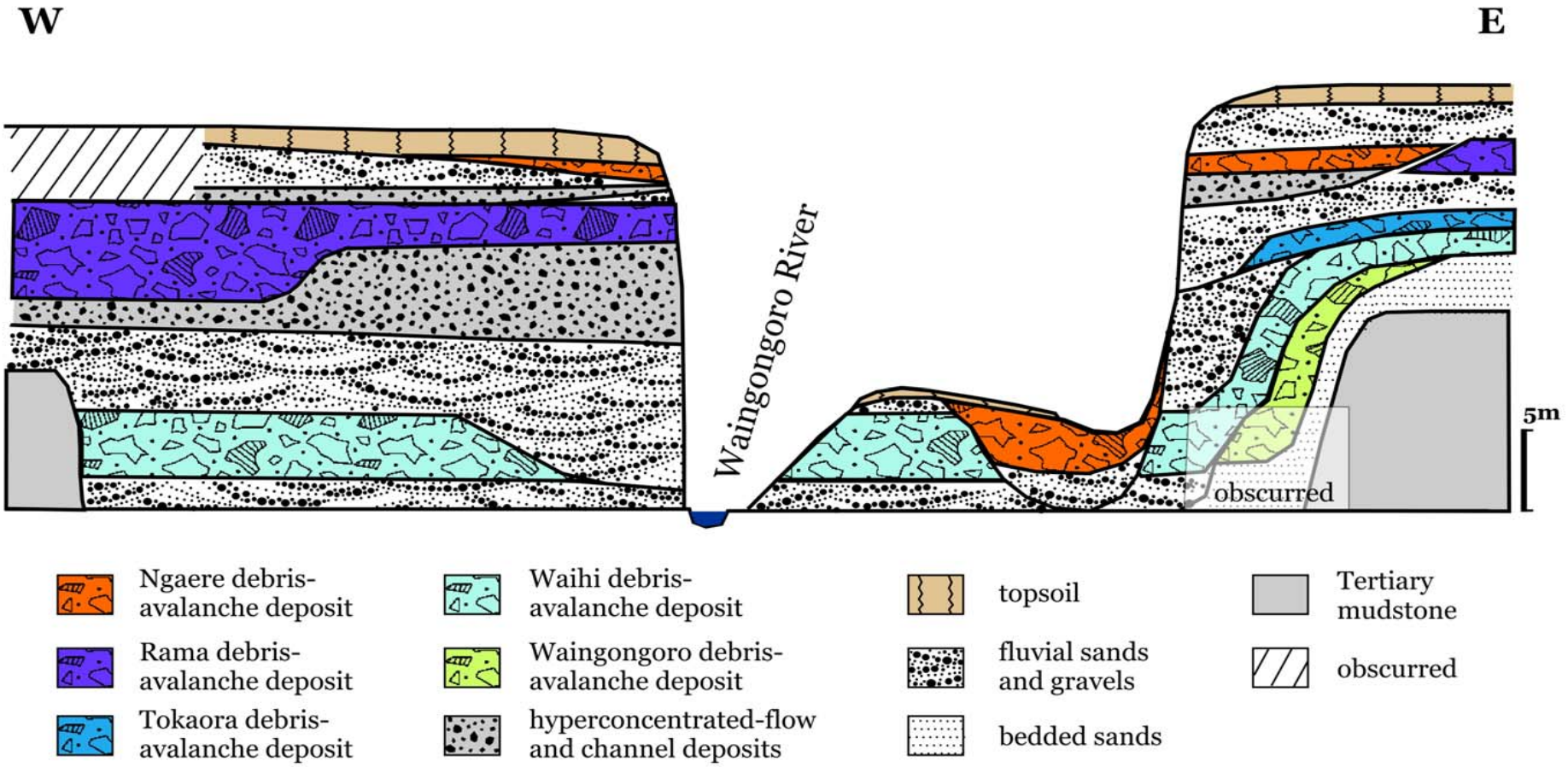

Figure 2.46. Schematic overview of the stratigraphy at the Waingongoro River mouth and Ohawe Beach. The complex valley sequence is the result of repeated incision and subsequent filling of these river channels with fluvial sediments and debris-avalanche deposits as well as intercalated hyperconcentrated-flow units. The profile is oriented west to east and c. 1.2 km in length. The mudstone sequence underlying the volcaniclastic succession is cut by the c. 127 ka Rapanui Marine Terrace in the eastern part of this cross-section and by the c. 105 ka Inaha Marine Terrace in the western part, resulting in a slight difference in thickness of the Tertiary basement.

Figure 2.47. Overview of the broad Waingongoro River valley at the coast (A), person for scale. Tertiary mudstone sequences form the side walls of an ancient, wider valley in the same location. Tertiary mudstones are c. 7 m thick at the western side (B) and c. 10 m thick at the eastern side (C). The confinement of the Waihi debris avalanche to this paleo-channel and its abrupt contact to the Tertiary basement confirms the long (>70 ka) existence of this valley (B).

2.5.11. Oeo debris-avalanche deposit (new unit)

The Oeo debris-avalanche deposit is a previously unrecognised unit, which was named after Oeo Stream in south-west Taranaki. It crops out at the very bottom of the cliff section in two locations, Oeo 4B and 7 (Fig. 2.50). At its type section Oeo 7, the deposit forms a c. 4.5 m-high and c. 20 m-wide mound at the bottom of the sequence (Fig. 2.48A). The deposit is characterised by a brecciated, almost clast-supported fabric with little matrix. Clasts range in size from a few cm to c. 1 m in diameter (Fig. 2.48B). The largest lava blocks are fractured and show characteristic jigsaw cracks. The deposit appears to consist of several monolithologic domains, which are even more obvious at Oeo 4B. The Oeo debris-avalanche deposit is directly overlain by a sequence of bedded dune sands with intercalated paleosols and peat beds, including the Puketapu buried forest, that wedges against the mound and is not exposed on its top (Fig. 2.51). The mound and the sand wedges either side are overlain by the Otakeho debris-avalanche deposit followed by a series of at least seven hyperconcentrated-flow deposits with interbedded paleosols. The upper part of the sequence consists of the Manaia debris-avalanche deposit in turn overlain by at least seven hyperconcentrated-flow deposits with intercalated soils that are capped by a thick soil.

A second debris-avalanche mound is exposed at reference locality Oeo 4B. The mound is larger than at the above described section, with a height of c. 5-6 m and a width of c. 40 m (Fig. 2.49A-B). The deposits wedging on either side of the mound consist of bedded sands with intercalated soil/peat beds and the prominent Puketapu buried forest, which is here characterised by a soil with a tree stump in growth position (Fig. 2.49C). The top of the sequence is mostly overgrown but appears very similar to Oeo 7. The Oeo debris-avalanche deposit is characterised by several monolithologic domains that represent individual megaclasts with different sedimentological characteristics (Fig. 2.49D). The top of the mound is clast-supported and consists exclusively of brecciated, strongly altered andesite. The shattered clasts range in size from a few cm to >1 m across. In contrast, a small megaclast and the domain below are characterised by a fine-grained matrix and angular-subangular clasts of various sizes (Fig. 2.49E). The bottom layer is matrix-rich and contains predominantly subrounded-rounded clasts. The base of the deposit is not exposed.

Due to its stratigraphic position and the thick overlying sequence, the uplift rates in South Taranaki were not sufficient to excavate the Oeo debris-avalanche deposit above the present day sea-level. Exposure of the top of the deposit is limited to two locations where it forms thick mounds that protrude out of the paleo-landscape with later deposits wedging against them. These debris-avalanche mounds typically occur near the main axis of dispersal, suggesting a

south-westerly distribution of the Oeo. The dispersal limit of the deposit is indicated by its absence in exposed sequences of assumed similar age above the Tertiary mudstones from Waiokura 5-7. The age range of the Oeo debris-avalanche deposit is given by the closely overlying c. 80 ka Puketapu buried forest and the cutting of the Inaha marine bench into the underlying Tertiary mudstone sequence at c. 105 ka. Its emplacement age is here estimated at c. 85-90 ka since it closely predates the formation of the Puketapu buried forest.

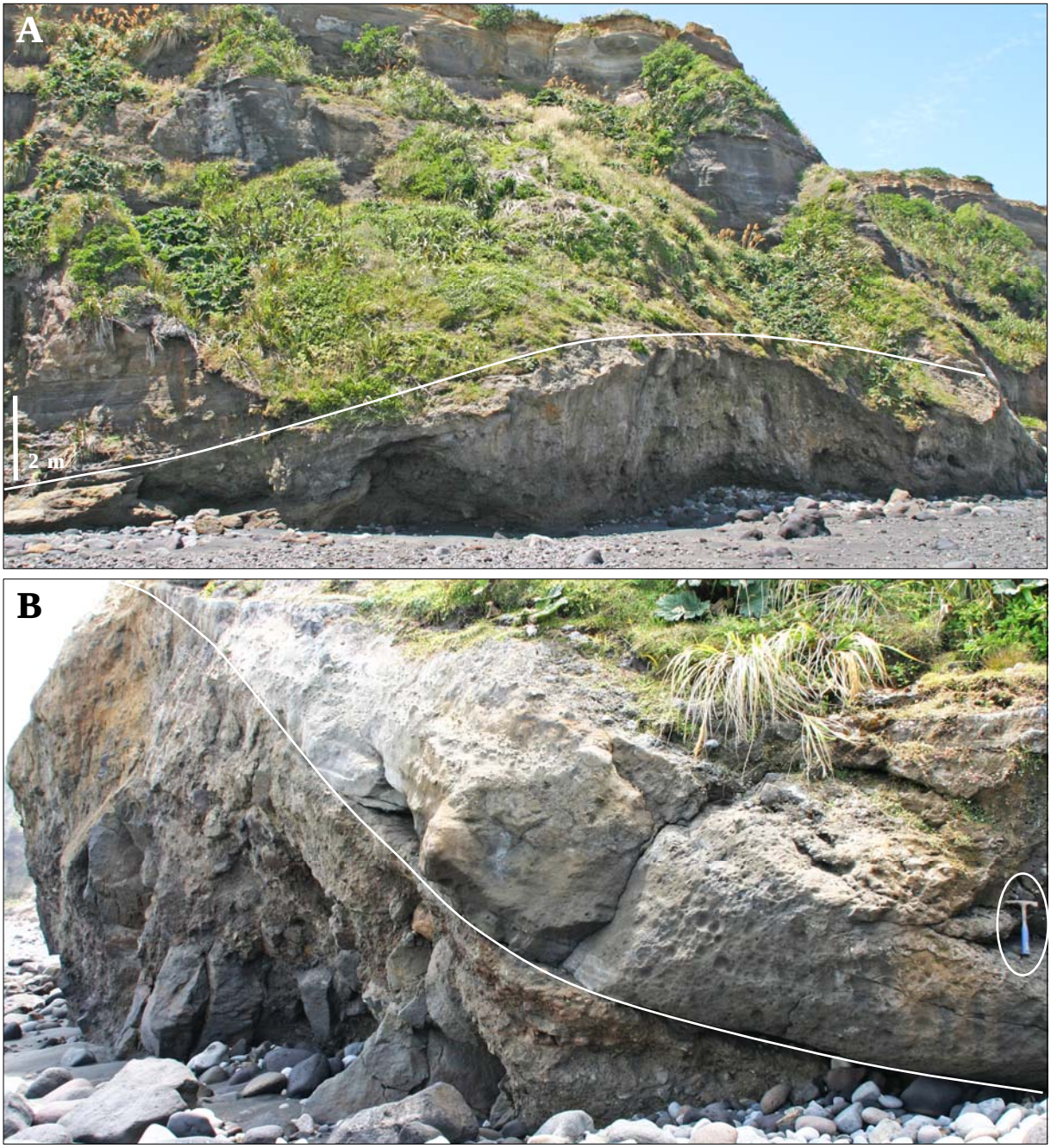

Figure 2. 48. A c. 4.5 m-thick mound of the otherwise buried Oeo debris-avalanche deposit crops out at the bottom of the cliff at its type section Oeo 7 (A). At this location (2593403/6184081) the deposit is characterised by a brecciated, almost clast-supported fabric (B). Hammer for scale, c. 30 cm long.

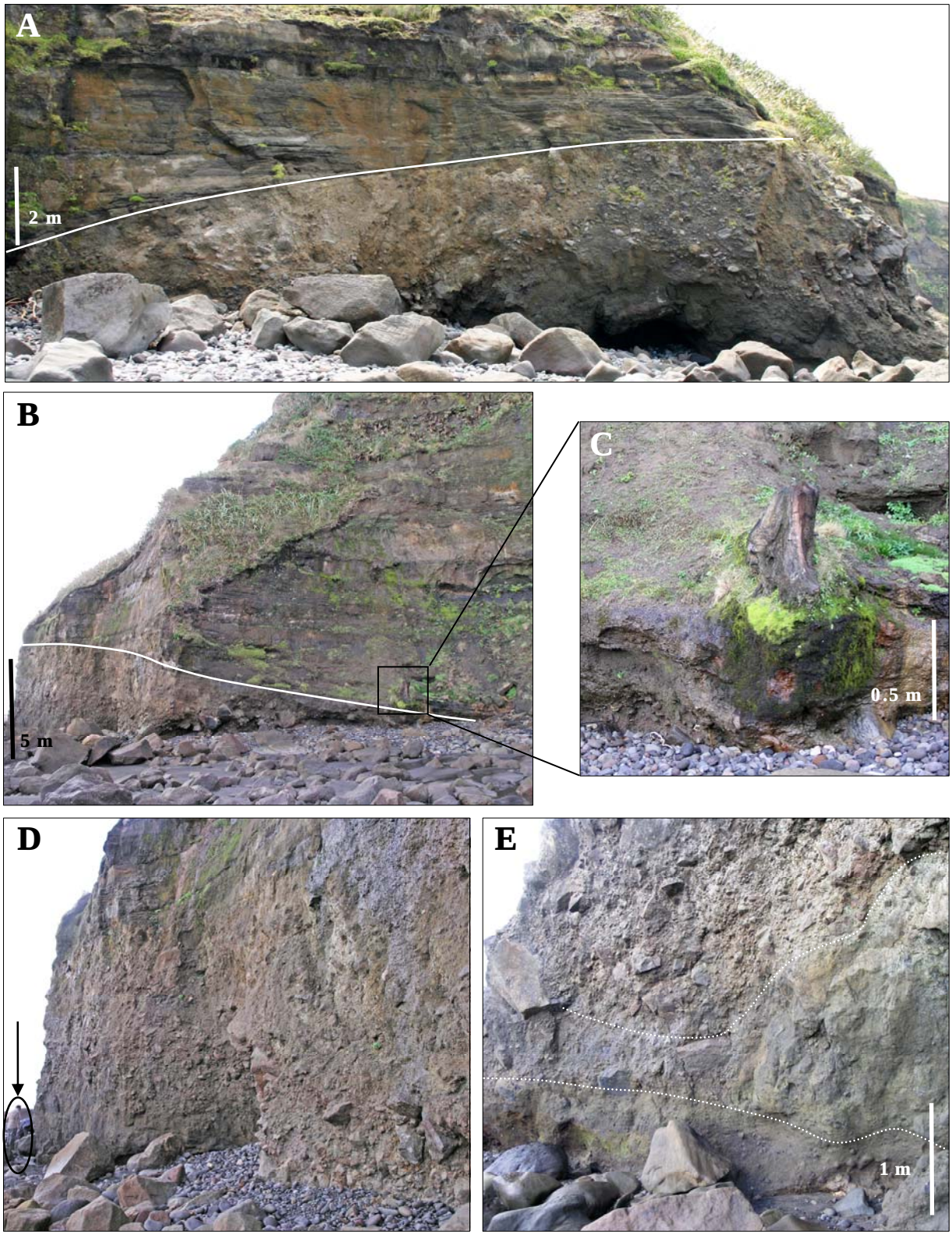

Figure 2.49. A second c. 6 m- high mound of the Oeo-debris avalanche deposit crops out at Oeo 4B (A-B). It is overlain by the distinct Puketapu buried forest, which is characterised by a soil with a preserved tree stump in growth position (C). The Oeo debris-avalanche deposit consists of several monolithologic megaclasts with different sedimentological characteristics (D), arrow points to person for scale. The top of the mound is brecciated and clast-supported, while other domains (marked by white dotted line) consist of fine-grained matrix and angular-subangular clasts of various sizes (E).

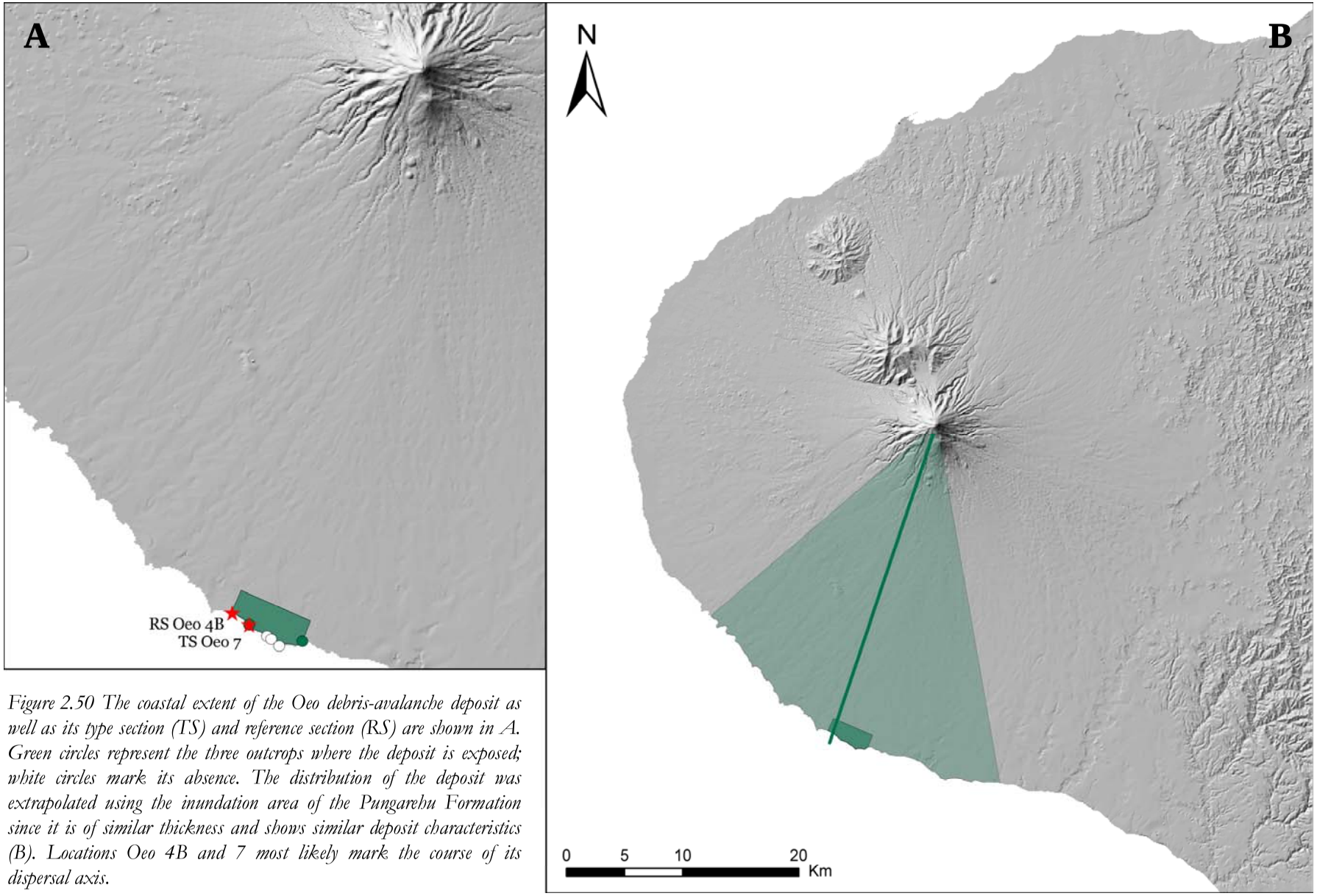

Figure 2.50 The coastal extent of the Oeo debris-avalanche deposit as well as its type section (TS) and reference section (RS) are shown in A. Green circles represent the three outcrops where the deposit is exposed; white circles mark its absence. The distribution of the deposit was extrapolated using the inundation area of the Pungarehu Formation since it is of similar thickness and shows similar deposit characteristics (B). Locations Oeo 4B and 7 most likely mark the course of its dispersal axis.

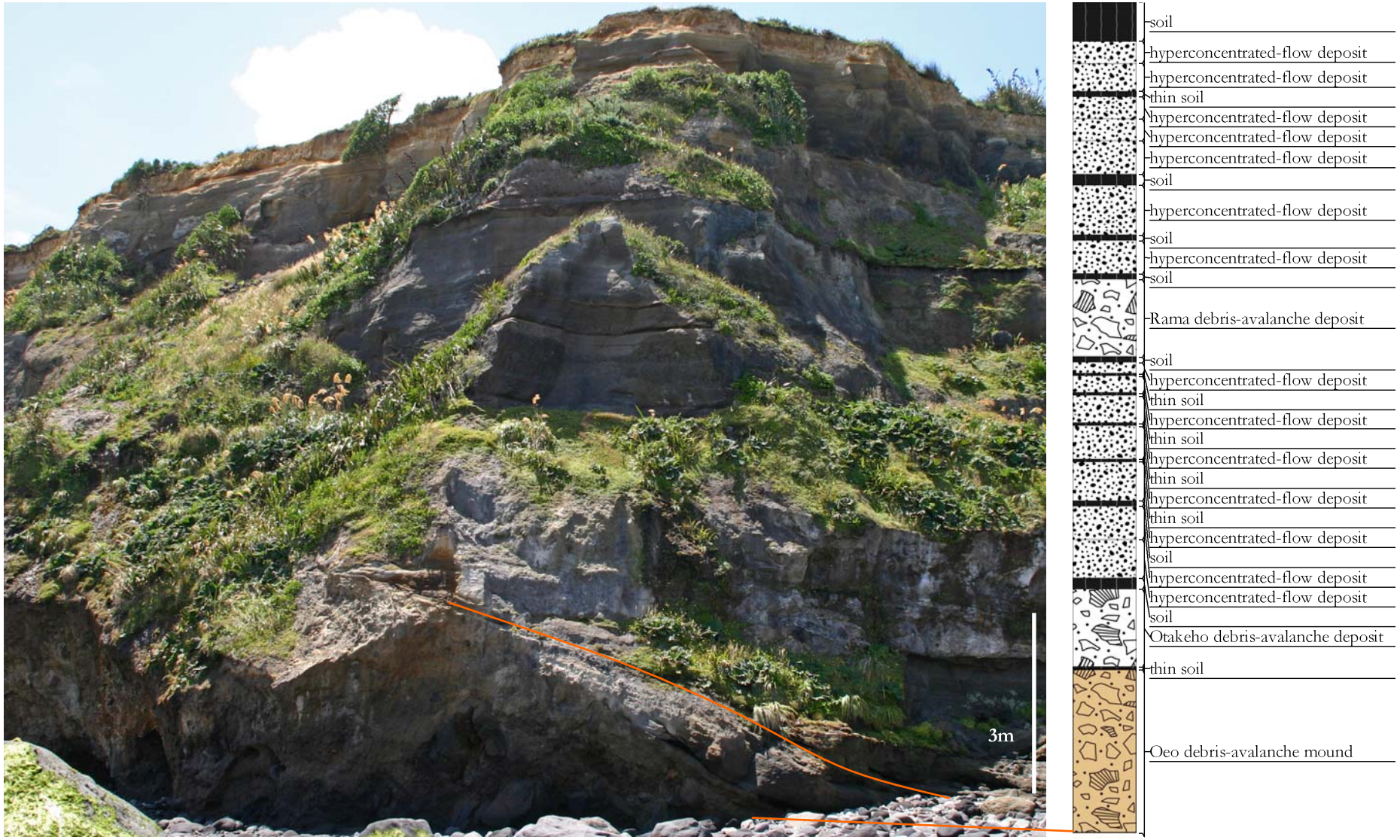

Figure 2.51. Stratigraphy of the type section for the Oeo debris-avalanche deposit (2593403/6184081). The deposit forms a mound that crops out at the bottom of the cliff and is overlain by the Puketapu buried forest. The upper part of the section consists of the Otakeho and Rama debris-avalanche deposits that are interbedded with hyperconcentrated-floow units and paleosols.

2.5.12. Mangati debris-avalanche deposit (redefined unit in north Taranaki)

An unnamed debris-avalanche deposit of unknown origin is exposed in coastal cliffs near Bell Block (Alloway 1989), which is here named Mangati debris-avalanche deposit after its occurrence east of the Mangati Stream. Its lateral extent was not mapped during this study since this project focused on the south-western ring-plain succession. However, the unit was included in the geochemical study of debris-avalanche deposits (cf. Chapter 4) in order to determine its origin. Therefore, the deposit was also studied in terms of its sedimentological characteristics over a coastal stretch of c. 2 km east of Bell Block. Here, the deposit is characterised by a maximum thickness of 6 m and coarse clasts in a clay-rich matrix (Fig. 2.52). Over most of its exposure along the coast north-east of Bell Block, its base is marked by a distinct layer of cobble- to boulder-sized rounded to subangular clasts. In some locations, large logs are found within this basal layer, which protrude from the deposit at a c. 90° angle, roughly parallel to flow direction. It is underlain by cemented, iron-stained, high-angle cross-bedded sands with occasional large tree stumps in growth position. These sands are part of the coverbed sequence of the NT3/Ngarino marine bench. The Mangati debris-avalanche deposit is separated from the overlying Motunui Formation by a thick peat with interbedded andesitic tephra layers.

Figure 2.52. The Mangati debris-avalanche deposit in north Taranaki is characterised by a basal zone of coarse cobble-to boulder-sized clasts and large protruding tree logs. It occurs above iron-stained cross-bedded sands and is overlain by a thick sequence of peat and andesitic tephra beds.

Some sedimentological characteristics indicate that the Mangati might represent a lateral equivalent of the Maitahi Formation, i.e. the occurrence of ripped-up fragments of mudstone and abundant large hornblende crystals within the matrix, in particular in the bottom part of the deposit. However, its stratigraphic position overlying the c. 210 ka NT3/Ngarino Marine Terrace (cf. Alloway 1989) and its geochemical characteristics (cf. Chapter 4) suggest that it is considerably younger. It seems unlikely that the Mangati debris avalanche was produced by a later failure of Pouakai Volcano since it was assumed that the enormous Maitahi collapse destroyed most of the previous edifice. Also, its distribution pattern and the geochemical composition of the contained clast assemblages (cf. Chapter 4) are similar to the overlying Motunui and Okawa Formations, suggesting that it most likely represents an early event from an ancestral Mt. Taranaki. Its apparent resemblance to the Maitahi Formation could be derived from incorporation of underlying Maitahi debris during transport.

TABLE 2.2. *Radiocarbon analytical data of selected Taranaki debris-avalanche deposits (DAD).*

Debris-avalanche unit	Sample number	Sample type, stratigraphic position	Laboratory number	Analysis method*	Radiocarbon date (a BP)	Inferred age (ka)
Pungarehu	AZ05-D01	Peat directly below DAD	Wk-16398/ NZA-22349	AMS	20 776 ± 170	c. 20
Te Namu	AZ05-D11	Organic soil above DAD	Wk-16401	LSC	25 198 ± 167	c. 29
	AZ05-D14b	Tree log from DAD	Wk-16402/ NZA-22895	AMS	29 074 ± 399	
Rama	AZ06-D06	Thick peat above DAD	Wk-19143	LSC	28 824 ± 237	> 35
Ihaia	AZ06-D04	Wood from DAD	Wk-19142	LSC	31 522 ± 381	c. 31
Otakeho	AZ06-D01	Wood from DAD	Wk-19140	LSC	background	c. 55
Waihi	AZ06-D02	Large log from DAD	Wk-19141	LSC	background	c. 70

*AMS = Accelerator Mass Spectrometry; LSC = Liquid Scintillation Counting.
Sample locations and grid references are given in Appendix 3A.

2.6. DISTRIBUTION OF KNOWN FORMATIONS IN THE STUDY AREA

2.6.1. Opua Formation

In the study area, the Opua debris-avalanche deposit makes up the top of the cliff sections over a wide stretch of coastline and has a maximal medial width of 14.6 km. It is exposed from Arawhata 3-Punehu 1 (11.3 km) with a small marginal lobe being confined to Ouri Stream, from Punehu 14-Ouri 1A (0.7 km). This observation matches the coastal distribution of the Opua Formation as marked on the geological map of Taranaki by Neall & Alloway (2004) (Fig. 2.54). The deposit is thickest (5-8 m) between Heimama and Otahi Streams, along its main dispersal axis. Here, it is characterised by abundant pebble- to boulder-sized clasts and large megaclasts in a clay-rich matrix (Fig. 2.53). Several small mounds <2 m in height occur in coastal cross-sections. Towards the margins, size and number of original clasts decrease while the number of rip-up clasts increases. The deposit is covered by a thick soil that makes up the present-day surface and typically overlies the distinct Oakura Tephra.

Figure 2.53. At Okaweu 10, the Opua debris-avalanche deposit is c. 4 m thick and characterised by cobble-to boulder-sized clasts in a clay-rich matrix.

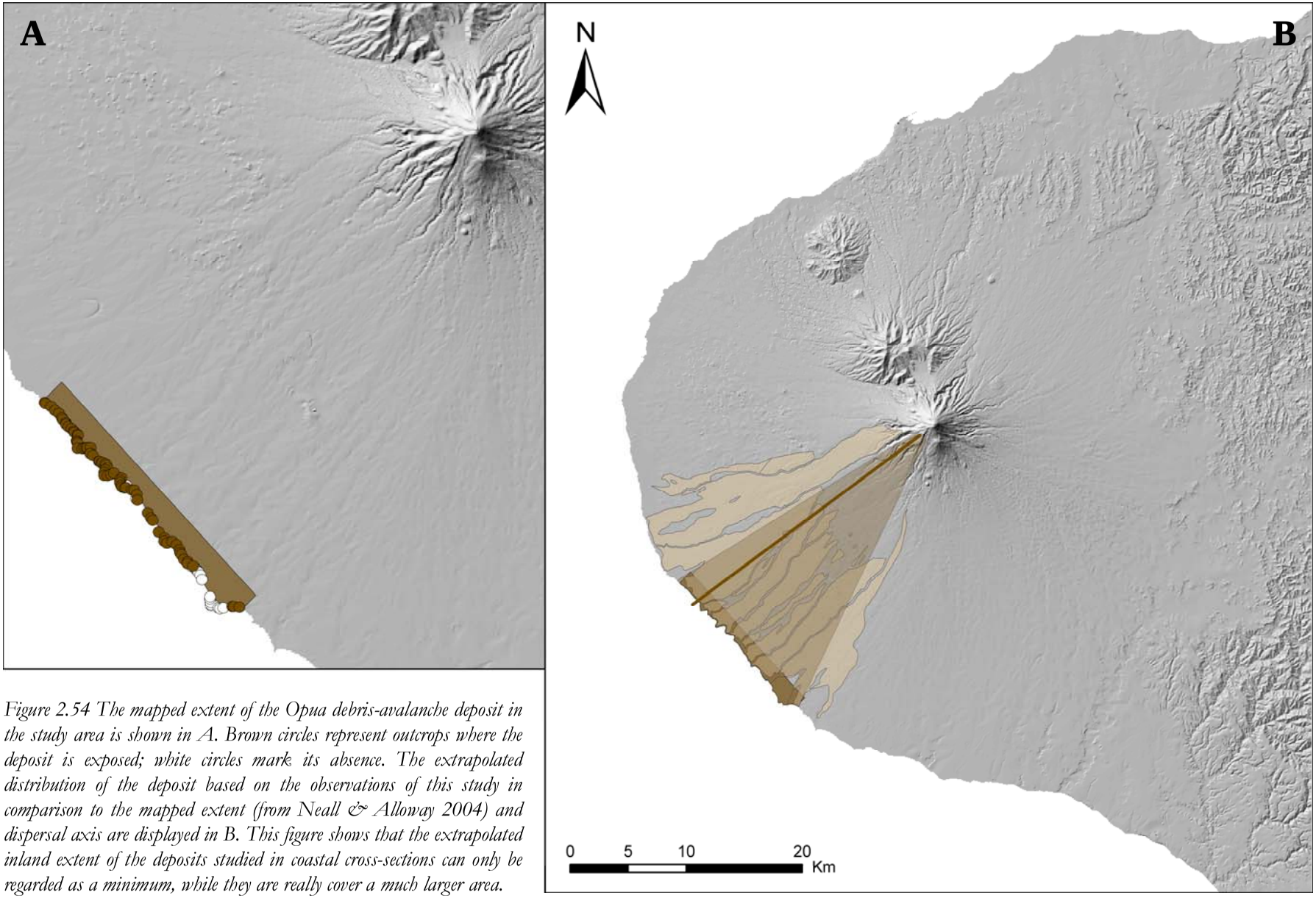

Figure 2.54 The mapped extent of the Opua debris-avalanche deposit in the study area is shown in A. Brown circles represent outcrops where the deposit is exposed; white circles mark its absence. The extrapolated distribution of the deposit based on the observations of this study in comparison to the mapped extent (from Neall & Alloway 2004) and dispersal axis are displayed in B. This figure shows that the extrapolated inland extent of the deposits studied in coastal cross-sections can only be regarded as a minimum, while they are really cover a much larger area.

2.6.2. Pungarehu Formation

The Pungarehu debris-avalanche deposit occurs in coastal cliff sections in the north-western part of the study area over c. 11.5 km. It is continuously exposed from Arawhata 1 to Okaweu 6 (2.3 km) and Middleton Bay 3 to Taungatara 2 (4.5 km) and is preserved in small channels at Heimama 10 and Otahi 5-7. It last appears in a small channel at Taungatara 9A (Fig. 2.56). The mapped extent of the Pungarehu debris-avalanche deposit in the study area complements the geological map of Neall & Alloway (2004) since the earlier work displays only the distribution of surficial deposits. The Pungarehu is thickest at the northern limit of the study area (4-8 m) and rapidly thins to c. 1 m at Okaweu 6. The deposit is characterised by abundant cobble- to boulder-sized clasts, shattered clasts and megaclasts that become less abundant and smaller with decreasing deposit thickness, while the matrix-content and the number of small rip-up clasts increase (Fig. 2.55). The second main lobe is characterised by a very matrix-rich deposit of orange-reddish colour with scattered small clasts and a varying thickness of c 0.8-2 m. The Pungarehu is separated from the overlying Opua Formation by the Okato Tephra, one or several thin, fine-grained hyperconcentrated-flow deposits of Warea age and the Oakura Tephra. It typically directly overlies a laminated soil that contains the Kawakawa Tephra.

Figure 2.55. In the second, marginal lobe of distribution, the Pungarehu debris-avalanche deposit is characterised by an orange-reddish matrix and few, predominantly pebble-sized clasts. It is c. 2 m thick at Mangahume 4.

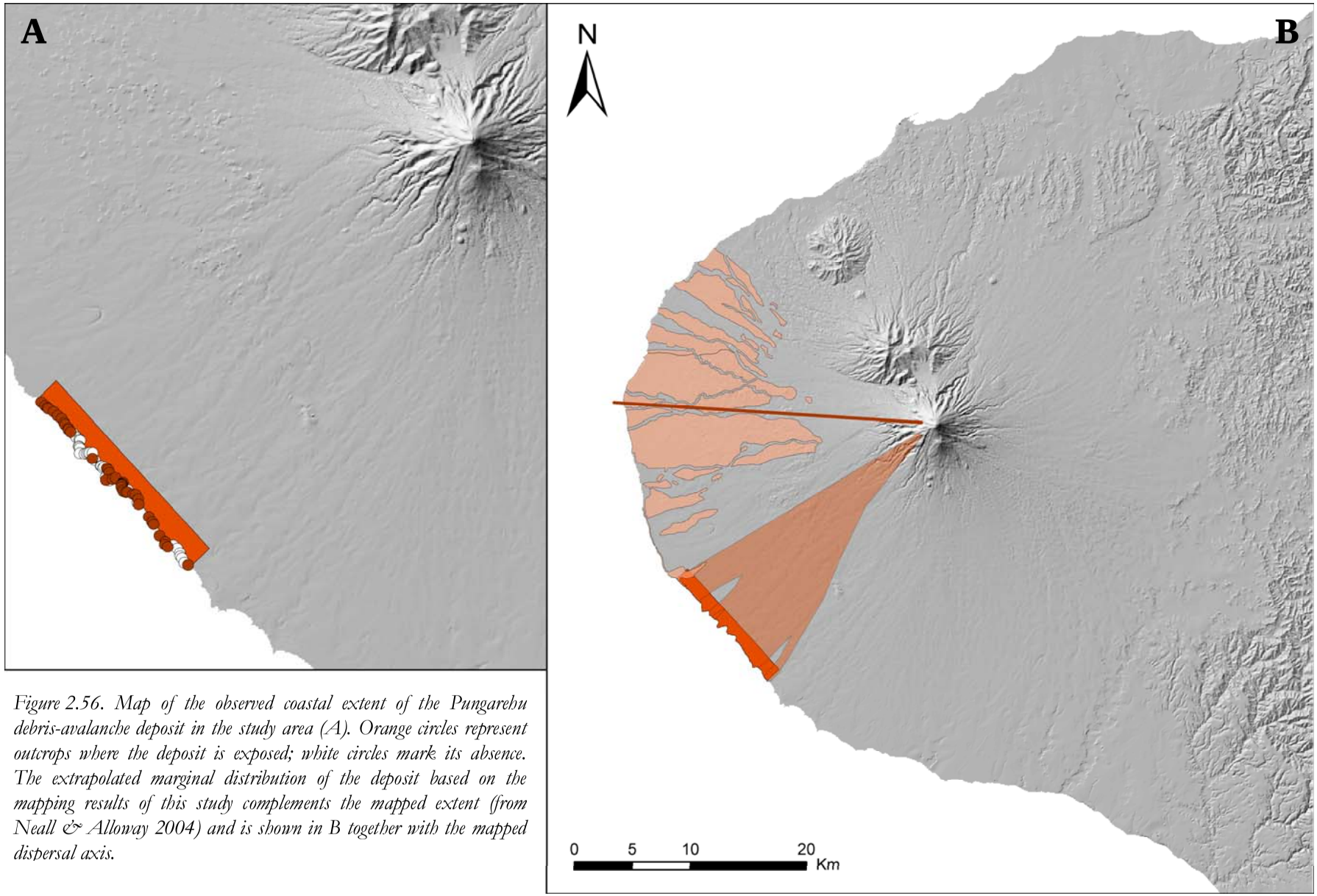

Figure 2.56. Map of the observed coastal extent of the Pungarehu debris-avalanche deposit in the study area (A). Orange circles represent outcrops where the deposit is exposed; white circles mark its absence. The extrapolated marginal distribution of the deposit based on the mapping results of this study complements the mapped extent (from Neall & Alloway 2004) and is shown in B together with the mapped dispersal axis.

2.6.3. Ngaere Formation

The Ngaere debris-avalanche deposit crops out in the southern part of the study area and was correlated over c. 10.7 km laterally. It is exposed continuously from Kaupokonui 5 to 9A (c. 4 km) and occurs as thin, matrix-rich, lenticular deposit at Waiokura 6AA (Inaha Stream), 6C, 8 and Waingongoro 1a-3 (Fig. 2.59). Previously, the Ngaere Formation was only mapped over a short stretch of coastline east of the Waingongoro River (Neall & Alloway 2004) but was here found to extent farther to the west. The distribution pattern suggests that the marginal parts of the debris avalanche were channelled down and reached the present-day coast along one larger (Waiokura Stream) and several small paleo-valleys.

The deposit is thickest (c. 4.5-5 m) at Kaupokonui 8, where it is characterised by pebble- to cobble- as well as boulder-sized clasts in a clay-rich matrix, and thins rapidly to 1.5 m towards the margins of this distal lobe (Fig. 2.57). It is overlain by fluvial and hyperconcentrated-flow deposits with intercalated paleosols/peat beds and in the westernmost locations by the Motumate debris-avalanche deposit. Below it is typically separated from the Rama debris-avalanche deposit by a series of hyperconcentrated-flow deposits with interbedded paleosols.

Figure 2.57. At Kaupokonui 6, the Ngaere debris-avalanche deposit is c. 3.5 m thick and characterised by coarse pebble- to boulder-sized clasts. It is overlain by the Motumate debris-avalanche deposit and separated from the underlying Rama by a thick hyperconcentrated-flow deposit.

Near the mouth of the Waingongoro River, the deposit is confined to a fluvial channel within the paleo-Waingongoro valley that was cut into the underlying Waihi debris-avalanche deposit (Fig. 2.58). Both debris-avalanche deposits are interbedded with a thick sequence of cross-bedded fluvial sands and gravel confirming the long-lasting existence of this deeply cut river valley. The large unconformity reflects filling of the paleo-valley since the Waihi collapse while subsequent erosion lead to incision of a new fluvial channel before the Ngaere event. This channel was cut into the Waihi unit and filled by the Nagere debris-avalanche deposit. Fluvial and volcaniclastic sediments that were deposited in the valley afterwards have been gradually eroded until present day.

Figure 2.58. Within the Waingongoro River valley, the Ngaere debris-avalanche deposit fills a small fluvial channel that was cut into the underlying Waihi debris-avalanche deposit and older fluvial sediments (A). The arrow marks the location of the cut and fill inset, which is shown as close-up in B.

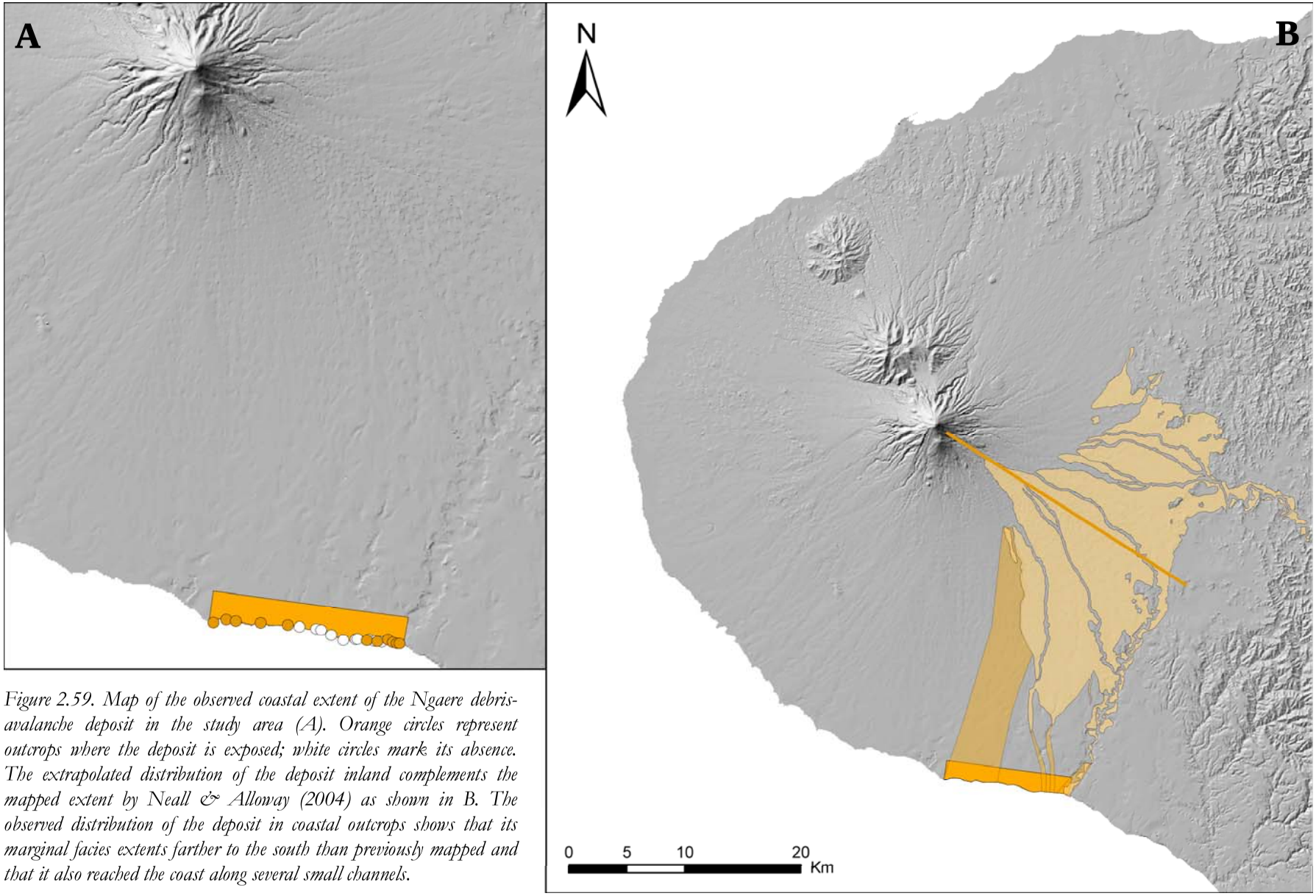

Figure 2.59. Map of the observed coastal extent of the Ngaere debris-avalanche deposit in the study area (A). Orange circles represent outcrops where the deposit is exposed; white circles mark its absence. The extrapolated distribution of the deposit inland complements the mapped extent by Neall & Alloway (2004) as shown in B. The observed distribution of the deposit in coastal outcrops shows that its marginal facies extents farther to the south than previously mapped and that it also reached the coast along several small channels.

2.7. FREQUENCY, VOLUME AND DISTRIBUTION OF TARANAKI DEBRIS-AVALANCHE DEPOSITS

At least 14 large and several smaller debris-avalanche deposits have been recognised in this and previous studies of the >200 ka record of volcanic activity at Mt. Taranaki (Table 2.3). This implies that major slope failures take place on-average every 13 ka. However, collapse events are not evenly spaced over time and appear to have become more frequent with maturity of the volcano, 6 having occurred in the last 35 ka. The number of debris-avalanche events shown here is considered a minimum and does not represent a true estimate of frequency. Other units might be buried in the ring-plain sediments, in particular to the east of the volcano where outcrops are rare and to the west where no significant uplift has occurred to view older parts of the succession. Apparent gaps in the reconstructed volcanic history may therefore simply reflect absence of preservation of units, or burial, rather than changes in volcanic behaviour.

The distribution of the pre-Ngaere debris-avalanche deposits in south-western and southern Taranaki was determined from correlation of deposits exposed in coastal cross-sections. Due to lack of longitudinal exposure towards the edifice and in some cases incomplete lateral exposure where the tilted strata dips below the surface, or the sequence is eroded by fluvial and lahar channels, the estimated distributions do not necessarily represent the maximum extent of the units. Also, it was not possible to determine the true run-out distances of the Taranaki debris avalanches. Their deposits are known to continue onshore for at least 25-45 km from source (Table 2.3), and a minimum of a further 6 km offshore to the north (Alloway 2005) and >8 km to the west (McDougall & Gibb 1970; Neall 1979). This prevented contouring the complete deposit thickness, so that deposit volumes could not be calculated with confidence. Hence, volume estimates are minimal and could only be based on comparison to known distributions, maximum recorded thicknesses and deposit characteristics of the better exposed surficial deposits in medial coastal exposures.

The deposit volumes of the studied debris-avalanche units were roughly classed in relation to the Opua, Pungarehu and Ngaere events (Table 2.3). The Ihaia and unnamed debris flows were of very small volume compared to the Opua debris avalanche and hence were restricted to small channels when reaching the present day coastline, resulting in thin matrix-rich deposits of limited lateral extent. The Motumate was produced by a debris avalanche that was confined to major paleo-channels in distal areas. It was significantly smaller than the Opua, but of larger volume than the clay-rich debris flows. The Te Namu and Otakeho debris-avalanche deposits show similar deposit characteristics, maximum medial thickness and lateral extent as the

TABLE 2.3. *Overview of some aspects of Mt. Taranaki debris-avalanche deposits.*

Debris avalanche / flow unit	Age (ka)	Direction of collapse	Max. medial thickness (m)	Max. medial width (km)	Calculated or estimated volume	Runout distance (km)
Opua	6.6*	SW	8/6*	25**	c. 0.35 km³ *	27+
Motumate	14-10†	S	3.5	10.8	<Opua	31+
Pungarehu	20§	W	8/>16*	35**	>7.5 km³ *	26+
Ngaere	23#	SE	5	10.7/40**	c. 5.85 km³ #	34+
Te Namu	29§	SW	>5	>8.8	~ Opua	26+
Ihaia	31§	SW	1.6	3.2	<<Opua	25+
Rama	>35§	S	12	25.5	<Pungarehu >2.6 km³ ††	34+
Unnamed dfd	35-50†	S	1.3	1	<<Opua	30+
Otakeho	c. 55§	S	>4	24.5	~ Opua >1.0 km³ ††	32+
Unnamed dfd	55-70†	SW	1	0.7	<<Opua	26+
Unnamed dfd	55-70†	S	0.5	0.1	<<Opua	30+
Tokaora	c. 60†	S	2.5	2	<<Ngaere	35+
Waihi	c. 70†	S	8	17.8	>Ngaere	45+
Waingongoro	c. 75†	S	5	16.6	~ Ngaere	44+
Oeo	c. 85-90†	S	>6	>21	~ Pungarehu?	34+
Okawa	c. 105#	NE	4	9**	c. 3.62 km³ #	39+
Motunui	>130#	NE	6	17**	>Okawa	41+
Mangati	>210#	NE	6	??	~ Okawa?	39+

* Neall (1979).
† Chronostratigraphy this study.
§ Radiocarbon dating this study (cf. Table 2.2).
# Alloway et al. (2005).
** Neall & Alloway (2004).
†† Palmer & Neall (1991); Palmer et al. (1991).

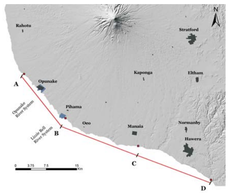

Age (ka)	Lithostratigraphic unit
c. 6.6	Opua Fm
c. 12	Motumate Fm
c. 20	Pungarehu Fm
c. 23	Ngaere Fm
c. 29	Te Namu Fm
c. 30-35	Hihiwera Peat
c. 32	Ihaia dfd
>35	Rama Fm
c. 45-50	unnamed dfd
c. 55	Otakeho Fm
c. 60-70	Pu/Kau
c. 60	Tokaora Fm
c. 70	Waihi Fm
c. 75	Waingongoro Fm
c. 80-60	sand dunes
c. 80	Pbf/ML
>80	Oeo Fm
>1.8 Ma	Tertiary

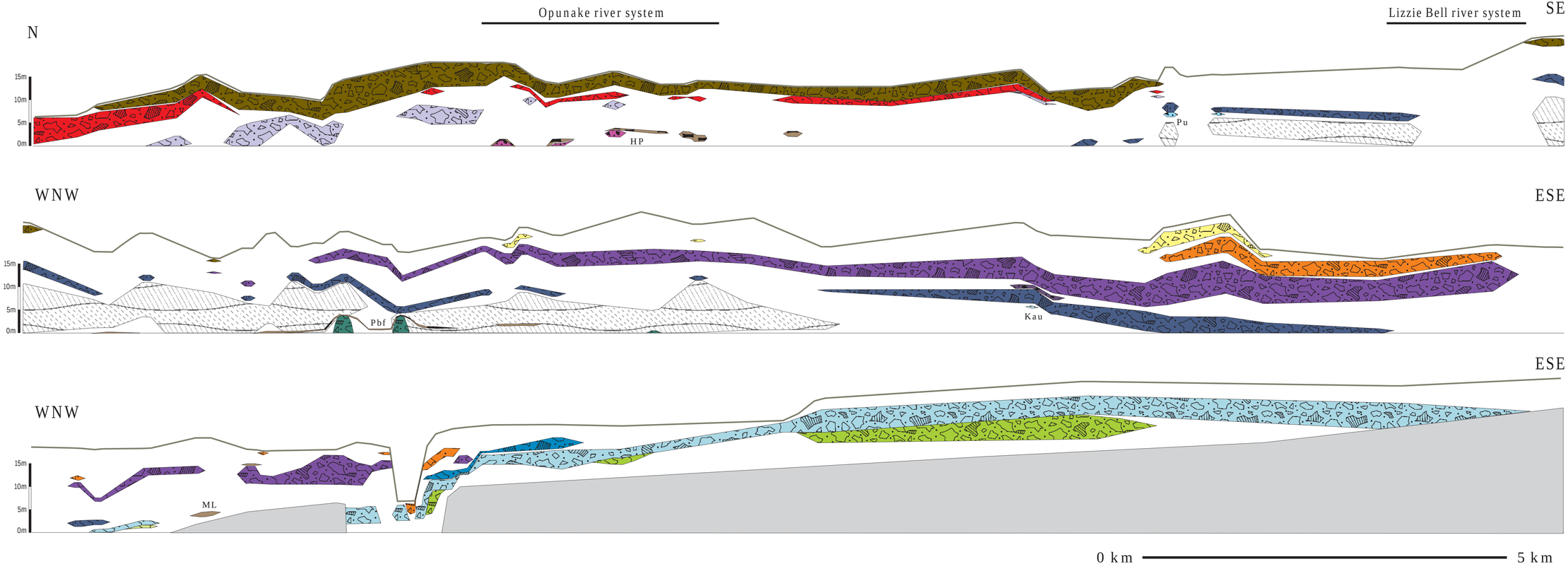

Figure 2.60. Cross-section of the medial Mt. Taranaki ring-plain succession, exposed in coastal cliff sections of the western to southern Taranaki peninsula. Displayed are the dominant marker horizons, including debris-avalanche and cohesive debris-flow deposits, prominent peat and soil layers that could be laterally correlated as well as Hauriri dune sands and the underlying Tertiary mudstone. The extent of the Opunake and Lizzie Bell river systems is also marked. Individual lahar deposits and channels could not be displayed due to their limited lateral extent. Pu = unnamed debris-flow deposit in Punehu catchement, Kau = unnamed debris-flow deposit in Kaupokonui catchement, Pbf = Puketapu buried forest, ML = Manaia lignite.

Opua Formation, indicating that they were of similar size, even though the Opua was calculated to have a volume of c. 0.35 km^3 (Neall 1979) compared to >1.0 km^3 for the Otakeho event (Palmer & Neall 1991; Palmer et al. 1991). The suggested deposit volume for the Opua Formation appears to be too low compared to estimates of the Pungarehu (Neall 1979), Ngaere (Alloway et al. 2005) and Otakeho (Stratford Fm. 3 of Palmer & Neall 1991; Palmer et al. 1991) events. Deposit characteristics and thickness of the Rama debris-avalanche deposit indicate that it is of larger volume than the Opua but considerably smaller than the Pungarehu Formation. A direct comparison to the 5.85 km^3 Ngaere is not possible due to the different dispersal directions of the two units, but the larger lateral extent of the Ngaere suggests that the size of the Rama debris-avalanche deposit lies between the Opua and Ngaere. This matches the calculated volume of >2.6 km^3 by Palmer & Neall (1991) and Palmer et al. (1991). The dispersal direction of the Waihi and the slightly smaller Waingongoro debris-avalanche deposits is similar to the Ngaere and their deposit thickness and lateral extent imply that they may have been at least of comparable if not larger volume. The maximum medial thickness and lateral distribution of the Oeo debris-avalanche deposit are unknown since it only crops out at a few locations at the bottom of the sequence. Similar deposit characteristics as the Pungarehu Formation close to its dispersal axis suggest that the Oeo event was of a comparable size. The oldest debris-avalanche deposits along the northern coast show a similar distribution, with the Motunui being thicker and laterally more extensive and hence of larger volume than the c. 3.62 km^3 Okawa Formation (Alloway et al. 2005).

The distribution of Mt. Taranaki debris-avalanche deposits was mainly controlled by the direction of collapse. Failures occurred on similar sectors of the edifice during certain periods, indicating that different parts of the edifice were more unstable and thus vulnerable to collapse at different times throughout the volcanic history (Table 2.3). The apparent distribution pattern of debris-avalanche deposits may reflect preservation and exposure of specific time packages of the succession or could indicate that the direction of collapse was influenced by internal and/or external processes, such as local stress regimes within the volcano resulting from its internal structure, a dominant direction of dike emplacement, the regional tectonic stress field or the slope of the subvolcanic basement (Siebert 1984; Vallance et al. 1995; van Wyk de Vries & Borgia 1996; Lagmay et al. 2000).

2.8. LAHAR STRATIGRAPHY AND CORRELATIONS

Hyperconcentrated-flow and debris-flow deposits were grouped into stratigraphic intervals, because they lack individual diagnostic properties, are numerous and the narrow distribution of single flow units did not allow distinction of individual events. These deposit packages were correlated by distinct marker horizons interbedded with them, including debris-avalanche deposits, continuous paleosols and peat layers but these were not sufficient to allow lateral correlation of deposits between catchments. Instead, it appears more likely that the grouped deposits were produced by separate groups of lahars, representing longer periods of sedimentation. In some cases, prominent lithological characteristics allowed the distinction of different series of hyperconcentrated-flow deposits, i.e. pumice-rich versus dense andesite-rich units.

At any one location, the ring-plain succession contains similar types of deposits, i.e. debris-avalanche and cohesive debris-flow deposits, hyperconcentrated-flow and non-cohesive debris-flow deposits with intercalated paleosols, peat layers and few thin tephra beds, channelised coarse non-cohesive debris-flow deposits, localised fluvial sediments, and dune sands, reflecting a repeating pattern of deposition. Hence, even though the studied coastal cross-sections represent only restricted insights into the lahar history at Mt. Taranaki, they provide an overview of reccurring types of flows and can be regarded as a window into the likely composition of buried parts of the succession.

A schematic overview of debris-avalanche marker beds, prominent peat layers and mappable sedimentary units is presented in Fig. 2.60. Hyperconcentrated-flow deposits and channelised debris-flow deposits are common in all parts of the studied volcaniclastic sequences in west, south-west and south Taranaki but could not be illustrated on this large scale because of their limited extent. The large number of identified events implies that lahars occurred frequently throughout the entire volcanic history of Mt. Taranaki.

2.9. REVISED STRATIGRAPHY OF THE MT. TARANAKI RING-PLAIN SUCCESSION

The stratigraphic overview of volcanic and volcaniclastic deposits at Mt. Taranaki has been established by several workers over the past 80 years, during which the understanding of volcanic successions has changed significantly. This is reflected in a patchwork of general to more

specific, details on the developing geologic map. Early mapping units such as the "Stratford and Opunake Lahars" were defined mainly based on their geomorphological properties and soil cover and contained a range of different types of deposits that were believed to have formed different "ring-plains" (Hay 1967; Grant-Taylor 1964a, 1964b; Grant-Taylor & Kear 1970). In contrast, later studies distinguished individual flow units according to their sedimentological characteristics, although also often grouping deposits of similar origin and age (Neall 1979; Alloway 1989; Neall & Alloway. 2004; Alloway et al 2005).

The different concepts resulted in a complex stratigraphic terminology for the ring-plain succession at Mt. Taranaki. A wide range of different stratigraphic elements were defined as individual formations:

- Single debris-avalanche deposits (Motunui, Okawa, Ngaere, Pungarehu, and Opua Formations).
- Groupings of deposits of the same or similar origin and thus with similar characteristics that were emplaced during a certain time span but in different areas, such as debris-flow and hyperconcentrated-flow deposits confined to different catchments (Warea, Kahui, Ngatoro, and Te Popo Formations).
- Groupings of different types of deposits that accumulated over a defined period of time (ring-plains of laharic agglomerate), distinguished by the geomorphology of the landscape (Opunake and Stratford Formations).

Other terms used to define groupings of deposits within the stratigraphic succession are based on origin, sedimentological or geomorphic characteristics, such as:

- Volcanic flow deposits (Kahui debris flows, Maero block-and-ash-flow deposits)
- Flood deposits (Hangatahua gravels and sands)
- Tephra beds (e.g. Inglewood Tephra, Burrell Lapilli, Saunders Ash, Newall Ash and Lapilli)
- Lava flows (e.g. Summit Group, Staircase Lavas, Warwicks Castle, The Turtle)

This inconsistent terminology has created a non-uniform stratigraphic view of the Mt. Taranaki volcanic succession. Also, remapping the former Opunake and Stratford Formations showed a greater complexity of volcaniclastic lithofacies and allowed a more detailed reconstruction of the past volcanic activity at Mt. Taranaki that needs to be added to the previously established stratigraphy (Table 2.4).

TABLE 2.4. *Previous lithostratigraphic units in comparison to new or redefined debris-avalanche deposits.*

Previous work			This study	
Formation	**Debris-avalanche deposits**	**Age**	**New and redefined debris-avalanche (DAD) and debris-flow (DFD) deposits**	**Age**
Opua Fm.	Opua	c. 6.6 ka[1]		c. 6.6 ka
Warea Fm.	Wr3 lobe	12-14 ka[2]	Motumate DAD	c. 12 ka
Pungarehu Fm.	Pungarehu	22.1 ka[1]		c. 20 ka
Ngaere Fm.	Ngaere	c. 23 ka[3,4]		c. 23 ka
Opunake Fm. 38-30 ka[5]	unnamed	33 ka[2]	Te Namu DAD	c. 29 ka
			Ihaia DFD	>31 ka
	unnamed	c. 50 ka[6]	Rama DAD	>35 ka
	Stratford Fm. debris avalanche 1	c. 48 ka[2]		
	Stratford Fm. debris avalanche 2		Unnamed DFD, Kaupokonui Stream	c. 40-50 ka
	Stratford Fm. debris avalanche 3	c. 80 ka[2]	Otakeho DAD	c. 55 ka
Stratford Fm. 80-50 ka[5]			Unnamed DFD, Punehu Stream	
			Unnamed DFD, Kaupokonui Stream	
			Tokaora DAD	c. 65 ka
			Waihi DAD	c. 70 ka
			Waingongoro DAD	c. 75 ka
			Oeo DAD	85-90 ka
Okawa Fm.		>105 ka[3,4]		>105 ka
Motunui Fm.		>130 ka[3,4]		>130 ka
	Unnamed	190 -210 ka[3]	Mangati DAD	c. 200 ka

[1] Neall 1979
[2] Palmer et al. 1991
[3] Alloway 1989
[4] Alloway et al. 2005
[5] Grant-Taylor & Kear 1970
[6] Neall et al. 1986

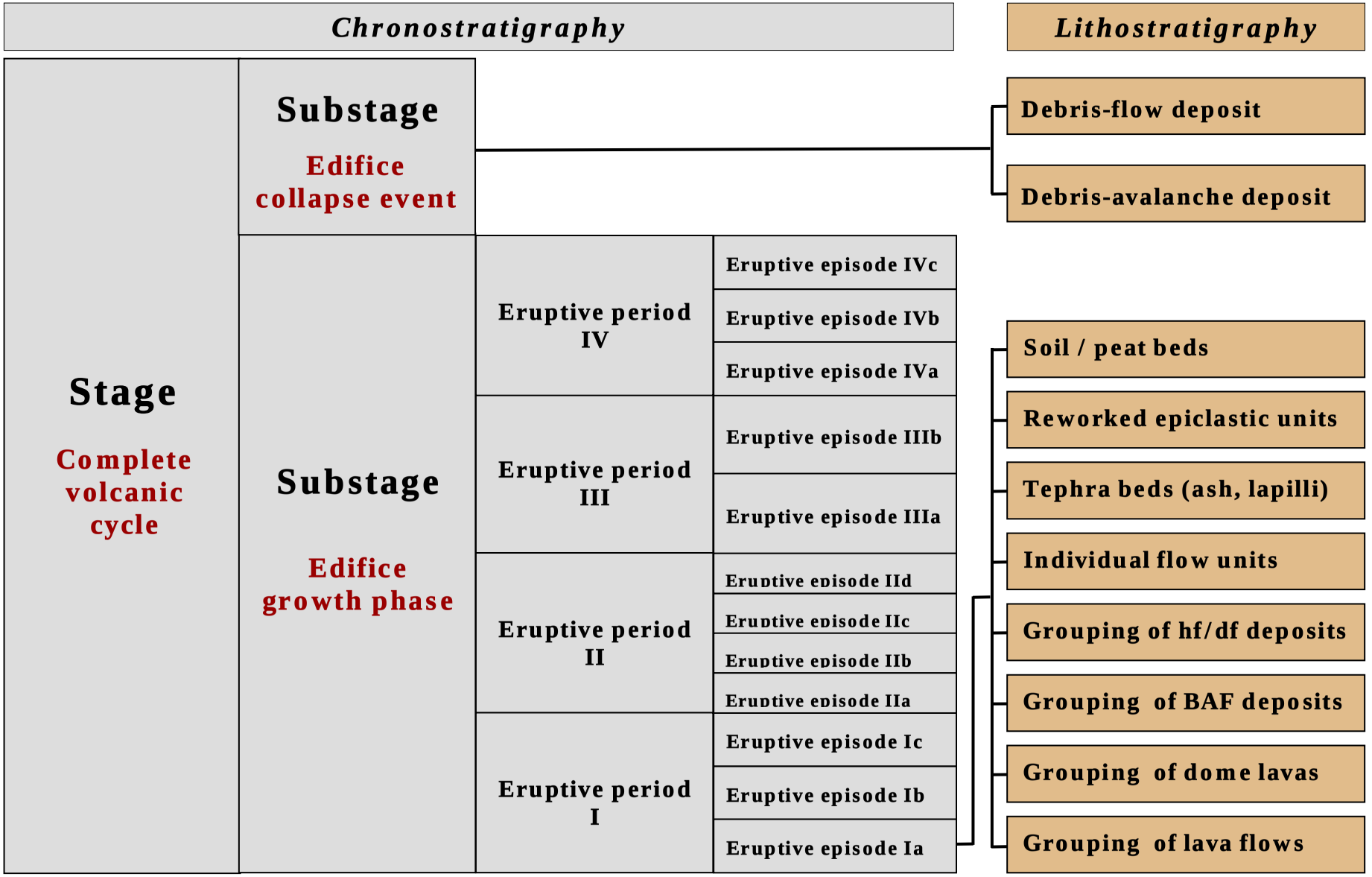

Figure 2.61 New stratigraphic conceptual scheme for the Mt. Taranaki volcanic succession, which combines a chronostratigraphic framework and lithostratigraphically defined units.

A larger number of debris-avalanche deposits were identified than formerly described, as well as a wide variety of volcanic mass-flow and reworked deposits. The different lithofacies show a repeating pattern of deposition, and can be related to phases of cone-construction or collapse events, depending on their sedimentological characteristics (cf. Palmer et al. 1991). This study illustrates that debris-avalanche deposits were produced frequently and regularly, and that the volcanic history of Mt. Taranaki was characterised by repeated edifice growth and destruction. Hence, basing the stratigraphic nomenclature of the volcanic (and volcaniclastic) succession at Mt. Taranaki on the apparently cyclic volcanic behaviour would provide a more uniform structure and clearer overview of past volcanic and sedimentary events.

A new concept that offers a more consistent and uniform nomenclature for the entire volcaniclastic succession is presented in Fig. 2.61. It also offers a more logical and intuitive way to understand the repeated sequence of events that have made up the geological history of Mt. Taranaki. It is based on chronostratigraphic time frames and mapped lithostratigraphic units (cf. Salvador 1994). Here, each Stage is defined as one complete volcanic cycle. Each cycle can be subdivided into a Substage that represents a phase of cone construction and a Substage that comprises the subsequent major edifice collapse event. The cone growth substage includes individual eruptive periods, which again consist of eruptive episodes. During the periods of edifice growth and collapse, a wide range of volcanic, volcaniclastic and other sedimentary deposits are produced, which can be mapped and distinguished based on their lithologic properties. These lithostratigraphic units can be classified as Formations, Members and single mappable units of different origin and then incorporated into the suggested chronostratigraphic framework.

This new structure is applied here to the known and newly identified volcanic and volcaniclastic events at Mt. Taranaki. The resulting revised stratigraphy of the entire known volcanic succession of Mt. Taranaki is shown in Fig. 2.62.

St	SS	EP	EE	Volcanics			Volcaniclastics SW Sector		Volcaniclastics SE Sector		Volcaniclastics NE Sector		Nonvolcanic	Age
				Lavas	PFs	Tephras	Lahars	Debris aval.	Lahars	Debris aval.	Lahars	Debris aval.	Sediments	(ka)
OAONUAN	Oa growth phase	Maero eruptive period	Pyramid Tahurangi Mangahume Burrell Puniho Waiweranui Newall Waingongoro Te Popo Hooker	Summit dome	P. rock avalanche T. BAFs & surges B. pumice flows B. BAF & surges P. pumice flows P. BAF & surges W. BAF & surges N. BAF & surges TP. BAF & surges	Pyramid Lapilli Tahurangi Ash Tahurangi B. a+b Mangahume L. Burrell Lapilli Burrell B. A+B Puniho Ash Puniho Breccia Waiweranui Ash Waiweranui B. Newall Ash a-c Newall Breccia Waingongoro Ash Te Popo Ash Te Popo Breccia Hooker Lapilli						Hangatahua Gravels & Sands c. 0.4 ka	1839-66 AD 1755 AD 0.23 1655 AD/ 0.31-0.4 0.45 0.3-0.38 0.45-0.47 0.39-0.65 0.47 0.88
			Kaupokonui Maketawa Manganui	Skeet Lavas Staircase Lavas Beehives, The Dome, Skinner hill Fanthams Lavas Peters Lavas	BAFs on eastern flank at least 3 PFs	Kaupokonui T. Maketawa Tephra Manganui T. a-c Inglewood T. a-b Korito Tephra a-b Mangatoki T a-b Tariki Tephra a-f Waiopuku Tephra			Warea4 DF/HF		Te Popo DF 3.1-2.9 ka Ngatoro DF			c. 1.4 < 1.7 c. 1.7 c. 2 2.9 3.2? <2.87 3.3-2.8 3.6-3.5 3.7-3.6 4.1-3.9 4.4 4.7-4.6 5.3-5 7-3.3
OPUAN	Collapse							Opua						c. 6.6
	Op growth phase		Kahui	Warwick Castle L.	Kahui BAFs on eastern & western flanks	Kaponga T. a-j Konini Tephra a-b Mahoe T. a-d Oakura Tephra	Kahui DFs		series of thin pumiceous HFs in S Taranaki local channelised DF in S Taranaki		Kahui DFs		accumulation of medial ash & soil formation in S Taranaki	c. 8 10.4-5.3 10.5-10.1 11.4-11.1 12.5-7 13-7
MOTUMATEAN	Collapse							Motumate						c. 12-14
	Mot growth phase			Pukeiti Lava Dome		Ahuahua Lapilli Kaihouri T a-h Okato Tephra Paetahi T a-f	Warea DFs /HFs in W, SW Taranaki		Warea DFs /HFs in E Taranaki series of pumiceous HFs in S Taranaki				thick peat in SSW Taranaki localised fluvial deposits in S Taranaki soil formation Opunake river system Katikara Sands	15 18.8-12.9 20-12.5 c. 20.7-13 ka 20.2-19.4 20.7-13
PUNGAREHUAN	Collapse							Pungarehu						c. 20.7
	Pu growth phase					Poto Tephra c-o *Kawakawa Tephra*	frequent HFs in W Taranaki some pumiceous channelised DFs in W Taranaki						Katikara Sands localised fluvial deposits accumulation of medial ash & soil formation Opunake river system	22.7-20.9 22.6 23-20.7 c. 22.7-20.7
NGAEREAN	Collapse									Ngaere				c. 22.6-23.4
	Ng growth phase					Poto T a-b Tuikonga T a-d Koru T a-b Pukeiti T Waitepuku T a-c	frequent HFs in W Taranaki HFs in S Taranaki channelised DFs in SSW Taranaki		pumiceous HFs in S Taranaki				double organic soil with inter-bedded tephras in W Taranaki localised fluvial deposits in S Taranaki Opunake river system	22.7 24-23.4 23.2-25.2 25.2-24.8 26.2 28-27.5 c. 29-22.7
TE NAMUAN	Collapse							Te Namu						c. 29
	TN growth phase					several tephra layers preserved in Hihiwera Peat	frequent HFs in W Taranaki some pumiceous channelised DFs in W Taranaki & along Opunake river system series of pumiceous HFs sandy HFs	Ihaia DF					Opunake river system localised fluvial deposits soil formation Hihiwera Peat in SW & S Taranaki Lizzie Bell river system	c. 30-29 c. 33-30 >33 c. 33-30
RAMAN	Collapse							Rama		Rama				c. 35
	Ra growth phase					several tephra layers preserved in thick peat in S Taranaki	channelised DFs in SW Taranaki & along Lizzie Bell river system frequent HFs in SW Taranaki some pumiceous	unnamed DF (Kaupokonui catchment)					thick peat in S Taranaki soil formation & localised peat accumulation localised fluvial deposits Lizzie Bell river system	c. 50-45 50-35
OTAKEHOAN	Collapse							Otakeho		Otakeho				c. 50
	Ot growth phase					*Rotoehu Tephra* Waitui Tephra in N Taranaki c. 55-60 ka BP	concentrated HFs in SW Taranaki series of pumiceous HFs in SW Taranaki channelised DFs in SW-S Taranaki	unnamed DF (Punehu catchment) unnamed DF (Kaupokonu catchment)					localised fluvial deposits bedded sands in S Taranaki Dune sands in SW Taranaki with interbedded peats Lizzie Bell river system	c. 55 c. 60-50
TOKAORAN	Collapse											Tokaora		c. 60
	To growth phase					several tephra layers preserved in thick peat in S Taranaki, possibly including Araheke Tephra in N Taranaki c. 60-75 ka BP							thick peat in S Taranaki fluvial deposits in S Taranaki Dune sands in SW Taranaki with interbedded peats	 c. 70-60
WAIHIAN	Collapse											Waihi		c. 70
	Wa growth phase					Te Ares Tephra in N Taranaki							Dune sands in SW Taranaki with interbedded peats	c. 75 c. 75-70
WAINGONGOROAN	Collapse											Waingongoro		c. 75
	Wai growth phase						some pumiceous transitional stream flow/HFs in S Taranaki						Dune sands in SW Taranaki Puketapu Buried Forest in SW Tar. Manaia lignite in S Taranaki Hauriri marine bench fluvial deposits in S Taranaki bedded sands in S Taranaki	c. 80 c. 85-75
OEOAN	Collapse							Oeo						c. 85
	Oeo growth phase					Epiha T a-e in N Taranaki							Thin peats and bedded sands in S Taranaki Thick peat in N Taranaki Inaha Terrace cover-beds Inaha Marine Bench	c.100-85 c.100-80 c. 100
OKAWAN	Collapse											Okawa		c. 105
	Ok growth phase					Ninia Tephra a-d in thick peat in N Taranaki							thick peat in N Taranaki massive/ bedded andesitic sands Rapanui Terrace cover-beds Rapanui Marine Bench	c. 105-115 c. 127
MOTUNUIAN	Collapse											Motunui		> 130
	Mo growth phase					several unnamed tephra layers in thick peat in N Taranaki							carbonaceous palesol bedded andesitic sands thick peat in N Taranaki	
MANGATIAN	Collapse											Mangati		c. 200
	Mg growth phase												cemented, iron-stained dune sands with tree stumps Ngarino Terrace cover-beds Ngarino Marine Bench	c. 210

Figure 2.62. Composite stratigraphic overview of the Mt. Taranaki volcanic succession. The chronostratigraphic units are defined based on the volcano's cyclic behaviour and represent phases of growth and collapse. Within this chronostratigraphic framework, the identified lithostratigraphic units from this and previous studies (Neall 1979; Neall et al. 1986; Alloway 1989; Alloway et al. 1995; Neall 2003; Alloway et al. 2005; Platz 2007) are distinguished based on their origin and emplacement mechanism. Volcanic units comprise edifice-building lava flows, pyroclastic flow deposits and tephras as well as satellite lava domes. The volcaniclastic units comprise lahar (hyperconcentrated-flow and debris-flow) and debris-avalanche deposits, which are shown based on their dispersal within the northeastern, southeastern and southwestern sector of the ring plain. Nonvolcanic sediments include flood deposits, fluvial sediments and aeolian sand dunes as well as peat layers. St = stage, SS = sub-stage, EP = eruptive period, EE = eruption episode, PF = pyroclastic flow.

2.10. CONCLUSIONS

Early geological maps of the Taranaki peninsula date back to the 1920s and were based on the concept that ring-plain aggradation was limited to glacial periods, while warm climates resulted in the cutting of marine benches. Later studies mapped individual units based on their sedimentological characteristics and subsequently added more detail to the geological map. The older units were mostly replaced except for remnants in south-west Taranaki that are still referred to as the Opunake and Stratford Formations. Remapping of these composite formations in coastal cliff exposures revealed a great complexity of volcaniclastic lithofacies and a larger number of debris-avalanche deposits than previously described. These represent distinct units that could be easily recognised and correlated laterally. Overall, five new debris-avalanche deposits were identified and named Te Namu, Tokaora, Waihi, Waingongoro and Oeo Formation. Four previously described units were renamed (Motumate, Rama, Otakeho and Mangati Formation), their stratigraphic position redefined and their lateral distribution mapped in more detail (except for the Mangati in north Taranaki). A number of cohesive debris flow-deposits were recognised, which most likely represent the distal runout of smaller, confined debris avalanches. Correlation of the known Opua, Pungarehu and Ngaere Formations showed a greater lateral extent in coastal cliff sections than displayed on the geological map.

Overall a minimum of 14 large debris-avalanche deposits occur within the volcaniclastic ring-plain record of Mt. Taranaki, indicating one major slope failure on average every 13 000 years. The deposits reflect a range in volume from small <0.1 km^3 debris flows to rare exceptionally large >7.5 km^3 debris avalanches. The exact run-out distance of Taranaki debris avalanches could not be determined, but the deposits extend c. 26-45 km onshore and at least another 6-8 km offshore. Their lateral width in coastal cross-sections ranges from c. 9-35 km with a medial deposit thickness of 2.5 to >16 m.

Hyperconcentrated-flow and non-cohesive debris-flow deposits are another common element of the studied volcaniclastic sequences, indicating that lahars occurred frequently at Mt. Taranaki. Lahar deposits were grouped into stratigraphic intervals since their large number and similar characteristics did not allow mapping of individual units. A stratigraphic overview of the older ring-plain succession was based on the correlation of directly and indirectly dated debris-avalanche marker beds and interbedded packages of lahar deposits. This chronological reconstruction of events showed that the same pattern of deposition was repeatedly produced throughout the existence of Mt. Taranaki.

The previously complex and non-uniform stratigraphic terminology in Taranaki is replaced with a suggested new stratigraphic scheme that is based on the identified repeating pattern of deposition. This model provides a more consistent nomenclature and chronostratigraphic framework that can be applied to the entire volcanic and volcaniclastic succession at Mt. Taranaki.

CHAPTER 3.

SEDIMENTARY CHARACTERISTICS OF MT. TARANAKI RING-PLAIN DEPOSITS

3.1. INTRODUCTION

This chapter concentrates on the interpretation of the accumulation history and characteristics of the Mt. Taranaki ring-plain succession based on the previously developed chronology of volcanic and other events.

The sedimentary sequences along the northern and southern Taranaki coast represent a cross-section through medial ring plain settings and show a variety of volcaniclastic and reworked epiclastic deposits, including debris-avalanche, lahar, tephra, fluvial and aeolian units (Neall 1979; Neall et al. 1986; Palmer & Neall 1991; Alloway 2005). The exposed deposits display a wide range in sedimentary characteristics between different lithofacies types and stratigraphic layers, as well as variations within individual units laterally and longitudinally. These sedimentological differences reflect the diverse origins of the deposits, varying emplacement mechanisms, depositional conditions, paleophysiography and paleoclimatic conditions.

The aims of this sedimentological study are:

a) To characterise and classify the different types of ring-plain deposits.

b) To relate sedimentological changes to the nature of volcanic activity and changes in eruptive style.

c) To determine the influence of paleogeomorphology and climate on the ring-plain depositional system.

d) To elucidate the evolution of the south-western and southern ring plain of Mt. Taranaki within the framework of a complex interaction of pyroclastic, volcaniclastic and other sedimentary events that reflect landscape construction and erosion during the last 100 ka.

3.2. CLASSIFICATION OF VOLCANIC MASS-FLOWS

A range of approaches have been developed in order to gain a better understanding of the behaviour of mass movements and subaerial flows of water-sediment mixtures ("lahars") on volcanoes. These encompass various scientific sub-disciplines based on morphology and sedimentology of deposits, direct observation and measurement of the processes, physical models of flow characteristics and dynamics, and theory of material behaviour and rheology (e.g. Takahashi 1981; Costa 1984; Costa & Williams 1984; Johnson & Rodine 1984; Pierson 1986; Qian & Wan 1986; Smith 1986; Iverson & Denlinger 1987; Pierson & Costa 1987; O'Brien & Julien 1988; Smith & Lowe 1991; Whipple & Dunne 1992; Coussot & Meunier 1996; Iverson 1997b; Cronin et al. 1999, 2000; Iverson & Vallance 2001; Pierson 2005). A variety of criteria were used by these authors to explain the wide range of characteristics of volcanic mass-flows, including triggering mechanism, sediment composition, solid fraction, relative bed roughness, velocity, duration, bed slope, material behaviour, and physical processes during flow. This has resulted in diverse mass-flow classifications that often contradict each other, especially when they are based only on individual quantitative criteria or are unable to cover all phenomena (Bradley & McCutcheon 1985). Classifications based on parameters related to flow dynamics are difficult to use for field studies (Smith 1986), and mechanical flow aspects can vary from one event to another or during a single event (Coussot & Meunier 1996). The following section gives an overview of existing classification models for volcanic mass-flows in order to illustrate relevant distinction criteria and their influence on the characteristics of the resulting deposits.

3.2.1. Depositional models

The morphology and sedimentology of deposits has been used by several authors to distinguish between different types of volcanic mass-flows (Pierson & Scott 1985; Smith 1986; Walton & Palmer 1988; Rodolfo 1989; Warresback & Turbeville 1990; Palmer & Neall 1991), mainly based on the concept of hyperconcentrated flow by Beverage & Culbertson (1964). Their empirical boundaries defined hyperconcentrated flow as having a sediment concentration between 40-80 wt% (20-60 vol.%) with a combination of increased viscosity, buoyancy and dispersive stress between grains as the primary grain-support mechanism.

Smith (1986, 1987a) noted that these concentration-based flow boundaries could not directly be applied to field records. Instead, he used field criteria to characterise the range of sediment-water flow with fully turbulent, dilute streamflow and viscous, laminar debris flow as end members (Fig. 3.1). Normal streamflow produces a variety of lithofacies ranging from

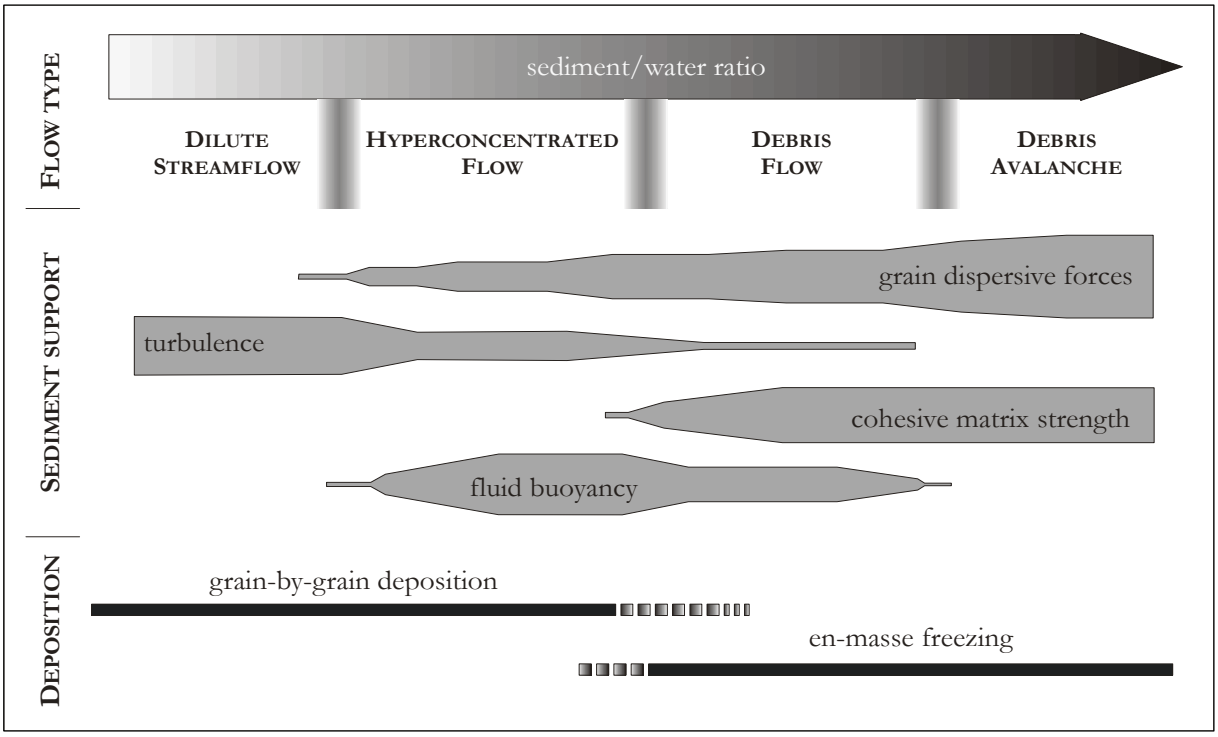

Figure 3.1. Schematic illustration of sediment/water ratio, corresponding flow type, transport and depositional mechanisms (from Smith & Lowe 1991).

cross- or horizontally bedded sands to massive, clast-supported, imbricated gravel, which reflect a traction-dominated, grain-by-grain sedimentation. Debris-flow deposits exhibit features characteristic of *en masse* emplacement and support of largest clasts by cohesive matrix strength, buoyancy, and dispersive pressure, i.e. matrix support, lack of stratification and grading or presence of reverse grading. Hyperconcentrated flow is regarded as intermediate between debris flow and normal streamflow. The resulting deposits show features that are incompatible with either debris-flow or normal streamflow deposition, including horizontal or no stratification, common normal grading, clast-support with a poorly sorted, polymodal matrix and poor imbrication. Deposition from these high-discharge, but relatively low concentration flows involves rapid grain-by-grain aggradation from both suspension and traction (Smith & Lowe 1991).

The depositional criteria used to interpret and identify different types of volcanic mass flows (Smith 1986; Scott 1988a) may not correspond to the flow conditions described by empirical or rheological definitions (Smith & Lowe 1991). Cases of direct observation and measurement of the flow event and comparison to the resulting deposits have allowed a better understanding of flow processes and depositional conditions.

Pierson & Scott (1985) observed the gradual transformation of the 19 March 1982 lahar at Mount St. Helens from debris flow into a hyperconcentrated flow and linked their observation to the characteristics of the resulting deposits. The flow transformation resulted from progressive downstream changes in sediment concentration mainly due to dilution by incorporation of overrun stream water in a turbulent mixing zone and progressive settling of the coarsest particles in the granular phase. The flow transition started at a sediment concentration of 78 wt.% (57 vol.%) at the head of the flow and worked its way back to the debris flow tail. It was marked by an improvement in sorting, decrease in sediment concentration, mean grain size, mean velocity and peak discharge. The hyperconcentrated streamflow phase had a peak sediment concentration of 61 wt.% (37 vol.%), which lagged behind peak discharge. Coarse sand and low density gravel were held in suspension. The high suspended sediment concentrations dampened turbulence and resulted in a laminar flow with an oily, glassy smooth surface but large-scale turbulence near the bed. With decreasing sediment concentrations turbulence increased, observed as the occurrence of large standing and breaking antidune waves.

Flow behaviour could be directly linked to the resulting sediments. The deposits produced by the debris flow phase showed an extremely wide range in grain size (clay to gravel), very poor to extremely poor sorting, total lack of cross-stratification, matrix-support, common inverse grading (coarsening upward) near bottom and normal grading (fining upward) near the top. The flow transformation was reflected in the progressive replacement of the debris-flow deposit from bottom upward by a hyperconcentrated-flow unit above a gradational, but locally sharp contact. The so-called lahar runout facies was characterised by a coarse sandy, clast-supported openwork texture with distinctly less fines than the debris-flow unit, poor sorting, faint horizontal stratification, with an overall massive appearance and locally small, isolated lenses of gravel at various levels especially near the margins, surface layers of logs, woody debris and pumice clasts.

Scott (1988a) links flow behaviour of the transforming lahar and deposit characteristics to the sediment support mechanisms of the different observed flow phases. He suggests that the textural changes record a continuous multiple physical support mechanism (dilatant flow and turbulent flow) in debris and hyperconcentrated flow. The sediment suspension in debris flows is a result of high yield strength, buoyancy and dispersive stress from particle interactions, with turbulence being limited to the flow front. With increasing dilution and sediment loss, yield strength and buoyancy decline and grain support and transport through internal grain collisions becomes progressively less effective. The smooth laminar nature and slick, oily appearance of the hyperconcentrated flow, together with the deposit characteristics, support the assumption that

turbulence was damped and subordinate during the main wave of sediment transport (cf. Cronin et al. 1997, 1999). The occurrence of standing waves, the surface expression of antidune bedforms, shows that turbulence played at least a local role and became more effective during later, more dilute parts of the hyperconcentrated flow phase.

A study by Cronin et al. (2000) based on flow observation, dip samples and the depositional record demonstrated that diluted channelised lahars can be vertically stratified. The developed depositional model divided the flow into a basal, mostly channel-confined, coarse, sediment-concentrated part with debris-flow-like rheology and a diluted, finer grained surface layer with hyperconcentrated flow properties. During observation of the event, the lahar surface showed features typical of hyperconcentrated flow, i.e. viscous and oily appearance with damped turbulence, periodical downstream-pointing V-shaped standing waves (Pierson & Scott 1985, Cronin et al. 1997, 1999; Pringle & Cameron 1997) and average sediment concentrations of 37 vol% (61 wt.%). The channel portion of the flow produced massive, bouldery, very poorly sorted, matrix-supported deposit wedges that pinched into voluminous, finer-grained, poorly sorted, faintly bedded upper and laterally contiguous marginal overbank deposits.

3.2.2. Physical models

Physical models to distinguish different types of volcanic mass-flows are based on flow dynamics as well as the mechanical properties of the solid components and the fluid.

In a geologic context, flow is the continuous, irreversible deformation of a material (typically a mixture of solids, water and air) in response to applied stress (gravity applied as a shear stress) (Pierson & Costa 1987). Newtonian fluids are single-phase liquids, like water, that flow under any applied stress (Pierson & Costa 1987) and their fluid viscosity (the ratio of applied stress to the rate of shear) depends on temperature and pressure (White 2006). Fluid mechanics are dominated by viscous fluid forces acting on the channel boundaries and on individual entrained sediment grains, but there are only negligible interactions with each other (Pierson 2005). Volcanic mass-flows, on the other hand, are often described as Bingham or viscoplastic fluids with uniform intrinsic shear strengths (Middleton & Hampton 1976; Pierson 1980; Major & Voight 1986; Blair & McPherson 1994; Kim et al. 1995; Coussot & Proust 1996; White 2006). These flows behave as a rigid body at low stresses and will only flow once a critical shear stress (or yield strength) has been exceeded (Pierson & Costa 1987; Coussot & Proust 1996). Resistance to flow is thus the result of viscosity and material strength (Vallance 2000). The viscosity increases with increasing sediment concentration and increasing clay content (Major 1993). The models describe the mechanical behaviour of a substance based on the concept of viscosity but

neglect other important flow properties such as particle interactions (Vallance 2000). These play a major role in the collisional grain flow theory of the Bagnold model, according to which flow only occurs if gravitational driving forces overcome grain-collision stresses (Bagnold 1954; Lowe 1976; Takahashi 1991; Major & Iverson 1999; Vallance 2000).

To characterise the bulk behaviour of two-phase sediment-water mixtures including the complicated interactions between solid and fluid forces, other rheological criteria need to be considered. The term rheology was introduced by Eugene Bingham, based on Heraclitus's famous expression *"panta rhei - everything flows"* (Bingham 1922) and deals with the deformation and flow behaviour of material under the influence of an applied stress. The rheologic character of a fluid is primarily a function of its composition, i.e. the relative proportions of components, grain-size distribution, physical and chemical properties of the contained solids (Pierson & Costa 1987).

Pierson & Costa (1987) developed a classification of sediment-water mixtures based on thresholds in rheologic behaviour according to deformation rate (mean flow velocity) and sediment concentration, with a constant composition of components (Fig. 3.2). The transition from "liquid" normal streamflow to "plastic" hyperconcentrated flow is marked by the acquisition of a yield strength. An abrupt, rapid increase in yield strength due to the onset of internal friction allows static suspension of gravel and inception of liquefaction behaviour, and thus represents the transition from hyperconcentrated flow to "slurry flow". Granular flow begins when the sediment concentration increases to the point where the mass loses the ability to liquefy and the bulk behaviour is dominated by friction and grain collisions. Even though rheology ignores some mechanistic details, rheological definitions of different types of flows can be compared to laboratory and experimental tests as well as field observations (Pierson 2005).

Experimental studies by Major & Pierson (1990, 1992) showed that the bulk rheological behaviour of fine-grained (<2 mm) debris flows is not only affected by the total sediment concentration but is also strongly influenced by the proportion of sand. At a given sediment concentration, a high sand content decreases the yield strength and viscosity of the mixture. In general, with increasing content of coarser particles, the sediment concentration has to increase to maintain the uniform integrity of the slurry. If the sediment concentration is too low, the slurry integrity is degraded by particle settling and the mixture separates into two independent phases: sediment in water. For fines-rich mixtures the sediment concentration required to maintain integrity is considerably lower (0.44) than for sand-rich flows (0.66). Where the sand concentration exceeds 0.2, the flow behaviour of the granuloviscous fluid is dominated by frictional interactions of sand grains, explained by changes in packing density, particle distribution

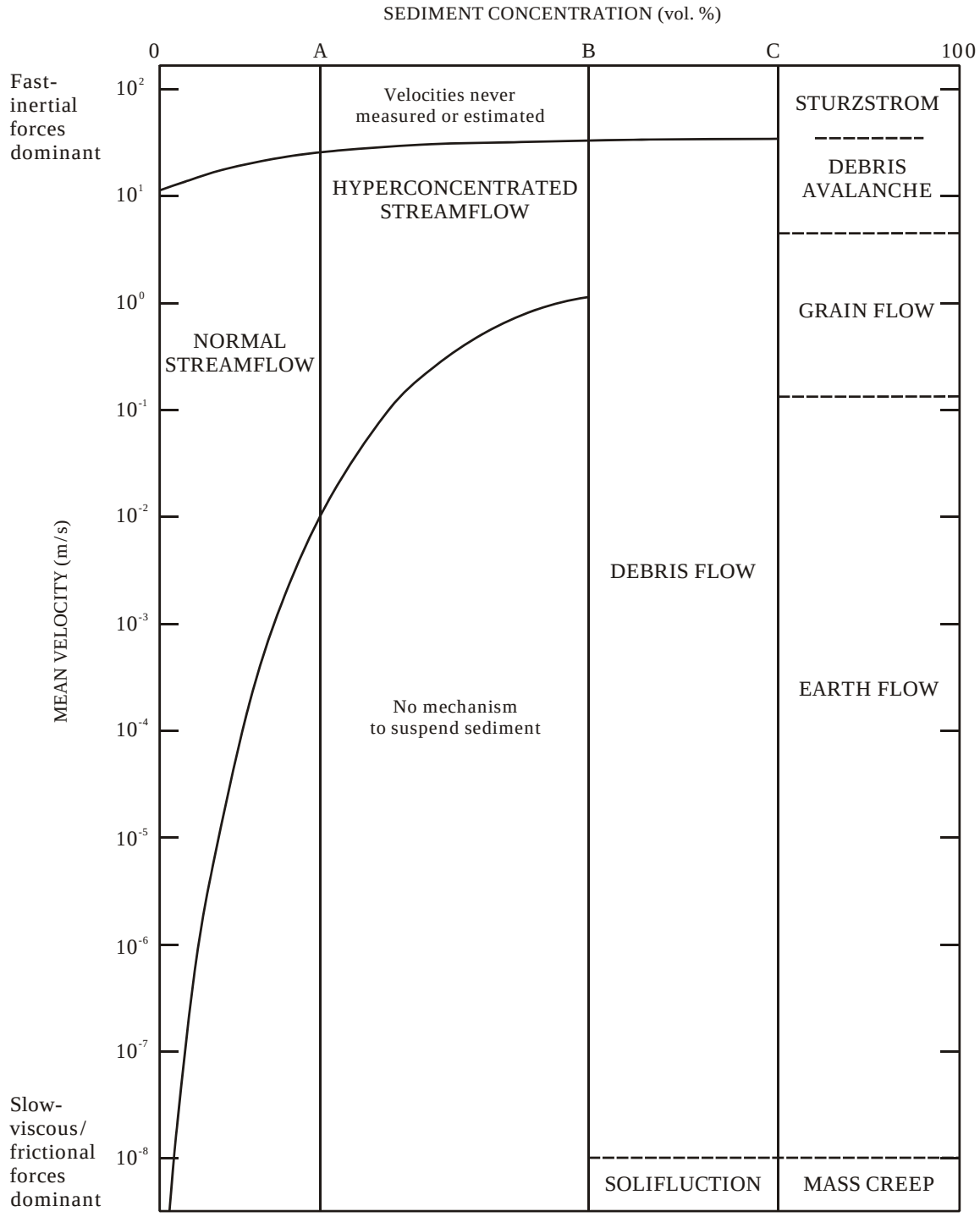

FLUID TYPE	NEWTONIAN	NON-NEWTONIAN		
INTERSTITIAL FLUID	WATER	WATER + FINES		WATER + AIR + FINES
FLOW CATEGORY		STREAMFLOW	SLURRY FLOW	GRANULAR FLOW
FLOW BEHAVIOUR	LIQUID	PLASTIC		

Figure 3.2. Rheologic classification of sediment-water flows from Pierson & Costa (1987).

and orientation as well as formation and destruction of coherent clusters of grains (Major & Pierson 1992).

Based on the two criteria discussed by Major & Pierson (1990, 1992), Coussot & Meunier (1996) developed a simple classification of mass-flows (Fig. 3.3). In addition to the sediment concentration they included the type of particles within the flow (fine, cohesive and/or coarse, cohesionless, granular material). The approximate limits between the different types of mass movements reflect common ideas on the main physical distinction between flow types. The transition from hyperconcentrated flow to debris flow corresponds to a critical percentage of solid fraction, which depends on the material type. The transition from debris flow to debris avalanche is marked by the critical percentage of solid fraction dependant on material type, upon which fracturing occurs in response to deformation.

Iverson (1997a, 1997b) developed a model for debris-flow motion and deposition based on fluid mechanical properties that contradicts intrinsic viscoplastic yield strength implied by the Bingham model, pervasive grain-collision stresses suggested by the Bagnold model, or the assumption of uniform dissipation of excess pore-fluid pressure. According to this newer theory,

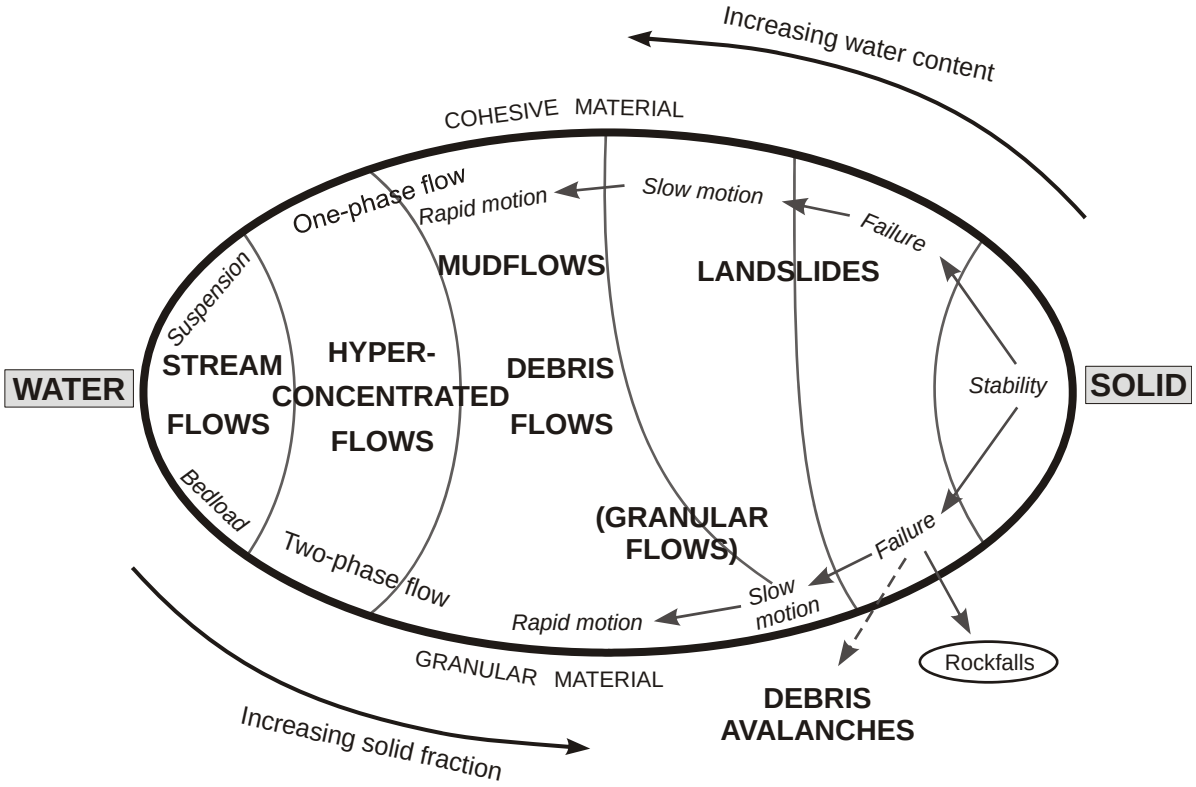

Figure 3.3. Classification of solid-water mixtures from Coussot & Meunier (1996).

debris flows behave primarily as variably liquefied Coulomb grain flows, in which intergranular friction, and thus flow resistance, is strongly influenced by the variable pressure of pore water containing suspended fine sediment. The wide range of potential pore-fluid pressure forces results in a deforming granular mass that can exhibit both solid and fluid behaviour. High pore-fluid pressures cause low material strength (liquefaction) and the liquefied mass behaves like a viscous fluid with low flow resistance, whereas in the absence of fluid pressure it acts like a deforming Coulomb material with high lateral stresses and flow resistance.

Experiments by Major & Iverson (1999) on the role of pore-fluid pressure for debris flow transport and deposition support Iverson's (1997a, 1997b) theory. Their study showed that the fluid pressure within the flow is high enough to liquefy the debris. Excess pore-fluid pressure dissipates significantly only during post-depositional consolidation (Major 2000), with debris-flow deposits >1m thick maintaining elevated fluid pressure and depressed frictional stress for several minutes to days, except at the margins (Pierson & Scott 1985; Major & Iverson 1999). Most natural debris flows are, thus, likely to deposit sediment that is mostly liquefied but impounded by high-friction debris at the flow margins. Pierson (1984) observed that coarse clasts moved to the front and margins of the flow, which stopped when the driving forces could no longer overcome the strength of the marginal rim. This observation was confirmed by Major & Iverson (1999) who showed that fluid pressure rises abruptly after the passage of the flow front, indicating that the leading edges of the flow exhibit very low pore-fluid pressure. Debris-flow deposition thus results from grain-contact friction and bed friction focused at the flow front and margins where high pore-fluid pressure is absent.

3.2.3. Transitions

Few studies link direct observation of flow behaviour and depositional processes to the characteristics of the resulting deposits. Most lack the observation and measurement of the flow event or only cover parts rather than the whole event from initiation to deposition, and the interpretation of the deposits is often not sufficient to fully understand the processes involved (Major 1997). Large-scale experimental studies can provide these linkages because they allow observation of flow processes and comparison of the results to "real-world" events and deposits (Iverson et al. 1992; Iverson 1997a; Major 1997; Major & Iverson 1999).

Experimental small-scale, cohesionless debris flows show behaviour similar to natural flows, e.g. a pulsing nature and transport in kinematic flow surges, as well as a leading flow edge marked by dry saltating, coarse particles, followed by a wet massive flow body (Major 1997). The depositional processes and geomorphological features of the resulting deposits were strongly

influenced by the water content of the source material. Unsaturated flows developed relatively thick lobes with a high aspect ratio, subtle to prominent arcuate ridges, steep, blunt margins and a gravel-dominated surface sedimentology. They were formed by successive surges that were partly overriding and partly shoving forward debris from previous waves. Debris emplacement migrated from the toe of the deposit upslope, i.e. from distally to proximally, and primarily through horizontal accretion. Saturated flows on the other hand, produced longer and thinner deposits with a low aspect ratio, low relief, flat surfaces, and variably shaped margins ranging from steep and blunt, especially distally, to tapered and wedge-shaped, with locally poorly developed levees, and clusters and streaks of coarse clasts at the surface that mark the boundary of flow surges. The deposits developed by incremental vertical rather than horizontal accretion from shallow, successively overlapping surges; later surges locally pushed into and shouldered aside sediment, and commonly overrode earlier debris or were deflected by it (Major 1997).

Within the flows there was typically an elongation of the source particle mass during transport. The general horizontal position of the source debris was retained even though progressive sedimentary accretion resulted in an exchange of the initial horizontal positions of source particles. The deposits were characterised by inverse grading of particles >8 mm, a lack of the coarsest particle fraction in the lowermost 5 cm of the deposit, better sorting of clasts at the surface and a massive, homogenous, unsorted internal texture. Longitudinal or lateral grain size variations do not occur due to the short runout and rapid, near-source deposition of the small-scale experimental debris flows. The complex depositional history and incremental accretion is only reflected in the deposit morphology and surface texture, while the internal texture of the deposits fails to provide a link between deposit character and flow behaviour. The only evidence of incremental vertical accretion can be found near the margins where finer-grained, poorly sorted debris locally overlies well-sorted gravel from the leading edge of the flow. Instead, the massive, matrix-supported nature of debris-flow deposits led to an apparent "misinterpretation" of *en masse* emplacement (Takahashi 1981; Fink et al. 1981; Pierson 1981; Innes 1983; Costa 1984; Major & Voight 1986; Blair & McPherson 1994; Kohlbeck et al. 1994; Kim et al. 1995).

Rheological properties, i.e. yield strength and viscosity, of the flow are often estimated from the deposits (Johnson & Rodine 1984) and the relation between the largest "suspended" clast and bed thickness has been used to infer processes of deposition, grain support mechanisms and strength properties (Walton & Palmer 1988; Collinson & Thompson 1989; Arguden & Rodolfo 1990). Experimental results show that the deposit thickness does not reflect flow strength and composition because the finest-grained flows produced the thinnest deposits (Major 1997). Interpretation of the deposit thickness based on the Bingham concept would suggest that

these flows had the lowest plastic yield strength, which contradicts rheometric experiments that show increasing yield strength with increasing content of fine-grained material (Major & Pierson 1992). Finer-grained debris flows spread out more thinly because they sustain a high pore-fluid pressure for longer, even near margins, due to lower permeability and greater compressibility (Major & Iverson 1999).

As shown by the experimental studies (Major 1997; Major & Iverson 1999), multiple flows of similar source material produce deposits that cannot be distinguished from each other due to a massive homogeneous texture, the lack of grain size variations and erosion surfaces, and thus appear to be the result of a single flow event. The lack of a stratigraphic contact between individual flow units is a result of the low effective stress state of the first unit and its unstable nearly liquefied character. Stacked deposits from separate flows might only be distinguished from each other by distinctive source material, facies variations over long travel distance, prolonged deposition by longitudinally sorted flows or sufficient time to develop unconformities. This is important for hazard implications as the frequency of events may be underestimated while their magnitude may be overestimated.

3.2.4. Spectrum of sediment-water flow

The wide range of models and classifications reflect the large variety of processes within the sediment-water flow spectrum that seem to grade from one to another without obvious boundaries (Pierson & Costa 1987). In the following, boundaries and distinction criteria of different flow types are summarised.

The original definition of hyperconcentrated flow was based on a sediment concentration of 40-80 wt.% (20-60 vol.%; Beverage & Culbertson 1964). Later studies showed that the concentration thresholds can only be used as an approximation as they vary depending on the grain-size distribution and grain density of the sediment mixtures (Pierson 2005). Hyperconcentrated flow behaviour was observed within sediment concentrations of 25-78 wt.% (11-57 vol.%; Pierson & Scott 1985), 36 -75 wt.% (18-54 vol.%) for silt- and clay-rich lahars (Cronin et al. 1999) and 8-11 to 19-37 vol.% for finer and better sorted mixtures from China (Pierson 2005).

Smith (1986) defined the boundaries of hyperconcentrated flow and debris flow based on deposit characteristics. Hyperconcentrated-flow deposits are distinguished from debris-flow deposits by the lack of matrix support or reverse grading and the occurrence of normal grading and horizontal stratification. Criteria of distinction from normal streamflow deposits are a lack of cross-stratification, very poor sorting, weak imbrication, and the occurrence of clast alignment in

gravel facies. These reflect sediment support in hyperconcentrated flows by grain-dispersive forces, turbulence and buoyancy and emplacement through grain-by-grain settling and traction along the channel bed. Sediment in debris flows is kept in suspension by matrix strength, buoyancy and grain-dispersive pressure and deposition has been misinterpreted to occur *en masse*. Large-scale experiments later showed that massive, unstratified debris-flow deposits were formed by a combination of vertical and horizontal incremental accretion from successively overlapping surges (Major 1997).

Some authors defined the boundary between normal streamflow and hyperconcentrated flow as transition from Newtonian to non-Newtonian fluid and the acquisition of a measurable yield strength (Qian et al. 1981; Pierson & Costa 1987). Normal streamflow has very low sediment concentration and larger particles are solely transported as bedload. Sediment in hyperconcentrated flows is held in suspension by a combination of processes (cf. Pierson & Scott 1985, Cronin et al 1997, 1999, 2000; Pringle & Cameron 1997; Major et al 2005; Pierson 2005). The suspended fines in water (carrier fluid) produce a yield strength and high fluid viscosity, which, in combination with turbulence and grain interactions, enables the intermittent, dynamic suspension of large quantities of coarse sediment (sand and fine gravel) at high concentrations (Cronin et al. 1997, 1999; Pierson 2005). Upwelling of fluid displaced by the downward settling of some of the grains adds an additional buoyancy mechanism that allows the mixture to hold more sand (Druitt 1995; Major 2003), which can be observed as a swirling reticulate pattern at the lahar surface (Cronin et al. 1999). The coarser grains move independent from finer particles and are selectively deposited during flow where velocity and, thus, turbulence are decreasing (channel margins with lower flow depth, in eddies or hydraulic jumps) or where dilution results in the loss of suspension competence (flow front or tributary inflows) (Pierson & Scott 1987; Cronin et al. 2000; Pierson 2005). Selective settling of suspended particles results in faintly stratified deposits with some degree of sorting (Smith 1986; Pierson & Scott 1986; Scott 1988a; Cronin et al. 1997, 1999). Furthermore, significant bedload transport occurs in a concentrated zone of intense bed shear, referred to as a traction carpet (Hanes & Bowen 1985; Todd 1989; Sohn 1997; Cronin et al. 2000; Manville et al. 2000). Traction carpet deposition occurs along channel thalwegs where flow velocities and thus bed shear stresses are high (Pierson 2005). The coarse bed load induces turbulence near the bed, while the upper part of the flow can be non-turbulent (observed as a smooth, oily appearance), or behave like a rigid plug depending on the sediment concentration (Pierson & Scott 1985; Cronin et al. 1997; Major et al. 2005; Pierson 2005). There appears to be no sharp boundary between the dense zone of sliding, rolling and

saltating bedload and the intermittently suspended load (Hanes & Bowen 1985; Todd 1989; Sohn 1997; Cronin et al. 2000; Manville et al. 2000; Pierson 2005).

The upper threshold and transition to debris flow is the point at which physical and electrochemical particle interactions start to dominate and selective deposition is hindered due to frictional forces between grains and dense grain packing (Coussot & Piau 1994; Coussot 1995; Druitt 1995; Iverson 1997b; Major 2003; Pierson 2005). This process produces massive, poorly sorted and unstratified deposits (Smith 1986; Pierson & Scott 1986; Scott 1988a; Cronin et al. 1997, 1999). Later studies showed that debris flows can be regarded as variably liquefied Coulomb grain flows in which pore-fluid pressure controls intergranular friction and the degree of liquefaction (Iverson 1997a, 1997b; Major & Iverson 1999). The transition to granular flow is marked by the loss of the ability to liquefy, i.e. pore-fluid pressures are no longer in excess of hydrostatic pressures and grain-to-grain contacts and particle collisions dominate (Pierson & Costa 1987).

3.3. TERMINOLOGY OF VOLCANIC MASS-FLOWS

In general, volcanic mass-flows are gravity-driven (sometimes accelerated by volcanic explosions), involve substantial volumes of poorly sorted rock particles as their primary solid component, and span a wide range of volumes, peak discharges, velocities, compositions, bulk rheologies, and flow hydraulics (Pierson 1998). The nomenclature used to distinguish different types of volcanic mass-flows is inconsistent and often misleading (Pierson & Costa 1987). Some terms include diverse geologic processes such as "mudflow", which was applied to different types of mass movements ranging from slow plastic deformation to rapid, turbulent sediment-water flow (Lowe 1979; Pierson & Costa 1987). On the other hand, a single flow can encompass a wide variety of fluid-dynamic characteristics and show transformations, which can lead to the use of diverse terms to describe the same event, such as lahar, debris flow, hyperconcentrated flow, mudflow, debris torrent, mud flood etc (Pierson & Scott 1985; Pierson & Costa 1987; Cronin et al. 1999; Major et al 2005). The puzzling variety of names and confusing nomenclature is mainly a result of the interdisciplinary character of volcanic mass-flow processes, and divergences in opinion. Scientists of different fields, i.e. sedimentology, physics and mechanics, deal with the problem from different points of view and apply a range of methods, including field characteristics, direct observation and measurement of the event, theoretical physical and mechanical models of flow and material behaviour, as well as depositional and physical experiments, in order to define the different flow types. The developed classification schemes are

used parallel in the literature and are often subject to the respective author's preference. The following section intends to clarify the meaning of terms and definitions used in this thesis.

3.3.1. Volcanic debris avalanches

Debris avalanches are very rapid, wet (but unsaturated), inertial, granular flows generated by large-volume landslides from the flanks of volcanoes (Varnes 1958, 1978; Ui 1983; Schuster & Crandell 1984; Pierson & Costa 1987). They involve large volumes of debris ranging from 0.05 to 45 km^3, may travel distances greater than 100 km and reach velocities as high as 78 m s^{-1} (Siebert et al. 1987; Crandell 1989; Stoopes & Sheridan 1992). The initial sliding motion of the rock mass involves non-turbulent translational transport of the material with relatively small deformations, mainly along internal fractures, and thus favours proximal preservation of the original strata that formed the failed edifice (Siebe et al. 1992; Coussot & Meunier 1996; Shea et al. 2008). The typically small water component does not play a major role during landslide transport, which is characterised by solid particle interactions such as collisions, adhesion and friction (Coussot & Meunier 1996; Iverson 2005). A transition from rockslide to flowing avalanche usually takes place at the base of the volcano and involves stronger deformation and disaggregation of the material (Siebe et al. 1992). Granular debris avalanches can also transform into cohesive debris flows through entrainment of water or water-saturated sediments (e.g. Palmer et al. 1991; Scott et al. 1995; Vallance & Scott 1997). Prior to the 1980 eruption of Mount St. Helens the resulting deposits were mostly termed "lahars" without distinction between debris-flow and debris-avalanche origin (e.g. Neall 1976a, 1976b, 1979; Crandell 1971).

In this thesis, the identification of debris-avalanche processes and deposits is based on distinctive sedimentary and geomorphic features such as the occurrence of shattered and jigsaw cracked clasts, megaclasts, large rip-up clasts, a clay-rich, matrix-supported fabric and the display of hummocks and mounds along the main axis of dispersal and closer to source (cf. Section 3.4.2.). These characteristics have been described in post-Mount St. Helens studies and allow the differentiation of debris-avalanche from other volcanic mass-flow deposits (e.g. Voight et al 1981, 1983; Siebert 1984; Ui 1983; Ui et al. 1986b; Crandell 1989; Glicken 1991; Stoopes & Sheridan 1992).

3.3.2. Lahars

The Indonesian term lahar has been used for a variety of volcanic mass-flows with different properties as well as for the generated deposits (Escher 1922; Van Bemmelen 1949; Neall 1976a, 1976b; Crandell 1971; Fisher & Schmincke 1984). Smith & Fritz (1989) redefined

lahar as "a general term for a rapidly flowing mixture of rock debris and water (other than normal streamflow) from a volcano. A lahar is an event; it can refer to one or more discrete processes, but does not refer to a deposit." The term lahar includes both debris flows and hyperconcentrated flows generated on volcanoes (Smith & Fritz 1989; Smith & Lowe 1991), because a single flow event can involve both rheologic flow types and multiple flow transformations (Pierson 1998).

Here, lahar is used as a general term to summarise gravity-driven, rapidly flowing mixtures of rock debris and water from a volcano, with a higher sediment concentration than normal streamflow, and includes non-cohesive debris flows as well as hyperconcentrated flows. The resulting volcaniclastic sediments are referred to as lahar deposits.

3.3.3. Debris flows

Debris flows are complex, flowing mixtures of sediment and water that exhibit an internal yield strength or resistance to shear, derived from grain collisions (frictional resistance to shear) and cohesion between clay-/silt-sized particles (Iverson & Denlinger 1987; Pierson & Costa 1987; Smith & Lowe 1991; Coussot & Meunier 1996). Cohesive debris flows contain more than 3-5 wt.% clay particles and were also referred to as mudflows or mudslides in the literature (cf., Varnes 1978; Coussot & Piaut 1994; Scott et al. 1995, 2001). Most volcanic debris flows, however, are clay-poor and non-cohesive; they can rather be regarded as water-saturated modified-granular flows (Costa & Williams 1984; Fisher & Schmincke 1984; Smith & Lowe 1991; Major 1996, 1997; Major et al. 2005). Debris flows are defined as highly concentrated, often >60 vol.% (80 wt.%) of solid fraction, relatively homogeneous, non-Newtonian, pseudo-single-phase gravitational flows of sediment and water in which a broad distribution of grain sizes, commonly including gravel, is vertically well mixed (Costa 1984, 1988; Pierson & Costa 1987; Wan & Wang 1994; Major 1997; Cronin et al. 2000; Vallance 2000; Pierson 2005). Debris flow motion is of a transient nature, typically comprising a series of surges that develop as a result of mechanical instability (Major & Pierson 1990; Coussot & Meunier 1996; Major 1997; Major & Iverson 1999; Iverson 2005). Flow behaviour is strongly influenced by interactions between the solid and fluid components, i.e. grain-grain collisions and viscous fluid flow (Wan & Wang 1994; Coussot & Piaut 1994; Coussot 1995; Iverson 1997; Major et al 2005).

In this study deposits from both cohesive and non-cohesive debris flows were identified that are interpreted to have been produced by various generation mechanisms. In Taranaki, debris-flow deposits associated with volcanic debris avalanches are characterised by considerable amounts of matrix clay (>3-5 wt. %) and can be classified as cohesive debris flows (Scott et al.

1995; Vallance & Scott 1997). In contrast, debris-flow deposits related to lahars are typically clay-poor (<3 wt. %) and are referred to as non-cohesive debris flows (Scott 1988a).

3.3.4. Hyperconcentrated flows

Hyperconcentrated flows are generated from floods through erosion and entrainment of sediment, or through transformation of large non-cohesive debris flows by dilution and selective deposition (Pierson & Scott 1985; Cronin et al. 1997; Major et al. 2005; Pierson 2005). The term was introduced by Beverage & Culbertson (1964) who described hyperconcentrated streamflows as having sediment concentrations between 40 and 80 wt% (20 to 60 vol.%). However, this definition can only serve as a rough guide, because the particle-size distribution, grain density and composition of the fine fraction within the flow also play important roles for the flow behaviour and flow transition thresholds (Pierson 1986; Cronin et al. 1999, 2000; Pierson 2005). Pierson & Costa (1987) redefined hyperconcentrated flow based on the sediment concentration required to generate the onset of a measurable internal yield strength and hence temporary suspension or hindered settling of coarse particles.

In general, hyperconcentrated flow is a turbulent, gravity-driven, non-Newtonian, two-phase flow of water and sediment, intermediate in sediment concentration between dilute, fully turbulent, normal streamflow and viscous, generally laminar flow (Smith 1986; Smith & Lowe 1991; Pierson 2005). Sediment is supported by grain-dispersive forces, turbulence and buoyancy and is emplaced through grain-by-grain settling and traction at the base of the flow (Hanes & Bowen 1985; Smith 1986; Smith & Lowe 1991; Sohn 1997; Pierson 2005).

This thesis deals with the resulting deposits rather than the actual flow, so the flow conditions can only be inferred. Thus, classifications based on deposit characteristics are included in addition to the above described flow observations and physical models.

3.3.5. Normal streamflow

Normal streamflow is fully turbulent, with sediment concentrations that are insufficient to change the Newtonian properties of flowing water. Turbulence is the principal sediment-support and transport mechanism (Smith 1986; Pierson & Costa 1987; Costa 1988). Transportation occurs by traction, in a grain-by-grain fashion and larger particles are transported as bedload, i.e. in traction carpets or by saltation (Hanes & Bowen 1985; Smith & Lowe 1991; Sohn 1997). The critical sediment concentration at which streamflow becomes a non-Newtonian fluid and thus grades into hyperconcentrated flow depends on the grain-size distribution, clay content and clay mineralogy, but is often around 20 % by volume (Pierson & Costa 1987).

In the Taranaki ring plain succession, normal streamflow behaviour is mainly reflected by deposits of major and minor fluvial systems as well as some transitional volcaniclastic flow deposits.

3.3.6. Flow transformations and transitions

Lahars are a common feature in volcanic terrains. Their formation requires an adequate water source, abundant unconsolidated debris, substantial relief at the source and a triggering event (Vallance 2000). Lahars may be of primary (syn-eruptive) or secondary (post-eruptive or unrelated to eruptive activity) origin and can be initiated by a variety of mechanisms (Neall 1976; Waitt et al. 1983; Cronin et al. 1997; Mothes et al. 1998; Hodgson & Manville 1999; Lavigne et al. 2000; Vallance 2000; van Westen & Daag 2005; Németh & Martin 2007). Lahars can be triggered by pyroclastic flows entering streams, phreatomagmatic explosions or directed blasts (Neall 1976b, Vallance 2000). Furthermore, lahars can form after sudden melting of a glacier or snow and ice by hot pyroclastics, lava flows, or growing lava domes, as well as an elevated heat gradient due to hydrothermal and magmatic fluids in the upper edifice (Janda et al. 1981, Pierson et al. 1990; Pierson & Janda 1994, Branney & Gilbert 1995, Cronin et al. 1996a, Thouret et al. 1998, Manville et al. 2000, Stern 2004; Major et al. 2005). Some flows are associated with existing crater lakes and are produced by an eruption through the crater lake or from a non-volcanic crater lake rim failure (Cronin et al. 1996a; 1999, Lecointre et al. 1998, Manville et al. 1998). Rain-triggered lahars often occur after large explosive eruptions, e.g. Mt. Pinatubo in the Philippines (Newhall & Punongbayan 1996; Chorowicz et al. 1997, van Westen & Daag 2005, Carranza & Castro 2006) or Mt. Merapi in Indonesia (Lavigne et al. 2000, Lavigne & Thouret 2002), and represent a major hazard especially in equatorial latitudes and temperate zones of high rainfall.

Debris flows can form by a variety of transformations from different kinds of flows, i.e. by water incorporation from pyroclastic flows and debris avalanches as well as from floods through sediment erosion and entrainment (Neall 1976a; Janda et al. 1981; Waitt et al. 1983; Scott 1988a; Pierson et al. 1990; Pierson & Janda 1994; Branney & Gilbert 1995; Newhall & Punongbayan 1996; Mothes et al. 1998; Thouret et al. 1998; Hodgson & Manville 1999; Lavigne et al. 2000; Vallance 2000; Lavigne & Thouret 2002; Major et al. 2005; van Westen & Daag 2005; Carranza & Castro 2006; Németh & Martin 2007). The sediment-water ratio within a flow can change longitudinally due to bulking or depositional processes as well as laterally, due to flow depth and velocity variations.

Confined lahars with low clay contents typically transform from debris flow to hyperconcentrated flow at some point along their path due to progressive incorporation of water

and continuous sedimentation (Janda et al. 1981; Pierson & Scott 1985, Lowe et al. 1986, Smith 1986, Major & Scott 1988; Scott 1988a, 1988b; Alloway 1989; Major & Newhall 1989; Smith & Lowe 1991; Scott et al. 1995; Major et al. 1996; Pringle & Cameron 1997; Thouret et al. 1998; Cronin et al. 1999, 2000; Lavigne et al. 2000; Lavigne & Suva 2004; Major et al. 2005). With distance and further dilution, more sediment is transported as bedload, deposits are more distinctly stratified and high-angle cross-bedding can be formed (Cronin et al 2000), which reflects gradation into normal streamflow (Pierson & Scott 1985; Scott 1988a; Scott et al. 1995). This gradual dilution and transformation process only affects lahars that are small compared to the volume of available water along the river catchment; it does not significantly influence the rheology and flow behaviour of large-volume lahars (Cronin 2000, Lavigne & Thouret 2000).

Pierson & Scott (1985) suggested that the progressive head to tail dilution of the lahar with stream water leads to the development of a hyperconcentrated flow phase preceding the main debris flow body. The fluid component of the flow separates from and outruns the sediment-rich component, producing a lag between the two flow components (Scott 1988a). A later study by Cronin et al. (1999) showed that the initial portion of a lahar wave is stream water pushed along the channel in front of the lahar rather than fluid separated from the bulk flow. The lahar is essentially an invading solution that contrasts with the resident stream water which is pushed ahead. The studied non-cohesive lahars showed four phases: resident stream water pushed ahead of the lahar, a downstream-lengthening mixing zone between stream water and the lahar, the relatively undiluted original lahar, and the tail of the lahar surge. The resident stream water portion indicates that lahars do not entrain and mix perfectly with water sources in their paths. The increasing lag between peak stage and peak sediment concentration described by Scott (1988a) is hence probably due to lengthening of the mixing interval between streamflow and lahar with distance from source.

A distinct change in slope or widening of the channel can cause a more abrupt transformation from debris flow to hyperconcentrated flow (Cronin et al. 2000). For example, the 25/09/95 lahar from Mt. Ruapehu, New Zealand, spread out over a broad area when it exited a confined gorge onto the Whangaehu fan, which led to a loss of flow competence and flow depth encouraging sediment deposition. In contrast to dilution by addition of water, this type of flow became water-rich through a sudden loss of velocity and a consequential loss of sediment load (Cronin et al. 2000). Under certain circumstances, i.e. strong erosive energy of the flow in combination with a high supply of loose sediment along the flow path, a hyperconcentrated flow can bulk up and transform into a debris flow (Costa 1984; Pierson & Scott 1985; Scott 1988a, 1988b; Smith & Lowe 1991; Scott et al. 1995; Major et al. 2005). A transition from

hyperconcentrated flow to debris flow can also occur due to rapid loss of water through infiltration into the surface of the underlying volcaniclastic and fluvial sequences (Smith 1986).

The Taranaki deposits appear to have been produced by a range of all the different flow types within the sediment-water spectrum described above. Their characteristics, transitions and lateral changes exposed in cross-section in the coastal cliffs of the Taranaki peninsula were documented in order to construct a spatial-temporal model of ring plain evolution, and to interpret the flow and sedimentation process operating over various time and spatial scales.

3.4. VOLCANIC MASS-FLOW DEPOSITS

3.4.1. Volcaniclastic ring-plain successions

The term "ring plain" was introduced from studies in New Zealand for "flat or nearly flat land in a nearly circular or annular area surrounding Mount Egmont" (Morgan & Gibson 1927). Subsequently the term was applied more generally to the low-relief alluvial plains and fans surrounding the volcanoes of the central North Island, i.e. Mt. Ruapehu and Mt. Tongariro (Palmer et al. 1993; Cronin et al. 1996; Cronin & Neall 1997; Lecointre et al. 1998; Donoghue & Neall 2001). Smith (1987a, 1987b) used the term volcaniclastic apron instead of ring plain to describe "relatively thin (<0.5 km) accumulations of volcaniclastic material adjacent to volcanoes that possess wedge-shaped cross-section thinning away from source". These sequences were dominated by debris-flow and flood deposits, which accumulated over fan-shaped segments of the apron and the sedimentary setting corresponds to relatively low-gradient alluvial plains.

Davidson & de Silva (2000) later defined volcanic ring plain as the circular area surrounding a centrally constructed volcanic edifice. However, a truly circular apron only develops around volcanic edifices that are more or less isolated from neighbouring volcanoes or mountainous terrain (Smith 1991). More commonly, volcanic settings are characterised by merging of deposits from individual edifices with those of their neighbours, or ancestral degraded volcanoes and thus a more irregular surrounding topography. This leads to the concentration of primary and reworked deposits in channels and drainage systems with wedge-shaped cross-sections that usually extend 10-30 km from the bases of the volcanoes (Neall 1979; Hackett & Houghton 1989). In the case of oceanic composite volcanoes of island arcs, for example, Augustine Volcano (Beget & Kienle 1992; Siebert et al. 1995) the immediate edifice is surrounded by the sea and a major part of the volcanic record accumulates below sea level without the development of an extensive onshore ring plain.

Volcanic ring-plain successions are progressively built up by deposition of syn- and post-eruptive volcaniclastics and minor primary products, as well as reworked deposits (Palmer & Neall 1991; Cronin et al. 1996; Cronin & Neall 1997; Lecointre et al. 1998; Donoghue & Neall 2001). Hence, the succession is dominated by various types of lahar deposits, and in some cases, debris-avalanche deposits and interbedded tephra layers. The most extensive pyroclastic flows and lava flows might also reach proximal parts of the ring plain but are otherwise confined to the edifice (Davidson & de Silva 2000). Major phases of ring-plain accumulation alternate with periods of dissection and landscape adjustment. The resulting fluvial and aeolian reworked deposits represent another major component of the sequence. The ring-plain depositional system contains the most complete chronostratigraphic record of volcanic activity and other sedimentary events (Palmer & Neall 1991; Smith 1991; Cronin et al. 1996; Cronin & Neall 1997; Lecointre et al. 1998; Donoghue & Neall 2001; Németh & Martin 2007). It is therefore essential to understand the depositional processes that contributed to the construction of the volcanic ring plain, in order to reconstruct the eruptive history of a stratovolcano in more detail.

The volcaniclastic sequences examined in this thesis represent "medial" portions of the Mt. Taranaki ring plain, 25-45 km from source. Proximal sites are typically <15 km and here distal is classified as >50 km (Smith 1987a; Beget & Kienle 1992; Scott et al. 1995; Belousov et al. 1999; Waythomas et al. 2000; Major et al. 2005). However, the nature of the studied volcanic mass-flow deposits depend not only on distance from source, but also on the type (debris avalanche vs. debris flow vs. hyperconcentrated flow) and volume of the depositing flow, the height of the edifice (e.g. early stage of regrowth phase vs. mature, high edifice) and the character of the surrounding landscape (unconfined vs. channelised). Most deposits of the south-western Mt. Taranaki ring-plain succession show medial facies characteristics (at c. 25-30 km from source), but coastal exposures may also show distal facies of some volcanic mass-flow deposits. This is particularly notable for hyperconcentrated-flow units, which show transitions to stream-flow deposits (distal run-out facies) in the south-eastern ring plain c. 40-45 km from source.

3.4.2. Debris-avalanche deposits

The younger parts of the Taranaki ring plain display a distinctive surface geomorphology of numerous hills and small mounds that have attracted the attention of geologists for more than a hundred years. The first geological surveyors in Taranaki interpreted these "conical hills" as individual volcanic vents formed by separate volcanic explosions (de Clarke 1912; Morgan & Gibson 1927), while Bossard (1928) considered them blisters on lava flows. Grange (1931) first postulated a laharic origin, based on their similarity to historic volcanic

mudflow deposits in Java and Japan. Neuman van Padang (1939) and van Bemmelen (1949) attributed similar hills at the base of several Indonesian volcanoes to "landsliding or avalanching" of a sector of the volcanic cone, but described the resultant deposits as laharic breccias.

Prior to the 1980 eruption of Mount St. Helens, Murai (1961) recognised "dry mudflows" in Japan that differed from lahars and suggested their emplacement by gravitational forces without the agency of water. Subsequently Mizuno (1964) distinguished fragmental avalanche-type deposits from those of flow-type. Ando & Yamagishi (1975) later related the formation of mudflow hills at the base of many Japanese volcanoes to either cold or hot avalanches. The term "volcanic dry avalanche" was introduced by Nakamura (1978) to describe the 1888 Bandai deposit.

The 1980 Mount St. Helens eruption presented the first opportunity to observe and document the generation and emplacement of a large volcanic debris avalanche (Voight et al. 1981, 1983; Glicken 1991, 1996). Observations of the eruption were integrated with studies of the deposits produced (Lipman & Mullineaux, 1981). This has provided a model for the interpretation of similar deposits elsewhere (Mimura et al. 1982; Crandell et al. 1984). As a direct consequence of the Mount St Helens event, debris-avalanche deposits were recognised at many volcanoes worldwide and their textural and morphological features described in more detail (e.g. Siebert 1984; Ui et al. 1986a; Crandell 1989; Beget & Kienle 1992; Vallance & Scott 1997; Belousov et al. 1999; Capra & Macias 2000).

The source area of debris avalanches is characterised by large, horseshoe-shaped amphitheatres that show a wide breach to one side and often extend into the core of the volcano (Voight et al. 1981; Ui 1983; Siebert 1984). The landscape at the base of the volcano below the avalanche scar typically shows a hummocky topography comprising numerous hills and mounds that are often surrounded by a flat surface (Ui 1983; Siebert 1984). The development of the secondary planar surface is attributed to immediate reworking of the debris-avalanche deposit after its emplacement by dewatering or by subsequent lahars (Janda et al. 1981; Ui 1983). With time the distinct surface expression of mounds is smoothed out due to long-term reworking and accumulation of debris from younger lahars that flow around the older debris-avalanche deposit as well as accretion of distal tephra (Alloway 1989; Alloway et al. 2005; Procter et al. 2009).

The internal structure of debris avalanches is characterised by three major components: megaclasts (>1 m in diameter), elsewhere described as megablocks or fragmental rock clasts, clasts (<1 m in diameter), and fine-grained material, referred to as matrix (Ui 1983; Crandell et al. 1984; Palmer et al. 1991; Glicken 1996; Alloway et al. 2005). Megaclasts represent relatively intact

former portions of the volcanic edifice that can be deformed and fractured into numerous clasts. The irregular cracks within megaclasts form a pattern that resembles a jigsaw puzzle and have been referred to as jigsaw cracks by Shreve (1968), Ui (1983) and Ui et al. (2000). The frequency of jigsaw cracks depends on rock type and travel distance (Ui et al. 1986a, 2000). Different types of megaclasts include lithologically homogeneous, shattered fragments of lava flows/domes and stratified material with preserved primary textures and original lithological contacts between layers (Ui 1983; Palmer et al. 1991; Alloway et al. 2005). The size and number of megaclasts decrease with distance from source and towards the lateral margins of the deposit, while the amount of matrix increases (Ui 1983). The lithology of megaclasts, clasts and matrix varies between debris-avalanche deposits and throughout each unit, even on a large exposure scale (Ui et al. 2000). The variations are influenced by the composition and structure of the original volcanic edifice as well as the topography underlying the deposit (Alloway et al. 2005).

The matrix consists of a mixture of smaller volcanic fragments ranging in size from clay to very coarse sand and includes all unsorted and unstratified parts of the deposit (Alloway et al. 2005; Ui et al. 2000). The matrix contains clasts of primary and secondary origin. Primary clasts are typically 2 mm - 1 m in diameter and show a wide range of lithologies, including fragments of lava, scoria, pumice, crystals or any other rock-type that were part of the volcanic edifice prior to avalanche initiation. Secondary or rip-up clasts are incorporated in the flow during transport and comprise variably rounded fluvial and other clasts, wood and fragments of the underlying strata, such as volcaniclastic and fluvial deposits, tephra, peat and soil beds (Palmer et al. 1991; Alloway et al 2005). The abundance of rip-up clasts increases with distance from source (Ui et al. 2000).

Since the relative proportion of matrix to megaclasts varies with distance from source and main axis of distribution, former workers used this ratio to subdivide a debris-avalanche deposit into mappable areas. The areas dominated by megaclasts and a characteristic hummocky surface was mapped as megablock facies by Mimura (1971), as axial facies by Neall (1979), and as block facies by Crandell et al. (1984). The topographically flat area that is characterised by the predominance of matrix was termed main facies by Mimura (1971) and Mimura & Kawachi (1981), marginal facies by Neall (1979), matrix mixture by Ui (1983), matrix facies by Crandell et al. (1984), and mixed facies by Glicken (1991). The terms "blocks" and "matrix" are ambiguous because they are applied to both individual components of debris-avalanche deposits as well as to describe different facies (Crandell et al. 1984). This thesis therefore adopts the nomenclature of Neall (1979) because it distinguishes descriptive mapping units from genetic sedimentological units. Based on Neall's (1979) concept, Alloway (1989) and Palmer et al. (1991) recognised three distinct lithofacies distributions that define distinct mapping units within the relatively

unconfined Taranaki debris-avalanche deposits that differ considerably from valley-confined debris avalanches described elsewhere (Siebe et al. 1992; Richards & Villeneuve 2001; Clavero et al. 2002; Pollet & Schneider 2004; Dunning et al. 2006).

These lithofacies developed in response to changes in the nature of flow as the debris avalanche travelled away from source (Fig. 3.4A). Axial-A and axial-B lithofacies correspond to the debris-avalanche phase of the landslide while the marginal lithofacies is attributed to the debris-flow phase. Axial-A facies forms lobes near source and is dominated by brecciated, self-supporting megaclasts with <30% sandy interclast matrix and a hummocky surface expression with closely spaced, large mounds up to 50 m high and basal diameters as much as 500 m (Fig. 3.4B, Fig. 3.5A-B). Axial-B facies is interclast matrix-rich (30-90%) and characterised by smaller, more widely spaced mounds ≤10 m high with basal diameters <25 m (Fig. 3.4C, Fig. 3.5C-D). Size and abundance of megaclasts decreases with increasing distance laterally from axial-A lithofacies, while the amount of rip-up clasts increases. The lateral transition from axial-B to marginal lithofacies is gradational and characterised by a decrease in overall unit thickness, clast size and abundance of larger megaclasts, an increase in matrix to clast ratio and in rip-up clasts. The marginal facies contains >90% of clay-rich matrix and is characterised by a predominantly planar surface with scattered small mounds <2 m high (Fig. 3.4D, Fig. 3.5E-F). The marginal facies is generally interpreted as being emplaced by debris flows that have transformed directly from debris avalanches (Palmer et al. 1991) although some may have been generated by contemporaneous smaller failures from the area of initial collapse (Palmer & Neall 1989). The flows have often been referred to as cohesive lahars. In this study they are described together with debris avalanches because their initiation mechanism, flow behaviour and the resulting clay-rich deposits relates them more closely to debris-avalanche processes and they differ significantly from the sand-rich non-cohesive types of lahars described in the next section.

The matrix of Mt. Taranaki debris-avalanche deposits contains amorphous and crystalline clay particles and minerals (Neall 1976c; Parfitt et al. 1981; Alloway et al. 2005; Procter pers. comm. 2009). The dominance of allophane indicates that this component was derived from soils eroded along the flow path, rather than representing hydrothermally altered material at source or products of diagenesis (Neall 1976; Alloway et al. 2005). Thick allophane-rich andic coverbeds on the ring plain represent the source for this clay. This mineral forms by rapid weathering of andesitic ash under the humid-temperate climate conditions of Taranaki (Neall 1976; Alloway et al. 2005). Granulometric data is only available for some Taranaki soils (Parfitt et al. 1981) and is very challenging to analyse due to the high amounts of very fine short-range-order and amorphous clays (Alloway et al. 1992c). The known thixotropic properties

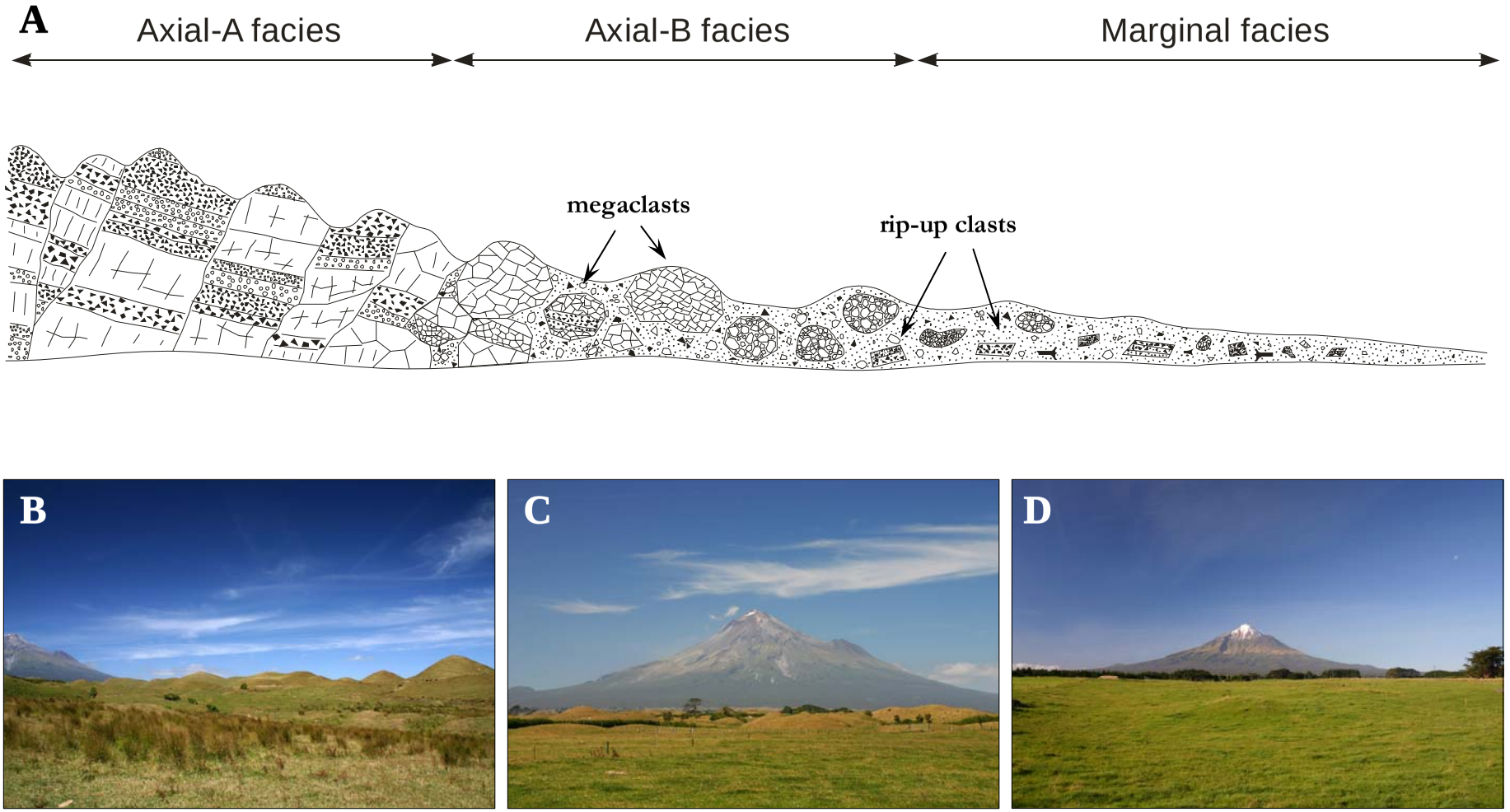

Figure 3.4. Characteristic lithofacies types and facies variations in Taranaki debris-avalanche deposits from source to medial/distal areas are illustrated in A (adapted from Palmer & Neall 1991). Photographs show the corresponding geomorphic characteristics of axial-A (A), axial-B (B) and marginal facies (C) of unconfined debris-avalanche deposits at Mt. Taranaki.

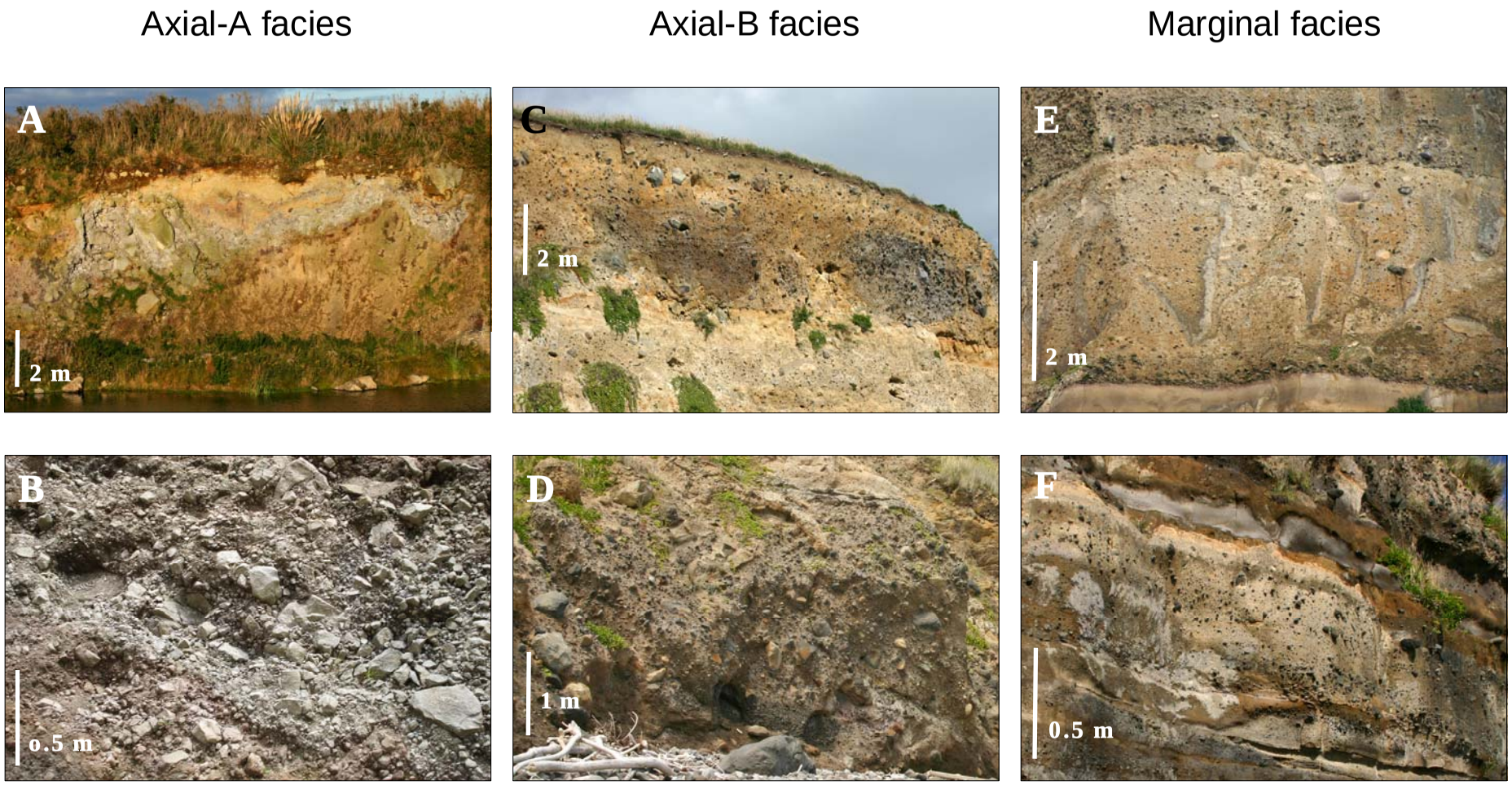

Figure 3.5. Fabric of axial-A (A -B), axial-B (C-D) and marginal (E-F) facies of Mt. Taranaki debris-avalanche deposits. The transition from axial-A to marginal facies is characterised by a decrease in overall clast size and thickness and an increase in matrix and megaclasts and large lava blocks are gradually disaggregated. Secondary rip-up clasts become more common.

of allophane and its high capacity for water storage probably engenders extremely high mobility for Taranaki debris avalanches that incorporate andic soils.

3.4.3. Lahar (debris-flow and hyperconcentrated-flow) deposits

The wide variety of lahar initiation mechanisms results in a broad range of deposits with diverse textures and fabrics (Fig. 3.6). Their composition, grain size and thickness depend on the type, size and origin of the flow as well as on the depositional environment (Fisher & Schmincke 1984; Scott 1988a, 1988b; Smith & Lowe 1991; Scott et al. 1995; Cronin et al. 1997; Vallance 2000; Major et al. 2005). The deposits from debris flows are recognised by their massive, poorly sorted texture, coarse grain-size, matrix-support of clasts and often inverse grading, which reflect the high sediment concentration, particle interaction, high yield strength, buoyancy and laminar flow of the transport medium. Hyperconcentrated-flow deposits are better sorted and finer-grained, show faint stratification, clast-support, normal, inverse or no grading indicating less yield strength and buoyancy and evidence of more turbulent flow behaviour. Normal streamflow deposits are produced by fully turbulent flow resulting in better sorting and distinct horizontal bedding to cross-stratification.

Lahar deposits can show several facies that reflect the lateral and longitudinal changes in flow dynamics. The progressive downstream transformation from debris flow to hyperconcentrated flow produces deposits that show a gradational vertical transition from a basal hyperconcentrated-flow deposit upward to a debris-flow unit (Pierson & Scott 1985; Cronin et al. 1999). With increasing dilution the basal horizontally bedded, poorly sorted, clast-supported hyperconcentrated-flow layer thickens, while the overlying massive, unbedded, coarse, very poorly sorted, matrix-supported debris-flow portion thins (Scott 1988a; Scott et al. 1995; Cronin et al. 1999). With increasing distance from source the horizontal stratification becomes more distinct and is eventually replaced by wavy cross-stratification as the flow transforms to normal streamflow. Some lahars are vertically stratified into a coarse, sediment-rich channel flow and an overlying dilute, finer grained surface layer, which results in accumulation of near-channel, wedge-shaped debris-flow deposits that are laterally equivalent to overbank hyperconcentrated-flow deposits (Cronin et al 2000).

Clasts within lahar deposits can be primary, mostly comprising angular to subangular volcanic rocks from the source region, or secondary angular to rounded clasts that were picked up along the lahar path (Major & Scott 1988; Scott 1988a, 1988b; Major et al 2005). The clast assemblage can be monolithologic but is more commonly polylithologic, with bimodal grain-size

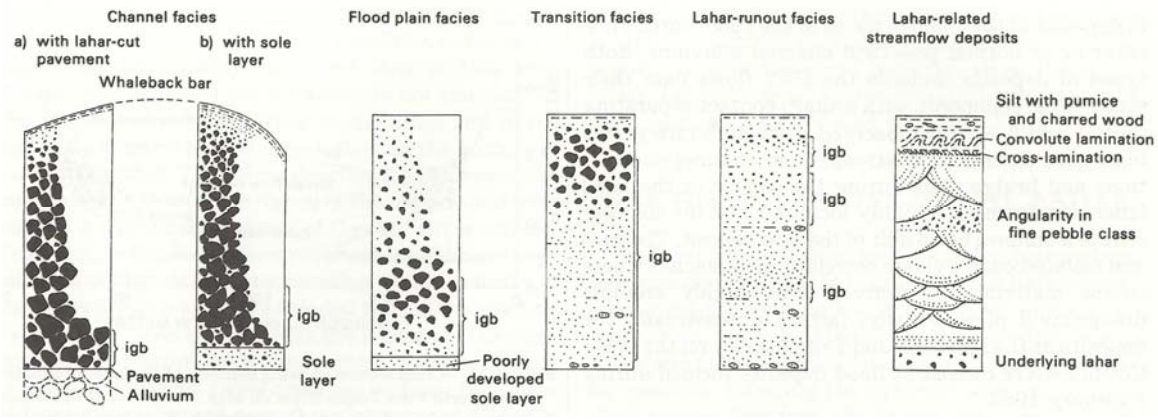

Figure 3.6. Facies types of lahar and lahar-related streamflow deposits (from Scott 1988a).

distributions (Vallance 2000). Vesicles commonly found in the matrix result from entrapment of air bubbles. Other components include wood fragments, casts of tree fragments, and charcoal.

Lahar deposits were recognised at an early stage as being a major component of the Taranaki ring-plain succession (Grant-Taylor 1964; Neall 1979; Neall et al. 1986; Palmer & Neall 1991). The distribution of the youngest (<20 ka) debris-flow and hyperconcentrated-flow deposits, which are exposed on the surface of the ring-plain succession, was mapped by Neall (1979) and Alloway (1989). Older lahar units >20 ka are buried by more-recent volcaniclastic deposits closer to source and are only exposed in cross-section along the Taranaki coast. Based on their lithofacies characteristics and lateral facies changes they were classified as diamicton sheets (DS), sandy bedforms (SB), channels (CH), gravely bedforms (GB) and overbank fines (OF) (Palmer & Neall 1991). DS includes sandy debris-flow units as well as clay-rich units related to debris avalanches, and corresponds to both cohesive and non-cohesive debris-flow deposits. Clast-supported debris-flow deposits (CH) grade laterally into a debris-flow plain dominated by DS and marginal sandy fluvial deposits (SB). The base of many channels is typically made up of fluvial gravel and sand (GB and SB), reflecting their fluvial origin. Intercalated with volcanic mass-flow and fluvial deposits are paleosols, peat and reworked tephra beds (OF).

(i) Debris-flow deposits

Debris-flow deposits are very poorly to extremely poorly sorted, massive, non-stratified, and the largest clasts are typically supported in a finer grained matrix (Smith 1986; Vallance 2000; Scott et al. 2001). Both matrix-supported and clast-supported frameworks occur but the latter is less common (Smith 1986). Debris-flow deposits may be graded or lack vertical grain size variation; grading can be reverse to normal, reverse throughout the deposit, or rarely coarse-tail normal (Smith 1986; Scott 1988a; Major 1997; Thouret et al. 1998; Major et al. 2005). Reverse grading of clay-poor debris-flow deposits is attributed to dispersive pressure and limited to the

basal portion; it can occur throughout deposits generated by cohesive debris flows as a result of upward-increasing yield strength (Smith 1986). Coarse-tail normal grading due to settling of clasts within the flow during transport is common especially in the upper half of the unit. Concentrations of coarse particles, in particular low-density pumice clasts, are common at the deposit top (Vallance 2000). Most deposits show a decrease in mean and maximum grain size as well as the development of better sorting with distance from source. Debris-flow deposits typically show a distinct basal subunit, which is attributed to boundary effects during the waxing-flow stages of the lahar (Alloway 1989; Scott 1988a, 1988b; Vallance 2000, Major et al. 2005). Sole layers of the channel facies consist of inversely graded, finer grained, texturally more uniform and more compacted sediment than the overlying debris, with locally primary foliation, while the floodplain facies typically shows sandy basal layers (Scott 1988a; Vallance 2000). The "ball-bearing bed" at Mt. St. Helens is an unusual clast-supported, fines deficient, concentrated basal unit of rounded pebbles and was interpreted as a sole layer of an exceptionally large lahar (Scott 1988a, 1988b).

The thickness of debris-flow deposits ranges from tens of centimetres to tens of metres, with thick deposits accumulating in valleys and on lowlands and thinner deposits on higher terraces and valley slopes, as well as thin veneers on steep slopes (Janda et al. 1981; Pierson 1985; Pringle & Cameron 1999; Cronin et al. 2000; Lavigne et al. 2000; Vallance 2000, Major et al. 2005). Lobate snouts, blunt margins, marginal levees, arcuate surface ridges and steep terminal flow fronts are common geomorphic features of deposits produced by unsaturated debris flows, but become less distinct with higher water contents of the flow (Major 1997; Vallance 2000). Some lahars accumulate clast-supported streamlined lags of poorly stratified gravel, so-called whaleback bars, in either expanding or constricting reaches of the channel due to changes in flow competence (Janda et al. 1981; Scott 1988)

(ii) Hyperconcentrated-flow deposits

Hyperconcentrated flows have properties that lie between debris flow and normal streamflow and thus produce deposits with intermediate characteristics (Pierson & Scott 1985; Smith & Lowe 1991; Pierson 2005). The deposits are typically finer-grained and better sorted than debris-flow deposits and often show a normally graded upper part. They can be non-stratified, relatively massive and well-sorted, faintly bedded or display strong horizontal bedding (cf. Cronin et al. 2000). Coarse deposits with more pronounced horizontal stratification as well as laminations without high-angle cross-bedding are the result of traction-carpet deposition (Cronin et al. 2000). Lenses or single outsized clasts of cobbles or boulders are common and represent

coarse bedload enveloped by accretionary strata or left stranded on surfaces of berms or terraces (Pierson 2005). In distal areas where sediment concentrations are decreasing, more sediment is transported as bedload, the deposits are more distinctly stratified; and high-angle cross-bedding can form as a result of transition to normal streamflow (Cronin et al. 2000).

When confined to channels, hyperconcentrated-flow deposits can show lateral facies variations from gravel-dominated valley-fill to sand-dominated floodplain or overbank deposits (Smith 1986; Scott 1988a; Palmer & Neall 1991; Cronin et al. 2000; Major et al. 2005). Channel-fill deposits are massive, very poorly sorted, usually clast-supported, only moderately compacted, and show a bimodal grain size distribution of sand and gravel (Cronin et al 2000; Vallance 2000). These gravel-dominated deposits commonly develop normal grading and lack reverse grading at the base. The poorly imbricated cobbles and boulders form a framework with poorly sorted, very coarse-grained sand and pebbles occupying the open spaces in between (Smith 1986). Vesicles might be present if the matrix is fine-grained (Vallance 2000). The grain size within floodplain deposits ranges from coarse- and medium-sand to silt with the occasional floating pebble, cobble, or boulder (Scott 1988a). These are better sorted and usually show a faint internal stratification, with thin horizontal or very low angle cross-beds of alternating well- to poorly sorted, relatively coarse- and fine-grained sands. Pumice clasts, if present, are usually concentrated at the top of the overbank portion (Vallance 2000). The deposits are often overlain by 1-2 cm of ripple cross-laminated sand, which is deposited by the low-energy, dilute waning stage of the flow (Smith 1986; Blair 2000; Cronin et al. 2000).

The thickness of hyperconcentrated-flow deposits varies from a few centimetres to several metres, with thicker deposits in channels or low areas grading into thinner deposits on higher ground. Scattered pebbles and larger clasts, especially pumice, are common towards the top of the deposit and are accompanied by thin layers of fine sand and silt that form due to compaction and dewatering (Cronin et al. 2000). Sedimentary features such as strong alignment or imbrication of elongate clasts, vertical variations in particle lithologies, similar clast compositions near margins and base of valley-fill deposits, tide lines indicating 5-10 times greater flow-depth than deposit thickness, and stratification indicate deposition within these currents through incremental accretion (Fisher & Schmincke 1984; Smith 1986; Smith & Lowe 1991; Vallance 2000).

3.5. FIELD CHARACTERISTICS OF VOLCANICLASTIC AND REWORKED EPICLASTIC DEPOSITS IN TARANAKI

Volcaniclastic deposition at Mt. Taranaki has formed a surrounding ring plain, which extends 25-40 km onshore from the current summit and at least a further 6 km offshore. Sequences along the northern and southern Taranaki coast represent a cross-section through medial ring-plain settings. The exposed units show a wide range of lithologies, which reflect the whole spectrum of sediment-water flow from highly concentrated debris flow to dilute streamflow. Based on their different sedimentological characteristics, the deposits were classified into volcaniclastic, fluvial and aeolian facies. Distinction criteria and main deposit features are summarised at the end of this section in Table 3.1.

3.5.1. Debris-avalanche and associated debris-flow deposits

Debris-avalanche and related deposits of at least 14 edifice failures have been recognised at Mt. Taranaki (Neall 1979, 1986; Alloway 1989; Alloway et al. 2005; this study). Eleven of these events are represented in the study area along the south-western Taranaki coast, including six newly identified units. Two distinctive types of debris-avalanche deposits occur: a dominant "granular-type" is distinguished from one "cohesive-type" unit, i.e. the Otakeho debris-avalanche deposit which contains significantly higher matrix clay contents.

In medial areas >25 km from source, only large-volume debris avalanches generated by major failures show axial-B facies, attributed to the landslide phase of the avalanche. Those produced by smaller collapse events had already transformed into run-out debris flows and deposited matrix-supported marginal facies. The physiographic expression of axial-B facies is only obvious for the youngest debris-avalanche deposits, which are exposed at the top of the ring-plain sequence. The medial facies of the Opua and Pungarehu events produced small, more widely spaced hummocks than the proximal axial-A facies, with variable basal diameters generally <25 m and extensive inter-mound areas (Palmer et al. 1991). In the case of the older debris-avalanche units, a few scattered hummocks can be found in cross-section in the coastal cliffs but the characteristic morphology is otherwise buried and the surface smoothed out by overlying younger parts of the sequence. Axial-B debris-avalanche units are typically up to 8 m thick in coastal outcrops with the exception of the Pungarehu Formation, which exceeds 15 m at medial coastal locations near its main axis of distribution (Palmer et al. 1991).

In general, Taranaki debris-avalanche deposits form a thick, laterally extensive cover of volcaniclastic debris and drape broad areas of the landscape. In medial areas, they display a

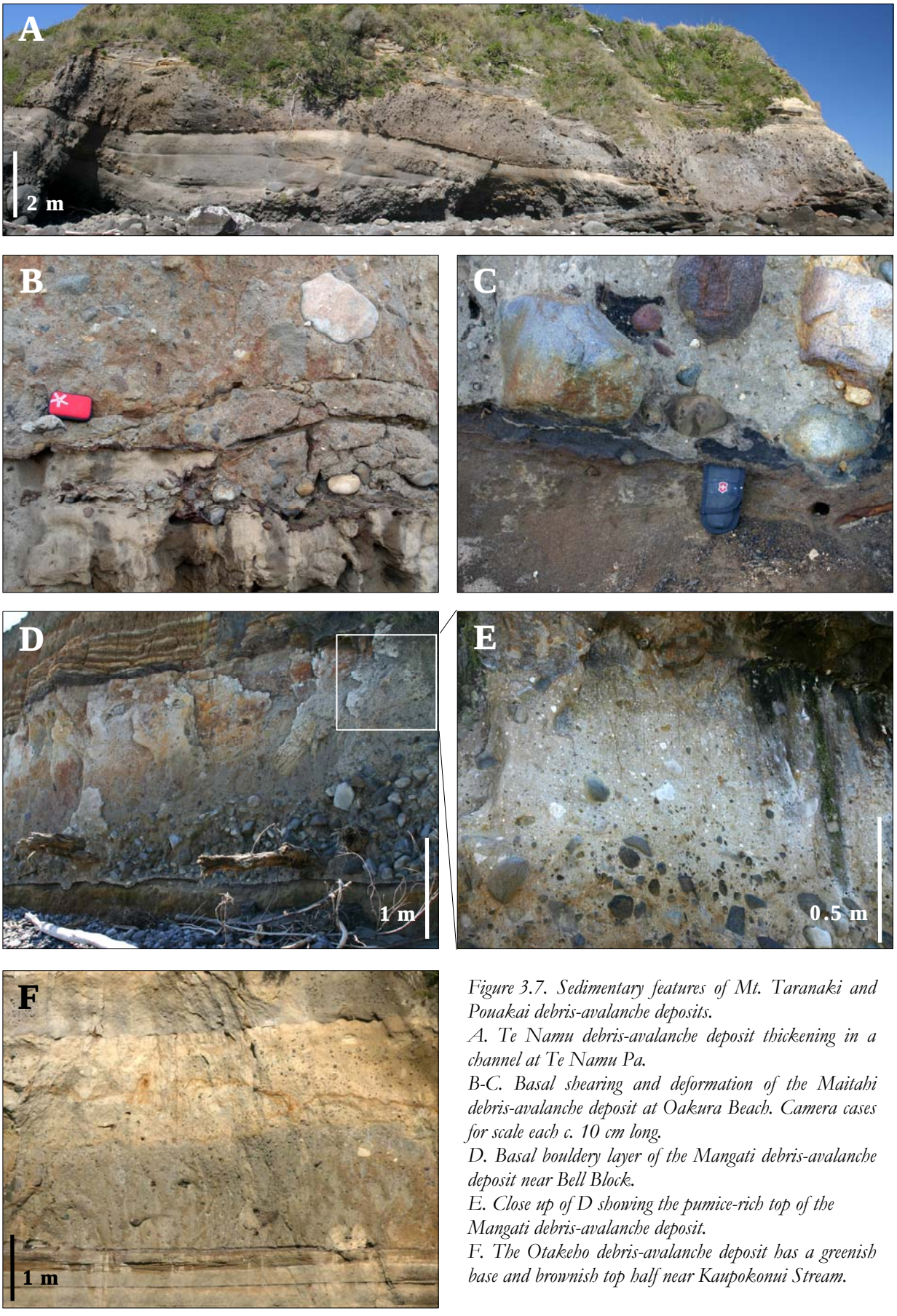

Figure 3.7. Sedimentary features of Mt. Taranaki and Pouakai debris-avalanche deposits.
A. Te Namu debris-avalanche deposit thickening in a channel at Te Namu Pa.
B-C. Basal shearing and deformation of the Maitahi debris-avalanche deposit at Oakura Beach. Camera cases for scale each c. 10 cm long.
D. Basal bouldery layer of the Mangati debris-avalanche deposit near Bell Block.
E. Close up of D showing the pumice-rich top of the Mangati debris-avalanche deposit.
F. The Otakeho debris-avalanche deposit has a greenish base and brownish top half near Kaupokonui Stream.

typically sharp, but non-erosive contact and fill former depressions or channels, resulting in up to 10 m-thick deposits in the central part of the channel (Fig. 3.7A). Evidence of shearing and *in situ* deformation of the underlying strata is rare and was only observed in the Mangati debris-avalanche deposit in north Taranaki (Fig. 3.7B-C).

A distinct basal layer of subangular to mostly rounded cobbles and boulders occurs locally in some deposits (Fig. 3.7D), which may indicate where the debris avalanche incorporated particles from river/stream beds or coastal areas. Many deposits have a basal part that appears greenish-brown in colour, which might reflect a higher content of dark, heavy minerals (ferromagnesian minerals or titanomagnetite) and small mafic clasts in the matrix (Fig. 3.7F) or more likely represents an oxidation/reduction effect. The top half of these deposits is yellow-brownish which contains correspondingly less dense clasts and a higher percentage of lighter clasts and matrix components (Fig. 3.7E).

(i) Granular type debris-avalanche deposits

The granular type is very coarse, polylithologic, very poorly sorted, and non-stratified (Fig. 3.8A). The deposits contain primary and secondary clasts as well as megaclasts in a matrix, which makes up >80% of the deposit and consists of small volcanic fragments and individual crystals from clay-size to very coarse sand (cf. Neall 1979; Palmer & Neall 1991; Alloway et al. 2005). A major primary component are disaggregated clasts, which can be up to 2 m in diameter and range in lithology from fragments of lava flows/domes, scoria and pumice to various types of xenoliths. Larger lava blocks are often fractured and show jigsaw cracks (Fig. 3.8B-C) of different dimensions, some containing matrix (cf. Ui et al. 1986a). Matrix is found to have infiltrated the cracks, indicating that they widened during transport, which allowed matrix to intrude into the developing gaps. This fracturing process gradually split the block into several smaller blocks and isolated clasts (Ui et al. 1986a). The fractured lava blocks are typically clustered and surrounded by smaller monolithologic clasts in the matrix.

Megaclasts were defined by Palmer et al. (1991) as "all components of the deposit >1 m maximum size that are bounded by an outer surface and show an internal lithological homogeneity". Here the term megaclast is size-independent and refers to relatively intact fragments of original edifice strata, which can be strongly brecciated or stratified and are bounded by an outer surface. In the coastal area they range in size from c. 0.2 m to 10 m and rarely up to 50 m (Fig. 3.8D) and include "brecciated clasts" (Fig. 3.8E), i.e. intensely brecciated single rock types <1 m in diameter (Palmer et al. 1991). Most megaclasts, in particular the smaller ones, are rounded and coated by rims that are several cm-thick and consist of finer-

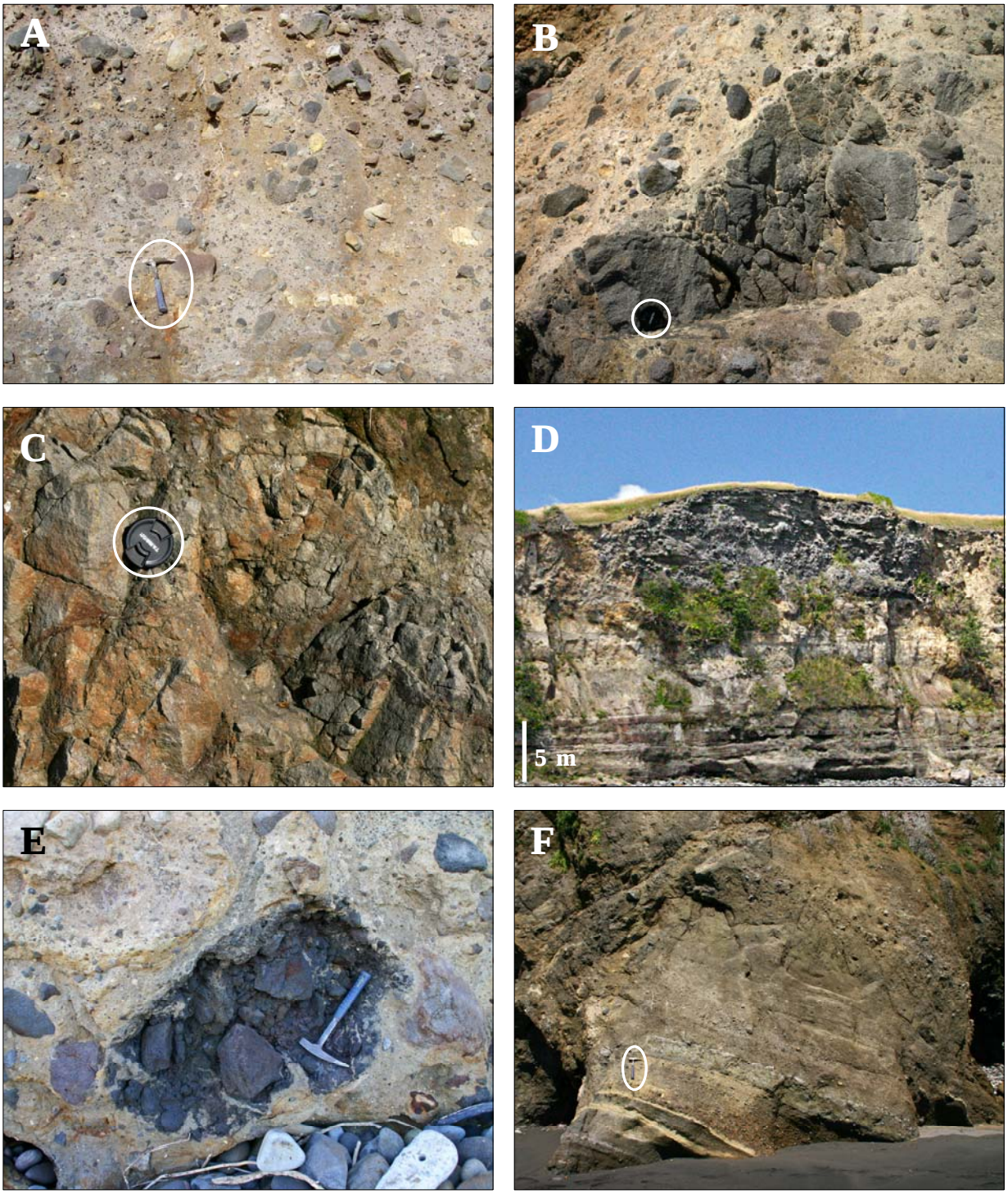

Figure 3.8. Characteristic components of Mt. Taranaki and Pouakai debris-avalanche deposits.
A. Matrix-rich fabric of the Opua Formation with coarse clasts as example of the granular type debris-avalanche deposit (2581607/6195365). Hammer for scale, handle c. 30 cm long.
B. Fractured clast with jigsaw cracks surrounded by clustered clasts of the same lithology within the Maitahi Formation north of Oakura Beach. Camera lens cap for scale c. 5 cm across.
C. Close-up of a fractured block with jigsaw cracks within the Pungarehu Formation. Lens cap for scale.
D. Large brecciated megaclast observed in the Opua Formation close to its main axis of dispersal (2582263/6195130).
E. Small "brecciated clast" within the Maitahi Formation, north of Oakura Beach.
F. Stratified megaclast in the Maitahi Formation, which preserved the original stratigraphy of the edifice (north of Oakura Beach). Circled hammer for scale.

grained inter-clast matrix. Lithologically homogeneous megaclasts composed of brecciated grey to dark grey basaltic andesite or andesite lava are the most common type. The lava is intensely shattered and is fractured into numerous irregular clasts, which range in size from a few mm to tens of cm, forming a characteristic jigsaw pattern (Shreve 1968, Ui 1983, Ui et al. 1986a; Ui et al. 2000). Clusters of smaller brecciated megaclasts of different sizes are often found in proximity to larger ones of identical lithology, indicating that these split up into smaller aggregates during transport. They continue to disaggregate until their fractured components are dispersed as discrete clasts in the matrix (Alloway et al. 2005). Stratified megaclasts that preserve the original stratigraphy and primary layering are rare in the studied medial debris-avalanche deposits. They are more common closer to source and are a significant component of the Axial-A facies (Palmer et al. 1991). They were also observed in coastal outcrops of the Maitahi debris-avalanche deposit (Fig. 3.8F).

With distance from source, the flows incorporated an increasing volume of secondary components during transport (Palmer et al. 1991; Alloway et al. 2005). The most common rip-up clasts are fragments of the underlying strata, including older debris-avalanche, debris-flow and hyperconcentrated-flow deposits, soil and peat beds, tephra layers, fluvial and aeolian sediments, as well as individual subrounded to rounded fluvial clasts (Fig. 3.9A-D). Some debris-avalanche units contain large quantities of entrained branches and tree stumps of a variety of lowland species, reflecting a warm climate and dense vegetation at the time of their deposition. The occurrence of rounded and often strongly deformed ripped-up pieces of mud- and sandstone, typically <1.5 m in diameter, within the oldest units (Motunui and Okawa Formation exposed along the northern coast (Alloway et al. 2005) as well as Waingongoro and Waihi debris-avalanche deposits in the south) indicate that the earliest debris avalanches at least partly travelled across exposed Tertiary substrate (Fig. 3.9E). Fragments of Tertiary rock are absent in the younger units, suggesting that they moved across a progressively thickening volcaniclastic substrate. The granular-type debris-avalanche deposits show interclast matrix-rich axial-B facies close to the axis of distribution and a maximum thickness of c. 8 m, with the exception of the Pungarehu Formation, which exceeds 15 m at medial coastal locations (Palmer et al. 1991).

The lateral transition from axial-B into matrix-supported marginal facies is gradational and marked by a decrease in overall thickness and clast size, an increase of matrix relative to clasts, decreasing abundance and size of primary megaclasts, and an increase in secondary clasts. These run-out debris-flow deposits are up to 4 m thick, have a non-erosive lower contact and a predominantly planar surface with scattered small mounds <2 m high (Palmer et al. 1991), which can be observed in coastal cross sections. They are characterised by >80-90% of allophane-rich

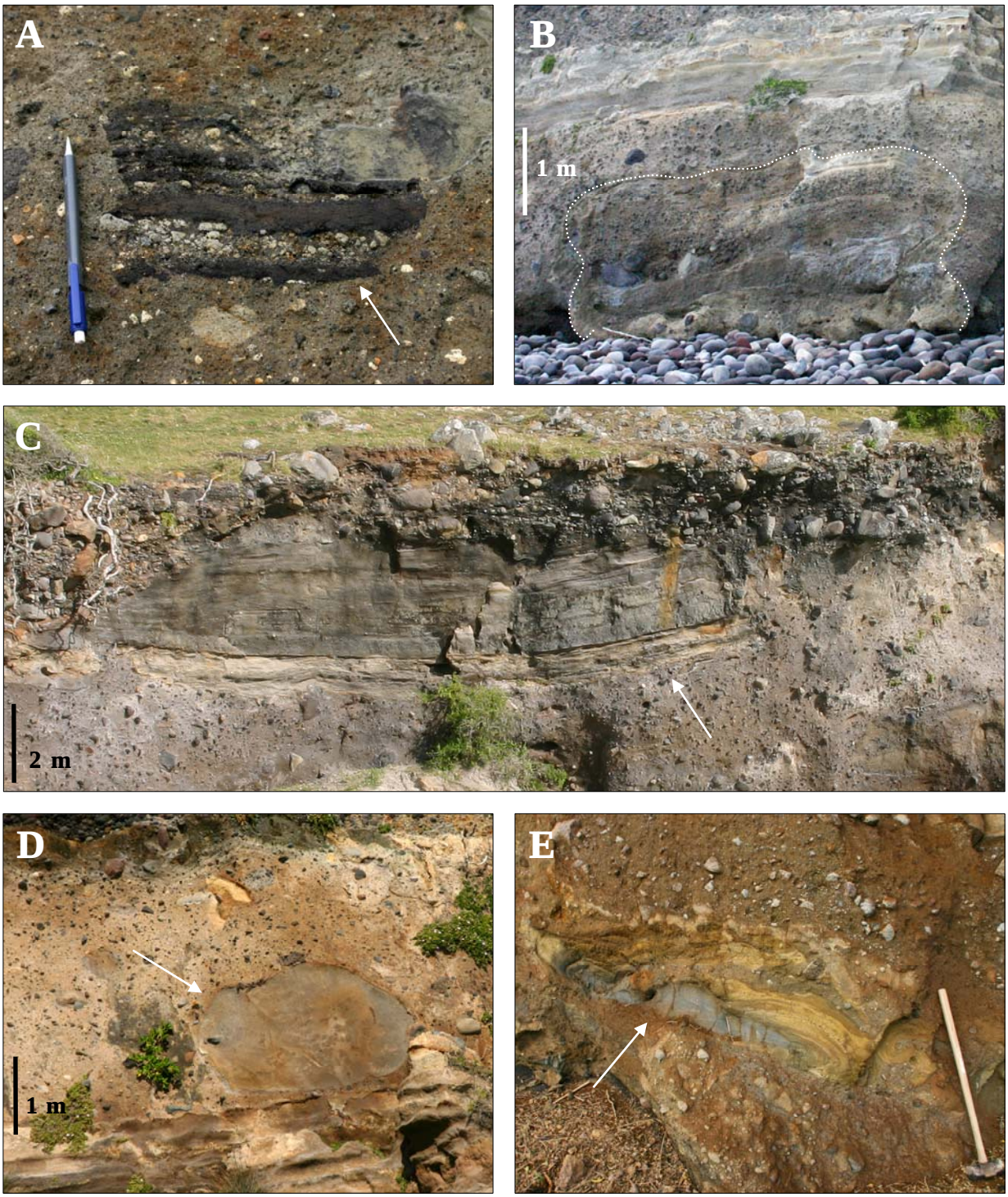

Figure 3.9. Photographs showing examples of rip-up clasts found within Mt. Taranaki and Pouakai debris-avalanche deposits. The most common types consist of soil fragments or peat with intercalated tephra beds (A; Waihi Formation), debris-flow deposits (B; Te Namu Formation), hyperconcentrated-flow deposits (C; Te Namu Formation) and less common fragments of underlying sandstone (D; Rama Formation). Ripped up and deformed pieces of Tertiary mudstone are limited to the older debris-avalanche deposits (E; Maitahi Formation). Pencil in A is c. 15 cm long; sledge hammer handle in E is c. o.8 m long.

matrix that contains disaggregated clasts, rare and smaller megaclasts <2 m and secondary clasts. The most distinctive feature of the marginal lithofacies is the increasing abundance of rip-up clasts compared to primary components. Small fragments, typically <1 m in diameter, of volcaniclastic material, soil/peat (often with interbedded layers of primary or reworked tephra), as well as fluvially subrounded to rounded clasts and wood (when available) are the most common type. Large stratified rip-up clasts made of debris-flow, hyperconcentrated-flow and cross-bedded fluvial deposits can be as much as 100 m across and generally occur at or near the base of the deposit (Palmer et al. 1991). The largest observed rip-up clast in the study area is c. 20 m in length (Fig. 3.9C). Number and size of clasts and rip-up clasts continuously decrease towards the marginal and distal limits of the deposits, until they become a relatively homogeneous mixture of clay-rich matrix and sparser gravel- to sand-sized volcanic particles. The deposits wedge out abruptly at their margins from <0.5 to 0 m within 10 m.

(ii) Cohesive type debris-avalanche deposits

The cohesive type is poorly sorted, polylithologic, and, in contrast to the granular-type, contains small (<5-10 cm in diameter) and completely disaggregated clasts in >95% allophane-rich matrix (Fig. 3.10A). Further components are abundant large logs and wood fragments (Fig. 3.10B) as well as small ripped-up pieces of underlying soil and tephra beds (Fig. 3.10B). Few brecciated clasts and rare, small rounded megaclasts occur (Fig. 3.10C). The deposits are more widespread than the granular type but of relatively constant thickness (typically 2-3 m) with a maximum observed medial thickness of 4 m. In coastal areas, only the marginal facies is exposed, which shows a slight increase in clast abundance and size (15-20 cm in diameter) closer to the main dispersal axis.

3.5.2. Channelised debris-flow and related overbank deposits

Where lahars were confined to pre-existing river channels they formed very coarse, very poorly to extremely poorly sorted, clast-supported, massive deposits with little sandy matrix. These are non-graded, lack internal stratification and often developed a thin matrix-supported base (cf. Scott 1988a; Vallance 2000). Boulders are rounded to angular and can be more than 2 m in diameter (Fig. 3.11A). Large angular-subangular boulders could be derived from older debris-avalanche deposits while the well-rounded clasts were probably picked up from the underlying river bed. Some units grade upward into moderately to poorly sorted, bedded, sandy hyperconcentrated-flow deposits. This has been described elsewhere and interpreted by several authors (cf., Pierson & Scott 1985; Smith 1986; Cronin et al. 2000) as reflecting deposition from the dilute waning stage of the flow. Intercalated lenses of bedded and cross-bedded sands fill

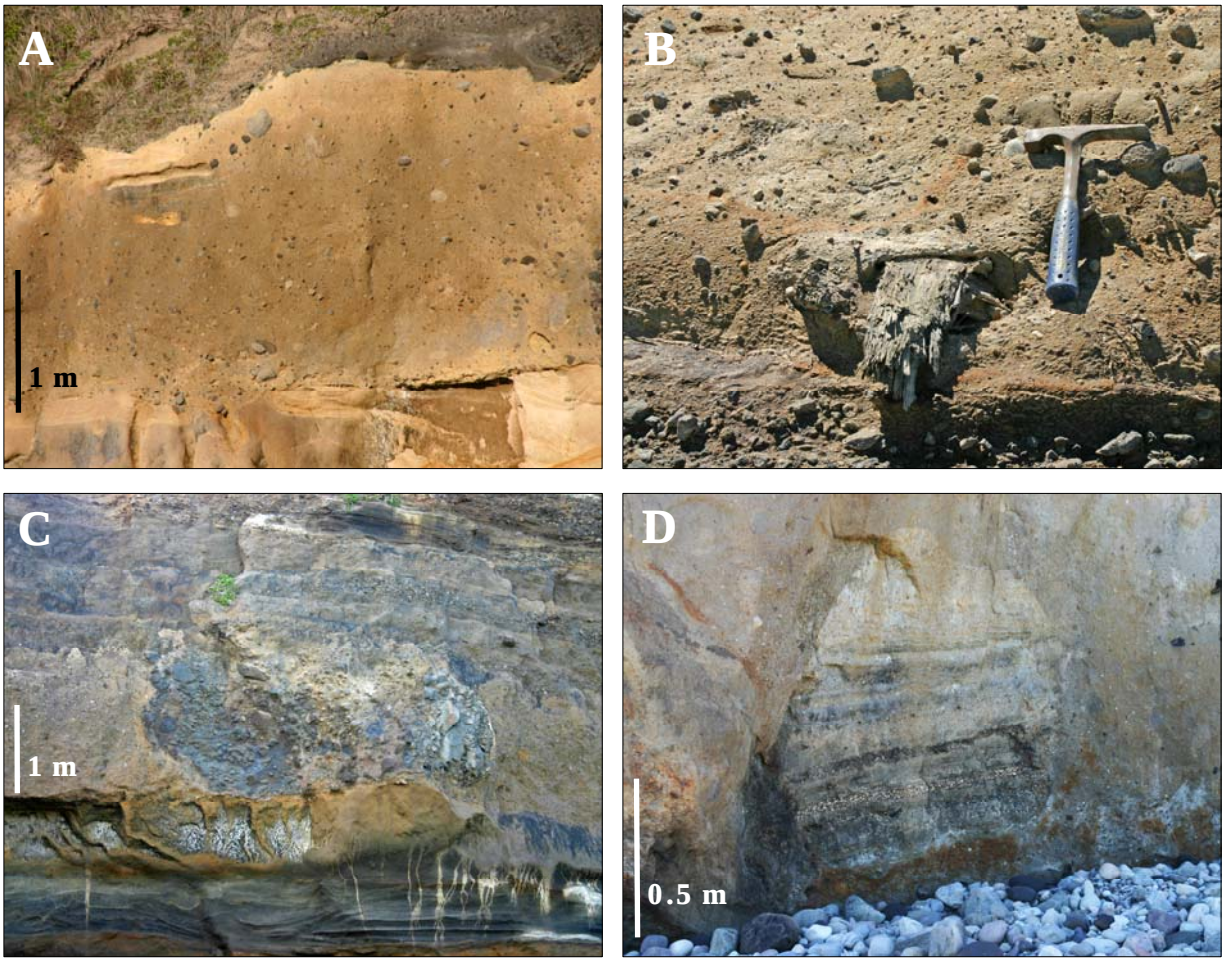

Figure 3.10. Cohesive-type debris-avalanche deposits are characterised by a matrix-rich fabric with only few and relatively small clasts (A; 2588351/6186992). The Otakeho Formation also contains abundant pieces of ripped-up wood up to log-size (B; 2602116/6180599). Megaclasts are rare, considerably rounded and small in size, like this example from the Otakeho debris-avalanche deposit (C; 2587165/6189163). Rip-up clasts are typically small and rounded and are often fragments of peat beds with interbedded tephras (D; 2603489/6180456).

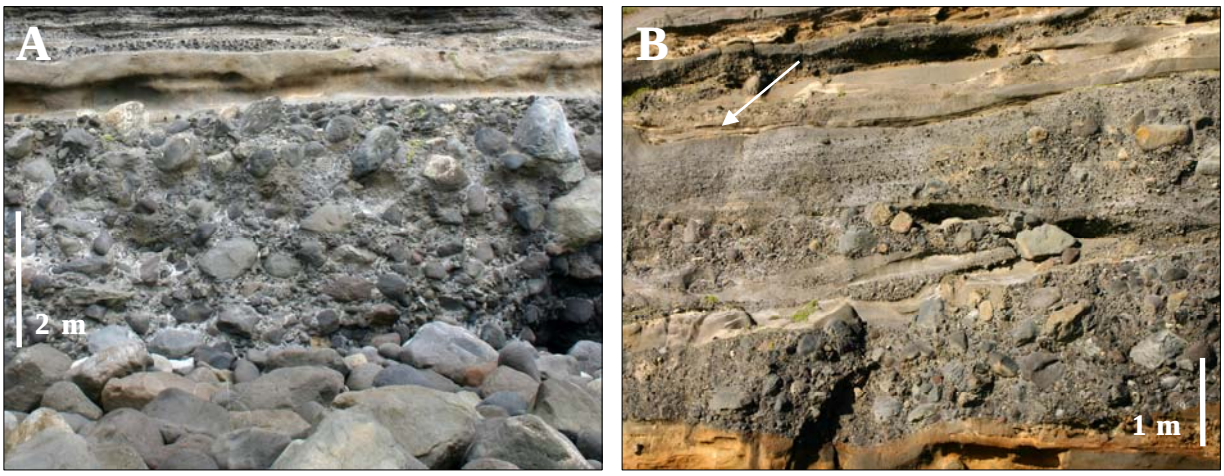

Figure 3.11. Channelised debris-flow deposits are characterised by a clast-supported fabric and large boulders (A; 2582945/6193712). Towards the channel margins they grade into thinner and finer-grained overbank deposits, marked by the white arrow (B; 2588351/6186992).

small surface channels that represent rapid post-depositional reworking of the deposit by fluvial processes. Typically, these channelised debris-flow deposits are lenticular with erosive basal and marginal contacts cut deeply into the underlying and abutting deposits.

Individual units are up to 5 m thick but extend only several tens of metres laterally before grading into thinner, more wide-spread overbank deposits (Fig. 3.11B). These tabular, overbank units drape the substrate with no erosional contacts and extend up to 250 m from the channel margin. They are better sorted than the channel facies and consist primarily of fine pebbly sands. The deposits become progressively finer-grained and better sorted with distance laterally from the channel margins, showing in outer reaches faint internal stratification with thin horizontal or very low-angle cross beds. The polylithologic character of most debris flows suggests that they were not directly produced during eruptive episodes but were probably generated by small collapse events.

3.5.3. Sheet-like hyperconcentrated-flow deposits

Distinct from the lahar overbank facies deposits are more widespread, pebbly sand-dominated tabular units that are interpreted to have been emplaced by hyperconcentrated flows with a wide range of sediment/water ratios and thus diverse flow behaviour. These deposits encompass features such as poor to moderate sorting, reverse-to-normal, normal or no grading, massive appearance to distinct bedding and can be tabular or lenticular with erosive basal contacts. They contain mostly subangular, predominantly monolithologic clasts. Monolithologic pumice and scoria-rich flows (Fig. 3.12A-B) are similar to those generated from remobilised tephra fall following explosive subplinian eruptions (cf., Pierson & Scott 1985; Scott 1988a; 1988b; Dorava & Meyer 1994; Meyer & Trabant 1995; Cronin et al. 1997; Waythomas 1999; Zanchetta et al. 2004; Major et al. 2005). Flows dominated by dense andesite clasts (Fig. 3.12C) appear to represent the reworking of dome-collapse block-and-ash-flow deposits, which are common in the volcanic history of Mt. Taranaki (Platz et al. 2007a). Juvenile breadcrust bombs were observed in only a few hyperconcentrated-flow deposits (Fig. 3.12D). Polylithologic flows (Fig. 3.12E) were probably not directly related to an eruption but represent the run-out of lahars and floods during periods of volcanic quiescence (cf., Zanchetta et al. 2004). The deposits can be traced up to 2.5 km in lateral exposure and thicken in small channels but do not show distinct transitions from confined coarse debris-flow to overbank facies.

Coarser units, produced by sediment-rich, high-competence flows transitional between debris and hyperconcentrated flow often show reverse-to-normal grading. The deposits are typically 0.4-0.6 m and rarely up to 1.5 m thick, consisting of an inversely graded, fine-grained

base and a coarse main body, which grades into a finer-grained top (Fig. 3.13A). The basal unit comprises fine angular to subangular pebbles and sand, can be faintly bedded and is sometimes underlain by a thin (c. 1 cm), well-sorted sole layer of fine to coarse sand. The overlying main part of the deposit is coarse, massive, poorly sorted with angular to subrounded, large pebble to small cobble-sized clasts in a sandy matrix and often shows normal grading into a finer-grained, bedded pebbly sandy top. These characteristics reflect the gradational vertical transition from a basal hyperconcentrated-flow deposit upward to a debris-flow unit (Pierson & Scott 1985; Cronin et al. 1999). The basal layer indicates passage of a watery front-wave with competence increasing over time. The following main body of the flow produces the overlying debris-flow unit. With increasing dilution downstream the basal layer thickens, while the overlying debris-flow portion thins (cf., Scott 1988; Scott et al. 1995). The top part of the deposit can be fine-grained and bedded, representing the transition to more dilute flow and decreasing energy. Typically, a thin silty layer develops on top after deposition due to settling and dewatering of the sediment (cf., Cronin et al. 2000).

Non-graded, poorly sorted, coarse deposits with pebble- to boulder-sized clasts in a sandy matrix also occur and likely represent the most concentrated of these non-cohesive debris-flow/hyperconcentrated-flow deposits (Fig. 3.13B). They lack internal stratification, are tabular and non-erosive, or lenticular with scoured basal contacts. Individual units can be up to 1.7 m thick.

Thinner and finer-grained sediments consisting of pebbly sands are also interbedded. These units are moderately to poorly sorted, show weak grain-size defined bedding on a cm to 20 cm scale (Fig. 3.13C), and commonly contain scattered clasts of cobble and boulder size. The basal contact of these deposits can be erosive or non-scoured. Upward-decreasing grain-size, better sorting and more distinct bedding indicate transition to higher water contents and a lower sediment concentration of the transport medium. The resulting deposits are moderately sorted and show horizontal lamination of fine and coarse sands with the occasional occurrence of isolated pebble- and rare cobble-sized clasts. The deposits are often lenticular with a wavy, erosive base.

Fine-grained, pumice-rich hyperconcentrated deposits can show pumice 'trains" and discontinuous beds of coarser particles aligned parallel to the depositional surface and bedding (Fig. 3.13D). Pebbles transported as bedload, cluster in front of larger clasts that represented a barrier during flow (Fig. 3.13E). The deposits are typically 0.2-0.5 m thick but can be as thick as c. 2 m (faintly bedded coarser units) or 1.2 m thickness (well-bedded fine-grained units).

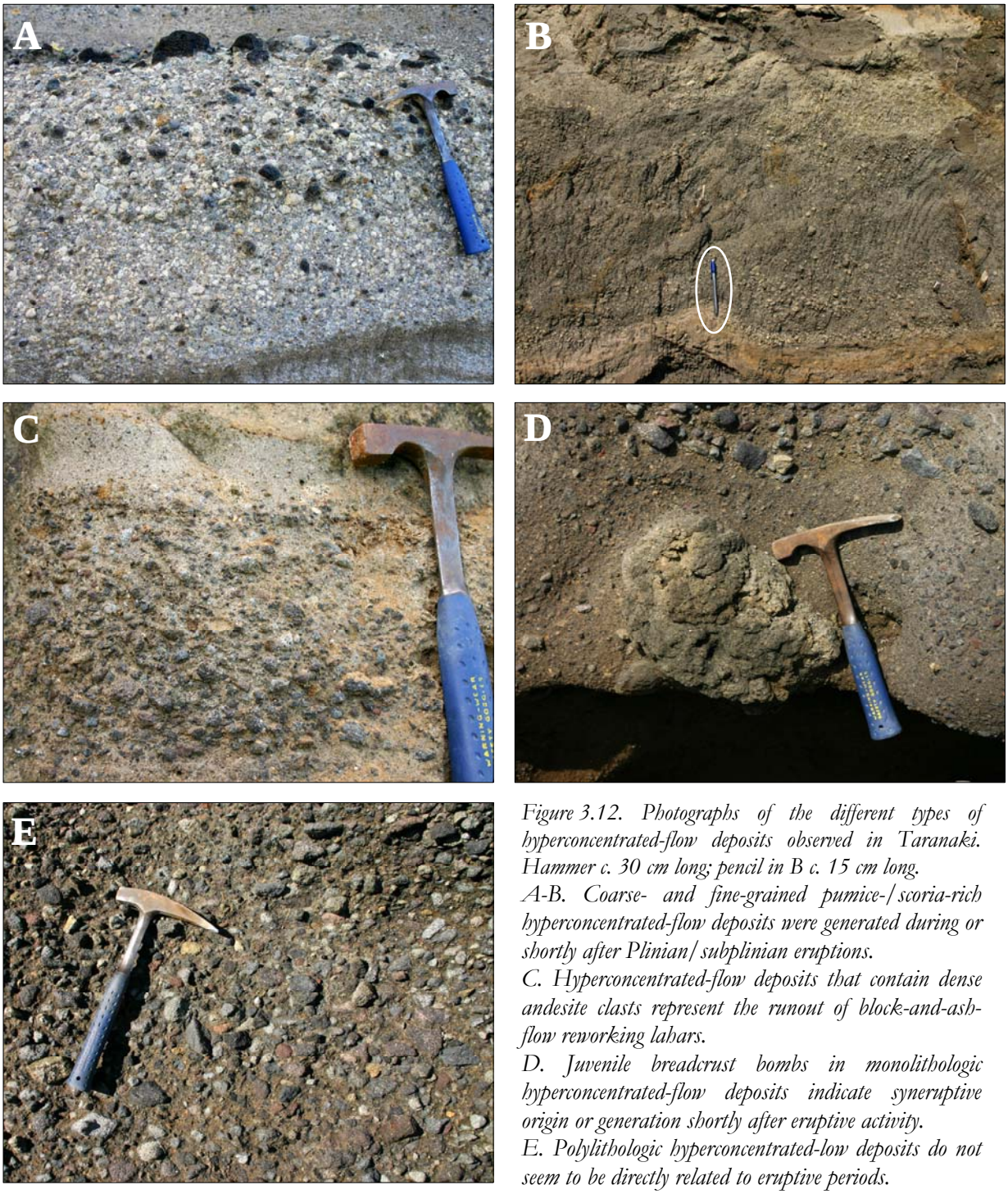

Figure 3.12. Photographs of the different types of hyperconcentrated-flow deposits observed in Taranaki. Hammer c. 30 cm long; pencil in B c. 15 cm long.
A-B. Coarse- and fine-grained pumice-/scoria-rich hyperconcentrated-flow deposits were generated during or shortly after Plinian/subplinian eruptions.
C. Hyperconcentrated-flow deposits that contain dense andesite clasts represent the runout of block-and-ash-flow reworking lahars.
D. Juvenile breadcrust bombs in monolithologic hyperconcentrated-flow deposits indicate syneruptive origin or generation shortly after eruptive activity.
E. Polylithologic hyperconcentrated-low deposits do not seem to be directly related to eruptive periods.

→

Figure 3.13. (next page) Sediment-rich hyperconcentrated flows at Mt. Taranaki emplaced coarse and reverse to normally graded (A) or massive and ungraded units (B), the latter showing transitions to debris-flow deposits. More dilute flows produced bedded, fine-grained hyperconcentrated-flow deposits (C). Pumice trains are common in finer-grained, faintly bedded, pumiceous hyperconcentrated-flow deposits (D). Pebble-sized clasts that were transported as bedload, cluster in front of larger clasts, which represented a barrier during flow (E). Dish and pillar structures (F) and load-induced flame structures (G-H) are common in Mt. Taranaki hyperconcentrated-flow deposits and are produced by post-depositional deformation and dewatering processes. Hammer c. 30 cm long; shovel handle in C c. 1 m long; lens cap in G c. 5 cm across.

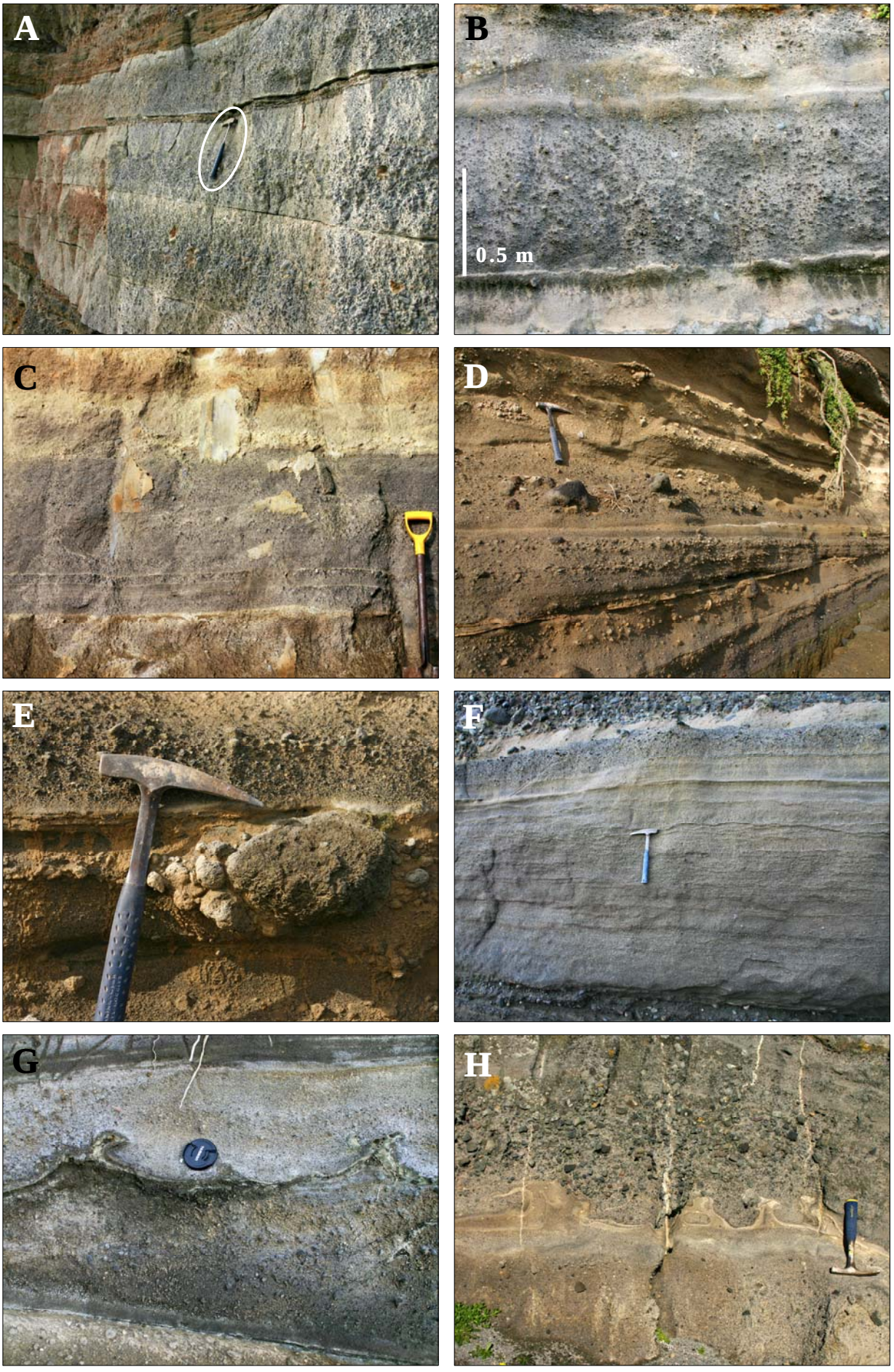
A
B
0.5 m
C
D
E
F
G
H

Post-depositional deformation and dewatering structures are common, such as dish and pillar structures (Fig. 3.13F) and load-induced flame structures (Fig. 3.13G-H). These features indicate that stacks of several units were probably emplaced in rapid succession. Dish and pillar structures form as a result of compaction and subsequent horizontal and vertical dewatering of commonly coarser sandy sediment after emplacement. Dish structures are thin, subhorizontal, flat to concave-upwards silty beds, typically a few mm thick and up to several tens of cm across, while pillars represent vertical fluid-escape paths (Wentworth 1967; Lowe & LoPiccolo 1974; Scott et al. 1995). Flame structures develop due to compression of underlying finer-grained, water-saturated material during and after accumulation of a coarser, sandy layer on top. The overload pushes out water and fine particles that form fingers or wedges ("flames") of sediment. Syn-depositional generated flames are oriented in flow direction while those developed post-depositional typically point upwards.

3.5.4. Transitional hyperconcentrated-flow/ normal streamflow deposits

Deposits representing runout and margins of hyperconcentrated flows are moderate to well-sorted, fine- to coarse-grained sands, typically with low-angle cross-bedding or strongly developed horizontal to wavy bedding (Fig. 3.14A). Lenses of cross-bedded fine sands and rounded pumice lapilli are common. The deposits are lenticular with very erosive basal contacts and often form steep, overlapping channels (Fig. 3.14B). Their thickness ranges from a few cm to 0.5 m.

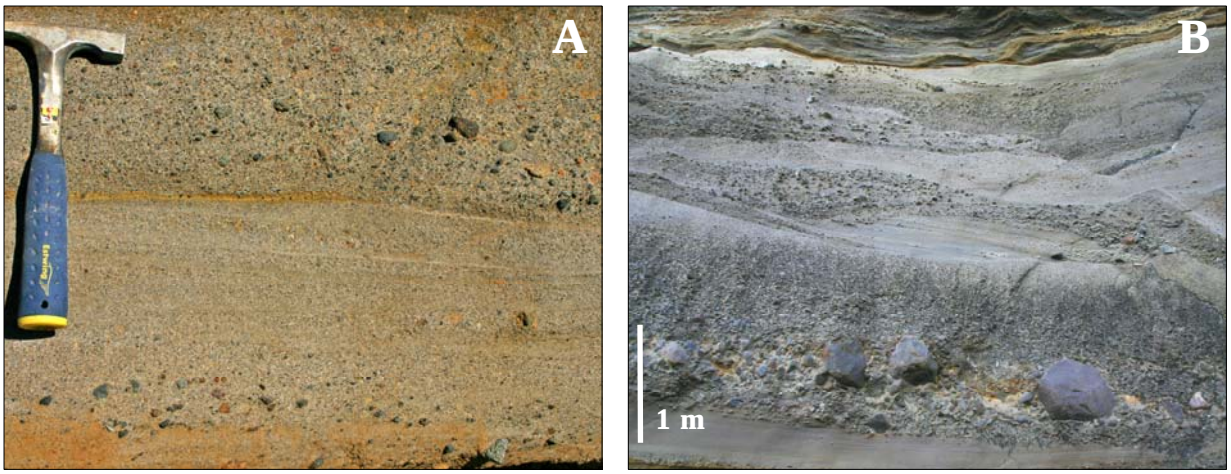

Figure 3.14 Flows transitional between hyperconcentrated flow and normal streamflow produce deposits with laminar bedding (A) or lenticular, cross-bedded units that can often steep channels.

3.5.5. Fluvial deposits

Different types of fluvial reworked equivalents of the volcaniclastic units above also occur in the medial sequences. The most common deposits consist of alternating lenses of well-sorted fine to coarse sands and moderately to poorly sorted, rounded to subrounded pebbles and sands separated by low-angle erosion surfaces (Fig. 3.15A-B). Individual sand beds are typically a few mm to 1 cm thick, while pebble layers are 1 to 10 cm thick. The deposits show horizontal lamination (sands), low-angle cross-stratification and prominent scour-fill cross-bedding. Contacts to the underlying deposits are erosive. The sequences are up to 4 m thick and highly localised in distribution, but can laterally extent up to 150 m. Complex sequences of overlapping channels that cover wider stretches of coastline reflect the locations of larger, long-lived river systems. These accumulated massive, sometimes >10 m thick, aggradational series of more poorly sorted sediments, made up of rounded volcanic clasts ranging from pebble- to boulder-size with intercalated cross-bedded lenses of small pebbles and sand (Fig. 3.15C-D).

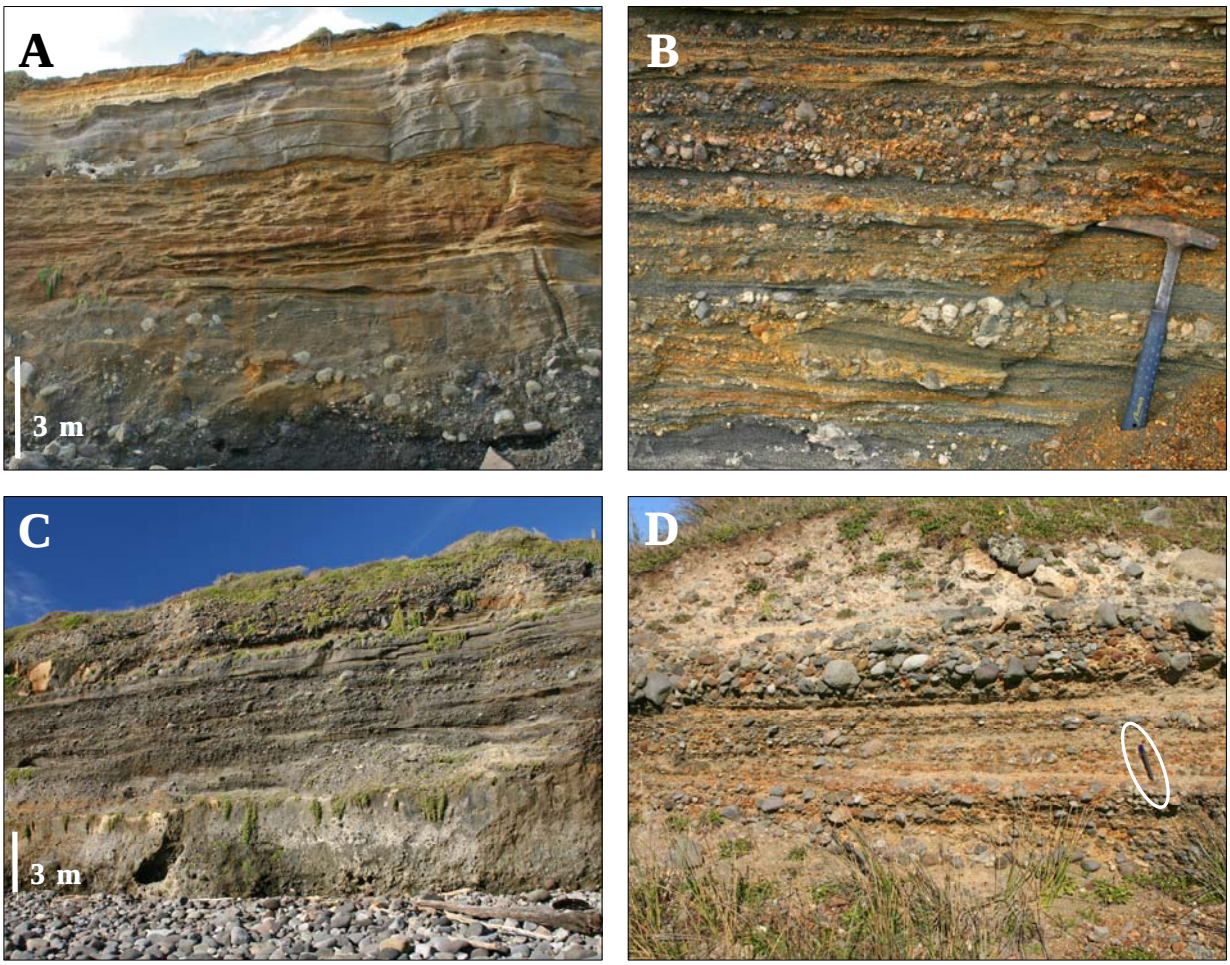

Figure 3.15. Fluvial deposits are common in the Taranaki ring-plain succession and typically consist of cross-bedded lenses of sand and beds of rounded pebbles (A-B). Aggradational river sequences are more poorly sorted and coarser, consisting of pebble- to boulder-sized rounded to subrounded volcanic clasts with intercalated cross-bedded lenses of small pebbles and sand (C-D). Pencil for scale in D is c. 15 cm long.

3.5.6. Aeolian deposits

In some areas, dune sands formed as a result of aeolian redeposition. These consist of alternating thin (0.5-1 cm) beds of dark grey, very well-sorted fine sands that are rich in dark, mafic, heavy minerals (i.e. ferromagnesian and titanomagnetite minerals) and thicker (up to 2 cm) beds of coarser, light yellow to brownish, well-sorted sands (Fig. 3.16A). Individual sets of dune sands are tens of cm to c. 1.5 m thick and show planar or high-angle cross-stratification (Fig. 3.16B). They form sequences that can be more than 12 m thick and are typically interbedded with thin (5-10 cm thick) organic-rich peat layers or iron-stained, weakly developed tephric soils as well as a number of sandy, often pumiceous hyperconcentrated sheet-flow deposits. Intercalated coarser beds of rounded, reworked pumice lapilli indicate rapid saltation and redeposition of these pumice-rich deposits within this area of aeolian reworking. Aerially exposed volcaniclastic and fluvial deposits provided further source material for dune sand formation.

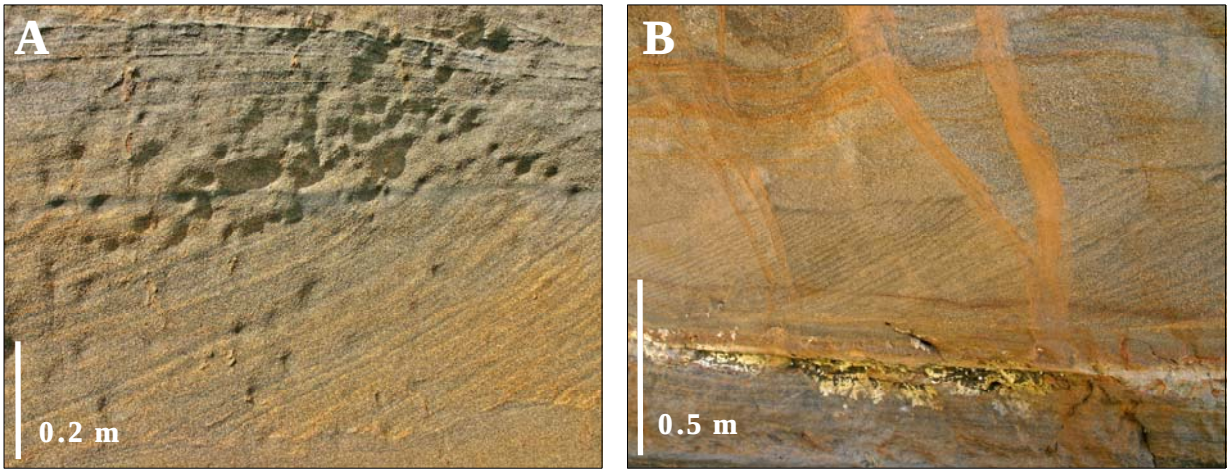

Figure 3.16. Paleo-sand dunes within the ring-plain succession consist of alternating thin beds of dark grey, very well-sorted fine sands and thicker beds of coarser, light yellow to brownish, well-sorted sands (A). They form sequences of >12 m thickness with individual sets of dune sands typically being tens of cm to c. 1.5 m thick and showing planar or high-angle cross-stratification (B).

TABLE 3.1. *Sedimentary characteristics and distinction criteria of different types of observed volcanic mass-flow, fluvial and aeolian deposits.*

Deposit type	Sedimentary characteristics	Contacts and geometry
Cohesive debris-flow deposits	Matrix-supported Pebble- to boulder-sized clasts in a clay-rich matrix Extremely poorly to very poorly sorted Massive, unstratified Typically ungraded, some deposits with coarse basal layer Shattered and fractured clasts, brecciated and stratified megaclasts, rip-up clasts, ripped-up wood Typically 4-6 m thick, maximum up to 10 m thick	Non-erosive, draping of irregularities Unconfined fan
Non-cohesive debris-flow deposits	Matrix-supported Pebble- to boulder-sized clasts in a sandy matrix Very poorly to poorly sorted Massive, unstratified Ungraded or reverse-to-normal grading Typically 0.4-0.6 m but up to 1.7 m thick Deposits often reflect transformation of debris to hyperconcentrated flow: they consist of an inversely graded, fine-grained layer with horizontal fabric and a coarse, massive, poorly sorted breccia unit that grades into a finer-grained, bedded top part	Typically tabular, non-erosive, some lenticular with scoured basal contacts
Channelised debris-flow	Clast-supported with little sandy matrix Very coarse, pebble to boulder-sized clasts Very poorly to extremely poorly sorted Massive, lack of internal stratification but often show a thin matrix-supported base Non-graded Up to 5 m thick Often upward transition to bedded, sandy deposits with weak horizontal fabric (hyperconcentrated flow) Intercalated lenses of cross-bedded and well sorted sands (fluvial) due to rapid post-depositional reworking	Erosive basal and marginal contacts Channel-confined, several tens of metres wide, lateral transition to overbank deposits
and associated overbank deposits	Fine pebbly sands but coarser near channel, occasional outsized clasts Poorly sorted near channel, becoming moderately to well-sorted with distance from channel margins Faint internal stratification near channel, becoming progressively more distinct with thin horizontal and often very low-angle cross beds near the deposit margin Ungraded Up to 2 m thick but pinch out over 20 to 250 m from the channel margins	Non-erosive Wedge-shaped, extend up to 250 m from channel margins

TABLE 3.1. continued. *Sedimentary characteristics and distinction criteria of different types of observed volcanic mass-flow, fluvial and aeolian deposits.*

Deposit type	Sedimentary characteristics	Contacts and geometry
Sheet-like hyper-concentrated-flow deposits	Pebbly sands, isolated pebble- to cobble-sized clasts, predominantly monolithologic components Poorly to moderately sorted Massive or bedded Reverse-to-normal grading, normal grading or no grading Typically 0.2-0.5 m thick, up to 2 m faintly bedded coarser units, up to 1.2 m well-bedded fine-grained units Occurrence of occasional outsized clasts, pumice 'trains" and aligned clasts Post-depositional deformation and dewatering structures (flame and dish and pillar structures)	Typically non-erosive, more dilute units lenticular with erosive basal contacts Sheets, up to 2.5 km wide
Transitional hyperconcen-trated flow / streamflow deposits	Fine- to coarse-grained sands Moderately to well-sorted Horizontal bedding to low-angle cross-bedding, lenses of cross-bedded fine sands and pebbles Ungraded Few-cm to 0.5 m thick units	Erosive, wavy basal contacts Lenticular, often steep, overlapping channels
Normal streamflow deposits	Clast-supported Fine to coarse sands, sands and rounded pebbles, pebble- to boulder-sized rounded clasts Well to moderately sorted in individual beds, poor sorting of aggradational deposits Horizontal lamination of sands, low-angle cross-stratification and prominent scour-fill cross-bedding of alternating thin lenses (few mm to 1 cm thick) of well-sorted sands and beds (1 to 10 cm thick) of moderately to poorly sorted pebbles and sands Massive to faintly bedded aggradational sequences of silts and sands with intercalated cross-bedded lenses of fine pebbles and sand Up to 4 m-thick sequences of alternating sandy and pebbly beds, >10 m thick aggradational series	Erosive Lenticular Complex sequences of overlapping channels up to 150 m wide
Aeolian deposits	Grain-supported Fine dark grey and coarse light yellow to brownish sands Well to very well-sorted Planar or high-angle cross-stratification of alternating thin (0.5-1 cm) beds of fine sands and thicker (up to 2 cm) beds of coarser sands Tens of cm to c. 1.5 m thick individual sets of dune sands, sequences up to 12 m thick	Non-erosive Extensive sand dune fields

3.6. LITHOFACIES ASSOCIATIONS OF VOLCANICLASTIC DEPOSITS

Medial ring-plain sequences are built of at least six different lithofacies elements that correspond to a range of transport and emplacement modes as well as various depositional environments.

3.6.1. Debris avalanche-dominated sequences

The gently dissected, flat nature of the ring plain around Mt. Taranaki resulted in relatively unconfined, very thick, laterally extensive debris-avalanche and related debris-flow deposits that buried large areas. Emplacement of these changed the focus of sedimentation dramatically, with subsequent deposition focussed to the lateral margins of these landscape-forming deposits. Hence sequences of stacked debris-avalanche and debris-flow units are formed with little accumulation of other deposits between them, apart from tephric soils and peat beds (Figs. 3.17 and 3.23A). The collapse events also significantly modified the pre-existing drainage system, with debris-avalanche units burying older river systems represented by underlying fluvial and channelised lahar deposits. Re-establishment of the drainage system is indicated by deep channels that were cut into and beside the avalanche deposits (Fig. 3.18) (cf. Procter et al. 2009). These accumulated coarse reworked material from the debris-avalanche units as well as being partially filled by later debris-flow deposits. Smaller stream systems reworked the surface of the avalanche to produce minor localised cross-bedded fluvial gravels and sands

3.6.2. Paleochannel-systems

Ring-plain locations record a network of separate and overlapping, laterally migrating paleo-channels that were repeatedly infilled. The channels were cut by rivers and streams as sometimes indicated by cross-bedded fluvial deposits at their base. They provided major flow paths for coarse, voluminous debris flows, which in most cases eroded the fluvial and underlying deposits and filled the central channel area. The sequence typically consists of several coarse, massive, poorly sorted debris-flow units that are separated from each other by unconformities. These are filled with thin cross-bedded lenses of sand and represent reworking by fluvial processes between lahar events. The central channel area can be as thick as 10 m but typically extends only 15-60 m laterally (Fig. 3.19). The lateral transition from channel area to floodplain is marked by a change into thinner, more-fine-grained, tabular hyperconcentrated-flow deposits. Vertically, the sequences fine upwards to a series of thin hyperconcentrated-flow deposits emplaced in shallow, broad channels (Fig. 3.23B). Interbedded fluvial sediments represent local re-establishment of paleo-streams and fluvial reworking.

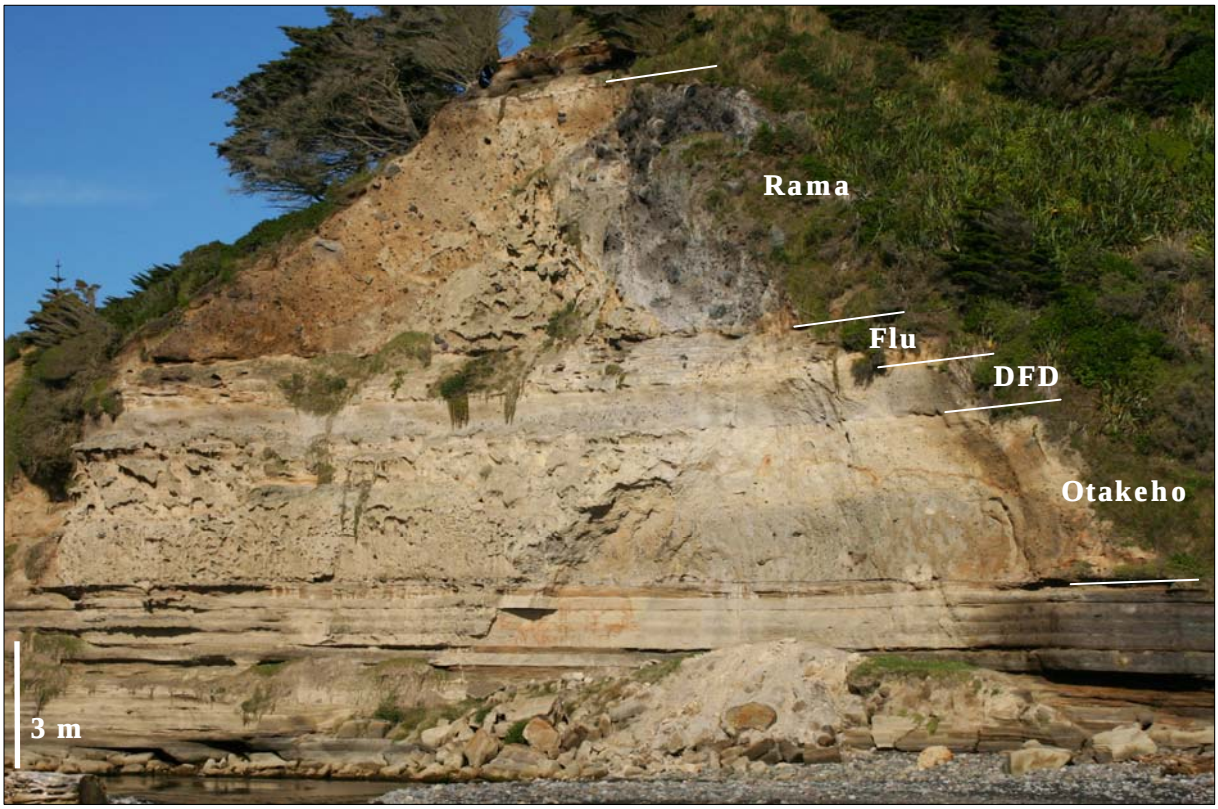

Figure 3.17. Sequence of stacked debris-avalanche (Rama and Otakeho) and debris-flow (DFD, unnamed) units at Kaupokonui 1 with little fluvial accumulation (Flu) between events.

Figure 3.18. Cliff section at Middleton Bay 3, which contains the Opua Formation near the top and the Ihaia debris-flow deposit at the bottom of the cliff. Channels were cut into the Pungarehu (Pu) and Te Namu (TN) debris-avalanche deposits and subsequently filled by debris-flow, hyperconcentrated-flow and fluvial deposits.

3.6.3. Sequences dominated by sheet-flow deposits

Hyperconcentrated-flow and transitional hyperconcentrated-/debris-flow facies associations are an important architectural element in broad flat interfluve areas of medial ring-plain locations. They occur as single depositional units of varying thickness or as a massive series, forming sequences up to 15 m thick (Fig. 3.20). Their wide range of sedimentary characteristics is a result of relatively minor variations in sediment concentration, volume and lithology of the depositing flow. Short breaks in volcaniclastic sedimentation are characterised by tephric soil and/or peat formation and localised fluvial deposition in paleo-stream locations (Fig. 3.23C). These tabular hyperconcentrated-flow deposits can be traced over lateral distances of up to 2.5 km. In other cases erosional surfaces and deep channels give them a seemingly lenticular appearance. Their unconfined, sheet-like distribution is related to the relief of the ring-plain, i.e. mostly infilled, shallow stream beds and wide coastal plains with broad terraces.

3.6.4. Fluvial facies associations

Fluvial deposits occur throughout all successions, representing periods of stream and river reworking and re-establishment (Figs. 3.21 and 3.23C.). They are typically highly localised and show bedding features that represent at least two different settings. The first is more common and characterised by relatively thin bedding, low relief of scours and low amplitude of cross-stratification, which suggests deposition by shallow, rapid streamflow in broad, braided channels (Smith 1987b). The stream channels in Taranaki are typically shallow but of relatively small lateral extent. Thicker aggradational series of mostly horizontally bedded fluvial gravel and sand are rare and steadily accumulated in deeper, wider river channels.

3.6.5. Sequences dominated by dune sands

Cross-bedded aeolian sands occur as sequences >12 m thick (Fig. 3.23D) and are exposed over a wide stretch of coastline (>15 km). In some areas they are interbedded with thin (<0.5 m thick) single or multiple volcaniclastic mass-flow deposits or localised fluvial sediments (Fig. 3.22). The dune sands accumulated during cool as well as mild climates indicated by different types of intercalated paleosols, i.e. tephric soils as well as peat beds between c. 50 ka to >80 ka. It is, thus, unlikely that they correspond to an earlier period of cold-climate aeolian redeposition such as the Katikara Formation that accumulated on the Pouakai ring plain in north Taranaki at the end of the Last Glaciation (Neall 1975; Alloway 1989).

Instead, the sand dunes are thought to have formed in a relatively undisturbed near-coastal environment as they are similar in extent and characteristics to present-day near-shore

Figure 3.19. Deposit sequence of a central channel area filled by coarse debris-flow and finer-grained hyperconcentrated-flow deposits towards the top (2583809/6193200). The coarser channel fill grades into finer-grained overbank deposits near the channel margins.

Figure 3.20. Cliff section (2584600/6192713) dominated by stacks of coarse- and fine-grained hyperconcentrated-flow deposit. Persons for scale.

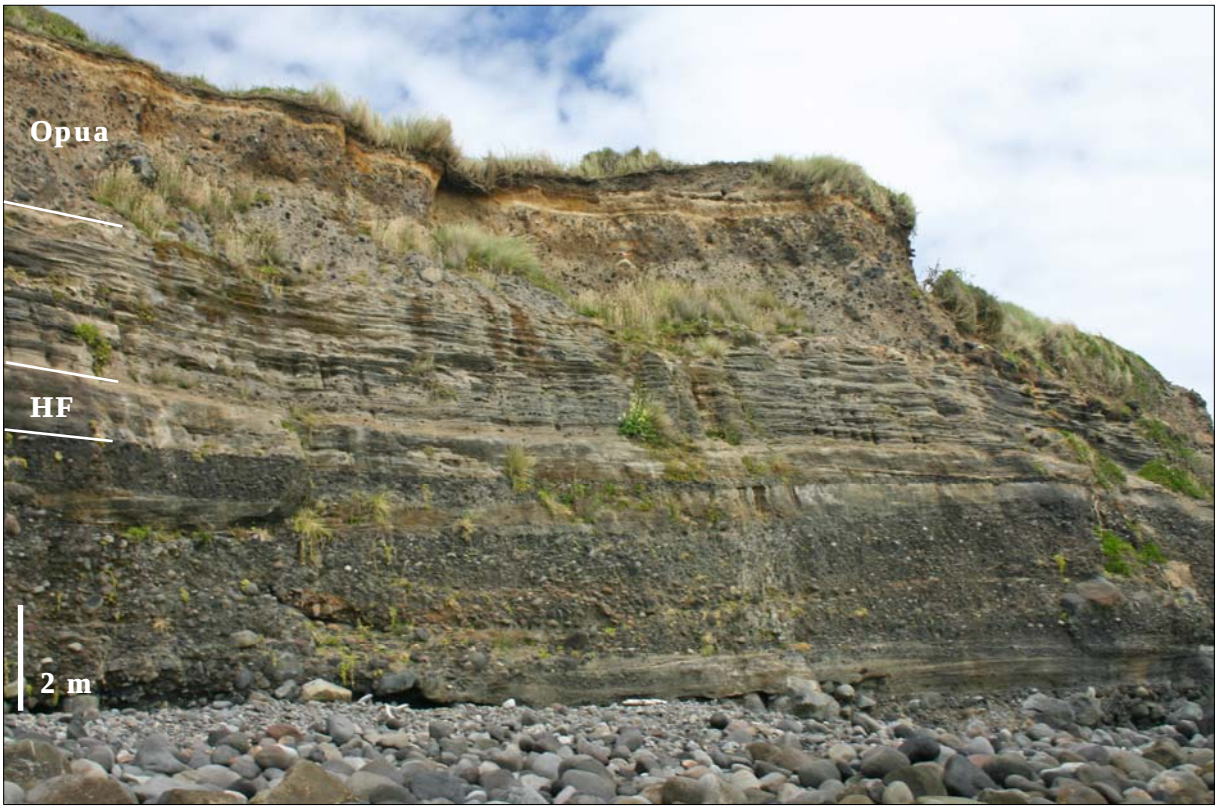

Figure 3.21. Fluvial deposit sequence characterised by aggradational, coarse sediments in the bottom half that are separated from overlying cross-bedded fluvial gravels and sands by several thin hyperconcentrated-flow deposits (HF). The cliff section (2583002/6193993) is capped by the Opua debris-avalanche deposit.

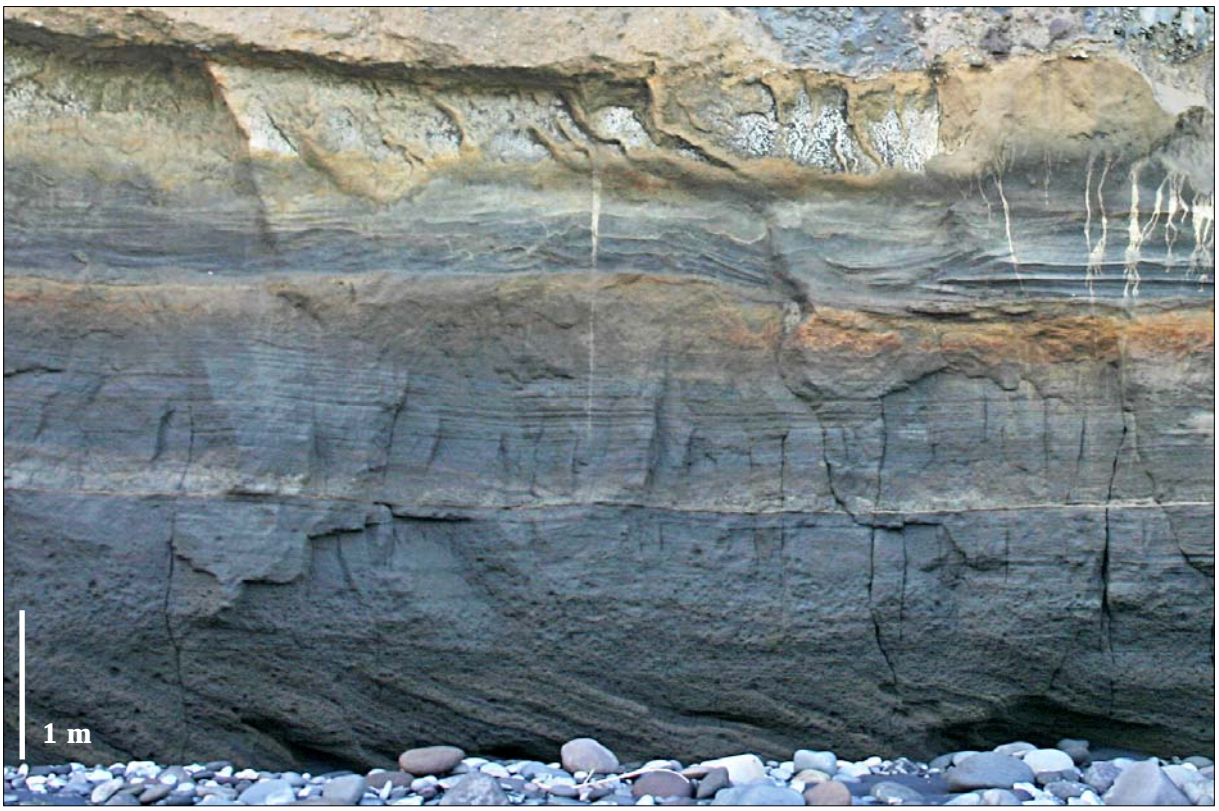

Figure 3.22. Deposit sequence dominated by several sets of cross- and planar bedded grey dune sands (2587165/6189163). Here, no paleosols formed within the sequence but some layers are characterised by weathered iron-stained tops.

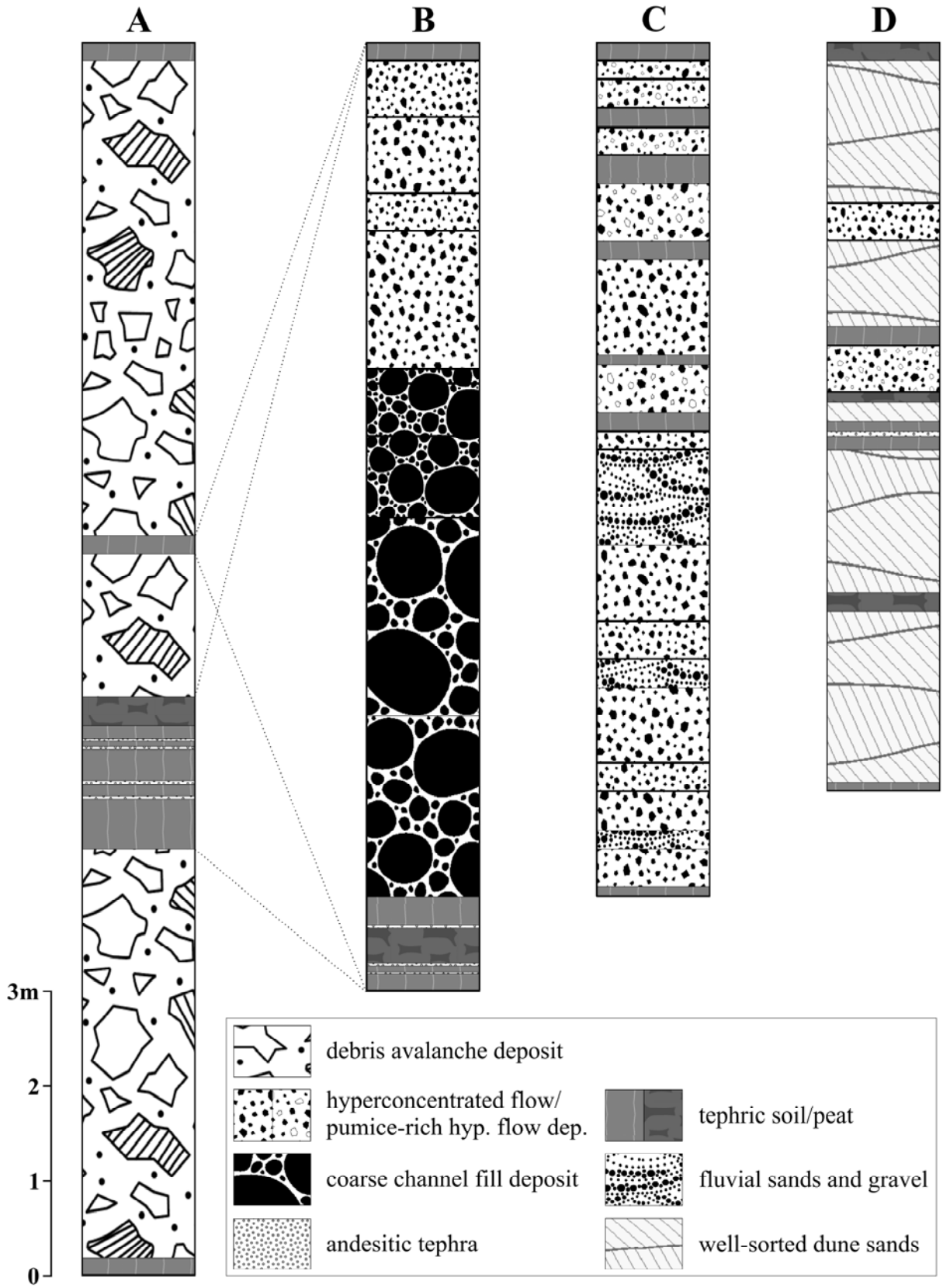

Figure 3.23. Stratigraphic columns of the different types of lithofacies associations occurring in the Taranaki ring-plain succession: debris-avalanche dominated sequence (A), channel system capped by hyperconcentrated-flow deposits (B), series of sheet-like hyperconcentrated-flow deposits with interbedded fluvial sediments (C) and sequence of dune sands with interbedded peat layers or sandy paleosols (D). Lithofacies elements B-D are typically found between debris-avalanche deposits, indicating different types of deposition between collapse events (as indicated by the dotted lines between A and B).

dune fields, indicating the presence of the paleo-strandline nearby. The assumed maximum age of the dune sands of just over 80 000 years correlates well with the high sea level that cut the Hauriri Marine Terrace in south Taranaki (Pillans 1983). At its type section south of Waverley, the coverbeds of the Hauriri wave-cut platform are c. 7.5 m thick and comprise a shelly conglomerate, overlain by laminated sand and silt, andesitic sandy conglomerate, c. 2 m massive grey tephric loess and c. 2.5 m andesitic sand with cross-beds (Pillans 1990). The observed dune sands in south-west Taranaki are most likely equivalent to the upper, terrestrial part of the described coverbeds, while the laminated sands and shellbed were deposited in a marine environment most likely a few hundred metres to several kilometres offshore of the present coastline.

3.6.6. Paleosol- and peat-dominated sequences

Paleosol-dominated stratigraphic intervals represent areas with relatively low sedimentation rates and periods of landscape stability. Soil development is faster than the rates of erosion, indicated by sequences made of alternating volcaniclastic deposits and preserved paleosols (cf. Zanchetta et al. 2004). These sequences are characterised by accumulation of thick layers of medial ash or peat and the preservation of (typically <2 cm) thick tephra beds (cf. Section 3.7, Fig. 3.25). Paleosols formed under cold climate conditions are developed within volcanic loess with intercalated thin, discrete tephra beds reaching up to 2.5 m thickness. Peat-dominated sequences up to 1.5 m thick formed in areas of poor drainage and are intercalated with medial ash and tephras. In some areas, the soil formation process is interrupted by infrequent emplacement events of single debris-flow or hyperconcentrated-flow units.

3.7. INFLUENCE OF PREVAILING CLIMATE CONDITIONS ON DEPOSIT CHARACTERISTICS

The extreme climate changes of the last 130 ka had a major impact on landscape development in New Zealand (Newnham et al. 1999). Periods of cold climate were characterised by seasonal frozen ground and the formation of glaciers in the Southern Alps (Porter 1975; Hellstrom et al. 1998) while periglacial conditions were dominant in the North Island. Here, only small areas were enveloped by glaciers. Instead, fluvial and wind erosion led to accumulation of thick alluvial sequences, aggradation of river terraces and deposition of loess (Suggate et al. 1978; Nelson et al 1988; Eden 1989; McArthur & Shepherd 1990; Alloway et al. 1992; Pillans et al. 1993; Palmer & Pillans 1996). Warm periods were marked by landscape stabilisation, river down-

cutting, soil development and the formation of marine terraces along the New Zealand coast due to glacioeustatic sea-level changes (Pillans 1983, 1988, 1990a, 1990b; Palmer 1987). These tectonically uplifted marine terraces are best developed in the south Taranaki-Wanganui coastal plain, where they run roughly parallel to the present coastline, rising to more than 300 m above present sea level and extending 20 km inland (Pillans 1983). Two terraces, NT1 and NT2, in the coastal sections of North Taranaki are correlated to the 100 ka Inaha (Neall & Alloway 2004) and the 127 ka Rapanui (Chappell 1975) Marine Terraces of south Taranaki, respectively (Dickson 1974; Pillans 1983, 1990). These represent important surfaces that allowed the approximate dating of the Motunui and Okawa debris-avalanche deposits (Alloway 1989; Alloway et al. 2005).

The present day climate in Taranaki changes from mild to warm-temperate conditions in coastal areas to a cooler inland region with higher rainfall, common frosts and fogs. Winds become stronger with elevation and are predominantly westerly. Annual rainfall ranges from 900-1600 mm but increases with altitude to about 8 000 mm above 2 000 m (Coulter 1976; Newnham & Alloway 2004). The climate pattern results in a distinct zonation of the vegetation from coast to summit with coastal forest up to 1 km inland, semicoastal forest up to 10 km inland and 150 m altitude, lowland forest up to 760 m, montane forest up to the treeline at 1050 m grading into subalpine shrubland up to 1280 m, a transitional shrubland-tussockland zone, and alpine tussockland from 1400 m (Druce 1970; Bayfield & Benson 1986; Newnham & Alloway 2004).

Pollen records suggest similar warm and moist conditions occurring during the last Interglacial around c. 127 ka (MISS 5e) with dense and extensive podocarp-angiosperm forest and beech forest farther inland (cf. Fig. 3.24) (Newnham & Alloway 2004). Oxygen isotope records of MISS 5d-5a show strong climate oscillations as the global climate deteriorated. MISS 5d and 5b were characterised by a cool climate, which caused the decline of podocarp-angiosperm forest and the expansion of low-growing shrubland-grassland with sparse woody vegetation (McGlone et al. 1984). MISS 5d represented cool and moist conditions while MISS 5b was considerably drier with incomplete vegetation cover and widespread erosion (McGlone et al. 1984; Newnham & Alloway 2004). MISS 5c and 5a conditions were warmer and moister, resulting in a decline of shrubland and the propagation of lowland podocarp forest. The high sea level stand during MISS 5c resulted in the formation of the Inaha Marine Terrace (McGlone et al. 1984) while the Hauriri Marine Terrace was cut at c. 80 ka during MISS 5a (Pillans 1983, 1990; Alloway 1989). Fully forested conditions are recorded in the Manaia Lignite and reflect significant warming during MISS 5a (McGlone et al. 1984). The assemblage of several tephra beds and overlying zones rich in pollen of seral shrubs and trees that are known to rapidly colonise fresh volcanic surfaces indicate a strong volcanic impact on the vegetation during that period

(Newnham & Alloway 2004). The occurrence of pieces of charcoal, two distinct charcoal layers and several tephra beds in the record of late MISS 5a indicate a period of environment instability with fire-ravaged vegetation possibly as a consequence of volcanic activity, lightning and frequent drought (McGlone et al. 1984; Newnham & Alloway 2004). The transition to MIS 4 began with a short dry period followed by harsh cool and moist stadial conditions with episodes of severe erosion. Conditions during interstadial MIS 3 were mild, leading to a partly forested landscape. The period around 40-30 ka was one of the wettest and warmest during the Last Glacial as recorded in pollen assemblages (McGlone et al. 1984) of the Hihiwera Peat. Conditions become colder and drier towards MIS 2. The Last Glacial Maximum (25-14 ka) was characterised by a cold and dry climate with widespread erosion along all stream channels draining the Pouakai Range (McGlone 1996) as well as widespread aeolian redeposition of tephras (Katikara Formation) (Neall 1975). Conditions during the late glacial (14-10 ka) become increasingly warmer and wetter with progressive afforestation and landscape stabilisation (McGlone et al. 1996). At c. 13.1 ka, grassland-shrubland and *Prumnopitys taxifolia*-dominated forest indicates cold and dry late-glacial climate with a shift to warm and moist climate from 12.9 to 11 ka (Alloway et al. 1992; McGlone & Neall 1994). In most sectors of the ring plain, the Okato Tephra (Neall 1979) is conformable with the present-day surface, indicating subsequent widespread stability on the flanks of the Taranaki volcanoes since c. 12.5 ka (McGlone 1996), with the exception of the Opua and Kahui events.

Climate and local weather strongly influence the nature of accumulation on volcaniclastic fans (e.g. Palmer et al. 1993; Davidson & De Silva 2000; Zanchetta 2004) because precipitation regimes control the rates of erosion, soil development, sediment yield in catchments and redistribution of volcanogenic material (e.g. Dorn et al. 1987; Frostick & Reid 1989; Ritter et al. 1995; Lavigne & Thouret 2002; Lavigne 2004; Zanchetta 2004; Scott et al. 2005; van Westen & Daag 2005). Vegetation type and growth as well as soil development play an important role for the stability of the landscape and depend on style (duration and intensity of rainfalls or amounts of snow accumulation) and amount of meteoric precipitation (Zanchetta 2004). Moist and mild or warm climate during interstadial and interglacial periods favour soil formation and forest vegetation, which leads to partial stabilisation of loose volcanic and volcaniclastic material. The sediment is stored on the edifice and the surrounding ring plain until periodically removed by mass-wasting processes (Zanchetta 2004). Cold, arid glacial and semiarid, cool stadial conditions are marked by a poorly vegetated and thus unstable landscape, resulting in rapid and vast remobilisation of loose material during infrequent intense rainfalls (e.g. Hubert & Filipov 1989;

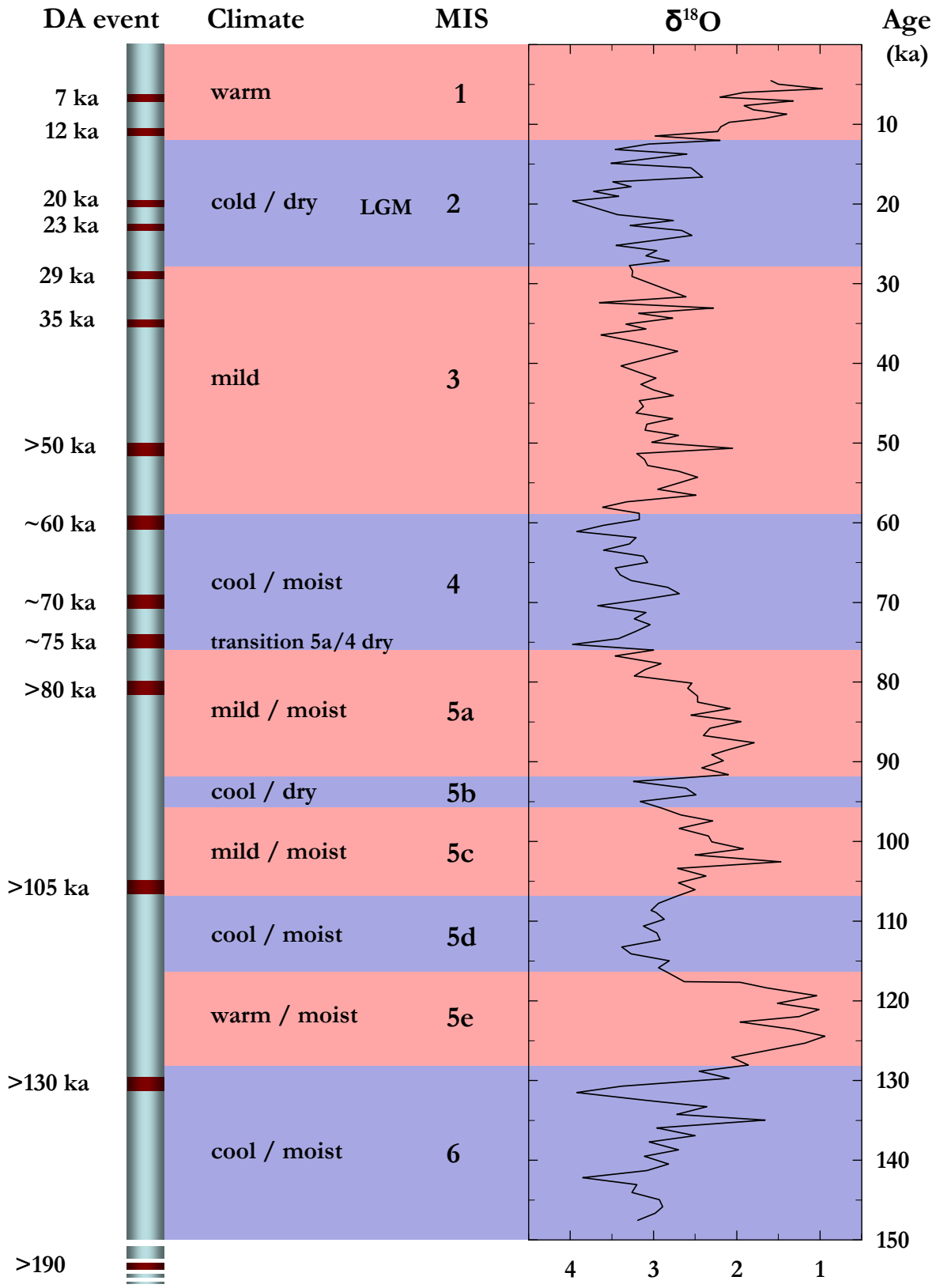

Figure 3.24. Correlation of debris-avalanche (DA) events with prevailing climate in Taranaki. Climate conditions from Newnham & Alloway (2004) and planctonic $\delta^{18}O$ isotope record at DSDP site 594 from Nelson et al. (1993).

Frostick & Reid 1989; Blair & McPherson 1994; Blair 2000). Large amounts of water rapidly infiltrate into unconsolidated, permeable volcanic debris due to the lack of a dense vegetation cover and the absence of, or only weakly developed, soils. This can lead to erosion by undercutting and entrainment, especially on the steep slopes of edifices, and remobilisation of the sediment as flash floods or lahars (e.g. Blair & McPherson 1994; Blair 1999, 2000; Zanchetta 2004). Similar conditions are observed after major explosive eruptions, which cover the surroundings with thick mantles of pyroclastic material and destroy the vegetation. This increases runoff and sediment availability and results in a phase of landscape instability marked by intense reworking of the bare and unprotected sediment for decades (e.g. Newhall & Punongbayan 1996; Major et al. 2000; Hayes 2002).

The sedimentary characteristics of the Taranaki ring-plain deposits not only vary according to lithofacies and type of volcanic mass-flow deposits but also show some differences in response to the above described climate fluctuations.

Debris-avalanche deposits that were emplaced during warm or mild climate typically contain abundant plant and tree fragments, indicating that they travelled across a densely vegetated landscape (cf. Fig. 3.24). Wood fragments range from small chips and a few centimetre-long twigs to several metre-long logs with diameters of up to 0.6 m (cf. Fig. 3.10B). Units produced during cool climate contain only sparse wood fragments, while those emplaced during cold glacial conditions appear completely free of significant organic components.

During warm climates, the episodic accretion and subsequent intense surficial weathering of aeolian redeposited fine-grained volcaniclastic sediment produced reddish, allophane-rich cover-beds and organic soils (Fig. 3.25A) (Alloway et al. 2005). These Andisols comprise friable to firmly friable material with moderately to well-developed soil structures, i.e. fine to medium block- or nut-structures (Alloway et al 1992). Cold climate soils (Fig. 3.25B) comprise firm to very firm, weakly developed, very coarse block- or massive-structured yellowish material (Alloway et al. 1992). The poorly developed soil structures are the result of only minor weathering processes and coincide with variations in soil mineralogy. A high influx of aeolian quartz grains in the non-quartzose volcanic soils of Taranaki is attributed to cold (full glacial) climate conditions, which exposed continental shelf quartzose-source areas (Stewart et al. 1977, 1986; Alloway 1989; Alloway et al. 1992). Rising sea levels during episodes of cool or warm climate resulted in low levels of aerially transported quartz grains (Alloway et al. 1992). During moist climate, thick peat beds, accumulated locally and were subsequently buried and preserved beneath volcaniclastic deposits (Alloway et al. 1992). Peat formed in wet, poorly drained areas, like enclosed depressions upon the initial depositional surface or at the margins of coalesced lahar

and debris-avalanche deposit fans that were not affected by large quantities of tephra accretion (Alloway et al. 1992). Numerous peat lenses and some more continuous peat layers were preserved in the study area along the south-western coast of Taranaki. They occur throughout the sequence from thin individual beds only a few cm thick to sequences of up to 1.5 m with interbedded organic and tephric soils, as well as thin andesitic tephras (Fig. 3.25C-D). The older peat beds identified in north and south Taranaki have become compacted to form lignite (e.g. McGlone et al. 1984; Alloway et al 2005).

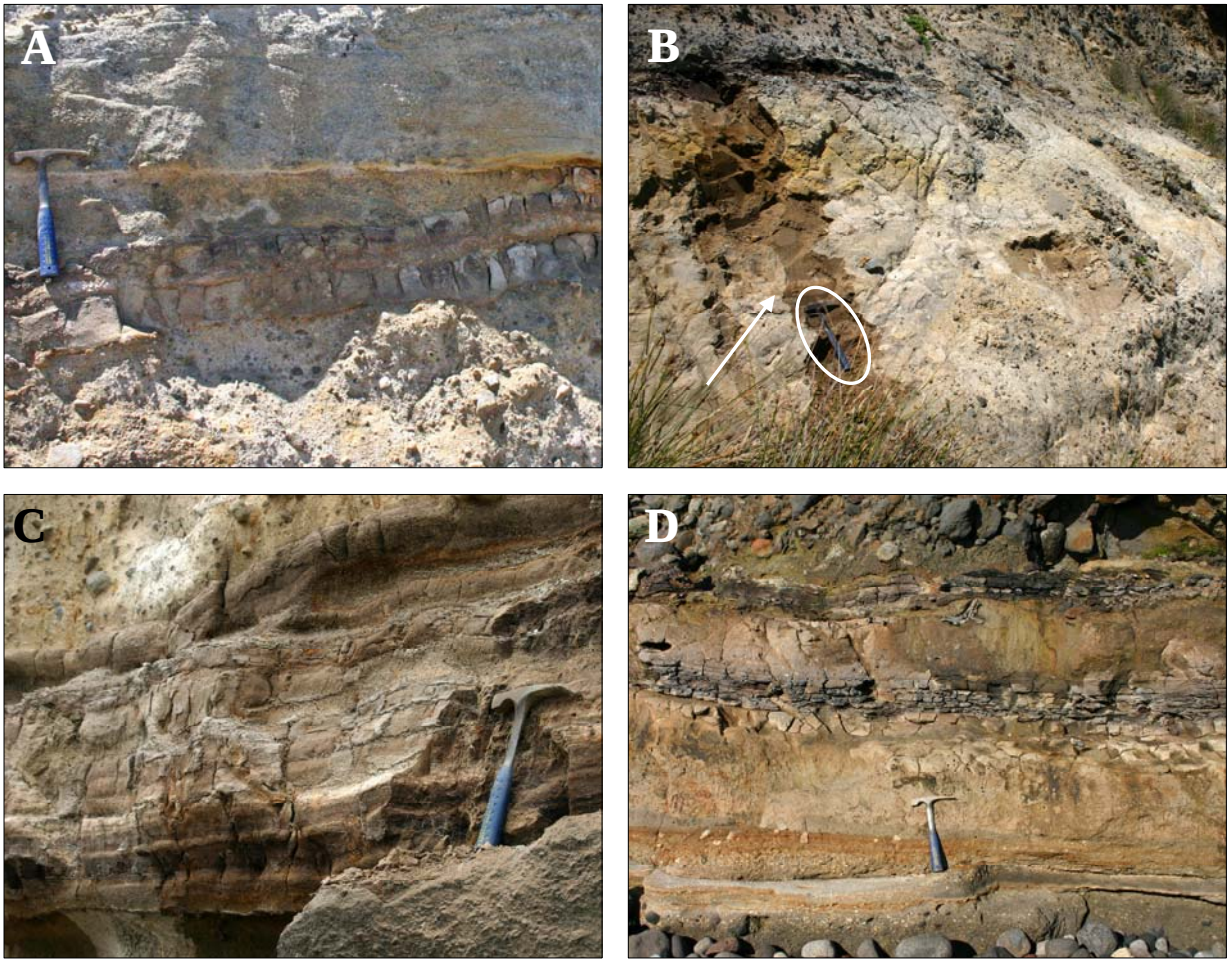

Figure 3.25. In Taranaki, warm climates are characterised by reddish-brown organic-rich paleosols with strongly developed soil structures (A; 2581551/6195488). In contrast, yellowish loess-rich tephric paleosols reflect cold climates (B; 2582247/6194848); the 22.5 ka Kawakawa Tephra is marked by a white arrow. Thick laminated peat deposits are common in the ring-plain succession and often preserve interbedded tephra beds (C; 2590428/6186143). The Hihiwera Peat is the most prominent peat accumulation of the south-western ring plain and at several locations it is interbedded with organic-rich and tephric soils (D; 2583809/6193200). Hammer for scale is c. 30 cm long.

3.8. PALEOGEOMORPHOLOGY OF THE TARANAKI RING PLAIN

3.8.1. Ring-plain paleogeomorphology

The present geomorphology of the Taranaki peninsula (Fig. 3.26.) was predominantly shaped by Quaternary volcanism, which produced an extensive ring plain of volcaniclastic debris around the volcanoes that unconformably overlies the Tertiary basement. The ring plain is only weakly dissected and gently dips from the prominent edifice of Mt. Taranaki to the sea. Its circular outline is only broken in the NNW where the eroded remnants of Pouakai and Kaitake Volcanoes form physiographic barriers. To the east the ring plain borders onto the Taranaki hill country consisting of upper Tertiary marine mudstone and sandstone sequences (Kamp et al. 2004), which restricted the extent of volcanic mass-flows due to an abrupt 100 m rise in elevation. Some of the streams that derive from the eastern flanks of Mt. Taranaki continue flowing eastwards into the hill country while others are redirected to the northern or southern coast. The Waingongoro River is deflected south once it meets the hilly terrain and flows through a deep but wide valley with steep side walls, which represents one of the longest living, most prominent river valleys of the Taranaki peninsula. Its relatively linear course and constant location suggests a fault-related origin. An older, elevated surface, previously referred to as Eltham Surface or Planeze (Grant-Taylor 1964; Hay 1967; Neall 1979, 1982; Alloway 1989) and renamed Old Surface (Neall & Alloway 2004), is preserved to the NE of Mt. Taranaki. It is strongly dissected near Inglewood but becomes less incised towards the coast with wide planar interfluves and the deeply entrenched north-south trending valleys of the Manganui River, Waitara River, Waiongana Stream, Mangaoreka Stream and Waiwhaikaiho River. Several uplifted marine terraces were cut into the northern and southern Taranaki coast during high sea-level stands and descend step-like from over 100 m to the present-day coast (Chappell 1975; Pillans 1983, 1990a, 1990b; Alloway 1989). Later debris-avalanche deposits draped the wave-cut surfaces in north and south Taranaki and smoothed out the otherwise prominent appearance of associated fossil cliffs. Though less distinct, the marine benches and terrace risers represent recognisable geomorphic surfaces, especially in coastal areas of south Taranaki.

The distribution and geometry of deposits within the ring-plain successions suggests a similar geomorphology of the ring plain with only minor modifications throughout the volcanic history of Mt. Taranaki. The oldest debris avalanches generated by collapse of the north-eastern sector of the volcano where channelised down confined paleo-valleys of the Manganui/Waitara River and Waiongana Stream until they spread out onto the broader coastal plains and marine terraces (Alloway et al 1989; Alloway et al. 2005). The sedimentary record along the western and

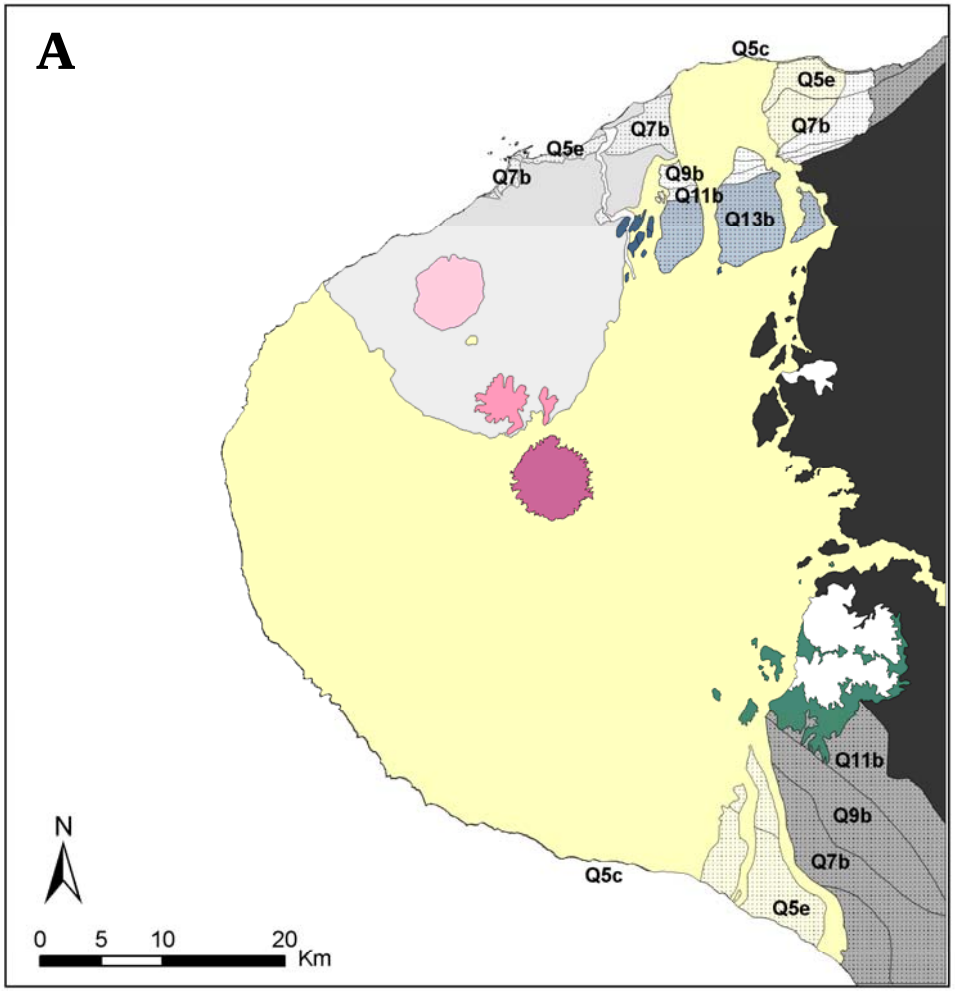

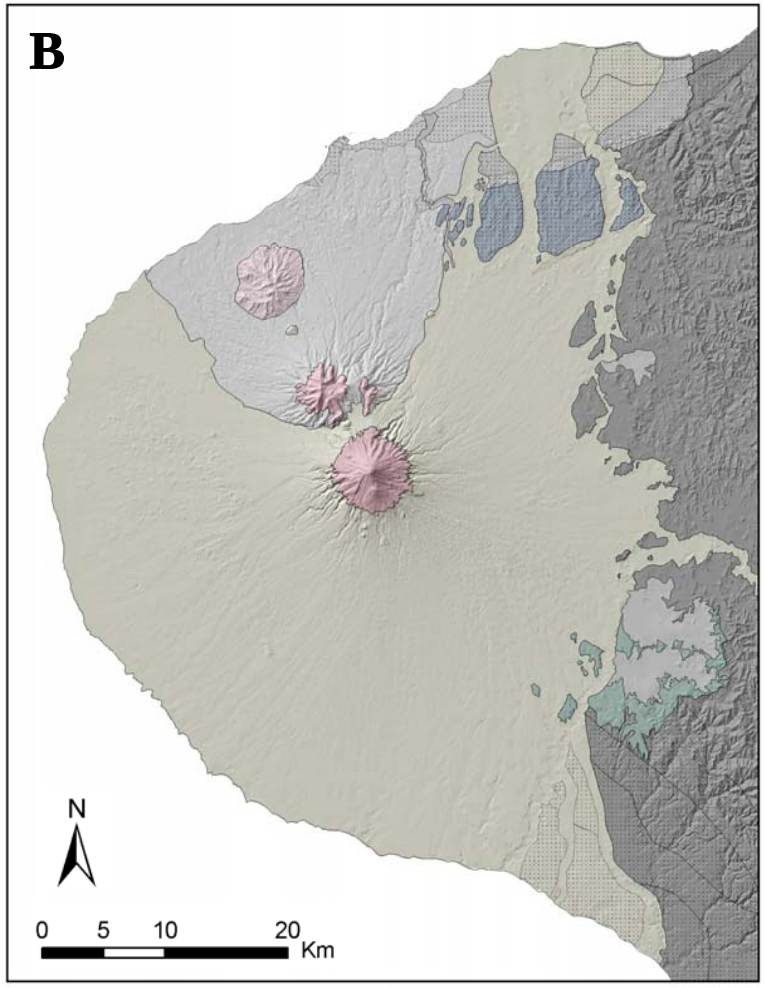

Figure 3.26. Map of the Taranaki peninsula showing distinct physiographic units: Taranaki ring plain, Pouakai ring plain, Old Surface, remnants of Kaitake and Pouakai Volcanoes, Mt. Taranaki edifice above 1100 m, marine terraces, and Taranaki hill country/Tertiary marine sediments (A). Swamp areas are shown in white. A digital elevation model (DEM) of the present-day geomorphology with these physiographic units is presented in B.

south-western coast suggests an unconfined distribution of debris avalanches with similar characteristics throughout the succession. The preservation of the Waihi debris-avalanche deposit at the base of the sequence within the Waingongoro River valley confirms the long-lasting existence (at least >70 ka) of this deep river channel.

The nature of the drainage pattern around Mt. Taranaki seems to have been similar throughout its history. The gently dipping ring plain was only weakly incised by a network of small, shallow streams that originated from the edifice. This is reflected in the frequent occurrence of relatively localised, cross-bedded fluvial deposits throughout the succession. Even though the character of stream channels continuously changed in response to varying sediment influx from syn- and inter-eruptive volcanic mass flows, their position shifted only slightly (cf. Major et al. 1996; Pierson et al. 1996; Rodolfo 1996 et al.; Major et al. 2005; Pierson 2005). Following periods of ring-plain aggradation, incision of new channels occurred along or near the margins of previous, infilled ones. The typically tabular, laterally widespread geometry of hyperconcentrated-flow deposits throughout the sequence confirms the existence of broad coastal or near-coastal plains.

3.8.2. Characterisation of paleo-river systems and lahar channels

Eruptive activity has a major influence on the depositional system surrounding the volcano and the nature of river and stream channels. Geomorphic alterations of the edifice such as deposition of lava flows, lava domes and pyroclastic deposits can result in modifications of stream/river origin and course due to a changed setting of the source area. High sediment input during and shortly after eruptions leads to considerable channel adjustment and instability as well as rapid aggradation due to frequent debris and hyperconcentrated flows (cf. Janda et al. 1981; Palmer et al. 1993; Major et al. 1996; Pierson et al. 1996; Rodolfo et al. 1996; Scott et al. 1996; Major 2003; Zanchetta et al. 2004; Major et al. 2005). However, the most significant influence on the drainage network are major edifice failures as they generate catastrophic debris avalanches and create large scarps, which redirect the majority of subsequent volcanic mass-flows. In Taranaki, the emplacement of voluminous debris-avalanche deposits buried large sectors of the ring plain and destroyed the pre-existing drainage system, as indicated by debris-avalanche units overlying fluvial deposits. Channel-development on debris-avalanche deposits has been observed to begin during the initial phase of liquefaction and dewatering, which triggers fill and spill of small ponds and erosion by associated cohesive debris flows (Major et al. 2005). The phenomenon of secondary debris flows is not recorded in medial sections of the Taranaki ring

plain. Some marginal debris-avalanche deposits show several units but similar characteristics suggest several pulses rather than secondary flow origin.

According to the type of disturbance (eruption versus collapse), the style of channel adjustment varied, but generally followed complex cycles of incision, aggradation and widening (cf. Major et al. 2005). After major edifice failures, re-establishment of initially shallow stream channels on the Taranaki debris-avalanche surfaces produced localised erosion contacts, filled by bedded fluvial deposits. In some locations, the continuous erosion and incision of the easily erodible volcaniclastic debris resulted in the development of larger stream and river channels. Larger river systems with deeper channels are common throughout the volcanic history of Mt. Taranaki and are not only restricted to debris-avalanche surfaces but were also cut into sequences dominated by hyperconcentrated-flow deposits, fluvial sediments or dune sands. They typically consisted of a central channel area that provided flow paths for the most voluminous and sediment-rich volcanic mass flows. Confinement of concentrated debris flows to these channels rapidly infilled them with massive, coarse, bouldery deposits, which raised the channel bed elevation and lowered the flow capacity. Once these were infilled, only more dilute and less confined hyperconcentrated flows inundated the increasingly shallower channel and the adjacent floodplain as indicated by accumulation of more widespread, finer-grained hyperconcentrated-flow deposits towards the top of the channel sequences (Fig. 3.27). As well as modifications of the channel morphology, the occurrence of different types of volcanic mass-flows in the same sites could also be a function of changing generation mechanisms (cf. Procter et al. 2009).

The basal debris-flow deposits show an unconformable, often wavy contact to the underlying strata indicating various degrees of vertical erosion (Fig. 3.27). Lahars can incise steep, narrow channels for tens of meters (cf. Pierson 2005); the higher the sediment concentration of the depositing flow, the deeper the channel relative to its width (Xu 1999). More dilute flows tend to laterally widen the channels rather than cutting into the underlying deposits (Pierson 2005). Individual channels of the Taranaki ring-plain succession typically extend 15-30 m laterally, can be as deep as 10 m and are often characterised by relatively steep slopes. This might reflect the high sediment concentration of the confined debris flows and their erosive ability compared to more dilute flows, which tend to horizontally erode the channel. Alternatively, these box-like structures could reflect an immature stage of the channels, which were preserved due to rapid filling by debris-flow deposits. Facies transitions from coarse channel fill to fine-grained overbank facies occur abruptly at the steep channel margins (Fig. 3.28A). Activity along these channels typically ceased after their filling or burial by later debris-avalanche deposits. Subsequent

channels often formed in similar locations, i.e. adjacent to previous settings or cut into the deposit sequence that filled the previous channel (Fig. 3.29).

Two large paleo-river systems near Opunake township and Puketapu Road ("Lizzie Bell") are an exception. These long-lived river systems are characterised by a laterally extensive network of overlapping channels that provided primary lahar paths over a long time-span and thus contain a more complete record of events than minor or shorter-lived channels (cf. Palmer et al. 1993). Wide channels typically cause rapid deposition and river-bed aggradation during syneruptive periods (cf. Major et al. 1996; Rodolfo 1996 et al.; Pierson 2005), which is indicated by stacked, massive, poorly sorted volcanic mass-flow deposits with no or small-scale erosional surfaces between events. Occasional interbedded, cross-stratified lenses of sands, or sands with rounded pebbles, suggest fluvial reworking and short-term re-establishment of normal river conditions. Major channels within these larger river systems are typically wider than the individual river channel described above and extend c. 30-60 m laterally. Most are characterised by gentle slopes and gradual facies changes towards the margins (Fig. 3.28B). The basal part of the individual channels typically contains the coarsest debris-flow deposits, which show erosional contacts to the underlying units. Steep, wavy erosion surfaces developed where the depositing flows cut into debris-avalanche deposits or dune sands. Vertical erosion was apparently less effective where the underlying strata was made of more resistant hyperconcentrated-flow and earlier bouldery debris-flow deposits. Repeated debris-flow events led to incremental infilling and lateral shifting of active channels, i.e. the formation of new channels at the margins of previous, completely infilled ones (cf. Pierson 2005). These are typically cut by more dilute and erosive flows as indicated by hyperconcentrated-flow deposits underlying younger coarser debris-flow units. Evidence of channel migration, i.e. lateral channel widening through bank erosion and burial of low-lying areas, was also observed and is a common process in low-gradient channels during aggradational phases (Major et al. 1996; Rodolfo et al. 1996; Pierson 2005). These laterally eroded channels are typically rectangular in cross-section due to undercutting and the formation of near-vertical banks in unconsolidated volcaniclastic deposits (Figs. 3.27, 3.29B) (cf. Pierson 2005).

Continuous aggradation, channel shifting and lateral migration resulted in a complicated network of overlapping channels, which cut into and eroded the underlying strata, often just preserving lenses of older lahar and fluvial deposits that formed in previous channels. Hence, it is often impossible to laterally trace and correlate individual flow units further than a few metres from the channel margins. Due to a lack of preserved paleosols or other marker beds no accurate age control, other than chronostratigraphic estimates, could be established on the formation of

Figure 3.27. A large channel with wavy basal and erosive lateral contacts is shown in photograph A (2588351/6186992). It is filled by a series of coarse channelised debris-flow deposits (Ch), which are overlain by several hyperconcentrated-flow units (HFD). A close-up of the channel shows the rectangular lateral contact (marked by black arrow) to the Otakeho debris-avalanche deposit (B). Vertical erosion stopped, when the channel encountered slightly cemented, iron-stained sands, resulting in a relatively straight basal contact (pointed out by white arrows).

Figure 3.28. Abrupt facies changes from coarse debris-flow deposits (DFD) filling a steep-sided channel to finer-grained overbank facies (OF) are shown in A (2587165/6189163). These facies changes are more gradational in wide, gently sloping channels observed within the larger river systems (B; 2583849/6193114).

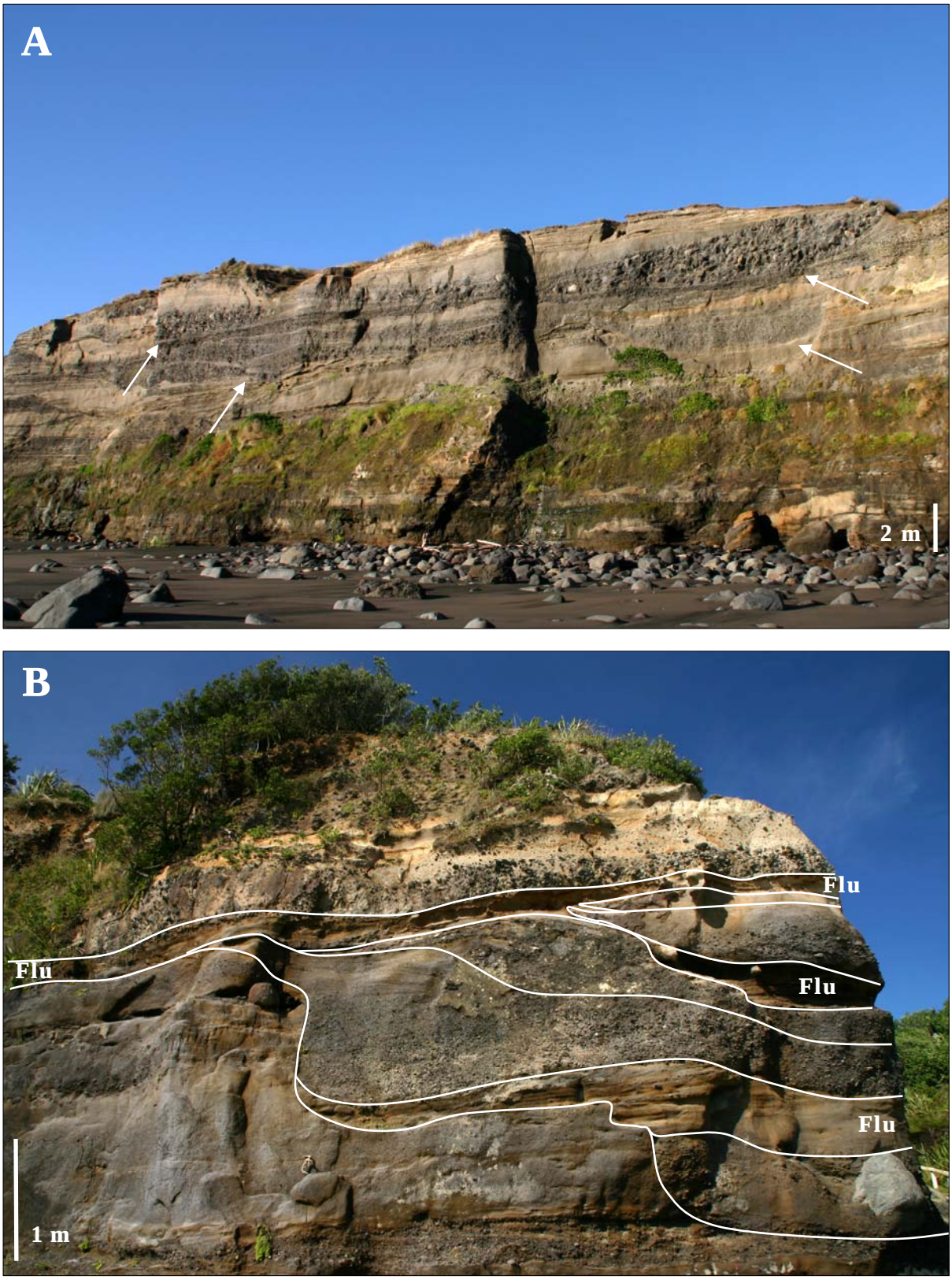

Figure 3.29. Cliff section showing a series of subsequent channels that were established in adjacent locations after previous ones had been filled as pointed out by arrows (A; 2584600/6192713). Other small channels were cut in the same location as previous ones (B; 2583057/6194247) and were subsequently filled with coarse hyperconcentrated-flow deposits, separated by fluvial sediments (Flu).

individual channels. An approximate age range of c. 33-13 ka for the Opunake river system is given by the stratigraphic position of channels and associated deposits. The lowermost channel fill units cut into and in some areas erode the top of the underlying 33-35 ka Hihiwera Peat but were not found below it. Only lenses of the Te Namu and Pungarehu debris-avalanche deposits were found within the network of channels, indicating that they were almost completely reworked within the river system. The channel sequences are capped by a set of hyperconcentrated-flow deposits of the Warea Formation, which thicken in remaining shallow channels. The river system ceased to exist after these last flows were deposited and is conformably overlain by the Oakura Tephra and the Opua Formation. The lateral extent of the Opunake river system in coastal cross-section is c. 1.8 km, while the Lizzie Bell system extends over c. 1.2 km laterally and is thought to have been active from >50 to at least 30 ka. A minimum age of the latter system is marked by a preserved lens of the Otakeho debris-avalanche deposit, which was strongly eroded by subsequent channelised debris flows confined to this paleo-valley. The debris-avalanche deposit overlies several older channelised debris flow deposits and its geometry reflects confinement to a small, shallow channel, indicating the existence of a channel system prior to deposition of the Otakeho debris-avalanche deposit. The post-Otakeho channel sequence is capped by a series of finer-grained hyperconcentrated-flow deposits intercalated with at least three distinct paleosols, which are possibly similar in age to the c. 33-35 ka Hihiwera Peat. At the north-western extent of the river system, these units are overlain and partly eroded by further channelised debris-flow and coarse hyperconcentrated-flow deposits. Hence, it is not clear when the activity of the Lizzie Bell river system ceased.

In Taranaki, the location of large river systems can often be identified based on the shape of the present-day coastline. Areas of major paleo-channels typically form small promontories according to the extent of the channelised bouldery debris-flow deposits. These seem to be more resistant to erosion than cliff sections dominated by finer-grained hyperconcentrated-flow and clay-rich debris-avalanche deposits, which produced relatively straight coastal stretches or small bays between points. The coastline in the area of the Opunake and Lizzie Bell paleo-river systems is characterised by numerous overlapping promontories.

The varying resistance of channel-fill debris-flow and hyperconcentrated-flow deposits compared to more easily erodible deposits finer-grained volcaniclastic material is also reflected in the pattern of the present-day drainage network. Re-establishment of the drainage system after filling of the river systems led to cutting of new river and stream channels adjacent to the previous channel systems. In the Opunake system, these new channels are represented by the present-day Otahi Stream to the northwest and the Waiaua River to the southeast. Only the

course of the small Hihiwera Stream lies within the older river system but it has not cut deeply into the channel deposits. The northwestern edge of the Lizzie Bell system is marked by the Punehu Stream and the Ouri Stream occurs at its southeastern margin. As is the case for the Opunake system, only a small, short stream occurs within the boundaries of the Lizzie Bell system and is deflected to its southeastern margin before entering the sea.

The location of these two large paleo-river systems is possibly related to nearby fault lines with tectonic activity leading to continuous re-establishment of river channels in the same area even after rapid filling or burial by large debris-avalanche deposits (Fig. 3.30). Two faults that were not mapped out to the coast but are leading roughly towards the northern and southern margins of the Opunake river system are marked on the recent 1:250000 scale Qmap (Rattenbury et al. 2007). The map also shows a recently identified fault just 0.4 km north of the Lizzie Bell system. The fault cuts the whole coastal cliff section and offsets the sequence by c. 2 m. Dating of paleosols and peat layers is currently being carried out by the Institute of Geological and Nuclear Sciences, Wellington (V. Mouslopoulou, GNS Science, pers. comm.). These radiocarbon dates will also provide time constraints for the activity of the nearby Lizzie Bell system.

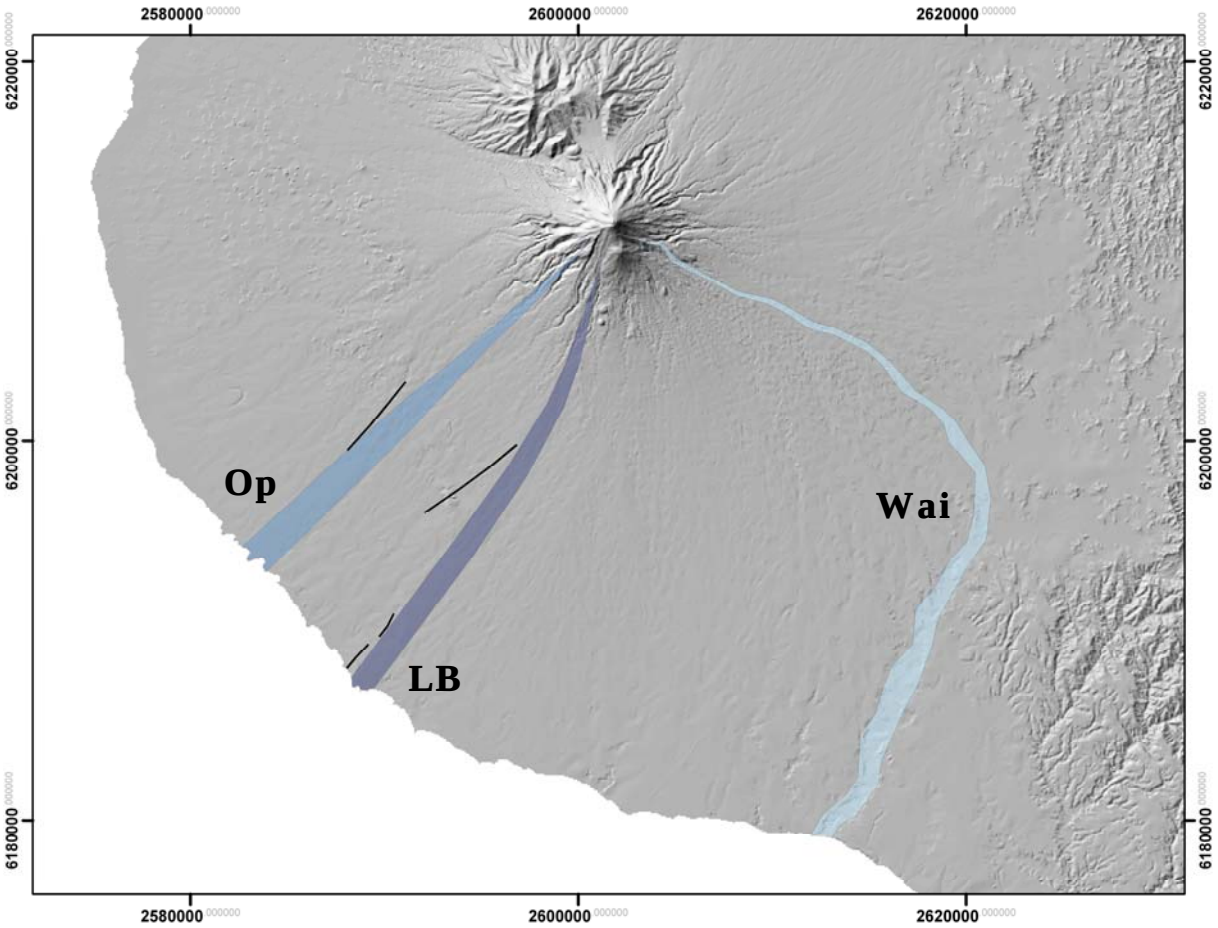

Figure 3.30. Location map of the Opunake (Op) and Lizzie Bell (LB) river systems and identified fault lines in their vicinity (from Rattenbury et al. 2007) as well as the course of the current Waingongoro River channel (Wai).

3.8.3. Frequency of volcanic mass-flows

The frequency of different types of volcanic mass-flow events in the Taranaki region is difficult to calculate due to low-resolution provided by available datable material. The occurrence of lahar deposits within the Taranaki ring-plain succession, however, appears not evenly distributed through time and space. The majority of volcanic mass-flows in Taranaki are related to eruptive activity, as indicated by monolithologic clast assemblages within the deposits. The lack of significant soil development or sediment redistribution between stacks of debris- and hyperconcentrated-flow deposits suggests that they were rapidly emplaced over relative short periods of time. The clusters of flow units correspond to individual eruptive episodes, which are separated from each other by longer intervals of quiescence, represented by occasional polylithologic lahar deposits, fluvial and aeolian redeposition as well as paleosols or peat layers. Furthermore, the distribution of lahar deposits varies according to the geomorphology of the ring plain and the edifice as well as the nature of the drainage network. Debris-flow deposits are restricted to the sites of deeper river channels, while hyperconcentrated-flow units are more wide-spread and occur at any of the coastal locations. They were emplaced on the shallower, broad floodplains, which represent the most active areas of the ring-plain depositional system. Furthermore, it was not possible to correlate individual flow units or time-equivalents over the entire cross-sectional exposure due to their large number and relatively limited lateral extent, a lack of individual diagnostic properties and significant marker horizons, as well as disturbance of the succession by complex, erosive channel systems. The studied medial ring-plain sequences also only represent part of the volcanic history of Mt. Taranaki and thus, cannot include a complete record of lahar events.

Hence, the simplified frequency presented here can only be considered a minimum estimate of recurrence. Calculations were carried out for a limited number of locations, where dated marker beds provided an age range for the recurring debris- and hyperconcentrated-flow deposits. The approximate frequency is based on the maximum number of flows over this specific time interval. The ring-plain record suggests that large channelised debris flows occur at least once every c. 2 ka, while sheet-like hyperconcentrated flows are more frequent events with a minimum recurrence of one event in 500 years. Large edifice failures and the generation of major debris avalanches are of lower frequency and occur on-average every 13 ka at Mt. Taranaki. Reconstruction of the number of debris-avalanche events was less problematic and provided a more complete record due to their distinct deposit characteristics, large volume, widespread distribution and thus easy recognition in the field. Even though the recurrence estimate for debris avalanches is more accurate, it only represents an approximation since collapse events are not

evenly spaced through time and more units could be buried within the older ring-plain succession.

Scott (1989) recognised the non-random occurrence and higher frequency of volcanic mass-flows during periods of eruption and suggested that a more useful way of calculating the average recurrence intervals of debris flows at Mount St. Helens is to consider only periods when the volcano was active. Unfortunately, a more accurate frequency estimate of lahar events cannot be established at Mt. Taranaki solely based on the record found within medial ring-plain sequences. However, Turner et al. (2008) developed more precise frequency-magnitude models for eruption events over the last 10 ka based on the number and volume of tephra beds preserved in lake core records. Their results provide a reconstruction of eruption recurrences in the younger volcanic history of Mt. Taranaki. Future correlation of these phases of eruptive activity with periods of lahar generation found in the more complete younger record would allow a better understanding of the relationship between these events. Eventually this might also provide a better insight into the time ranges of the older volcanic mass-flow records within the medial ring-plain succession.

3.9. DISCUSSION

3.9.1. Internal and external controls on ring-plain accumulation

(i) Influence of volcanic activity

Alluvial fan growth in volcanic and non-volcanic areas is controlled by a combination of processes that vary according to tectonic setting, slope, aspect and size of the drainage system, local climate, lithology and erodibility of the sediment cover, all of which affect the rate of sediment supply (Smith et al. 1987a; Frostick & Reid 1989; Smith 1991; Palmer et al. 1993; Ritter et al. 1995; Blair 1999, 2000; Zanchetta et al. 2004). High sediment input leads to fan aggradation, while low quantities of sediment result in erosion and dissection (Palmer et al. 1993). Sediment influx in volcanic areas is strongly influenced by the type, frequency and magnitude of volcanic activity (Smith 1991; Palmer & Neall 1991; Palmer et al. 1993; Zanchetta 2004). Major explosive eruptions and long-lasting eruptive periods produce large volumes of easily erodible, often predominantly sand-sized pyroclastic material that is rapidly reworked. The sedimentary and geomorphic response to such events has been studied in detail following the Plinian eruptions of Mount St. Helens (Lipman & Mullineaux 1981) and Mount Pinatubo (Newhall & Punongbayan 1996). Similar processes of resedimentation are interpreted from volcaniclastic sequences that

accumulated after large-volume ignimbrite eruptions, although these were not directly observed (RCM Smith 1991; Segschneider 2002a, 2002b; Kataoka & Nakajo 2002; Manville & Wilson 2004; Manville et al. 2005).

A high volume and high rate of sediment influx after large explosive eruptions is a consequence of a sudden supply of loose volcanic material, which mantles large areas of the surrounding landscape, destroys stabilising vegetation, reduces water infiltration capacity and hence results in increased run-off and erosion (Swanson et al. 1983; Collins & Dunne 1986; Leavesley et al. 1989; Pierson et al. 1992, 1996; Major et al. 1996; Hayes et al. 2002; Major 2003). The resulting accelerated sediment yields induce significant changes in the drainage networks and the alluvial plain/ring-plain depositional system (Smith 1986, 1987, 1991; Smith & Lowe 1991; Smith & Swanson 1987; Waresback & Turbeville 1990; Buesch 1991; Palmer & Neall 1991; Palmer et al. 1993; Major et al. 1996; Sulpizio et al. 2000; Zanchetta 2004). Continuous aggradation of volcanic mass-flow deposits rapidly fill channels, resulting in an abrupt transformation of river systems from meandering to wider, gravel- and sand-dominated, braided, aggrading systems with "flashy discharge" (Smith 1991) and unconfined spreading of subsequent flows as well as channel migration (Palmer et al. 1993; Hayes et al. 2002; Zanchetta 2004; Major 2005; Pierson 2005). The geomorphic response seen in historic examples is also reflected in the depositional record of the Taranaki ring-plain system. High sediment inputs following eruptive activity resulted in rapid aggradation of debris-flow and hyperconcentrated-flow deposits that filled pre-existing channels. A resulting channel shifting and migration occurred along larger river channels and in the Opunake and Lizzie Bell river systems. It also led to unconfined spreading of subsequent flows to generate widespread, sheet-like deposits that typically cap confined channel sequences.

The rapid post-eruptive remobilisation of eruptive material influences the nature of the resulting volcaniclastic deposits. The sequences are characterised by stacked, homogeneous debris-flow and hyperconcentrated-flow deposits, which typically lack important erosive surfaces between units due to their rapid accretion (Smith 1987a, 1987b; Smith & Lowe 1991; Palmer & Walton 1990; Waresback & Turbeville 1990; Palmer 1991; Palmer et al. 1993; Zanchetta 2004). Syneruptive volcaniclastic sediments may also be intercalated with primary pyroclastic fall or flow deposits, depending on the site of deposition in relation to prevailing wind direction, course of pyroclastic flows and distance from source (Smith 1991; Cronin 1996). Interbedded layers of medial ash reflect slow accumulation of fine ash from small-scale eruptions as well as wind-blown, reworked ash (Cronin 1996). Series of monolithologic hyperconcentrated-flow and transitional non-cohesive debris-flow deposits with little intermediary deposits between individual

units are a common feature of the Taranaki ring-plain succession. Their lithology indicates generation during or shortly after phases of volcanic activity. The laterally widespread, sheet-like distribution of these units is a result of rapid aggradation, infilling and overwhelming of channels, resulting in a smoothed, flat physiography and subsequent unconfined spreading of dominantly hyperconcentrated flows. Primary eruptive products such as pyroclastic flow or thick fall deposits were not observed within the syneruptive volcaniclastic sequences at coastal regions 25-40 km away from source. Pyroclastic fallout was mainly distributed eastwards in downwind direction and pyroclastic flows apparently did not reach the studied area. The occurrence of thin tephra layers interbedded with paleosols and peats indicate either a change of wind direction during certain periods or, more likely, existence of ideal environments for their preservation. During aggradational phases, the preservation potential of thin tephras was probably very low due to rapid erosion by volcanic mass-flows and low vegetative cover.

High aggradation rates with frequent generation of debris flows, hyperconcentrated flows and floods can continue for decades or centuries following eruptions depending on the frequency and magnitude of the volcanic activity as well as precipitation rates (Scott 1989; Rodolfo & Arguden 1991; Smith 1991; Scott et al. 1995; Newhall & Punongbayan 1996; Major et al. 2000; Manville et al. 2000; Pareschi et al. 2000a). Moderate annual rainfall and engineering measures at Mount St. Helens and other Cascade volcanoes resulted in predominantly fluvial erosion and transport of primary deposits and the accumulation of thick alluvial fills in the drainage systems (Major 2004; Major et al. 2005). This contrasts with observations of predominantly debris flow transport at other volcanoes, in particular those located in tropical climates (Major et al. 1996, 2000; Pierson et al 1996; Rodolfo et al. 1996; Lavigne et al. 2000; Lavigne & Thouret 2002; Thouret et al. 2007). Present annual precipitation rates on the Taranaki peninsula are high, especially on the edifice and increasing with altitude (Coulter 1976). The climate throughout most of Mt. Taranaki's volcanic history, even during the colder stadial periods, has been characterised by moist conditions except for relatively short, dry phases during MISS 5b, the beginning of MIS 4 and the Last Glacial Maximum (MIS 2). The abundant water supply for generating volcanic mass-flows is reflected in the dominance of debris-flow and hyperconcentrated-flow deposits within the volcaniclastic succession. This indicates that post- and syneruptive reworking in Taranaki is controlled by volcanic mass-flows rather than fluvial processes. Fluvial resedimentation dominates only once sediment yields have returned to normal in relation to stabilisation of the vegetation cover. Pre-eruption conditions are restored when the reservoir of loose debris on the volcanic flanks is exhausted or stabilised (Smith 1991; Palmer et al. 1993; Zanchetta 2004).

(ii) Influence of non-volcanic processes

Syneruptive sedimentary episodes have a high impact on the ring-plain depositional system but are typically relatively brief compared to periods of quiescence when volcanism has little influence on fan aggradation (Smith & Vincent 1987; Smith 1991). Sedimentation during inter-eruptive periods is influenced by processes such as regional climate and vegetational changes, geomorphology, as well as short- and long-term modifications in edifice or ring-plain sediment budget (Palmer et al. 1993; Cronin et al. 1996; Donoghue & Neall 2001; Zanchetta et al. 2004).

Re-establishment of a full vegetation cover after large eruptions stabilises volcanic deposits over long periods because plant roots cause cohesion and rain is intercepted and absorbed, reducing erosion (Zanchetta 2004). Types of vegetation and regrowth rates strongly depend on the local climate and are influenced by long-term climate changes. Stabilisation of the sediment cover results in longer storage of volcaniclastic material on the edifice and the surrounding ring plain. Flows are less frequent and are limited to periods of overall landscape instability (Cronin et al. 1995). These can originate from short-term changes in climate, or extreme weather conditions such as periods of heavy and/or prolonged rainfall, which enhance erosion and resedimentation (Palmer et al. 1993). Precipitation regimes not only influence the rate of erosion and sediment yield in watersheds but also control weathering processes and subsequent soil development (Dorn et al. 1987; Frostick & Reid 1989; Ritter et al. 1995). Soils typically form in sectors characterised by sediment starvation (Wright & Alonzo Zarza 1990; Smith 1992; Palmer et al. 1993; Zanchetta 2004), while peats accumulate in wet locations during warm or mild, moist climates (Alloway et al. 1992).

The influence of precipitation rates on alluvial processes has been described in Huntington's Principle (Huntington 1907; Fairbridge 1968). Increased aridity has similar effects as eruptive activity, because it results in the loss of the vegetation cover and increased mass wasting. Arid areas are characterised by aggradation, excessive load, reduced discharge and braided rivers. Higher precipitation maintains a stabilising vegetation cover that inhibits mass-wasting, promotes infiltration and leads to a more sustained flow of rivers. Rivers are typically meandering and erode valley-deepening channels with more gentle gradients. For some regions, Huntington's Principle can also be applied to changes in the nature of sedimentation during Quaternary climate fluctuations. The unstable conditions of arid areas are comparable to processes during colder climates, while warmer climates result in greater landscape stability (Bloom 1998).

The fluctuating climate conditions of the last >130 ka are also recorded in the Taranaki ring-plain succession. Weathering processes and soil formation were more intense during warm and mild climates as indicated by allophane-rich, reddish Andisols with strongly developed soil structures (cf. Alloway et al. 2005). Colder conditions resulted in weakly developed loess-rich, yellowish paleosols (cf. Alloway et al. 1992). Overall, the climate impacts can be seen as a secondary over-printing onto volcanically-driven processes, in particular the exacerbating sediment supply and slowing rates of revegetation.

Accumulation rates and sedimentation loci on the ring plain are also controlled by the degree of dissection (Palmer et al. 1993). During eruptive periods, channels are rapidly infilled and the flatter surfaces result in relatively unconfined flows and sheet-like sediment deposition. In contrast, the initial stages of inter-eruptive periods are characterised by dissection, including lateral channel shifts and entrenchment of new channels in the freshly deposited volcaniclastic debris (Smith 1991; Palmer et al. 1993). This results in a significant change in the nature and dispersal pattern of deposits on the ring plain. A strongly incised fan leads to confinement of volcanic mass-flows or floods and sediment transport to more distal depositional sites (Smith 1991; Palmer et al. 1993). Subsequently, the interchannel areas are marked by little sediment influx and the formation of soils as well as stabilisation by vegetation (Smith 1992; Palmer et al. 1993, Zanchetta 2004). Streams and rivers are confined to channels that can be steep and incised or wide and shallow depending on subsidence/uplift rates of the region and/or eruption frequencies and magnitudes (Smith 1991). Meandering rivers typically dominate in contrast to the shallower, braided systems during syneruption phases. Fluvial facies are dominated by gravel-bedload and polylithologic debris (Smith 1991). The landscape surrounding Mt. Taranaki is and has been characterised by a weakly dissected physiography, resulting in a similar dispersal pattern of fluvial and volcaniclastic deposits in most sectors of the ring plain. The gentle slopes and low gradient of the ring plain resulted in high rates of aggradation in proximal and medial areas. Small, shallow and mostly straight streams deposited cross-bedded fluvial sands and polylithologic pebbles. Larger rivers cut deeper channels and incrementally accumulated coarser sequences built up of rounded, polylithologic gravels. These deeper channels provided paths for coarse, confined, eruption- or collapse-related debris flows. The location and nature of stream and river channels was strongly influenced by volcanic activity and changed during eruptive episodes. Channel shifting and lateral migration were common, as well as rapid filling and subsequent incision of new channels. In contrast, hyperconcentrated flows were mostly unconfined and spread out sheet-like onto the broad coastal or near-coastal plains due to either

being large enough to overwhelm channels or because they were deposited during later stages of post-eruption response once channels were already filled.

In addition to eruptions, the ring-plain sediment budget can also be strongly modified by collapse events (Smith 1991). These range from small slips to large-scale sector or edifice failures. Small slips typically generate confined, coarse, polylithologic non-cohesive or cohesive debris flows, depending on the nature of the source material. Non-cohesive debris flows often transform into hyperconcentrated flows further downstream. A catastrophic collapse event partly destroys the volcanic edifice and leads to the formation of an amphitheatre and the generation of a volcanic debris avalanche. The avalanche scarp is characterised by steep, often vertical walls and represents a site of ongoing instability (Voight et al. 1981; Siebert 1984; Siebert et al. 1987). Emplacement of the debris-avalanche deposit devastates large portions of the surrounding landscape, burying the pre-existing drainage system and vegetation under several tens of metres of debris. The contribution of such large volumes of volcaniclastic debris to the lower ring plain leads to long-term landscape instability and conditions that may be even more severe than during syneruptive periods. Subsequently, redistribution of this massive sediment input produces frequent volcanic mass flows. Debris avalanches are common in the volcanic history of Mt. Taranaki (cf. Chapter 2). Due to their unconfined distribution, they reshape large areas of the ring-plain, resulting in major modification of the nature and focus of sedimentation (cf. Procter et al. 2000). Hence, landscape adjustment following these large collapse events shows similar cycles of channel incision, volcaniclastic aggradation accompanied by channel widening, braiding of streams and cutting and meandering of rivers as has been observed after large explosive eruptions (Lipman & Mullineaux 1981; Newnham & Punongbayan 1996; Major et al. 2005; Manville et al. 2005).

Some studies suggest that climate conditions, in particular heavy rainfalls, may influence the potential of the volcano to fail, or even trigger a collapse (McGuire 1996; Sheridan et al. 1999; Kerle et al. 2003; Scott et al. 2005). Capra (2006) attributed several edifice collapses worldwide, including the Pungarehu and Opua debris-avalanche events and the Warea lahars, to an abrupt change of climate following the Last Glacial Maximum. This theory contrasts with the findings of this study, which demonstrate that edifice failures at Mt. Taranaki are not directly related to abrupt climate changes, but have occurred repeatedly during its history. Irrespective of prevailing climate conditions, the occurrence of collapse events instead seems to be influenced by other factors such as the nature and magnitude of volcanic activity, rate of eruptions, reaching critical edifice heights and flank oversteepening.

However, it appears that some of the exceptionally large debris avalanches such as the Pungarehu, Ngaere, and possibly the Waihi were generated during cool or cold periods, compared to more frequent smaller and only a few larger events during warm or mild periods, such as the Rama and possibly the Oeo (cf. Fig. 3.23). This trend might be deceiving due to the imperfect age control for the older events (cf. Chapter 2). Yet, larger debris avalanches during cold periods could be the result of several factors. The type and elevation of vegetation lines may have played an important role in edifice stability with grass- and shrubland dominating during cooler periods and vegetation cover being restricted to lower altitudes than during warm climates. Hence, a larger area of the edifice was bare and unprotected by vegetation, resulting in greater instability of the volcano flanks and possibly greater saturation and deeper water infiltration. Snow and ice cover may have been also higher during colder periods with freeze and thaw processes increasing physical weathering of the volcanic products (cf. Cronin & Neall 1997). These climatic impacts could have increased the instability of the edifice and may have lead to a lowered stable height and slope angle than during warmer periods. Also, edifice failures may have been more deep-seated, and involved larger volumes of the cone. Further studies are needed to investigate the implications of variable climate conditions on the size of edifice failures and the volume of the resulting debris-avalanche deposits.

3.9.2. Comparison to other volcaniclastic successions

Volcaniclastic sediments have been described in detail at volcanoes worldwide. Previous work often concentrated on the sedimentary characteristics of the exposed deposits in order to infer their origin, possible trigger mechanisms, mode of transport and depositional conditions. This aimed towards developing a better general understanding of the flow dynamics and behaviour of volcanic mass flows. Reconstruction of short periods of the volcanic history, typically within the younger, more easily accessible record, and the characterisation of individual events are typically used as the basis for future hazard assessments (e.g. Siebert et al. 1995; Thouret et al. 1995; Scott et al. 1997; Belousov et al. 1999; Waythomas 1999; Waythomas & Miller 1999; Reid et al. 2001). In addition to these works, only a few studies have described in a holistic sense the setting, detailed accumulation history and overall evolution of volcaniclastic aprons in the surroundings of long-lived stratovolcanoes (Palmer & Neall 1991; Smith 1991; Cronin et al. 1996; Davidson & de Silva 2000; Donoghue & Neall 2001; Borgia & van Wyk de Vries 2003). The volcaniclastic apron surrounding Mt. Taranaki represents a volcanic ring plain *sensu stricto* according to the definition of Davidson & de Silva (2000). Similar settings are rare, since most long-lived stratovolcanoes form parts of volcanic mountain ranges or are enclosed by neighbouring volcanoes. Their surroundings are typically characterised by a deeply incised

physiography with steep valleys, in contrast to the gently incised landscape of the Taranaki peninsula. This leads to confinement of volcanic mass-flows and limited preservation or exposure of the volcanic and volcaniclastic record. Due to the varying physiographic setting and often different climatic background, origin and emplacement mechanisms of the deposits and in particular depositional conditions can differ significantly from the Taranaki succession. Also, the reconstruction of the accumulation history is often based on the interpretation of the youngest, surficially exposed succession, while the Taranaki depositional system provides a more complete record that spans almost the entire history of this volcano. The following section discusses aspects of the Taranaki ring-plain succession in comparison to relevant other modern and ancient analogues.

(i) Active and Quaternary volcanoes

Volcanoes of the Cascade Range and their products have been studied in detail (e.g. Crandell 1989; Scott et al. 1995; WE Scott et al. 1995; Hildreth & Fierstein 1997; Vallance & Scott 1997; Hoblitt et al. 1998; Thouret 2005). The 1980 eruption of Mount St. Helens provided important and revolutionary insights into origin, transport and emplacement mechanisms of volcanic mass-flows (Lipman & Mullineaux 1981). Even though the physiographic setting of Mount St. Helens differs significantly from Mt. Taranaki with mass-flows being confined to large valleys, similar deposits were generated. Hence, the St. Helens depositional and physical models (cf. Section 3.2.) were helpful tools in interpreting the observed types of volcanic mass-flow deposits in Taranaki and the range of sedimentary characteristics. The geomorphic response following the Mount St. Helens eruption also provided a better understanding of syneruptive volcaniclastic sedimentation and subsequent channel behaviour and alterations that could be related to observations within the Taranaki ring-plain record (cf. Section 3.8.2.). In contrast to Taranaki, restricted exposure of the older geologic record at most Cascade volcanoes only allows the study of individual events or eruptive episodes of the younger history with a focus on hazard assessments as well as eruption and sedimentary processes rather than the long-term reconstruction dynamics of the volcano-sedimentary system.

Lahar and debris-avalanche deposits are described at many stratovolcanoes worldwide, but only a few long-lived examples are known to have experienced similar recurrence rates of collapse events as observed at Mt. Taranaki. Mount St. Augustine in Alaska and Shiveluch Volcano in Kamchatka show the highest frequencies of debris-avalanche events known, i.e. 11 events within the last 2 ka and 8-14 collapses during the past 10 ka, respectively (Beget & Kienle 1992, Siebert et al. 1997; Ponomareva et al. 1998; Belousov et al. 1999). The instability and high

frequency of collapse events at both volcanoes is attributed to extremely high magma supply rates and very viscous, volatile-rich magmas, which resulted in repeated formation of overlapping lava domes and explosive eruptions (Beget & Kienle 1992; Belousov et al. 1999). At the low-profile dome complex of Mount St. Augustine, debris avalanches were emplaced on unconfined, low-angle slopes and formed a thick volcaniclastic apron around the island volcano that extends c. 4-10 km from the crater area. Due to the restricted onshore extent of the ring-plain only hummocky facies-A is observed at Augustine Volcano (Beget & Kienle 1992) without lateral or longitudinal facies changes typical of Mt. Taranaki debris-avalanche deposits. Collapse events at Shiveluch Volcano mostly occurred at Young Shiveluch, a Holocene cone that formed within a horse-shoe shaped caldera of the old Pleistocene stratovolcano Old Shiveluch (Belousov et al. 1999). Debris avalanches and pyroclastic flows were thus directed and built up a semi-circular volcaniclastic apron in the open southern sector. The scale of collapse events at both volcanoes (except for the Old Shiveluch debris-avalanche deposit) is significantly smaller than at Mt. Taranaki. Volume and run-out distance of debris-avalanche deposits at Augustine Volcano are 0.1-0.5 km^3 and >4-10 km respectively (Beget & Kienle 1992; Siebert et al. 1997), 1-2.5 km^3 and 11-20 km at Young Shiveluch, 28-35 km^3 and c. 35 km for the Old Shiveluch event (Belousov et al. 1999), compared to 0.1-7.5 km^3 and 25-39 km for those at Mt. Taranaki (Ui et al. 1986a; Palmer et al. 1991; Alloway et al. 2005). Lithofacies associations are characterised by debris avalanche, pyroclastic flow, block-and-ash-flow and pumiceous airfall deposits, while lahar units are absent from the Augustine ring-plain and seem to be rare within the Shiveluch record. This contrasts strongly with the hyperconcentrated flow and debris flow-dominated medial Taranaki ring-plain succession and most likely reflects the more proximal location of the studied sequences, the predominant eruptive style, as well as the scale of volcaniclastic events at Augustine and Shiveluch Volcanoes.

Zanchetta et al. (2004) studied the development of late Pleistocene-Holocene alluvial fans in the Campanian plain, Italy, in order to evaluate the relative roles of volcanic activity and climate. Even though not a classic ring-plain, the hillslope drainage system in this volcanic hinterland setting was influenced by similar processes due to its location 20-30 km downwind from Somma-Vesuvius and Campi Flegrei volcanoes. Each episode of explosive volcanic activity resulted in emplacement of pyroclastic material and subsequently a phase of volcaniclastic sedimentation in the downwind hillcountry. Syneruptive periods were dominated by rapid accumulation of lithologically homogeneous hyperconcentrated-flow deposits during the late Pleistocene and occasional debris-flow deposits with mixed lithologies during the Holocene. These sedimentological and lithological differences are attributed to varying climate conditions at

a relatively constant rate of sediment influx. Semi-arid, poorly vegetated conditions resulted in the rapid and almost complete remobilisation of loose pyroclastic material during infrequent but intense rainfalls, while retarding soil stabilisation. More humid conditions during Holocene times favoured soil formation and thus partial stabilisation and longer storage of loose debris, which was periodically removed by slips.

These findings contrast with an earlier study by de Rita et al. (2002) that described the interplay of explosive volcanism and glacio-eustatic sea-level changes on volcaniclastic sedimentation in coastal lowlands near the volcanic districts of Vulsini and Vico, Central Italy. Eruptive activity during high sea level (warm climate) produced thick sequences dominated by debris-flow deposits, hyperconcentrated-flow deposits and monolithologic fluvial sediments in a medial basin, while the distal coastal areas accreted volcanic-rich sands with interbedded volcanic units. In inter-eruptive periods diatomitic lacustrine and polylithologic fluvial deposits accumulated with coastal sands being depleted in volcanic particles. Syneruptive sedimentation during low sea-level (cold climate) filled deeply eroded valleys with thick volcaniclastic deposits in medial as well as distal areas. Erosion prevailed during phases of quiescence resulting in partial excavation of the volcanic and volcaniclastic succession and terrace formation. This study explained how the interplay of changing sea-levels, uplift and cutting of marine terraces affected the setting of the near-coastal areas. The sedimentary signatures of the generated volcaniclastic deposits did not directly reflect climate conditions, but their varying geometry and distribution was rather a result of climatically induced changes in geomorphology.

This example of volcaniclastic sedimentation appears to be more relevant to Taranaki than the downwind hillcountry, due to a comparable near-coast depositional environment with changing sea-levels and hence changing stream gradients and similar volcanic products, i.e. pyroclastic-flow and minor fallout deposits compared to the tephra-dominated Campanian setting. Syneruptive volcaniclastic remobilisation at Mt. Taranaki resulted in rapid accumulation of monolithologic hyperconcentrated-flow and debris-flow deposits. Coarse, polylithologic debris-flow deposits confined to channels were most likely triggered by small collapse events during inter-eruptive periods. Due to the limited age control of the Taranaki ring-plain succession, the role of climate conditions could not be evaluated unambiguously. However, similar sedimentation patterns throughout the sequence suggest that volcanic activity was the dominant control on the accumulation style of the ring-plain depositional system. Climate variations and resulting fluctuations in sea level might have affected the paleogeomorphic setting but seem to have had only minor influence on deposit characteristics and type of sedimentation.

Ruapehu Volcano and its surrounding volcaniclastic apron represent the geographically closest comparator to the Taranaki ring-plain system, with similar characteristics of the exposed deposits and overall setting. The Ruapehu ring plain is dominated by lahar deposits interbedded with local andesitic tephras derived from Ruapehu, Tongariro and Ngauruhoe Volcanoes, fluvial sediments, paleosols / peat layers and distal rhyolitic tephras from the Taupo Volcanic Zone (Palmer & Neall 1989; Palmer 1991; Palmer et al. 1993; Donoghue et al 1995; Cronin et al. 1996; Cronin & Neall 1997; Lecointre et al. 1998; Donoghue & Neall 2001). In addition, four debris-avalanche deposits were recognised, the >120 ka Hautapu and Whangaehu Formations to the south (Te Punga 1952; Hodgson 1993, Thouret et al. 2006), the c. 9.5-12.5 ka Murimotu Formation to the west (Palmer & Neall 1989), and the c. 4.6 ka Mangaio Formation (Donoghue & Neall 2001). The ring plain was constructed during syn- as well as inter-eruptive periods with variations of sedimentation style according to frequency and magnitude of eruptions, climate, sediment reservoir and degree of fan dissection (Palmer et al. 1993; Cronin et al. 1996; Donoghue & Neall 2001). During major eruptive episodes, volcanism was the primary control on sedimentation, with little influence of climate variations (Palmer et al 1993). The continuous, high sediment supply during and shortly after major eruptions resulted in rapid, sector-wide aggradation of lahar (debris- and hyperconcentrated-flow) deposits with little time breaks between events (Palmer 1991; Palmer et al. 1993; Cronin et al. 1996; Cronin & Neall 1997; Donoghue & Neall 2001). Ring-plain aggradation continued during minor eruptive activity and inter-eruptive episodes but sedimentation was more localised and strongly affected by non-volcanic processes, in particular regional climate and vegetational changes. The two coolest periods of the last Glacial, i.e. MIS 2 (23-14 ka) and 4 (75-65 ka), were characterised by large-scale aggradation and the most widespread and voluminous accumulation of debris-flow and hyperconcentrated-flow deposits (Cronin et al. 1996; Cronin & Neall 1997). The high frequency of lahar events was attributed to the interplay of a large supply of loose debris through increased physical weathering on higher slopes, as well as large volumes of snow and ice that provided the required water for lahar formation. Likely triggering mechanisms were eruptive activity, frequent storm events, slope failures, avalanches and glacier collapses (Cronin & Neall 1997). In milder periods, the ring-plain sequences were dominated by tephra (lapilli and medial ash) deposits and one eruption-triggered, pumiceous lahar unit, indicating greater landscape stability and less control of non-volcanic factors on the accumulation style. Volcaniclastic resedimentation continued after eruptive activity until the supply of loose debris on the volcanic flanks was exhausted (Palmer et al. 1993). Subsequent ring-plain dissection led to sediment starvation and soil formation and/or aeolian reworking in interfluve and minor channel areas. Fluvial

sedimentation and infrequent, collapse-related debris flows were restricted to major channels (Palmer et al. 1993).

The ring-plain depositional systems of both Mt. Ruapehu and Mt. Taranaki are dominated by lahar deposits and influenced by similar factors. At Taranaki, climate changes are reflected in deposit characteristics but do not drive aggradation, nor dominate the style of volcaniclastic sedimentation as observed at Ruapehu during cold periods. Instead, eruptive activity appears to be the primary control of ring-plain accumulation at Mt. Taranaki during mild as well as colder climates. This is indicated by the consistent pattern of volcaniclastic deposits within the relatively monotonous ring-plain succession. Variations are mainly the result of sedimentation loci due to modifications in paleogeomorphology and changes in sea level. As mentioned above, the nature of major river channels most likely varied during low sea-level with a higher degree of incision at the studied sites.

(ii) Ancient successions

Similar lithofacies associations are identified in several older volcaniclastic apron successions, which help interpreting the Taranaki ring-plain sequences. Middle Miocene volcanism at the Börzsöny Mountains in Hungary began with submarine eruptions that accumulated voluminous pumiceous volcaniclastic mass-flow deposits in a shallow marine basin (Karatson & Nemeth 2001). The subsequent emergent stage was characterised by subaerial eruptive activity from several silicic centres. Pyroclastic flows, dome-collapse block-and-ash-flows and small-scale debris avalanches transformed into various types of debris flows and hyperconcentrated flows, which rapidly built up an emerging ring-plain system. Due to subtropical climate conditions, debris flows were generated frequently during syn- as well as inter-eruptive periods. The ring-plain succession consists of tabular and channelised debris-flow deposits, hyperconcentrated-flow units, fluvial channel fills and cross-bedded fluvial sands, lithofacies associations typically observed in subaerial volcaniclastic aprons and common in the Taranaki ring-plain succession.

The Miocene Ellensburg (Washington) and Deschutes Formations (Oregon) represent ancient volcaniclastic aprons that formed adjacent to the volcanic Cascade Range in basins and lowlands, respectively. They are important because the well-exposed lateral and vertical lithofacies relationships were used to develop a conceptual model for facies geometry and sequence in volcaniclastic aprons (Smith 1987b, 1991) that can be applied to the Taranaki ring-plain succession. The Ellensburg Formation is the result of episodic accumulation of syneruptive sheets of monolithologic, pumice-rich hyperconcentrated-flow deposits in broad shallow braided

streams with intercalated ash fall tuffs (Smith 1988). Inter-eruptive periods were marked by paleosol formation on floodplains and channel-fill conglomerates deposited by a gravel-bedload river that flowed through the basin (Smith 1991). Distal facies assemblages are dominated by cross-bedded, monolithologic fluvial sandstones, less common polylithologic gravel bedload facies, and rare debris-flow and flood deposits. The Deschutes Formation is probably a more comparable example of volcaniclastic sedimentation to Taranaki since large volumes of volcaniclastic material were deposited over broad areas and long distances from source over extended periods of time. The main depositional setting was an eastward-wedging apron, which accumulated lava flows, airfall tuffs, ignimbrites, and volcaniclastic deposits, derived from the Cascades from 7.4 to 4.0 Ma (Smith 1986b). Continuous high-sediment load aggradation of hyperconcentrated-flow, debris-flow, and sheetflood deposits produced a broad, low-relief plain. Sedimentation between volcanism-induced depositional episodes was focused in gravel-bedload braided streams, which incised only shallow channels due to frequent volcanic activity and high subsidence rates (Smith et al 1987; Smith 1988, 1991). The upper part of the succession is dominated by cycles of episodic aggradation of hyperconcentrated-flow, debris-flow, and sheetflood deposits and degradation, characterised by deep incision and subsequent infilling of channels with fluvial conglomerates, lava flows, ignimbrites and lahar deposits. When the narrow, steep-sided channels were filled, continued sedimentation generated broad sheets of sand and gravel on the floodplain (Smith 1987b). The occurring lithofacies association of hyperconcentrated-flow, debris-flow, fluvial channel, floodplain and sheetflood deposits as well as paleosols with interbedded tephras are very similar to the Taranaki ring-plain sequences. Although no ignimbrites were produced at Mt. Taranaki, the frequent debris avalanches had a similar effect on the depositional system by supplying large volumes of unconsolidated volcanic debris. The nature of depositional episodes and environments at different stages of the Deschutes apron can be related to variations in lithofacies associations and settings observed within the Taranaki succession. The morphology of the low-relief, gently sloping Taranaki ring-plain is similar to the first stage broadplain setting of the Deschutes Formation, resulting in episodic accumulation of tabular, widespread hyperconcentrated-flow deposits during volcanic activity. Degradation during periods of volcanic quiescence was characterised by incision of shallow streams as well as deeper river channels, which were subsequently filled by fluvial as well as later debris flow and hyperconcentrated-flow deposits.

A larger magnitude of volcaniclastic resedimentation was studied in Japan, following an extremely large explosive ignimbrite-producing eruption that occurred at the Plio-Pleistocene boundary (Nakayama & Yoshikawa 1997; Kataoka & Nakajo 2002). The effects of the sediment

influx, i.e. the style of volcaniclastic reworking, were similar to eruptions of smaller magnitude but affected larger areas. Remobilisation of the volcanic material produced a variety of different lithofacies, ranging from debris-flow, hyperconcentrated-flow, channel-fill and floodplain deposits to distal fluvially dominated sequences (Nakayama & Yoshikawa 1997; Kataoka & Nakajo 2002). Sedimentary variations between volcaniclastic sequences of different basins were the result of differing rates of sediment input, distance from source, distribution pattern of pyroclastic-flow deposits and the drainage pattern. The depositional processes observed in medial areas support the conceptual model of Smith (1991). Following the eruption, pre-existing small-scale meandering rivers were replaced by low-sinuosity braided river systems in wide channels, which were inundated by debris and hyperconcentrated flows. Once sediment input returned to normal, rivers started cutting into the volcaniclastic sequence and returned to meandering streams. The changes in sedimentation in response to volcanic activity are also obvious in the Taranaki succession. Syneruptive deposition of sheet-like hyperconcentrated-flow deposits occurred on broad plains and infilled, shallow channels, followed by inter-eruptive re-establishment of drainage networks and incision of deeper channels. The observed confined non-cohesive debris-flow deposits in medial ring-plain settings accumulated in channels that were typically cut into massive, predominantly syneruptive sequences of hyperconcentrated-flow deposits. Most debris-flow deposits consist of polylithologic rounded to angular clasts and are hence interpreted to be derived from small-scale collapse events. Demonstrably, eruption-related debris-flow deposits are rare, typically of smaller volume, and contain subangular-angular clasts. The areas of the Opunake and Lizzie Bell system are dominated by accumulation of debris-flow units and coarser hyperconcentrated-flow deposits, in a wider, long-lived channel system, where syn- and inter-eruptive depositional signatures cannot be clearly distinguished.

3.10. CONCLUSIONS

Volcaniclastic sedimentation at Mt. Taranaki has formed a surrounding ring-plain of volcaniclastic deposits that extends 25-40 km onshore from the current summit. This apron holds a detailed chronostratigraphic record of volcanic activity, other sedimentary, and geomorphic events. Medial ring-plain sequences contain a spectrum of deposit types, reflecting transport modes that range from dry debris avalanche, highly concentrated debris flow, hyperconcentrated flow to dilute streamflow as well as transitions between these processes. Differences in sedimentary characteristics are the result of different flow source regions, flow dynamics and emplacement conditions as well as diversity in paleo-depositional environments. Vertical facies

transitions of individual units reflect variations in flow regime and sediment load with time, while lateral facies variations are attributed to distance from source, dispersal axes or channel geometry and capacity.

Debris avalanches produced wide-spread, massive, polylithologic, very coarse, and very poorly sorted deposits that contain disaggregated, shattered clasts, megaclasts and secondary components in a clay-rich matrix. Margins and medial locations show a gradational transition into thinner cohesive debris-flow deposits with increasing matrix contents and decreasing clast size. Channelised, non-cohesive debris-flow deposits are very coarse, poorly sorted, clast-supported with little sandy matrix and typically unstratified. They grade laterally into thinner, better sorted, faintly bedded overbank deposits that consist of fine pebbly sands. Distinct from the lahar overbank deposits are tabular hyperconcentrated-flow deposits that can be traced up to 2.5 km in lateral exposure. They typically contain pebbly clasts in a sandy matrix and show a variety of different characteristics ranging from poorly to moderately sorted, massive to bedded, and graded to non-graded.

The style of ring-plain accumulation, and hence lithofacies associations and deposit characteristics, were strongly influenced by the nature of volcanic activity of Mt. Taranaki. Syn-eruptive periods were characterised by rapid, continuous aggradation of thick packages of predominantly monolithologic, hyperconcentrated-flow and cohesive debris-flow deposits. Their clast assemblages vary in response to the predominant eruptive style: pumice-dominated lahar deposits and tephra layers indicate vigorous subplinian and/or Plinian eruptions, while those rich in dense, glassy, monolithologic andesite clasts correspond to dome-building and associated block-and-ash-flow activity. Polylithologic debris- and hyperconcentrated-flow deposits were probably not directly related to an eruption, but may represent conditions where dilute mass flows gained momentum via erosion and incorporation of sediment along their paths. The high sediment supply during or shortly after episodes of eruptive activity had a major impact on the ring-plain depositional system and the drainage network. Repeated volcanic mass-flow events led to incremental infilling, widening and/or shifting of active stream and river channels. Subsequent intervals of quiescence were marked by landscape re-adjustment and dissection along with steady accretion of medial ash, soil formation and/or peat accumulation. Fluvial erosion and reworking of primary deposits produced sediments ranging from localised cross-bedded, well-sorted sand and pebble beds, to aggradational series of river gravels interbedded with lenses of fluvial sand. Some coastal areas accumulated massive sequences of well-sorted dune sands during periods of extensive aeolian redeposition. Channelised, polylithologic debris flows were generated by small

collapse events during periods of quiescence or at the beginning of eruptive activity, when river channels were not yet filled by syneruptive mass-flow deposits.

Sedimentation during these inter-eruptive periods was influenced by non-volcanic processes such as sea-level variations, regional climate, and vegetational changes as well as short- and long-term modifications in the edifice/ring-plain sedimentary budget and geomorphic setting. The relief around Mt. Taranaki was the primary control on the distribution of lahar and fluvial deposits. The distribution and geometries of volcaniclastic deposits within the ring-plain succession indicate a similar ring-plain geomorphology, with only minor modifications throughout the known volcanic history of Mt. Taranaki. The ring-plain setting was characterised by small, shallow stream channels and wide coastal plains with broad terraces resulting in the predominance of largely unconfined and extensive sheet-like volcanic mass-flows. Some larger, long-lived river systems provided consistent flow paths for channelised lahars. Climate fluctuations are to some degree reflected as a secondary influence in the Taranaki ring-plain succession. Cold climates with lower vegetation levels resulted in larger areas of bare, unprotected volcanic debris inducing greater landscape instability and remobilisation processes, producing elevated sediment supplies as indicated by stacks of polylithologic hyperconcentrated- and debris-flow deposits. Andisols with strongly developed soil structures reflect periods of warm and mild climate while weakly developed, loess-rich paleosols represent colder climate conditions. Repeated edifice failures at Mt. Taranaki generated an unusually high frequency of debris-avalanche deposits. The rapid and intense input of loose volcanic debris strongly affected the sediment budget of large sectors of the ring-plain system and each resulted in a subsequent phase of mass wasting and redeposition.

Despite distinct climate changes during the last 100 ka, the sedimentation pattern of volcaniclastic deposits within the Taranaki succession is consistent, which suggests that volcanic activity and debris-avalanche events were the primary control on the accumulation style of the ring-plain depositional system. Climate variations and resulting sea level changes influenced the paleogeomorphic setting and hence geometry and distribution of deposits, but had only secondary and minor overprinting effects on deposit characteristics and type of sedimentation.

CHAPTER 4.

GEOCHEMISTRY OF DEBRIS-AVALANCHE CLASTS

4.1. INTRODUCTION

Geochemical work at Mt. Taranaki has mainly been based on the well-known succession of the last 20 ka and comparisons with products from the andesitic centres of the TVZ (Price et al. 1992, 1999, 2005; Stewart et al. 1996). Most geochemical studies focused on the <10 ka present-day edifice (Price et al. 1992; Stewart et al. 1996; Platz et al. 2007a, 2007b), which is primarily made up of steeply dipping, interstratified pyroclastic breccia and lava flow deposits. Only a few samples from the surrounding ring plain were included (Price et al. 1999) even though clast assemblages within these volcaniclastic sediments record variations in magma compositions over a much wider time span.

The stratigraphy developed in this and previous studies (Neall 1979; Alloway 1989; Neall et al. 1986; Alloway et al. 2005) for the older ring-plain succession and the identified debris-avalanche record (cf. Chapter 2) provided the context for extending geochemical studies into the early magmatic history of the volcano. Major, trace, and rare earth element analyses as well as stable isotope characteristics of debris-avalanche clasts allow an insight into the composition of pre-20 ka edifices. This chapter presents new geochemical data from the collected debris-avalanche sample suites in order to characterise the early magmatic system of Mt. Taranaki and to establish a better understanding of the overall magmatic evolution since inception of volcanism as well as the origin of Mt. Taranaki magmas. Compositional changes with time from the early to recent Mt. Taranaki magma systems are discussed and related to the constructional and destructional history of the volcano. The geochemical composition of clast assemblages is also evaluated as a tool for distinguishing and identifying stratigraphic units.

4.2. PREVIOUS WORK

Previous studies have used the classification scheme of Gill (1981) to conclude that the Mt. Taranaki lavas range in composition from medium- to high-K basalts and basaltic andesites through to high-K, high-Si andesites (Neall et al. 1986; Price et al. 1992, 1999; Stewart et al. 1996). Overall, the volcanics become progressively more potassic and show higher mean silica contents with decreasing age (Price et al. 1992; Stewart et al. 1996). In general, Mt. Taranaki lavas show distinctly higher K_2O abundances than equivalent andesites at Mt. Ruapehu (Neall et al. 1986; Price et al. 1992, 1999). Their relatively low Mg# (in this thesis calculated as $MgO*100/(MgO+FeO_{total}$; based on $FeO_{total}=Fe_2O_3*0.8998165$) and low Ni and Cr contents indicate that Taranaki rocks are highly evolved and lack the characteristics of primitive arc magmas (Price et al. 1992). The few rocks that were found to have elevated MgO, Ni, and Cr concentrations might be contaminated with xenocrystic olivine rather than representing primary melts (Stewart et al. 1996).

Trace element distributions are characterised by relatively high proportions of large ion lithophile elements (LILE) such as Cs, Rb, Ba, Th and K and light rare earth elements (LREE) with deficiencies in high field strength elements (HFSE) such as Ta, Nb and Zr (Price et al. 1992, 1999, 2005). The strong depletion in Nb relative to La, K, Th and Pb, enrichment in Pb and Sr over Ce, enrichment of LREE over heavy rare earth elements (HREE) and Y, is a distinct arc-signature (Price et al. 1992, 1999), characteristic of subduction-related magmas (e.g. Pearce 1982; Sun & McDonough 1989; McCulloch & Gamble 1991).

Isotope data from the Mt. Taranaki suite is relatively uniform with $^{87}Sr/^{86}Sr$, $^{143}Nd/^{144}Nd$ and Pb isotope ratios displaying only a very narrow compositional range (Price et al. 1992, 1999, 2005). No apparent systematic change in $^{143}Nd/^{144}Nd$ isotopic ratio with stratigraphic position or major and trace element chemistry was observed but $^{87}Sr/^{86}Sr$ ratios of edifice-building lavas increase slightly as the lavas become younger (Price et al. 1992, 1999). Oxygen isotope studies are consistent with the Sr, Nd and Pb data and indicate that genesis of Taranaki magmas involved partial melting of lower crustal material due to interaction with mantle-derived magmas (Price et al. 1992; 1999). The isotopic composition of Taranaki lavas overlaps with basalts from the TVZ but they are generally less radiogenic than Ruapehu andesites (Price et al. 1992; 1999, 2005).

The geochemical characteristics of Taranaki magmas are attributed to an origin in a complex "subduction factory" system initially as low-degree partial melts from a depleted mantle wedge fluxed by slab-derived fluids (Price et al. 1999). These parental magmas ponded at the

crust-mantle boundary, where they evolved from relatively undersaturated, hydrous, oxidised high-Mg basalts to high-Al basalts and basaltic andesite melts through a combination of crystal fractionation and interaction with underplated material (Foden & Green 1992; Stewart et al. 1996; Price et al. 1999). A small fraction of high-Al basalt melt rose to the surface and evolved to fractionated basaltic andesites and low-Si andesites. The basaltic andesite magmas are believed to have fed small, high-level magma chambers, where the complex interplay of fractional crystallisation, crystal accumulation, magma mingling and mixing (Smith et al. 1996) resulted in the formation of relatively hydrous, evolved magmas (Price et al. 1999).

Based on the comparison of Taranaki volcanism with andesite and rhyolite magmatism in the TVZ, Price et al. (2005) proposed that Taranaki and Ruapehu andesite magmas are generated through the interaction of mantle-derived arc magmas with the lower crust. Further modification of these melts occurred at varying times and various levels through assimilation and fractional crystallisation (AFC; de Paolo 1981) processes during migration within a complex, dispersed plumbing system. This evolution is reflected in the observed geochemical and mineral textural variations within andesitic rocks through time (Price et al. 2005). While andesitic systems develop at modest heat flow and magma supply, a shift to much higher heat flow and hence more extensive crustal melting likely results in transition to rhyolite volcanism and the production of large volumes of rhyolite magmas as found in the TVZ (Price et al. 2005).

4.3. METHODS OF SAMPLE COLLECTION

The new stratigraphy that has been developed (cf. Chapter 2) provides the basis for sampling the volcanic products of Mt. Taranaki for petrographic and geochemical analysis. As part of this study, twelve debris-avalanche deposits generated by large collapse events have been sampled from coastal ring-plain successions around the volcano, including the Maitahi Formation from Pouakai Volcano. Between 10 and 31 rock samples were analysed from selected debris-avalanche deposits, depending on accessibility of the sample location, availability of suitable clasts and variety of lithologies. Due to restricted outcrops and strong weathering, only four samples were collected from the Oeo debris-avalanche deposit. Grid references of sampling locations and sample numbers are listed in Appendix I.

The debris-avalanche deposits are used as a window into the composition of past edifices, since the contained clast assemblages represent the diversity of lithologies that built up the then existing volcanic edifice. Furthermore, they span the complete known age range of the

volcano as they occurred from earliest stages of volcanism onward. Mt. Taranaki debris-avalanche deposits are distinct, widespread and form a more complete stratigraphic record than the observed lahar units, which represent only short, spatially restricted time packages that are difficult to correlate and date.

For each individual debris-avalanche sample suite, a range of as many different lithologies as available was collected in order to cover as much of the spectrum of existing rock types and geochemical compositions at the time of deposition as possible. This method has not been applied before but appears to be a good approach to determine long-term magmatic trends even though there could be an overlap in samples and age ranges, since younger debris avalanches are likely to have picked up material from older units.

Geochemical data of all collected rock samples was acquired by X-ray fluorescence analysis (XRF) and inductively coupled plasma mass spectrometry (ICP-MS). In addition Sr, Nd and Pb isotope analyses were carried out for selected samples. Thin-sections were prepared for petrographic classification and electron microprobe (EMP) analysis of mineral compositions of clasts from the oldest debris-avalanche samples (cf. Chapter 5). A detailed description of analytical methods applied during this study can be found in Appendix II.

4.4. BULK ROCK COMPOSITION

The wide variety of volcanic lithologies represented by the debris-avalanche samples display a range in vesicularity reflecting both explosive and effusive origins. The analysed clasts have compositions ranging from basalt to andesite with the majority being basaltic andesite (Fig. 4.1; Table 4.1). SiO_2 content varies from 48.65 wt.% for the most primitive to 60.54 wt.% for the most evolved rocks. The oldest suites from Mt. Taranaki (Mangati, Motunui and Okawa debris-avalanche deposits) display the broadest range of compositions (48.6-58.8 wt.% SiO_2) that overlap with samples from the Maitahi Formation from Pouakai Volcano (Fig. 4.2A). They also include more primitive rocks that are generally absent from the younger suites, except for a basalt clast found within the Ngaere debris-avalanche deposit and basaltic lava flows from the Fanthams Peak satellite vent (cf. Price et al. 1992, 1999; Rosenthal 2005). In contrast, the younger units comprise a markedly higher proportion of andesite (Fig. 4.2B). Table 4.1 includes lithology data, SiO_2- and K_2O-ranges of the youngest, <10 ka edifice-building lavas and pyroclastic deposits for comparison as well as lava flow data of the satellite vent Fanthams Peak.

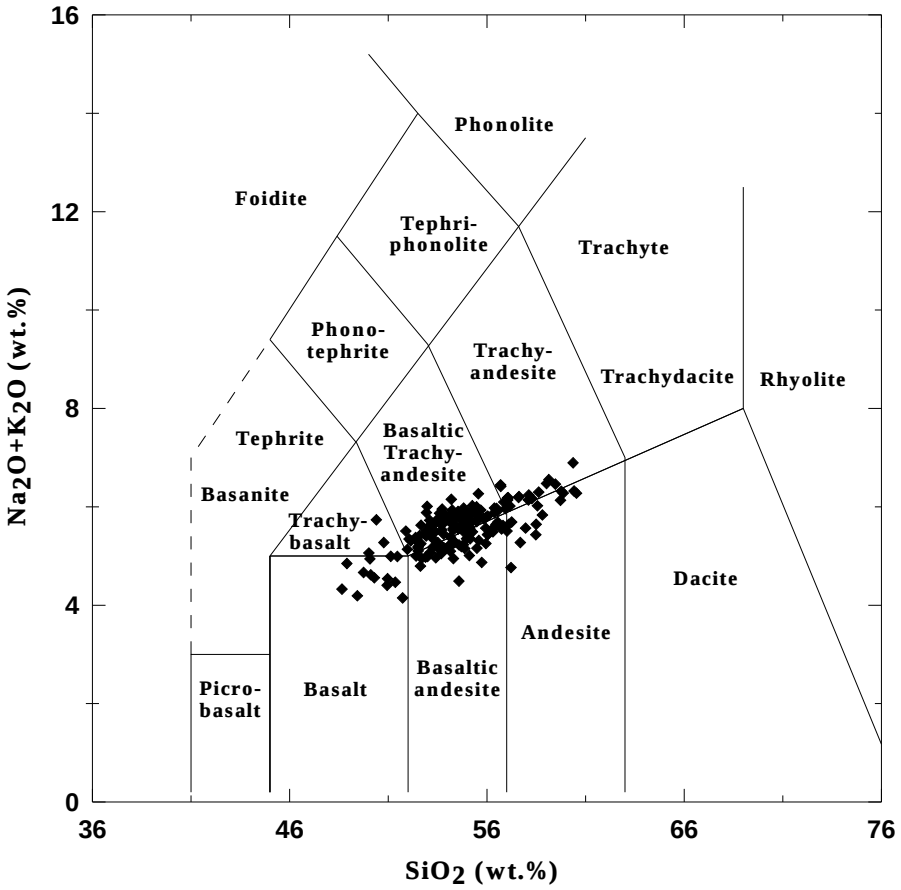

Figure 4.1. TAS discrimination diagram (after Le Maitre et al. 1989) of analysed debris-avalanche clasts showing their range in composition from basalt through to andesite.

TABLE 4.1. *Lithologies, SiO_2 and K_2O ranges of debris-avalanche and edifice sample suites.*

DA sample suite	Age (ka)	No. of samples	Basalt	Basaltic andesite	Andesite	SiO_2 range (wt.%)	K_2O range (wt.%)
Opua	7	13	0	9	4	52.1-59.5	1.79-2.43
Pungarehu	20	22	0	20	2	52.5-57.6	1.71-2.15
Ngaere	23	11	1	3	7	50.8-57.2	1.77-2.27
Te Namu	29	25	0	22	3	52.6-59.1	1.57-2.44
Rama	35	15	0	9	6	53.1-60.5	1.77-2.50
Otakeho	55	12	0	8	4	53.2-59.7	1.72-2.04
Waihi	70	8	0	8	0	51.9-55.9	1.78-2.00
Oeo	85	4	0	4	0	52.4-54.5	1.70-1.97
Okawa	105	16	6	8	2	48.7-58.6	1.26-2.07
Motunui	130	31	3	23	5	49.8-58.8	1.17-1.94
Mangati	200	15	1	13	1	48.9-57.1	1.16-2.09
Maitahi	270	12	2	7	3	49.4-58.5	1.27-1.66
Edifice*	<10	181	0	111	70	52.3-60.2	1.79-3.25
Fanthams**	<3.3	32	11	21	0	49.8-54.6	1.54-2.11

* Data of lava flow, BAF deposit and tephra samples from Price et al. (1999), Platz (2007) and Turner (2008).
** Data of Fanthams Peak lava flows from Price et al. (1999) and Rosenthal (2005).

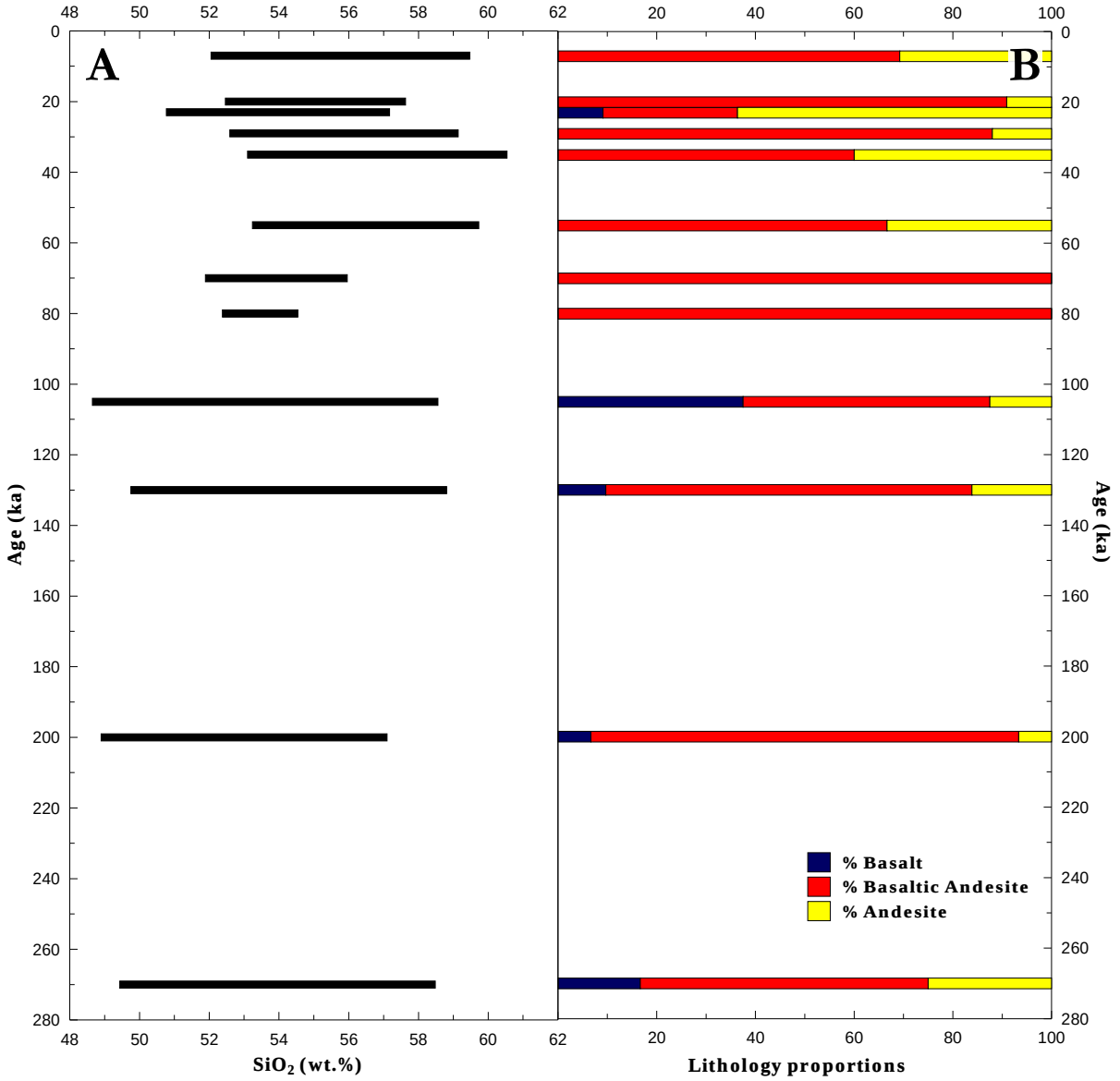

Figure 4.2. Variations in SiO_2 and lithological proportions for debris-avalanche clasts. The oldest debris-avalanche sample suites show the widest range in SiO_2 content (A). They also contain more primitive, basaltic rocks, which are rare in the younger deposits (B). By contrast, the latter comprise a higher proportion of andesite. The total number of analysed samples for each suite is given in Table 4.1.

The evolution to more evolved compositions is characterised by increasing K_2O with decreasing age. Potassium contents vary from 1.16 wt.% in older up to 2.5 wt.% in younger rocks (cf. Table 4.1). On a Gill (1981) classification diagram, debris-avalanche clasts range in composition from medium-K, low-Si basalts to high-K, high-Si andesites with the majority of samples plotting in the field of high-K, low-Si basaltic andesites (Fig. 4.3). The overall sequence shows a positive correlation between K_2O and SiO_2.

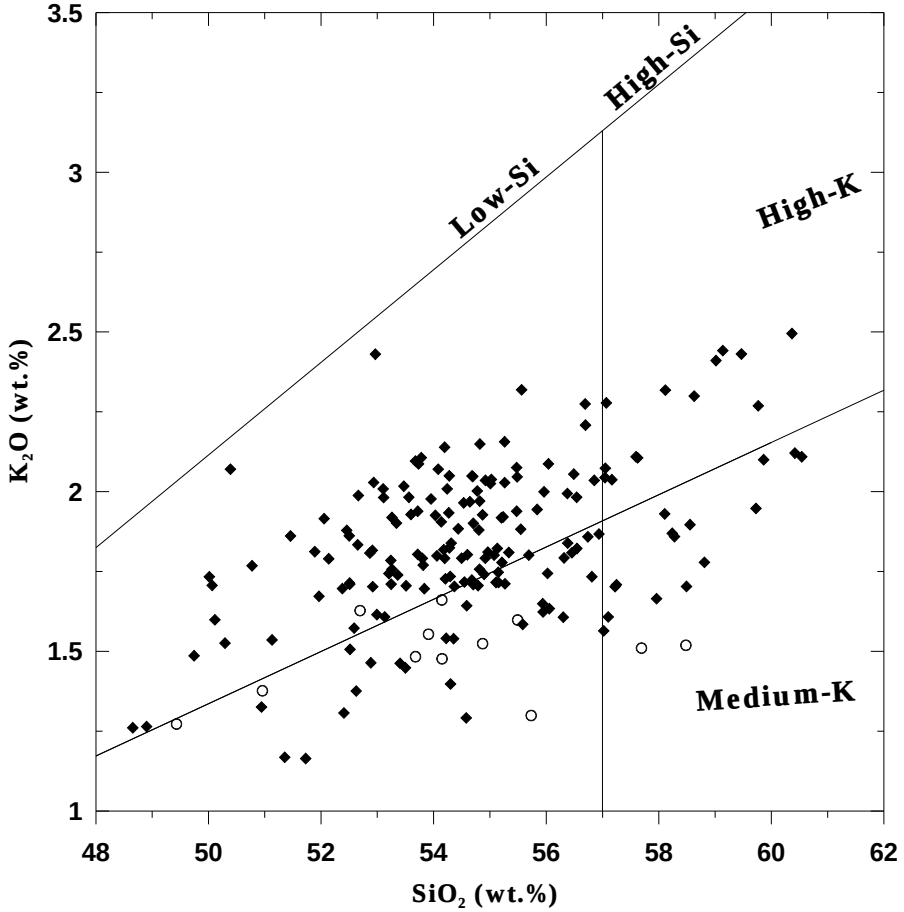

Figure 4.3. K_2O vs. SiO_2 variation diagrams for Mt. Taranaki (filled diamond) and Pouakai (open circle) debris-avalanche clasts. According to the classification of Gill (1981) the volcanics range from medium-K, low-Si to high-K, high-Si rocks, with Pouakai clasts showing predominantly lower-K contents than Mt. Taranaki.

4.4.1. Major elements

Major element abundances of Mt. Taranaki and Pouakai sample suites were obtained by XRF analyses and are illustrated in Fig. 4.4, using silica variation diagrams. TiO_2, FeO_{total}, CaO and MgO behave compatibly and show systematic decreases with increasing SiO_2 content, while Na_2O and K_2O (cf. Fig. 4.3) are incompatible and characterised by a positive correlation with SiO_2. The Pouakai data seem to indicate no change in K_2O with increasing SiO_2, which contrasts with Mt. Taranaki samples. Al_2O_3 appears to increase with increasing SiO_2 in samples <52 wt.% while Al_2O_3 in samples with >52 wt.% SiO_2 is constant. The highest-silica samples show the narrowest range of Al_2O_3. MnO contents and P_2O_5 abundances are relatively constant at varying SiO_2 contents. Generally, there appears to be a wider scatter of major element distributions at lower SiO_2 abundances, except for FeO_{total} with a very narrow range and K_2O with an overall wider array (Fig. 4.3).

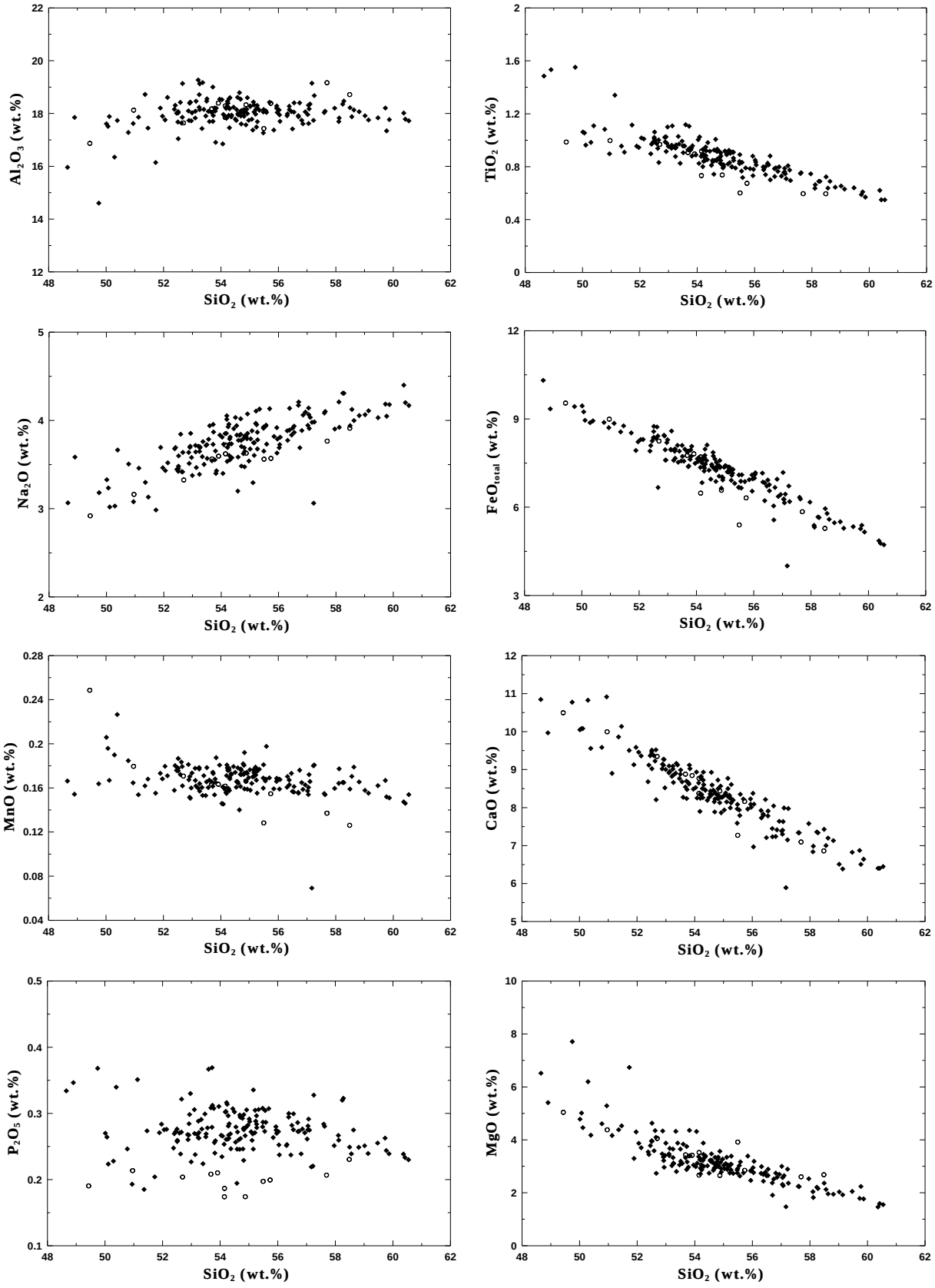

Figure 4.4. Major element variation as a function of SiO_2 content for Mt. Taranaki (filled diamond) and Pouakai (open circle) debris-avalanche samples.

The negative correlation of TiO_2 content with SiO_2 abundance is attributed to fractionation of titanomagnetite and possibly amphibole to a minor extent. A more rapid decrease at lower SiO_2 contents might indicate a higher rate of titanomagnetite crystallisation. Fractionation of olivine (at lower SiO_2 abundances), clinopyroxene, titanomagnetite as well as amphibole resulted in the systematic decrease of FeO_{total} in relation to SiO_2. CaO is predominantly bound in plagioclase and clinopyroxene and, to a minor extent, in amphibole, resulting in a negative correlation with SiO_2. The negative relationship between MgO and SiO_2 is mainly the result of olivine, clinopyroxene and amphibole fractionation with the more rapid decrease of MgO abundance at lower SiO_2 contents reflecting a greater influence of olivine. The content of MnO is relatively constant with a slight negative correlation to SiO_2 possibly due to its compatibility in clinopyroxene.

The increase of Na_2O and K_2O with increasing SiO_2 is a result of their incompatible behaviour and enrichment in the residual melt. P_2O_5 displays a relatively wide scatter when plotted against SiO_2 with Pouakai clasts having distinctly lower P_2O_5 contents than the Mt. Taranaki suites, which show a slightly negative relationship with SiO_2.

4.4.2. Trace elements

The variation of trace elements in Taranaki debris-avalanche samples is displayed in SiO_2 variation diagrams (Fig. 4.5). The geochemical abundances of all trace elements except Ni were acquired by more precise ICP-MS analyses. Due to a technical error the wrong Ni isotope was analysed; as a result, XRF-determined Ni values are reported here instead.

Rubidium, Ba and Zr behave incompatibly and hence their abundances increase systematically with increasing SiO_2 contents. Rubidium and Ba variation is similar to the distribution of K_2O (cf. Price et al. 1999). These elements show a strong positive correlation, with Pouakai samples generally displaying lower concentrations. Zirconium abundances in Pouakai rocks appear relatively constant with increasing SiO_2 and lack the distinct positive correlation displayed by Mt. Taranaki sample suites. Strontium contents show a wide scatter and overall no correlation with SiO_2 abundance in both the Mt. Taranaki and Pouakai debris-avalanche data, but Pouakai samples plot at distinctively lower Sr concentrations.

The systematic decrease of Sc and V with increasing SiO_2 is similar to MgO, FeO, CaO and TiO_2 but with a narrower range at low-Silica abundances. Nickel and Cr show a wide scatter and rapid decrease at low-silica contents, indicating olivine and clinopyroxene fractionation, and a weak negative correlation with SiO_2 at medium- to high-silica abundances. Nickel and Cr

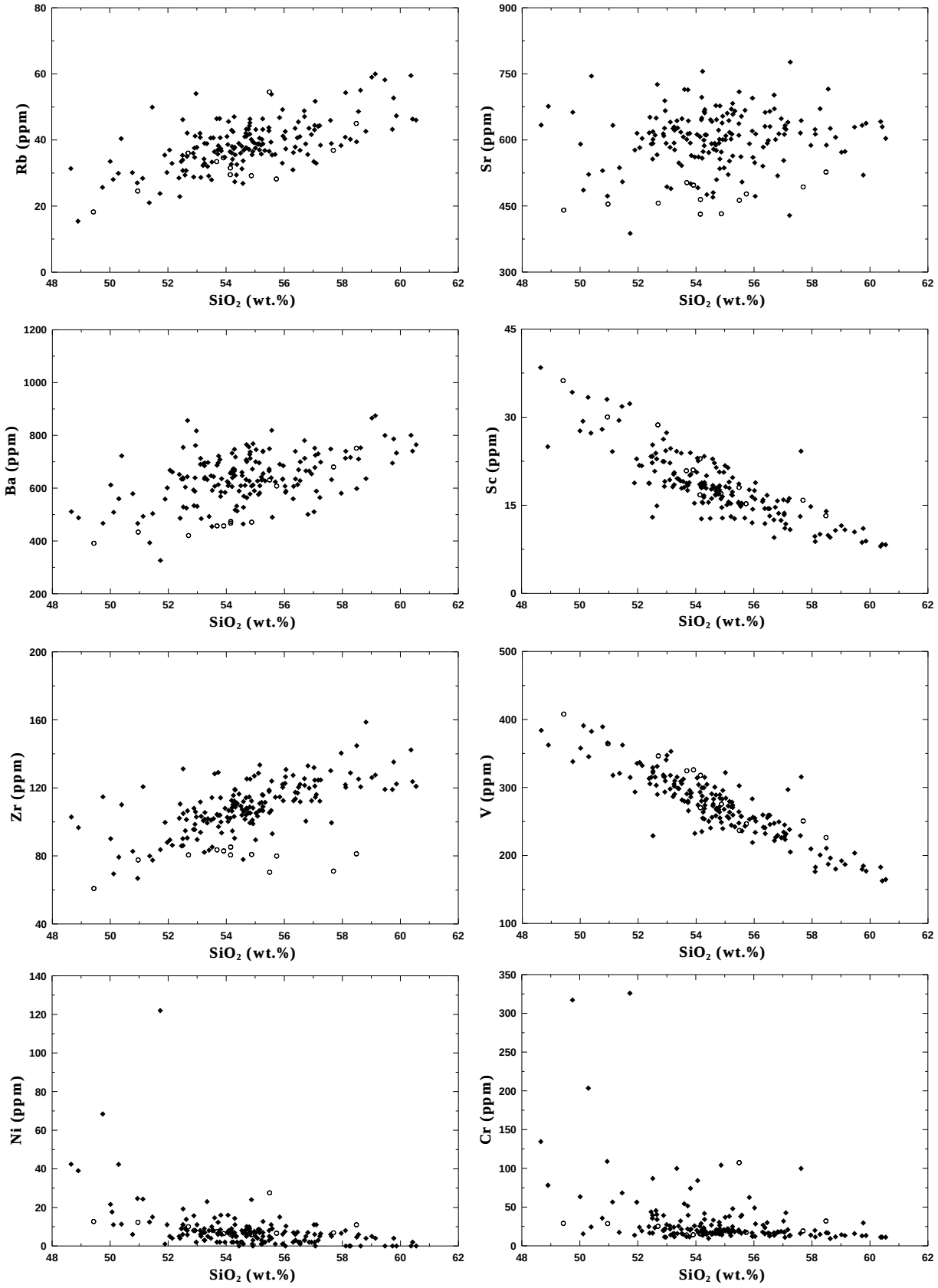

Figure 4.5. Trace element variation versus SiO_2abundance for Mt. Taranaki (filled diamond) and Pouakai (open circle) debris-avalanche samples.

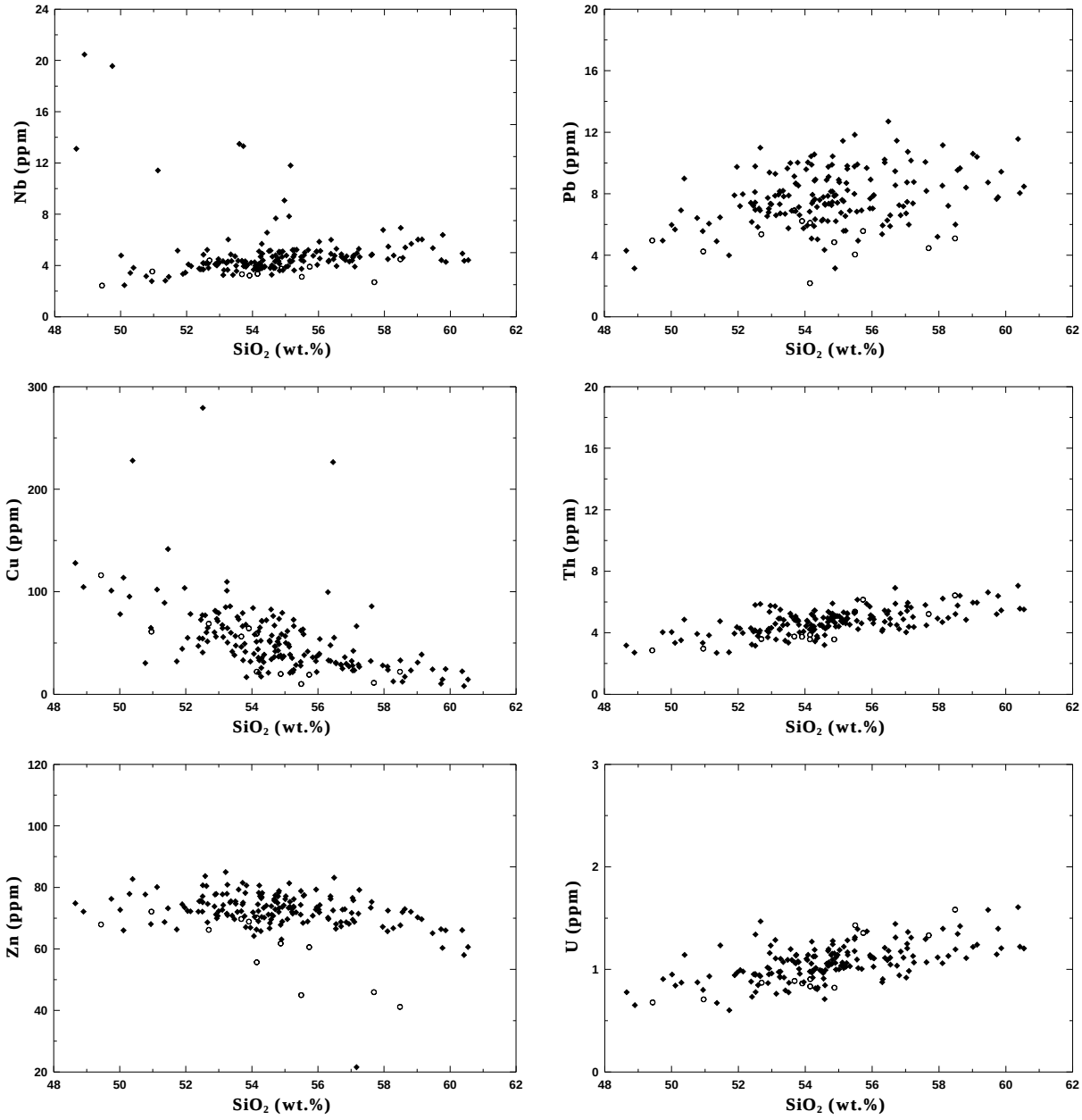

Figure 4.5. (continued) Trace element variation versus SiO_2abundance for Mt. Taranaki (filled diamond) and Pouakai (open circle) debris-avalanche samples.

contents are generally low, reflecting the evolved nature of Taranaki magmas (cf. Price et al. 1999). Nickel abundance is <16 ppm for most samples, ranging up to 68 ppm with one sample showing an exceptionally high content of 188 ppm. Most samples contain <50 ppm Cr, a few up to 203 ppm and two rocks show high Cr contents of 317 and 326 ppm, respectively. Copper variation displays a systematic decrease with increasing SiO_2 with three samples having higher concentrations. Mt. Taranaki sample suites show relatively constant Zn contents with a change to decreasing abundances for high-silica rocks. Pouakai samples are distinct with significantly lower Zn contents that decrease systematically with increasing SiO_2.

Niobium variation is complex and abundances are generally low (<6 ppm). Pouakai samples have lower Nb contents (<4.5 ppm) than Mt. Taranaki debris-avalanche clasts and show a weak positive relationship with SiO_2. Some samples scatter at higher Nb contents with a few low-Si rocks containing up to 20 ppm Nb

Uranium, Pb and Th behave incompatibly and hence their abundances increase with increasing SiO_2. They are also strongly correlated with K_2O. The variation of Pb is most similar to K_2O with a wide scatter and the oldest units showing the lowest Pb abundances. Pouakai rocks have distinctly lower Pb contents than Mt. Taranaki sample suites.

4.4.3. Fractionation trends

Dominantly linear trends of major and some trace element variation within the whole rock analyses of the analysed debris-avalanche sample suites are consistent with a broad control by crystal/melt fractional processes (cf., Bowen 1928; Gill 1981; Gamble et al. 1990). Early fractionation or accumulation of olivine and clinopyroxene is reflected in the rapid decrease of FeO*, MgO, Ni and Cr within the more primitive compositions. Further fractionation of olivine and clinopyroxene results in the systematic depletion in FeO*, MgO, Ni and Cr and enrichment in SiO_2, Na_2O and K_2O. The high rate of CaO-decrease at lower SiO_2 also reflects clinopyroxene fractionation with the change to a gentler slope marking the onset of plagioclase crystallisation. The increase of Al_2O_3 at lower SiO_2 abundances could indicate initial plagioclase repression due to high P_{H2O}, while relatively constant Al_2O_3 contents together with falling CaO abundance reflect clinopyroxene fractionation. Hornblende fractionation systematically reduces TiO_2, Sc and V abundances, which are also compatible in titanomagnetite. The variability of Sr abundance is likely to reflect variable amounts of plagioclase some of which appears to be xenocrystic. LILE, HFSE and REE are incompatible in the early crystallising phases and hence increase with increasing SiO_2.

The interpretation of geochemical trends within these samples might allow some indication of crystal/melt fractional processes and the above described fractionation trends are consistent with the major mineral phases (plagioclase, hornblende, clinopyroxene, olivine and titanomagnetite) observed in Taranaki debris-avalanche clasts (cf. Chapter 5). However, crystal/melt fractional processes are more complex and whole rock compositional trends do not correspond directly to simple liquid lines of descent. Instead, there is strong evidence that large proportions of the contained crystals may be xenocrysts that formed in the lower crust and are not directly related to the surrounding melt during ascent (Stewart et al. 1996). Hence,

geochemical variation is not the result of simple crystal fractionation but reflects mixing of melts with crystals from various sources.

Mineral textures are therefore a more useful indicator of crustal processes at Mt. Taranaki since they preserve evidence of crystal fractionation, later crystal resorbtion and assimilation (AFC; DePaolo 1981) processes as well as magma mixing or mingling (Smith et al. 1996; Stewart et al. 1996; Price et al. 1999; Turner 2008). Furthermore, a new model by Turner (2008) suggests that a two-stage magmatic system operates beneath Mt. Taranaki with much of the magma differentiation occurring at lower levels within the crust, from where melt-crystal mixtures subsequently rise to recharge a mid-crustal system (at c. 7-10 km depth). Hence, geochemical (and petrographic) variations within Mt. Taranaki rocks are mainly generated by AFC processes within the deeper part of the plumbing system and during subsequent ascent. Further fractional crystallisation and magma mingling at shallow levels may have overprinting effects on the magma characteristics (Smith et al. 1996; Stewart et al. 1996). Petrographic and mineralogical characteristics of the debris-avalanche sample suites will be further discussed in Chapter 5.

4.4.4. Rare earth elements

The chondrite-normalised REE patterns of analysed debris-avalanche clasts (Fig. 4.6) are characterised by enrichment of light rare earth elements (LREE) relative to heavy rare earth elements (HREE) with $(La/Yb)_n$ = 3.1-10.0 for Mt. Taranaki samples and $(La/Yb)_n$ = 4.1-9.5 for Pouakai rocks. Concentrations of HREE form a relatively flat profile with a gentle decrease in normalised abundances from Eu to Dy and almost constant proportions of Ho-Lu. Pouakai samples typically have lower concentrations of REE than Mt. Taranaki suites (Fig. 4.6B). Three andesite clasts (AZ06-57, -60 and -61) are distinct and show similar low concentrations of La-Pr but markedly lower abundances of Nd, Sm and HREE than the rest of the Pouakai suite, which might be due to their high contents of very large xenocrystic plagioclase. This could also explain why these three andesites, and some other samples, lack the weakly developed negative Eu anomaly that is present in the normalised REE pattern of most Mt. Taranaki and Pouakai debris-avalanche samples.

The composite normalised extended element diagrams for Mt. Taranaki sample suites (Fig. 4.7.A) show a strong enrichment of large ion lithophile elements (LILE) such as Cs, Rb, Ba and K and, to a lesser extent, Sr relative to normal mid-ocean ridge basalts (MORB). Niobium is strongly depleted relative to K, Th, U and Pb. Lead and, to a lesser extent, Sr are enriched over

TABLE 4.2. *XRF and ICP-MS whole-rock analyses for selected Mt. Taranaki and Pouakai debris-avalanche samples.*

DAD	**Maitahi**		**Mangati**		**Motunui**		**Okawa**		**Waihi**	**Rama**		**Te Namu**		**Ngaere**		**Pungarehu**		**Opua**
Sample	**AZ06-60**	**AZ06-65**	**AZ06-68**	**AZ06-73**	**AZ04-20**	**AZ04-30**	**AZ04-1**	**AZ04-6**	**AZ06-32**	**AZ06-10**	**AZ06-12**	**AZ05-21**	**AZ05-22**	**AZ06-84**	**AZ06-93**	**AZ05-33**	**AZ05-55**	**AZ06-51**
XRF analyses of major elements (wt%)																		
SiO_2	58.48	49.43	51.73	48.90	52.88	56.46	58.56	48.65	55.21	60.37	54.24	53.51	55.26	56.49	50.77	54.64	52.51	58.63
TiO_2	0.60	0.99	1.11	1.53	0.99	0.83	0.64	1.48	0.80	0.62	0.89	0.91	0.87	0.81	1.08	1.01	0.99	0.69
Al_2O_3	18.72	16.87	16.14	17.85	17.74	18.07	17.88	15.96	18.15	18.02	18.39	18.56	18.30	17.41	17.28	18.79	18.03	18.13
Fe_2O_3	5.87	10.60	9.48	10.39	9.36	7.47	6.43	11.46	7.68	5.40	8.19	8.59	7.95	7.69	9.87	8.49	9.31	6.21
FeO_{total}	5.28	9.54	8.53	9.35	8.42	6.72	5.79	10.31	6.91	4.86	7.37	7.73	7.16	6.92	8.88	7.64	8.38	5.59
MnO	0.13	0.25	0.16	0.15	0.17	0.17	0.17	0.17	0.17	0.15	0.18	0.18	0.16	0.16	0.18	0.14	0.18	0.18
MgO	2.68	5.04	6.74	5.41	4.33	2.78	2.13	6.52	2.75	1.46	2.87	3.19	2.86	2.65	4.61	2.85	3.96	1.96
CaO	6.86	10.50	9.51	9.97	9.15	8.21	7.00	10.85	8.25	6.40	8.34	8.99	8.24	7.21	9.58	8.46	9.51	7.20
Na_2O	3.91	2.92	2.99	3.58	3.51	3.83	4.12	3.07	4.11	4.40	3.93	3.57	3.87	3.91	3.51	3.83	3.48	4.00
K_2O	1.52	1.27	1.16	1.26	1.46	1.81	1.90	1.26	1.78	2.50	2.01	1.71	2.16	2.06	1.77	1.97	1.71	2.30
P_2O_5	0.23	0.19	0.20	0.35	0.26	0.24	0.24	0.33	0.30	0.24	0.31	0.27	0.30	0.28	0.25	0.26	0.26	0.27
H_2O	0.30	1.02	0.49	0.41	0.05	0.00	0.09	0.08	0.06	0.06	0.13	0.05	0.02	0.50	0.43	0.00	0.15	0.07
LOI	0.41	0.32	-0.02	0.01	-0.10	0.02	0.56	0.20	0.04	-0.26	-0.06	0.28	-0.17	0.21	0.25	-0.10	-0.28	-0.03
Total	99.70	99.41	99.68	99.82	99.81	99.89	99.71	100.03	99.31	99.35	99.42	99.79	99.81	99.39	99.58	99.66	99.81	99.60
Mg# *	33.67	34.57	44.14	36.65	33.98	29.28	26.87	38.73	28.44	23.14	28.00	29.20	28.58	27.69	34.16	27.15	32.09	25.97
ICP-MS analyses of trace elements (ppm)																		
Ba	751.47	391.32	326.29	487.82	533.58	613.46	710.46	511.02	631.09	800.40	673.53	591.47	738.13	669.74	579.04	610.32	754.89	753.25
Rb	44.98	18.23	23.78	15.42	28.80	40.65	48.62	31.35	35.72	59.47	42.49	33.32	46.40	45.47	30.11	41.00	46.15	55.02
Sr	527.01	440.59	387.77	676.31	609.23	592.28	715.61	633.69	670.06	641.57	573.45	648.16	482.83	598.63	530.31	592.15	618.89	625.98
Pb	5.09	4.96	3.99	3.15	7.73	6.27	9.53	4.60	5.60	11.56	7.52	7.88	9.81	12.70	6.42	8.89	9.78	9.66
Th	6.43	2.86	2.73	2.71	3.71	5.22	5.77	3.17	4.61	7.06	5.11	3.88	5.27	5.41	3.93	4.34	5.80	6.41
La	34.04	29.44	29.69	33.65	15.98	18.88	18.86	16.54	36.61	46.75	34.97	14.53	15.65	26.57	31.22	13.19	19.53	37.39
Ce	25.95	21.75	21.84	28.54	32.88	36.28	37.33	32.30	35.33	39.94	34.45	28.20	31.67	26.89	26.12	27.16	39.52	37.98
Y	11.32	18.00	18.25	17.82	20.85	22.44	19.74	19.86	19.03	18.57	21.74	20.02	19.09	20.43	18.89	20.50	23.06	21.73
Zr	81.24	60.82	83.67	96.67	107.99	117.03	125.22	102.87	111.49	142.36	115.58	85.22	106.61	120.43	82.71	101.60	131.22	120.61
Nb	4.49	2.43	5.16	20.46	4.08	4.49	4.60	13.11	5.21	4.94	4.69	3.57	3.62	4.76	3.16	3.79	4.84	5.40
Sc	13.21	36.22	32.29	24.98	26.26	16.70	9.89	38.44	13.08	8.01	15.40	17.90	17.27	14.42	27.94	22.20	12.96	9.52
V	226.42	407.93	314.89	362.48	315.91	255.76	187.29	384.02	244.50	182.77	263.83	281.70	273.85	259.20	389.26	300.66	229.01	196.19
Cr	32.04	28.98	325.98	78.17	39.27	29.94	16.53	134.51	17.93	11.29	13.77	15.93	21.03	16.61	35.80	16.67	16.48	9.35
Ni **	8	10	122	39	15.7	7.2	5.9	42.4	3	0	2	8	7	2	6	8	11	0
Cu	21.94	116.10	32.12	106.64	81.51	226.46	12.25	127.98	35.34	22.38	35.12	47.54	72.68	55.19	30.44	76.40	40.81	17.15
Zn	41.15	67.94	66.35	72.12	77.68	72.53	71.96	74.84	72.03	66.10	77.16	74.69	73.79	83.16	77.72	70.74	75.18	72.95

* Mg# calculated as $MgO*100/(MgO+FeO_{total})$ based on $FeO_{total} = Fe_2O_3*0.8998165$.
**Ni data from XRF analyses.

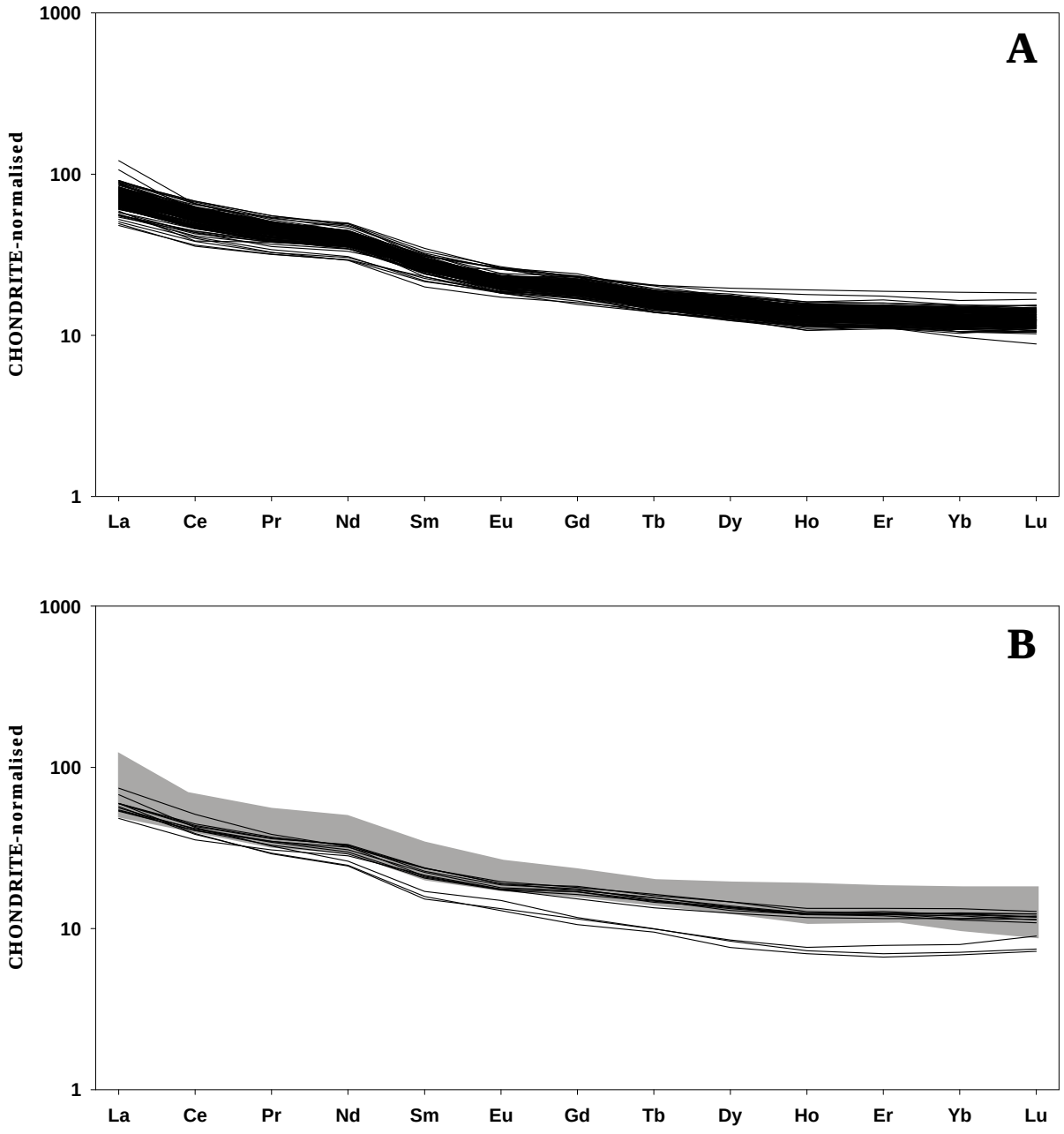

Figure 4.6. Chondrite-normalised rare earth element diagrams (normalising values from Sun & McDonough, 1989).

A: Mt. Taranaki sample suites show enrichment of LREE over HREE, a feature characteristic of arc magmas.

B: In comparison, Pouakai samples have lower REE contents than Mt. Taranaki rocks (shaded in grey). Three samples are distinct with similar abundances of La-Pr but markedly lower concentrations of Nd, Sm and HREE.

Ce. Titanium, Y and Yb are depleted relative to N-MORB. Overall, LILE show significantly greater abundances than high field strength elements (HFSE) such as Nb, Zr, Ti, Y and REE.

The normalised trace element pattern of most basaltic clasts is parallel to that of the analysed andesites, with the exception of basalts having lower Zr and higher Ti abundances (Fig. 4.6B). Some of the oldest, more primitive rocks are characterised by a smoother trace and rare earth element pattern (Fig. 4.6C), in particular sample AZ06-73 of the Mangati suite, marked in red. Three additional basalt clasts, two of the Okawa series and one of the Motunui suite, also show a more subdued arc signature.

Most Pouakai samples display a similar normalised trace and rare earth element distribution to Mt. Taranaki basalts (Fig. 4.7). One Pouakai basalt (AZ06-65) has a slightly different geochemistry with LILE concentrations similar to AZ06-73 and a distinctly lower Zr content and one basaltic andesite (AZ06-59) shows lower Pb abundances. The three andesites (AZ06-57, -60 and -61) with low HREE contents are also characterised by lower abundances of other HFSE such as Zr, Ti and Y and higher Ba, Th, and U concentrations than the rest of the Pouakai suite.

→

Figure 4.7 (next page). Composite normalised extended element diagram of selected trace and rare earth elements normalised to N-MORB for Mt. Taranaki sample suites (normalising values from Sun & McDonough 1989).

A: Mt. Taranaki rocks show a typical arc signature, characterised by enrichment of LILE relative to normal MORB, strong depletion in Nb relative to K, Th, U and Pb and enrichment of Pb and Sr over Ce.

B: Andesitic and most basaltic samples of the Mt. Taranaki suites show parallel trends of trace and rare earth element with the latter generally having lower concentrations of incompatible trace elements. The normalised trace element distributions of some basalt clasts are distinct from the overall observed pattern.

C: One basaltic sample of the Mangati suite (AZ06-73) shows a significantly more subdued arc signature than the average Mt. Taranaki rocks (shaded in grey). Two basaltic rocks of the Okawa series (AZ04-06 and -07) and one clast of the Motunui suite (AZ04-27) show a weak but yet more distinct subduction-related trace and rare earth element pattern.

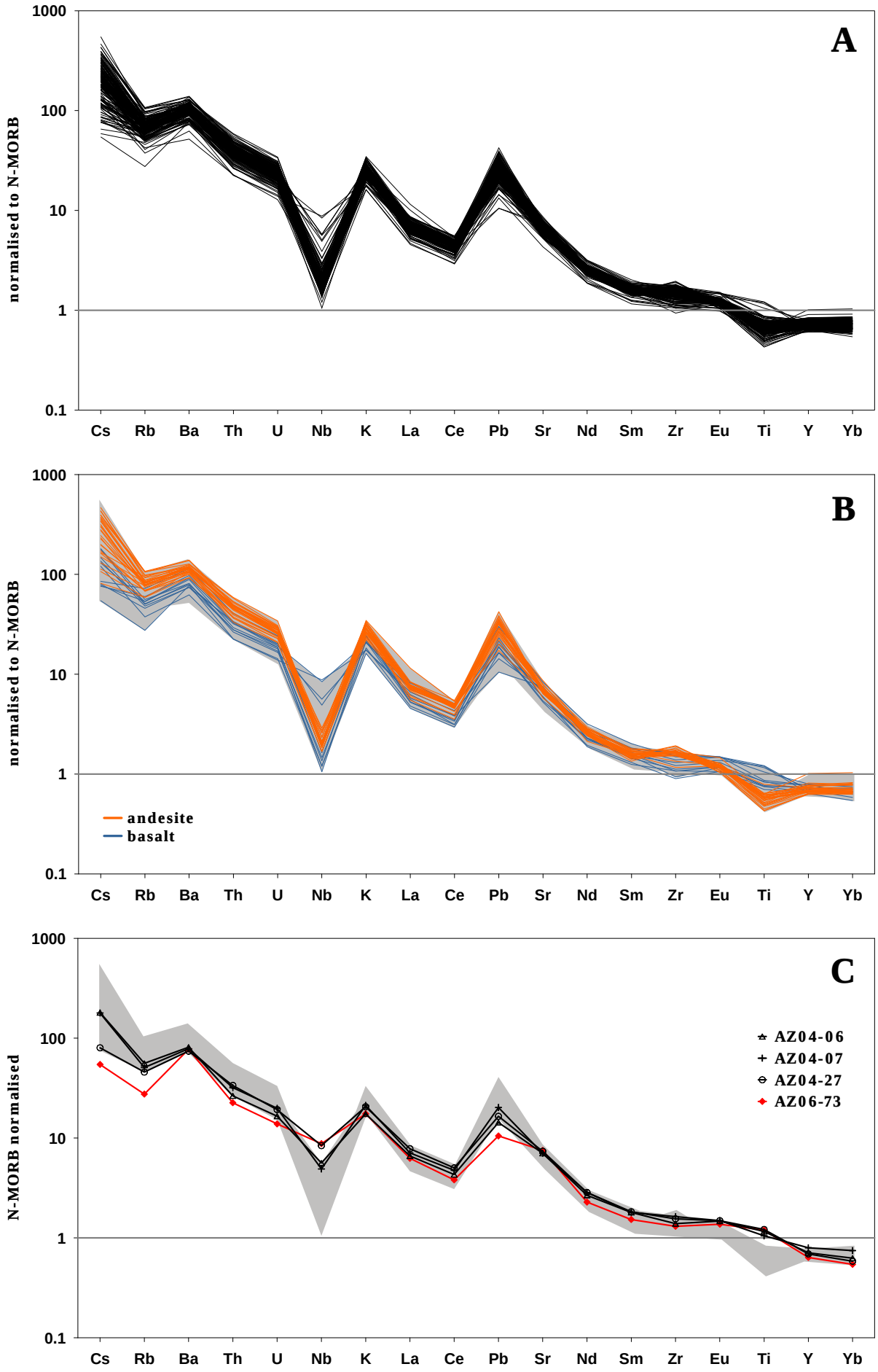
A
normalised to N-MORB
1000
100
10
1
0.1
Cs Rb Ba Th U Nb K La Ce Pb Sr Nd Sm Zr Eu Ti Y Yb
B
normalised to N-MORB
andesite
basalt
C
N-MORB normalised
AZ04-06
AZ04-07
AZ04-27
AZ06-73

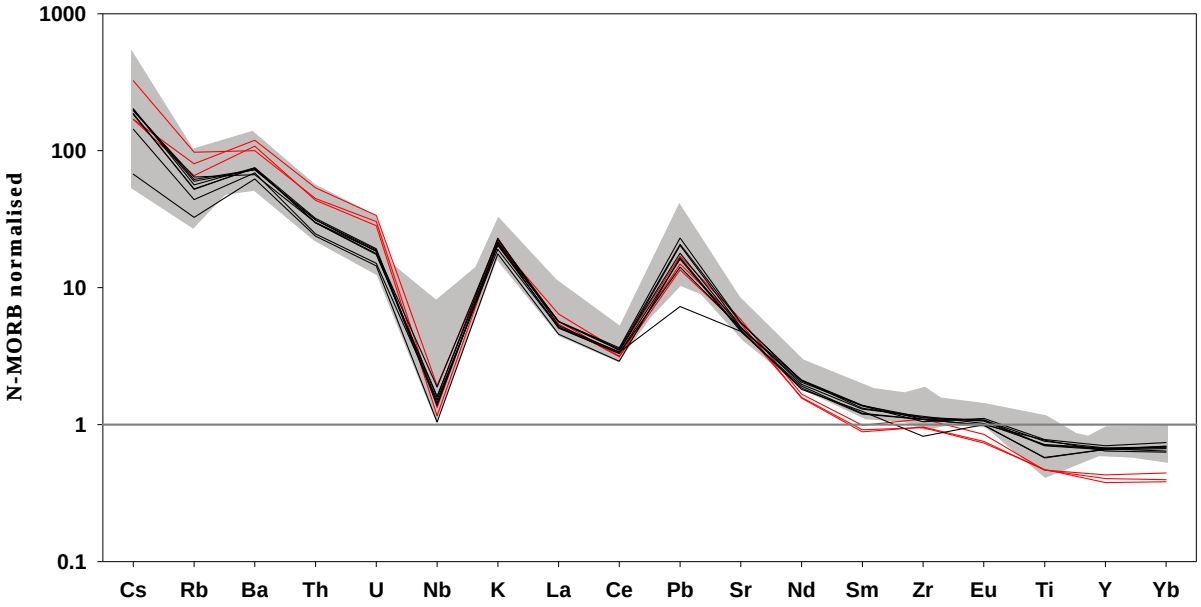

Figure 4.8. Composite normalised extended element diagram of selected trace and rare earth elements normalised to N-MORB (normalising values from Sun & McDonough 1989) for Pouakai samples in comparison to Mt. Taranaki suites (shaded in grey). The three distinct andesite samples AZ06-57, -60 and -61 with markedly lower HREE contents are shown in red.

4.5. ISOTOPIC SIGNATURES

The most primitive basalts and basaltic andesite clasts from the oldest debris-avalanche deposits and, because primitive compositions are absent, some basaltic andesite samples from several younger units were selected for Sr and Nd isotope analysis. Some of these were also analysed for Pb isotope geochemistry. The results are presented in Table 4.3.

$^{87}Sr/^{86}Sr$ ratios show little variation and range from 0.703605-0.704742 for Mt. Taranaki samples. Pouakai clasts lie within the same narrow range (0.704639-0.704839). Three basalts of the oldest Mt. Taranaki debris-avalanche deposits have markedly lower isotope ratios compared to the rest of the suites. There is no obvious correlation between $^{87}Sr/^{86}Sr$ isotopic composition and SiO_2 contents in the analysed suites (Fig. 4.9A), which contrasts with the behaviour observed in the lava flow sequences of the young (post-10 ka) Mt. Taranaki edifice (Price et al. 1999). Overall, and with the exception of the three distinct basalt samples, the strontium isotopic ratios of the debris-avalanche rocks become slightly less radiogenic with decreasing age (Fig. 4.9B).

Both, the Mt. Taranaki and Pouakai $^{143}Nd/^{144}Nd$ isotopic compositions are also constrained within a narrow range and vary from 0.512831 (εNd = 3.76) to 0.512987 (εNd = 6.81) (cf. Table 4.3). Despite the restricted range of observed values, Sr isotopic compositions correlate negatively with $^{143}Nd/^{144}Nd$ (Fig. 4.10).

The sample suites show only a limited range in Pb isotopic compositions, with $^{206}Pb/^{204}Pb$ ratios ranging from 18.740 to 18.792, $^{207}Pb/^{204}Pb$ ratios from 15.580 to 15.606 and $^{208}Pb/^{204}Pb$ ratios from 38.539 to 38.639 (cf. Table 4.3). The youngest samples have the highest $^{207}Pb/^{204}Pb$ contents and higher $^{208}Pb/^{204}Pb$ ratios than most other analysed clasts but their $^{206}Pb/^{204}Pb$ ratios overlap with the older suites (Fig. 4.11). As is the case for the Sr and Nd isotopic data, other trends or correlations with major and trace elements could not be recognised due to the restricted range in variation in isotopic composition and the limited number of analysed samples.

TABLE 4.3. *Isotope data of analysed debris-avalanche samples.*

DAD	Sample	$^{87/86}Sr$	$^{143/144}Nd$	εNd	$^{206/204}Pb$	$^{207/204}Pb$	$^{208/204}Pb$
Pungarehu	AZ05-43	0.704488	0.512864	4.41			
Te Namu	AZ05-12	0.704718	0.512837	3.88			
Rama	AZ06-09	0.704661	0.512856	4.25			
Rama	AZ06-16	0.704742	0.512838	3.90	18.760	15.606	38.622
Otakeho	AZ06-41	0.704639	0.512831	3.76	18.758	15.605	38.615
Okawa	AZ04-03	0.704548	0.512884	4.80			
Okawa	AZ04-04	0.704574	0.512922	5.54	18.743	15.599	38.585
Okawa	AZ04-06	0.704015	0.512951	6.11	18.792	15.596	38.608
Motunui	AZ04-27	0.703834	0.512930	5.70	18.788	15.591	38.591
Motunui	AZ04-31	0.704602	0.512876	4.64	18.740	15.591	38.593
Mangati	AZ06-68	0.704622	0.512849	4.12	18.751	15.599	38.639
Mangati	AZ06-73	0.703605	0.512987	6.81	18.781	15.580	38.539
Mangati	AZ06-80	0.704584	0.512873	4.58			
Maitahi	AZ06-63	0.704839	0.512826	3.67			
Maitahi	AZ06-65	0.704639	0.512879	4.70	18.743	15.590	38.588

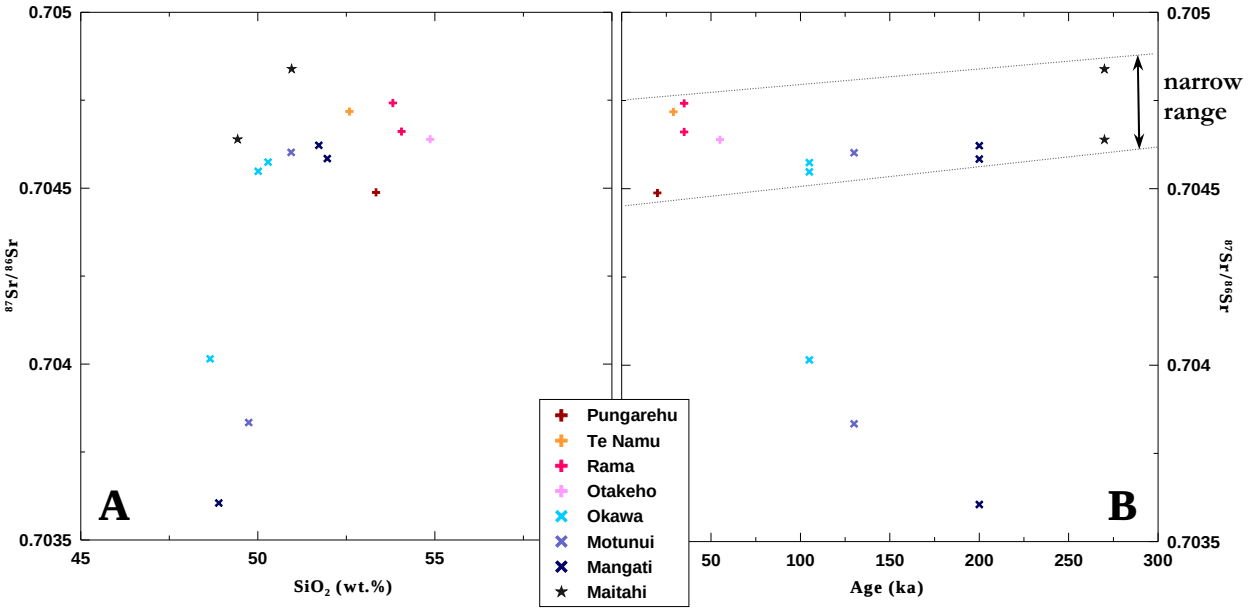

Figure 4.9. Variation of $^{87}Sr/^{86}Sr$ in relation to SiO_2 content (A) and age (B) of selected Taranaki debris-avalanche samples. Most samples are within a narrow range of $^{87}Sr/^{86}Sr$ isotopic compositions but three basalts from the oldest Mt. Taranaki suites are distinct with lower $^{87}Sr/^{86}Sr$ ratios.

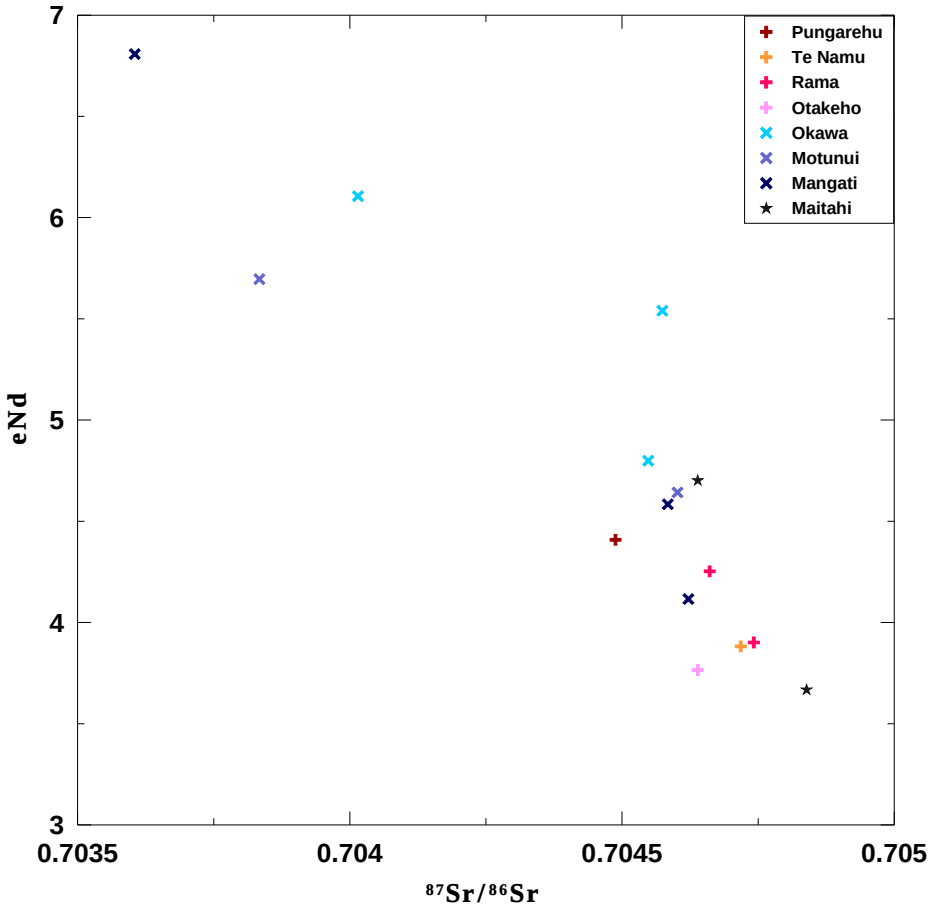

Figure 4.10. Taranaki debris-avalanche clasts show a distinct negative correlation between $^{87}Sr/^{86}Sr$ and $^{143}Nd/^{144}Nd$ isotopic compositions.

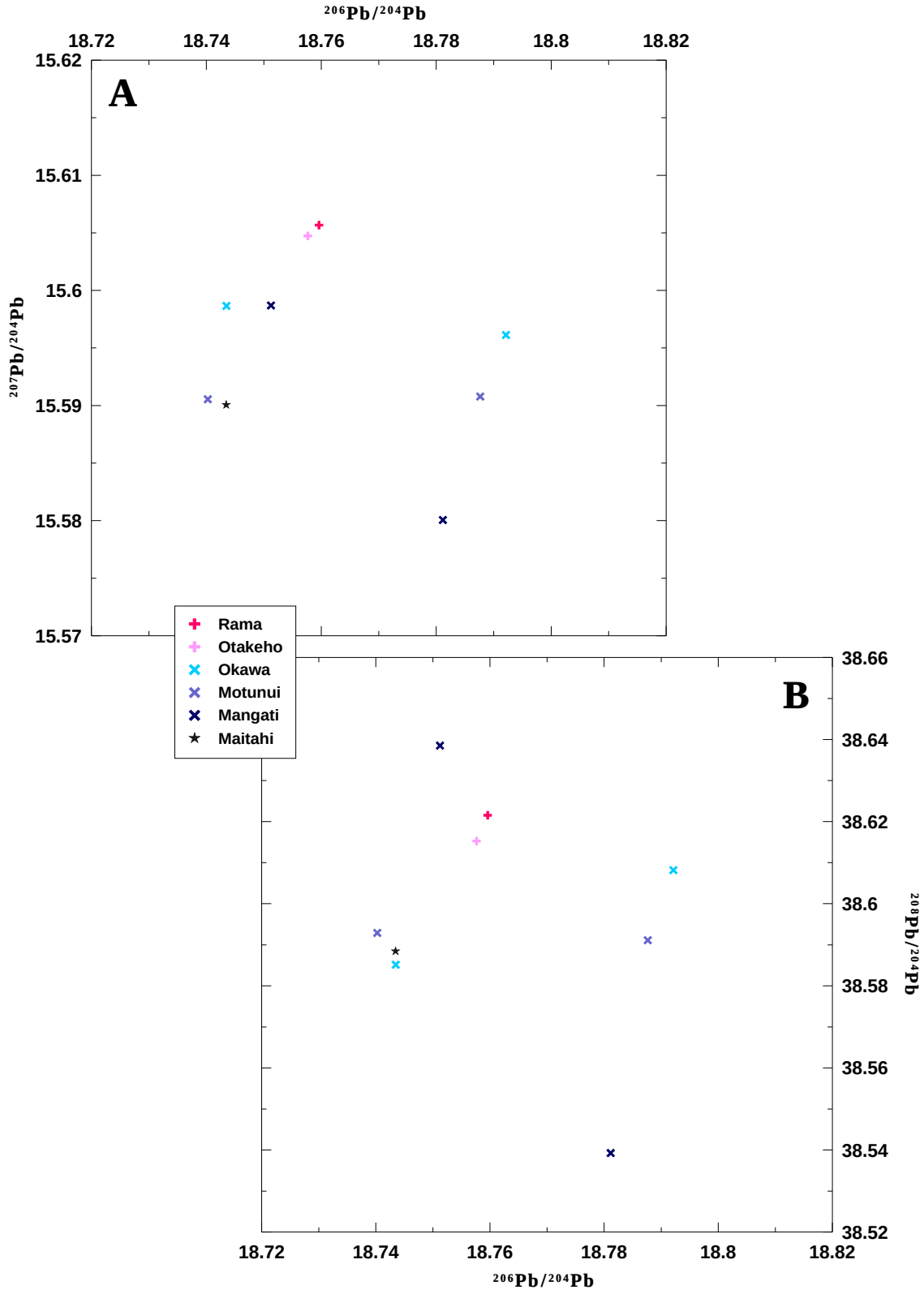

Figure 4.11. Lead isotope composition of selected Mt. Taranaki and Pouakai debris-avalanche clasts.
A: Variation of $^{207}Pb/^{204}Pb$ in relation to $^{206}Pb/^{204}Pb$.
B: Plot of $^{208}Pb/^{204}Pb$ versus $^{206}Pb/^{204}Pb$.

4.6. COMPOSITIONAL VARIATION WITH TIME

Mt. Taranaki is recognised as a high-K arc volcano and was originally used to develop the concept of the K-*h* relationship of increasing K_2O with increasing depth to the slab by Dickinson & Hatherton (1967). Later studies showed that K_2O behaviour in the Taranaki volcanics is time rather than slab depth-dependent (Price et al 1992, 1999, 2005; Stewart et al. 1996). The debris-avalanche sample suites described here allow a more detailed reconstruction of systematic changes in the magmatic composition of eruptives over a long period and differentiation of individual stratigraphic units as well as Mt. Taranaki and Pouakai suites. Variations in K_2O-contents continue to show up as the most distinct time-dependent geochemical trend observed.

Figure 4.12 shows a K_2O versus SiO_2 compilation of debris-avalanche data from this study and data from previous studies of younger volcanic eruptives that built up the present-day cone of Mt. Taranaki (Price 1999; Platz 2007; Turner 2008). Each stratigraphic suite is distinct, although there is some overlap for units of similar age (Fig. 4.3B), which is expected because a major debris-avalanche event may sample variably older rocks. The Pungarehu and Ngaere Formations were deposited less than 5 ka apart and show considerable similarity in clast composition. The compositions of clasts found within the Opua Formation overlap with those of <10 ka eruptives that form the present-day edifice. This is to be expected since the Opua debris avalanche was generated from the modern edifice by partial collapse at c. 6.6 ka (Neall 1979). The linear regression fits of each sample suite not only display a progressive increase of K_2O abundance with time but also show successively steeper trajectories on the SiO_2 versus K_2O plot. The Maitahi suite from Pouakai Volcano contains the least fractionated samples with relatively constant K_2O abundances. In contrast, a dramatic jump and steepening of slope occurs from the Opua suite to the youngest rocks (<1.7 ka) of the Maero eruptive period, which have the highest potassium contents known from Mt. Taranaki (Platz 2007).

The anomalously steep regression lines of the Mangati and Te Namu sample suites might reflect sampling of a wider range of lithologies with distinctly different geochemical compositions, while the steep, short fit of the Oeo suite is a result of the small number of samples with a limited compositional range.

In order to illustrate the changes in K_2O with time, K55 values, i.e. the K_2O value of each sample suite at 55 wt.% SiO_2, were employed (Fig. 4.13). This has the advantage of minimising the effect of wide scatter in slope gradient. K55 increases from 1.51 wt.% K_2O for

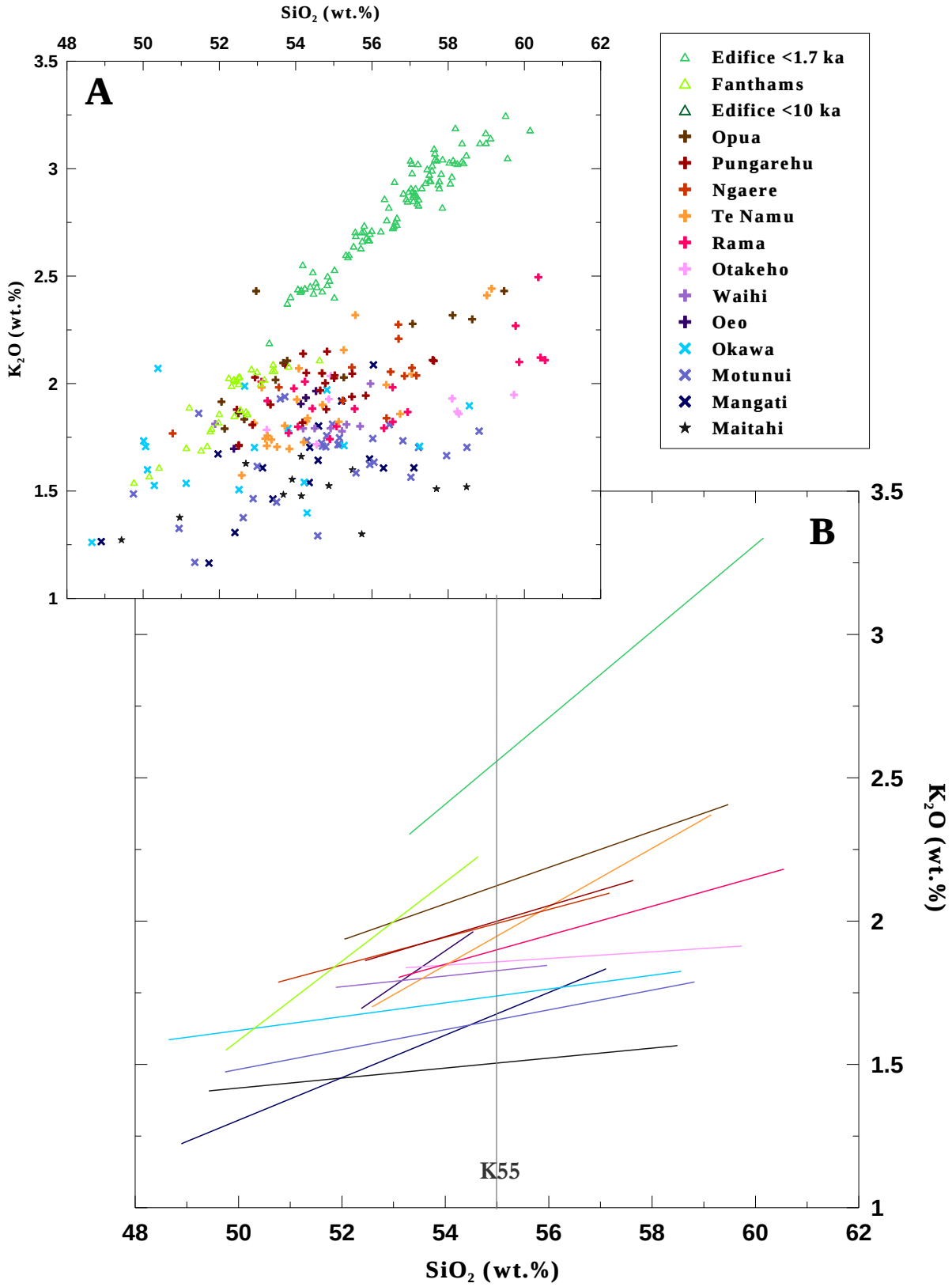

Figure 4.12. K_2O vs. SiO_2 variation diagrams for Taranaki eruptives. Each sample suite is distinct (A) and the linear fits of the stratigraphic units show a progressive increase in K_2O with decreasing age (B).

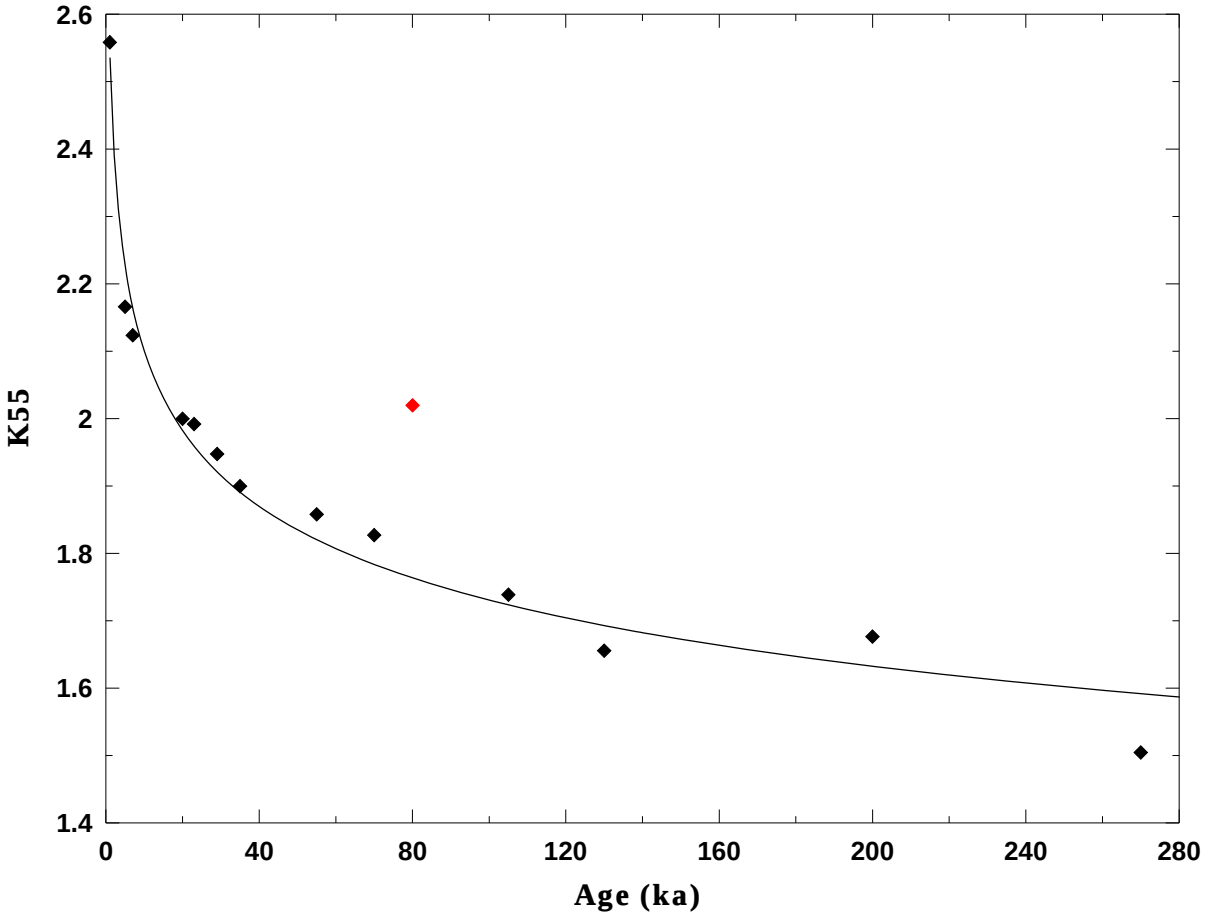

Figure 4.13. When plotted versus age, K55 values of the individual sample suites conform closely to an exponential curve of increasing K_2O with decreasing age. The unusually high K55 value of the Oeo suite (marked in red) is a result of the limited number of samples and the resulting steep, short fit on the K_2O vs. SiO_2 plot (Fig. 4.1). Hence, the unrepresentative value was not included in the calculation of the exponential fit.

samples from Pouakai Volcano, to 1.67 wt.% for the oldest rocks from Mt. Taranaki, and up to 2.17 wt.% for the mid-Holocene suite, with a dramatic rise to 2.56 wt.% for the latest eruptives (<1 ka). When plotted against age, K55 values conform closely to an exponential curve of increasing potassium with decreasing age, showing the largest increase in the youngest units (<10 ka). The Pouakai data is consistent with the overall trend of the Mt. Taranaki rock suites.

Abundance patterns for most LILE are coupled with those of K_2O and display similar trends with time; this is particularly so for Rb, Ba and Th. Barium abundance shows a systematic increase with decreasing age and the closest similarity to K_2O behaviour. Individual stratigraphic suites can be distinguished with a slight overlap between 35-100 ka and distinct youngest and oldest units with the latter (Mangati, Motunui and Okawa suites) also displaying the widest scatter (Fig.4.14A, Fig. 4.16B). Rubidium and Th contents behave similarly and also increase with time, although there is a stronger overlap between the abundances observed in individual units from

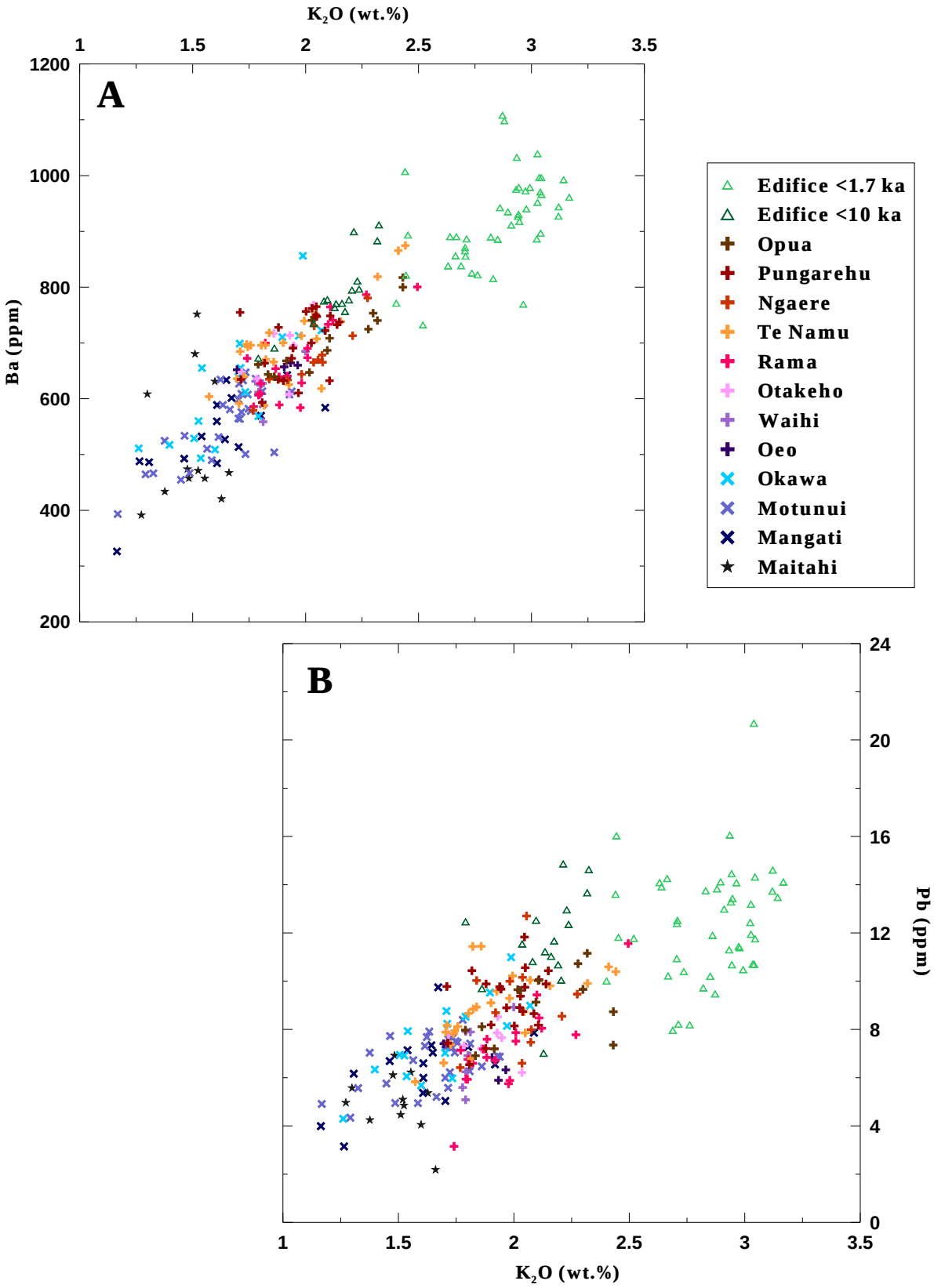

Figure 4.14. Most LILE are coupled with K_2O. On a plot of Ba versus K_2O individual stratigraphic suites form distinct clusters due to increasing concentrations in these elements with decreasing age (A). Lead concentrations show a greater spread of data with age but still define a trend of increasing Pb and K_2O with decreasing age, which allow a clear distinction between the oldest and youngest units (B).

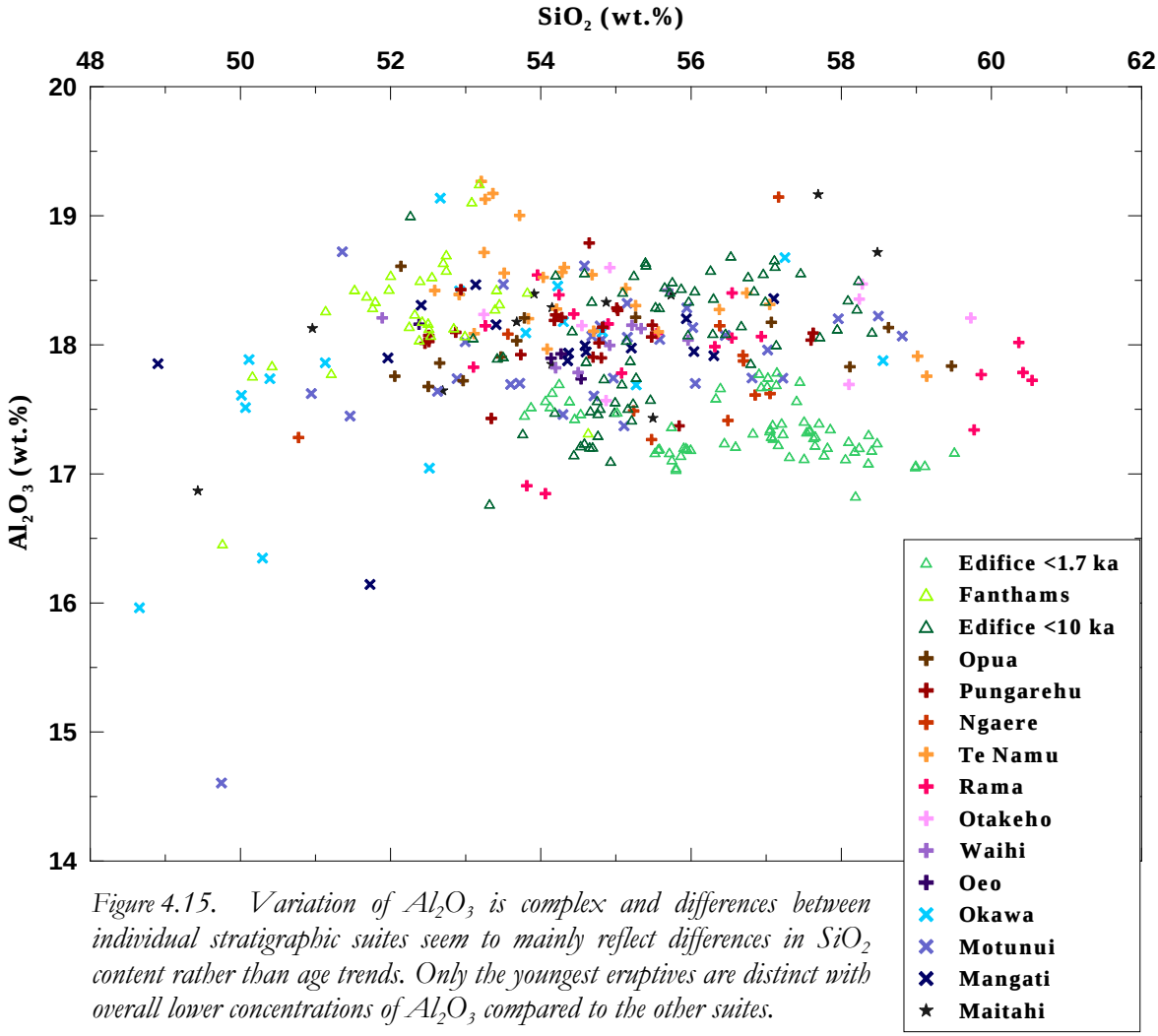

Figure 4.15. Variation of Al_2O_3 is complex and differences between individual stratigraphic suites seem to mainly reflect differences in SiO_2 content rather than age trends. Only the youngest eruptives are distinct with overall lower concentrations of Al_2O_3 compared to the other suites.

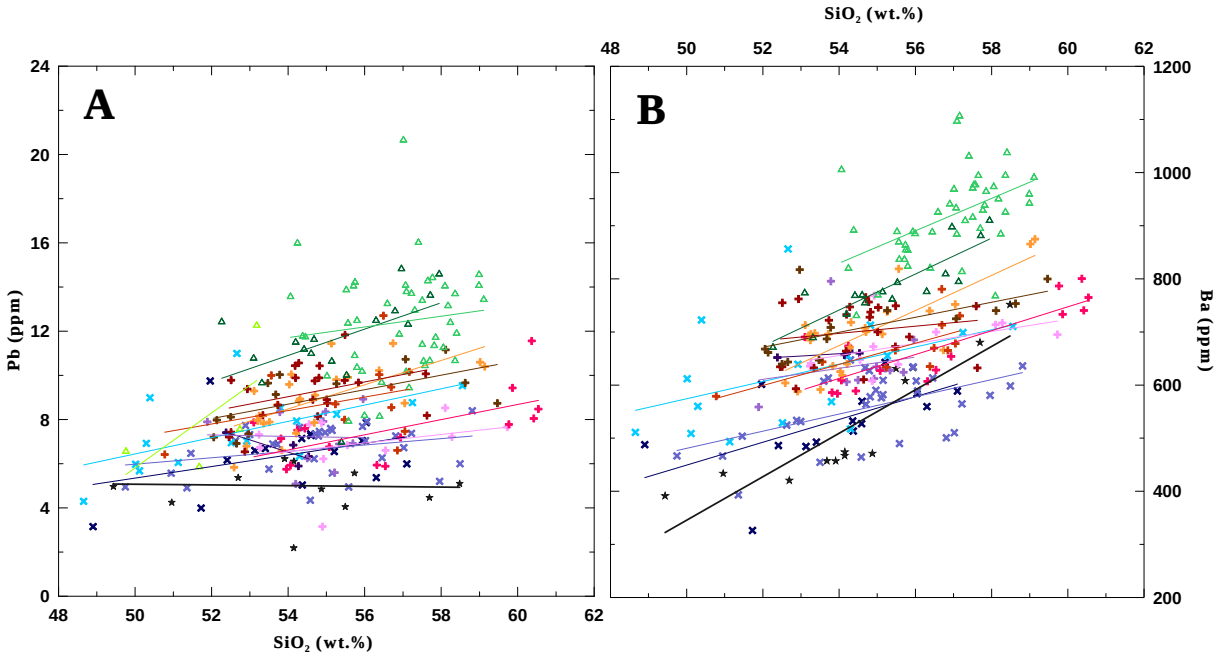

Figure 4.16. Debris-avalanche samples from Pouakai show lower concentrations in Pb than the Mt. Taranaki suites and a constant trend with increasing SiO_2 (A). Barium contents are lower for low-silica compositions but overlap with the oldest suites from Mt. Taranaki towards higher SiO_2 abundances (B). The Maitahi suite also shows a steeper fractionation trend than the other sample suites.

35-130 ka. The youngest suites show the most distinct increase and steeper fractionation trends, while the oldest units display the widest range of Rb and Th abundances. Other LILE, such as Pb as well as Cs and U, show a more subdued correlation with age and an overall greater overlap of sample compositions. Only the oldest suites and samples younger than 30 ka show distinct clusters based on age (Fig. 4.14B, Fig. 4.16A).

Other incompatible components and elements such as Na_2O, Sr, Be and some HFSE such as Zr, Hf, Nb and Ta do not show these distinct age-related trends, instead individual stratigraphic suites form strongly overlapping fields. The oldest >100 ka units, in particular the Motunui suite, display the widest scatter and contain some samples with higher concentrations of Sr, Be, Zr, Nb, and Ta. The younger suites have lower abundances and a tighter range of Zr abundances. Light rare earth elements (La-Sm) show similar trends of increasing abundances with increasing SiO_2-content and typically a wider range within the oldest units with lower SiO_2 contents. The Mangati suite has slightly lower concentrations of La, Ce and Pr compared to the rest of the Mt. Taranaki samples. Individual stratigraphic suites display relative constant proportions of HREE (Eu-Lu) and Y although some show a slight decrease in the abundances of these elements with increasing SiO_2. High-silica samples of the youngest eruptives and the Rama suite appear to have a weak negative correlation of Sm, Gd, Tb and Lu abundances with SiO_2-content. In contrast to the LREE and Y, the youngest suite shows the widest scatter in Er and Lu.

The variation of Al_2O_3 is complex and contrasts between individual stratigraphic suites seem to reflect different fractionation trends at varying SiO_2 contents or, more likely, different degrees of plagioclase accumulation rather than age trends (Fig. 4.15). The oldest debris avalanche suites (Maitahi, Mangati, Motunui and Okawa) and Fanthams Peak lavas show a positive correlation of Al_2O_3 with increasing SiO_2 for low-silica compositions. Abundances of Al_2O_3 at >51 wt.% SiO_2 in these units are relatively constant and similar to those observed in the Waihi, Otakeho, Rama, Te Namu and Ngaere suites. Edifice samples show a wider scatter of Al_2O_3 abundance at medium-silica contents and the youngest eruptives have lower Al_2O_3 abundances, implying a negative correlation.

Compatible elements behave in a similar way for all age groups and do not distinguish individual stratigraphic units. Ranges for FeO*, CaO, TiO_2, V and Sc form similarly decreasing trends with increasing SiO_2, although the oldest units appear to have slightly higher abundances of FeO*. MgO, Cr, Ni and Cu abundances show an overall negative correlation with SiO_2 content but a wider scatter and higher values for low-silica samples results in steeper trends for the old suites and Fanthams lavas.

4.6.1. Distinction of stratigraphic suites

The results of this study show that the geochemical composition of debris-avalanche sample suites can be used to roughly differentiate stratigraphic units at Mt. Taranaki. Although trends with age are observed for most LILE, individual suites are best distinguished based on their K_2O (and Ba) content. In this regard, sampling of an unknown debris-avalanche deposit at Waihi Beach allowed its identification as Ngaere Formation. Although the sedimentary characteristics and its stratigraphic position could have suggested an older age, equivalent to the Tokaora debris-avalanche deposit, geochemical analysis of the sample suite revealed higher K_2O contents and a perfect overlap with the Pungarehu Formation samples.

The K_2O abundances of Mt. Taranaki sample suites can be helpful for estimating the approximate age of any stratigraphic unit; the K55 value can be compared with the K55-age curve of Fig. 4.13. For this purpose, the suite needs to consist of at least 10 samples, including a large variety of compositions and lithologies that provide a reasonable range in K_2O abundances. As demonstrated by the Oeo suite, the K55 value becomes more representative as the number of samples increases and their compositional range widens. This concept could be applied to newly identified debris-avalanche deposits at Mt. Taranaki or possibly to series of lahar deposits of unknown age, especially where stratigraphic correlation is not possible.

The overall evolution of Mt. Taranaki magmas is characterised by a gradual, continuous increase of K_2O and Ba abundances. Hence, significant differences in K_2O and Ba contents for individual debris-avalanche suites indicate that large sectors of the volcano were removed by collapse, which was subsequently rebuilt with new lava flows and pyroclastic deposits that show a slightly different geochemical signature. Overlapping compositions of debris-avalanche sample suites suggest that similar material, which was produced during a restricted time range, was involved in the collapse. Hence, compositional overlap can be generated by (1) smaller collapses of neighbouring parts of the edifice, producing a similar dispersal of relatively small-volume debris-avalanche deposits and (2) small or large collapse of different parts of the same edifice, resulting in debris avalanches of varying volumes that are directed in different directions. In contrast, distinct differences between debris-avalanche sample suites are the result of involvement of material that was part of a completely different (removed and rebuilt) Mt. Taranaki edifice, suggesting significant time between collapse events.

Clasts from the Rama and Otakeho debris-avalanche deposits show some overlap in composition. The collapses occurred in the same direction but the older event was smaller in size. Hence, the subsequent larger Rama collapse involved parts of the 'old' edifice as well as new

material. In addition, the debris avalanche could have picked up material of the underlying Otakeho deposit during transport. A different example is the collapse of the eastern sector of a previous Mt. Taranaki edifice during the Ngaere event, followed by collapse of the western sector of the same edifice to generate the Pungarehu debris avalanche. The geochemical composition of clast assemblages within these two large-volume debris-avalanche deposits is almost identical, indicating involvement of edifice material that was produced during the same time range. Also, the derivation of the youngest (Opua) debris-avalanche deposit from collapse of the present-day edifice is shown by the overlapping geochemistry of debris-avalanche clasts and edifice-forming lavas.

4.7. FINGERPRINTING OF POUAKAI AND MT. TARANAKI SUITES

The debris-avalanche sample suite displays compositional changes with time and a distinct difference between samples derived from Pouakai Volcano and Mt. Taranaki. Potassium and most LILE show a gradual, systematic increase with decreasing age and the Maitahi suite typically has the lowest contents of these elements. Pouakai samples are distinctly lower in K and Pb than Mt. Taranaki rocks (Fig. 4.16A) and for Pouakai these elements also show relatively constant abundances with increasing SiO_2. Barium, Th and U abundances form significantly steeper regression lines on silica variation diagrams than is the case for the Taranaki suites and abundances overlap with those observed in the Mangati and Motunui samples (Fig. 4.16B), while Cs and Rb abundances cannot be distinguished from those of Taranaki samples.

Contents of HFSE differ significantly between Pouakai and Mt. Taranaki samples. The Maitahi suite shows overall lower abundances in TiO_2 but these overlap slightly with those of Mt. Taranaki rocks (cf. Fig. 4.4). Pouakai samples are also characterised by markedly lower concentrations of Zr and Hf and relatively constant abundances of these elements with increasing SiO_2. This contrasts with the distinct positive fractionation trends defined by the Taranaki suites (Fig. 4.17A, cf. Fig. 4.5). These differences are slightly more subdued for Nb and Ta (Fig. 4.17B, cf. Fig. 4.5), but concentrations of these elements are overall lower in Pouakai rocks than for Mt. Taranaki samples. The Maitahi suite also forms a tighter range in Nb and Ta contents without a clear trend on silica variation diagrams.

The distribution of Be is similar to those observed for Zr and Hf with distinctly lower concentrations for Maitahi samples and a narrow, relatively constant range. Individual Taranaki sample suites show a wide scatter in Zr, in particular the Motunui suite, similar to the behaviour

noted for Nb and Ta. Strontium abundance is also lower in Pouakai samples and is less scattered than for Mt. Taranaki suites (cf. Fig. 4.5).

Some significant differences between Pouakai and Mt. Taranaki rocks can also be found in the distribution of LREE. The Maitahi samples show lower La contents and there is only a minor overlap with those observed in Mt. Taranaki samples. There is, however a similar positive correlation between La and SiO_2 abundances in all suites (Fig. 4.18A). Concentrations of Ce and Pr are markedly lower in Maitahi samples and there is only a slight increase in Ce abundance with increasing SiO_2 content. Praesodymium contents show a weak negative correlation with SiO_2 abundance, which contrasts with the positive fractionation trends observed for the other suites. On a plot of Pr versus Ce, the Maitahi samples cluster in a field that is distinct from that defined by data for Mt. Taranaki rocks (Fig. 4.18C). The youngest eruptives from Mt. Taranaki also show a slightly different trend to older suites. The diverging trends between the two volcanoes become even more obvious for Nd and Sm which have distinctly lower abundances in Pouakai rocks where they also show a clear negative correlation with increasing SiO_2 (Fig. 4.18B). The sample suites form two separate fields with different slopes on a plot of Sm versus Nd with only minor overlap of some more primitive rocks from the oldest Mt. Taranaki debris-avalanche deposits (Fig. 4.18D). Concentrations of Eu and Gd are similarly lower in Pouakai rocks and show a steep negative correlation with SiO_2. These differences become less distinct for the heavier REE. The three Pouakai andesites have significantly lower contents in Tb-Lu and Y while most other samples overlap with the Mt. Taranaki field.

Other elements also show distinctly different trends for the Pouakai and Mt. Taranaki suites. Pouakai samples display a strong negative correlation between MnO and SiO_2 contents, whereas most Mt. Taranaki rocks have relatively constant abundances with only the youngest eruptives and high-silica rocks of the Rama suite forming a similar negative trend. Abundances of P_2O_5 are markedly lower in the Maitahi suite (cf. Fig. 4.4) and show a slightly positive relationship with SiO_2 compared to Mt. Taranaki suites, for which P_2O_5 concentrations are relatively constant or decrease with increasing SiO_2. Pouakai samples also have distinctly lower concentrations of Zn (cf. Fig. 4.5) and Zn contents decrease rapidly with increasing SiO_2 content, in contrast to constant abundances for the Pungarehu, Opua and >100 ka Mt. Taranaki debris-avalanche samples.

These geochemical differences between the Maitahi and the other debris-avalanche suites allow a clear distinction between Pouakai and Mt. Taranaki-derived rocks. Until now the origin of the Mangati debris-avalanche deposit was unknown and it has only been speculated that the Motunui Formation originated from Mt. Taranaki (Alloway et al. 2005). The sample suites of

both debris-avalanche deposits strongly overlap with the other Mt. Taranaki suites and show similar characteristics or progressive trends with time. Based on the geochemical signatures of clast assemblages within the Mangati Formation, it is here suggested that it originated from a proto-Mt. Taranaki edifice and thus represents the oldest known deposit recognised from this volcano. The nature of the deposit, i.e. volume and thickness, implies that this ancestral Mt. Taranaki was already a high unstable stratocone at the time. The contained range of lithologies indicates that the edifice was of an apparently similar composite structure to the present cone and volcanic activity involved a similar wide range of eruptive styles as identified in the Holocene record (cf. Neall et al. 1986; Alloway et al. 1995, 2005; Platz 2007; Turner 2008). The emplacement of the Mangati debris-avalanche deposit between 190-210 ka hence gives a new minimum age for Mt. Taranaki, indicating that the volcano is considerably older than previously thought.

4.7.1. Interpretation of compositional differences

The trace element distribution within Mt. Taranaki and Pouakai debris-avalanche clasts is characterised by the same overall pattern. The two suites are also similar in terms of trace element ratios that might indicate different degrees of slab input into the source, e.g. Ce/Yb, Nb/Yb, Ba/Nb. Together with their very similar isotopic compositions, this suggests a similar mantle source for magmas parental to Mt. Taranaki and Pouakai eruptives. However, Pouakai debris-avalanche samples are less enriched in K, Rb and Ba, have lower Zr, lower REE and HFSE than is generally the case for equivalent Mt. Taranaki rocks.

These observations are consistent with:

a) Derivation of magmas parental to Pouakai debris-avalanche clasts by larger degrees of partial melting of a mantle source that was compositionally the same as that from which Mt. Taranaki eruptives were derived.

b) Less interaction between Pouakai parental magmas and young amphibolitic underplated material within a lower crustal "hot zone" (cf., Annen& Sparks 2002; Annen et al. 2006) than was the case for Mt. Taranaki.

c) Some combination of these processes.

Here, a combination of different degrees of partial melting and varying interaction with the lower crust are believed to be responsible for the compositional differences between Pouakai and Mt. Taranaki debris-avalanche clasts. Higher degrees of partial melting produced parental

Figure 4.17. Plots showing the differences in HFSE between Mt. Taranaki and Pouakai samples suites.

A: The Maitahi suite has distinctly lower contents of Hf and marks a relatively constant trend with increasing SiO_2.

B: Pouakai samples have distinctly lower contents of Zr and Hf than Mt. Taranaki rocks, resulting in a distinct cluster for each volcano with only minor overlap.

C: The differences in Nb and Ta contents are less distinct, with Pouakai samples plotting towards lower concentrations but overlapping with Mt. Taranaki rocks. Within ring-plain samples, Nb and Ta are linearly correlated, in contrast to the youngest eruptives that have relatively constant Nb at varying Ta abundances.

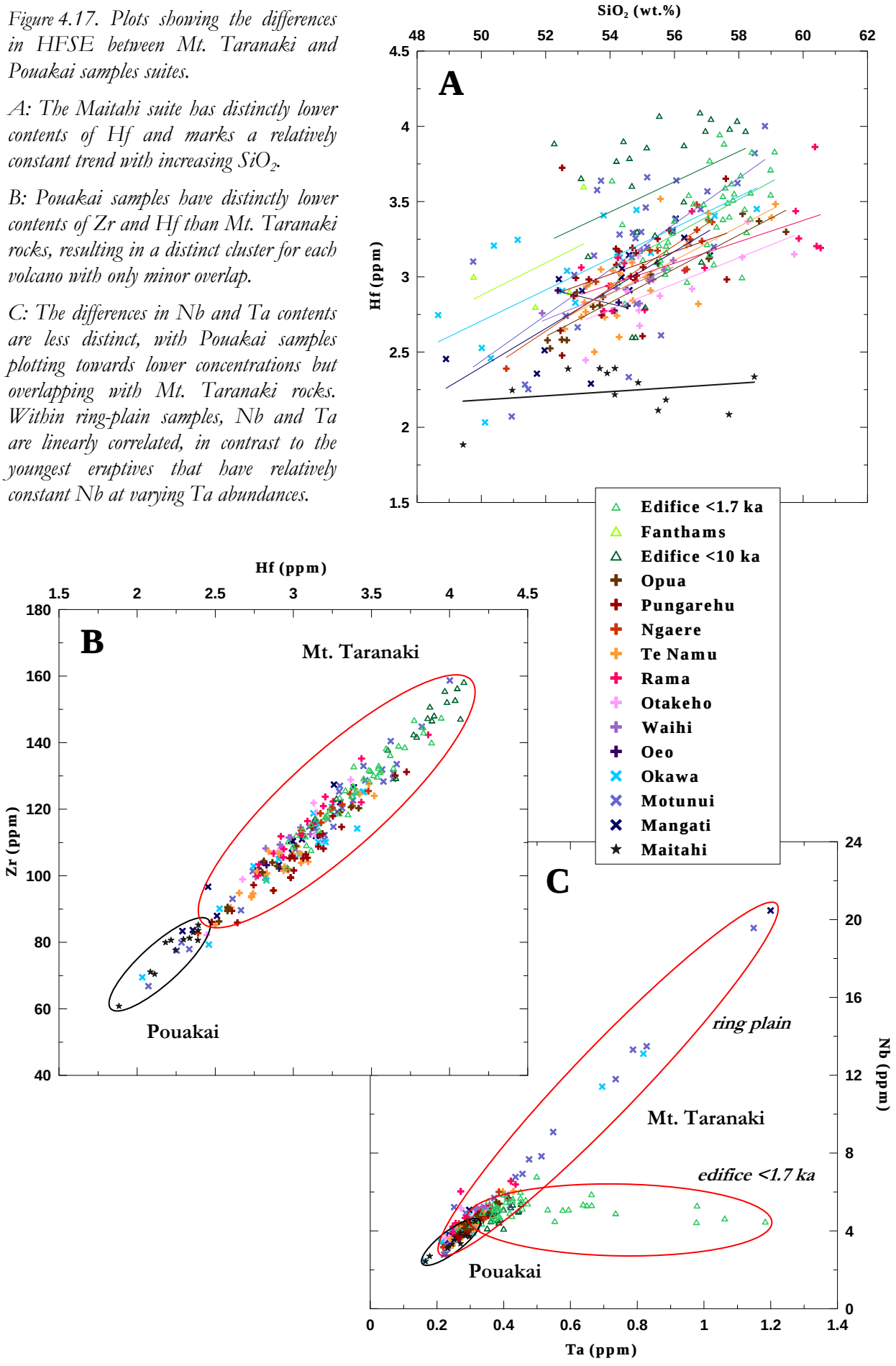

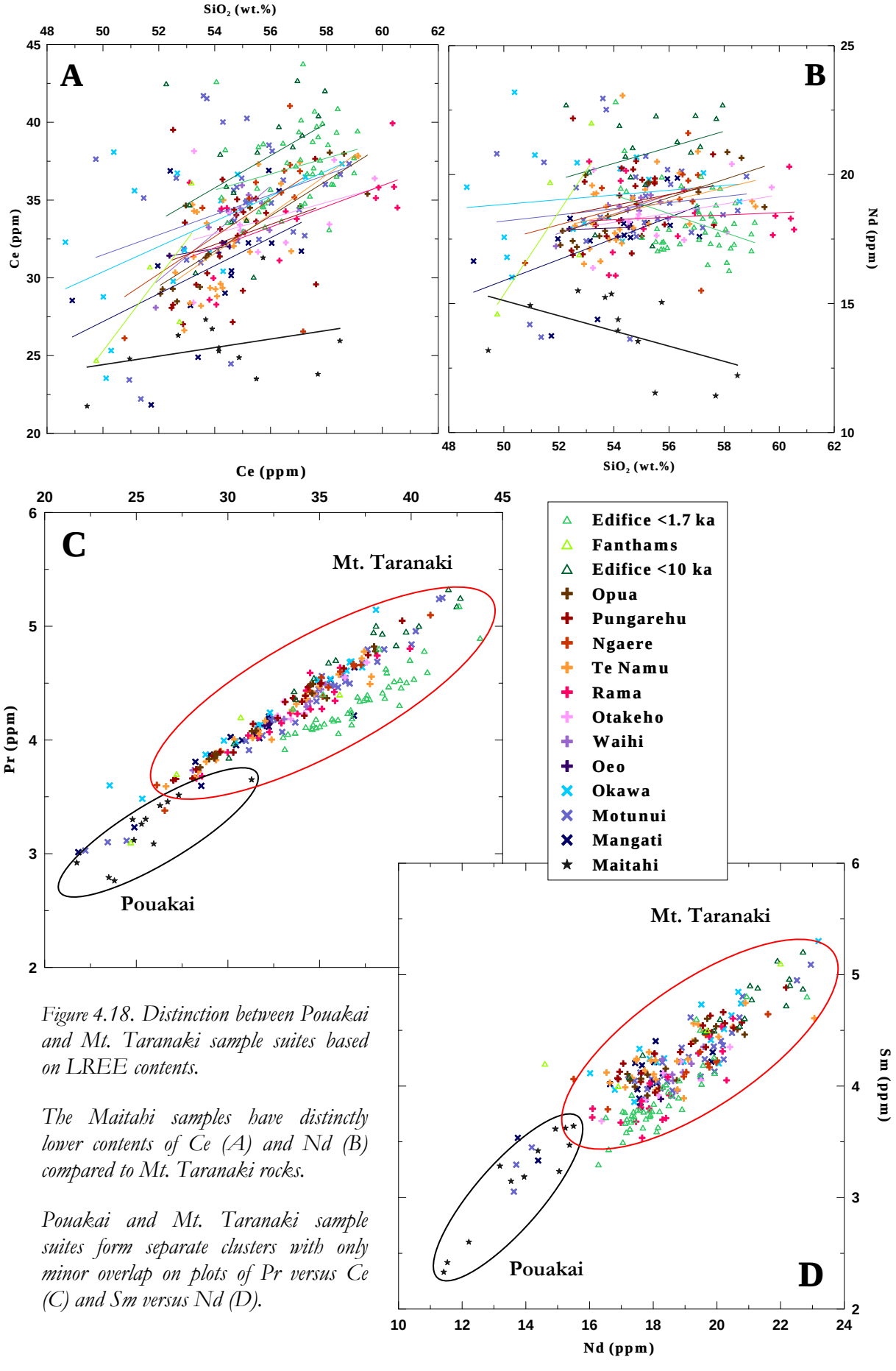

Figure 4.18. Distinction between Pouakai and Mt. Taranaki sample suites based on LREE contents.

The Maitahi samples have distinctly lower contents of Ce (A) and Nd (B) compared to Mt. Taranaki rocks.

Pouakai and Mt. Taranaki sample suites form separate clusters with only minor overlap on plots of Pr versus Ce (C) and Sm versus Nd (D).

magmas that differ slightly in abundances of LILE, REE and HFSE. These mantle-derived magmas were subsequently modified within the lower crustal hot zone (cf., Annen & Sparks 2002; Annen et al. 2006) where less interaction with underplated material during the early stages resulted in lower concentrations of LILE (cf. Stewart et al. 1996). As a consequence of the raising geothermal gradient and continuous intrusions of mantle-derived magmas within the evolving hot zone, increasing interaction of parental magmas with lower crustal material occurred, generating magmas with gradually increasing abundances of LILE. However, variations in the degrees of partial melting appear to be the controlling mechanism for generation of compositionally different magmas, because large degrees of melt involvement from the crustal underplate would most likely also result in modification of the "arc" indicative trace element ratios.

The Maitahi debris-avalanche clasts provide only a limited insight into the geochemical composition of Pouakai eruptives since they do not cover the whole lifetime of this volcano from beginning of volcanic activity to its extinction. Instead, they most likely represent a mature stage and older eruptives from this volcano could have had different trace element compositions and K contents. Three samples from Pouakai analysed by Price et al. (1999) have similar geochemical compositions to Mt. Taranaki rocks of this study, while one Kaitake sample overlaps with the fields defined by Maitahi debris-avalanche clasts. One explanation could be that their three rocks represent magmas from earlier stages of the volcanic system, while the Maitahi clasts were produced at a mature stage through higher degrees of partial melting in the mantle. It seems unlikely that the similarities of the Kaitake sample and the Maitahi clasts indicate a generation of the Maitahi debris avalanche from Kaitake, because the age, dispersal pattern and sedimentary characteristics of the deposit are consistent with an origin from Pouakai (cf., Gaylord et al. 1993).

4.8. ORIGIN OF MT. TARANAKI MAGMAS

It has been well established that subduction-related magmas have an ultimate origin in the mantle wedge above the subducting slab (e.g. Grove & Kinzler 1986; Crawford et al. 1987; Hawkesworth et al. 1991; McCulloch & Gamble 1991; Tatsumi & Eggins 1995) where transformations of mineral phases and related dehydration reactions in the descending slab result in the release of fluids into the asthenospheric mantle. These slab-derived fluids initiate partial melting of the overlying mantle wedge to produce primitive basaltic magmas (e.g. Ringwood 1973, 1974; Hawkesworth et al. 1979; Arculus & Powell 1986; Davies & Stevenson 1992; Tatsumi

& Eggins 1995; Schmidt & Poli 1998; Ulmer 2001; Grove et al. 2002; Forneris & Holloway 2003). The involvement of these metasomatic fluids results in partitioning of trace elements between fluids and residual phases (e.g. Perfit et al. 1980; Saunders et al. 1980; McCulloch & Perfit 1981; Pearce 1982; Sun & McDonough 1989; McCulloch & Gamble 1991), which produces the characteristic trace element patterns of subduction-related magmas.

Trace element abundances at Mt. Taranaki are marked by relatively high proportions of LILE such as K, Rb, Cs, Ba, and Th as well as LREE, accompanied by deficiencies in HFSE such as Ta, Nb, Zr and Hf (cf. Price et al. 1992, 1999, 2005). The high LILE/HFSE ratio found in arc magmas is attributed to melting of the mantle wedge, which has been metasomatised due to dehydration of subducted sediments and oceanic crust (e.g. Tatsumi & Kogiso 2003; Miskovic & Francis 2006). It reflects the contrasting behaviour of these elements, i.e. relative mobility of LILE and immobility of HFSE in the slab-derived fluids (e.g. Tatsumi et al. 1986; Brenan et al. 1995; Keppler 1996). These, as well as other trace element characteristics including strong depletion of Nb relative to La, K, Th and Pb and enrichment of Pb and, to a lesser extent, Sr relative to Ce as well as enrichment of LREE over HREE and Y are typical of subduction-related magmas (e.g. Gill 1981; Pearce 1982; Sun & McDonough 1989; Hawkesworth et al. 1991, 1993; McCulloch & Gamble 1991; Grove et al. 2002). The depletion in Nb, Ta and other HFSE is regarded as an intrinsic feature of subduction related magmas arising from the immobility of these elements in fluids and their retention in residual Fe-Ti-oxides during melting or during dehydration processes of the slab (e.g. Perfit et al. 1980; Gill 1981; Pearce 1982; Tatsumi et al. 1986; Vukadinovic & Nicholls 1989; McCulloch & Gamble 1991; Saunders et al. 1991; Brenan et al. 1995; Tatsumi & Eggins 1995; Keppler 1996). The enrichment of Pb has been related to the involvement of subducted sediment (e.g. Plank & Langmuir 1993; Ewart et al. 1998). Price et al. (2007a) pointed out that although these trace element characteristics are commonly interpreted to reflect slab-fluid influences, they are also specific to continental crust. Hence, magmas that evolved through AFC processes in complex dispersed crustal storage and feeder systems show a similar 'arc' signature.

Mt. Taranaki rocks all have similar trace element distributions but the arc pattern is developed to varying degrees. Typically, Mt. Taranaki andesites show a stronger 'arc signature' than basalt samples with greater enrichment of LILE over HFSE and NMORB and a narrower range of trace element concentrations. Also, some of the oldest, more primitive rocks display a more subdued subduction signature (cf. Fig. 4.7) similar to the basalt sample T90/42A described by Price et al. (1999). Variations in slab input or lower crustal interaction can be further illustrated using ratios of K/Nb and Ce/Pb (Fig. 4.19A). The oldest sample suites from Mt. Taranaki have

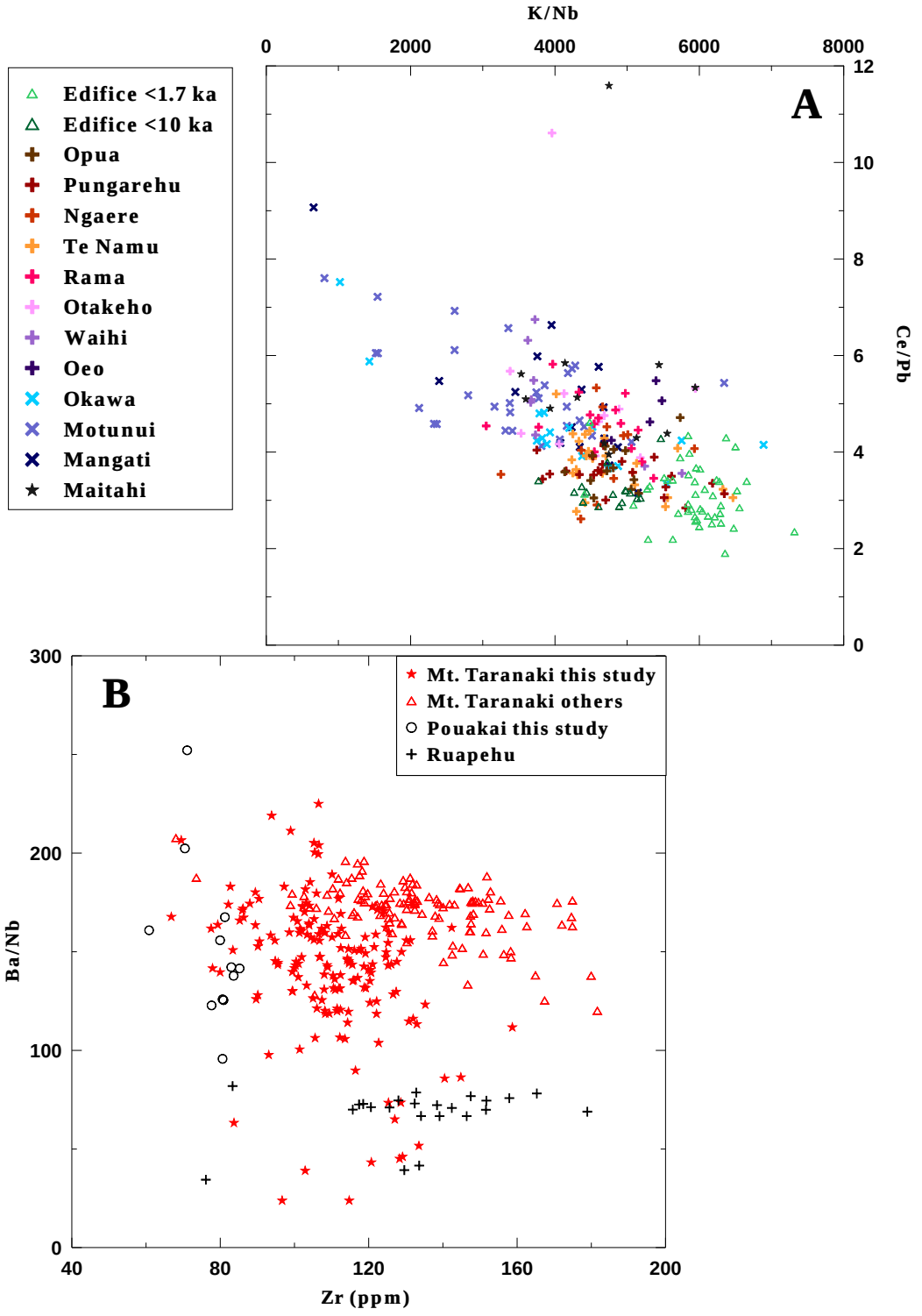

Figure 4.19. A: The plot of K/Nb ratios versus Ce/Pb ratios highlights the increasing slab influences or lower crustal interactions with time within the Mt. Taranaki sample suites. The oldest Mt. Taranaki debris-avalanche samples show the highest Ce/Pb and lowest K/Nb ratios, while Pouakai samples overlap with the 80-10 ka sample suites. One Pouakai rock and one Otakeho clast plot at unusually high Ce/Pb ratios.

B: The generally higher Ba/Nb ratios of Mt. Taranaki and Pouakai eruptives indicate lower degrees of partial melting and more interaction with underplated lower crustal material than at Ruapehu although there is some overlap with older Taranaki samples. Mt. Taranaki data from Price et al. (1999), Platz (2007) and Turner (2008); Mt. Ruapehu data from Gamble et al. (1993 & 1999) and Waight et al. (1999).

relatively low ratios of K/Nb that gradually increase with decreasing age with the youngest eruptives showing the strongest depletion of Nb. The ratio of Ce/Pb decreases with decreasing age, corresponding to the increasing enrichment of Pb over Ce. This indicates that either the influence of slab-derived fluids becomes more dominant with time or there is increasing interaction with the lower crust, which is augmenting the arc signature. Pouakai rocks overlap with the 80-10 ka Mt. Taranaki units (Fig. 4.19A), suggesting similar processes to the more mature Mt. Taranaki system, although their normalised trace element pattern is similar to the older Mt. Taranaki basalts (cf. Fig. 4.8).

Compared to Ruapehu, Mt. Taranaki rocks are enriched in REE and strongly enriched in LREE relative to HREE with overall similar trace element patterns (Price et al. 1999). Ratios of Ba/Nb (Fig. 4.19B) and Ba/La (cf. Price et al. 1999) are generally higher at Mt. Taranaki, especially in later Taranaki eruptives, indicating more substantial involvement of a slab-derived component at source. Price et al. (1999) also argued that the fluids involved in the sources of the two volcanoes are compositionally different due to the declining influence of sediment on slab-derived fluids with increasing slab depth. Higher contents of K, Ba, LREE, LILE and HFSE in Mt. Taranaki rocks were thought to reflect higher abundances in parental magmas, possibly due to lower degree of partial melting. In contrast, larger degrees of partial melting at Ruapehu possibly diluted the arc signature but resulted in similar patterns (Price et al. 1999).

Higher Ti/Zr ratios at low Zr abundances and elevated K/Rb and Cs/Rb ratios of Mt. Taranaki eruptives compared to Ruapehu have been interpreted to indicate a more depleted mantle source for parental magmas and/or more interaction with underplated lower crust (Price et al. 1999). Lower $^{86}Sr/^{87}Sr$ and higher $^{143}Nd/^{144}Nd$ ratios for Taranaki eruptives also suggest derivation of parental magmas from a more depleted mantle than is the case for Ruapehu magmas (Fig. 4.20). In the $^{143}Nd/^{144}Nd$ versus $^{86}Sr/^{87}Sr$ isotopic ratio diagram, most Mt. Taranaki samples lie within the field defined by TVZ basalts and plot between lavas from the Kermadec-Tonga-Arc segment and Ruapehu. Three basalt samples from the oldest units (AZ04-06, -27 and AZ06-73) overlap with the Kermadec-Tonga field and are distinct from the rest of the Taranaki debris-avalanche suites as well as previously analysed rocks. The different isotopic composition of these basalts appears to indicate variability in the mantle source. Several other samples, predominantly basalts as well as some basaltic andesites from the older sample suites, also show a range in compositions that differ significantly from the rest of the Taranaki suites.

These samples, i.e. AZ06-68 and -73 from the Mangati suite, AZ04-25, -26, -27, -28, -34, -35 and -37 from the Motunui suite and AZ04-06 and -07 from the Okawa suite are characterised by different degrees of LREE enrichment and a strong depletion in HREE relative

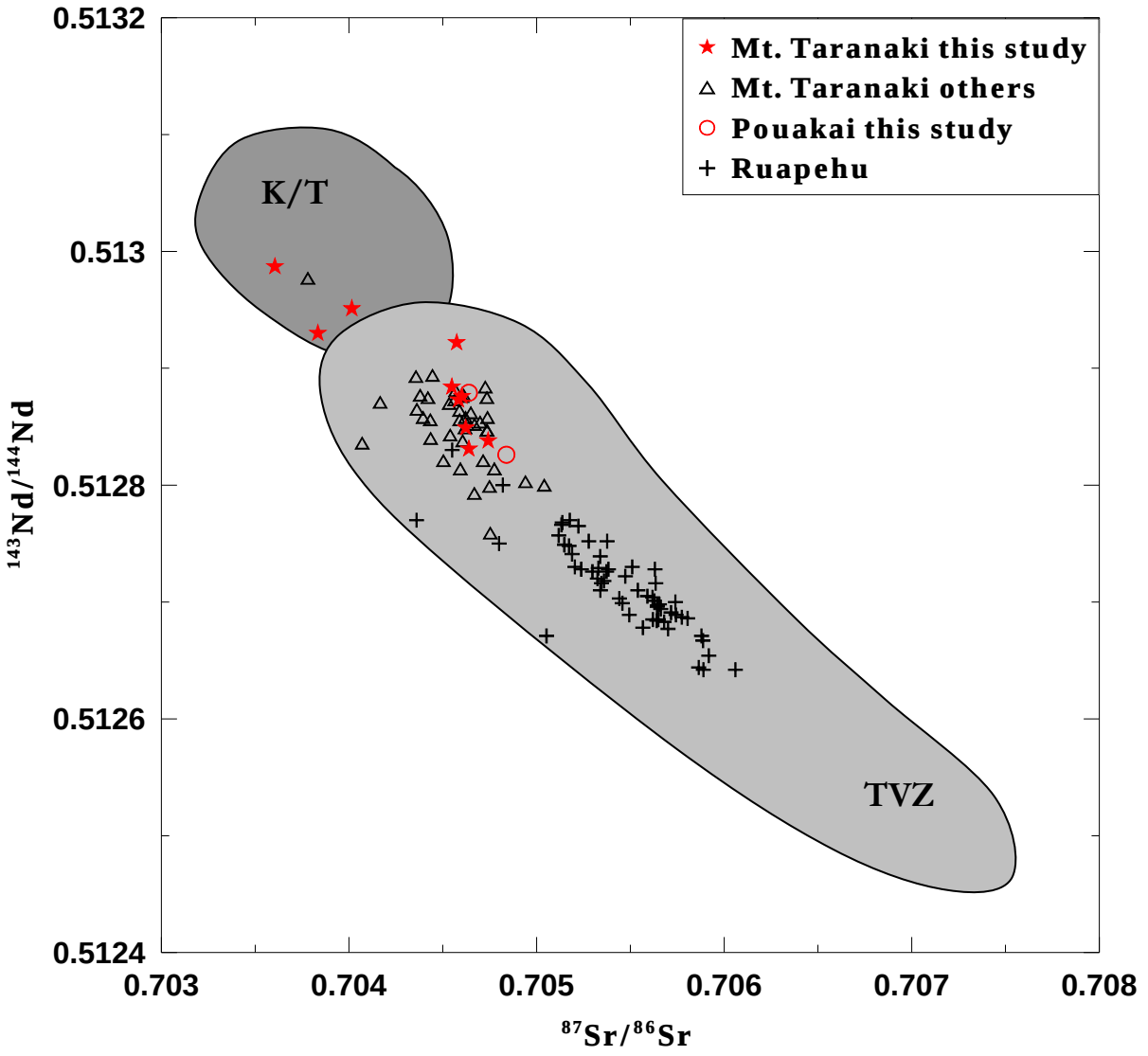

Figure 4.20. $^{86}Sr/^{87}Sr$ *versus* $^{143}Nd/^{144}Nd$ *diagram for Mt. Taranaki and Pouakai sample suites in comparison with data from Ruapehu as well as fields defined by rhyolites and basalts from the Taupo Volcanic Zone (TVZ) and Kermadec/Tonga lavas (K/T). Data sources: Graham & Hackett 1986; Gamble et al 1993, 1999; Ewart et al. 1998; Price et al. 1999; Waight et al 1999.*

to NMORB (Fig. 4.21A). They also show overall lower abundances of LILE, especially Ba, Pb, Th and U, and a range of HFSE concentrations (Fig. 4.21B). In addition, some of these rocks have lower Al_2O_3 and higher TiO_2, MgO, Cr and Ni than the rest of the suite (cf. Figs. 4.4 and 4.5). Together with T90/42A, T95/2A and T90/4D from Price et al. (1999), these samples can be best distinguished on a Ce/Yb versus Nb/Yb diagram, where they plot at higher Nb/Yb ratios outside the field defined by Mt. Taranaki and Pouakai sample suites (Fig. 4.22). Some transitional compositions, represented by andesites from the Maitahi Fm (AZ06-60), Motunui Fm (AZ04-22 and -29), Rama debris avalanche-deposit (AZ06-01 and -02) and the Ngaere Fm (AZ06-90), overlap with data from Ruapehu.

Andesite sample AZ06-83 from the Ngaere Formation also shows a unique major and trace element geochemistry that differs significantly from the rest of the suites, including the samples listed above (cf. Figs. 4.21 and 22). The rock has the lowest contents of FeO_{tot}, CaO, MnO and MgO observed (cf. Fig. 4.4) and is characterised by a relatively flat REE profile with low abundances of LREE and unusually high concentrations of HREE that are similar to NMORB (Fig. 4.21A). Despite these differences, it still shows a typical arc signature with strong enrichment of LILE relative to NMORB, depletion of Nb over K and U, as well as enrichment of Pb relative to Ce (Fig. 4.21B). The characteristics of this highly evolved rock might not only reflect a different source for the parental magma but also larger degrees of interaction with lower crustal rocks. In addition, the sample is characterised by an almost aphyric texture, hence the lower contents of FeO_{tot}, CaO, MnO and MgO could be explained by absence or smaller amounts of cumulate clinopyroxene and to some extent plagioclase.

The range of compositions and the various degrees of arc signature, in particular the strong variation in HFSE, indicate variability in the mantle source of Mt. Taranaki magmas. Price et al. (2007b) suggested that arc signatures in the mantle are not necessarily related to present-day subduction systems but might in some cases reflect the effects of past subduction events on the lithospheric mantle. Miocene arc magmatism could have preconditioned the mantle beneath the Taranaki volcanoes, resulting in a heterogeneous, more depleted source region for Taranaki magmas. This is implicit in the geophysically-based tectonic model developed by Stern et al. (2006) who suggested that Taranaki magmatism is not directly related to the present-day subduction but is instead associated with lithospheric delamination.

Differences in crustal structure and heat flow beneath Mt. Taranaki and Ruapehu resulted in varying degrees of assimilation and crystal fractionation within the crust (Price et al. 1999). Mt. Taranaki magmas are more evolved, which has been attributed to ascending magmas being more likely to become trapped and fractionated beneath a thicker crust (c. 25 km; Stern et al. 1987; Price et al. 1999). Thinner crust (15 km; Stern & Davey 1987) and higher heat flow (Hochstein et al. 1993) at Ruapehu resulted in hotter, drier and less evolved magmas, which ponded at higher levels where they were contaminated by interaction with the basement (Price et al. 1999). Magmas from both volcanoes form a continuous trend of increasing $^{207}Pb/^{204}Pb$ and $^{208}Pb/^{204}Pb$ ratios at slightly increasing $^{206}Pb/^{204}Pb$ with Taranaki magmas extending to less radiogenic compositions (Fig. 4.23), suggesting that the basements beneath the two volcanoes have similar Pb isotopic compositions but that crustal contamination was more significant at Ruapehu (cf. Price et al. 1999). Differences in the geochemical composition of Mt. Taranaki and Ruapehu eruptives were interpreted to reflect the complex interplay between different mantle

sources and crustal assimilants as well as magmatic processes such as variations in storage and feeder systems (Price et al. 1999). Various degrees of arc signature reflect different degrees of crustal involvement, i.e. assimilation and contamination with an inhomogeneous crust.

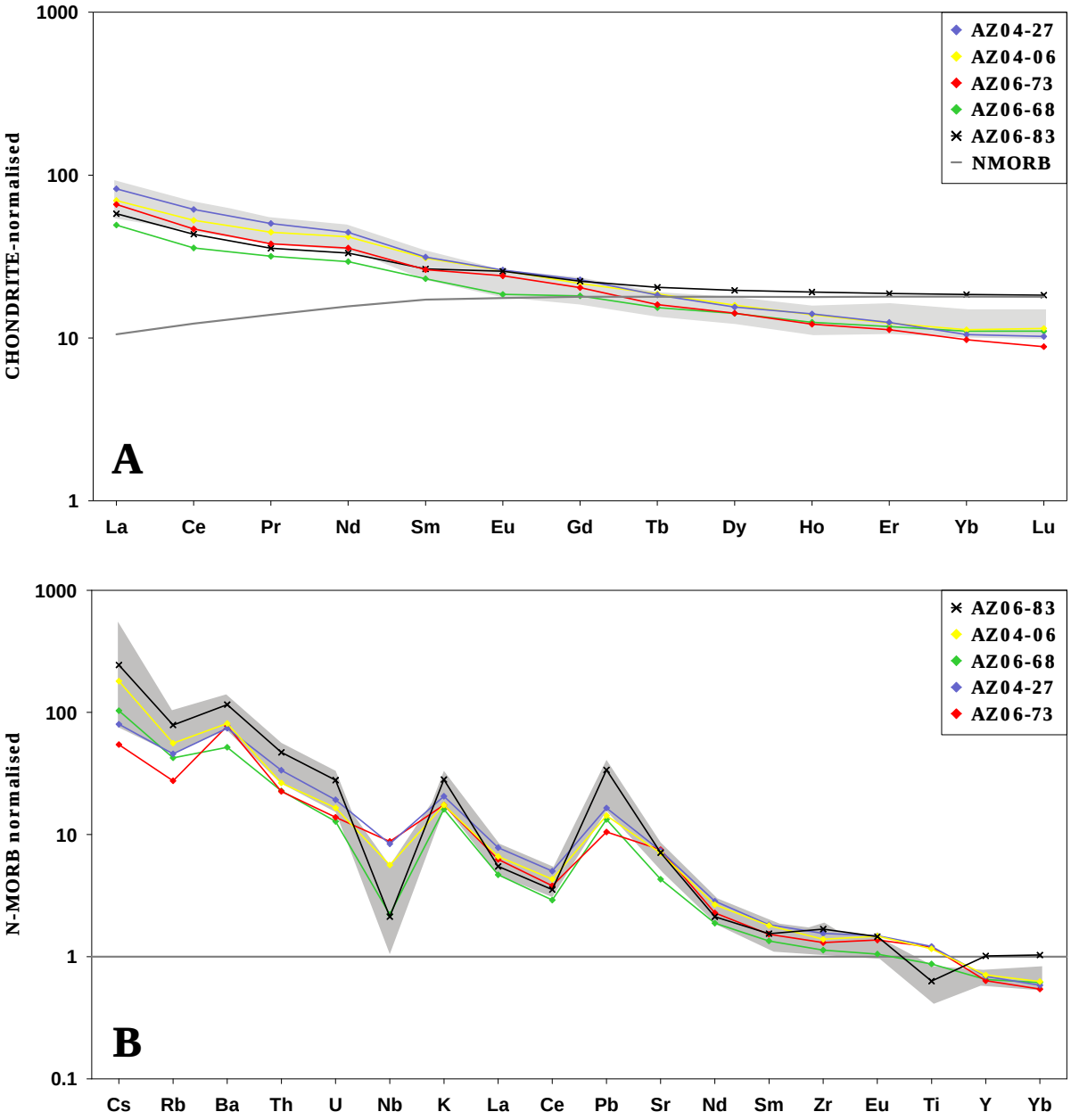

Figure 4.21. Trace element characteristics of distinct samples from Mt. Taranaki compared to the rest of the sample suites. They show a range of LREE abundances and depletion of HREE compared to NMORB with the exception of andesite sample AZ06-83 from the Ngaere Formation (A). Various degrees of arc signature suggest more than one mantle source for Taranaki magmas (B).

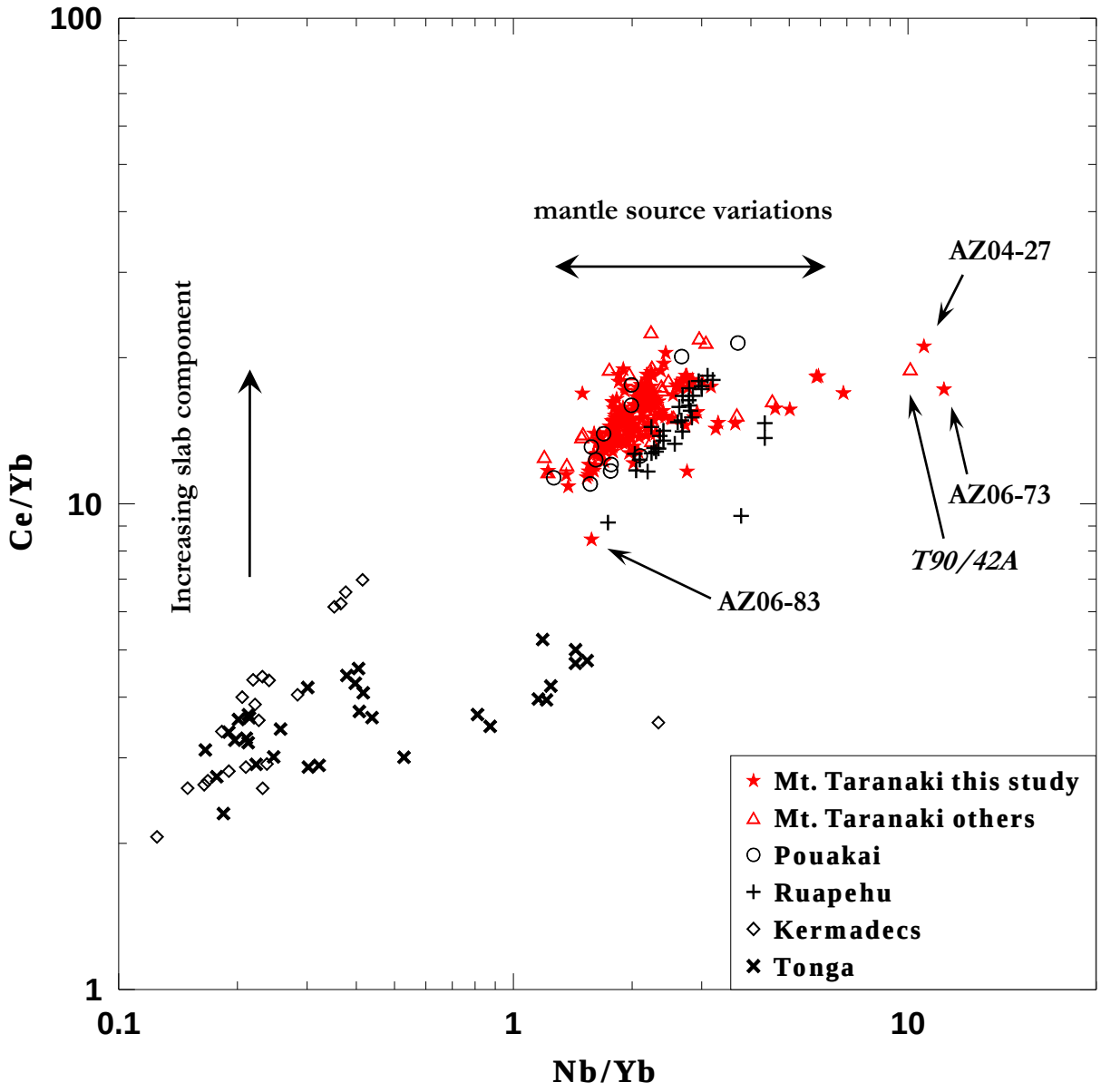

Figure 4.22. The influence of the slab component increases from the Kermadecs/Tonga to the Taranaki volcanoes and Ruapehu. Taranaki eruptives show a wide range in Nb/Yb ratios, which reflects variations in the mantle source, and some overlap with Ruapehu. Mt. Taranaki data from Price et al. (1999), Platz (2007) and Turner (2008). Ruapehu data from Gamble et al. (1993, 1999) and Waight et al. (1999). Kermadec/Tonga data from Ewart et al. (1998).

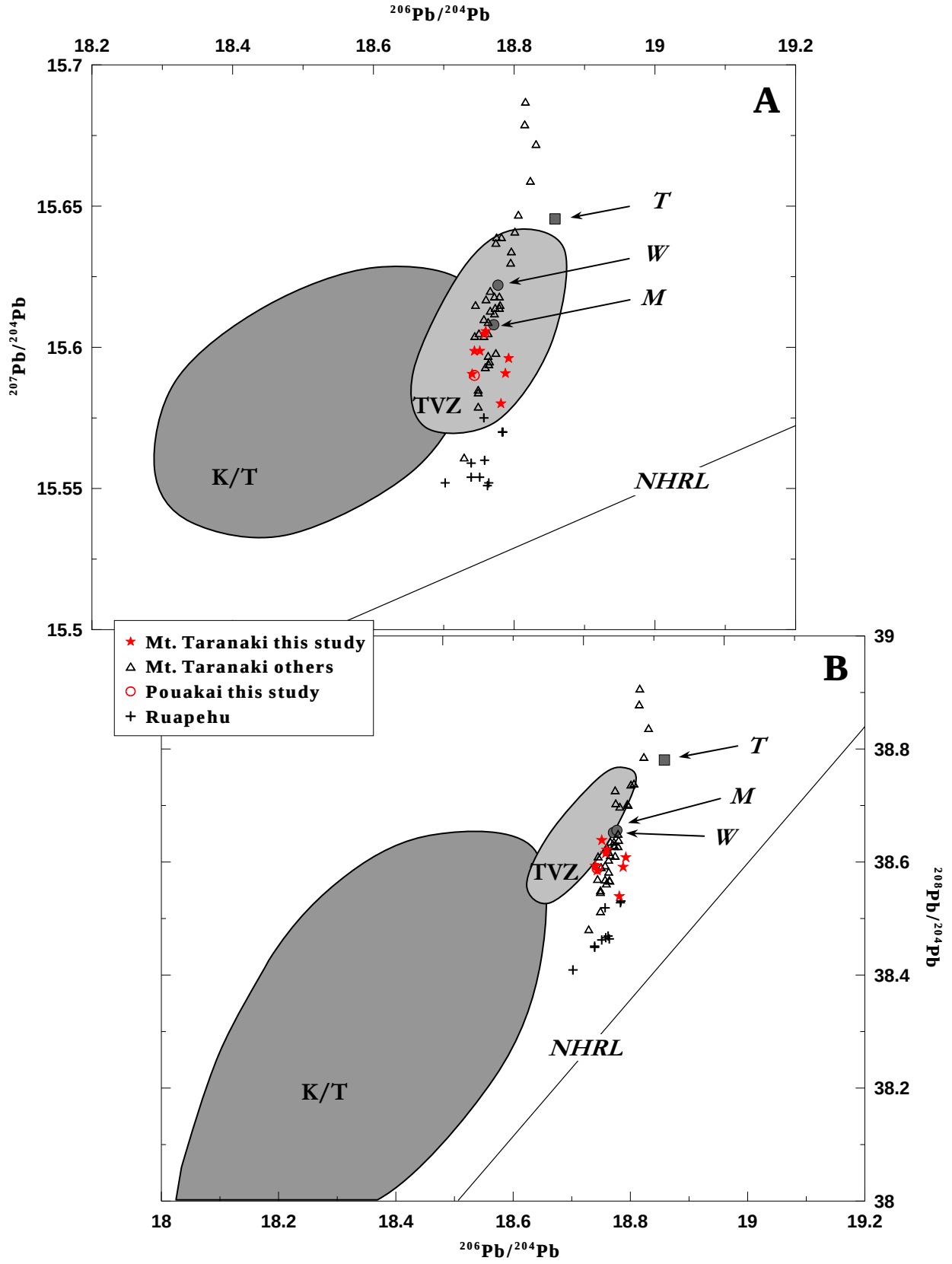

Figure 4.23. Pb isotopic data for Mt. Taranaki and Pouakai samples in comparison with Ruapehu, data fields of TVZ and Kermadec-/Tonga-arc (K/T) and the Northern Hemisphere Reference Line (NHRL) from Hart (1984). Magmas from both volcanoes form a continuous trend of increasing $^{207}Pb/^{204}Pb$ (A) and $^{208}Pb/^{204}Pb$ (B) ratios at slightly increasing $^{206}Pb/^{204}Pb$. Ruapehu rocks are more radiogenic and cluster in a small field, while Taranaki magmas show a wider range of $^{207}Pb/^{204}Pb$ and $^{208}Pb/^{204}Pb$ ratios and extend to less radiogenic compositions. Circles W and M represent average data (from Price et al. 1999) for Taranaki basement rocks of Waipapa terrane and Median Tectonic Zone. The square labelled T represents Ruapehu basement made of Torlesse terrane. Other data sources: Gamble et al (1993, 1999) and Price et al. (1999).

4.9. MAGMATIC EVOLUTION OF MT. TARANAKI

4.9.1. Models of andesite magma generation

Primitive basaltic magmas in arc systems are generated by partial melting of the mantle wedge through some combination of fluxing by slab-derived, H_2O-rich fluids (e.g. Tatsumi 1982; Davies & Stevenson 1992; Tatsumi & Eggins 1995; Schmidt & Poli 1998; Blatter & Carmichael 2001; Ulmer 2001; Grove et al. 2002; Carmichael 2002, 2004; Forneris & Holloway 2003; Parman & Grove 2004) and decompression melting resulting from subduction-induced corner flow (e.g. Sisson & Bronto 1998; Elkins-Tanton et al. 2001; Hasegawa & Nakajima 2004). Models for the generation of andesite magmas have focused on two main processes, i.e. magma differentiation through fractional crystallisation in shallow crustal magma chambers (e.g. Sisson & Grove 1993; Grove et al. 1997; Pichavant et al. 2002b) or in the lower crust at or close to the Moho (Müntener et al. 2001; Annen & Sparks 2002; Mortazavi & Sparks 2003; Prouteau & Scaillet 2003; Turner 2008) and partial melting of older crustal rocks (e.g. Smith & Leeman 1987; Atherton & Petford 1993; Tepper et al. 1993; Rapp & Watson 1995; Petford & Atherton 1996; Chappell & White 2001; Izebekov et al. 2004).

Previously developed models for the generation of intermediate and silicic magmas at Mt. Taranaki suggest that mantle-derived, parental magmas were undersaturated, relatively hydrous, oxidised high-Mg basalts (Stewart et al. 1996; Price et al 1999). These are not represented in the Taranaki sample suites. Instead, ponding of these primary melts at the upper mantle/lower crust boundary is hypothesised, which drove the magma composition to high-Al basalts through fractionation of olivine, pyroxene and spinel (Stewart et al. 1996). Further fractionation and the crystallisation of amphibole buffered the melt composition to basaltic andesite, leading to progressive underplating of the crust with amphibole, olivine and pyroxene cumulates (Foden & Green 1992; Stewart et al. 1996; Price et al. 1999). Some high-Al basalt melts rose to the surface, evolving to fractionated basaltic andesites and low-silica andesites through continued fractionation of olivine, clinopyroxene and eventually plagioclase. The melts were further modified in small, high-level magma chambers through the complex interplay between magma extraction and recharge, crystal fractionation, magma mingling and mixing, and plagioclase accumulation (Smith et al. 1996).

A recent model developed by Annen et al. (2006) combines the above described concept of underplating (cf. Huppert & Sparks 1988; Bergantz 1989; Raia & Spera 1997; Petford & Gallagher 2001; Jackson et al. 2003) and basalt differentiation at high pressures (Gill 1981;

Grove et al. 2002) with the ideas of AFC (DePaolo 1981) and MASH (Hildreth & Moorbath 1988). It suggests that repeated intrusions of mantle-derived hydrous high-Mg magmas into the lower crust gradually raise the geothermal gradient, resulting in the development of a lower crustal 'hot zone'. This hot zone is regarded as a layered mixture of partially crystallised basalt, partially molten crustal rocks and volatiles derived from the solidifying basalt intrusions. In this environment, silicic and intermediate magmas are generated by incomplete crystallisation of the underplated basaltic material (Annen & Sparks 2002; Prouteau & Scalillet 2003), dehydration partial melting of earlier, partly crystallised basalt intrusions and/or meta-basalts (amphibolite) by the intrusion of new hot mantle-derived magma (Smith & Leeman 1987; Annen & Sparks 2002, Price et al. 2005) and crustal assimilation (DePaolo et al. 1981, 1992). The rate of melt production and hence the composition of magmas that ascend to upper crustal levels is controlled by the intrusion rate and depth of mantle-derived basalts, the prevailing geotherm and volatile content in the lower crust (Annen et al. 2006).

Detailed mineralogical studies of the younger Mt. Taranaki eruptives indicate that a two-stage magmatic system of storage, crystallisation and fractionation operates beneath the volcano (Turner 2008). Mantle-derived magmas are differentiated within a lower crustal hot zone, as suggested by Stewart et al. (1996) and Annen et al. (2006), and subsequently rise and assemble at mid-crustal levels prior to eruption. Andesitic melts that segregated from the lower crust are believed to stall within the Tertiary sandstone and mudstone basement at depth of 6-7 km, while more mafic basaltic andesite melts, including basalt melts of Fanthams Peak, stalled at slightly lower levels (up to 10 km) within greywacke basement (Turner 2008).

As shown by geophysical studies of the subvolcanic basement (Sherburn & White 2005), the suggested 'hot zone' of partial melts extends from the lower crust at c. 25 km to the brittle-ductile transition zone at approximately 10-7 km depth beneath Mt. Taranaki. A further implication of the hot zone model for Taranaki is the significant thickening of the crust as a consequence of continuous basalt emplacement. Melt extraction from these basalts results in the formation of residual dense mafic cumulates, which can eventually lead to delamination and recycling into the less dense underlying mantle (Kay & Kay 1993; Jull & Keleman 2001).

4.9.2. Compositional trends with time and geochemical variation

The temporal geochemical changes within Taranaki eruptives, particularly in K_2O, have been explained by two different concepts (Price et al. 1999). (1) Progressively lower degrees of partial melting in the mantle source and changes in the nature of slab-derived fluids. This also generates a more significant fluid trace element signature, and a dilution of the depleted mantle

wedge signature. (2) Increasing thickness of underplated and intruded amphibole-bearing lower crust. Progressive underplating would gradually raise the geothermal gradient, so that subsequently intruding basaltic magmas could incongruently melt previously emplaced amphibole-bearing assemblages (cf., Foden & Green 1992; Stewart et al. 1996). This would have resulted in increasingly more amphibolite assimilation in later mantle-derived basalts, giving rise to increasingly more potassic magmas over time (Price et al. 1992, 1999; Stewart et al. 1996; cf. Dufek & Bergantz 2005).

The debris-avalanche suites illustrate a gradual increase in K_2O and most LILE with time as well as a shift to more evolved magmas and the absence of more primitive compositions with increasing maturity of the volcanic system but no significant changes in the nature of the arc signature were observed. Hence, the data supports the second concept, which is also in agreement with the model by Annen et al. (2006). As the lower crustal hot zone evolves, the geothermal gradient gradually rises leading to increased partial melting of previously crystallised basalt intrusions and underplated amphibolite. Increasingly higher proportions of remelted amphibolite in relation to residual melts from crystallising intrusions generate the progressively more potassic and LILE-enriched compositions observed within the Taranaki debris-avalanche sample suites.

It has been hypothesised that Mt. Taranaki has evolved to its present state from a much more basic system with a more restricted range in compositions (Price et al. 1999). But despite including more primitive eruptives, the variety of rock types (including pumice and scoria lithologies) found in the early debris-avalanche deposits show that Mt. Taranaki was producing a similar range of eruptive compositions and eruption styles to the modern volcano. Each debris-avalanche sample suite contains similar lithologies of basaltic andesites and andesites with basalts being restricted to the oldest units and the Ngaere Formation. The basalt clasts of the Maitahi Formation and the >100 ka Mt. Taranaki debris-avalanche deposits as well as sample T90/42A from Price et al. (1999) are not only characterised by low SiO_2 abundances (48.65-51.73 wt.%) but several also have relatively high MgO (up to 7.71 wt.%), Ni (up to 122 ppm) and Cr (up to 326 ppm) concentrations. The trace element distributions of these unusual samples display a more subdued arc signature with lower La/Nb ratios, higher Ce/Pb ratios and unusually high Nb contents. They have lower $^{87}Sr/^{86}Sr$ and higher $^{144}Nd/^{143}Nd$ isotopic ratios and a relatively unradiogenic Pb isotopic composition compared to other analysed Taranaki samples. This type of rock has been interpreted to represent relatively low-degree melts from a depleted mantle source that has undergone less fractionation during ascent and eruption (Price et al. 1999).

These oldest, most primitive rocks appear to have formed within a more immature volcanic system and reflect the early stages of hot zone development, when more primitive melts could ascend through the lower crust with little interaction. As the hot zone evolved, the likelihood of mantle-derived magmas passing through without some degree of processing was reduced, which is also reflected in the scarcity of mantle-derived magmas in mature arc systems (Annen et al. 2006). The rising geotherm associated with the development of the hot zone beneath Taranaki promoted generation of more silicic and intermediate melts as more primitive melts were trapped in the lower crust where they were modified through crystallisation and mixing with more silicic melts. In addition, the increasingly complex crustal structure with a more dispersed plumbing system resulted in magma assembly and storage at different mid- to shallow crustal levels, where the melts were further modified by fractional crystallisation, magma mingling and mixing (Smith et al. 1996; Stewart et al. 1996; Turner 2008). The interplay of these processes resulted in a gradual shift to more evolved and potassic compositions with increasing maturity of Mt. Taranaki.

The lavas erupted from Fanthams Peak between 3-1.5 ka contain low-silica compositions similar to the early basalt magmas but they have higher contents of K_2O and LILE. The almost identical trace element geochemistry of Fanthams lavas and the youngest Mt. Taranaki eruptives indicates derivation from a similar source but Fanthams magmas reflect a stronger mantle input with less modification in the crust. This might be the consequence of a higher magma supply rate of mantle-derived intrusions into the hot zone, resulting in hotter magmas that were buoyant enough to rapidly ascend through the crust with less interaction. The basalt sample of the Ngaere suite was most likely generated by similar processes and might have been erupted in a similar setting from a proto-Fanthams Peak or a previously existing satellite vent.

The hot zone model suggests that a wide range of melt compositions is produced when intrusions occur over a wide range of depths, i.e. the thicker the crust the greater the potential diversity of melt compositions (Annen et al. 2006). Further compositional and textural diversity of magmas can be generated through entrainment and dissolution of restite or cumulates from their source region and/or incorporate wall-rock during ascent (Annen et al. 2006). Turner (2008) suggested that geochemical variation in Taranaki magmas is the result of varying degrees of amphibole fractionation and/or breakdown of pre-existing amphibolite/gabbro assemblages within the lower crustal hot zone. Recent studies of younger Mt. Taranaki eruptives also showed that during any given eruption cycle, variations across the whole spectrum of compositions may occur (Turner 2008). Broad 1500-2000 year long geochemical cycles at Mt. Taranaki represent

individual magma batches, characterised by initial eruption of a relatively mafic end member followed by progressively more evolved compositions. Further variation within each batch or during eruption is the result of late-stage magma mixing, assimilation and fractional crystallisation processes (Price et al. 2005; Annen et al. 2006). A similar compositional evolution has been observed in the mafic magmas from Fanthams Peak, which become progressively less magnesian with time (Turner 2008).

In the early stages of hot zone development, mantle-derived basaltic melts intruded into a colder, less complex crust. Less interaction with the colder crust resulted in less modification of the new hot mantle-derived magma through dehydration partial melting of earlier intrusions or crustal assimilation. Magmas most likely also intruded at a wider range of depths within the c. 22-25 km thick crust beneath Taranaki (Stern et al. 1987; Sherburn & White 2005). As a consequence, a wider range in compositions with a wider scatter in most major and trace elements, in particular HFSE and LREE, was produced during the early stages of Mt. Taranaki volcanism. Early volcanic products included more primitive basaltic material with a less diluted mantle component. As the volcanic system evolved, continuous basaltic intrusions gradually heated up the hot zone, resulting in more interaction and partial melting of the amphibolised crust and later magmas becoming trapped at similar depths within the lower crust. This resulted in the gradual increase in K_2O and LILE with time and a narrower, more homogenised range of compositions and trace element variations, as observed in the <100 ka Mt. Taranaki eruptives. Only these more evolved melts were buoyant enough to rise through a crust which had become progressively more modified.

4.9.3. Correlation of geochemical and sedimentary cycles

Throughout the volcanic history of Mt. Taranaki a consistent depositional pattern has generated similar types of deposits that contain similar lithologies (cf. Chapter 3). The progressive change to more evolved compositions and the absence of more primitive basalts with increasing maturity of the volcanic system is displayed in the clast assemblages of debris-avalanche deposits. Despite the gradual change in magma composition, the eruptive style and erupted volcanic products reflected in the oldest and youngest debris-avalanche deposits are similar. The occurrence of pumice and scoria lithologies in early deposits indicates Plinian/subplinian style eruptions similar to the ones observed in the Holocene record (cf. Neall 1972; Alloway et al. 1995; Turner 2008). The frequency of lahars and the resulting deposit characteristics (i.e. pumiceous vs. dense vs. polylithologic) depends on the eruptive style with rapid emplacement of stacks of lahar deposits occurring during and after major eruptive activity.

Since changes reflected in the geochemical trends were gradational, they did not result in any abrupt changes in volcanic behaviour and sedimentary pattern. Also, the frequency and timing of edifice failures shows no relation to the geochemical evolution of Mt. Taranaki but rather to its regrowth rate and structure. Eruption frequency and magnitude as well as eruptive style do not appear to be linked to the overall magmatic evolution of Mt. Taranaki over long periods of tens of thousands of years. However, it is known that they are controlled by processes in the upper-crustal plumbing system and shorter geochemical cycles (Platz 2007; Turner 2008).

Overall, the gradual shift to more siliceous magmas may have resulted in more dome-forming eruptions and associated generation of block-and-ash flows in the younger past, compared to earlier longer lava flow extrusion. This may have led to an increasingly unstable summit region of Mt. Taranaki, which may lead to the generation of more frequent but lower volume debris avalanches, as observed for example at St. Augustine (Beget & Kienle 1992) or Shiveluch (Belousov et al. 1999).

4.10. CONCLUSIONS

Debris-avalanche clasts provide useful indicators of past edifice compositions and this method is a novel way to examine what proto-Mt. Taranaki edifices were like.

Mt. Taranaki has evolved to a high-K andesite magmatic system over the last >190 ka. In addition to the progressive enrichment in K_2O and LILE, temporal trends observed within the debris-avalanche sample suite include a gradual shift to more evolved magmas. Throughout the volcanic history, eruptives show a relatively constant arc signature. This new data supports the model of mantle-derived basaltic magmas ponding at the base of the crust where they evolve through a combination of fractionation and interaction with underplated material (cf. Stewart et al. 1996). Repeated intrusions of primitive melts into the lower crust gradually raised the geothermal gradient, resulting in the development of a lower crustal 'hot zone' (cf. Annen et al. 2006). As the hot zone evolved, larger proportions of the underplated basaltic material were partially remelted and generated the progressively more potassic and LILE-enriched compositions observed within the Taranaki debris-avalanche sample suites. Older sample suites include relatively unfractionated basalts with higher MgO, Cr and Ni contents. The trace element distributions of these samples show the most subdued arc signature observed at Mt. Taranaki and they represent more primitive magmas that were able to rise through the crust without intense modification during the early stages of hot zone development. The compositional variations of

these more primitive compositions also reflect a heterogeneous mantle source for parental Mt. Taranaki magmas.

Trace element and some major characteristics allow a distinction to be made between Pouakai- and Mt. Taranaki-derived units. Pouakai samples have distinctly lower contents of K_2O, Rb and Ba, lower Zr, REE and HFSE but similar arc signatures and isotopic compositions to Mt. Taranaki reflect derivation of parental magmas from the same mantle source. Compositional differences between Mt. Taranaki and Pouakai debris-avalanche clasts are the result of higher degrees of partial melting and less interaction with the lower crust for the latter.

Until now, the origin of the Mangati debris-avalanche deposit was unknown and it was assumed that the Motunui event originated from Mt. Taranaki (Alloway et al. 2005). This study has demonstrated that, in contrast to the Maitahi series, both suites overlap in composition with the Mt. Taranaki sample suite and show similar or progressive trends with time. Based on these geochemical characteristics, the Mangati Formation now represents the oldest known deposit derived from Mt. Taranaki. Hence, its emplacement between 190-210 ka gives a new minimum age for the commencement of eruptive activity at Mt. Taranaki, considerably older than previously thought. The nature of the deposit and the range of lithologies present also imply that ancestral Mt. Taranaki was already a high, unstable composite stratocone at this time. The similar range of lithologies represented in debris-avalanche clast assemblages reflects similar eruptive styles throughout the volcanic history, illustrating a long-term sustainability of the volcanic system.

Individual debris-avalanche sample suites can be distinguished based on their geochemical characteristics, in particular differences in K_2O and Ba contents. This indicates that after large sectors of the volcano had been removed by collapse, the edifice was rebuilt by new material with a slightly different geochemical signature before collapsing again. This observation is also important for evaluating the size of collapse and the volume of the subsequent debris-avalanche deposit, in particular for units with limited data of distribution. Major differences in the geochemical character of clast assemblages in comparison to previous debris-avalanche deposits suggest a significant failure and removal of large sectors of the edifice.

This study shows that debris-avalanche clast assemblages can be used as windows into the volcanic past, in some cases back to the earliest stages in the development of the volcanic system. Their geochemical characteristics are a useful tool to distinguish individual stratigraphic units and characterise the overall magmatic evolution. This is an important line of research,

especially at long-lived stratovolcanoes where the older records are incomplete and the full range of products is not exposed.

CHAPTER 5.

PETROGRAPHY AND MINERAL CHEMISTRY OF DEBRIS-AVALANCHE CLASTS

5.1. INTRODUCTION

Previous petrographic and mineralogical studies at Mt. Taranaki concentrated on the <10 ka edifice-forming lavas, but also included a number of samples from younger ring-plain deposits (Warea and Pungarehu Formations). Due to the lack of stratigraphic control, the older parts of the succession have been mostly neglected. Clasts were collected from deposits overlying the Inaha marine bench (c. 105-50 ka), but were studied from a geochemical rather than mineralogical perspective (Price et al. 1999, 2006). The new stratigraphic framework established in this study (cf. Chapter 2) allows a more systematic sampling of the ring-plain succession with tighter age control. This chapter describes clast lithologies and their petrographic characteristics from samples throughout the debris-avalanche deposit record to compare and contrast to the known younger units of the volcanic succession. Clasts from the oldest debris-avalanche deposits at Mt. Taranaki (Motunui and Okawa Formations), were examined in greater detail, to expose the maximum expected differences to the youngest known eruptives.

5.2. PREVIOUS WORK

Mt. Taranaki eruptives range from vesicular red and black scorias and black glassy porphyritic rocks to dense, hard, grey porphyric lavas (Neall et al. 1986; Stewart et al. 1996). Xenoliths are common (Price et al. 1999) and include a diverse set of rocks representing the subvolcanic crust, mostly showing textural evidence of metamorphism. The suite can be grouped into four components that represent different crustal levels beneath the volcano; supra-crustal rocks, upper to mid-crustal basement (Median Tectonic Zone), mid to lower crustal cumulates and granulites, along with gabbros and ultramafic xenoliths (Gründer 2006).

In thin-section, Mt. Taranaki rocks are holocrystalline to hypocrystalline, some show seriate textures but most are porphyritic (Neall et al. 1986; Stewart et al. 1996; Price et al. 1999; Platz 2007). The first petrological classification of Mt. Taranaki volcanics by Gow (1968) was based on ferromagnesian mineral assemblages. He recognised five gradational types of andesite: augite-andesite, augite-hornblende andesite (augite>hornblende), augite-hornblende andesite (augite~hornblende), augite-hornblende andesite (augite<hornblende), and augite-olivine andesite (olivine ≤7%) with augite-hornblende andesite being the most common type.

Phenocryst contents range from 25 to 55% and include (in order of abundance) plagioclase, clinopyroxene, titanomagnetite, and hornblende (Neall et al. 1986; Stewart et al. 1996; Price et al. 1999; Platz 2007). Hornblende can occasionally form large (>100 mm) crystals (Stewart et al. 1996). Olivine occurs in small amounts in most lavas whereas biotite and orthopyroxene are rare. Glomerocrysts typically comprise clinopyroxene ± titanomagnetite ± plagioclase ± olivine with rare amphibole and orthopyroxene. Groundmass constituents are glass, plagioclase, clinopyroxene, Fe-Ti-oxides, rare orthopyroxene and traces of olivine (Stewart et al. 1996; Price et al. 1999; Platz 2007). Accessory apatite and zircon are common.

5.3. SAMPLE LITHOLOGIES

Rock types collected from 12 Mt. Taranaki and 1 Pouakai debris-avalanche deposit, comprise compositions from basalt to evolved andesite with most samples being basaltic andesites (cf. Chapter 4). Andesite clasts range from light grey to dark grey, are mostly dense and hard and rarely vesicular. Rock textures vary from glassy and aphyric to crystal-rich with fine- to coarse-grained crystals. Hornblende can be fresh or resorbed and commonly occurs as large

phenocrysts (up to 20 mm). Some samples contain large, up to 10 mm long, macroscopically zoned plagioclase crystals; large clinopyroxene phenocrysts are rare. Hornblende-feldspar-andesites with no macroscopically visible clinopyroxene are common.

Basaltic andesite samples occur in a variety of lithologies, reflecting their wide range of SiO_2-contents (from 52.1-56.8 wt.%) and geochemical compositions. Lithologies include pumice/scoria and lavas with grey to black clasts, some are reddish and oxidised. The clasts are mostly glassy and range from dense and hard to very vesicular, and aphyric to crystalline. Basaltic andesite rocks contain a variety of different mineral assemblages including hornblende- to clinopyroxene assemblages and olivine-clinopyroxene-bearing rocks. Texturally they are coarse- to fine-grained (according to IUGS sizes: coarse >3 mm, medium 1-3 mm and fine <1 mm), some with large clinopyroxenes (up to 12 mm) and/or large olivines of similar size, some with large hornblende crystals; all have generally smaller plagioclase (up to 4 mm). Hornblende and olivine phenocrysts can be unaltered or show reaction textures.

Lithologies of basalt samples range from dark grey to black, aphyric to crystalline and dense to vesicular. A large proportion of rocks are hard and glassy. Most basaltic clasts are coarsely crystalline and contain olivine phenocrysts, which are fresh to strongly weathered or resorbed. Clinopyroxene phenocrysts can be up to 20 mm in length, while larger plagioclase is less common and macroscopic hornblende is very rare and strongly resorbed.

5.4. PETROGRAPHIC OBSERVATIONS

5.4.1. Mineral assemblages and characteristic textures

Mineral phases that occur within the studied debris-avalanche clasts include plagioclase (Plg), hornblende (Hbl), clinopyroxene (Cpx), Olivine (Ol), titanomagnetite (Tm) and rare phlogopite (Phl), biotite (Bt), and orthopyroxene (Opx). The most abundant mineral assemblage comprises:

1) Plg-Cpx-Hbl-Tm with mineral proportions varying from Cpx>Hbl to Hbl>Cpx

   Other commonly observed assemblages are:

2) Plg-Cpx-Hbl-Ol-Tm
   (with varying proportions of Cpx, Hbl, Ol and varying degrees of Hbl resorption)

3) Plg-Cpx-Ol-Tm

The rarest assemblages are:

4) Plg-Cpx-Tm

5) Plg-Cpx-Ol-Phl-Tm

6) Plg-Hbl-Cpx-Bt-Tm

In thin-section, the rocks range from holocrystalline to more common hypocrystalline textures and are typically microcrystalline with a cryptocrystalline or mostly hyaline groundmass. The major mineral phases (Plg, Cpx, Hbl, Ol, and Tm) occur as euhedral to subhedral phenocrysts to microphenocrysts in seriate to porphyritic textures. Fluidal and intersertal textures are also present. Glomerocrysts are common and consist of Cpx-Tm (± Plg, Ol, Hbl), Cpx-Plg (± Ol), Hbl-Cpx, Plg, Hbl, Hbl-Plg, Ol-Tm, Hbl-Tm, Hbl-Ol-Plg, and less common Hbl-Plg-Bt. The studied samples range from dense lavas to very vesicular pumice-clasts.

5.4.2. Mineral characteristics

Plagioclase is the most abundant mineral phase and forms euhedral to subhedral phenocrysts, groundmass microphenocrysts, and inclusions in hornblende and clinopyroxene. It also occurs within glomerocrysts associated with clinopyroxene and titanomagnetite (± Ol, Hbl), or with hornblende (± Ol, Bt). Plagioclase phenocrysts are typically strongly zoned and large crystals often show multiple rims or thick coronas. Oscillatory, convolute and continuous zoning occurs that include bands rich in melt inclusions and multiple zoning patterns. Inclusions of melt, clinopyroxene, and hornblende, and sieve textures are common and typically occur along zone boundaries in rims or in crystal cores. The sieve texture is either void space or filled with a more sodic plagioclase (Neall et al. 1986), glass, secondary minerals, or in rare cases clinopyroxene or phlogopite. Larger plagioclase crystals commonly show fractures, strongly developed sieve texture and/or embayed or rounded rims and can appear skeletal. Carlsbad, albite, or carlsbad-albite twinning is common. Occasionally, intergrowth and cross hatched patterns were observed, the latter reflecting a combination of albite- and pericline-twins.

Clinopyroxene occurs as euhedral to subhedral crystals that are green to brown in colour. It is present as phenocrysts, groundmass microphenocrysts, inclusions in hornblende, and as clinopyroxene aggregates. Occasionally, clinopyroxene mantles orthopyroxene cores. Clinopyroxene also forms abundant glomerocryst clusters with titanomagnetite, plagioclase and sometimes hornblende. Some larger crystals and aggregates may represent xenocrysts and/or small xenolithic fragments. Oscillatory, continuous and discontinuous zoning with distinct (in some cases greenish) cores and single or multiple rims were frequently observed with sector and

melt inclusion zoning being less common. Twinning and exsolution lamellae are also characteristic features. Titanomagnetite is the most abundant inclusion mineral found in clinopyroxene, commonly found along zone boundaries or fractures. Inclusions of hornblende, apatite, plagioclase and rare olivine also occur. Large clinopyroxene crystals sometimes exhibit resorbed or embayed rims, coronas and cracks. Resorbed cores and skeletal clinopyroxene crystals are less common. Cores were occasionally observed to be replaced by opaque oxides, plagioclase and titanomagnetite grains or recrystallised clinopyroxene and plagioclase.

Hornblende is present in most samples and forms euhedral to subhedral crystals. These commonly exhibit the characteristic 60°/120° cleavage of amphiboles and are dark brown to reddish brown and rarely greenish in colour. The reddish brown colour is produced by rapid oxidation during the slow cooling of the lavas, while fresh greenish hornblende typically occurs in rapidly chilled pumice clasts (Stewart et al. 1996; Platz 2007). Hornblende occurs as phenocrysts, microphenocrysts in the groundmass, inclusions in other larger hornblende crystals and plagioclase, and in glomerocrysts associated with clinopyroxene, titanomagnetite, plagioclase, rarely biotite and sometimes plagioclase (± Ol). In low-silica rock types of the studied sample suites, hornblende is an accessory mineral and strongly corroded. Some crystals show discontinuous zoning with distinct cores, thin middle rim and thick outer rims or multiple rims. Hornblende phenocrysts commonly contain small plagioclase, infrequent melt inclusions and rare clinopyroxene. Hornblende shows varying degrees of resorption and opacitisation (cf. Platz 2007). Fresh crystals with sharp boundaries and no reaction rim are rare. More commonly they are mantled by black opacite alteration rims of variable thickness or appear skeletal due to strongly resorbed and/or substituted rims and cores, some containing patches of plagioclase, clinopyroxene, or titanomagnetite. Strongly altered hornblende crystals are partially or fully replaced by opaque oxides and are only preserved as pseudomorphs. Occasionally, strongly resorbed crystals were found to be mantled by grains of plagioclase, clinopyroxene, and titanomagnetite (± Ol) or even completely replaced by fine-grained aggregates of clinopyroxene, plagioclase and titanomagnetite (± Ol) that formed due to amphibole breakdown in response to decompression during magma ascent (cf. Stewart 1975; Devine et al. 1998).

Olivine is common in the lower silica rock types of the studied sample suites. It is present as euhedral to subhedral, and less common anhedral, phenocrysts, groundmass microphenocrysts and in glomerocrysts associated with titanomagnetite, clinopyroxene-titanomagnetite (± Plg, Hbl) or plagioclase-hornblende. Small phenocrysts are typically euhedral. Some larger olivine crystals might represent xenocrysts (cf. Stewart et al. 1996). Olivine also occurs as small inclusions in clinopyroxene. Crystals were observed to be mantled by

clinopyroxene and titanomagnetite grains and rarely by opaque oxides. Larger crystals commonly show resorbed rims and distinct fractures. The latter can be unfilled or filled with small plagioclase grains and titanomagnetite or secondary (in some cases carbonate) minerals. Inclusions of clinopyroxene were observed in fractured olivine. Occasionally, olivine crystals are strongly resorbed and mostly replaced by small grains of hornblende, clinopyroxene, plagioclase and olivine.

The most abundant Fe-Ti oxide in Mt. Taranaki rocks is titanomagnetite. In debris-avalanche samples it forms fresh, homogeneous, euhedral microphenocrysts in the groundmass and also occurs as larger grains 1-1.5 mm in size that are clustered near or occur as inclusions in clinopyroxene phenocrysts and Cpx-aggregates. Titanomagnetite is also commonly associated with clinopyroxene (± Plg, Ol, Hbl) in glomerocrysts or, in more primitive samples, with olivine.

Orthopyroxene is rare in the studied debris-avalanche clasts. It was found in one sample mantling xenocrystic clinopyroxene and olivine as well as in a resorbed hornblende crystal. The thin-section of another sample contains honey-coloured orthopyroxene cores that were mantled by clinopyroxene, a texture that has been described previously from Taranaki (cf. Neall et al. 1986).

Biotite has been described as a minor phenocryst and as a phase in microphenocryst assemblages in the lavas that form the current summit dome (Platz 2007). In the studied sample suites, biotite is rare and was only observed within a resorbed hornblende crystal in one higher-silica andesite. Phlogopite is also rare and was microscopically identified in a rock of basaltic composition where it occurs as anhedral, interstitial phenocrysts and as inclusions in large plagioclase crystals. The observed phlogopite is pleochroic from light yellow to orange-brown and has a distinct mica cleavage.

A common accessory is apatite which occurs mainly as small inclusions in clinopyroxene, but chalcopyrite and Fe-Mn-rich carbonate were also found in a few samples. Zircon has been described as a common accessory phase in younger Taranaki rocks (Neall et al. 1986) but was not observed in the older, more primitive sample suites.

In most samples examined as part of this study, the groundmass is largely hypocrystalline and consists of microphenocrysts and small proportions of interstitial colourless or pale to dark brownish glass. Some samples exhibit a hyaline groundmass with only few microphenocrysts. Most of the minerals described above also occur as microphenocrysts in the groundmass, with plagioclase being the most dominant phase. Clinopyroxene and

titanomagnetite are also common, as is olivine in rocks with lower silica contents. Hornblende is rare and orthopyroxene, biotite and phlogopite have not been identified as groundmass phases.

5.5. VARIATIONS IN MINERAL COMPOSITIONS

The mineral chemistry of selected samples from within the two oldest Mt. Taranaki debris-avalanche deposits, the Motunui and Okawa Formations, were studied in more detail. Thin sections were prepared for the complete range of lithologies and whole-rock compositions represented in these formations and used for electron-microprobe analysis of the constituent mineral phases. Variations in mineral compositions of these oldest known rocks are described in the following sections and the results compared with previously obtained mineral data from the youngest (<10 ka), edifice-forming deposits (Stewart et al. 1996; Platz 2007; Turner 2008) to highlight differences between early and late stages of the Mt. Taranaki magma system.

5.5.1. Plagioclase

The variety of observed textures of plagioclase crystals is reflected in the broad range of compositions from An_{92-33} (Fig. 5.1A, Table 5.1). Phenocrysts are strongly zoned, particularly the larger crystals, which typically consist of substantial cores and multiple rims. The composition of large crystals ranges from An_{92-71} in cores to An_{73-33} in rims while smaller crystals show cores with An_{86-48} and rims with An_{74-38} (Fig. 5.1B). Reverse and reverse-to-normal zoning is common and reflects disequilibrium of the crystal and the residual melt. The most calcic plagioclase compositions (An_{92-88}) are found in cores of large strongly zoned crystals and these may be of xenocrystic origin. The lowest An contents (An_{39-33}) were observed in plagioclase rims and smaller crystals within the groundmass of andesite rock compositions.

Fanthams Peak lavas and the youngest Mt. Taranaki eruptives (Burrell Lapilli and summit dome lavas) show a similar range of plagioclase compositions to the >100 ka debris-avalanche samples (Fig. 5.1C) with An_{37-83} and An_{36-87}, respectively (Turner 2008; Platz 2007). In contrast, a wider compositional range of An_{93-9} has been described for <5 ka volcanics with the most sodic, also having up to Or_{43} (Turner 2008). Similar plagioclase compositions (An_{91-6}) were observed in Mt. Taranaki lavas (<10 ka) with the most sodic crystals being rich in Or and the most calcic plagioclase occurring as inclusions in amphibole (Stewart et al. 1996). Plagioclases in clinopyroxene phenocrysts and associated with clinopyroxene in glomerocrysts contained high proportions of An (An_{84-80} and An_{89-74}, respectively). Resorbed cores showed two populations

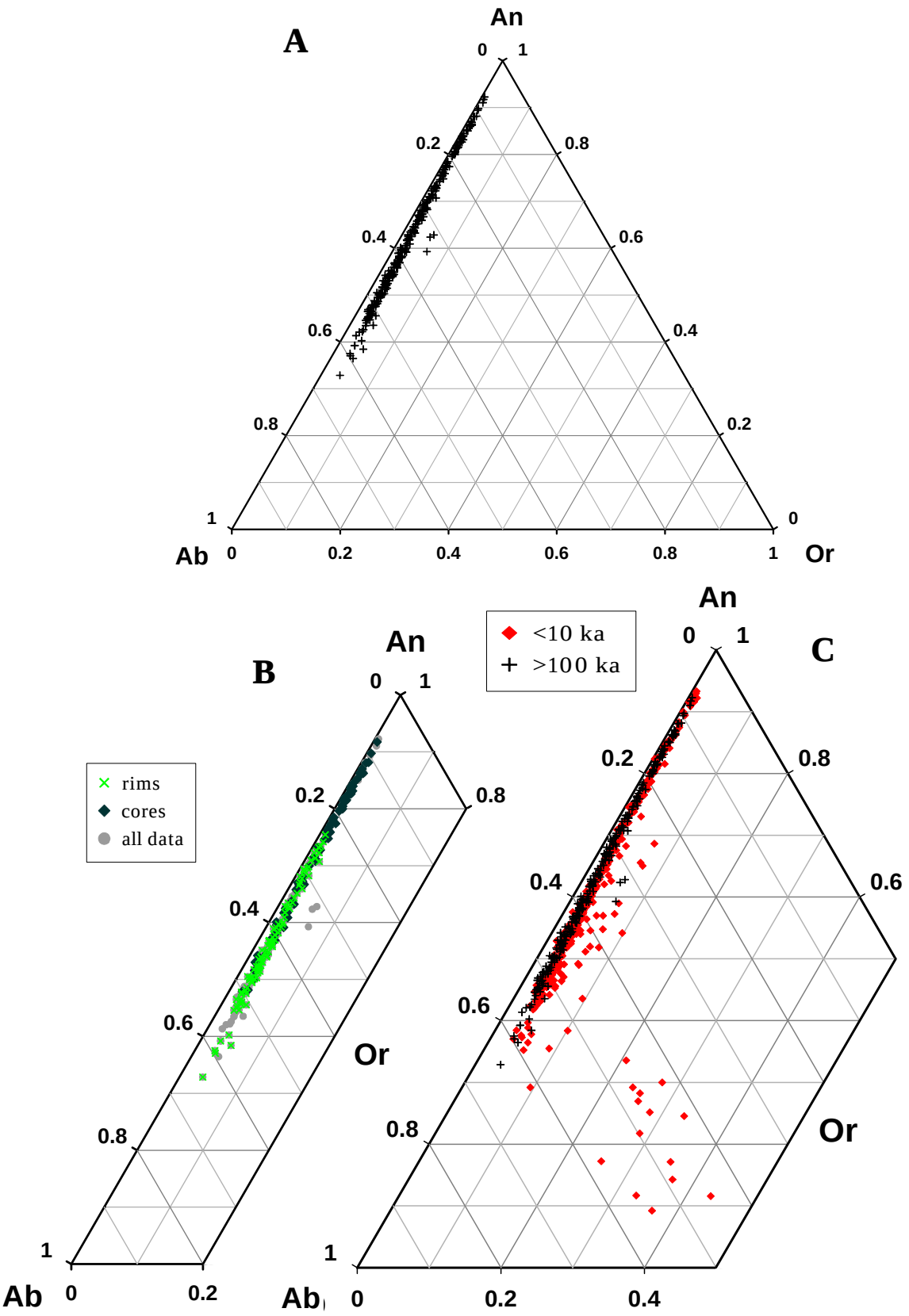

Figure 5.1. Composition of feldspars in Mt. Taranaki rocks. A: Compositional range of plagioclase in 100-130 ka debris-avalanche clasts. B: Rim and core analyses of plagioclase in debris-avalanche samples. C: Comparison of plagioclase composition in >100 ka and <10 ka rocks (data from Platz 2007, Turner 2008).

TABLE 5.1. *Compositions of selected plagioclases of the Motunui and Okawa sample suites.*

	Plg	Zoned Plg		Zoned Plg		Large Plg with calcic core and multiple zoned rims						Large zoned Plg with zoned calcic core				
	Small	Core	Rim	Core	Rim	Core	Rim1	Rim2	Rim3	Rim4	Rim5	Core	Core2	Core3	Rim1	Rim2
sample no.	*AZ04-08*	*AZ04-41*		*AZ04-06*		*AZ04-09*						*AZ04-20*				
analysis no.	*7538*	*7651*	*7653*	*7459*	*7460*	*7362*	*7367*	*7366*	*7365*	*7364*	*7363*	*8250*	*8247*	*8248*	*8249*	*8246*
SiO_2	53.38	54.44	51.77	48.28	52.26	45.95	57.63	56.08	55.60	59.73	58.13	46.82	47.15	48.68	51.34	52.55
TiO_2	0.13	0.09	0.05	0.11	0.01	0.00	0.00	0.00	0.11	0.10	0.09	0.00	0.12	0.11	0.10	0.08
Al_2O_3	28.82	28.03	29.48	31.59	29.13	33.37	25.92	26.82	26.68	24.52	25.33	32.55	32.79	31.59	29.31	28.53
FeO	0.42	0.61	0.64	0.73	0.87	0.40	0.44	0.47	0.32	0.26	0.45	0.53	0.38	0.57	0.69	0.87
MnO	0.00	0.00	0.00	0.00	0.07	0.06	0.09	0.02	0.01	0.12	0.00	0.04	0.12	0.00	0.01	0.00
MgO	0.03	0.15	0.17	0.16	0.01	0.00	0.07	0.00	0.00	0.00	0.07	0.00	0.00	0.00	0.06	0.15
CaO	12.09	11.37	13.05	15.53	12.62	0.00	8.37	9.45	9.59	6.87	7.76	16.40	16.65	15.65	12.95	11.98
Na_2O	4.42	5.17	4.14	2.65	4.25	1.59	6.81	5.99	5.80	7.35	6.90	2.16	1.97	2.36	4.06	4.89
K_2O	0.31	0.21	0.19	0.17	0.33	0.14	0.55	0.44	0.44	0.62	0.59	0.17	0.10	0.25	0.27	0.44
P_2O_5	0.00	0.00	0.00	0.00	0.08	0.26	0.00	0.00	0.00	0.02	0.00	0.00	0.00	0.01	0.00	0.00
SO_3	0.11	0.16	0.00	0.01	0.00	0.00	0.00	0.00	0.09	0.00	0.08	0.02	0.00	0.01	0.07	0.04
Cl	0.02	0.02	0.00	0.00	0.00	0.00	0.05	0.02	0.00	0.03	0.03	0.00	0.00	0.00	0.01	0.01
V_2O_3	0.09	0.00	0.00	0.00	0.13	0.10	0.00	0.00	0.01	0.00	0.06	0.00	0.00	0.00	0.04	0.14
Cr_2O_3	0.02	0.00	0.06	0.10	0.07	0.00	0.20	0.06	0.04	0.08	0.00	0.07	0.00	0.10	0.00	0.02
NiO		0.04	0.00									0.00	0.15	0.00	0.00	0.00
Total	99.75	100.29	99.55	99.29	99.73	99.27	99.99	99.06	98.64	99.56	99.34	98.76	99.43	99.33	98.91	99.70
Ab	0.39	0.45	0.36	0.23	0.37	0.14	0.58	0.52	0.51	0.64	0.60	0.19	0.18	0.21	0.36	0.41
An	0.59	0.54	0.63	0.76	0.61	0.85	0.39	0.45	0.47	0.33	0.37	0.80	0.82	0.77	0.63	0.56
Or	0.02	0.01	0.01	0.01	0.02	0.01	0.03	0.03	0.03	0.04	0.03	0.01	0.01	0.01	0.02	0.02

ranging from An_{89-70} and An_{65-55}. More Ab-rich outer rims with up to Or_{27} and K-rich feldspar ($Or_{45}An_{6}$) as an interstitial phase in some glomerocrysts were also observed.

5.5.2. Pyroxene

Clinopyroxenes are predominantly augites with some, mostly crystal cores, being diopsidic in composition. Clinopyroxene crystals in the Motunui and Okawa sample suites are relatively homogeneous and range in composition from Wo_{39-47}:En_{33-51}:Fs_{4-18} (Fig. 5.2A, Table 5.2). They are either unzoned or slightly zoned from Mg-rich cores to Fe-enriched rims (Fig. 5.2B). Reverse zoning is common. The most ferrous compositions (Fs_{14-18}) occur in a basaltic andesite that contains only microphenocrystic clinopyroxene and in the two highest-silica andesite rocks of the analysed sample suite. More magnesian clinopyroxene (En_{49-51}) is limited to lower-silica basaltic andesite or basalt.

Clinopyroxenes in young eruptives do not span the same compositional range as is observed in the studied >100 ka debris-avalanche clasts (Fig. 5.2C). The young volcanics cover a similar spectrum of En proportions with fewer analyses plotting at the highest and the lowest En contents. They also lack the most ferrous compositions observed in the older rocks (up to Fs_{18}). Samples <1.7 ka (from the summit dome lavas, Burrell Lapilli, Minirapa and Lizard lavas) and eruptives <5 ka have Wo_{36-47}:En_{40-52}:Fs_{5-16} contents (Platz 2007; Turner 2008), while Fanthams lavas contain clinopyroxene of a smaller compositional range with Wo_{46-48}:En_{41-45}:Fs_{9-11} (Turner 2008). Similar zoning patterns from Mg-rich cores to Fe-enriched rims with a change of only 1-2 mol% En and sometimes reversed zoning were described by Stewart et al. (1996).

Orthopyroxene is a rare component of Mt. Taranaki volcanics (cf. Neall et al. 1986; Stewart et al. 1996) and was only found in two rocks of the studied sample suites. In a basaltic andesite it occurs in the core of a resorbed hornblende as well as mantling clinopyroxene and olivine crystals and has a tight range in composition from En_{75-76} (Fig. 5.2A, Table 5.2). Orthopyroxene associated with olivine in a basalt sample is slightly less magnesian (En_{72}).

More orthopyroxene analyses have been obtained from the younger Mt. Taranaki volcanics (Fig. 5.2D). Orthopyroxene in volcanics <5 ka have compositions of En_{75-77} (Turner 2008) similar to the older samples. In contrast, eruptives <1.7 ka show a variety of En contents ranging from En_{58-79} (Platz 2007). Stewart et al. (1996) pointed out that orthopyroxene cores (En_{74-79}) mantled by clinopyroxene differ in composition from groundmass microlites, microphenocrysts and rare phenocrysts (En_{60-66}).

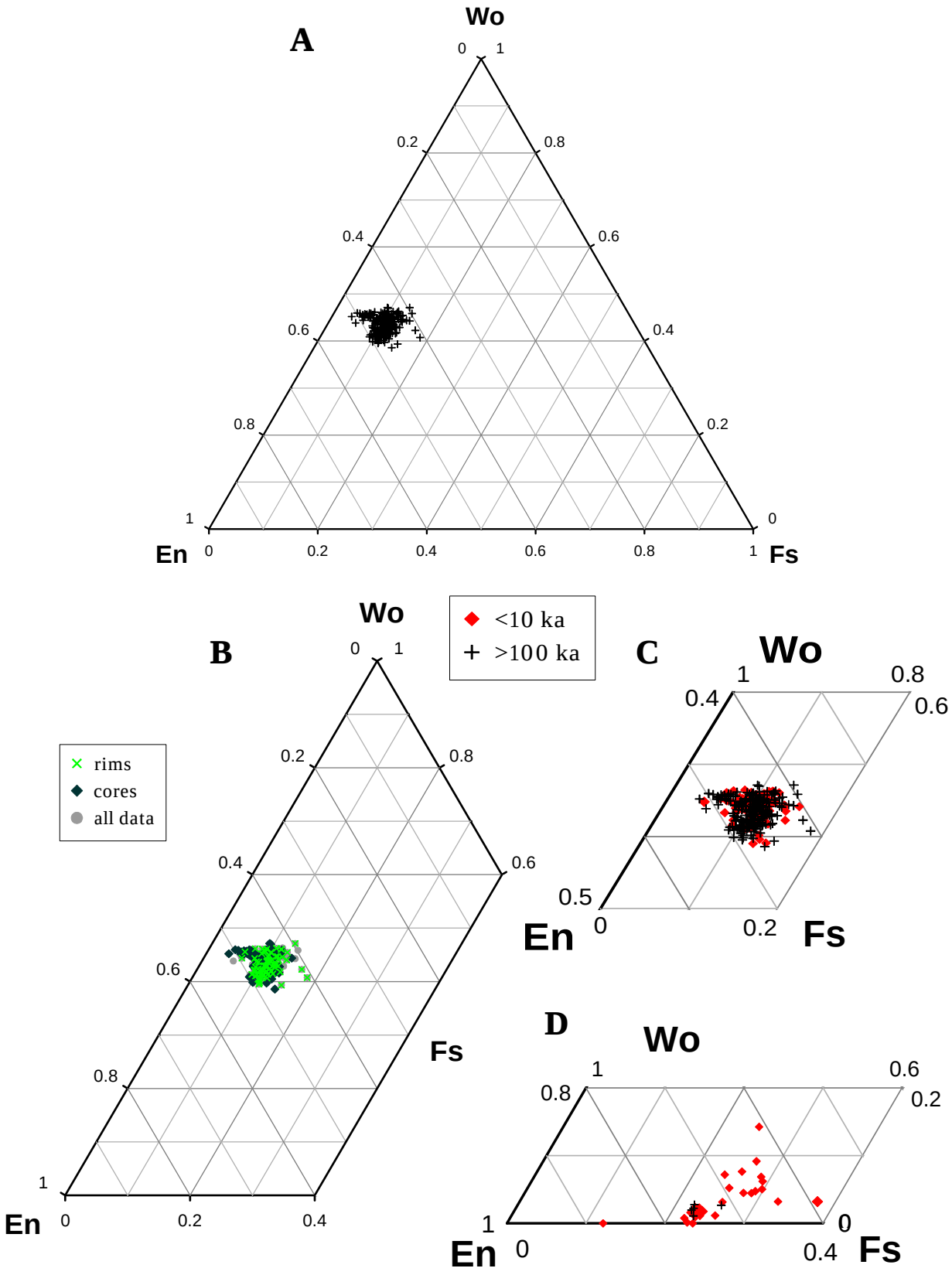

Figure 5.2. Composition of pyroxenes in Mt. Taranaki rocks. A: Clinopyroxene and orthopyroxene compositions in 100-130 ka debris-avalanche clasts. B: Rim and core analyses of clinopyroxenes in debris-avalanche samples. Comparison of clinopyroxene and orthopyroxene compositions in >100 ka and 10 ka rocks is shown in C and D, respectively (data from Stewart et al. 1996, Platz 2007, Turner 2008).

TABLE 5.2. *Composition of selected pyroxenes of the Motunui and Okawa sample suites.*

	Large cpx		**Large cpx**		**Small cpx**	**Cpx rim**	**Opx**	**Opx rim**
	Core	**Rim**	**Core**	**Rim**	**Green**	**around Ol**	**Core**	**around Ol**
Sample no.	*AZ04-33*		*AZ04-06*		*AZ04-09*		*AZ04-41*	*AZ04-28*
Analysis no.	*8011*	*8010*	*7454*	*7455*	*7360*	*7650*	*7665*	*7466*
SiO_2	51.57	47.99	49.3	47.63	52.61	50.67	54.5	54.64
TiO_2	0.46	1.11	0.79	1.44	0.34	0.78	0.28	0.15
Al_2O_3	2.13	5.36	4.19	6.25	1.38	2.76	1.21	1.23
FeO	7.60	9.65	6.22	7.23	7.16	8.58	16.52	14.77
MnO	0.55	0.45	0.14	0.22	0.65	0.30	0.77	0.77
MgO	14.6	11.87	14.76	13.63	15.2	15.28	25.69	27.26
CaO	21.47	21.85	22.53	22.18	21.46	20.41	1.96	1.11
Na_2O	0.37	0.42	0.14	0.19	0.53	0.31	0.06	0.14
K_2O	0.02	0.07	0.03	0.08	0.14	0.07	0.15	0.08
P_2O_5	0.00	0.04	0.17	0.12	0.05	0.00	0.00	0.00
SO_3	0.00	0.10	0.01	0.01	0.00	0.01	0.10	0.00
Cl	0.00	0.05	0.00	0.00	0.01	0.04	0.05	0.05
V_2O_3	0.03	0.07	0.18	0.13	0.15	0.00	0.00	0.02
Cr_2O_3	0.08	0.16	0.15	0.04	0.24	0.19	0.07	0.03
NiO	0.00	0.08				0.00	0.12	0.00
Total	98.88	99.27	98.6	99.11	99.92	99.4	101.48	100.25
En	45	42	48	47	47	48	72	76
Fs	11	13	07	08	09	11	26	23
Wo	44	45	45	44	45	41	03	01

5.5.3. Hornblende

Hornblende is present in most samples and shows various degrees of resorption/reaction and recrystallisation. It ranges in composition from Mg# 59-78 with most analysed hornblende being pargasitic (Fig. 5.3A, Table 5.3); only some classify as magnesiohastingsites (after Leake et al. 1997a, 1997b, 2003). Some crystals plot in the field of edenite. Hornblende phenocrysts are zoned optically but only show weak Mg-Fe-zoning with cores ranging from Mg# 62-76 and rims from Mg# 59-77 (Fig. 5.3B). Core and rim compositions differ more distinctly in Al_2O_3 (cores: 11.23-13.1 wt.% and rims: 9.2-14.4 wt.%) and TiO_2 (cores: 1.3-3.78 wt.% and rims: 2.12-3.64 wt.%). Similar characteristics have been observed

previously with crystals only showing weak Mg-Fe-zoning and most change occurring in Ti and Al (Stewart et al. 1996).

Hornblende shows a similar range of Mg# and Si in younger eruptives (Fig. 5.3C) with Mg# 62-75 and Si 6-6.5 for eruptives <1.7 ka (Platz 2007), Mg# 63-69 and Si 5.9-6.5 for Fanthams Peak lavas and Mg# 55-74 and Si 5.8-6.6 for volcanics <5 ka (Turner 2008), compared to Mg# 59-78 and Si 5.8-6.6 for >100 ka rocks. Hornblende compositions of the sample suites show more distinct differences in TiO_2 and Al_2O_3 contents (Fig. 5.4A). The oldest rocks have the broadest range in TiO_2 and Al_2O_3 contents with 1.3-3.8 wt.% and 9.2-15 wt.%, respectively, compared to 1.9-3.4 wt.% TiO_2 and 8.8-13.7 wt.% Al_2O_3 for <1.7 ka rocks (Platz 2007), 2.5-5.8 wt.% TiO_2 and Al_2O_3 9.2-13.5 wt.% in Fanthams Peak lavas and 2.1-4.1 wt.% TiO_2 9.4-14.8 wt.% Al_2O_3 for tephras <5 ka (Turner 2008). Plots of Ti (cpf = calculated per formula unit) versus tetrahedral and octahedral Al again show that the oldest rocks exhibit the widest range in hornblende compositions but also reveal two distinct populations (Fig. 5.4B-C).

Figure 5.4C displays a large group of analyses from all sample suites plotting at higher Ti and corresponding lower Al^{VI} contents. The youngest rocks (<1.7 ka) do not contain hornblende with compositions near the upper Ti/lower Al^{VI} spectrum ($Ti \leq 0.38$, $Al^{VI} \geq 0.18$). Instead, a large number of hornblende analyses from the youngest (and oldest) studied rocks cluster at low Ti and corresponding high Al^{VI} contents, while only few hornblende compositions from <5 ka eruptives plot in this field.

Hornblende crystals in edifice-building lavas <10 ka show a similar mineral chemistry to the oldest and youngest eruptives. They were found to be of magnesiohastingsitic composition with Mg# ranging from 72-92, low SiO_2 and high Al_2O_3 contents, Si near 6 and Al^{IV} 1.7-2 (Stewart et al. 1996).

5.5.4. Biotite

Biotite is a minor mineral phase in Mt. Taranaki rocks (Platz 2007). Based on Al^{IV} and Mg#, the biotite found in one thin-section of the debris-avalanche sample suite is classified within the annite-phlogopite series (cf. Rieder et al 1998). It contains 71.7-72.2% phlogopite component (Table 5.3). These values lie in the compositional range of biotite phenocrysts and microphenocrysts observed in samples from the summit dome (Platz 2007), which show 62-81% phlogopite component.

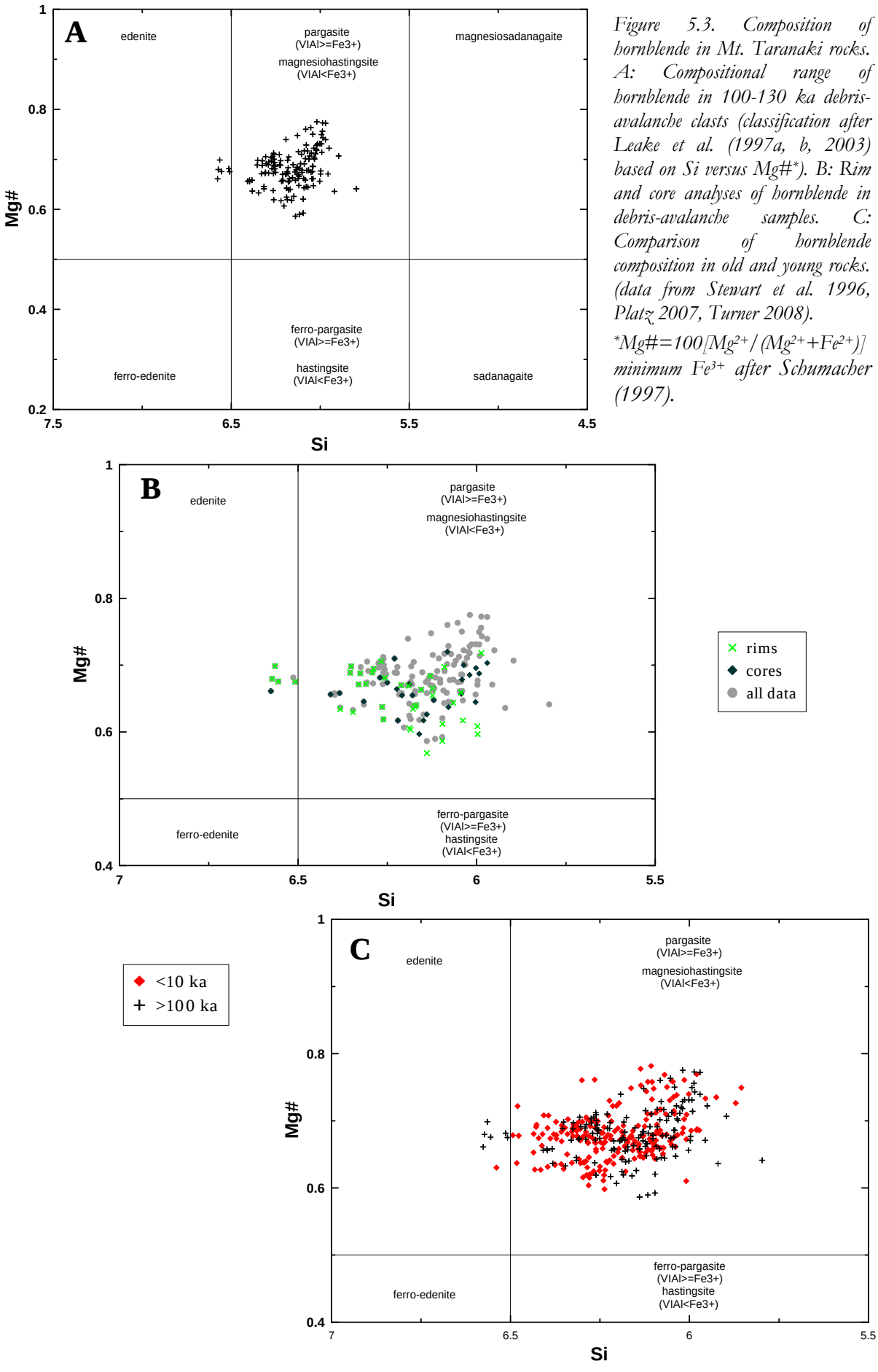

Figure 5.3. Composition of hornblende in Mt. Taranaki rocks. A: Compositional range of hornblende in 100-130 ka debris-avalanche clasts (classification after Leake et al. (1997a, b, 2003) based on Si versus Mg#). B: Rim and core analyses of hornblende in debris-avalanche samples. C: Comparison of hornblende composition in old and young rocks. (data from Stewart et al. 1996, Platz 2007, Turner 2008).*

**Mg#=100[Mg^{2+}/(Mg^{2+}+Fe^{2+})] minimum Fe^{3+} after Schumacher (1997).*

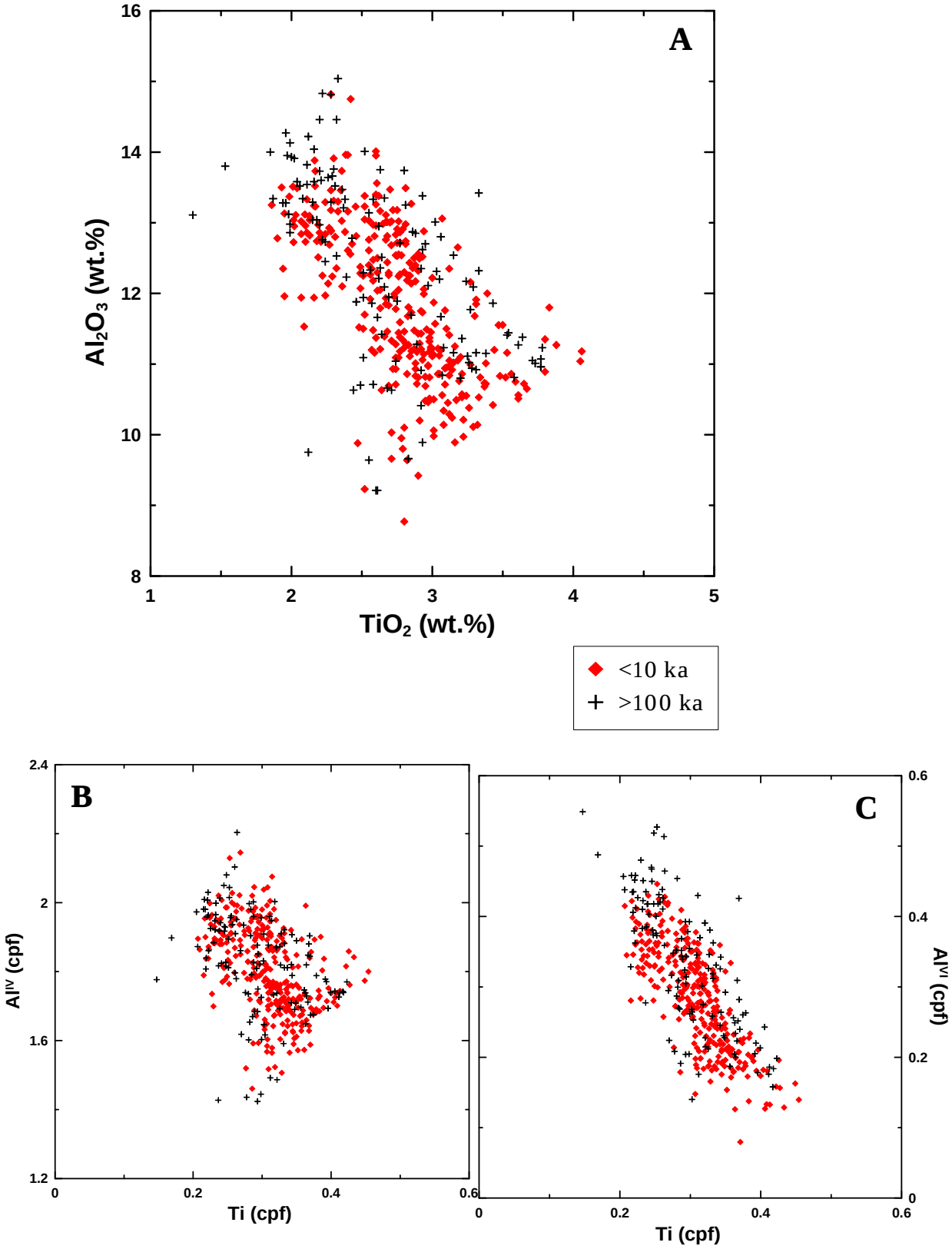

Figure 5.4. Comparison of Ti and Al proportions in hornblende within 100-130 ka debris-avalanche clasts and rocks <10 ka. A: TiO_2 (wt.%) versus Al_2O_3 (wt.%) of hornblende crystals. B: Ti versus tetrahedral Al^{IV} and C: Ti versus octahedral Al^{VI}.

TABLE 5.3. *Composition of selected hornblendes and biotite of the old sample suites.*

	Unaltered Hbl		**Rel. unaltered Hbl**		**Hbl**	**Hbl**	**Bt**
	Core	**Rim**	**Core**	**Rim**	**Resorbed**	**Resorbed**	
Sample no.	*AZ04-13*		*AZ04-01*		*AZ04-20*	*AZ04-31*	*AZ04-09*
Analysis no.	*7687*	*7686*	*7176*	*7177*	*8261*	*7441*	*7339*
SiO_2	42.38	42.75	40.96	41.65	41.81	40.92	37.45
TiO_2	3.71	3.31	2.20	2.22	3.02	2.02	5.10
Al_2O_3	11.05	11.16	13.73	12.76	13.01	13.91	14.48
FeO	10.52	11.25	13.73	14.20	12.29	10.86	11.62
MnO	0.21	0.22	0.28	0.36	0.34	0.34	0.11
MgO	14.60	14.35	12.10	12.12	13.73	14.44	16.91
CaO	11.06	11.26	11.85	11.66	11.02	12.16	0.00
Na_2O	2.61	2.46	2.04	2.27	2.68	2.38	1.16
K_2O	0.86	0.84	0.87	0.77	0.76	0.78	8.41
P_2O_5	0.05	0.27	0.00	0.01	0.00	0.00	0.19
SO_3	0.00	0.05	0.00	0.00	0.00	0.12	0.01
Cl	0.12	0.15	0.05	0.02	0.02	0.02	
V_2O_3	0.09	0.08	0.12	0.13	0.03	0.05	0.00
Cr_2O_3	0.01	0.07	0.00	0.00	0.00	0.01	0.00
NiO					0.05	0.00	0.01
Total	97.27	98.22	97.93	98.17	98.76	98.01	95.45
Si	6.26	6.29	6.07	6.18	6.12	5.97	6.18
Al^{IV}	1.74	1.71	1.93	1.82	1.88	2.03	1.41
Al^{VI}	0.19	0.22	0.47	0.42	0.36	0.36	0.00
Fe^{3+}	0.00	0.00	0.23	0.11	0.00	0.40	
Fe^{2+}	1.30	1.38	1.48	1.65	1.50	0.93	1.60
Mg#	71	69	64	62	67	77	72
Annite							28
Phlog							72
OH,F							1.84
Cl							0.05

5.5.5. Olivine

Olivine occurs in basalts and basaltic andesites of the analysed debris-avalanche sample suites and shows compositions of Fo_{61-86} (Fig. 5.5A, Table 5.4). Distinct (c. 4-8 mol%, e.g. core/rim $Fo_{86/79}$ or $Fo_{72/64}$) to weak zoning (c. 1-3 mol%, e.g. core/rim $Fo_{79/77}$ or $Fo_{69/68}$) is common with rare inversely zoned or unzoned crystals (Fig. 5.5B). CaO content of the olivines is low, ranging from 0.04-0.39 wt.%.

The <1.7 ka eruptives contain only sparse olivine which is less compositionally varied, ranging from Fo_{61-74} (Platz 2007). Forsterite-rich compositions that are observed in the oldest samples are missing. Olivines in <10 ka lava flows were found to be predominantly Mg-rich Stewart et al. (1996). Most magnesian olivines are believed to be xenocrysts, which occasionally contain chromite and are zoned from Fo_{82-87} cores to Fo_{71-77} rims. Some olivine crystals are mantled by clinopyroxene, which was also observed in the older sample suites. Smaller, more Fe-rich olivines (Fo_{62-74}) occur throughout the basaltic andesites and overlap with the compositional range of xenocryst rims. CaO contents of the high-magnesian olivines in edifice-building lava flows were described as being very low, in particular in chromite-bearing olivines. Less forsteritic olivines and rims, on the other hand, contain up to 0.3 wt.% CaO, similar to debris-avalanche clasts. Despite a smaller range in forsterite contents, olivines of the youngest eruptives show a wider range of CaO contents up to 0.61 wt.% (Fig. 5.5C).

5.5.6. Fe-Ti-Oxides

The most abundant Fe-Ti oxide in the studied debris-avalanche samples and in Mt. Taranaki rocks in general, is titanomagnetite. Titanomagnetites contain 6-43 mol% ulvöspinel (Fig. 5.6A, Table 5.4) and show a wide range in Fe^{3+}# from 82.8-97.5 with corresponding Ti/Al ratios from 2.9-4.5 (Fig. 5.7D).

In the young Mt. Taranaki volcanics, titanomagnetites show similar ulvöspinel and magnetite proportions (Fig. 5.6B-C) with uvsp 6-45 in <1.7 ka eruptives (Platz 2007) and uvsp 5-49 in <5 ka samples (Turner 2008). Rare ilmenite has also been found in young rocks and contains 84-88 mol% ulvöspinel. The data set of Turner (2008) contains more than 3000 analyses, which most likely cover the whole spectrum of titanomagnetite compositions produced at Mt. Taranaki. This provides a good basis for comparison and allows the identification of more distinct compositional differences in titanomagnetites of the studied sample suites (Fig. 5.7).

Titanomagnetite analyses of the >100 ka rocks scatter across most of the composition spectrum and show the widest range of Fe^{2+} (calculated) at low Al contents (Fig. 5.7A-B); high-Al

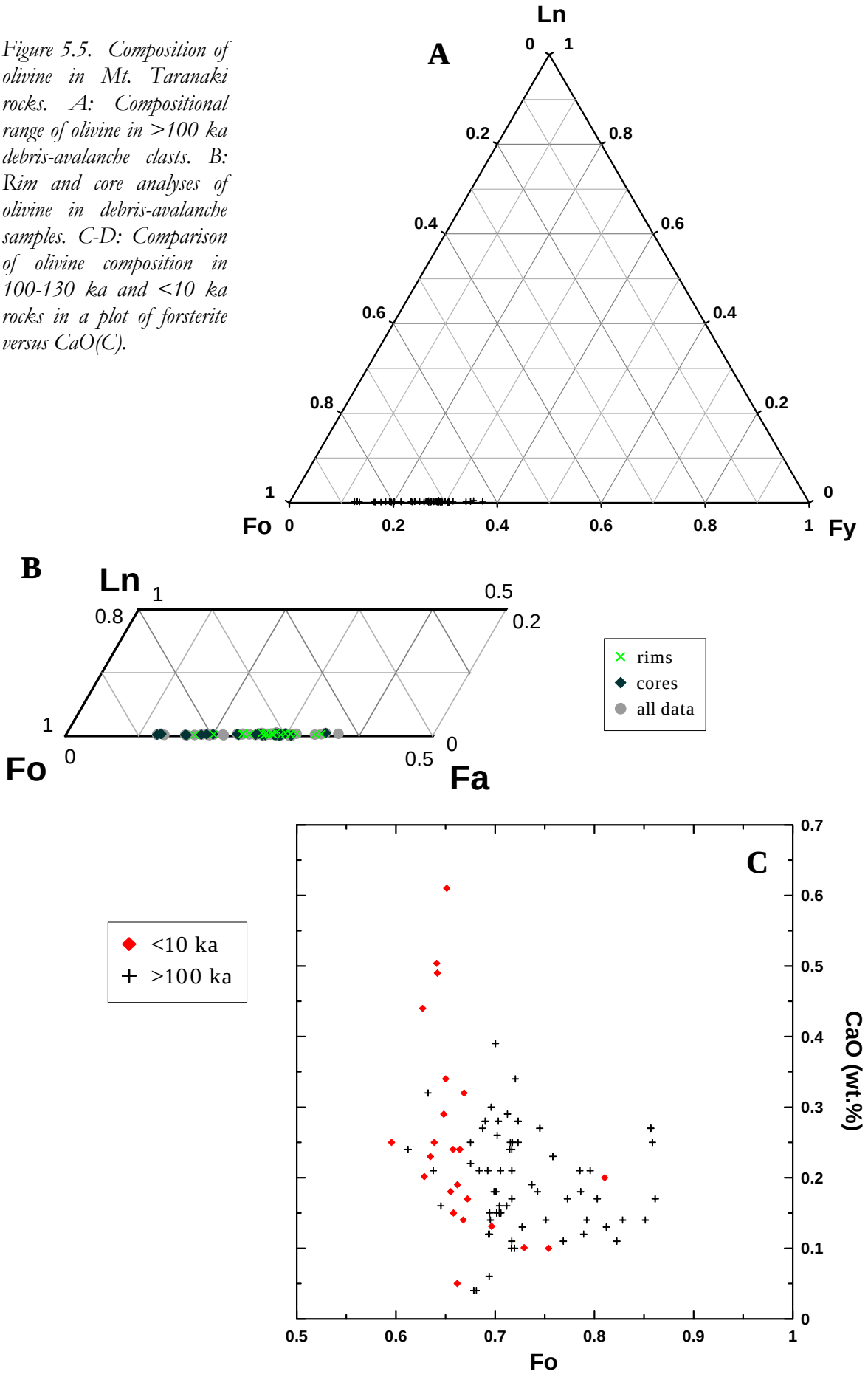

Figure 5.5. Composition of olivine in Mt. Taranaki rocks. A: Compositional range of olivine in >100 ka debris-avalanche clasts. B: Rim and core analyses of olivine in debris-avalanche samples. C-D: Comparison of olivine composition in 100-130 ka and <10 ka rocks in a plot of forsterite versus CaO(C).

compositions are lacking (Fe_{tot} 17.4-21.2, Fe^{2+} 5.1-10.4, Al 0.34-2.05 cpf). The sample set of Turner (2008) shows a wide range of Al (0.23-2.74 cpf) and the highest Fe_{tot} and Fe^{2+} contents (Fe_{tot} 15.8-22.7, Fe^{2+} 7.23-9.08). Titanomagnetites in rocks <1.7 ka show a scatter across a similar range, including some with the lowest Fe_{tot} and Fe^{2+} and the highest Al compositions (Fe_{tot} 15.5-21.1, Fe^{2+} 3.7-10.2, Al 0.4-3.1 cpf). Several groups are recognised with the most distinct cluster at low Al and high Fe and Fe^{2+}contents. On an Al versus Mg plot (Fig. 5.7C), titanomagnetites of the debris-avalanche samples show a similar range of compositions with some higher Mg contents at low Al than the other groups. The youngest rocks show a wide scatter in both elements with only a few titanomagnetite analyses having high Al and high Mg contents, while the bulk of the data shows lower Mg for high Al contents. Most titanomagnetites cluster near the low Al and Mg end of the spectrum.

Titanomagnetites show exponentially increasing Ti/Al ratios with increasing Fe^{3+}# (Fig. 5.7D). The data set from Turner (2008) displays the widest scatter with a few points plotting at higher Ti/Al (Fe^{3+}#78-98, Ti/Al 0.2-11.5), while three distinct groups of titanomagnetite compositions were recognised within the youngest samples (Platz 2007). Titanomagnetite in hornblende showed a large variety in Fe^{3+}# (76.1-90) with Ti/Al ratios of up to 1.7, compared to a narrow range in Fe^{3+}# (91.1-94.4) and Ti/Al (1.3-1.9) for inclusions in clinopyroxene. In contrast, phenocrysts displayed the broadest array of Ti/Al ratios (1.2-5.4) over a narrow range of Fe^{3+}# (90.1-96.6). The oldest sample suite show similar, though less distinct clusters of data points corresponding to the different types of titanomagnetite and an overall wide scatter of Ti/Al ratios and lack examples with the lowest Fe^{3+}# of the other groups.

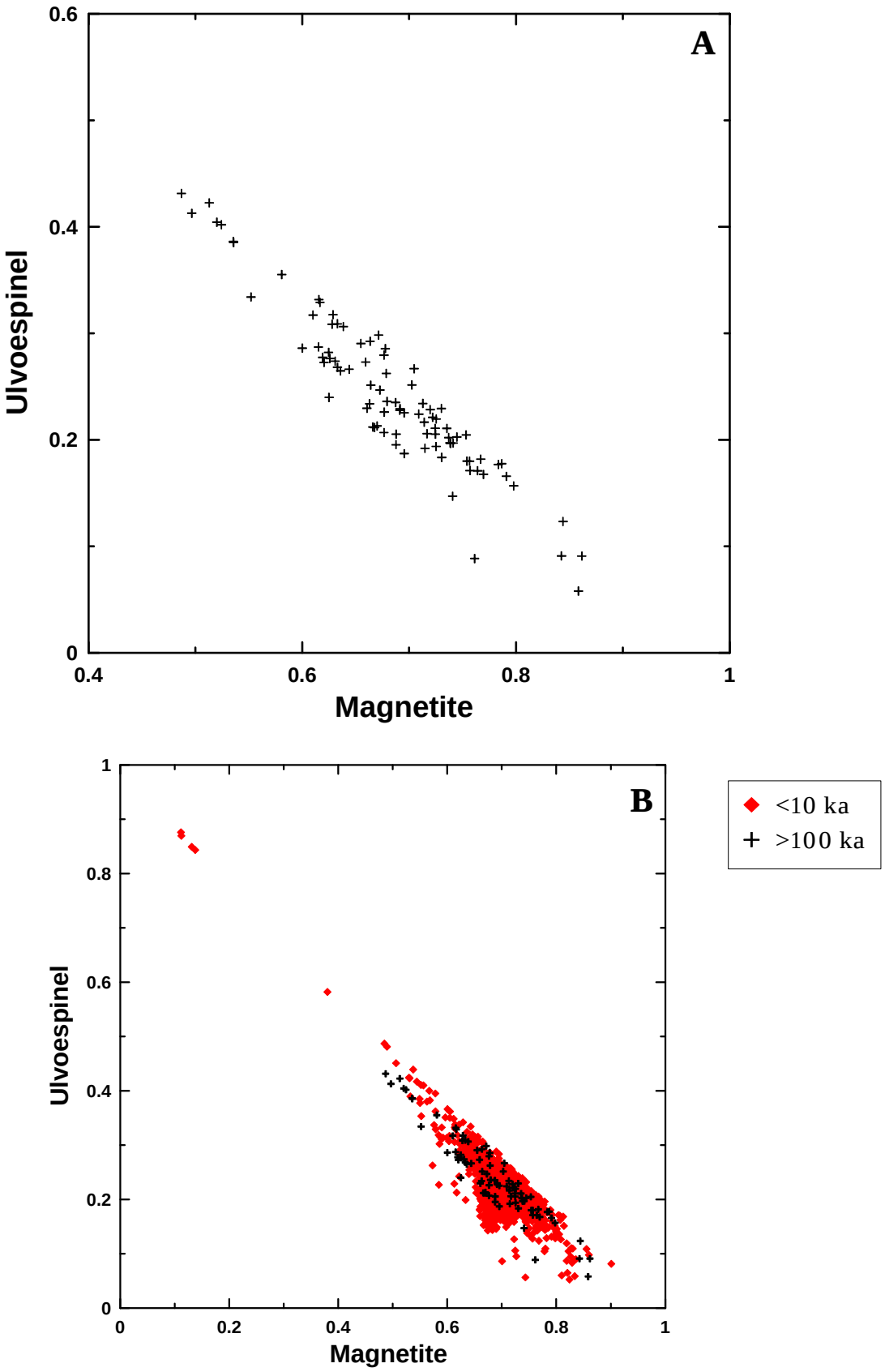

Figure 5.6. Composition of Fe-Ti-oxides in Mt. Taranaki rocks. A: Compositional range of titanomagnetite in >100 ka debris-avalanche clasts. B: Comparison of titanomagnetite and ilmenite compositions in >100 ka and <10 ka rocks.

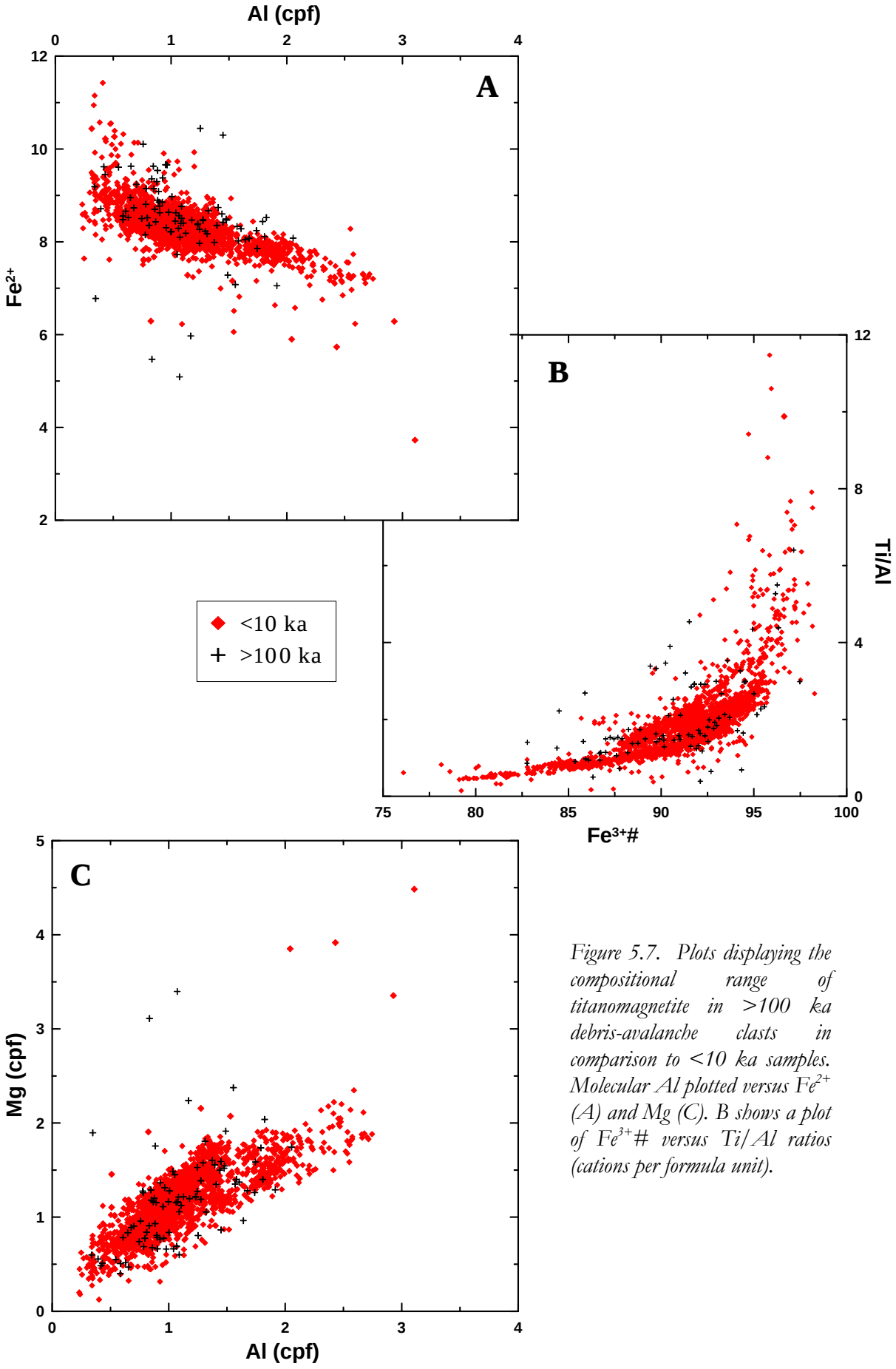

Figure 5.7. Plots displaying the compositional range of titanomagnetite in >100 ka debris-avalanche clasts in comparison to <10 ka samples. Molecular Al plotted versus Fe^{2+} (A) and Mg (C). B shows a plot of Fe^{3+}# versus Ti/Al ratios (cations per formula unit).

TABLE 5.4. *Composition of selected olivines and titanomagnetites of the >100 ka sample suites.*

	Large Ol		**Large Ol**		**Small Ol**	**Tm**	**Tm**	**Tm**
	Core	**Rim**	**Core**	**Rim**	**Euhedral**	**in Cpx**	**Small**	**Large**
Sample no.	*AZ04-31*		*AZ04-25*		*AZ04-25*	*AZ04-28*	*AZ04-33*	*AZ04-06*
Analysis no.	*7452*	*7453*	*7512*	*7513*	*7522*	*7505*	*8009*	*7461*
SiO_2	40.82	40.16	38.58	38.05	37.01	0.01	0.18	0.25
TiO_2	0.00	0.07	0.00	0.00	0.04	4.67	7.27	11.73
Al_2O_3	0.00	0.01	0.06	0.10	0.00	1.00	3.61	5.33
FeO	12.10	16.49	24.39	26.40	30.23	79.63	76.78	69.25
MnO	0.25	0.32	0.32	0.82	0.73	0.91	0.69	0.49
MgO	47.07	43.43	36.76	34.75	30.98	4.31	2.92	4.71
CaO	0.17	0.13	0.17	0.27	0.32	0.11	0.18	0.04
Na_2O	0.26	0.18	0.13	0.00	0.00	0.06	0.16	0.00
K_2O	0.01	0.01	0.00	0.00	0.07	0.04	0.00	0.00
P_2O_5	0.01	0.00	0.02	0.00	0.00	0.05	0.00	0.04
SO_3	0.02	0.05	0.01	0.03	0.01	0.00	0.00	0.00
Cl	0.02	0.03	0.07	0.00	0.00	0.00	0.00	0.00
V_2O_3	0.04	0.01	0.00	0.00	0.00	0.49	0.42	0.14
Cr_2O_3	0.20	0.00	0.00	0.02	0.00	0.01	0.01	0.06
NiO	0.00	0.08	0.17	0.02	0.00	0.02	0.01	
Total	100.97	100.97	100.68	100.46	99.39	91.31	92.23	92.04
Fo	0.86	0.81	0.72	0.69	0.63			
Fa	0.12	0.17	0.27	0.29	0.35			
Ln	0.0022	0.0017	0.0024	0.0038	0.0047			
Mg#	0.87	0.82	0.73	0.70	0.65	8.55	6.16	10.51
Uvsp						0.12	0.19	0.33
Magn						0.84	0.71	0.55
Al						0.35	1.25	1.82
Ti						1.04	1.60	2.56
Mg	1.72	1.62	1.43	1.37	1.26	1.90	1.27	2.04
Fe_{tot}	0.25	0.35	0.53	0.59	0.69	20.28	19.41	17.36
Fe^{2+}	0.24	0.35	0.53	0.59	0.69	6.78	7.97	8.52
Fe^{3+}#						97.47	90.16	82.78

5.5.7. Glass

Groundmass glass of samples with a hyaline matrix has silica contents ranging from 51.5-75 wt.% compared to slightly higher SiO_2 (57.7-76.5 wt.%) for glass inclusions in hornblende and clinopyroxene phenocrysts (Table 5.5). Glass inclusions show a narrower range of Al_2O_3 contents (12.2-17.5 wt.%) than analysed groundmass glass (12.6-29.4 wt.%). Similar compositions for glass inclusions (SiO_2 54.9-73.4 wt.%, Al_2O_3 12.7-19.6 wt.%) and groundmass glass (SiO_2 65.28-69.17 wt.%, Al_2O_3 15.9-18.1 wt.%) were observed in eruptives <10 ka (Price et al. 2005; Platz 2007). Platz (2006) also showed compositional differences between clinopyroxene and hornblende melt inclusions (SiO_2 64.5-71.6 and 59.7-66.3 wt.%, respectively) in summit dome lavas.

TABLE 5.5. *Selected glass analyses of the Motunui and Okawa sample suites.*

	Glass Inclusion in Hbl	**Glass Inclusion in Cpx**	**Glass Groundmass**	**Glass Groundmass**
Sample no.	*AZ04-20*	*AZ04-10*	*AZ04-05*	*AZ04-13*
Analysis no.	*8321*	*7700*	*7604*	*7679*
SiO_2	59.19	66.98	70.87	63.35
TiO_2	1.00	0.36	0.71	0.62
Al_2O_3	17.08	14.49	12.88	18.22
FeO	2.59	1.48	1.64	2.58
MnO	0.15	0.06	0.17	0.18
MgO	3.79	0.00	0.04	0.59
CaO	4.06	0.26	0.66	3.71
Na_2O	6.01	4.03	4.34	5.87
K_2O	2.91	4.59	5.45	3.15
P_2O_5	0.28	0.10	0.25	0.40
SO_3	0.11	0.06	0.00	0.04
Cl	0.17	0.34	0.21	0.27
V_2O_3	0.00	0.01	0.02	0.04
Cr_2O_3	0.14	0.00	0.00	0.23
NiO	0.10			
Total	97.58	92.75	97.24	99.25

5.5.8. Accessories

Apatite has been described as a common accessory in Mt. Taranaki rocks (Neall et al. 1986; Stewart et al. 1996; Price et al. 1999; Platz 2007). Contents of Cl and SO_3 in apatite found in debris-avalanche samples range from 0.8-2.4 wt.% and 0.0-0.4 wt.%, respectively (Table 5.6). In summit dome lavas, apatite occurs as inclusions in clinopyroxene, hornblende and Fe-Ti oxides as well as in the groundmass and shows similar compositions to the older samples with Cl ranging from 0.8-3 wt.% and SO_3 from 0.3-1.7 wt.% (Platz 2007).

Selected compositions of accessory pyrite and Fe-Mn-rich carbonates are also shown in Table 5.6. The observed carbonates are solid solutions between siderite and rhodochrosite end-members.

TABLE 5.6. *Composition of selected accessories of the Motunui and Okawa sample suites.*

	Apatite in Cpx	**Apatite in Cpx**	**Pyrite in Cpx**	**Pyrite in Carb.**	**Carbonate in Hbl**	**Carbonate in Hbl**
Sample no.	*AZ04-33*	*AZ04-28*	*AZ04-28*	*AZ04-20*	*AZ04-20*	*AZ04-20*
Analysis no.	*8418*	*7502*	*7490*	*8256*	*8254*	*8276*
SiO_2	0.00	0.00	0.00	0.00	0.29	0.10
TiO_2	0.00	0.03	1.68	2.73	0.00	0.25
Al_2O_3	0.00	0.04	0.00	0.00	0.01	0.08
FeO	0.22	0.32	46.03	59.81	26.20	46.66
MnO	0.17	0.03	0.00	0.48	22.02	5.23
MgO	0.11	0.54	0.00	0.00	0.12	0.30
CaO	53.55	52.91	0.07	0.16	7.79	3.76
Na_2O	0.00	0.05	0.00	0.24	0.18	0.19
K_2O	0.11	0.07	0.02	0.15	0.02	0.03
P_2O_5	42.64	41.74	0.12	0.00	0.46	0.33
SO_3	0.27	0.41	85.18	137.23	0.24	0.00
Cl	1.00	1.30	0.00	0.00	0.00	0.02
V_2O_3	0.05	0.00	0.00	0.00	0.02	0.12
Cr_2O_3	0.00	0.01	0.05	0.00	0.02	0.00
NiO	0.00	0.12	0.85	0.00	0.00	0.12
Total	98.12	97.57	134.00	200.80	57.08	57.09
Ca	9.15	9.10				
P	5.76	5.67				

5.6. DISCUSSION

Compositions and types of mineral phases are sensitive to pre- and syn-ascent conditions and record responses to variations in pressure, oxygen fugacity, melt composition, temperature and rise rate. These changes are reflected in crystal textures, i.e. resorption features, oxidisation, mineral breakdown and recrystallisation, compositional zoning of individual crystals, inclusions as well as the compositional range of the individual mineral phases. Aspects of magma generation and crystallisation conditions in Taranaki magmas were discussed in more detail by Stewart et al (1996), who used the mineral chemistry of <10 ka lavas to determine melt processes occurring during early stages of magma evolution, and Turner (2008), who studied processes of magma storage and modification at shallower depth during magma recharge events. Their results and interpretations of the petrology and textures of young eruptives are compared to the mineralogical findings for the older debris-avalanche sample suites.

5.6.1. Plagioclase

The compositional and textural zoning of plagioclase phenocrysts within Mt. Taranaki debris-avalanche clasts and younger eruptives are similar to those described from andesite volcanoes elsewhere (e.g. Stewart & Fowler 2001; Landi et al. 2004). Large plagioclase crystals within the studied debris-avalanche lithologies consist of larger cores and thinner, mostly multiple oscillatory rims. The boundary between core and rim is typically sharp and characterised by major and minor discordances, indicating resorption of the core-forming plagioclase before growth of the rims. The sharp contact and subsequent oscillatory growth reflects near equilibrium diffusion-controlled crystallisation (Pearce & Kolisnik 1990; Pearce 1993; Stewart et al. 1996). Oscillatory zoning has been attributed to small-scale thermal and compositional changes due to replenishment of new melt to the surface of the growing crystal (Ginibre et al. 2002) as well as to the complex interplay between decompression and heating during plagioclase growth (Blundy et al. 2006). Major resorption surfaces, with abrupt compositional and textural changes, reflect dramatic changes of crystallisation conditions due to variation in temperature, pressure, volatile content or melt composition or a combination of these (Pearce & Kolisnik 1990; Singer et al. 1995). Sieve textures and skeletal textures form when small melt inclusions become trapped between the overgrowth and typically larger-scale resorption surfaces (Stewart & Fowler 2001), which can be due to decompression over relatively short time periods (Nelson & Montana 1992), reheating effects or increased P_{H2O} during crystallisation (cf. Morrice & Gill 1986; Stewart et al.

1996), attributed to mixing with hotter magmas (Stewart & Fowler 2001; Couch et al. 2003; Zellmer et al. 2003; Landi et al 2004; Turner 2008).

The majority of plagioclase phenocrysts within the oldest Mt. Taranaki debris-avalanche clasts as well as in younger eruptives are characterised by large, resorbed calcic cores, suggesting that they crystallised at depth and were partially resorbed during ascent (cf. Stewart et al. 1996; Turner 2008). More sodic rims and plagioclase microphenocrysts reflect lower volatile contents and temperatures and indicate crystallisation at shallower levels (Smith et al. 1997; Stewart et al. 1996; Turner 2008).

Plagioclase phenocrysts in the older debris-avalanche clasts and <10 ka eruptives show consistent mineral characteristics and a similar compositional range, indicating that crystallisation conditions for plagioclase have not changed significantly at Mt. Taranaki over the last 130 ka. A noticeable difference is, however the occurrence of Or-rich rims and interstitial Or-rich plagioclase in the younger lavas, which are thought to reflect high K_2O-contents of the residual melt at advanced stages of crystallisation. No Or-rich plagioclase has been found in the old sample suites with Or_6 being the most potassic composition. This is consistent with less potassic whole-rock and glass compositions of the older sample suites and increasing K_2O-contents of the Mt. Taranaki magmas with time (cf. Chapter 4).

5.6.2. Pyroxene

(i) Clinopyroxene

Larger clinopyroxene crystals within Mt. Taranaki debris-avalanche clasts have diffusively zoned cores, surrounded by rims with fine oscillatory zoning. Compositional changes within individual crystals are subtle and involve variations in Al_2O_3 and Mg#. Their relatively narrow compositional range with only weakly developed zoning and commonly observed sector zoning indicates rapid crystal growth (cf. Stewart et al. 1996). Ratios of Al/Ti (cpf) are consistent with polybaric clinopyroxene crystallisation under pressures ranging from crustal to upper mantle (cf. Stewart et al. 1996). En-rich clinopyroxene also show various degrees of resorption and some show melt inclusions that separate the core from the rims, reflecting disequilibrium conditions. Normal zoning from Mg-rich cores to Fe-rich rims indicates decreasing temperature and oxygen fugacity, while the occasionally observed reverse zoning, i.e. increasing Mg# and decreasing Al_2O_3 in rims, was interpreted as an increase in magmatic temperature and fO2 (Nakagawa et al. 2002) and reduction of Al_2O_3 availability in the melt due to plagioclase crystallisation (Cortes et al. 2005; Humphreys et al. 2006). The reversely zoned rims of clinopyroxene phenocrysts were

interpreted to reflect recharge events with hotter magmas in shallow crustal storage systems (Turner 2008).

Mg-rich cores of the young lavas were also described to contain higher proportions of stoichiometric Fe^{3+} consistent with high fO_2 at the time of crystallisation, while rims and less magnesian clinopyroxenes have little or no Fe^{3+}. This contrasts with clinopyroxene crystals in the older samples since they do not contain significant stoichiometric Fe^{3+} and no correlation between En and Fe^{3+} contents were observed. Also no evidence was found that clinopyroxene and olivine/chromite crystallised from similar host magma compositions and during similar conditions as was assumed by Stewart et al. (1996). Olivine and chromite fractionation is likely to have occurred prior to clinopyroxene crystallisation as is also suggested by the absence of chromite in clinopyroxene and the presence of low Cr-titanomagnetite in young (and old) samples.

A major difference between the data collected in this study and previously described clinopyroxene characteristics is the much wider range of clinopyroxene compositions in the older rocks. This might reflect the broader compositional range of host magmas and crystallisation over a wider spectrum of pressures and temperatures as also implied by the whole-rock geochemistry of the older sample suites.

(ii) Orthopyroxene

Orthopyroxene is a rare component of Mt. Taranaki rocks (Stewart et al. 1996; Turner 2008) and was only observed in two samples of the debris-avalanche suite. Orthopyroxene cores mantled by clinopyroxene show En-contents equivalent to the large crystals observed in the young lavas (Stewart et al. 1996). These cores most likely represent remnant orthopyroxene that originated at lower P_{H2O} in the mantle and the overgrowths is the result of its subsequent metasomatic reaction with hydrous high-silica melts derived from partial melting in the lower crustal hot zone, or during further differentiation within the upper crustal storage system (cf., Stewart et al. 1996). In contrast, less magnesian orthopyroxene in a basalt sample was found to be associated with olivine and might reflect mantling of mantle/upper crust-derived olivine during late-stage crystallisation at lower levels.

In the young Mt. Taranaki lavas, orthopyroxene has also been observed as rare individual phenocrysts, microphenocrysts, in the groundmass or in glomerocrysts associated with clinopyroxene and plagioclase (Stewart et al. 1996). The presence of microphenocrysts and more Fe-rich acicular orthopyroxene were interpreted to indicate that silica contents were high enough

for orthopyroxene to form (Stewart et al. 1996). Its absence in the older samples might reflect the less evolved compositions and a lower silica activity of the early magmas.

5.6.3. Hornblende

Hornblende phenocrysts of varying size and degrees of resorption occur in both the old debris-avalanche samples and young eruptives (cf., Stewart et al. 1996; Turner 2008), ranging from thin to thick opaque rims or complete replacement of the crystals by magnetite, pyroxene and plagioclase. These rims form when pressure changes shift the crystallisation conditions out of the hornblende stability field (Rutherford & Devine 1988; Rutherford & Hill 1993; Browne & Gardener 2006). Rim thickness and size of replacement crystals depend on the storage depth and time the magmas resides at this depth before ascending/erupting (Browne & Gardener 2006).

Hornblende was found to mantle clinopyroxene in young Mt. Taranaki lavas, particularly in aggregates, sometimes replacing large parts of the clinopyroxene crystal to form thick rims, and more rarely it mantled olivine, probably due to interaction with partial melts in the lower crust (Stewart et al. 1996). In the older rocks, hornblende was not observed to mantle clinopyroxene or olivine suggesting no significant late-stage hornblende crystallisation at shallower depth. Instead, resorbed clinopyroxene cores commonly contain patches of recrystallised hornblende and strongly resorbed olivine is occasionally replaced by small grains of recrystallised hornblende, clinopyroxene, plagioclase and olivine. Plagioclase inclusions are common in the old suites but only few hornblende crystals of the young eruptives were observed to contain inclusions of Mg-rich titanomagnetite and Ca-rich plagioclase (Stewart et al. 1996).

Similarly to clinopyroxene, a broader range of hornblende compositions was observed in the >100 ka rocks than was described for young Mt. Taranaki eruptives (cf., Stewart et al. 1996; Turner 2008). In particular Al_2O_3 and TiO_2 contents show a wider variation, corresponding to the wide range of melt compositions (cf. Chapter 4). The high abundance of compositions with higher Al_2O_3 and lower TiO_2 in the older sample suites indicates that large proportions of hornblende crystallised at high P_{H2O}, reflecting an origin at greater depth (cf. Foden & Green 1992) and the existence of more primitive melt compositions. In contrast, the mostly high TiO_2 and low Al_2O_3 hornblende compositions of the younger eruptives indicate significant high-level crystallisation under lower pressure, which does not appear to be a major process in the older rocks. Fanthams Peak lavas have higher Ti/Al ratios than the summit lavas, consistent with higher pressure during hornblende fractionation. In contrast, crystallisation at shallow depth produced green hornblende in the Shark's Tooth lava, which is the most Ti-rich and Al-poor hornblende observed at Mt. Taranaki (Platz 2007).

5.6.4. Olivine

Olivine in the debris-avalanche sample suites shows a similar range of compositions and characteristics as was observed in the young lavas (cf., Stewart et al. 1996). The most forsteritic olivines in the old suites are interpreted to represent xenocrysts that most likely crystallised at mantle pressures. Similar magnesian olivines within the young lavas occasionally contained chromite and were mantled by clinopyroxene (Stewart et al. 1996). Very low CaO contents in these Mg-rich olivine cores, especially in chromite-bearing ones, suggested that they may have formed at high (P >15 kbar) mantle pressures (cf. Stormer 1973; Finnerty & Boyd 1978; Jurewicz & Watson 1988). These xenocrysts have been in equilibrium with neither the host whole-rock compositions nor the mantle assemblages as indicated by their low-Ni contents, suggesting that their source magmas have already undergone substantial fractionation (Stewart et al. 1996). In contrast, more Fe-rich olivines in debris-avalanche clasts are typically smaller and their higher CaO contents suggest that they formed under crustal conditions (cf. Jurewicz & Watson 1988; Stewart et al. 1996).

5.6.5. Fe-Ti-oxides

Titanomagnetite in the >100 ka debris-avalanche clasts was observed as inclusions in or clustered near magnesian olivine and clinopyroxene, indicating coeval and hence early crystallisation (cf., Stewart et al. 1996). A second, smaller grain size population of titanomagnetite is represented in the groundmass, where it forms small euhedral microphenocrysts. The two grain size populations also show compositional differences. In young Mt. Taranaki eruptives, early titanomagnetite showed higher MgO and Al_2O_3 contents and lower ulvospinel proportions than groundmass microphenocrysts, the latter reflecting lowering fO_2 during crystallisation (cf. Morrice & Gill 1986). The differences in grain size and composition were interpreted to reflect a hiatus in crystallisation of titanomagnetite between the two populations. Estimates of fO_2 showed a drop from early titanomagnetite to groundmass oxides, indicating decreasing fO_2 during crystallisation, a process typical for differentiating magmas (cf., Frost & Lindsley 1992). A similar compositional range and grain size characteristics of titanomagnetites in the older sample suites reflect similar processes, i.e. an early crystal population that formed at greater depth under higher fO_2 and a second population that crystallised at lower crustal levels with lower fO_2.

Titanomagnetite crystals of young Mt. Taranaki tephras were also found to show different textures and oxidation-induced exsolution features depending on the prevailing crystallisation conditions prior to and during eruptions. These were used by Turner et al. (2008)

to identify eruption styles of tephras and distinguish fast- from slow-ascent eruptions. Slow-ascent eruptions, characterised by near-stagnant magma bodies and slow effusion of lava domes with associated block-and-ash-flows, were found to show solid-state exsolution of titano-hematite/ilmenite lamellae within titanomagnetite hosts. Fast-ascent eruptions, marked by rapid chilling of magma in subplinian eruptions, contain titanomagnetite without such features. This differentiation is only likely to develop in pyroclastics rocks and is not observed in the >100 ka debris-avalanche clasts.

5.6.6. Magmatic processes and fractionation trends

The mineral data obtained from Motunui and Okawa debris-avalanche clasts support the model developed by Stewart et al. (1996) and indicate that a lower crustal hot zone (c.f. Annen et al. 2006) had developed at Mt. Taranaki already at the known onset of volcanism. Together with the previously described mineral compositions and textures of young Mt. Taranaki eruptives, they also complement the model of magma evolution at Mt. Taranaki developed in Chapter 4.

A large proportion of crystals in Mt. Taranaki rocks represent 'xenocrysts' that were entrained from the upper mantle/lower crust, including the most magnesian olivines, especially the chromite-bearing ones, clinopyroxene and titanomagnetite cumulates as well as calcic plagioclase cores. Mg-rich olivines and chromite crystallised early from highly oxidised primitive magmas and were therefore largely segregated. The hydrous parent magmas are thought to have been derived from melting of a metasomatised and depleted (lherzolite) mantle source (Stewart et al. 1996). These mantle-derived magmas ponded at the base of the lower crust, where they evolved from a high-Mg basalt composition to high-Al basalt through a combination of olivine, clinopyroxene, titanomagnetite and amphibole fractionation and interaction with underplated material (cf., Stewart et al. 1996). Plagioclase also formed relatively early, after olivine and clinopyroxene, with most plagioclase crystallisation occurring from the more evolved high-Al basalt melts. Drier melts crystallised plagioclase and orthopyroxene, although typically crystallisation of the fractionating magmas at the base of the crust and partial melting of previously intruded basalts increased the water content of the melt, resulting in more hydrous magmas (Stewart et al. 1996). Ascending magmas entrained wall rock xenoliths and xenocrysts that were gradually melted and resorbed into the melt. These mixtures of melt and crystals rose to lower levels in the upper crust, where further fractionation of plagioclase and late-stage amphibole occurred at lower pressures, eventually joined by crystallisation of biotite and possibly orthopyroxene (Stewart et al. 1996).

During early stages of volcanism, a less-well developed hot zone allowed more primitive magma compositions to rise to the surface with considerably less crustal interaction/overprinting during ascent. This is reflected in the older suite containing a broad range of clinopyroxene and hornblende compositions that crystallised over a wide spectrum of pressures and temperatures, including high-pressure compositions of hornblende that have not been described from the young lavas. As the hot zone evolved, a more complex crustal structure developed with a more dispersed plumbing system, resulting in magma assembly and storage at different mid- to shallow-crustal levels. The young Mt. Taranaki eruptives show evidence of a two-stage magma differentiation system that involved crystallisation in the lower crust and a subsequent second stage at upper-crustal levels, where magmas were further modified by fractional crystallisation, magma mingling and mixing during recharge events (Turner 2008).

Continuous intrusion and crystallisation of mantle-derived magmas in the lower crust resulted in a thickening zone of underplated, amphibole-bearing material and a gradually rising geothermal gradient. Increasing amounts of incongruent partial melting of the previously intruded, underplated material formed clinopyroxene and produced progressively K_2O-rich melts (Stewart et al. 1996), that are reflected in the occurrence of Or-rich plagioclase in younger eruptives.

5.7. CONCLUSIONS

The emplacement of the Motunui and Okawa debris-avalanche deposits imply that ancestral Mt. Taranaki was already a high and unstable stratocone at these times. The observed variety of rock types found in the deposits shows that a broad range of lithologies was present, including more primitive eruptives. Along with these, however, were more evolved andesites and rock textures including pumice lithologies that reflect a similar range of eruption styles from magmatic explosive to effusive like those represented on the modern volcano.

The distinct differences in whole-rock geochemistry between the oldest and youngest volcanic products (cf. Chapter 4) are also reflected in the mineral chemistry of these units, although the differences are very subtle. The overall composition of mineral phases in Mt. Taranaki volcanics has not changed significantly over the last 130 ka, with phenocrysts of the Motunui and Okawa debris-avalanche suites and the youngest eruptives mostly plotting in similar compositional fields to the young samples.

The most distinct differences in mineralogy are related to the broader range of erupted magma compositions observed in the older rock suites, including more primitive, basaltic compositions. Clinopyroxene shows a wider range of compositions with greater variety in En-contents as well as more ferrous minerals, which could imply crystallisation at greater depth than during later stages of volcanism. The compositional range of hornblende is also broader in the debris-avalanche clasts and includes a higher abundance of early phases with higher Al_2O_3 and lower TiO_2. Fresh, euhedral olivine is more abundant than in the young eruptives and phlogopite also occurs occasionally. The occurrence of these mineral phases reflects the immature state of the early magmatic system and eruption of more primitive melts with a more distinct mantle signature. As indicated by the whole-rock geochemistry, the lower crustal 'hot zone' was significantly thinner and colder >130 000 years ago, allowing less interaction of melt with amphibolised, underplated material. Early stages of hot zone development were most likely characterised by "normal" upper mantle/lower crustal conditions, resulting in more extensive fractionation of high-pressure mineral phases at greater depth.

In contrast to the younger eruptives, evolved high-silica compositions are less abundant in the oldest sample suites. This is also reflected in the composition and occurrence of some late-stage mineral phases that typically form at shallower depth under lower pressures. Very few hornblende compositions in the old debris-avalanche clasts have the higher TiO_2 and lower Al_2O_3 contents characteristic of late-crystallisation at upper crustal levels. Biotite is rare in the old samples and only occurs in more evolved rocks, while Fe-rich groundmass orthopyroxene is either completely absent or very rare since it has not been observed. This suggests that late-stage crystallisation in zoned upper-crustal storage levels was not a significant process during the early stages of Mt. Taranaki volcanism. Their rare occurrence or absence in the older sample suites together with the lower abundance of more evolved magma compositions indicate that early magmas typically rose rapidly through the crust and only rarely stalled at shallow levels to further differentiate.

The occurrence of Or-rich plagioclase in young Mt. Taranaki lavas was attributed to the high K_2O-content of residual melts during late-stage crystallisation (Stewart et al. 1996). Its absence from the Motunui and Okawa sample suites and plagioclase compositions with a maximum of Or_6 indicate significantly lower proportions of K_2O in the melts, which is also shown by whole-rock and glass data. These less potassic compositions of early melts confirm the overall magma evolution established in Chapter 4 and the recognised trend of increasing K_2O-contents with time.

This mineralogical study of the oldest known rocks from Mt. Taranaki focused on differences between the youngest eruptives rather than detailed aspects of magma generation and differentiation processes. More detailed mineralogical work is needed to better understand variations and systematic changes in melt generation processes and crystallisation conditions at Mt. Taranaki over the last 200 ka.

CHAPTER 6.

CYCLIC GROWTH AND DESTRUCTION OF STRATOVOLCANOES

6.1. INTRODUCTION

The formation of debris avalanches resulting from the failure of an unstable volcanic edifice has been described at many volcanoes worldwide (e.g. Voight et al. 1981; Siebert 1984; Ui et al. 1986; Crandell et al. 1984; Glicken 1996; Vallance et al. 1995; van Wyk de Vries et al. 2000; Capra et al. 2002; Waythomas & Wallace 2002; Concha-Dimas et al. 2005). Yet from most stratovolcanoes only one major lateral collapse is known with possible older events being hidden or eroded. Repeated debris-avalanche events have been inferred from just a few long-lived examples, e.g. St. Augustine (Beget & Kienle 1992), Colima (Stoopes & Sheridan 1992), Mt. Rainier (Vallance & Scott 1997), Shiveluch (Belousov et al. 1999), as well as from a number of ocean island volcanoes, e.g. Stromboli (Kokelaar & Romagnoli 1995, Tibaldi et al. 2001), Reunion (Lenat et al. 1989, Labazuy, 1996), Canary Islands (Holcomb & Searle 1991, Carracedon 1994, 1996; Walter & Schmincke 2002), and Hawaii (Fornari & Campbell 1987; Moore et al. 1994), which have been studied by oceanographic methods. However, in many of these locations the oldest units are deeply buried by more recent volcaniclastic deposits or are only preserved below sea-level and therefore inaccessible. Consequently, reconstruction of the volcanic history for hazard analysis is usually based on interpretations of the Holocene record. This brief interval may fail to identify longer-term influences on the activity, stability and evolution of stratovolcanoes. Detailed, continuous records from these volcanoes are needed to understand the processes behind their evolution in order to truly characterise the potential volcanic hazard.

The most complete chronostratigraphic record of volcanic activity and other sedimentary events is recorded in volcanic ring-plain successions/alluvial plains, which are progressively built up by deposition of syn- and post-eruptive volcaniclastics and minor primary products, as well as reworked deposits (Smith 1987; Palmer & Neall 1991; Smith 1991; Cronin et

al. 1996; Donoghue & Neall 2001; Borgia & van Wyk de Vries 2003). Hence, in order to reconstruct the eruptive history of a stratovolcano in more detail and to recognise its true hazard potential, it is important to understand the depositional processes that contributed to the construction of the volcanic ring plain.

Unusually, at Mt. Taranaki/Egmont, New Zealand, a stratigraphic record is exposed in medial ring-plain successions for most of the life of the volcano (Neall 1979), which is due to continuous coastal erosion of the tectonically uplifted Taranaki peninsula (Pillans 1994). These circumstances allowed the reconstruction of volcanic and other landscape-forming events operating over the life-span of this stratovolcano, based on the correlation of the exposed ring-plain deposits and their sedimentological classification. The unique long-term record of this repeatedly collapsing volcano provides a better understanding of the nature and processes behind the volcano's behaviour and was here used to develop a model of cyclic behaviour and sedimentation that can be applied to stratovolcanoes in general.

6.2. VOLCANIC CYCLES AT MT. TARANAKI

More than 200 ka of volcaniclastic deposition at Mt. Taranaki have produced a surrounding ring-plain that extends 25-45 km onshore from the current summit. Cliff sequences along the northern, western and in particular the southern Taranaki coast represent a cross-section through medial ring-plain settings. Exposed are a wide range of lithologies, which reflect the whole spectrum of sediment-water flow from "dry" debris avalanche, highly concentrated debris flow, hyperconcentrated flow to dilute streamflow as well as transitions between these processes. Based on their different sedimentological characteristics, the deposits were classified into volcaniclastic, fluvial and aeolian facies.

The medial ring-plain succession contains at least six different lithofacies elements: debris-avalanche dominated sequences, paleo-channel systems, series of sheet-flow deposits, fluvial facies associations, dune sands and paleosol-/peat-dominated sequences. These lithotype associations correspond to a range of transport and emplacement modes as well as various depositional environments and can be linked to specific periods within a repeating pattern of deposition in the areas surrounding unstable stratovolcanoes.

A generalised volcanic cycle at Mt. Taranaki arbitrarily starts after the destruction of large portions of the edifice by collapse (Fig. 6.1). This event is followed by long-term regeneration of the deeply scarred edifice. The early stages of (re-) growth are characterised by

small-scale pyroclastic eruptions, dome-building and localised lava flows, background activity typical of this centre (Platz et al. 2007; Turner 2008). Medial areas accumulate thick tephric soils or peat with interbedded tephra layers that reflect the proximal activity. Mass-flows produced during this period are mostly restricted to proximal areas due to the lower elevation of the source area. With increasing height of the growing edifice, eruption-generated mass-flows start to reach greater distances of >25 km. Subsequently, medial accumulation is characterised by massive sequences of mainly monolithologic debris-flow and hyperconcentrated-flow deposits with intercalated tephra beds. These are sheet-like on broad terraces and coastal plains or confined to channels where the landscape has been incised by rivers and streams. Volcanic activity is not

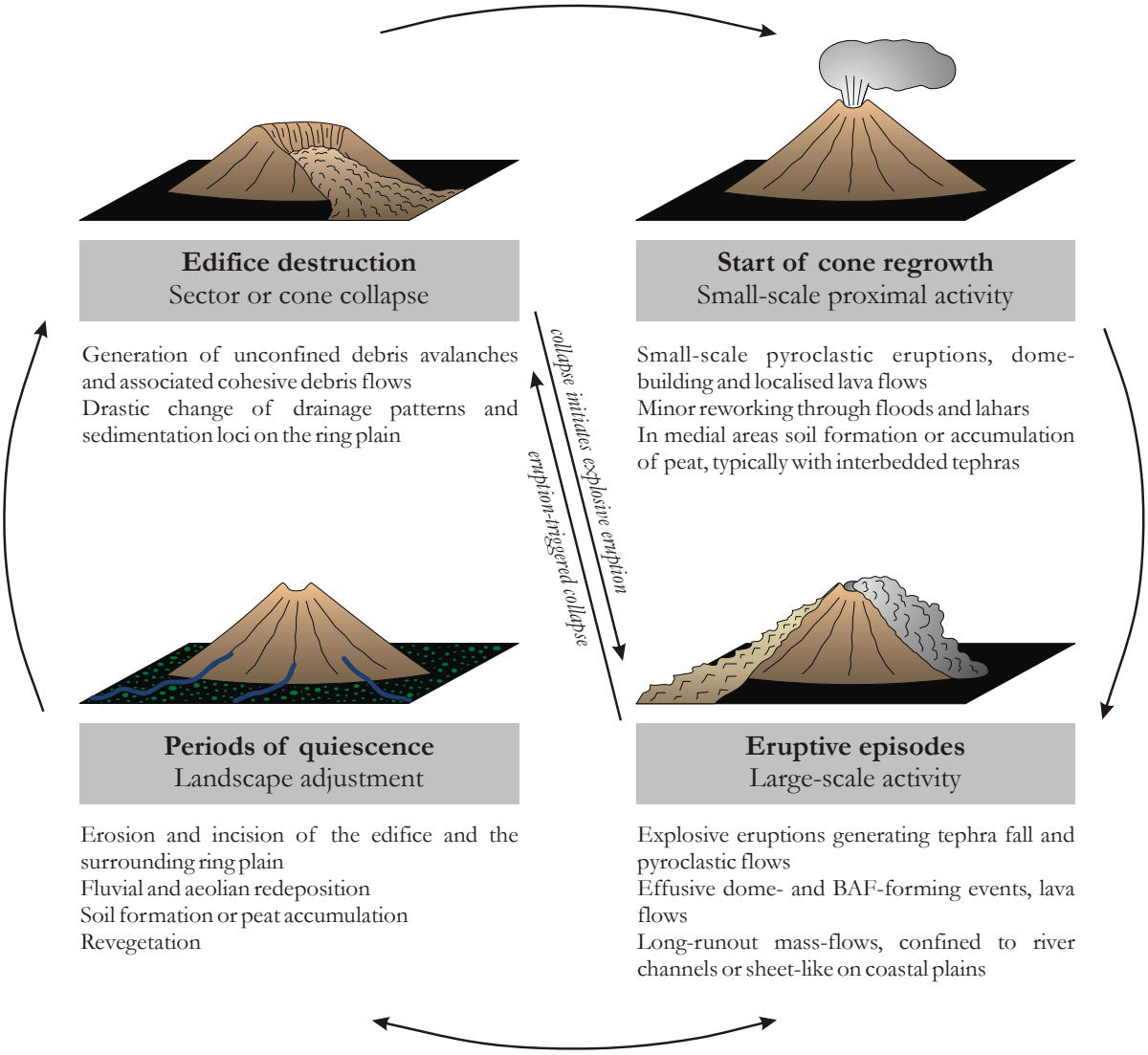

Figure 6.1. Simplified model of cyclic behaviour of stratovolcanoes in general and associated volcanic and volcaniclastic sedimentation as observed at Mt. Taranaki.

constant and deposition loci change resulting in frequent periods of apparent quiescence for variable sectors of the ring plain. These are recorded by soil, medial ash, or peat accumulation, along with landscape adjustment through fluvial and aeolian processes. Small collapse events can be triggered during eruptive episodes or occur during periods of volcanic quiescence. In medial areas, they are represented as channelised cohesive debris-flow deposits of limited extent and thickness.

The similar extent and run-out distance of major Taranaki debris avalanches suggest that the edifice is regenerated to a similar size before it collapses again. Edifice growth is ultimately limited to a critical point at which its structure becomes sufficiently unstable that even a weak disturbance may cause it to fail. The average size of composite volcanoes is typically between 2000-2500 m (Davidson & de Silva 2000), indicating that this height might represent a natural limit. Although, a strong seismic or magmatic event can trigger the collapse of a more stable edifice before this critical height and / or slope is attained (Siebert 1984; Belousov et al. 1999). The volcanic cycle is closed with a major sector or cone collapse, represented by debris-avalanche and long run-out debris-flow deposits in medial areas. These major debris avalanches bury extensive areas of the ring-plain and reshape the landscape. They significantly modify the drainage system and change the focus of sedimentation before and after the collapse (cf. Procter et. al 2009).

6.3. CONTROLS ON THE CHARACTERISTICS OF VOLCANIC CYCLES

The characteristics and sedimentary signatures of a volcanic cycle at repetitively collapsing volcanoes are controlled by the interplay of several internal and external factors.

6.3.1. Factors leading to instability

The tendency of stratovolcanoes to collapse depends on the rate and extent of destabilisation. Various structural, magmatic and external processes can lead to the increasing instability of a volcanic edifice (e.g. McGuire et al. 1996; Elsworth 2000; see Table 6.1 for more references). A combination of processes has contributed to an inherently unstable structure of present and proto Mt. Taranaki edifices. This is mostly a result of a high content of unconsolidated pyroclastic and volcaniclastic deposits (cf. Siebert 1984; Vallance et al. 1995), interbedded with lava flows. Megaclasts of intact, layered fragments of edifice strata within the debris avalanches suggest a similar structure for proto-edifices (Neall et al. 1986). Another

important structural factor at Mt. Taranaki is the development of steep upper slopes (cf. Siebert 1984; Beget & Kienle 1992). The absence of hydrothermally altered components within the Taranaki debris avalanche deposits indicates that hydrothermal processes did not affect large parts of the edifice as has been observed at other volcanoes (cf. Siebert et al. 1987; Lopez & Williams 1993; Vallance & Scott 1997; Voight & Elsworth 1997). Instead, hydrothermal alteration was probably restricted to the area around the central conduit, leading to a progressively weaker core.

Further factors that are recognised to contribute to the instability of volcanoes are their growth on a sloping or weak substrate (Wooller et al. 2004; Carrasco-Nunez et al. 2006), subsidence or uplift of the sub-volcanic basement (Firth et al. 1996; McGuire 2003) as well as frequent tectonic activity (Francis & Self 1987). These processes also play an important role in Taranaki where the sub-volcanic basement consists of a Tertiary marine-basin sequence of dominantly poorly consolidated mudstone with interbedded sandstone (Kamp et al. 2004). The substrate is cut by several Quaternary and active faults, some of which extend through the modern edifice (Neall 1979; Alloway 1989; Sherburn & White 2006). Structural alignments, i.e. the SSE migration of the Taranaki volcanoes and the younger N-S alignment of Mt. Taranaki summit, Fanthams Peak and several lava domes (<3 ka) (Neall 1971; Neall et al. 1986) reflect the more recent tectonic stress field (Sherburn & White 2006) and might have also contributed to the instability of the volcano (cf. Vallance et al. 1995). The high annual precipitation in Taranaki (>8 m rainfall per year on the north flank of the volcano) is likely to cause saturation of the porous deposits that build up the edifice, enhance alteration and eventually weaken the rocks (cf. Scott et al. 2005; Carrasco-Nunez et al. 2006). It is not known in which way the global climatic changes of the last 200 kyrs affected Mt. Taranaki because no correlation between edifice failures and abrupt climate changes could be found as was postulated by Capra (2006). Volcano-tectonic gravity-driven processes such as gravitational spreading can deform and destabilise a volcanic edifice, resulting in the generation of a slump that can develop into a large flank collapse (Van Bemmelen 1949, Borgia et al. 1992, van Wyk de Vries et al. 1996b, 1997, 2000, 2003, Reid et al. 2001, Cecchi et al. 2004). Evidence of buttressing, spreading or slumping (cf. Borgia 1994; van Wyk de Vries & Francis 1997; Borgia & van Wyk de Vries 2003) is absent at Mt. Taranaki.

In addition to the above described slow processes that lead to progressive instability of the edifice, magmatic processes can have similar effects on a much shorter time-scale. The intrusion of fresh magma can result in oversteepening and lateral displacement of the flank, as occurred during the 1980 eruption of Mount St. Helens (Voight et al. 1981), as well as fracturing

TABLE 6.1. *Factors leading to instability of volcanic edifices.*

Structural factors	
Steepening of slopes	Siebert 1984; Beget & Kienle 1992; Murray & Voight 1996
High proportion of weak unconsolidated pyroclastics	Siebert 1984; Vallance et al. 1995; McGuire 2003
Hydrothermal activity within the edifice leading to alteration and a general increase in pore pressure	Frank 1983; Siebert et al 1987; Carrasco-Nunez et al. 1993; Lopez & Williams 1993; Day 1996; Elsworth & Voight 1996; Iverson et al. 1997; Vallance & Scott 1997; Voight & Elsworth 1997
Gravitational spreading and slumping	Borgia et al. 1992; Borgia 1994; van Wyk de Vries et al. 1996b, 1997, 2000, 2003; van Wyk de Vries & Francis 1997; Borgia et al. 2000; Reid et al. 2001; Borgia & van Wyk de Vries 2003; Cecchi et al. 2004
Structural alignments and buttressing	Siebert 1987; Vallance et al. 1995
Buried faults of past structural failures or scars	Normark et al. 1993; Lipman 1995
Magmatic processes	
Oversteepening, mechanical push and lateral flank displacement	Voight et al. 1981; Labazuy 1996 Donnadieu & Merle 1998; Donnadieu et al. 2001
Fracturing and pore-fluid pressure enhancement	Elsworth & Voight 1996
Persistent dike emplacement	Elsworth & Voight 1992, 1995; Lipman 1995; Tibaldi 1996
Change in magma composition and eruptive style	Belousov et al. 1999
Flank overloading from accumulation of eruptive products	Voight et al 1983; Murray 1988; Elsworth & Voight 1995; McGuire 2003
Tectonic factors	
Regional tectonic stress field	Siebert 1984; Ui et al. 1986; Vallance et al. 1995; Capra et al. 2002: Tibaldi & Lagmay 2006
Growth on a sloping or weak substrate	Wooller et al. 2004; Carrasco-Nunez et al. 2006
Subsidence or uplift of the sub-volcanic basement	Firth et al. 1996, McGuire 2003
Rifting	Carracedo 1994, 1996
Frequent tectonic activity	Francis & Self 1987
Climate / weather influences	
Increase in pore water pressure from high-intensity rainstorms	Sheridan et al. 1999; Iverson 2000; van Wyk de Vries et al. 2000; Scott et al. 2005; Carrasco-Nunez et al. 2006
Peripheral erosion of island volcanoes due to sea-level changes	Moore et al. 1994; Nunn 1994; Ablay & Hurliman 2000
Glacial activity / ice cap	Capra et al. 2002

and pore-fluid pressure enhancement within the edifice (Elsworth & Voight 1996). A change in the magma composition can also influence edifice stability, like at Shiveluch volcano where an abrupt shift to a higher SiO_2-content of the erupting magma changed the predominant eruptive style to the production of lava domes (Belousov et al. 1999).

6.3.2. Trigger mechanisms of edifice collapse

The sedimentary signatures of individual volcanic cycles at repetitively collapsing volcanoes are also controlled by the process causing edifice destruction. Bezymianny-type failures were defined by Gorshkov (1959) as being associated with the intrusion of fresh magma (e.g. Glicken et al. 1981; Voight et al. 1981, 1983; Siebert et al. 1987; McGuire et al 1990; Elsworth & Voight 1995; Belousov 1996; Donnadieu & Merle 1998; Elsworth & Day 1999; Donnadieu et al. 2001). They can be triggered by magmatically-induced seismicity, mechanical push, temperature-related changes in pore pressure or gravity loading of erupted material (Voight et al 1983; Elsworth & Voight 1995). The collapse can be accompanied by magmatic activity or trigger explosive eruptions. Thus, regeneration of the edifice starts immediately after its destruction with growth of a new lava dome in the amphitheatre, e.g. St. Augustine (Beget & Kienle 1992), or with a Plinian eruption followed by lava dome formation, e.g. Mount St. Helens and Shiveluch (Lipman & Mullineaux 1981, Bogoyavlenskaya et al. 1985, Belousov et al. 1999). In contrast, Bandai-type collapse events (Siebert et al. 1987) are associated with solely phreatic eruptions, which cease after debris-avalanche generation. Unzen-type slope failures occur without any volcanic activity and are triggered by tectonic earthquakes like nonvolcanic landslides (Voight et al 1983; Siebert et al. 1987; Voight & Sousa 1994). These can be caused by movement of basement faults (Vidal & Merle 2000), active rift zones surrounding or underlying the volcano (van Wyk de Vries & Merle 1996; Day et al. 1999), strike-slip faulting (Lagmay et al. 2000) or caldera collapse (Hurlimann et al. 1999).

The trigger mechanism of failures at Mt. Taranaki is not known except for the Ngaere event, which Alloway et al. (2005) postulated as being of Bezymianny-type because it is immediately preceded by a magmatic fall unit and is directly overlain by several tephra layers. In contrast, there is no evidence to indicate that magmatic activity initiated or immediately followed the other identified edifice failures. However, the large volume of the 80-35 ka southern debris avalanches and a high content of pumice clasts suggest that they were generated during periods of intensified explosive magmatic activity (cf. McPhie et al. 1993). The derivation of these large amounts of pumice from incorporation of substrate or cutting of voluminous pumice deposits by the failure (van Wyk de Vries et al. 2001; Shea et al. 2008) is unlikely at Taranaki due to the

absence of ignimbrites and the typically small size (<<1 km^3) of eruptions (Alloway et al. 1995). Direct evidence such as blast deposits and tephra layers associated with debris avalanches is otherwise absent, due to distance from source, prevailing (north-east) wind direction as well as erosion. Tectonic triggers such as large-scale fault movements or gravitational settling-related faulting may represent significant triggering mechanisms once the volcano reaches a metastable height (cf. Lagmay et al 2000; Vidal & Merle 2000). In addition, environmental factors such as high-intensity rainstorms, which can cause a reduction in strength of the edifice due to saturation (McGuire 2003; Scott et al. 2005; Carrasco-Nunez et al. 2006), could have initiated smaller collapse events.

6.3.3. Frequency of growth and collapse cycles

The frequency of growth and collapse at a stratovolcano is strongly influenced by the magma supply and the magma ascent rate, which determine the repose times between eruptions and the time it takes to (re)build an edifice. Very high lava effusion rates at Mount St. Augustine, for example, are responsible for rapid regeneration of the edifice after a collapse and recurrence of large debris avalanches approximately every 150-200 years (Beget & Kienle 1992). A similar conclusion is reached for Shiveluch Volcano, which produced at least 8 debris avalanches in the last 10 ka (Belousov et al. 1999). The averaged 13 ka between major collapses at Mt Taranaki suggest slower growth phases, and overall lower magma recharge rates.

The apparent increase in debris-avalanche abundance in the recent record, if real, may have a number of causes, including: a change in magma composition or eruptive style (Belousov et al. 1999), an increase of the magma supply rate (Beget & Kienle 1992: Belousov et al. 1999), progressive weakening of the core due to hydrothermal alteration around the conduit (Vallance & Scott 1997; van Wyk de Vries et al. 2000) or persistent dike intrusion (Siebert 1984). Structural aspects such as regrowth of the edifice on former scars seem to have strongly added to the increasing instability and, together with major climate changes, could be responsible for a higher frequency of collapses. Furthermore, a gradual shift to more evolved high-K magma composition (Price et al. 1999) may have resulted in the extrusion of more viscous andesite and basaltic-andesite lavas, which presumably produced steeper upper slopes and a higher percentage of lava domes than in the early history of the volcano. This happened on a larger scale at Shiveluch volcano where an abrupt shift to a higher SiO_2-content of the erupting magma changed the predominant eruptive style to the production of lava domes (Belousov et al. 1999).

6.3.4. Eruptive style and type of products

Phases of edifice construction consist of major eruptive periods separated by intervals of quiescence and landscape adjustment. The predominant eruptive style during edifice-building periods varies between volcanoes or even between cycles on a single volcano. It is controlled by magmatic differentiation processes, which determine physical properties of the magma such as composition, density and viscosity as well as volatile contents and hence explosive vs. effusive behaviour (Davidson & de Silva 2000). The nature of eruptive activity is recorded in the clast assemblages of long run-out debris-flow and hyperconcentrated-flow deposits, which are typically generated in response to a high sediment supply during or after eruptive activity. The clasts vary according to the type of erupted products and hence reflect the predominant eruption mechanism at the time of lahar generation. At Mt. Taranaki some growth phases are characterised by pumice-dominated lahars and tephra layers indicating vigorous subplinian and / or Plinian eruptions. Other mass-flow depositional series are rich in dense, glassy, monolithologic andesite clasts, corresponding to dome-building and associated block-and-ash-flow activity. Polylithologic flows are probably not directly related to an eruption, but may represent conditions where mass-flows gained momentum via erosion and incorporation of sediment along their paths.

The frequency, nature and volume of flows may also depend on the prevailing local and global climate, i.e. rainfall intensity and duration in the source region, vegetation patterns and related slope-stability or sediment supply (e.g. Lavigne et al. 2000; Waitt et al. 1983; Mothes et al. 1998; Hodgson & Manville 1999; Vallance 2000). Syn- and post-eruptive lahars and floods initiated by rain are common at stratovolcanoes with high precipitation rates, e.g. Pinatubo (Pierson et al. 1997; van Westen & Daag 2005) or Indonesian volcanoes such as Merapi (Lavigne et al. 2000; Lavigne & Thouret 2002), Semeru (Lavigne & Suwa 2004; Thouret et al. 2007) and Kelud (Thouret et al. 1998). The average annual rainfall in Taranaki is high, especially on and around the mountain (up to 8 m/yr) but rainfall amount and intensity varied according to climate changes over the last 200 ka.

6.3.5. Distribution of deposits

The distribution of tephra is mainly controlled by the prevailing wind direction while that of volcanic mass-flows (debris avalanches and lahars) depends strongly on the location of the source area (i.e. direction of collapse, site of lahar initiation or position of vent or lava dome), the morphology of the edifice (crater breaches, amphitheatres or deep gullies) and the nature of the landscape surrounding the volcano. A deeply incised topography leads to confinement of debris

avalanches and lahars, as is the case at most volcanoes in the Cascades, e.g. the Osceola Mudflow at Mt. Rainier (Vallance & Scott 1997) and the 1980 debris avalanche at Mount St. Helens as well as subsequent lahars (Voight et al. 1981; Janda et al. 1981). In contrast, Mt. Taranaki debris avalanches form broad fans on the weakly dissected ring-plain. Through most of Taranaki's history the ring-plain setting resembled the present landscape, which is characterised by mostly shallow stream beds and wide coastal plains with broad terraces resulting in the predominance of relatively unconfined and extended sheet-like volcanic mass-flows. Some larger, long-lived river systems provided flow paths for channelised lahars but were commonly infilled and covered by sheet-like flows. Subsequent fluvial erosion again incised some valleys that formed new paths to guide younger flows (cf. Procter et al. 2009). The thickness of mass-flows at any one location in Taranaki increased with growing height and volume of the edifice. In general, the travel-distance of lahars is expected to depend on the elevation and nature of the source region, origin of the flow, slope angle, type and grain-size of the transported material, sediment/water ratio as well as the volume of the flow (Fisher & Schmincke 1984; Scott 1988; Pierson et al. 1990; Mothes 1992; Scott et al. 1995; Vallance 2000).

Mt. Taranaki debris-avalanche deposits form broad fans on the weakly dissected ring-plain (Neall et al. 1986; Palmer et al. 1991; Alloway et al. 2005) and their distribution is mainly controlled by the direction of collapse. Several models have tried to relate volcano morphology and the direction of edifice failures to the regional tectonic stress field. Nakamura (1977), Moriya (1980) and Siebert (1984) suggested that where volcanoes respond to an existing stress regime, the preferred orientation of the axis of the avalanche scarp is perpendicular to the regional σ_{Hmax} or to the strike of normal faults (Francis & Self 1987). Second generation collapse events may be parallel to the previous axes, or at a high angle, i.e. c.135° (Siebert 1984). Later studies showed that volcanoes respond in different ways to the tectonic stress and have varying orientations of amphitheatres in relation to σ_{Hmax} depending on their geodynamic setting (Lagmay & Valdivia 2006). Failure directions were found to occur at an angle to σ_{Hmax} with the highest frequency at 20°-30° and 40°-50° (Lagmay & Valdivia 2006) and are mainly influenced by temporal and local stress-fields within the edifice (Ui et al. 1986b), the geometry and nature of faults (Tibaldi 1995; Lagmay et al. 2000; Vidal & Merle 2000) and the subvolcanic basement (van Wyk de Vries & Borgia 1996; Wooller et al. 2004; Tibaldi et al. 2005). The NE-SW orientation of the numerous active and inactive Quaternary faults that cut the Taranaki peninsula (Fig. 1B) dates from the initial formation of the Tasman Sea c. 80 Ma ago (Hull & Dellow 1993) and does no longer reflect the current stress field (Sherburn & White 2006). The NNW-SSE alignment of the Taranaki volcanoes and the younger N-S trend of Mt. Taranaki and flank vents (Neall 1971)

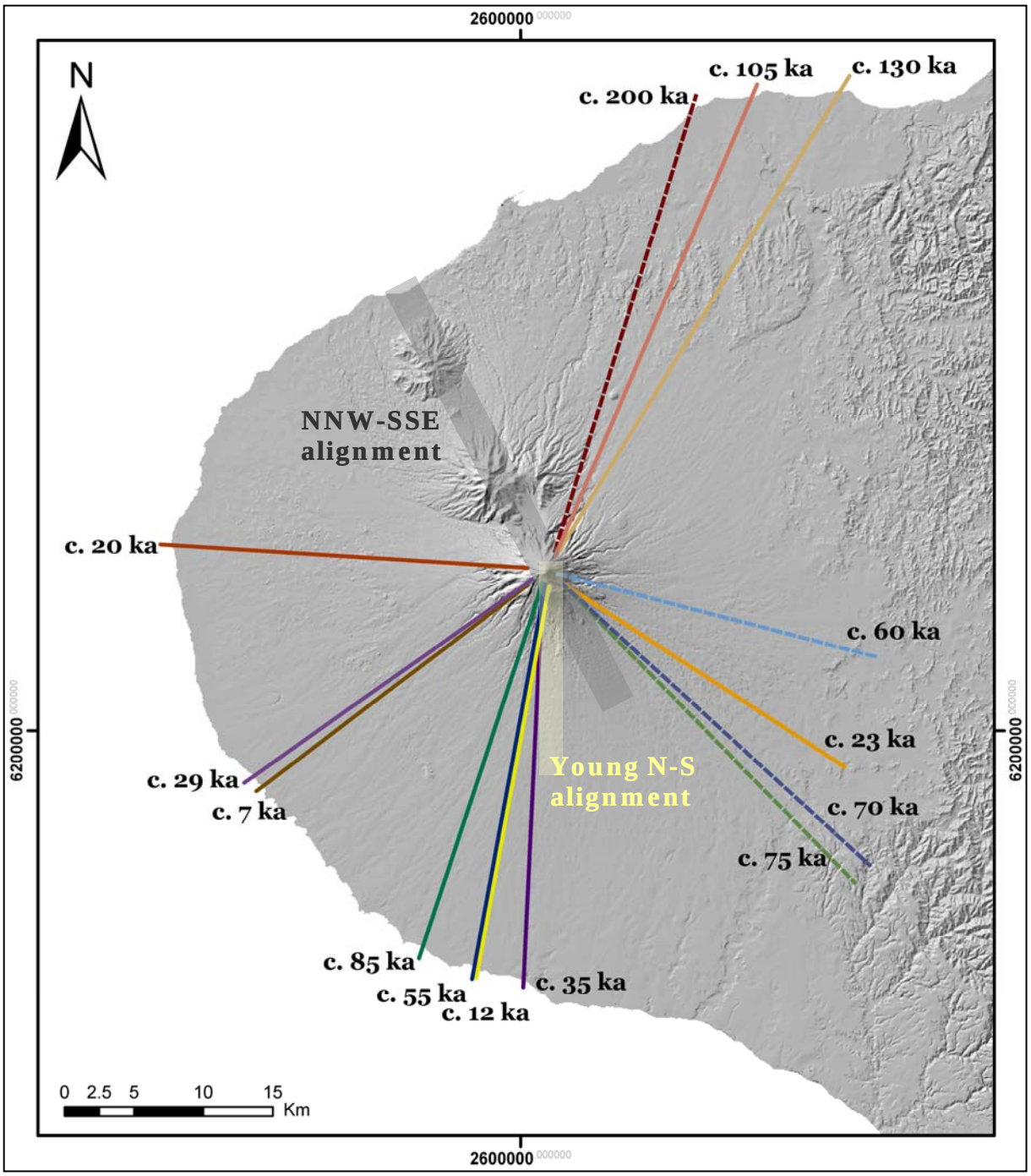

Figure 6.2. DEM of the Taranaki peninsula showing the direction of collapse that produced the identified debris-avalanche deposits in the Mt. Taranaki ring-plain succession. Failures have occurred on similar sectors of the edifice during certain time periods, indicating that different parts of the edifice were more unstable and thus vulnerable to collapse at different times throughout the volcanic history. Dashed axes are based on assumed dispersal of the south-eastern and the oldest northern debris-avalanche deposits. Shaded areas illustrate the direction of the two main volcanic alignments. Grid references are NZ map grid.

differ significantly from the NE-SW orientation of the observed faults, indicating that magmatic intrusions are responsible for the long-term change of the stress direction (Sherburn & White 2006). The distribution axes of debris avalanches at Mt. Taranaki are oriented at various angles to the main structural lineament, and the regional σ_{Hmax} without obvious pattern. Most probably the direction of collapse at Mt. Taranaki was influenced by the trigger mechanisms, i.e. magmatic intrusions / large-scale explosive eruptions and large fault movements in combination with the apparent structural alignments and the morphology of the edifice at the time of failure.

6.3.6. Ring-plain sedimentation between eruptive episodes

The sedimentation as well as erosion and redeposition between eruptive episodes vary according to climate and setting as well as sediment supply. In south-west Taranaki, organic-rich soil and peat beds accumulated during warm periods, while loess-rich tephric soils formed in cooler climate. Fluvial erosion and reworking of primary deposits produced sediments ranging from localised cross-bedded, well-sorted sand and pebble beds to aggradational series of river gravel interbedded with lenses of fluvial sand. Some near-coastal areas accumulated massive sequences of well-sorted dune sands due to near-shore aeolian redeposition during periods of sea level high-stands. Interbedded coarser beds entirely made up of rounded pumice lapilli were most likely formed shortly after explosive eruptive activity.

6.4. HAZARD IMPLICATIONS

Overall, the hazard potential varies strongly at different parts of the cycle, because each phase generates distinctive types of mass-flows. Although large edifice failures and the generation of debris avalanches individually represent the greatest hazard at repetitively collapsing volcanoes, they are usually of low frequency, i.e. on-average every 13 ka at Mt. Taranaki. During construction phases, mass-flows are by far more frequent and are not only confined to stream valleys but can inundate wide areas and travel long distances. The majority of past volcanic mass-flows in Taranaki are related to eruptive activity with individual units being rapidly emplaced over relative short periods of time. Intervals of quiescence separating these eruptive episodes produce occasional polylithologic lahar and flood deposits. Large debris flows are restricted to the sites of deeper river channel and occur at least once in c. 2 ka. In contrast, sheet-like hyperconcentrated flows are more widespread and inundate the shallower, broad floodplains and coastal terraces. They represent the most frequent event recorded in medial ring-plain locations, with a minimum recurrence of one event in 500 years. Due to the large number and narrow distribution range of

single flow units and the lack of individual diagnostic properties, hyperconcentrated-flow and debris-flow deposits were grouped into composite stratigraphic units and correlated as packages rather than separate flow events. The given frequency is thus only an approximate minimum estimate.

Understanding the cyclic nature of stratovolcanoes and the frequency of their cyclicity will be critical for developing realistic probabilistic hazard models. Potential lahar inundation areas can be determined from previous events at a volcano and evaluation of the modern topography. The nature of eruptive activity and deposits produced in the younger past can help to evaluate which part of the cycle the volcano is currently in and if a collapse is likely to occur in the near future. Forecasting models have to not only consider return periods of debris avalanches but also the preconditioning of the edifice to failure. The historic record can provide information on the nature, extent and recurrence of past collapse events. Regional tectonic stress fields sometimes produce a preferred direction of slope failure (Siebert 1984; Vallance et al. 1995) but often it is influenced by local stress regimes within the volcano. Hence, in order to assess timing and location of a possible next collapse future surveillance is needed to identify weak parts of the edifice that are susceptible to failure.

6.5. DRIVING FORCES BEHIND THE CYCLIC BEHAVIOUR OF STRATOVOLCANOES

6.5.1. External forces: Correlation with the climatic background

Climate conditions have been recognised as an important influence on the nature of volcaniclastic sedimentation around volcanoes (e.g. Palmer et al. 1993; Davidson & de Silva 2000; de Rita et al. 2002; Zanchetta 2004). Local precipitation regimes control soil development, vegetation patterns, rates of erosion, the degree of landscape dissection and hence the sediment supply during inter-eruptive periods as well as the frequency of syn- and post-eruptive lahar generation (e.g. Dorn et al. 1987; Frostick & Reid 1989; Palmer et al. 1993; Ritter et al. 1995; Davidson & de Silva 2000; Lavigne & Thouret 2002; Lavigne 2004; Zanchetta 2004; Scott et al. 2005; van Westen & Daag 2005). Some studies furthermore suggest that extreme weather conditions such as intense or prolonged rainfalls as well as abrupt climate changes and glaciations may influence the potential of the volcano to fail, or even trigger a collapse (McGuire 1996; Sheridan et al. 1999; Kerle et al. 2003; Scott et al. 2005; Capra 2006).

To evaluate the possible role of major climate changes behind cyclic volcanic behaviour, the occurrence of debris-avalanche events at Mt. Taranaki was compared to the global climate fluctuations of the last 150 ka (cf. Chapter 3). Since edifice failures have occurred repeatedly during the volcanic history during both warm interglacial as well as cold glacial periods, the timing of major collapse events does not seem to be directly related to global climate changes. Irrespective of prevailing climate conditions, the occurrence of edifice failures was influenced by other factors such as the nature and magnitude of volcanic activity, rate of eruptions, edifice height and flank oversteepening (c.f. Section 6.3.2). However, it appears that the size of failures and the volume of the resulting debris-avalanche deposits might have been larger during cool or cold periods, possibly due to greater instability of the barely vegetated, less protected volcano flanks and greater saturation and deeper water infiltration into the edifice.

Even though major climate fluctuations do not seem to have triggered the frequent edifice collapses of Mt. Taranaki, they are reflected in deposit characteristics of the medial ring-plain succession. Debris avalanches that were generated during warm climate travelled across a densely vegetated landscape and the resulting deposits typically contain abundant tree fragments ranging from small chips to large tree logs. Units emplaced during cool climate contain only sparse wood fragments, while those produced during cold glacial conditions are free of significant organic components. More intense weathering processes during warm and mild climates produced allophane-rich, reddish Andisols in contrast to weakly developed, loess-rich soils that formed during cold climate (cf. Alloway et al. 1992, 1995). During moist conditions peat beds of variable thickness accumulated locally in wet, poorly drained areas and occur frequently throughout the sequence (cf. McGlone et al. 1984; Alloway et al. 1992, 2005). Less vegetation cover during cold glacial and cool stadial conditions resulted in larger areas of bare, unprotected volcanic debris, susceptible to erosion and intense reworking (c.f. Zanchetta 2004). Within the Mt. Taranaki ring-plain succession, the rapid remobilisation of a high supply of unconsolidated sediment is reflected in stacks of polylithologic hyperconcentrated-flow and debris-flow deposits. In contrast, mild or warm climate during interstadial and interglacial periods are typically characterised by stabilisation of loose volcanic and volcaniclastic material and sediment storage on the edifice and the surrounding ring plain (c.f. Hubert & Filipov 1989; Frostick & Reid 1989; Blair & McPherson 1992; Blair 1999, 2000; Zanchetta 2004).

Global climate changes of the last >150 ka not only affected vegetation patterns and landscape stability but associated sea-level fluctuations had severe impacts on near-coastal environments (c.f. de Rita et al. 2002), in particular island volcanoes (e.g. Moore et al. 1994; Nunn 1994; Ablay & Hurliman 2000). Falling sea level during cold periods is inferred to have

increased the rate of marine abrasion and steep cliff development onshore, hence reducing the support for the base of the subaerial flank and favouring edifice failure of island volcanoes (Ablay & Hurliman 2000). Dropping sea levels also significantly change the geomorphology of near-coastal areas (de Rita et al. 2002). In Taranaki, present day coastal areas were characterised by more deeply incised stream valleys at low sea-level stands, compared to a weakly dissected landscape with shallow channels during warm climates such as today. The change in geomorphology resulted in different deposit geometries and facies characteristics, in Taranaki represented by thick, bouldery channelised debris flow deposits compared to more widespread sheet-like hyperconcentrated flow deposits during high sea-level stands.

Despite major climate fluctuations during the last >150 ka, the overall sedimentation pattern of volcaniclastic deposits within the Mt. Taranaki ring-plain succession is consistent, suggesting that climate variations were not the driving force behind Mt. Taranaki's cyclic behaviour. This is supported by the occurrence of repeated collapse and regrowth described at volcanoes in different climate zones and various tectonic settings, such as St. Augustine, Alaska (Beget & Kienle 1992), Shiveluch, Kamtchatka (Ponomareva et al. 1998; Belousov et al. 1999); Colima (Stoopes & Sheridan 1992) and several other Mexican volcanoes (Vallance et al. 1995; Capra et al. 2002), Mt. Rainier, Cascades (Vallance & Scott 1997) as well as ocean island volcanoes like Stromboli (Kokelaar & Romagnoli 1995, Tibaldi et al. 2001), Reunion (Lenat et al. 1989, Labazuy, 1996), Canary Islands (e.g. Holcomb & Searle 1991, Carracedon 1994, 1996; Ablay & Hurliman 2000; Walter & Schmincke 2002), and Hawaii (Fornari & Campbell 1987; Moore et al. 1994). Instead, volcanically-driven processes such as volcanic activity and collapse events were the primary control on the accumulation style of the ring-plain depositional system. Climate fluctuations on the other hand influenced the sediment supply during inter-eruptive periods and the rates of revegetation while associated sea-level changes controlled the paleogeomorphic near-coastal setting and hence geometry and distribution of deposits, but had only secondary, overprinting effects on deposit characteristics and type of sedimentation. Varying climate conditions are also responsible for some of the differences in the sedimentary signatures of cyclic growth and destruction of volcanoes in different settings.

6.5.2. Internal forces: Relationship between sedimentary and geochemical cycles

To elucidate the role of the magmatic system behind the frequent recurrence of edifice failures at Mt. Taranaki, clasts within debris-avalanche deposits were used as a series of windows into the composition of previous successive edifices.

The diversity of lithologies and their geochemical composition is similar throughout the volcanic history, with the oldest sample suites displaying a slightly broader range of compositions including more primitive rock types. The evolution to less primitive compositions is accompanied by an increase in K_2O with decreasing age, indicating progressive interaction with an increasingly hotter amphibolitic underplated crust. The gradual changes in the geochemical composition of Mt. Taranaki eruptives are a result of the long-term stability of the magmatic system. The preservation of similar internal conditions during the volcano's evolution suggests that volcanic processes are the main driving force behind its cyclic behaviour and sedimentation.

Although the geochemical data shows that the evolution of the magmatic system was not controlling the repeated failures of Mt. Taranaki, it revealed certain aspects that strongly support the model of cyclic growth/collapse/(re-)growth. The magmatic evolution of Mt. Taranaki magmas is characterised by gradual compositional changes, yet individual debris-avalanche sample suites show geochemical differences that allow their distinction. This indicates that after very large sectors of the volcano had been removed by collapse, lava flows and pyroclastic material of a different geochemical composition rebuilt the edifice during the following growth phase. A subsequent failure would involve the compositionally distinct, 'new' material that was part of a completely different edifice, generating a different geochemical signature of the resulting debris-avalanche deposit. In contrast, overlapping compositions of debris-avalanche sample suites show that similar material was involved in the collapses. This could be the result of failures of different sectors of the volcano that removed part of the same edifice. Smaller collapses of similar sectors that occur within a shorter period of time most likely also contain clast assemblages with similar compositions.

6.6. CONCLUSIONS

Cyclic growth and collapse represent a natural frequency in the life of stratovolcanoes. This behaviour is often difficult to identify because of long time-scales of cycles or incomplete stratigraphic records. The cyclic evolution of Mt. Taranaki produced a repeating pattern of deposition in the volcaniclastic sequences of the surrounding ring-plain. The reconstruction of volcanic events at this example allowed the study of processes operating over the life-span of collapsing stratovolcanoes.

Individual volcanic cycles may vary in detail between different volcanoes as well as during the life-time of a single volcano. Their characteristics are influenced by various internal

and external factors, including frequency and nature of collapse events, magmatic composition and hence style and magnitude of eruptive activity, recurrence and duration of eruptive periods, as well as the surrounding topography and climate conditions.

Volcanic hazards vary strongly at different parts of the cycle since each phase generates distinctive types of mass-flows ranging from catastrophic debris avalanches to channelised and unconfined lahars. Large edifice failures and the generation of debris avalanches individually represent the greatest hazard at repetitively collapsing volcanoes but are usually of low frequency compared to more frequent eruption-related lahars during construction phases. Smaller events are typically confined to stream valleys while large lahars can be relatively unconfined and travel long distances, hence affecting wide areas.

Edifice failures at Mt. Taranaki occurred during both warm interglacial as well as cold glacial periods, indicating that the timing of major collapse events was not directly related to global climate changes. Although major climate fluctuations did not control the frequent edifice collapses of Mt. Taranaki, resulting variations in the vegetation pattern, precipitation regimes and geomorphic setting had overprinting effects on deposit characteristics, type of volcaniclastic ring-plain sedimentation as well as the distribution of deposits.

The long-term stability of the magmatic system and preservation of similar internal conditions during the evolution of Mt. Taranaki also suggest that volcanically-driven processes, such as nature and magnitude of volcanic activity, rate of eruptions, edifice height and flank oversteepening, are the main driving force behind its cyclic behaviour and sedimentation.

CHAPTER 7.

CONCLUSIONS

7.1. CONCLUSIONS

Volcanic activity at Mt. Taranaki has produced a surrounding volcaniclastic ring-plain that contains the most complete chronostratigraphic record of volcanic activity and other sedimentary events at this volcano. Cliff sections along the northern, western, and southern Taranaki coast show a cross-section through medial to distal ring-plain settings and expose sedimentary records of volcanic mass-flow deposits and epiclastic sediments that extend back to c. 200 ka. This study focused on mapping the ring-plain succession through identification and correlation of key units, such as widespread debris-avalanche deposits, as well as continuous soil and peat layers, and intercalated composite stratigraphic packages of hyperconcentrated-flow and debris-flow deposits. Altogether 14 debris-avalanche deposits were identified as being sourced from Mt. Taranaki, including five new units and four previously described deposits that were redefined in this study. This implies a minimum of one major slope failure on average every 13 000 years. Several clay-rich debris flow-deposits were also recognised, which are interpreted to represent the distal runout of smaller, confined debris avalanches. Deposits range in volume from <0.1 km^3 to rare exceptionally large units of >7.5 km^3 and exhibit a minimum run-out distance of c. 26-45 km onshore and at least another 6-8 km offshore. Their lateral width in coastal cross-sections ranges from c. 9 to 35 km with deposit thickness in medial areas (>20 km from source) of 2.5 to >16 m. Hyperconcentrated-flow and non-cohesive debris-flow deposits are another common element of the studied volcaniclastic sequences, indicating that lahars occurred frequently at Mt. Taranaki between collapse events.

The exposed deposits were emplaced by a very broad spectrum of sediment-water flows, ranging from dry debris avalanche, highly concentrated debris flow, hyperconcentrated flow to dilute streamflow as well as intermediaries between these categories. These deposit types and lithologies contained within, were not randomly emplaced. By reconstructing the chronology volcanic events and other landscape-forming processes a repeating pattern of deposition was

recognised continuously since the known inception of Mt. Taranaki volcanism. These repeated sedimentary signatures were used to develop a model of cyclic volcaniclastic sedimentation for medial to distal areas surrounding stratovolcanoes. A generalised volcanic cycle at Mt. Taranaki begins after the destruction of large portions of the edifice by collapse, followed by long-term regeneration of the deeply scarred edifice. The early stages of re-growth are characterised by small-scale pyroclastic eruptions, dome-building and localised lava flows. These produce few if any long-runout mass-flows and hence medial areas accumulate thick paleosols of medial ash and/or peat, with interbedded tephra layers. With growing height of the edifice, larger mass-flows reach greater distances and the medial accumulation is characterised by massive sequences of mainly monolithologic (both pumice- or dense-andesite clast rich) debris-flow and hyperconcentrated-flow deposits that intercalate with tephra beds. These represent redistribution of voluminous near-vent explosive pyroclastic deposits or those derived from collapses of lava domes. Periods of quiescence separating these eruptive episodes are recorded by soil, medial ash, or peat accumulation, along with landscape adjustment through fluvial and aeolian processes. Edifice growth was ultimately limited to a possibly similar critical point at which it failed. The cycle is thus closed with a major sector collapse, which in medial areas is represented by clay-rich debris-flow and most characteristically debris-avalanche deposits.

The new stratigraphy developed during this study identified the major debris-avalanche record for the older ring-plain succession. This provided a framework for sampling the older volcanic products of Mt. Taranaki. Up to this point, only easily accessible lavas from the present edifice had been sampled, limiting most studies to the rocks of only the lattermost 5% of the known lifespan of Mt. Taranaki volcanism. To extend geochemical studies into the early magmatic history of the volcano samples taken from identified debris-avalanche deposits were used as a series of "snap shots" into the composition of proto-edifices at the time immediately preceding the debris-avalanche collapse. Individual sample suites from the debris-avalanche deposits demonstrate a consistent pattern of evolution with time, indicating that the volcanic edifice was substantially destroyed and rebuilt between the major debris-avalanche events. The data shows that Mt. Taranaki has evolved to a high-K andesite magmatic system over the last c. 190 ka. A progressive enrichment in whole-rock K_2O concentrations and those of Large Ion Lithophile Elements (LILE) was observed along with a gradual shift to more evolved magmas. Throughout this sequence there was a constant arc-fluid component signature. The evolving magma characteristics imply the existence of an evolving "hot zone" (cf. Annen et al. 2006) in the lower crust. This was derived through repeated intrusions and underplating of mantle-derived melts (generated with a slab-fluid component) into and below the lower crust, gradually raising

the geothermal gradient. As the "hot zone" evolved, larger proportions of the underplated and intruded basaltic magmas were partially re-melted to generate progressively more potassic and LILE-enriched magmas over time. Relatively weakly fractionated basalt clasts with subdued arc signatures occurred only within the older sample suites and show evidence for the ability of more primitive magmas to rise through the crust without intense modification during the early stages of hot zone development beneath Mt. Taranaki. Other compositional variations of these more primitive compositions also indicate that there is a heterogeneous mantle source for parental Mt. Taranaki magmas.

Individual debris-avalanche sample suites can be distinguished based on their geochemical characteristics, in particular differences in K_2O and Ba contents. This suggests that after large sectors of the volcano had been removed by collapse, the edifice was rebuilt by new material with a slightly different geochemical signature before collapsing again. Major differences in the geochemical character of clast assemblages in comparison to previous debris-avalanche deposits suggest: (1) major failure resulting in removal of large sectors of the edifice and (2) significant time between collapses. Trace element characteristics also show a strong distinction between clasts within Pouakai- and Mt. Taranaki-derived debris-avalanche deposits. Lower contents of K_2O, Rb and Ba, Zr, Rare Earth Elements (REE) and High Field Strength Elements (HFSE) in Pouakai samples imply there was higher degrees of partial melting and even less modification in the lower crustal hot zone than for early Mt. Taranaki magmas. Based on these distinct differences, it was demonstrated that the Mangati and Motunui Formations are the oldest known deposits derived from Mt. Taranaki. The emplacement of the Mangati debris-avalanche deposit between 190-210 ka gives a new minimum age for the commencement of eruptive activity at Mt. Taranaki, which is around 70 ka older than previously thought.

Some of the magmatic trends shown in the whole-rock geochemistry are reflected in mineralogical differences between the oldest debris-avalanche units and the youngest eruptives at Mt. Taranaki. The overall composition of mineral phases in Mt. Taranaki volcanics has not changed significantly over the last 130 ka with the most distinct differences being related to the broader range of erupted magma compositions observed in the older rock suites, including more primitive, basaltic compositions. Clinopyroxene and hornblende compositions are consistent with crystallisation over a wider range of pressures and at greater depth than during later stages of volcanism. This reflects the immature state of the early magmatic system and eruption of more primitive melts with a more distinct mantle signature. As indicated by the whole-rock geochemistry, the lower crustal "hot zone" was significantly thinner and colder >200 000 years ago, allowing less interaction of melt with amphibolised, underplated material. During early stages

of hot zone development more extensive fractionation of high-pressure mineral phases at greater depth occurred. In contrast, mineral phases, such as biotite, and compositions that are produced during differentiation at shallower levels are rare, suggesting that late-stage crystallisation in zoned upper-crustal storage levels was not a significant process during the early stages of Mt. Taranaki volcanism. Instead, early magmas typically rose rapidly through the crust and only rarely stalled at shallow levels to further differentiate. The occurrence of Or-rich plagioclase in young Mt. Taranaki lavas and higher K_2O-content in residual melts are consistent with the magmatic evolution reflected in whole-rock compositions and the recognised trend of increasing K_2O-contents with time.

The geochemical data and field records combined were used to elucidate the relative roles of internal and external driving forces behind the volcano's behaviour. Edifice failures at Mt. Taranaki occurred frequently and during both warm as well as cold periods, indicating that climate variations did not control the timing of major collapse events. Instead, major climate fluctuations had overprinting effects on deposit characteristics, type of volcaniclastic ring-plain sedimentation as well as the distribution of deposits. Together with the long-term stability of the magmatic system and preservation of similar internal conditions during the evolution of Mt. Taranaki, this suggests that volcanically-driven processes, such as nature and magnitude of volcanic activity, rate of eruptions, edifice height and flank oversteepening, were the main driving force behind its cyclic behaviour and sedimentation.

It has also been recognised that cyclic growth and collapse represents a natural frequency in the life of stratovolcanoes worldwide. Individual cycles may vary in detail between different volcanoes as well as during the life-time of a single volcano. Their characteristics are influenced by various internal and external factors, including frequency and nature of collapse events, magmatic composition and hence style and magnitude of eruptive activity, recurrence and duration of eruptive periods, as well as the surrounding topography and climate conditions. Understanding the long-term cyclic nature of the stability and behaviour of stratovolcanoes worldwide is important in order to develop more holistic and accurate forecast of hazards, since the probabilities of various hazardous processes will vary greatly at different periods within the cycle.

7.2. RECOMMENDATIONS FOR FUTURE RESEARCH

The outcomes of this study provided important new insights into the cyclic behaviour of andesite stratovolcanoes such as Mt. Taranaki, most notably pointing out the sedimentary signatures of repeated growth and collapse and their implications for volcanic hazards. It is recognised that this work represents only a small step towards a more comprehensive understanding of volcanic behaviour, sedimentation and magmatic evolution. Upon completion of this study, there remain several lines of inquiry that would benefit from further, focused study. The following avenues of future research could help significantly improve our knowledge of volcanic behaviour and future risk from Mt. Taranaki and other repeatedly collapsing volcanoes:

a) The volcaniclastic succession from west to south Taranaki has been studied in detail and recorded volcanic and sedimentary events were mapped and correlated. But this covered only one sector of the extensive ring plain surrounding the volcano. In order to develop a comprehensive overview of the entire volcanic history and to establish a more complete stratigraphic framework, ring-plain sequences in southeast and east Taranaki need further research. Lahar and debris-avalanche deposits that are exposed surficially have been identified and mapped but as was shown by the study of coastal cliffs in west-south Taranaki, these only represent the 'tip of the iceberg' and more units are buried. Borehole data from oil and gas companies as well as the collection of carefully located new cores would enable a better reconstruction of event magnitude and volume. These may also help to constrain the age of the known 14 debris-avalanche events, using the radiocarbon method for younger units and also K-Ar and Ar-Ar dates of clasts within the older units.

b) Several studies at volcanoes worldwide focus on the factors that lead to volcanic instability and processes that trigger edifice failures. A better understanding of the processes involved in repeated collapse allows specific monitoring of these volcanoes and the possible identification of warning signs before a collapse happens. More work needs to be done on factors that lead to the instability of Mt. Taranaki and trigger mechanisms of past edifice failures. Also, geophysical studies and monitoring of the edifice using permanent tiltmeters or GPS systems may allow the recognition of weak zones and possible slow movements and deformations preceding collapse, which could prevent a major disaster in the future.

c) Turner (2008) identified a 1 500-2 000 year cyclic eruption frequency in the Holocene record of Mt. Taranaki that involved geochemically defined magma batches. Series of monolithologic lahar deposits in the ring plain are believed to be linked to individual eruption episodes and hence represent time series of individual eruption cycles. Now that it is recognised that the debris-avalanche clasts successfully provide an insight into proto Taranaki edifices, systematic sampling of the intervening deposits for geochemical analysis could provide important information on eruption cycles that represent edifice growth to complement what is known about the latest Mt. Taranaki edifice. Exploring geochemical trends within these series of lahar deposits would also allow a reconstruction of the magmatic evolution during growth phases to complement what is known from the debris-avalanche sample suites.

d) The new geochemical and mineralogical data obtained during this study could provide the basis for further and more detailed research on long-term magma generation processes and subsequent crystallisation conditions within the framework of previous concepts, i.e. models of andesite petrogenesis by Stewart et al. (1996) and Price et al. (1999, 2005) and the concept of a lower crustal "hot zone" by Annen et al. (2006). Detailed petrography and mineral chemistry of all debris-avalanche sample suites samples could represent a valuable time-series to identify systematic changes in crystallisation conditions and origin of the volcanic rocks. Phenocryst textures furthermore allow the reconstruction of magmatic processes over the last 190 ka at Mt. Taranaki and their implications for the complex storage system in mid- to upper crustal levels (cf. Annen et al. 2006; Turner 2008).

e) The method of sampling clast assemblages from debris-avalanche deposits clearly provided a snap-shot view of proto-edifices in this study. Hence, this could be easily applied to units from collapsing stratovolcanoes worldwide to provide longer views into the volcanic and magmatic system that are typically overlooked when concentrating on the youngest volcanic edifice. The insights gained into the long-term magmatic evolution provided in this way allow important new information of possible subsequent magmatic processes (and implicit hazards).

REFERENCES CITED

Ablay G, Hurlimann M (2000) Evolution of the north flank of Tenerife by recurrent giant landslides. Journal of Volcanology and Geothermal Research 103: 135-159.

Adams RD, Ware DE (1977) Structural earthquakes beneath New Zealand: location determined with a laterally inhomogeneous velocity model. New Zealand Journal of Geology and Geophysics 20: 59-83.

Aitken JF, Campbell IB, Wilde RH (1978) Soils of Stratford County, North Island, New Zealand. New Zealand soil survey report 42.

Alloway B (1989) Late Quaternary cover-bed stratigraphy and tephrochronology of north-eastern and central Taranaki, New Zealand. Unpublished PhD thesis, Massey University, Palmerston North, New Zealand.

Alloway BV, Stewart RB, Neall VE, Vucetich CG (1992a) Climate of the last glaciation in New Zealand, based on aerosolic quartz influx in an andesitic terrain. Quaternary Research 38: 170-179.

Alloway BV, McGlone MS, Neall VE, Vucetich CG (1992b) The role of Egmont-sourced tephra in evaluating the paleoclimatic correspondence between the bio- and soil-stratigraphic records of central Taranaki, New Zealand. Quaternary International 13-14: 187-194.

Alloway BV, Neall VE, Vucetich CG (1992c) Particle size analyses of late Quaternary Allophane-dominated andesitic deposits from New Zealand. Quaternary International 13/14: 167-174.

Alloway BV, Lowe DJ, Chan RPK, Eden DN, Froggatt PC (1994) Stratigraphy and chronology of a c. 4000 year old distal silicic tephra from Taupo Volcanic Centre, New Zealand. New Zealand Journal of Geology and Geophysics 37: 37-47.

Alloway BV, Neall VE, Vucetich CG (1995) Late Quaternary tephrostratigraphy of north-east and central Taranaki, New Zealand. Journal of the Royal Society of New Zealand 25: 385-458.

Alloway B, McComb P, Neall V, Vucetich C, Gibb J, Sherburn S, Stirling M (2005) Stratigraphy, age, and correlation of voluminous debris avalanche events from an ancestral Egmont Volcano: implications for coastal plain construction and regional hazard assessment. Journal of the Royal Society of New Zealand 35: 229-267.

Ando S, Yamagishi H (1975) Hill Topography on the Nuee Ardente deposits of Shikaribetsu Volcano, Hokkaido. Bulletin of the Volcanological Society of Japan 20: 31-36.

Arculus RJ, Wills KJA (1980) The petrology of plutonic blocks and inclusions from the Lesser Antilles island arc. Journal of Petrology 21: 105-122.

Arculus R J, Powell R (1986) Source component mixing in the regions of arc magma generation. Journal of Geophysical Research 91: 5913–5926.

Annen C, Sparks RSJ (2002) Effects of repetitive emplacement of basaltic intrusions on thermal evolution and melt generation in the crust. Earth and Planetary Science Letters 203: 937–955.

Annen C, Blundy JD, Sparks RSJ (2006) The Genesis of Intermediate and Silicic Magmas in Deep Crustal Hot Zones. Journal of Petrology 47: 505–539

Arguden AT, Rodolfo KS (1990) Sedimentological and dynamic differences between hot and cold laharic debris flows of Mayon Volcano, Phillipines. Bulletin of the Geological Society of America 102: 865-876.

Arnold HC (1959) The Sugar Loaf intrusions near New Plymouth. New Zealand Journal of Geology and Geophysics 2: 735-745.

Atherton M.P, Petford N (1993) Generation of sodiumrich magmas from newly underplated basaltic crust. Nature 362: 144–146.

Bagnold RA (1954) Experiments on a gravity free dispersion of large solid spheres in a Newtonian fluid under shear. Proceedings of the Royal Society London A 225: 49-63.

Ballance PF, Pettinga JR, Webb C (1982) A model of the Cenozoic evolution of northern New Zealand and adjacent areas of the southwest Pacific. Tectonophysics 87: 37-48.

Beavan JM, Moore M, Pearson C, Henderson M, Parsons B, Bourne S, England P, Walcott D, Blick G, Darby D, Hodgkinson K (1999) Crustal deformation during 1994-1998 due to oblique continental collision in the central Southern Alps, New Zealand, and implications for seismic potential of the Alpine fault. Journal of Geophysical Research 104: 25,233-25,255.

Beget JE, Kienle J (1992) Cyclic formation of debris avalanches at Mount St Augustine volcano. Nature 356: 701-704.

Belousov A (1996) Deposits from the 30 March 1956 directed blast at Bezimianny volcano, Kamchatka, Russia. Bulletin of Volcanology 57: 649-662.

Belousov A, Belousova M, Voight B (1999) Multiple edifice failures, debris avalanches and associated eruptions in the Holocene history of Shiveluch volcano, Kamchatka, Russia. Bulletin of Volcanology 61: 324-342.

Bemmelen RW van (1949) Geology of Indonesia. The Hague, The Netherlands, Government Printing Office, 732 p.

Bergantz G (1989) Underplating and partial melting: implications for melt generation and extraction. Science 245: 1093-1095.

Beverage JP, Culbertson JK (1964) Hyperconcentrations of suspended sediment. American Society of Civil Engineers, Proceedings, Hydraulics Division Journal 90, no. HY6: 117-128.

Bevis M, Taylor FW, Schutz BE, Recy J, Isacks BL, Helu S, Singh R, Kendrick E, Stowell J, Taylor B, Calmantli S (2002) Geodetic observations of very rapid convergence and back-arc extension at the Tonga arc. Nature 374: 249-251.

Bibby HM, Caldwell TG, Davey FJ, Webb TH (1995) Geophysical evidence on the structure of the Taupo Volcanic Zone and its hydrothermal circulation. Journal of Volcanology and Geothermal Research 68: 29-58.

Bingham EC (1922) Fluidity and Plasticity. McGraw-Hill Book Co., New York. 440 p.

Blair TC (1999) Sedimentology of the debris-flow-dominated Warm Spring Canyon alluvial fan, Death Valley, California. Sedimentology 46: 941-965.

Blair TC (2000) Sedimentology and progressive tectonic unconformities of the sheetflood-dominated Hell's Gate alluvial fan, Death Valley, California. Sedimentary Geology 132: 233-262.

Blair TC, McPherson JG (1994) Alluvial fans and their natural distinction from rivers based on morphology, hydraulic processes, sedimentary processes, and facies assemblages. Journal of Sedimentary Research 3: 450-489.

Blatter DL, Carmichael ISE (1998). Plagioclase-free andesites from Ziticuaro (Michoacan), Mexico: petrology and experimental constraints. Contributions to Mineralogy and Petrology 132: 121-138.

Borgia A, van Wyk de Vries B (2003) The volcano-tectonic evolution of Concepcion, Nicaragua. Bulletin of Volcanology 65: 248-266.

Borgia A, Ferrari L, Pasquarè G (1992) Importance of gravitational spreading in the tectonic and volcanic evolution of Mount Etna. Nature 357: 231-235.

Borgia A, Delaney PT, Denlinger RP (2000) Spreading volcanoes. Annual Reviews in Earth and Planetary Science 28: 539-70.

Bossard L (1928) Origin of the conical hills in the neighbourhood of Mt. Egmont, New Zealand. Journal of Science and Technology 10: 119-124.

Bowen NL, (1928) The evolution of the igneous rocks. New York: Dover reprinted 1956, 334 p.

Bradley JB, McCutcheon SC (1985) The effects of high sediment concentration on transport processes and flow phenomena. International Symposium of Erosion, Debris Flow and Disaster Prevention. Tsukuba, Japan, p. 219-225.

Bradshaw JD (1993) A review of the Median Tectonic Zone: terrane boundaries and terrane amalgamation near the Median Tectonic Line. New Zealand Journal of Geology and Geophysics 36: 117-125.

Branney M, Gilbert J (1995) Ice-melt collapse pits and associated features in the 1991 lahar deposits of Volcán Hudson, Chile: criteria to distinguish eruption-induced glacier melt. Bulletin of Volcanology 57: 293-302.

Brenan JM, Shaw HF, Ryerson FJ, Phinney, DL (1995) Mineral-aqueous fluid partitioning of trace elements at 900°C and 2.0 GPa: Constraints on the trace element chemistry of mantle and deep crustal fluids. Geochimica et Cosmochimica Acta 69: 3331-3350.

Briggs RM, Itaya T, Lowe DJ, Keane AJ (1989) Ages of the Pliocene-Pleistocene Alexandra and Ngatutura Volcanics, western Noah Island, New Zealand, and some geological implications. New Zealand Journal of Geology and Geophysics 32: 417-427.

Browne BL, Gardner JE, (2006) The influence of magma ascent path on the texture, mineralogy and formation of hornblende reaction rims. Earth and Planetary Science Letters 346: 161-176.

Buesch DC (1991) Changes in depositional environments resulting from emplacement of a large-volume ignimbrite. In: Fisher RV, Smith GA (Eds.) Sedimentation in Volcanic Settings. SEPM Special Publication 45: 139-153.

Bussell MR, Pillans B (1992) Vegetational and climatic history during oxygen isotope stage 9, Wanganui district, New Zealand, and correlation of the Fordell Ash. Journal of the Royal Society of New Zealand 22: 41-60.

Capra L (2006) Abrupt climatic changes as triggering mechanisms of massive volcanic collapses. Journal of Volcanology and Geothermal Research 155: 329-333.

Capra L, Macias JL (2000) Pleistocene cohesive debris flows at Nevado de Toluca Volcano central Mexico. Journal of Volcanology and Geothermal Research 102: 149-168.

Capra L, Macias JL (2002) The cohesive Naranjo debris-flow deposit (10 km3): A dam breakout flow derived from the Pleistocene debris-avalanche deposit of Nevado de Colima Volcano (México). Journal of Volcanology and Geothermal Research 117: 213-235.

Capra L, Macias JL, Scott KM (2002) Debris avalanches and debris flows transformed from collapses in the Trans-Mexican Volcanic Belt, Mexico behaviour, and implications for hazard assessment. Journal of Volcanology and Geothermal Research 113: 81-110.

Carmichael ISE (2002) The andesite aqueduct: perspectives on the evolution of intermediate magmatism in west–central (105–99_W) Mexico. Contributions to Mineralogy and Petrology 143: 641-663.

Carmichael ISE (2004) The activity of silica, water, and the equilibration of intermediate and silicic magmas. American Mineralogist 89: 1438–1446.

Carranza EJM, Castro OT (2006) Predicting Lahar-Inundation Zones: Case Study in West Mount Pinatubo, Philippines. Natural Hazards 37: 331-372.

Carrasco-Nuñez G, Vallance JW, Rose WI (1993) A voluminous avalanche-induced lahar from Citlaltepetl volcano, Mexico: implications for hazard assessment. Journal of Volcanology and Geothermal Research 59: 35-46.

Cecchi E, van Wyk de Vries B, Lavest JM (2004) Flank spreading and collapse of weak-cored volcanoes. Bulletin of Volcanology 67: 72-91.

Chanier F, Ferriere J, Angelier J (1999) Extensional deformation across an active margin, relations with subsidence, uplift, and rotations: the Hikurangi subduction, New Zealand. Tectonics 18: 862-876.

Chappell B W, White J.R (2001) Two contrasting granite types: 25 years later: Australian Journal of Earth Sciences 48, 489499. Izebekov, P., Gardner, J. E. & Eichelberger, J. C. (2004). Comagmatic granophrye and dacite from Karymsky volcanic center, Kamchakta; experimental constraints and magma storage conditions. Journal of Volcanology and Geothermal Research 131: 1-18.

Chappell J (1975) Upper Quaternary warping and uplift rates in the Bay of Plenty and West Coast, North Island, New Zealand. New Zealand Journal of Geology and Geophysics 18: 129-155.

Chase CG (1978) Extension behind island arcs and motions relative to hot spots. Journal of geophysical Research 83: 5385-5387.

Chorowicz J, Lopez E, Garcia F, Parrot J-F, Rudant J-P, Vinluan R (1997) Keys to analyze active lahars from Pinatubo on SAR ERS imagery. Remote Sensing Environment 62: 20-29.

Clavero JE, Sparks RSJ, Huppert HE (2002) Geological constraints on the emplacement mechanism of the Parinacota avalanche, northern Chile. Bulletin of Volcanology 64: 40-54.

Clavero JE, Polanco E, Godoy E, Aguilar G, Sparks S, van Wyk deVries B, Pérez de Arce C, Matthews S (2004) Substrata influence in the transport and emplacement mechanisms of the Ollagüe debris avalanche (Norhern Chile). Acta Vulcanologica 16: 31-8.

Cole JW (1978) Andesites of the Tongariro Volcanic Centre, North Island, New Zealand. Journal of Volcanology and Geothermal Research 3: 121-153.

Cole JW (1979) Structure, petrology and genesis of Cenozoic volcanism, Taupo Volcanic Zone, New Zealand: a review. New Zealand Journal of Geology and Geophysics 22: 631-657.

Cole JW (1982) Tonga-Kermadec-New Zealand. In: Thorpe RS (ed.) Andesites: Orogenic andesites and related rocks. Wiley, New York.

Cole JW (1986) Distribution and tectonic setting of late Cenozoic volcanism in New Zealand. In: Smith IEM (ed.) Late Cenozoic Volcanism in New Zealand. Bulletin of the Royal Society of New Zealand 23: 7-20.

Cole JW, Graham IJ, Hackett WR, Houghton BF (1986) Volcanology and petrology of the Quaternary composite volcanoes of Tongariro Volcanic Centre, Taupo Volcanic Zone. Royal Society of New Zealand Bulletin 23: 224-250.

Cole JW, Darby DJ, Stern TA (1995) Taupo Volcanic Zone and Central Volcanic Region: Backarc Structures of North Island, New Zealand. In: Taylor B (ed.) Backarc Basins: Tectonics and Magmatism, Springer Heidelberg, p. 1-24.

Collins BD, Dunne T (1986) Erosion of tephra from the 1980 eruption of Mount St. Helens. Bulletin of the Geological Society of America 97: 905-986.

Collinson JD, Thompson DB (1989) Sedimentary Structures. Unwin Hyman London, 207 p.

Collot J-Y, Delteil J, Lewis KB, Davy B, Lamarche G, Audru J-C, Barnes P, Chanier F, Chaumillon E, Lallemand S, Mercier de Lépinay B, Orpin A, Pelletier B, Sosson M, Toussaint B, Uruski C (1996) From oblique subduction to intra-continental transpression: structures of the southern Kermadec-Hikurangi margin from multibeam bathymetry, side scan sonar and seismic reflection. Marine Geophysical Researches 18: 357-381.

Concha-Dimas A, Cerca M, Rodríguez SR, Watters RJ (2005) Geomorphological evidence of the influence of pre-volcanic basement structure on emplacement and deformation of volcanic edifices at the Cofre de Perote-Pico de Orizaba chain and implications for avalanche generation. Geomorphology 72: 1-4.R

Cortes JA, Wilson M, Condliffe E (2005) A Calibration of an oxygen geobarometer based on clinopyroxene stoiciometry. Geophysical Research Abstracts 7:02888.

Costa JE (1984) Physical geomorphology of debris flows. In: Costa JE, Fleischer PJ (Eds.) Developments and applications of geomorphology, Springer, Berlin, p. 269-317.

Costa JE (1988) Rheologic, geomorphic, and sedimentologic differentiation of water floods, hyperconcentrated flows, and debris flows. In: Baker VR, Kochel RC, Patton PC (Eds.) Flood Geomorphology. Wiley, New York, p. 113-122.

Costa JE, Williams GP (1984) Debris-flow dynamics (videotape, 22.5 min). US Geological Survey Open-File Report 84-606.

Couch S, Harford CL, Sparks RSJ, Carroll MR (2003) Experimental constraints on the conditions of formation of highly calcic plagioclase microlites at the Soufrie`re Hills Volcano, Montserrat. Journal of Petrology 44: 1455–1475.

Coulter JD (1976) Weather in the Park. In: Fullarton JH (Ed.) Egmont National Park. Egmont National Park Board, New Plymouth, p. 51-55.

Coussot P (1995) Structural similarity and transition from Newtonian to non-Newtonian behavior for water-clay suspensions. Physical Review Letters 74: 3971-3974.

Coussot P, Piau J-M (1994) On the behaviour of fine mud suspensions. Acta Rheologica 33: 175-184.

Coussot P, Meunier M (1996) Recognition, classification and mechanical description of debris flows. Earth-Science Reviews 40: 209-227

Coussot P, Proust S (1996) Slow unconfined spreading of a mudflow. Journal of Geophysical Research 101: 25,217-25,229.

Crandell DR (1971) Post-glacial lahars from Mt. Rainier volcano, Washington. US Geological Survey Professional Paper 1444, 91 p.

Crandell DR (1989) Gigantic debris avalanche of Pleistocene age from ancestral Mount Shasta volcano, California, and debris-avalanche hazard zonation. US Geological Survey Bulletin 1861, 29 p.

Crandell DR, Miller CD, Glicken HX, Christiansen RL, Newhall CG (1984) Catastrophic debris avalanche from ancestral Mount Shasta Volcano, California. Geology 12: 143-146.

Crawford A J, Falloon,TJ, Eggins S (1987) The origin of island arc high alumina basalts. Contributions to Mineralogy and Petrology 97: 417–430.

Cronin SJ, Neall VE (1997) A late Quaternary stratigraphic framework for the northeastern Ruapehu and eastern Tongariro ring plains, New Zealand. New Zealand Journal of Geology and Geophysics 40: 185-197.

Cronin SJ, Neall VE, Palmer AS (1996) Geological history of the northeastern ring plain of Ruapehu volcano, New Zealand. Quaternary International 35: 21-28.

Cronin SJ, Neall VE, Lecointre JA, Palmer AS (1999) Dynamic interactions between lahars and stream flow: A case study from Ruapehu Volcano, New Zealand. Bulletin of the Geological Society of America 111: 28-38.

Cronin SJ, Lecointre JA, Palmer AS, Neall VE (2000a) Transformation, internal stratification, and depositional processes within a channelised, multi-peaked lahar flow. New Zealand Journal of Geology and Geophysics 43: 117-128.

Cronin SJ, Neall VE, Lecointre JA, Palmer AS (2000b) Dynamic interactions between lahars and stream flow: A case study from Ruapehu Volcano, New Zealand: Discussion and reply. Bulletin of the Geological Society of America 112: 1151-1152.

Cronin SJ, Stewart RB, Neall VE, Platz T, Gaylord D (2003) The AD1040 to present Maero Eruptive Period of Egmont Volcano, Taranaki, New Zealand. Geological Society of New Zealand Miscellaneous Publications 16A: 43.

Davey FJ (1982) The structure of the South Fiji Basin. Tectonophysics 87: 185-241.

Davidson JP & De Silva S (2000) Composite volcanoes. In: Sigurdsson H, Houghton B, McNutt S, Rymer H, Stix J (Eds.) Encyclopedia of Volcanoes, Academic Press, San Diego, p. 663-681.

Davies JH, Stevenson DJ (1992) Physical model of source region of subduction zone volcanics. Journal of Geophysical Research 97: 2037-2070.

Davies TRH (1986) Large debris flows: A macro-viscous phenomenon. Acta Mechanica 63: 161-178.

Davies TRH, McSaveney MJ (2002) Dynamic simulation of the motion of fragmenting rock avalanches. Canadian Geotechnical Journal 39: 789-798.

Davies TRH, McSaveney MJ, Hodgson KA (1999) A fragmentation spreading model for long run-out rock avalanches. Canadian Geotechnical Journal 36: 1096-1110.

Day SJ (1996) Hydrothermal pore fluid pressure and the stability of porous, permeable volcano. In: McGuire WJ, Jones AP, Neuberg J (eds.) Volcano Instability on the Earth and other Planets. Geological Society of London Special Publication 110: 77-93.

De Clarke E (1912) The Geology of the New Plymouth subdivision. New Zealand Geological Survey Bulletin NS 14.

De Rita D, Fabbri M, Mazzini I, Paccara P, Sposato A, Trigari A (2002) Volcaniclastic sedimentation in coastal environments: the interplay between volcanism and Quaternary sea level changes (central Italy). Quaternary International 95-96: 141-154

DeMets C, Gordon RG, Argus DF, Stein S (1990) Current plate motions. Geophysical Journal International 101: 425-478.

DePaolo DJ (1981) Trace-element and isotopic effects of combined wallrock assimilation and fractional crystallisation. Earth and Planetary Science Letters 53: 189–202.

DePaolo DJ, Perry FV, Baldridge WS (1992) Crustal versus mantle sources of granitic magmas—a 2-parameter model based on Nd isotopic studies. Transactions of the Royal Society of Edinburgh, Earth Sciences 83: 439–446.

Devine JD, Rutherford MJ, Gardner JE (1998) Petrologic determination of ascent rates for the 1995-97 Soufriere Hills volcano andesitic magma. Geophysical Research Letters 25: 3673-3676.

Dickinson WR, Hatherton T (1967) Andesitic Volcanism and Seismicity around the Pacific. Science 157: 801-803.

Dickson M, Fleming CA, Grant-Taylor TL (1974) Ngarino Terrace: an addition to the Late Pleistocene standard sequence in the Wanganui-Taranaki District. New Zealand Journal of Geology and Geophysics 17: 789-798.

Donnadieu F, Merle O (1998) Experiments on the indentation process during cryptodome intrusions: new insights into Mount St. Helens deformation. Geology 26:79–82

Donnadieu F, Merle O, Besson JC (2001) Volcanic edifice stability during cryptodome intrusion. Bulletin of Volcanology 63:61–72

Donoghue SL, Neall VE (1996) Tephrostratigraphic studies at Tongariro Volcanic Centre, New Zealand: an overview. Quaternary International 34: 13-20.

Donoghue SL, Neall VE (2001) Late Quaternary constructional history of the southeastern Ruapehu ring plain, New Zealand. New Zealand Journal of Geology and Geophysics 44: 439-466.

Donoghue SL, Palmer AS, McClelland E, Hobson K, Stewart RB, Neall VE, Lecointre JA, Price R (1999) The Taurewa Eruptive Episode: evidence for climatic eruptions at Ruapehu volcano, New Zealand. Bulletin of Volcanology 60: 223-240.

Dorava JM, Meyer DF (1994) Hydrologic hazards in the lower Drift River basin associated with the 1989-1990 eruptions of Redoubt Volcano, Alaska. Journal of Volcanology and Geothermal Research 62: 387-407.

Dorn RI, DeNiro MJ, Ajie HO (1987) Isotopic evidence for climatic influence on alluvial-fan development in Death Valley, California. Geology 15: 108-110.

Downey WS, Kellett RJ, Smith IEM, Price RC, Stewart RB (1994) New paleomagnetic evidence for the recent eruptive activity of Mt Taranaki, NZ. Journal of Volcanology and Geothermal Research 60: 15-28.

Druce AP (1966) Tree-ring dating of recent volcanic ash and lapilli, Mt. Egmont. New Zealand Journal of Botany 4: 3-41.

Druce AP (1970) The vegetation. In: Scanlan AB (Ed.) Egmont National Park handbook. New Plymouth, Egmont National Park Board.

Druitt TH (1995) Settling behaviour of concentrated dispersions and some volcanological applications. Journal of Volcanology and Geothermal Research 65: 27-39.

Dufeck J, Bergantz GW, (2005). Lower Crustal Magma Genesis and Preservation: a Stochastic Framework for the Evaluation of Basalt- Crust Interaction. J. Petrol. 46:2167-2195.

Dunning SA, Rosser NJ, Petley DN, Massey CR (2006) Formation and failure of the Tsatichhu landslide dam, Bhutan. Landslides 3: 107-113

Eden DN (1989) River terraces and their loessial cover beds, Awatere River valley, South Island, New Zealand. New Zealand Journal of Geology and Geophysics 32: 487-497.

Elkins-Tanton LT, Grove TL, Donnelly-Nolan J (2001) Hot shallow melting under the Cascades volcanic arc. Geology 29: 631–634.

Elsworth D, Voight B (1992) Theory of dike intrusion in a saturated porous solid. Journal of Geophysical Research 97: 9105-9118.

Elsworth D, Voight B (1995) Dike intrusion as a trigger for large earthquakes and the failure of volcano flanks. Journal of Geophysical Research 100: 6005-6024.

Elsworth D, Voight B (1996) Evaluation of volcano flank stability triggered by dyke intrusion. In: McGuire WJ, Jones AP, Neuberg J (eds.) Volcano Instability on the Earth and other Planets. Geological Society of London Special Publication 110: 281-292.

Escher BG (1922) On the hot "lahar" (mud flow) of the Valley of Ten Thousand Smokes (Alaska). Proceedings Koninklijke Nederlandse Akademie van Wetenschappen, Amsterdam 24: 282-293.

Ewart A, Brothers RN, Mateen A (1977) An outline if the geology and geochemistry, and the possible petrogenetic evolution of the volcanic rocks of the Tonga-Kermadec-New Zealand island arc. Journal of Volcanology and Geothermal Research 2: 205-250.

Ewart A, Bryan WB, Chappell BW, Rudnick RL (1994a) Regional geochemistry of the Lau–Tonga arc and back-arc systems. In: Hawkins J, Parson L, Allan J (Eds) Proceedings of the Ocean Drilling Program, Scientific Results 135. College Station, TX: Ocean Drilling Program, pp. 385–425.

Ewart A, Hawkesworth CJ (1987) The Pleistocene-Recent Tonga-Kermadec arc lavas: interpretation of new isotopic and rare earth data in terms of a depleted mantle source model. Journal of Petrology 28: 495-530.

Ewart A, Bryan WB, Gill J (1973) Mineralogy and geochemistry of the younger volcanic islands of Tonga, southwest Pacific. Journal of Petrology 14: 429-465.

Ewart A, Hergt JM, Hawkins JW (1994) Major element, trace element, and isotope (Pb, Sr and Nd) geochemistry of Site 839 basalts and basaltic andesites: implications for arc volcanism. In: Hawkins J, Parson L, Allan J (Eds) Proceedings of the Ocean Drilling Program, Scientific Results 135. College Station, TX: Ocean Drilling Program, pp. 519-531.

Ewart A, Collerson KD, Regelous M, Wendt JI, Niu Y (1998) Geochemical Evolution within the Tonga–Kermadec–Lau Arc–Back-arc Systems: the Role of Varying Mantle Wedge Composition in Space and Time. Journal of Petrology 39: 331-368.

Fink J, Malin M, D'Alli RE, Greeley R (1981) Rheological properties of mudflows associated with the spring 1980 eruption of Mount St. Helens volcano, Washington. Geophysical Research Letters 8: 43-46.

Finnerty AA, Boyd FR (1978) Pressure-dependent solubility of calcium in forsterite coexisting with diopside and andesite. Carnegie Institute Yearbook 77: 713-717.

Firth C, Stewart I, McGuire WJ, Kershaw S, Vita-Finzi C (1996) Coastal elevation changes in eastern Sicily; implications for volcano instability at Mount Etna. In: McGuire WJ, Jones AP, Neuberg J (eds.) Volcano Instability on the Earth and other Planets. Geological Society of London Special Publication 110: 153-167.

Fisher RV, Schmincke H-U (1984) Pyroclastic rocks. Springer, Heidelberg, 472 p.

Flemming CA (1953) The geology of Wanganui Subdivision. New Zealand Geological Survey Bulletin 52.

Foden JD, Green DH (1992) Possible role of amphibole in the origin of andesite: some experimental and natural evidence. Contributions to Mineralogy and Petrology 109: 479-493.

Forneris JF, Holloway JR (2003) Phase equilibria in subducting basaltic crust: implications for H2O release from the slab. Earth and Planetary Science Letters 214: 187–201.

Francis P, Self S (1987) Collapsing volcanoes. Scientific American 256: 72-90.

Frank D (1983) Origin, distribution, and rapid removal of hydrothermally formed clay at Mount Baker. US Geological Survey Professional Paper, Washington, 1022-B, p 31.

Froggatt PC, Lowe DJ (1990) A review of late Quaternary silicic and some other tephra formations from New Zealand: their stratigraphy, nomenclature, distribution, volume and age. New Zealand Journal of Geology and Geophysics 33: 89-109.

Frost BR, Lindsley D.H. (1992) Equilibria among Fe-T1 oxides. pyroxene, olivine and quartz: Part II. Application. Am. Mineral., 77: 1004-1020.

Frostick LE, Reid I (1989) Climatic versus tectonic controls of fan sequences: lessons from the Dead Sea, Israel. Journal of the Geological Society London 146: 527-538.

Gamble JA, Smith IEM, Graham IJ, Kokelaar BP, Cole JW, Houghton BF, Wilson CJN (1990) The petrology, phase relations and tectonic setting of basalts from the TVZ, New Zealand and Kermadec Island Arc-Havre Trough. Journal of Volcanology and Geothermal Research 43: 253-270.

Gamble JA, Smith IEM, McCulloch MT, Graham IJ, Kokelaar BP (1993a) The geochemistry and petrogenesis of basalts from the Taupo Volcanic Zone and Kermadec Island arc, SW Pacific. Journal of Volcanology and Geothermal Research 54: 265-290.

Gamble JA, Wright IC, Baker JA (1993b) Sea floor geology and petrology in the oceanic to continental transition zone of the Kermadec/Havre/Taupo Volcanic Zone arc system, New Zealand. New Zealand Journal of Geology and Geophysics 36: 417-435.

Gamble JA, Woodhead J, Wright I, Smith I (1996) Basalt and sediment geochemistry and magma petrogenesis in a transect from oceanic island arc to rifted continental margin arc: The Kermadec-Hikurangi margin, S.W. Pacific. Journal of Petrology 37: 1523-1546.

Gamble JA, Wood P, Price RC, Smith IEM, Waight TE (1999) A fifty year perspective of magmatic evolution on Ruapehu Volcano, New Zealand: verification of open system behaviour in an arc volcano. Earth and Planetary Science Letters 170: 30-314.

Gamble JA, Price RC, Smith IEM, McIntosh WC, Dunbar NW (2003) 40Ar/39Ar geochronology of magmatic activity, magma flux and hazards at Ruapehu volcano, Taupo Volcanic Zone, New Zealand. Journal of Volcanology and Geothermal Research 120: 271-287.

Gaylord DR, Neall VE, Palmer AS (1993) The Maitahi Formation, A Mid-Pleistocene volcanic debris avalanche assemblage, Taranaki, New Zealand. Abstract in: Volcanic activity and the environment, abstracts of the IAVCEI, Puerto Vallarta, Mexico 1997 General Assembly. Gobierno de Jalisco, Unidad Editorial, Guadalajara, Mexico.

Geddes AM, Neall VE, Stewart RB (1981) Recent discovery of the westernmost occurrences of Aokautere Ash and implications for the late Quaternary in Taranaki. In: Howorth R et al. (eds) Proceedings of Tephra Workshop. Geology Department, Victoria University of Wellington. Publication 20: 29-32.

Gibson W, Morgan PG (1927) The Geology of the Egmont subdivision. New Zealand Geological Survey Bulletin, N.S. 29.

Gill JB (1981) Orogenic Andesites and Plate Tectonics, Springer-Verlag.

Ginibre C, Worner G, Kronz A, (2002) Minor- and trace element zoning in plagioclase: implications for magma chamber processes at Parinacota Volcano, Northern Chile. Contrib. Mineral Petrol. 143:300-315 (DOI: 10.1007/s00410-002-0351-z).

Glicken H (1991) Sedimentary architecture of large volcanic debris avalanches. In: Fisher RV, Smith GA (Eds.) Sedimentation in Volcanic Settings, SEPM Special Publication 45: 99-106.

Glicken H (1996) Rockslide-debris avalanche of May 18, 1980, Mount St. Helens volcano, Washington, US Geological Survey, Open File Report 96-677, 90 p.

Gorshkov GS (1959) Gigantic eruption of the Volcano Bezymianny. Bulletin of Volcanology 20: 77-109

Gow AJ (1968) Petrographic and petrochemical studies of Mt. Egmont andesites. New Zealand Journal of Geology and Geophysics 11: 166-190.

Graham IJ, Hackett WR (1987) Petrology of calc-alkaline lavas from Ruapehu Volcano and related vents. Journal of Petrology 28: 531-567.

Grange LI (1931) Conical hills on Egmont and Ruapehu Volcanoes, New Zealand. Journal of Science and Technology 12: 376-384.

Grant-Taylor TL (1964a) Volcanic history of Western Taranaki. New Zealand Journal of Geology and Geophysics 7: 78-86.

Grant-Taylor TL (1964b) Geology of Egmont National Park. In: Scanlan AB (ed) Egmont National Park. Egmont National Park Board, New Plymouth, p. 13-26.

Grant-Taylor TL, Kear D (1970) Geology. In: Land Inventory Survey, Waimate West Country. Department of Lands and Survey, Wellington, p. 20-33.

Grant-Taylor TL, Rafter TA (1971) New Zealand radiocarbon measurements - 6. New Zealand Journal of Geology and Geophysics 14:364-402

Grove TL, Kinzler RJ (1986) Petrogenesis of andesites. Annual Review of Earth and Planetary Sciences 14: 417–454.

Grove TL, Donnelly-Nolan JM, Housh T (1997) Magmatic processes that generated the rhyolite of Glass Mountain, Medicine Lake volcano, N California. Contributions to Mineralogy and Petrology 127: 205–223.

Grove TL, Paman SW, Bowring SA, Price RC, Baker MB (2002) The role of an H2O-rich fluid component in the generation of primitive basaltic andesites and andesites from the Mt. Shasta region, N California. Contributions to Mineralogy and Petrology 142: 375-392.

Gründer K (2006) Petrography and mineral chemistry of a xenolith suite from Mt. Taranaki, New Zealand: Insights into the sub-volcanic lithosphere of an arc volcano. Unpublished Diploma thesis. Johannes-Gutenberg-Universität Mainz, Bundesrepublik Deutschland.

Hackett WR, Houghton BF (1989) A facies model for a Quaternary andesitic composite volcano - Ruapehu, New Zealand. Bulletin of Volcanology 51: 51-68

Hanes DM, Bowen AJ (1985) A granular-fluid model for steady intense bed-load transport. Journal of Geophysical Research 90: 9,149-9,158.

Hasegawa A, Nakajima J (2004) Geophysical constraints on slab subduction and arc magmatism. In: Sparks, R. S. J. & Hawkesworth, C. J. (eds) The State of the Planet: Frontiers and Challenges in Geophysics. Washington, DC: American Geophysical Union, pp. 81-94.

Hatherton T (1969) The geophysical significance of calc-alkaline andesites in New Zealand. New Zealand Journal of Geology and Geophysics 12: 436-459.

Hawkesworth CJ, Norry MJ, Roddick, JC, Baker PE, Francis PW, Thorpe RS (1979) $^{143}Nd/^{144}Nd$, $^{87}Sr/^{86}Sr$, incompatible element variations in calc-alkaline andesites and plateau lavas from South America. Earth and Planetary Science Letters 42: 45-57.

Hawkesworth CJ, Hergt JM, Ellam RM, McDermott F (1991) Element fluxes associated with subduction related magmatism. Philosophical Transactions of the Royal Society of London 335: 393-405.

Hawkesworth CJ, Gallagher K, Hergt JM, McDermott F (1993) Mantle and slab contributions in arc magmas. Annual Reviews of Earth and Planetary Science 21: 175-204.

Hay RF (1967) Sheet 7 Taranaki. Geological map of New Zealand 1:250,000. Department of Scientific and Industrial Research, Wellington, New Zealand.

Hayes SK, Montgomery DR, Newhall CG (2002) Fluvial sediment transport and deposition following the 1991 eruption of Mount Pinatubo. Geomorphology 45: 211-224.

Hayward BW (1993) The tempestuous 10 million year life of a double arc and intra-arc basin – New Zealand's Northland Basin in the Early Miocene. In: Balance PF (Ed.) South Pacific sedimentary basins. Sedimentary basins of the World 2. Amsterdam, Elsevier, pp. 113-142.

Hellstrom J, McCulloch M, Stone J (1998) A detailed 31,000-year record of climate and vegetation change from the isotope geochemistry of two New Zealand speleotherms. Quaternary Research 50: 167-178.

Herzer RH (1995) Seismic stratigraphy of a buried volcanic arc, Northland, New Zealand and implications for Neogene subduction. Marine and Petroleum Geology 12: 511-531.

Hildreth W, Moorbath S (1988) Crustal contribution to arc magmatism in the Andes of Central Chile. Contributions to Mineralogy and Petrology 98: 455-489.

Hildreth W, Fierstein J (1997) Recent eruptions of Mount Adams, Washington Cascades, USA. Bulletin of Volcanology 58: 472-49.

Hobden BJ, Houghton BF, Lanphere MA, Nairn IA (1996) Growth of the Tongariro volcanic complex: new evidence from K–Ar age determinations (Note). New Zealand Journal of Geology and Geophysics 39: 151-154.

Hoblitt RP, Walder JS, Driedger CL, Scott KM, Pringle PT, Vallance JW (1998) Volcano hazards from Mount Rainier, Washington, revised 1998. U.S. Geological Survey Open-File Report 98-428, 11p.

Hochstein MP (1995) Crustal heat transfer in the Taupo Volcanic Zone (New Zealand): comparison with other volcanic arcs and explanatory heat source models. Journal of Volcanology and Geothermal Research 68: 117-151.

Hodgson KA, Manville VR (1999) Sedimentology and flow behaviour of a rain-triggered lahar, Mangatoetoenui Stream, Ruapehu volcano, New Zealand. Bulletin of the Geological Society of America 5: 743-754.

Holt WE, Haines AJ (1995) The kinematics of northern South Island, New Zealand, determined from geologic strain rates. Journal of Geophysical Research 100: 17,991-18,010.

Houghton BJ, Nairn IA (1991) The 1976-1982 Strombolian and phreatomagmatic eruptions of White Island, New Zealand: eruptive and depositional mechanisms at a 'wet' volcano. Bulletin of Volcanology 54: 25-49.

Houghton BJ, Wilson CJN, McWilliams MO, Lanphere MA, Weaver SD, Briggs RM, Pringle MS (1995) Chronology and dynamics of a large silicic magmatic system: Central Taupo Volcanic Zone, New Zealand. Geology 23: 13-16.

Hubert JF, Filipov AJ (1989) Debris flow deposits in alluvial fans of the west flank of the White Mountains, Owens Valley, California, USA. Sedimentary Geology 61: 177-205.

Hull AG, Dellow G (1993) Earthquake hazards in the Taranaki region. Institute of Geological and Nuclear Sciences Client Report 1993/03, Institute of Geological and Nuclear Sciences Ltd, Lower Hutt.

Humphreys MCS, Blundy JD, Sparks RSJ (2006) Magma evolution and open-system processes at Shiveluch Volcano: Insights from phenocrysts zoning. Journal of Petrology 47: 2303-2334.

Huppert HE, Sparks SJ (1988) The generation of granitic magma by intrusion of basalt into continental crust. Journal of Petrology 29: 599-624.

Imbrie J, Hays JD, Martinson DG, McIntyre A, Mix AC, Mortley JJ, Pisias NG, Prell WL, Shackleton NJ (1984) The orbital theory of Pleistocene climate: support from a revised chronology of the marine δ18O record. In: Berger AL, Imbrie J, Hays H, Kukla G, Saltzman B (Eds.) Milankovitch and climate, Part I. Reidel Publishing, Dordrecht, p. 269-305.

Innes JL (1983) Debris flows. Progress in Physical Geography 7: 469-501.

Isacks BL, Barazangi M (1977) Geometry of Benioff zones: Lateral segmentation and downwards bending of the subducted lithosphere. In: Talwani M, Pittman III WC (eds.) Island Arcs, Deep Sea Trenches and Back Arc Basins. American Geophysical Union, Maurice Ewing Series 1, p. 94-117.

Issac MJ, Herzer R, Brook FJ, Hayward B (1994) Cretaceous and Cenozoic geology of Northland, New Zealand. Institute of Geological and Nuclear Sciences Monograph 8, Institute of Geological and Nuclear Sciences Ltd, Lower Hutt, 203 p.

Iverson RM (1997a) Hydraulic modelling of unsteady debris-flow surges with solid-fluid interactions. In: Chen CL (Ed.) Debris-flow Hazards Mitigation: Mechanics, Prediction, and Assessment. American Society of Civil Engineers, p. 550-560.

Iverson RM (1997b) The physics of debris flows. Reviews of Geophysics 35: 245-296.

Iverson RM (2005) Debris-flow mechanics. In: Jakob M, Hungr O (Eds.) Debris-flow Hazards and Related Phenomena, Springer, Heidelberg, p. 105-134.

Iverson RM, Denlinger RP (1987) The physics of debris flows - A conceptual assessment. In: Beschta RL, Blinn T, Grant, GE Ice GG, Swanson FJ (Eds.) Erosion and Sedimentation in the Pacific Rim. International Association of Hydrological Sciences Publication 165: 155-165.

Iverson RM, Vallance JW (2001) New views of granular mass flows. Geology 29: 115-118.

Iverson RM, Costa JE, LaHusen RG (1992) Debris flow flume at H. J. Andrews Experimental Forest, Oregon: US Geological Survey Open-File Report 92-483, 2 p.

Iverson RM, Reid ME, La Husen RG (1997) Debris-flow mobilization from landslides. Annual Reviews in Earth and Planetary Science 25: 85-138.

Jackson MD, Cheadle MJ, Atherton MP (2003) Quantitative modeling of granitic melt generation and segregation in the continental crust. Journal of Geophysical Research 108: 2332.

Janda RJ, Scott KM, Nolan KM. Martinson HA (1981) Lahar movement, effects, and deposits. In: Lipman PW & Mullineaux DR (Eds.) The 1980 eruptions of Mount St. Helens, Washington, US Geological Survey Professional Papers 1250: 347-377.

Jarrard RD (1986) Relations among subduction parameters. Reviews of Geophysics 24: 217-284.

Johnson AM, Rodine JR (1984) Debris flow. In: Brunsden D, Prior DB (Eds.) Slope Instability. Wiley, New York, p. 257-361.

Jull M, Kelemen PB (2001) On the conditions for lower crustal convective instability. Journal of Geophysical Research 106: 6423-6446.

Jurewicz AJG, Watson EB (1988) Cations in olivine Pt I: calcium partitioning and calcium-magnesium distribution between olivines and coexisting melts, with petrologic applications. Contributions to Mineralogy and Petrology 99: 176-185.

Kamp PJJ, Vonk AJ, Bland KJ, Hansen RJ, Hendy AJW, McIntyre AP, Ngatai M, Cartwright SJ, Hayton S, Nelson CS (2004) Neogene stratigraphic architecture and tectonic evolution of Wanganui, King Country, and eastern Taranaki Basins, New Zealand. New Zealand Journal of Geology and Geophysics 47: 625-644.

Karatson D (1996) Rates and factors of stratovolcano degradation in a continental climate: a complex morphometric analysis for nineteen Neogene-Quaternary crater remnants in the Carpathians. Journal of Volcanology and Geothermal Research 73: 65-78.

Karig DE (1970) Kermadec Arc-New Zealand tectonic confluence. New Zealand Journal of Geology and Geophysics 13: 21-29.

Kataoka K, Nakajo T (2002) Volcaniclastic resedimentation in distal fluvial basins induced by large-volume explosive volcanism: the Ebisutoge–Fukuda tephra, Plio-Pleistocene boundary, central Japan. Sedimentology 49: 319-334.

Kay RW, Kay SM (1993) Delamination and delamination magmatism. Tectonophysics 219: 177-189.

Keppler H (1996) Constraints from partitioning experiments on the composition of subduetion-zone fluids. Nature 380: 237-240.

Kim SB, Chough SK, Chun SS (1995) Bouldery deposits in the lowermost part of the Cretaceous Kyokpori Formation, SW Korea: Cohesionless debris flows and debris falls on a steep-gradient delta slope. Sedimentary Geology 98: 97-119.

Kimbrough DL, Tulloch AJ, Coombs DS, Landis CA, Johnston MR, Martinson JM (1994) Uranium-lead zircon ages from the Median Tectonic Zone, South Island, New Zealand. New Zealand Journal of Geology and Geophysics 37: 393-419.

King PR (1991) Physiographic maps of the Taranaki Basin - Late Cretaceous to Recent. New Zealand Geological Survey report, G155.

King PR (2000) Tectonic reconstructions of New Zealand: 40 Ma to the present. New Zealand Journal of Geology and Geophysics 43: 611-638.

King PR, Thrasher GP (1996) Cretaceous–Cenozoic geology and petroleum systems of the Taranaki Basin, New Zealand. I Institute of Geological and Nuclear Sciences Monograph 13, Institute of Geological and Nuclear Sciences Ltd, Lower Hutt, 243 p.

King PR, Scott GH, Robinson PH (1993) Description, correlation and depositional history of Miocene sediments outcropping along the North Taranaki coast. Institute of Geological and Nuclear Sciences Monograph 5, Institute of Geological and Nuclear Sciences Ltd, Lower Hutt, 199 p.

Kohlbeck F, Mojica J, Scheidegger AE (1994) Clast orientation of the 1985 lahars of the Nevado del Ruiz, Colombia and implications for depositional processes. Sedimentary Geology 88: 175-183.

Labazuy P (1996) Recurren landslide events on the submarine flank of Piton de la Fournaise Volcano (Reunion Island). In: McGuire WJ, Jones AP, Neuberg J (eds.) Volcano Instability on the Earth and other Planets. Geological Society of London Special Publication 110: 295–306.

Lagmay AMF, Valdivia W (2006) Regional influence on the opening direction of crater amphitheatres in Southeast Asian volcanoes. Journal of Volcanology and Geothermal Research 158: 139-150.

Lagmay AMF, van Wyk de Vries B, Kerle N, Pyle DM (2000) Volcano instability induced by strike-slip faulting. Bulletin of Volcanology 62: 331-346.

Landi P, Metrich N, Bertagnini A, Rosi M, (2004) Dynamics of magma mixing and degassing recorded in plagioclase at Stromboli (Aeolian Archipelago, Italy). Contributions to Mineralogy and Petrology 147: 629-631.

Lavigne F (2004) Rate of sediment yield following small-scale volcanic eruptions: a quantitative assessment at the Merapi and Semeru stratovolcanoes, Java, Indonesia. Earth Surfaces and Landform Processes 29: 1045-1058.

Lavigne F, Thouret JC (2000) Les lahars: dépôts, origines et dynamique. Bulletin de la Société Géologique de France 171: 545-557.

Lavigne F, Thouret JC (2002) Sediment transportation and deposition by rain-triggered lahars at Merapi volcano, central Java, Indonesia. Geomorphology 49: 45-69.

Lavigne F, Suva H (2004) Contrasts between debris flows, hyperconcentrated flows and stream flows at a channel of Mount Semeru, East Java, Indonesia. Geomorphology 61: 41-58.

Lavigne F, Thouret JC, Voight B, Suwa H, Sumaryono A (2000) Lahars at Merapi volcano, Central Java: an overview. Journal of Volcanology and Geothermal Research 100: 423-456.

Le Maitre RW, Bateman P, Dudek A, Keller J, Lameyre J, Le Bas ML, Sabine PA,. Scmid R, Sørensen H, Streckeisen A, Woolley AR, Zanettin.B (1989) A classification of igneous rocks and glossary of terms. Blackwell Scientific Publications, Oxford, UK.

Leake BE, Woolley AR, Arps CES, Birch WD, Gilbert MC, Grice JD, Hawthorne FC, Kato A, Kisch HJ, Krivovichev VG, Linthout K, Laird J, Mandarino J, Maresch WV, Nickel EH, Rock NMS, Schumacher JC, Smith DC, Stephenson NCN, Ungaretti L, Whittaker EJW,, Youzhi G (1997a) Nomenclature of amphiboles: report of the Subcommittee on amphiboles of the International Mineralogical Association Commission on new minerals and mineral names. Mineralogical Magazine 61: 295-321.

Leake BE, Woolley AR, Arps CES, Birch WD, Gilbert MC, Grice JD, Hawthorne FC, Kato A, Kisch HJ, Krivovichev VG, Linthout K, Laird J, Mandarino JA, Maresch WV, Nickel EH, Rock NMS, Schumacher JC, Smith DC, Stephenson NCN, Ungaretti L, Whittaker EJW, Guo YZ (1997b) Nomenclature of amphiboles: report of the Subcommittee on amphiboles of the International Mineralogical Association Commission on new minerals and mineral names. American Mineralogist 82: 1019-1037.

Leake BE, Woolley AR, Birch WD, Burke EAJ, Ferraris G, Grice JD, Hawthorne FC, Kisch HJ, Krivovichev VG, Schumacher JC, Stephenson NCN, Whittaker EJW (2003) Nomenclature of amphiboles: additions and revisions to the International Mineralogical Association's 1997 recommendations. Canadian Mineralogist 41: 1355-1362.

Leavesley GH, Lusby GC, Lichty RW (1989) Infiltration and erosion characteristics of selected tephra deposits from the 1980 eruption of Mount St. Helens, Washington, USA. Hydrological Sciences 34: 339-353.

Lecointre JA, Neall VE, Palmer AS (1998) Quaternary lahar stratigraphy of the western Ruapehu ring plain, New Zealand. New Zealand Journal of Geology and Geophysics 41: 225-245.

Lensen GJ (1959) Sheet 10 Wanganui. Geological map of New Zealand 1:250,000. Department of Scientific and Industrial Research, Wellington, New Zealand.

Lian OB, Shane PA (2000) Optical dating of paleosols bracketing the widespread Rotoehu tephra, North Island, New Zealand. Quaternary Science Reviews 19: 1649-1662.

Lipman PW (1995) Declining growth of Mauna Loa during the last 100,000 years: rates of lava accumulation vs. gravitational subsidence. In: Rhodes JM, Lockwood JP (Eds.) Mauna Loa

Revealed, Structure, Composition, History and Hazards. American Geophysical Union, Washington, D.C., Geophysical Monograph 92: 45-80.

Lipman PW, Mullineaux DR (Eds.) (1981) The 1980 eruptions of Mount St. Helens, Washington. US Geological Survey Professional Papers 1250, 844 p.

Lopez DL, Williams SN (1993) Catastrophic volcanic collapse: relation to hydrothermal processes. Science 260: 1794-1796.

Lowe DR (1979) Sediment gravity flows - Their classification and some problems of application to natural flows and deposits. In: Doyle LJ, Pilkey OH Jr (Eds.) Geology of continental slopes. Society of Economic Paleontologists and Mineralogists Special Publication 27: 75-82.

Lowe DR, LoPiccolo RD (1974) The Characteristics and Origins of Dish and Pillar Structures Journal of Sedimentary Petrology 44: 484-501.

Major JJ (1993) Rheometry of natural sediment slurries. In: Proceedings of ASCE National Conference on Hydraulic Engineering 1993, San Francisco. American Society of Civil Engineers, New York. 7 pp.

Major JJ (1996) Experimental studies of deposition by debris flows: Process, characteristics of deposits and effects of pore-fluid pressure, Unpublished PhD Thesis, University of Washington, Seattle, 341 pp.

Major JJ (1997) Depositional processes in large-scale debris-flow experiments. Journal of Geology 105: 345-366

Major JJ (2000) Gravity-driven consolidation of granular slurries - Implications for debris-flow deposition and deposit characteristics. Journal of Sedimentary Research 70: 64-83.

Major JJ (2003) Post-eruption hydrology and sediment transport in volcanic river systems. In: Water Resources IMPACT 5: 10-15.

Major JJ (2004) Posteruption suspended sediment transport at Mount St. Helens: Decadal-scale relationships with landscape adjustments and river discharges. Journal of Geophysical Research 109: doi:10.1029/2002JF000010.

Major JJ, Voight B (1986) Sedimentology and clast orientations of the 18 May 1980 southwest-flank lahars, Mount St. Helens, Washington. Journal of Sedimentary Petrology 56: 691-705.

Major JJ, Scott KM (1988) Volcaniclastic sedimentation in the Lewis River Valley, Mount St. Helens, Washington; processes, extent, and hazards: US Geological Survey Bulletin 1383-D, 38p.

Major JJ, Newhall CG (1989) Snow and ice perturbation during historical volcanic eruptions and the formation of lahars and floods. Bulletin of Volcanology 52: 1-27

Major JJ, Pierson TC (1990) Rheological analysis of fine-grained natural debris-flow material. In: French RH (Ed.) Hydraulics/Hydrology of Arid Land (H2AL). ASCE, New York, pp. 225-231.

Major JJ, Pierson TC (1992) Debris flow rheology: Experimental analysis of fine-grained slurries. Water Resources Research 28: 841-857.

Major, JJ, Iverson RM (1999) Debris-flow deposition - Effects of pore-fluid pressure and friction concentrated at flow margins. Bulletin of the Geological Society of America 111: 1424-1434.

Major JJ, Mark LE (2006) Peak flow responses to landscape disturbances caused by the cataclysmic 1980 eruption of Mount St. Helens, Washington. Bulletin of the Geological Society of America 118: 938-958.

Major JJ, Janda RJ, Daag AS (1996) Watershed disturbance and lahars on the east side of Mount Pinatubo during the mid-June 1991 eruptions. In: Newhall CG, Punongbayan RS (Eds.) Fire and mud: Eruptions and lahars of Mount Pinatubo, Philippines. Philippine Institute of Volcanology and Seismology, Quezon City and University of Washington Press, Seattle, pp. 895-919.

Major JJ, Pierson TC, Scott KM (2005) Debris flows at Mount St. Helens, Washington, USA. In: Jakob M and Hungr O (Eds.) Debris-flow hazards and related phenomena. Springer Berlin Heidelberg, p. 685-731.

Manville V (2002) Sedimentary and geomorphic responses to a large ignimbrite eruption: readjustment of the Waikato River in the aftermath of the A.D. 181 Taupo eruption, New Zealand. Journal of Geology 110: 519-542.

Manville V, Wilson CJN (2004) The 26.5 ka Oruanui eruption, New Zealand: a review of the roles of volcanism and climate in the post-eruptive sedimentary response. New Zealand Journal of Geology and Geophysics 47: 422-442.

Manville VR, Hodgson KA, White JDL (1998) Rheological properties of a remobilised tephra lahar associated with the 1995 eruptions of Ruapehu volcano, New Zealand. New Zealand Journal of Geology and Geophysics 41: 157-165.

Manville V, White JDL, Hodgson KA (2000) Dynamic interactions between lahars and stream flow: A case study from Ruapehu Volcano, New Zealand: Discussion and reply. Bulletin of the Geological Society of America 112: 1149-1151.

Manville V, Newton EH, White JDL (2005) Fluvial responses to volcanism: resedimentation of the 1800a Taupo ignimbrite eruption in the Rangitaiki River catchment, North Island, New Zealand. Geomorphology 65: 49-70

McArthur JL, Shepherd MJ (1990) Late Quaternary glaciation of Mt. Ruapehu, North Island, New Zealand. Journal of the Royal Society of New Zealand 20: 287-296.

McCulloch MT, Gamble JA (1991) Geochemical and geodynamic constraints on subduction zone magmatism. Earth and Planetary Science Letters 102: 358-374.

McCulloch MT, Perfit MR (1981) $^{143}Nd/^{144}Nd$, $^{87}Sr/^{86}Sr$ and trace element constraints on the petrogenesis of Aleutian island arc magmas. Earth and Planetary Science Letters 56: 167-169.

McDougall JC, Gibb JG (1970) Patea sediments. New Zealand Oceanographic Institute chart, coastal series 1:200,000.

McGlone MS, Neall VE (1994) The late Pleistocene and Holocene vegetation history of Taranaki, North Island, New Zealand. New Zealand Journal of Botany 3: 251-269.

McGlone MS, Neall VE, Pillans BJ (1984) Inaha terrace deposits: a late Quaternary terrestrial record in South Taranaki, New Zealand. New Zealand Journal of Geology and Geophysics 27: 35-49.

McGlone MS, Neall VE, Clarkson BD (1988) The effect of recent volcanic events and climate changes on the vegetation of Mt Taranaki (Egmont), New Zealand. New Zealand Journal of Botany 26: 123-144.

McGlone MS, Mildenhall DC, Pole MS (1996) History and paleoecology of New Zealand Nothofagus forests. In: Veblen TT, Hill RS, Read J (Eds.) The ecology and biogeography of Nothofagus forest Yale University Press, New Haven, USA, p. 83-130.

McGuire WJ (1996) Volcano instability: a review of contemporary themes. In: McGuire WJ, Jones AP, Neuberg J (Eds.) Volcano Instability on the Earth and other Planets. Geological Society of London Special Publication 110: 1-24.

McGuire WJ (2003) Volcanic instability and lateral collapse. Revista 1: 33-45.

McGuire WJ, Jones AP, Neuberg J (Eds.) (1996) Volcano Instability on the Earth and other Planets. Geological Society of London Special Publication 110, 388 pp

Meyer DF, Trabant DC (1995) Lahars from the 1992 eruptions of Crater Peak, Mount Spurr Volcano, Alaska. In: Keith TEC (Ed.) The 1992 Eruptions of Crater Peak Vent, Mount Spurr Volcano, Alaska. US Geological Survey Bulletin 2139, p. 183-198.

Middleton GV, Hampton MA (1976) Subaqueous sediment transport and deposition by sediment gravity flows. In: Stanley DJ, Swift DJP (Eds.) Marine Sediment Transport and Environment Management vol. 11. Wiley, New York, pp. 197-218.

Middleton GV, Southard JB (1984) Mechanics of sediment movement. Society of Economic Palaeontologists and Mineralogists, Eastern Section, Short Course 3, 401 p.

Mimura K, Kawachi S (1981) Nirasaki debris-avalanche, a catastrophic event at the Yatsugatake volcanic chain, central Japan (abstract). In: Proceedings IAVCEI Symposium. Tokyo and Hakone, p. 237.

Mimura K, Kawachi S, Fijimoto U, Taneichi M, Hyuga T, Ichikawa S, Koizumi M (1982) Debris-avalanche hills and their natural remnant magnetisation - Nirasaki debris-avalanche, central Japan. Journal of the Geological Society of Japan 88: 653-663.

Miskovic A, Francis D (2006) Interaction between mantle-derived and crustal calc-alkaline magmas in the petrogenesis of the Paleocene Sifton Range volcanic complex, Yukon, Canada. Lithos 87: 104-134.

Mizuno Y (1964) Landforms associated with volcanic debris flows at the foot of Zao Volcano. Hirosaki University Faculty Bulletin 13: 23-32.

Monzier M, Robin C, Samaniego P, Hall ML, Cotten J, Mothes P, Arnaud N (1999) Sangay volcano, Ecuador: structural development, present activity and petrology. Journal of Volcanology and Geothermal Research 90: 49-79.

Moore JG, Normark WR, Holcomb RT (1994) Giant Hawaiian landslides. Annual Reviews of Earth and Planetary Sciences 22: 119-144.

Morgan PG, Gibson W (1927) The geology of the Egmont subdivision, Taranaki. New Zealand Geological Bulletin 29: 92 p.

Morimoto (1989) Nomenclature of pyroxenes. Canadian Mineralogist 27: 143-156.

Moriya I (1980) Bandaian eruption and landforms associated with it. In: Collection of articles in memory of retirement of Prof. Hishimura, 66. Tohoku University, Tokyo, 214-219.

Morrice MG, Gill JB (1986) Spatial patterns in the mineralogy of island arc magma series: Sangihe Arc, Indonesia. Journal of Volcanology and Geothermal Research 29: 311-353.

Mortazavi M, Sparks RSJ (2004) Origin of rhyolite and rhyodacite lavas and associated mafic inclusions of Cape Akrotiri, Santorini: the role of wet basalt in generating calcalkaline silicic magmas. Contributions to Mineralogy and Petrology 146: 397–413.

Mortimer N, Tulloch AJ, Ireland TR (1997) Basement geology of Taranaki and Wanganui Basins, New Zealand. New Zealand Journal of Geology and Geophysics 40: 223-236.

Mortimer N, Herzer RH, Gans PB, Parkinson DL, Seward D (1998) Basement Geology from Three Kings Ridge to West Norfolk Ridge, southwest Pacific Ocean: evidence from petrology, geochemistry and isotopic dating of dredge samples. Marine Geology 148: 135-162.

Mothes PA, Hall ML, Janda RJ (1998) The enormous Chillos Valley Lahar: an ash-flow-generated debris flow from Cotopaxi Volcano, Ecuador. Bulletin of Volcanology 59: 233-244.

Muntener O, Kelemen PB, Grove TL (2001) The role of H2O during crystallisation of primitive arc magmas under uppermost mantle conditions and genesis of igneous pyroxenites: an experimental study. Contributions to Mineralogy and Petrology 141: 643–658.

Murai I (1961) A study of the textural characteristics of pyroclastic flow deposits in Japan. Bulletin of the Earthquake Research Institute, Tokyo University 39: 133-248.

Murray JB (1988) The influence of loading by lavas on the sitting of volcanic eruption vents on Mt. Etna. Journal of Volcanology and Geothermal Research 35: 121-139.

Murray JB, Voight B (1996) Slope stability and eruption preduction on the eastern flank of Mount Etna. In: McGuire WJ, Jones AP, Neuberg J (Eds.) Volcano Instability on the Earth and other Planets. Geological Society of London Special Publication 110: 111-114.

Naish TR, Kamp PJJ, Alloway BV, Pillans BJ, Wilson GS, Westgate JA (1995) Tephrostratigraphy and integrated chronology for Pliocene-Pleistocene marine cyclothemic strata, Wanganui Basin: implications for the Pliocene-Pleistocene boundary in New Zealand. Quaternary International 34-36: 29-49.

Nakagawa M, Wada K, Thordarson T, Wood CP, Gamble JA (1999) Petrologic investigations of the 1995 and 1996 eruptions of Ruapehu volcano, New Zealand: formation of discrete and small magma pockets and their intermittent discharge. Bulletin of Volcanology 61: 15-31.

Nakagawa M, Wada K, Wood CP (2002) Mixed magmas, mush chambers and eruption triggers: Evidence from zoned clinopyroxene phenocrysts in andesitic scoria from the 1995 eruption of Ruapehu Volcano, New Zealand. Journal of Petrology 43: 2279-2303.

Nakamura K (1977) Volcanoes as possible indicators of tectonic stress orientation - principle and proposal. Journal of Volcanology and Geothermal Research 2: 1-16.

Neall VE (1971) Volcanic domes and lineations in Egmont National Park. New Zealand Journal of Geology and Geophysics 14: 71-81.

Neall VE (1972) Tephrochronology and tephrostratigraphy of western Taranaki (N108-109), New Zealand. New Zealand Journal of Geology and Geophysics 15: 507-57.

Neall VE (1975) Climate-controlled tephra redeposition on Pouakai ring plain, Taranaki, New Zealand. New Zealand Journal of Geology and Geophysics 18: 317-326.

Neall VE (1976a) Lahars as major geological hazards. Bulletin of the International Association of Engineering Geology 14: 233-240.

Neall VE (1976b) Lahars - Global occurrence and annotated bibliography. Victoria University Wellington, New Zealand, Publication 5, 18 p.

Neall VE (1976c) Genesis and weathering of Andosols in Taranaki, New Zealand. Soil Science 123: 400-408.

Neall VE (1979) Sheets P19, P20 and P2l New Plymouth, Egmont and Manaia, Geological Map of New Zealand 1:50,000. 3 maps and notes, 36 p. New Zealand Department of Science and Industrial Research, Wellington.

Neall VE (2003) The volcanic history of Taranaki. Institute of Natural Resources - Massey University, Soil & Earth Sciences Occasional Publication No. 2.

Neall VE, Alloway BE (2004) Quaternary Geological Map of Taranaki. Institute of Natural Resources - Massey University, Soil & Earth Sciences Occasional Publication No. 4.

Neall VE, Stewart RB, Smith IEM (1986) History and petrology of the Taranaki volcanoes: Royal Society of New Zealand Bulletin 23: 251-263.

Nehlig P, Leyrit H, Dardon A, Freour G, de Goer de Herve A, Huguet D, Thieblemont D (2001) Constructions et destructions du stratovolcan du Cantal. Bulletin de la Société Géologique de France 172: 295-308.

Nelson CS, Mildenhall DC, Todd AJ, Pocknall DT (1988) Subsurface stratigraphy, palaeoenvironments, palynology and depositional history of the late Neogene Tauranga Group at Ohinewai, lower Waikato lowland, south Auckland, New Zealand. New Zealand Journal of Geology and Geophysics 31: 21-40.

Nelson CS, Cooke PJ, Hendy CH, Cuthbertson AM (1993) Oceanographic and climatic changes over the past 160 000 years at Deep Sea Drilling Project Site 594 off southeastern New Zealand, Southwest Pacific Ocean. Paeloceanography 8 (4): 435-458.

Nelson ST, Montana A (1992) Sieve textured plagioclase produced in volcanic rocks by rapid decompression. American Mineralogist 77: 1242-1249.

Németh K, Martin U (2007) Practical Volcanology. Occasional Papers of the Geological Institute of Hungary, Budapest, v. 207.

Neumann van Padang M (1939) Ueber die vielen tausend Huegel im westlichen Vorlande des Raoeng-Vulkans (Ostjava). Ing Ned Indies 6: 35-41.

Newhall CG, Punongbayan RS (Eds.) (1996) Fire and mud: Eruptions and lahars of Mount Pinatubo, Philippines. Philippine Institute of Volcanology and Seismology, Quezon City and University of Washington Press, Seattle, 1126 p.

Newnham RM, Alloway BV (2004) A terrestrial record of interglacial climate preserved by voluminous debris-avalanche inundation in Taranaki, Western North Island, New Zealand. Journal of Quaternary Science 19: 299-314.

Newnham RM, Lowe DJ, Williams PW (1999) Quaternary environmental change in New Zealand: A review. Progress in Physical Geography 23: 567-610.

Normark WR, Moore JG, Torresan ME (1993) Giant volcano-related landslides and the development of the Hawaiian Islands. In: Schwab WCH, Lee J, Twichell DC (Eds.) Submarine Landslides: Selected Studies in the U.S. Exclusive Economic Zone. US Geological Survey Bulletin 2002, pp. 184-196.

Norris RJ, Cooper AF (2000) Late Quaternary slip rates and slip partitioning on the Alpine Fault, New Zealand. Journal of Structural Geology 23: 507-520.

Nunn PD (1994) Oceanic Islands. Blackwell, Oxford. 413 pp.

O'Brien JS, Julien PY (1988) Laboratory analysis of mudflows properties. Journal of Hydraulic Engineering 14: 877-887.

Palmer AS (1987) Late Pleistocene loess in southern North Island New Zealand. In: Liu T (Ed.) Aspects of Loess Research, China Ocean Press, Beijing, pp. 204-215.

Palmer AS, Pillans BJ (1996) Record of climatic fluctuations from ca. 500 ka loess deposits and paleosols near Wanganui, New Zealand. Quaternary International 34-36: 155-162.

Palmer BA, Neall VE (1989) The Murimotu Formation, 9500-year old deposits of a debris avalanche and associated lahars, Mount Ruapehu, North Island, New Zealand. New Zealand Journal of Geology and Geophysics 32: 477-486.

Palmer BA, Neall VE (1991) Contrasting lithofacies architecture in ring plain deposits related to edifice construction and destruction, the Quaternary Stratford and Opunake Formations, Egmont Volcano, New Zealand. Sedimentary Geology 74: 71-88.

Palmer BA, Alloway BV, Neall VE (1991) Volcanic-debris-avalanche deposits in New Zealand - lithofacies organisation in unconfined, wet-avalanche flows. In: Fisher RV, Smith GA (Eds.) Sedimentation in Volcanic Settings, SEPM Special Publication 45: 89-98.

Palmer BA, Purves AM, Donoghue SL (1993) Controls on accumulation of a volcaniclastic fan, Ruapehu composite volcano, New Zealand. Bulletin of Volcanology 55: 176-189.

Pareschi MT, Favalli M, Giannini F, Sulpizio R, Zanchetta G, Santacroce R (2000) May 5, 1998, debris flows in circum-Vesuvian areas (southern Italy): insights for hazard assessment. Geology 28: 639-642.

Parfitt R, Pollok JA, Furkert RJ (Eds) (1981) Guide Book for Tour 1, Pre-Conference North Island. Soils with Variable Charge Conference, Palmerston North New Zealand. PD Hasselberg, Government Printer, Wellington, New Zealand, 153 p.

Parish A (1994) Petrology and Provenance of the O'Leary Conglomerate, North East Wanganui, New Zealand. Unpublished B.Sc. Thesis, Victoria University of Wellington, 89 pp.

Parman SW, Grove T L (2004) Harzburgite melting with and without H2O: experimental data and predictive modeling. Journal of Geophysical Research 109. doi:10.1029/2003JB002566.

Parson LM, Wright IC (1996) The Lau-Havre-Taupo back-arc basin: A southward-propagating, multi-stage evolution from rifting to spreading. Tectonophysics 263: 1-22.

Patterson DB, Graham IJ (1988) Petrogenesis of andesitic lavas from Mangatepopo Valley and Upper Tama Lake, Tongariro Volcanic Centre, New Zealand. Journal of Volcanology and Geothermal Research 35: 17-29.

Pearce JA (1982) Trace element characteristics of lavas from destructive plate boundaries. In: Thorpe RS (ed.) Orogenic Andesites and Related Rocks. Wiley. p. 525-548.

Pearce TH, Kolisnik AM (1990) Observations of plagioclase zoning using interference imaging. Earth Science Reviews 29: 9-26.

Perfit MR, Gust DA, Bence AE, Arculus RJ, Taylor SR (1980). Chemical characteristics of island arc basalts: implicationsfor mantle sources. Chemical Geology 30: 227–256.

Petford, N. & Atherton M (1996) Na-rich partial melts from newly underplated basaltic crust: the Cordillera Blanca Batholith, Peru. Journal of Petrology 37: 1491–1521.

Petford N, Gallagher K (2001) Partial melting of mafic (amphibolitic) lower crust by periodic influx of basaltic magma. Earth and Planetary Science Letters 193: 483-489.

Pichavant M, Martel C, Bourdier JL, Scaillet B (2002a) Physical conditions, structure, and dynamics of a zoned magma chamber: Mount Pelée (Martinique, Lesser Antilles Arc). Journal of Geophysical Research 107, article number 2093.

Pierson TC (1980) Erosion and deposition by debris flows at Mount Thomas, North Canterbury, New Zealand. Earth Surface Processes 5:227-247.

Pierson TC (1981) Dominant particle support mechanisms in debris flows at Mt. Thomas, New Zealand, and implications for flow mobility. Sedimentology 28: 49-60.

Pierson TC (1984) Why debris flows stop (abstract). Geological Society of America Abstracts with Programs 16: 623.

Pierson TC (1986) Flow behavior in channelized debris flows, Mount St. Helens, Washington. In: Abrahams AD (Ed.) Hillslope processes. Boston, Allen and Unwin, p. 269-296.

Pierson TC (1998) An empirical method for estimating travel times for wet volcanic mass flows. Bulletin of Volcanology 60: 98-109.

Pierson TC (2005) Hyperconcentrated flow - transitional process between water flow and debris flow. In: Jakob M, Hungr O (Eds.) Debris-flow Hazards and Related Phenomena, Springer, Heidelberg, p. 159-202.

Pierson TC, Scott KM (1985) Downstream dilution of a lahar: transition from debris flow to hyperconcentrated streamflow. Water Resource Research 12: 1511-1524.

Pierson TC, Costa JE (1987) A rheologic classification of subaerial sediment-water flows. Geological Society of America Reviews in Engineering Geology 7: 1-12.

Pierson TC, Janda RJ (1994) Volcanic mixed avalanches: a distinct eruption-triggered mass-flow process at snow-clad volcanoes. Bulletin of the Geological Society of America 106: 1351-1358.

Pierson TC, Janda RJ, Thouret J-C, Borrero CA (1990) Perturbation and melting of snow and ice by the 13 November 1985 eruption of Nevado del Ruiz, Colombia and consequent mobilization, flow and deposition of lahars. Journal of Volcanology and Geothermal Research 41: 17-66.

Pierson TC, Janda RJ, Umbal JV, Daag AS (1992) Immediate and long-term hazards from lahars and excess sedimentation in rivers draining Mt. Pinatubo, Philippines. U.S. Geological Survey Water-Resources Investigations Report 92-4039, 35 p.

Pierson TC, Daag AS, Delos Reys PJ, Regalado MTM, Solidum R, Tubianosa BS (1996) Flow and deposition of posteruption hot lahars on the east side of Mount Pinatubo, July-October 1991. In: Newhall CG, Punongbayan RS (Eds.) Fire and mud: Eruptions and lahars of Mount Pinatubo, Philippines. Philippine Institute of Volcanology and Seismology, Quezon City and University of Washington Press, Seattle, p. 921-950.

Pillans BJ (1983) Upper Quaternary marine terrace chronology and deformation South Taranaki, New Zealand. Geology 11: 292-297.

Pillans B (1986) A late Quaternary uplift map for North Island, New Zealand. Royal Society of New Zealand Bulletin 24: 409-417.

Pillans BJ (1988) Loess chronology in Wanganui Basin, New Zealand. In: Eden DN & Furkett RJ (Eds.), Loess, Its Distribution, Geology and Soils. Balkema, Rotterdam, pp. 175-191.

Pillans BJ (1990a) Late Quaternary marine terraces, south Taranaki- Wanganui (NZMS sheet Q22 and part sheets Q20, Q21, R21 and R22) 1:100,000. New Zealand Geological Survey Miscellaneous Series Map, 18. New Zealand Department of Scientific and Industrial Research, Wellington.

Pillans BJ (1990b) Pleistocene terraces in New Zealand: a review. New Zealand Journal of Geology and Geophysics 33: 219-231.

Pillans BJ (1994) Direct marine-terrestrial correlations, Wanganui Basin, New Zealand: the last 1 million years. Quaternary Science Reviews 13: 189-200.

Pillans BJ, McGlone MS, Palmer AS, Mildenhall D, Alloway BV, Berger GW (1993) The Last Glacial Maximum in central and southern North Island, New Zealand: a palaeoenvironmental reconstruction using the Kawakawa Tephra Formation as a chronostratigraphic marker. Palaeogeography, Palaeoclimatology, Palaeoecology 101: 283-304.

Plank T, Langmuir CH (1988) An evaluation of the global of arc magmas: evidence from high-pressure experiments and natural variations in the major element chemistry of arc basalts. Planetary Science Letters 90: 349–370.

Plank T, Langmuir CH (1993) Tracing trace elements from sediment input to volcanic output at subduction zones. Nature 362: 739-742.

Platz T (2007) Aspects of Dome-forming Eruptions from Andesitic Volcanoes through the Maero Eruptive Period (1000 yrs BP to Present) Activity at Mt. Taranaki, New Zealand. Unpublished PhD Thesis, INR, Massey University, New Zealand.

Platz T, Cronin SJ, Cashman KV, Stewart RB, Smith IEM (2007a) Transition from effusive to explosive phases in andesite eruptions - A case-study from the AD1655 eruption of Mt. Taranaki, New Zealand. Journal of Volcanology and Geothermal Research 161: 15-34.

Platz T, Cronin SJ, Smith IEM, Turner MB, Stewart RB (2007b) Improving the reliability of microprobe-based analyses of andesitic glasses for tephra correlation. The Holocene 17: 573-583.

Pollet N, Schneider JL (2004) Dynamic disintegration processes accompanying transport of the Holocene Flims sturzström (Swiss Alps). Earth and Planetary Science Letters 221: 433-448.

Ponomareva VV, Pevzner MM, Melekestsev IV (1998) Large debris avalanches and associated eruptions in the Holocene eruptive history of Shiveluch Volcano, Kamchatka, Russia. Bulletin of Volcanology 59: 490-505.

Ponomareva VV, Melekestsev IV, Dirksen OV (2006) Sector collapses and large landslides on Late Pleistocene–Holocene volcanoes in Kamchatka, Russia. Journal of Volcanology and Geothermal Research 158: 117-138

Porter SC (1975) Equilibrium line altitudes of late Quaternary glaciers in the Southern Alps, New Zealand. Quaternary Research 5: 27-47.

Price RC, McCulloch MT, Smith IEM, Stewart RB (1992) Pb-Nb-Sr isotopic compositions and trace element characteristics of young volcanic rocks from Egmont Volcano and comparisons with basalts and andesites from the Taupo Volcanic Zone, New Zealand. Geochimica et Cosmochimica Acta 56: 941-953.

Price RC, Stewart RB Woodhead JD, Smith IE (1999) Petrogenesis of High-K Arc Magmas: Evidence from Egmont Volcano, North Island, New Zealand. Journal of Petrology 40: 167-197.

Price RC, Gamble JA, Smith IEM, Stewart RB, Eggins S, Wright IC (2005) An integrated model for the temporal evolution of andesites and rhyolites and crustal development in New Zealand's North Island. Journal of Volcanology and Geothermal Research 140: 1-24.

Price RC, Smith IEM, Gamble JA, Zernack AV, and Stewart RB (2007a) Magmatic processes and the evolution of crust: Insights from the New Zealand/Kermadec subduction system. Abstract A810 in: 17th Annual VM Goldschmidt Conference, Cologne, Germany.

Price R, Zernack AV, Smith IE, Gamble J, and Stewart RB (2007b) Mantle source compositions for the basaltic component in North Island andesitic volcanoes – A lithospheric source for Taranaki andesites? In: Geological Society of New Zealand Miscellaneous Publication 123A, p. 134.

Pringle PT, Cameron KA (1997) Eruption-triggered lahar on May 14, 1984. In: Pierson TC (Ed.) Hydrologic consequences of hot rock/snowpack interactions at Mount St. Helens Volcano, Washington. US Geological Survey Open-File Report 96-179: 81-103.

Procter JN, Cronin SJ, Zernack AV (2009) Landscape and Sedimentary Response to Catastrophic Debris Avalanches, Western Taranaki, New Zealand. *In*: K. Nemeth, V. Manville, and K. Kano (Eds.) Source to sink: from volcanic eruptions to volcaniclastic deposits, *Sedimentary Geology Special Volume. (In Press)*

Prouteau G, Scaillet B (2003) Experimental constraints on the origin of the 1991 Pinatubo dacite. Journal of Petrology 44: 2203-2241.

Qian N, Wan Z (1986) A critical review of the research on the hyperconcentrated flow in China. International Research Training Centre on Erosion and Sedimentation Publication, China.

Qian Y, Yang W, Zhao W, Cheng X, Zhang L, Xu W (1981) Basic characteristics of flow with hyperconcentration of sediment. In: Proceedings of International Symposium on River Sedimentation. Chinese Society of Hydraulic Engineering, Beijing, p. 175-184.

Raia F, Spera FJ (1997) Simulation of the growth and differentiation of continental crust. Journal of Geophysical Research 102: 22629–22648.

Rapp RP, Watson EB (1995) Dehydration melting of metabasalt at 8–32 kbar - implications for continental growth and crust–mantle recycling. Journal of Petrology 36: 891–931.

Rattenbury M, Begg J, Edbrooke S, Heron D, Lee J, Townsend D (2007) The Qmap 1:250,000 geological map of New Zealand: Linking Cape Reinga to Stewart Island. In: Geological Society of New Zealand Miscellaneous Publication 123A, p. 137.

Reading AM, Gubbins D, Mao W (2001) A multiphase seismic investigation of the shallow subduction zone, southern North Island, New Zealand. Geophysical Journal International 147: 215-226.

Reid ME, Sisson TW, Brien DL (2001) Volcano collapse promoted by hydrothermal alteration and edifice shape, Mount Rainier, Washington. Geology 29: 779-782.

Richards JP, Villeneuve M (2001) The Llullaillaco volcano, northwestern Argentina: construction by Pleistocene volcanism and destruction by edifice collapse. Journal of Volcanology and Geothermal Research 105: 77-105

Rieder M, Cavazzini G, D'Yakonov Y, Frank-Kamenetskii VA, Gottardi G, Guggenheim S, Koval PV, Müller G, Neiva AMR, Radoslovich EW, Robert J-L, Sassi FP, Takeda H, Weiss Z, Wones DR (1998) Nomenclature of the micas. Canadian Mineralogist 36: 905-912.

Ringwood A.E (1974) Petrological evolution of island arc systems. Journal of the Geological Society, London 130: 183–204.

Ritter JB, Miller JR, Enzel Y, Wells SG (1995) Reconciling the roles of tectonism and climate in Quaternary alluvial fan evolution. Geology 23: 245-248.

Rodolfo KS (1989) Origin and early evolution of lahar channel at Mabinit, Mayon volcano, Philippines. Bulletin of the Geological Society of America 101: 414-426.

Rodolfo KS, Arguden AT (1991) Rain-lahar generation and sediment-delivery systems at Mayon volcano, Philippines. In: Fisher RV, Smith GA (Eds.) Sedimentation in Volcanic Settings. SEPM Special Publication 45: 71-87.

Rodolfo KS, Umbal JV, Alonso RA, Remotique CT, Paladio-Melosantos ML, Salvador JHG, Evangelista D, Miller Y (1996) Two years of lahars on the western flank of Mount Pinatubo: Initiation, flow processes, deposits, and attendant geomorphic and hydraulic changes. In: Newhall CG, Punongbayan RS (Eds.) Fire and mud: Eruptions and lahars of Mount Pinatubo, Philippines. Philippine Institute of Volcanology and Seismology, Quezon City and University of Washington Press, Seattle, pp. 989-1013.

Rosenthal A (2005) Mapping and characterisation of the eastern Fanthams Peak lavas, Egmont Volcano, Taranaki, New Zealand. Unpublished Diploma mapping thesis. Technische Universitaet Bergakademie Freiberg, Freiberg, Bundesrepublik Deutschland.

Rutherford MJ, Devine JD (1988) The May 18, 1980, eruption of Mount St. Helens, 3. Stability and chemistry of amphibole in the magma chamber. Journal of Geophysical Research 93: 11,949-11,959.

Rutherford MJ, Hill PM (1993) Magma ascent rates from amphibole breakdown—an experimental study applied to the 1980– 1986 Mount St. Helens eruptions. Journal of Geophysical Research 98: 19,667-19,685.

Salvador A (Ed.) (1994) International stratigraphic guide. A guide to stratigraphic classification, terminology, and procedure (2nd ed.). Subcommission on Stratigraphic Classification of IUGS International Commission on Stratigraphy and Geological Society of America. Boulder, Colorado, 214 pp.

Saunders AD, Tarney J, Weaver SD (1980) Transverse geochemical variations across the Antarctic Peninsula: Implications for the genesis of calc-alkaline magmas. Earth and Planetary Science Letters 46: 344–360.

Saunders AD, Norry MJ, Tarney J (1991) Fluid influence Formation, Mt Egmont, New Zealand. Journal of Volcanology and Geothermal Research 27: 255–264.

Schmidt MW, Poli S (1998) Experimentally based water budgets for dehydrating slabs and consequences for arc magma generation. Earth and Planetary Science Letters 163: 361–379.

Schumacher JC (1997) The estimation of ferric iron in electron-microprobe analysis of amphiboles. Appendix 2. In: Leake BE Woolley AR, Arps CES, Birch WD, Gilbert MC, Grice JD, Hawthorne FC, Kato A, Kisch HJ, Krivovichev VG, Linthout K, Laird J, Mandarino JA, Maresch WV, Nickel EH, Rock NMS, Schumacher JC, Smith DC, Stephenson NCN, Ungaretti L, Whittaker EJW, Youzhi G (eds.) Nomenclature of amphiboles: report of the Subcommittee on amphiboles of the International Mineralogical Association, Commission on new minerals and mineral names. Canadian Mineralogist 35: 238-246.

Schuster RL, Crandell DR (1984) Catastrophic debris avalanches from volcanoes. Proceedings IV Symposium on landslides, Toronto 1: 567-572.

Scott KM (1988a) Origins, behaviour, and sedimentology of lahars and lahar-runout flows in the Toutle-Cowlitz River system. US Geological Survey Professional Paper 1447-A, 74 p.

Scott KM (1988b) Origin, behaviour, and sedimentology of prehistoric catastrophic lahars at Mount St. Helens, Washington. Geological Society of America Special Paper 229: 23-36.

Scott KM (1989) Magnitude and frequency of lahars and lahar runout flows in the Toutle-Cowlitz river system. US Geological Survey Professional Paper 1447-B: 1-33.

Scott KM (2001) Catastrophic debris flows transformed from landslides in volcanic terrains: mobility, hazard assessment and mitigation strategies. US Geological Survey Professional Paper 1630, 59 p.

Scott KM, Vallance JW, Pringle PT (1995) Sedimentology, behaviour, and hazards of debris flows at Mount Rainier, Washington. US Geological Survey Professional Paper 1547, 56 p.

Scott KM, Janda RJ, de la Cruz EG, Gabinete E, Eto I, Isada M, Sexon M, Hadley KC (1996) Channel and sedimentation responses to large volumes of 1991 volcanic deposits on the east flank of Mount Pinatubo. In: Newhall CG, Punongbayan RS (Eds.) Fire and mud: Eruptions and lahars of Mount Pinatubo, Philippines. Philippine Institute of Volcanology and Seismology, Quezon City and University of Washington Press, Seattle, pp. 971-988.

Scott KM, Macías JL, Naranjo J, Rodriguez S, McGeehin JP (2001) Catastrophic debris flows transformed from landslides in volcanic terrains: mobility, hazard assessment and mitigation strategies. US Geological Survey Professional Papers 1630, 59 p.

Scott KM, Vallance JW, Kerle N, Macías JL, Strauch W, Devoli G (2005) Catastrophic precipitation-triggered lahar at Casita volcano, Nicaragua: occurrence, bulking and transformation. Earth Surface Processes and Landforms 30: 59-79.

Scott WE, Iverson RM, Vallance JW, Hildreth W (1995) Volcano Hazards in the Mount Adams Region, Washington. U.S. Geological Survey Open-File Report 95-492, 11 p.

Scott WE, Pierson TC, Schilling SP, Costa JE, Gardner CA, Vallance JW, Major JJ (1997) Volcano hazards in the Mount Hood region, Oregon. U.S. Geological Survey Open-File Report 97-89, 14 pp.

Sdrolias M, Müller RD (2006) Controls on back-arc basin formation. Geochemistry, Geophysics, Geosystems 7, Q04016, doi:10.1029/2005GC001090.

Segschneider B, Landis CA, Manville V, White JDL, Wilson CJN (2002a) Environmental response to a large, explosive rhyolite eruption: lithofacies and physical sedimentology of post-1.8 ka pumice-rich Taupo volcaniclastics in the Hawke's Bay region, New Zealand. Sedimentary Geology 150: 275-299.

Segschneider B, Landis CA, White JDL, Wilson CJN, Manville V (2002b) Resedimentation of the 1.8 ka Taupo ignimbrite in the Mohaka and Ngaruroro river catchments, Hawke's Bay, New Zealand. New Zealand Journal of Geology and Geophysics 45: 85-102.

Shackleton NJ, Berger A, Peltier WR (1990) An alternative astronomical calibration of the lower Pleistocene timescale based on ODP Site 677. Transactions of the Royal Society of Edinburgh Earth Sciences 81: 251-261.

Shane P, Sandiford A (2003) Paleovegetation of marine isotope stages 4 and 3 in northern New Zealand and the age of the widespread Rotoehu tephra. Quaternary Research 59: 420-429.

Shea T, van Wyk de Vries B, Pilato M (2008) Emplacement mechanisms of contrasting debris avalanches at Volcán Mombacho (Nicaragua), provided by structural and facies analysis. Bulletin of Volcanology DOI 10.1007/s00445-007-0177-7

Shell, BP and Todd Oil Services Ltd (1974) Maui Development. Environmental Impact Report 1, June 1974. Shell, BP and Todd Oil Services Limited, New Plymouth.

Sherburn S, White RS (2005) Crustal seismicity in Taranaki, New Zealand using accurate hypocentres from a dense network. Geophysical Journal International 162: 494-506.

Sherburn S, White RS (2006) Tectonics of the Taranaki region, New Zealand: earthquake focal mechanisms and stress axes. New Zealand Journal of Geology and Geophysics 49: 269-279.

Sheridan MF, Bonnard C, Carreo R, Siebe C, Strauch W, Navarro M, Calero JC, Trujilo NB (1999) Report of the 30 October 1998 rock fall/ avalanche and breakout flow of Casita volcano, Nicaragua, triggered by Hurricane Mitch. Landslide News 12: 2-4.

Shreve RL (1968) The Blackhawk landslide. Geological Society of America Special Paper 108: 1-47.

Siebe C, Komorowski J-C, Sheridan MF (1992) Morphology and emplacement of an unusual debris-avalanche deposit at Jocotitlan volcano, Central Mexico. Bulletin of Volcanology 54: 573-589.

Siebert L (1984) Large volcanic debris avalanches: Characteristics of source area, deposits, and associated eruptions. Journal of Volcanology and Geothermal Research 22: 163-197.

Siebert L (1996) Hazards of large volcanic debris avalanches and associated eruptive phenomena. In: Scarpa R, Tilling RI (Eds.) Monitoring and mitigation of volcano hazards. Springer-Verlag, Berlin Heidelberg, p. 541-572.

Siebert L, Glicken H, Ui T (1987) Volcanic hazards from Bezymianny- and Bandai-type eruptions. Bulletin of Volcanology 49: 435-459.

Siebert L, Beget JE, Glicken H (1995) The 1883 and late-prehistoric eruptions of Augustine volcano, Alaska. Journal of Volcanology and Geothermal Research 66: 367-395.

Singer BS, Dungan MA, Layne GD, (1995) Texturees and Sr, BA, Mg, Fe, K andTi Compositional Profiles in Plagioclase – Clues to the Dynamic of Calc-Alkaline Magma Chambers. Am Mineral 80:776-798.

Sisson TW, Grove TL (1993) Experimental investigations of the role of H2O in calc-alkaline differentiation and subduction zone magmatism. Contributions to Mineralogy and Petrology 113: 143–166.

Sisson TW, Bronto S (1998) Evidence for pressure-release melting beneath magmatic arcs from basalt at Galunggung, Indonesia. Nature 391: 883–886.

Smith DR, Leeman WP (1987) Petrogenesis of Mount St. Helens dacitic magmas. Journal of Geophysical Research 92: 10313–10334.

Smith EGC, Stern T, Reyners M (1989) Subduction and back-arc activity at the Hikurangi convergent Margin, New Zealand. 129: 203-231.

Smith GA (1986) Coarse-grained nonmarine volcaniclastic sediment: Terminology and depositional process. Bulletin of the Geological Society of America 97: 1-10.

Smith GA (1987a) Sedimentology of volcanism-induced aggradation in fluvial basins: Examples from the Pacific Northwest, USA. In: Ethridge FG, Flores RM, Harvey MG (Eds.) Recent developments in fluvial sedimentology. Society of Economic Palaeontologists and Mineralogists Special Publication 39: 217-228.

Smith GA (1987b) The influence of explosive volcanism on fluvial sedimentation: The Deschutes Formation (Neogene) in central Oregon. Journal of Sedimentary Petrology 57: 613-629.

Smith GA (1991) Facies Sequences and geometries in continental volcaniclastic settings. In: Fisher RV, Smith GA (Eds.) Sedimentation in Volcanic Settings, SEPM Special Publication 45: 109-121.

Smith GA, Vincent KR (1987) Rates of sedimentation, subsidence, and volcanism as controls on facies architecture in terrestrial volcaniclastics. Geological Society of America Abstracts with Programs 19: 845.

Smith GA, Fritz WJ (1989) Volcanic influences on terrestrial sedimentation. Geology 17: 375-376.

Smith GA, Lowe DR (1991) Lahars: Volcano-hydrologic events and deposition in the debris flow-hyperconcentrated flow continuum. In: Fisher RV, Smith GA (Eds.) Sedimentation in Volcanic Settings. SEPM Special Publication 45: 60-70.

Smith GM, Davies TR, McSaveney MJ, Bell DH (2006) The Acheron rock avalanche, Canterbury, New Zealand - morphology and dynamics. Landslides 3:62–72

Smith IEM, Price RC (2006) The Tonga–Kermadec arc and Havre–Lau back-arc system: Their role in the development of tectonic and magmatic models for the western Pacific. Journal of Volcanology and Geothermal Research 156: 315-331.

Smith IEM, Price RC, Stewart RB (1996) Young eruptives from Taranaki: a window into a magma chamber. Geological Society of New Zealand Miscellaneous Publication 91A, 157.

Smith RCM (1991) Landscape response to a major ignimbrite eruption, Taupo Volcanic Center, New Zealand. In: Fisher RV, Smith GA (Eds.) Sedimentation in volcanic settings. SEPM Special Publication 45: 123-137.

Smith RD, Swanson FJ (1987) Sediment routing in a small drainage basin in the blast zone at mount St. Helens, WA, USA. Geomorphology 1: 1-13.

Sohn YK (1997) On traction-carpet sedimentation. Journal of Sedimentary Research 67: 502-509.

Stern CR (2004) Active Andean volcanism: its geologic and tectonic setting. Revista Geologica de. Chile 31: 161-206.

Stern TA (1985) A back-arc basin formed within continental lithosphere: the Central Volcanic Region of New Zealand. Tectonophysics 112: 385-409.

Stern TA (1987) Asymmetric back-arc spreading, heat flux and structure associated with the Central Volcanic Region of New Zealand. Earth and Planetary Science Letters 85: 265-276.

Stern TA, Stratford WR, Salmon ML (2006) Subduction evolution and mantle dynamics at a continental margin: Central North Island, New Zealand. Reviews of Geophysics 44: 1-36.

Stewart DC (1975) Crystal clots in calc-alkaline andesites as breakdown product of high-Al amphiboles. Contributions to Mineralogy and Petrology 53: 195-204.

Stewart ML, Fowler AD (2001) The nature and occurrence of discrete zoning in plagioclase from recently erupted volcanic rocks, Montserrant. Journal of Volcanology and Geothermal Research 106:243-253.

Stewart RB, Neall VE, Pollock JA, Syers JK (1977) Parent material stratigraphy of an Egmont loam profile, Taranaki, New Zealand. Australian Journal of Soil Research 15: 177-190.

Stewart RB, Neall VE, Syers JK (1986) Origin of quartz in selected soils and sediments, North Island, New Zealand. New Zealand Journal of Geology and Geophysics 29: 147-152.

Stewart RB, Price RC, Smith IE (1996) Evolution of high-K arc magma, Egmont volcano, Taranaki, New Zealand: evidence from mineral chemistry. Journal of Volcanology and Geothermal Research 74: 275-295.

Stipp JJ (1968) The geochronology and petrogenesis of Cenozoic volcanics of the North Island, New Zealand. Unpublished PhD thesis, Australian National University, Canberra, 438 pp.

Stoopes GR, Sheridan MF (1992) Giant debris avalanches from the Colima Volcanic Complex, Mexico: Implication for long-runout landslides (>100 km). Geology 20: 299-302.

Stormer JC (1973) Calcium zoning in olivine and its relationship to silica activity and pressure. Geochimica Cosmochimica Acta 37: 1815-1821.

Suggate RP, Stevens GR, Te Punga MT (1978) The geology of New Zealand. Government Printer, Wellington, 2 volumes, 820 p.

Sulpizio R, Zanchetta G, Paterne M, Siani G (2003) A review of tephrostratigraphy in central and southern Italy during the last 65 ka. Il Quaternario, Italian Journal of Quaternary Science 16: 91-108.

Sun S-S, McDonough WF (1989) Chemical and isotopic systematics of oceanic basalts: Implications for mantle composition and processes. In: Saunders AD, Norry MJ (eds) Magmatism in the Ocean Basins. Geological Society Special Publication 42: 313-345.

Sutherland R (1999) Basement geology and tectonic development of the greater New Zealand region: an interpretation from regional magnetic data. Tectonophysics 308: 341-362.

Swanson FJ, Collins B, Dunne T, Wicherski BP (1983) Erosion of tephra from hillslopes near Mt. St. Helens and other volcanoes. In: Proceedings of the Symposium on Erosion Control in Volcanic Areas. Technical Memorandum of the Public Works Research Institute, vol. 1908. Ministry of Construction, Japan, pp. 183-221.

Sykes LR (1966) The seismicity and deep structure of island arcs. Journal of Geophysical Research 71: 2981-3005.

Takahashi T (1981) Debris flows. Annual Reviews of Fluid Mechanics 13: 57-77.

Tanaka H, Kawamura K, Nagao K, Houghton BF (1997) K-Ar ages and paleosecular variation of direction and intensity from Quaternary Lava Sequences in the Ruapehu Volcano, New Zealand. Journal of Geomagnetism and Geoelectricity 49: 587-599.

Tatsumi Y (1982) Origin of high-magnesian andesites in the Setouchi Volcanic Belt, Southwest Japan, 2. Melting phase-relations at high pressures. Earth and Planetary Science Letters 60: 305–317.

Tatsumi,Y, Eggins S (1995) Subduction Zone Magmatism. Oxford: Blackwell Scientific.

Tatsumi,Y Kogiso T (2003) The subduction factory: its role in the evolution of the Earth's crust and mantle. Geological Society of London Special Publications 219: 55-80.

Tepper JH, Nelson BK, Bergantz GW, Irving AJ (1993) Petrology of the Chiilwack batholith, North Cascades, Washington. Generation of calc-alkaline granitoids by melting of mafic lower crust with variable water fugacity. Contributions to Mineralogy and Petrology 113: 333–351.

Thouret JC (2005) The stratigraphy, depositional processes, and environment of the late Pleistocene Polallie-period deposits at Mount Hood Volcano, Oregon, USA. Geomorphology 70: 12-32.

Thouret JC, Cantagrel J-M , Robin C, Murcia A, Salinas R, Cepeda H (1995) Quaternary eruptive history and hazard-zone model at Nevado de Tolima and Cerro Machin Volcanoes, Colombia. Journal of Volcanology and Geothermal Research 66: 397-426.

Thouret JC, Abdurachman KE, Bourdier JL, Bronto S (1998) Origin, characteristics, and behaviour of lahars following the 1990 eruption of Kelud volcano. Bulletin of Volcanology 59: 460-480.

Thouret JC, Lecointre JA, Neall VE, Cronin SJ, Wallace RC (2006) The Whangaehu Formation: a massive debris-avalanche from ancestral Ruapehu? In: Geological Society of New Zealand Miscellaneous Publication 122A, p. 103.

Thouret JC, Lavigne F, Suwa H, Sukatja B, Surono (2007) Volcanic hazards at Mount Semeru, East Java (Indonesia), with emphasis on lahars. Bulletin of Volcanology 70: 221-244.

Tibaldi A (1995) Morphology of pyroclastic cones and tectonics. Journal of Geophysical Research 100: 24521-24535.

Tibaldi A (1996) Mutual influence of dyking and collapses at Stromboli volcano, Italy. In: McGuire WJ, Jones AP, Neuberg J (Eds.) Volcano Instability on the Earth and other Planets. Geological Society of London Special Publication 110: 55-63.

Tibaldi A (2001) Multiple sector collapses at Stromboli volcano Italy: how they work. Bulletin of Volcanology 63: 112-125.

Tibaldi A, Lagmay AMF (2006) Interaction between volcanoes and their basement. Journal of Volcanology and Geothermal Research 158: 1-5.

Tibaldi A, Lagmay AMF, Ponomareva V (2005) Effects of basement structural and stratigraphic heritages on volcano behaviour and implications for human activities. Episodes 28: 158-170.

Todd SM (1989) Stream-driven, high-density gravelly traction carpets: possible deposits in the Trabeg Conglomerate Formation, SW Ireland and some theoretical consideration of their origin. Sedimentology 36: 513-530.

Tschuiyama A (1985) Dissolution kinetics of plagioclase in the melt of the system di-ab-an and the origin of dusty plagioclase in andesite. Contributions to Mineralogy and Petrology 81: 1-16.

Turner MB (2008) Eruption cycles and magmatic processes at a reawakening volcano, Mt. Taranaki, New Zealand. Unpublished PhD Thesis, INR, Massey University, New Zealand.

Turner MB, Cronin SJ, Bebbington MS, Platz T (2008a) Developing a probabilistic eruption forecast for dormant volcanoes; a case study from Mt Taranaki, New Zealand. Bulletin of Volcanology 70: 507-515. DOI: 10.1007/s00445-007-0151-4.

Turner MB, Cronin SJ, Stewart RB, Bebbington M, Smith IEM (2008b) Using titanomagnetite textures to elucidate volcanic eruption histories. Geology 36: 31-34.

Ui T (1983) Volcanic dry avalanche deposits: identifications and comparison with nonvolcanic debris stream deposits. Journal of Volcanology and Geothermal Research 18: 135-150.

Ui T (1989) Discrimination between debris avalanches and other volcaniclastic deposits. In: Latter JH (Ed.) Volcanic Hazards. Springer, Heidelberg, 625 p.

Ui T, Kawachi S, Neall VE (1986a) Fragmentation of debris avalanche material during flowage - evidence from the Pungarehu Formation, Mount Egmont, New Zealand. Journal of Volcanology and Geothermal Research 27: 255-264.

Ui T, Yamamoto H, Suzuki-Kamata K (1986b) Characterisation of debris avalanche deposits in Japan. Journal of Volcanology and Geothermal Research 29: 231-243.

Ui T, Takarada S, Yoshimoto M (2000) Debris avalanches. In: Encyclopedia of Volcanoes, p. 617-626.

Ulmer P (2001) Partial melting in the mantle wedge - the role of H_2O in the genesis of mantle-derived 'arc-related' magmas. Physics of the Earth and Planetary Interiors 127: 215–232.

Vallance JW (2000) Lahars. In: Sigurdsson H, Houghton B, McNutt S, Rymer H, Stix J (Eds.) Encyclopedia of Volcanoes, Academic Press, San Diego, p. 601-616.

Vallance JW, Scott KM (1997) The Osceola Mudflow from Mount Rainier; sedimentology and hazard implications of a huge clay-rich debris flow: Bulletin of the Geological Society of America 109: 143-163.

Vallance JW, Siebert L, Rose WI Jr, Giron JR, Banks NG (1995) Edifice collapse and related hazards in Guatemala. Journal of Volcanology and Geothermal Research 66: 337-355.

Vames DJ (1978) Slope movement types and processes. In: Schuster RL, Krizek RJ (Eds.) Landslides: Analysis and Control. National Academy of Sciences, Washington, D.C. Transportation Research Board Special Report 176: l-33.

Van Benmelen (1949) The geology of Indonesia, vol. IA. General geology of Indonesia and adjacent archipelagos, 732 pp, vol. IB (portfolio), 60 pp.

Van Dissen R, Yeats RS (1991) Hope fault, Jordan thrust, and uplift of the Seaward Kaikoura Range, New Zealand. Geology 19: 393-396.

Van Steijn H (1988) Debris flows involved in the development of Pleistocene stratified slope deposits. Zeitschrift fuer Geomorphologie NF 71: 45-58.

Van Westen CJ, Daag AS (2005) Analysing the relation between rainfall characteristics and lahar activity at Mount Pinatubo, Philippines. Earth Surface Processes and Landforms 30: 1663-1674.

Van Wyk de Vries B, Borgia A (1996) The role of basement in volcano deformation. In: McGuire WJ, Jones AP, Neuberg J (eds.) Volcano Instability on the Earth and other planets. Geological Society of London Special. Publication 110: 95-110.

Van Wyk de Vries B, Merle O (1996) The effect of volcanic constructs on rift fault patterns. Geology 24: 643-646.

Van Wyk de Vries B, Francis PW (1997) Catastrophic collapse at statovolcanoes induced by gradual volcano spreading. Nature 387: 387-390.

Van Wyk de Vries B, Kerle N, Petley D (2000) Sector collapse forming at Casita volcano, Nicaragua. Geology 28: 167-170.

Van Wyk de Vries B, Self S, Francis PW, Keszthelyi L (2001) A gravitational spreading origin for the Socompa debris avalanche. Journal of Volcanology and Geothermal Research 105: 225-247.

Varnes DJ (1958) Landslide types and processes. In: Eckel EB (Ed.) Landslides and engineering. Highway Research Board Special Report 29: 20-47.

Vidal N, Merle O (2000) Reactivation of basement faults beneath volcanoes: a new model for flank collapse. Journal of Volcanology and Geothermal Research 99: 9-26.

Voight B, Sousa J (1994) Lessons from Ontake-san: a comparative analysis of debris avalanche dynamics. Engineering Geology 38: 261-297.

Voight B, Elsworth D (1997) Failure of volcano slopes. Geotechnique 47: 1-31.

Voight B, Glicken H, Janda RJ, Douglass PM (1981) Catastrophic rockslide avalanche of May 18. In: Lipman PW & Mullineaux DR (Eds.) The 1980 eruptions of Mount St. Helens, Washington, US Geological Survey Professional Papers 1250: 347-377.

Voight B, Janda RJ, Glicken H, Douglass PM (1983) Nature and mechanism of the Mount St. Helens rockslide-avalanche of May 1980. Geotechnique 33: 243-273.

Vucetich CG, Pullar WA (1969) Stratigraphy and chronology of late Pleistocene volcanic ash beds in central North Island, New Zealand. New Zealand Journal of Geology and Geophysics 12: 784-837.

Vukadinovic D, Nicholls IA (1989) The petrogenesis of island arc basalts from Gunung Slamet volcano, Indonesia: trace element and 87Sr/86Sr constraints. Geochimica et Cosmochimica Acta 53: 2349–2363.

Waight TE, Price RC, Stewart RB, Smithe IEM, Gamble J (1999) Stratigraphy and geochemistry of the Turoa area, with implications for andesite petrogenesis at Mt Ruapehu, Taupo Volcanic Zone, New Zealand. New Zealand Journal of Geology and Geophysics 42: 513-532.

Waitt RB Jr, Pierson TC, MacLeod NS, Janda RJ, Voight B, Holcomb RT (1983) Eruption-triggered avalanche, flood and lahar at Mount St. Helens: effects of winter snowpack. Science 22: 1394-1397.

Wallace LM, Beavan J, McCaffrey R, Darby D (2004) Subduction zone coupling and tectonic block rotations in the North Island, New Zealand. Journal of Geophysical Research 109: B12406, doi:10.1029/2004JB003241.

Walton AW, Palmer BA (1988) Lahar facies of the Mount Dutton Formation (Oligocene-Miocene) in the Marysvale volcanic field, southwestern Utah. Bulletin of the Geological Society of America 100: 1078-1091.

Wan Z, Wang Z (1994) Hyperconcentrated flow. AA Balkema, Rotterdam, 290 pp.

Waresback DB, Turbeville BN (1990) Evolution of a Plio-Pleistocene volcanogenic–alluvial fan: the Puye formation, Jemez Mountains, New Mexico. Bulletin of the Geological Society of America 102: 298-314.

Waythomas CF (1999) Stratigraphic framework of Holocene volcaniclastic deposits, Akutan Volcano, east-central Aleutian Islands, Alaska. Bulletin of Volcanology 61: 141-161.

Waythomas CF, Miller TP (1999) Preliminary volcano-hazard assessment for Iliamna Volcano, Alaska. U.S. Geological Survey Open-File Report 99-373, 31 pp.

Waythomas CF, Miller TP, Beget JE (2000) Record of Late Holocene debris avalanches and lahars at Iliamna Volcano, Alaska. Journal of Volcanology and Geothermal Research 104: 97-130.

Waythomas CF, Wallace KL (2002) Flank collapse at Mount Wrangell, Alaska, recorded by volcanic mass-flow deposits in the Copper River lowland. Canadian Journal of Earth Sciences 39: 1257-1279.

Wellman HW (1962) Holocene of the North Island of New Zealand: a coastal reconnaissance. Transactions of the Royal Society of New Zealand Geology 1: 29-99.

Wentworth CM (1967) Dish structure, a primary sedimentary structure in coarse turbidites. Bulletin of the American Association of Petroleum Geologists 51: 485.

Whipple K, Dunne T (1992) The influence of debris-flow rheology on fan morphology, Owens Valley, California. Bulletin of the Geological Society of America 104: 887-900.

White FM (2006) Viscous Fluid Flow. New York, NY: McGraw Hill.

Wilson CJN (1993) Stratigraphy, chronology, styles and dynamics of late Quaternary eruptions from Taupo volcano, New Zealand. Philosophical Transactions of the Royal Society of London A343: 205-305.

Wilson CJN (2001) The 26.5 ka Oruanui eruption, New Zealand: An introduction and overview. Journal of Volcanology and Geothermal Research 112: 133-174.

Wilson CJN, Houghton BF, McWilliams MO, Lanphere MA, Weaver SD, Briggs RM (1995) Volcanic and structural evolution of Taupo Volcanic Zone, New Zealand: a review. Journal of Volcanology and Geothermal Research 68: 1-28.

Wilson CJN, Switsur VR, Ward AP (1988) A new 14C age for the Oruanui (Wairakei) eruption, New Zealnad. Geological Magazine 125: 297-300.

Wooller L, van Wyk de Vries B, Murray JB, Rymer H, Meyer S (2004) Volcano spreading controlled by dipping substrata. Geology 32: 573-576.

Wright VP, Alonzo Zarza AM (1990) Pedostratigraphic models for alluvial fan deposits: a tool for interpreting ancient sequences. Journal of the Geological Society of London 147: 8-10.

Zanchetta G, Sulpizio R, Di Vito MA (2004) The role of volcanic activity and climate in alluvial fan growth at volcanic areas: an example from southern Campania (Italy). Sedimentary Geology 168: 249-280.

Zellmer GF, Hawkesworth CJ, Sparks RSJ, Thomas LE, Harford CL, Brewer TS, Loughlin SC (2003a)Geochemical evolution of the Soufriere Hills volcano, Montserrat, Lesser Antilles volcanic arc. Journal of Petrology 44: 1349-1374.

APPENDICES (ON DISC)

I. STRATIGRAPHIC SECTION DESCRIPTIONS

II. METHODOLOGY

A. Mineralogy (EMP)

B. Bulk Rock Geochemistry (XRF)

C. Trace Element Geochemistry (ICP-MS)

D. Isotope Analysis

III. RESULTS

A. Radiocarbon dating

B. List of samples for geochemical analyses

C. EMP analyses

D. XRF analyses

E. ICP-MS analyses

F. Isotope data

IV. PAPERS:

A. Sedimentary signatures of cyclic growth and destruction of stratovolcanoes: A case study from Mt. Taranaki, New Zealand.

(Accepted in Sedimentary Geology special volume "Source to sink: from volcanic eruptions to volcaniclastic deposits")